CHEM 212/213: INORGANIC CHEMISTRY



Chip Nataro
Lafayette College

LibreTexts™

Lafayette College: CHEM 211



This text is disseminated via the Open Education Resource (OER) LibreTexts Project (https://LibreTexts.org) and like the thousands of other texts available within this powerful platform, it is freely available for reading, printing, and "consuming."

The LibreTexts mission is to bring together students, faculty, and scholars in a collaborative effort to provide an accessible, and comprehensive platform that empowers our community to develop, curate, adapt, and adopt openly licensed resources and technologies; through these efforts we can reduce the financial burden born from traditional educational resource costs, ensuring education is more accessible for students and communities worldwide.

Most, but not all, pages in the library have licenses that may allow individuals to make changes, save, and print this book. Carefully consult the applicable license(s) before pursuing such effects. Instructors can adopt existing LibreTexts texts or Remix them to quickly build course-specific resources to meet the needs of their students. Unlike traditional textbooks, LibreTexts' web based origins allow powerful integration of advanced features and new technologies to support learning.



LibreTexts is the adaptable, user-friendly non-profit open education resource platform that educators trust for creating, customizing, and sharing accessible, interactive textbooks, adaptive homework, and ancillary materials. We collaborate with individuals and organizations to champion open education initiatives, support institutional publishing programs, drive curriculum development projects, and more.

The LibreTexts libraries are Powered by NICE CXone Expert and was supported by the Department of Education Open Textbook Pilot Project, the California Education Learning Lab, the UC Davis Office of the Provost, the UC Davis Library, the California State University Affordable Learning Solutions Program, and Merlot. This material is based upon work supported by the National Science Foundation under Grant No. 1246120, 1525057, and 1413739.

Any opinions, findings, and conclusions or recommendations expressed in this material are those of the author(s) and do not necessarily reflect the views of the National Science Foundation nor the US Department of Education.

Have questions or comments? For information about adoptions or adaptions contact info@LibreTexts.org or visit our main website at https://LibreTexts.org.

This text was compiled on 01/12/2026

TABLE OF CONTENTS

Licensing

1: Atoms

- 1.1: Mass Spectrometry
- 1.2: Rutherford's Atom
- 1.3: Bohr's Atom
- 1.4: Hydrogen Atom
- 1.5: Slater Rules

2: Molecules

- 2.2: Molecular Shapes
- 2.3: The VSEPR Model
- 2.4: Hybrid Orbitals
- 2.5: Molecular Orbitals
  - 2.5.1: Molecular Shape and Molecular Polarity
  - 2.5.2: Prelude to Molecular Orbital Theory
  - 2.5.3: Constructing Molecular Orbitals from Atomic Orbitals
  - 2.5.4: Orbital Symmetry
  - 2.5.5: Molecular Orbital Diagrams
  - 2.5.6: π Orbitals and Diatomic Molecules
  - 2.5.7: Orbital Filling
  - 2.5.8: δ orbitals
- 2.6: The Range of Bonding
- 2.7: Advanced Bonding
  - 2.7.1: Symmetry Elements and Operations
  - 2.7.2: Point Groups
    - 2.7.2.1: Other Groups
    - 2.7.2.2: Groups of Low and High Symmetry
  - 2.7.3: Ligand Group Orbitals and Generator Functions
  - 2.7.4: Expanded Octets and Molecular Orbitals
- 2.8: Nuclear Magnetic Resonance (NMR)
  - 2.8.1: The Origin of the NMR Signal
  - 2.8.2: Chemical Equivalence
  - 2.8.3: The 1H-NMR experiment
  - 2.8.4: Spin-Spin Coupling
  - 2.8.5: The Basis for Differences in Chemical Shift
- Index
- Glossary
- Detailed Licensing

3: Solid state

- 3.1: Prelude to Metals and Alloys
- 3.2: Unit Cells and Crystal Structures
- 3.3: Crystal Structures of Metals
- 3.4: Conduction in Metals
- 3.5: Atomic Orbitals and Magnetism
- 3.6: Ferro-, Ferri- and Antiferromagnetism
- 3.7: Hard and Soft Magnets
- 3.8: Defects in Metallic Crystals
- 3.9: X-ray Crystallography
- 3.10: Miller Indices (hkl)
- 3.11: Powder X-ray Diffraction
- 3.12: Prelude to Ionic and Covalent Solids - Structures
- 3.13: Close-packing and Interstitial Sites
- 3.14: Structures Related to NaCl and NiAs
- 3.15: Tetrahedral Structures
- 3.16: Layered Structures and Intercalation Reactions
- 3.17: Ionic Radii and Radius Ratios
- 3.18: Structure Maps
- 3.19: Energetics of Crystalline Solids- The Ionic Model
- 3.20: Born-Haber Cycles for NaCl and Silver Halides
- 3.21: Lattice Energies and Solubility
- 3.22: Spinel, Perovskite, and Rutile Structures
- 3.23: Kapustinskii Equation

4: Acid-Base Theories

- 4.1: Bronsted-Lowry acids and bases
- 4.2: Lewis Acids and Bases
- 4.3: Acidity of the Hexaaqua Ions
- 4.4: Hard-soft Acids and Bases
- 4.5: Quantitative Measures of Hardness and Softness

5: Coordination Chemistry

- 5.1: Introduction to Coordination Chemistry
- 5.2: Ligands and Nomenclature
- 5.3: Coordination Numbers and Geometry
- 5.4: Bonding with d-orbitals
- 5.5: Isomers
  - 5.5.1: Structural Isomers - Ionization Isomerism in Transition Metal Complexes
  - 5.5.2: Structural Isomers - Geometric Isomerism in Transition Metal Complexes
  - 5.5.3: Stereoisomers - Optical Isomerism in Transition Metal Complexes
  - 5.5.4: Structural Isomers - Linkage Isomerism in Transition Metal Complexes
- 5.6: Crystal Field Theory
  - 5.6.1: Crystal Field Theory
  - 5.6.2: Colors of Coordination Complexes
  - 5.6.3: Crystal Field Stabilization Energy
  - 5.6.4: Factors That Affect the Magnitude of Δo
  - 5.6.5: Jahn-Teller Distortions

- 5.6.6: Magnetic Moments of Transition Metals
- 5.6.7: Magnetism
- 5.6.8: Thermodynamics and Structural Consequences of d-Orbital Splitting
- 5.7: Ligand Field Theory
- 5.8: Ligand Exchange Reactions (Thermodynamics)
- 5.9: Electronic Spectra of Coordination Compounds

6: Bioinorganic Chemistry

- 6.1: Biological Significance of Iron, Zinc, Copper, Molybdenum, Cobalt, Chromium, Vanadium, and Nickel
- 6.2: Introduction to Amino Acids and Proteins
- 6.3: Redox Reactions
  - 6.3.1: Introduction to Redox Reactions
  - 6.3.2: Balancing Redox Reactions
  - 6.3.3: Electrochemical Potentials
  - 6.3.4: Prelude to Redox Stability and Redox Reactions
  - 6.3.5: Latimer and Frost Diagrams
  - 6.3.6: Pourbaix Diagrams
- 6.4: Associative Ligand Substitution
- 6.5: Dissociative Ligand Substitution
- 6.6: Biological Significance of Iron, Zinc, Copper, Molybdenum, Cobalt, Chromium, Vanadium, and Nickel
- 6.7: Ferrodoxins, Hydrogenases, and Nitrogenases - Metal-Sulfide Proteins
  - 6.7.1: Iron-sulfur Proteins and Models
  - 6.7.2: Iron-sulfur Proteins and Models (Part 2)
  - 6.7.3: Iron-sulfur Proteins and Models (Part 3)
  - 6.7.4: Iron-sulfur Proteins and Models (Part 4)
- 6.8: Overview of Hemoglobin and Myoglobin
  - 6.8.1: Myoglobin, Hemoglobin, and their Ligands
  - 6.8.2: Oxygen Transport by the Proteins Myoglobin and Hemoglobin

Index

Glossary

Glossary

Detailed Licensing

Licensing

*A detailed breakdown of this resource's licensing can be found in **Back Matter/Detailed Licensing**.*

CHAPTER OVERVIEW

1: Atoms

1.1: Mass Spectrometry
1.2: Rutherford's Atom
1.3: Bohr's Atom
1.4: Hydrogen Atom
1.5: Slater Rules

1: Atoms is shared under a not declared license and was authored, remixed, and/or curated by LibreTexts.

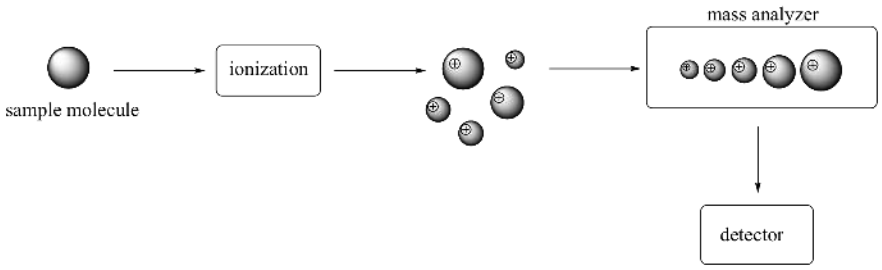
1.1: Mass Spectrometry

Mass spectrometry (MS) is a powerful analytical technique widely used by chemists, biologists, medical researchers, and environmental and forensic scientists, among others. With MS, we are looking at the mass of a molecule, or of different fragments of that molecule.

The basics of a mass spectrometry experiment

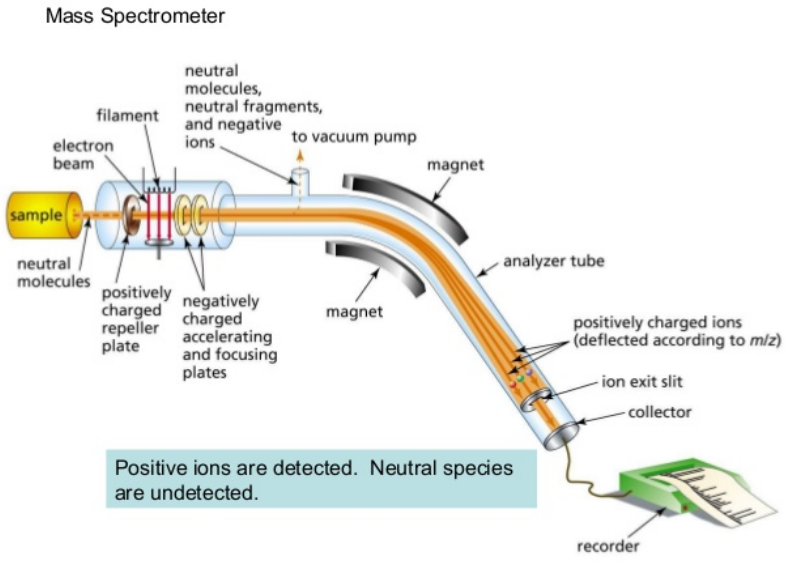
There are many different types of MS instruments, but they all have the same three essential components. First, there is an ionization source, where the molecule is given a positive electrical charge, either by removing an electron or by adding a proton. Depending on the ionization method used, the ionized molecule may or may not break apart into a population of smaller fragments. In the figure below, some of the sample molecules remain whole, while others fragment into smaller pieces.

Next in line there is a mass analyzer, where the cationic fragments are separated according to their mass.



Finally, there is a detector, which detects and quantifies the separated ions.

One of the more common types of MS techniques used in the organic laboratory is **electron ionization**. In the ionization source, the sample molecule is bombarded by a high-energy electron beam, which has the effect of knocking a valence electron off of the molecule to form a **radical cation**. Because a great deal of energy is transferred by this bombardment process, the radical cation quickly begins to break up into smaller fragments, some of which are positively charged and some of which are neutral. The neutral fragments are either adsorbed onto the walls of the chamber or are removed by a vacuum source. In the mass analyzer component, the positively charged fragments and any remaining unfragmented **molecular ions** are accelerated down a tube by an electric field.

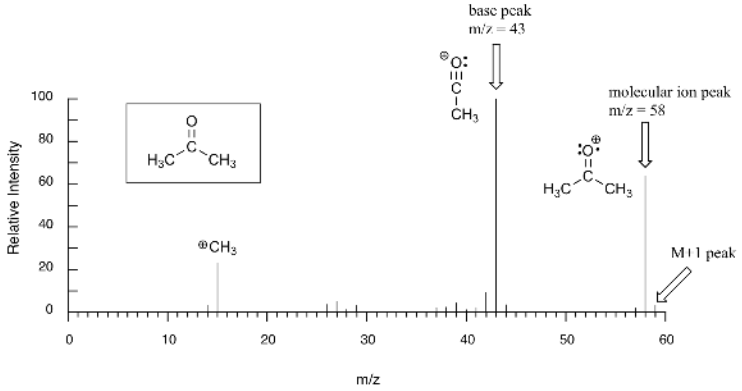


(Image from Wikipedia Commons)

This tube is curved, and the ions are deflected by a strong magnetic field. Ions of different mass to charge (m/z) ratios are deflected to a different extent, resulting in a 'sorting' of ions by mass (virtually all ions have charges of z = +1, so sorting by the mass to charge ratio is the same thing as sorting by mass). A detector at the end of the curved flight tube records and quantifies the sorted ions.

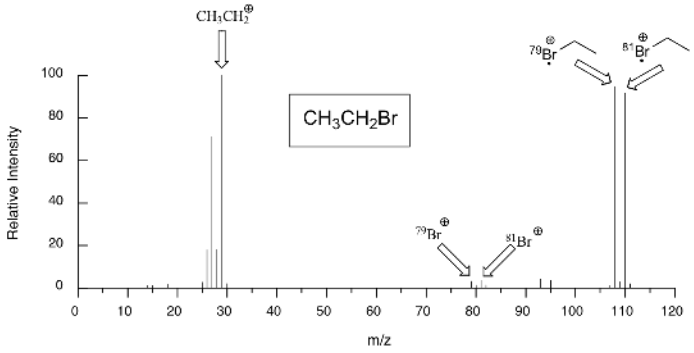
Looking at mass spectra

Below is typical output for an electron-ionization MS experiment (MS data in the section is derived from the Spectral Database for Organic Compounds, a free, web-based service provided by AIST in Japan.



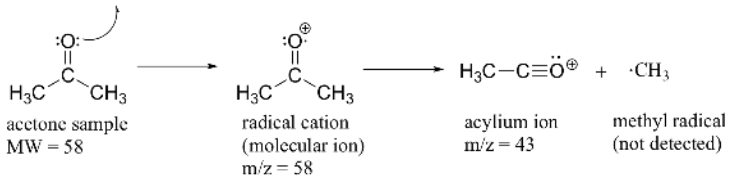
The sample is acetone. On the horizontal axis is the value for m/z (as we stated above, the charge z is almost always +1, so in practice this is the same as mass). On the vertical axis is the relative abundance of each ion detected. On this scale, the most abundant ion, called the **base peak**, is set to 100%, and all other peaks are recorded relative to this value. For acetone, the base peak is at m/z = 43 - we will discuss the formation of this fragment a bit later. The molecular weight of acetone is 58, so we can identify the peak at m/z = 58 as that corresponding to the **molecular ion peak**, or **parent peak**. Notice that there is a small peak at m/z = 59: this is referred to as the **M+1 peak**. How can there be an ion that has a greater mass than the molecular ion? Simple: a small fraction - about 1.1% - of all carbon atoms in nature are actually the ^{13}C rather than the ^{12}C isotope. The ^{13}C isotope is, of course, heavier than ^{12}C by 1 mass unit. In addition, about 0.015% of all hydrogen atoms are actually deuterium, the ^{2}H isotope. So the M+1 peak represents those few acetone molecules in the sample which contained either a ^{13}C or ^{2}H.

Molecules with lots of oxygen atoms sometimes show a small **M+2 peak** (2 m/z units greater than the parent peak) in their mass spectra, due to the presence of a small amount of ^{18}O (the most abundant isotope of oxygen is ^{16}O). Because there are two abundant isotopes of both chlorine (about 75% ^{35}Cl and 25% ^{37}Cl) and bromine (about 50% ^{79}Br and 50% ^{81}Br), chlorinated and brominated compounds have very large and recognizable M+2 peaks. Fragments containing both isotopes of Br can be seen in the mass spectrum of ethyl bromide:

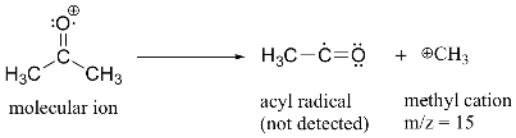


Much of the utility in electron-ionization MS comes from the fact that the radical cations generated in the electron-bombardment process tend to fragment in predictable ways. Detailed analysis of the typical fragmentation patterns of different functional groups is beyond the scope of this text, but it is worthwhile to see a few representative examples, even if we don't attempt to understand the exact process by which the fragmentation occurs. We saw, for example, that the base peak in the mass spectrum of acetone is

m/z = 43. This is the result of cleavage at the 'alpha' position - in other words, at the carbon-carbon bond adjacent to the carbonyl. Alpha cleavage results in the formation of an acylium ion (which accounts for the base peak at m/z = 43) and a methyl radical, which is neutral and therefore not detected.



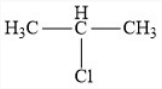
After the parent peak and the base peak, the next largest peak, at a relative abundance of 23%, is at m/z = 15. This, as you might expect, is the result of formation of a methyl cation, in addition to an acyl radical (which is neutral and not detected).



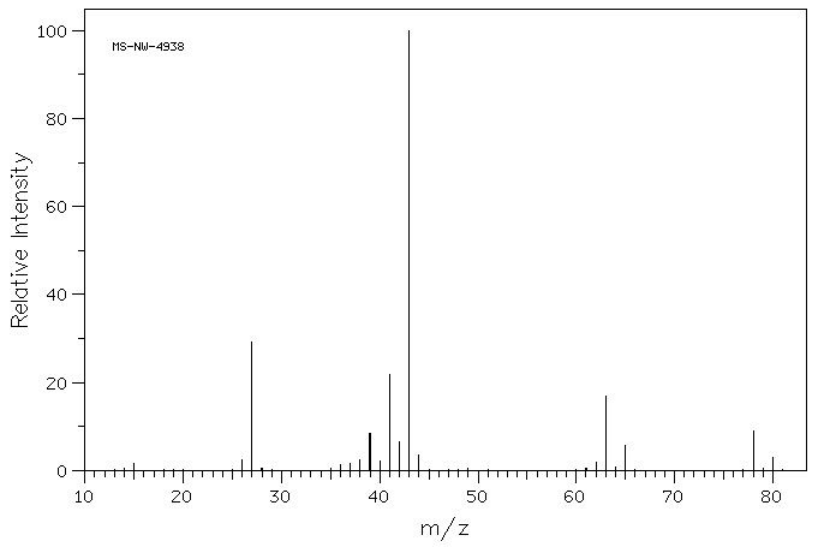
You can see many more actual examples of mass spectra in the Spectral Database for Organic Compounds

Exercise 1.1

Predict some signals that you would expect to see in a mass spectrum of 2-chloropropane.



Answer



There are two isotopes of Cl, Cl-35 and Cl-37.

The molecular ion appears at 78 which would contain Cl-35 and the peak at 80 contains Cl-37.

This pattern can be quite indicative of a fragment still containing a chlorine atom.

The next major peak grouping occurs at 63 and 65. The relative abundance values of the peaks and the difference of 2 in terms of mass suggest that there is still a chlorine atom in this fragment. The difference in mass from the molecular ion is 15, which based on the molecular formula can only be accounted for by the loss of a CH_3 unit. This suggests that these two peaks are due to the fragments $CH_3CH\text{-}^{35}Cl$ and $CH_3CH\text{-}^{37}Cl$.

There is a cluster of peaks around 40. This is a little tougher to interpret. Thinking about the starting molecule, one might consider breaking the C-Cl bond. That would give a fragment of H_3CCHCH_3 which would have a mass of 43 matching the highest intensity peak.

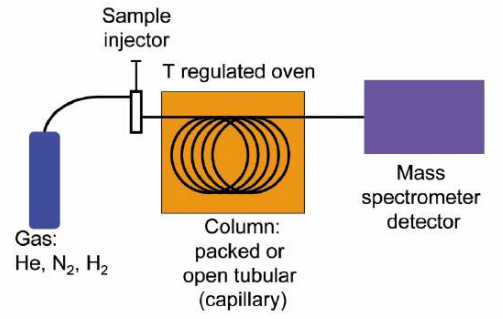
The mass of chlorine on the periodic table is closer to 35 than 37 indicating that the Cl-35 isotope is more abundant that Cl-37. This can also be seen in the molecular ion. One might consider saying that the peak at 41 is just due to the other isotope of chlorine. However, the peak at 43 does not contain chlorine and the relative ratio of 43 to 41 does not support the presence of chlorine. It is much more likely that the peak at 41 is due to loss of two hydrogen atoms from the fragment with a mass of 43. Which specific hydrogen atoms is well beyond the scope of this course, so we will just say the fragment is C_3H_5.

The final major peak has a mass of 27. This would correspond to a fragment of C_2H_3.

The spectrum was obtained from SDBSWeb. (National Institute of Advanced Industrial Science and Technology, 1/18/21).

Gas Chromatography - Mass Spectrometry

Quite often, mass spectrometry is used in conjunction with a separation technique called gas chromatography (GC). The combined GC-MS procedure is very useful when dealing with a sample that is a mixture of two or more different compounds, because the various compounds are separated from one another before being subjected individually to MS analysis. We will not go into the details of gas chromatography here, although if you are taking an organic laboratory course you might well get a chance to try your hand at GC, and you will almost certainly be exposed to the conceptually analogous techniques of thin layer and column chromatography. Suffice it to say that in GC, a very small amount of a liquid sample is vaporized, injected into a long, coiled metal column, and pushed though the column by helium gas. Along the way, different compounds in the sample stick to the walls of the column to different extents, and thus travel at different speeds and emerge separately from the end of the column. In GC-MS, each purified compound is sent directly from the end of GC column into the MS instrument, so in the end we get a separate mass spectrum for each of the compounds in the original mixed sample. Because a compound's MS spectrum is a very reliable and reproducible 'fingerprint', we can instruct the instrument to search an MS database and identify each compound in the sample.



Gas chromatography-mass spectrometry (GC-MS) schematic

(Image from Wikipedia by K. Murray)

The extremely high sensitivity of modern GC-MS instrumentation makes it possible to detect and identify very small trace amounts of organic compounds. GC-MS is being used increasingly by environmental chemists to detect the presence of harmful organic contaminants in food and water samples. Airport security screeners also use high-speed GC-MS instruments to look for residue from bomb-making chemicals on checked luggage.

Contributors

- Organic Chemistry With a Biological Emphasis by Tim Soderberg (University of Minnesota, Morris)

This page titled 1.1: Mass Spectrometry is shared under a CC BY-NC-SA 4.0 license and was authored, remixed, and/or curated by Tim Soderberg.

1.2: Rutherford's Atom

Learning Objectives

- Introduce the initial attempts to explain the structure of atoms.

The Gold Foil Experiment

In 1911, Rutherford and coworkers Hans Geiger and Ernest Marsden initiated a series of groundbreaking experiments that would completely change the accepted model of the atom. They bombarded very thin sheets of gold foil with fast moving **alpha particles**. Alpha particles, a type of natural radioactive particle, are positively charged particles with a mass about four times that of a hydrogen atom.

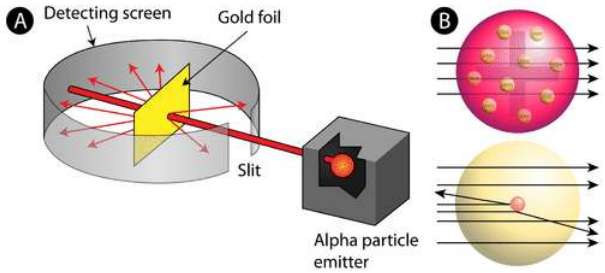


Figure **1.2.1**: *(A) The experimental setup for Rutherford's gold foil experiment: A radioactive element that emitted alpha particles was directed toward a thin sheet of gold foil that was surrounded by a screen which would allow detection of the deflected particles. (B) According to the plum pudding model (top) all of the alpha particles should have passed through the gold foil with little or no deflection. Rutherford found that a small percentage of alpha particles were deflected at large angles, which could be explained by an atom with a very small, dense, positively-charged nucleus at its center (bottom).*

According to the accepted atomic model, in which an atom's mass and charge are uniformly distributed throughout the atom, the scientists expected that all of the alpha particles would pass through the gold foil with only a slight deflection or none at all. Surprisingly, while most of the alpha particles were indeed undeflected, a very small percentage (about 1 in 8000 particles) bounced off the gold foil at very large angles. Some were even redirected back toward the source. No prior knowledge had prepared them for this discovery. In a famous quote, Rutherford exclaimed that it was "as if you had fired a 15-inch [artillery] shell at a piece of tissue and it came back and hit you."

Rutherford needed to come up with an entirely new model of the atom in order to explain his results. Because the vast majority of the alpha particles had passed through the gold, he reasoned that most of the atom was empty space. In contrast, the particles that were highly deflected must have experienced a tremendously powerful force within the atom. He concluded that all of the positive charge and the majority of the mass of the atom must be concentrated in a very small space in the atom's interior, which he called the nucleus. The **nucleus** is the tiny, dense, central core of the atom and is composed of protons and neutrons.

Rutherford's atomic model became known as the **nuclear model**. Most of the α-particles were not scattered; they passed unchanged through the thin metal foil. Some of the few that were scattered were scattered in the backward direction; i.e. they recoiled. This backward scattering requires that the foil contain heavy particles. When an α-particle hits one of these heavy particles it simply recoils backward, just like a ball thrown at a brick wall. Since most of the α-particles don’t get scattered, the heavy particles (the nuclei of the atoms) must occupy only a very small region of the total space of the atom. Most of the space must be empty or occupied by very low-mass particles. These low-mass particles are the electrons that surround the nucleus. It is worth emphasizing just how small the nucleus is compared to the rest of the atom. If we could blow up an atom to be the size of a large professional football stadium, the nucleus would be about the size of a marble.

Rutherford's Failed Planetary Atom

There are some basic problems with the Rutherford model. The Coulomb force that exists between oppositely charge particles means that a positive nucleus and negative electrons should attract each other, and the atom should collapse. To prevent the collapse, the electron was postulated to be orbiting the positive nucleus. The Coulomb force (discussed below) is used to change the direction of the velocity, just as a string pulls a ball in a circular orbit around your head or the gravitational force holds the

moon in orbit around the Earth. The origin for this hypothesis that suggests this perspective is plausible is the similarity of gravity and Coulombic interactions. The expression for the force of gravity between two masses (Newton's Law of gravity) is

$$F_{gravity} \propto \frac{m_1 m_2}{r^2} \tag{1.2.1}$$

with m_1 and m_2 representing the **mass** of object 1 and 2, respectively and r representing the distance between the objects centers

The expression for the Coulomb force between two charged species is

$$F_{Coulomb} \propto \frac{Q_1 Q_2}{r^2} \tag{1.2.2}$$

with Q_1 and Q_2 representing the **charge** of object 1 and 2, respectively and r representing the distance between the objects centers.

However, this analogy has a problem too. An electron going around in a circle is constantly being accelerated because its velocity vector is changing. A charged particle that is being accelerated emits radiation. This property is essentially how a radio transmitter works. A power supply drives electrons up and down a wire and thus transmits energy (electromagnetic radiation) that your radio receiver picks up. The radio then plays the music for you that is encoded in the waveform of the radiated energy.

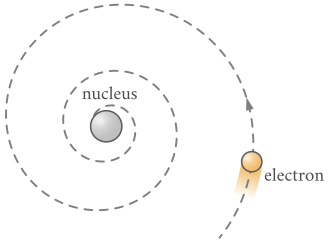


Figure 1.2.2: The classical death spiral of an electron around a nucleus. (CC BY-NC; Ümit Kaya)

If the orbiting electron is generating radiation, it is losing energy. If an orbiting particle loses energy, the radius of the orbit decreases. To conserve angular momentum, the frequency of the orbiting electron increases. The frequency increases continuously as the electron collapses toward the nucleus. Since the frequency of the rotating electron and the frequency of the radiation that is emitted are the same, both change continuously to produce a continuous spectrum and not the observed discrete lines. Furthermore, if one calculates how long it takes for this collapse to occur, one finds that it takes about 10^{-11} seconds. This means that nothing in the world based on the structure of atoms could exist for longer than about 10^{-11} seconds. Clearly something is terribly wrong with this classical picture, which means that something was missing at that time from the known laws of physics.

Conservative Forces can be explained with Potentials

A conservative force is dependent only on the position of the object. If a force is conservative, it is possible to assign a numerical value for the potential at any point. When an object moves from one location to another, the force changes the potential energy of the object by an amount that does not depend on the path taken. The potential can be constructed as simple derivatives for 1-D forces:

$$F = -\frac{dV}{dx}$$

or as gradients in 3-D forces

$$F = -\nabla V$$

where ∇ is the vector of partial derivatives

$$\nabla = \left(\frac{\partial}{\partial x}, \frac{\partial}{\partial y}, \frac{\partial}{\partial z}\right)$$

The most familiar conservative forces are gravity and Coloumbic forces.

The Coulomb force law (Equation 1.2.2) comes from the corresponding Coulomb potential (sometimes call electrostatic potential)

$$V(r) = \frac{kQ_1Q_2}{r} \tag{1.2.3}$$

and it can be easily verified that the Coulombic force from this interaction ($F(r)$ is

$$F(r) = -\frac{dV}{dr} \tag{1.2.4}$$

As r is varied, the energy will change, so that we have an example of a potential energy curve $V(r)$ (Figure 1.2.2;). If Q_1 and Q_2 are the same sign, then the curve which is a purely **repulsive potential**, i.e., the energy increases monotonically as the charges are brought together and decreases monotonically as they are separated. From this, it is easy to see that like charges (charges of the same sign) repel each other.

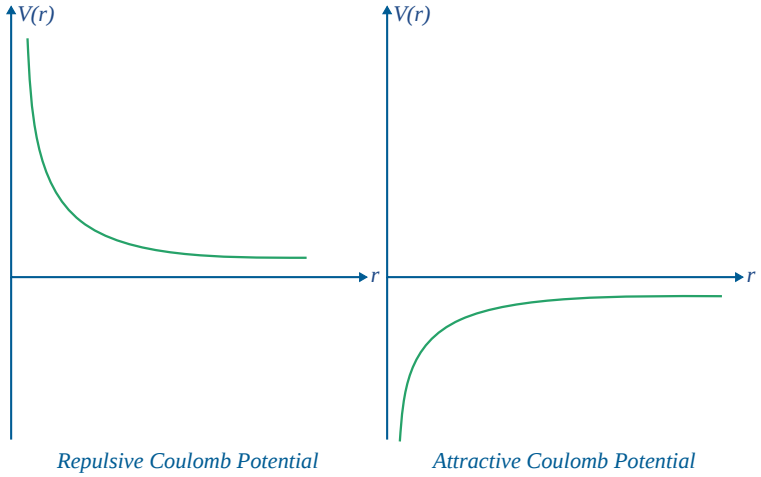


Figure 1.2.3: Potential energy curve for the Coulomb interactions between two charges of same sign (left) and opposite signs (right). (CC BY-NC; Ümit Kaya)

If the charges are of opposite sign, then the curve appears roughly Figure 1.2.2; and this is a purely **attractive potential**. Thus, the energy decreases as the charges are brought together, implying that opposite charges attract.

Contributors and Attributions

- CK-12 Foundation by Sharon Bewick, Richard Parsons, Therese Forsythe, Shonna Robinson, and Jean Dupon.
- Mark Tuckerman (New York University)
- David M. Hanson, Erica Harvey, Robert Sweeney, Theresa Julia Zielinski ("Quantum States of Atoms and Molecules")
- Template:Contriboundless

1.2: Rutherford's Atom is shared under a not declared license and was authored, remixed, and/or curated by LibreTexts.

1.3: Bohr's Atom

Review Necessary Skills

- Relate the wavelength (λ) and frequency (ν) of light to the velocity of light (c) ($c = \lambda\nu$) and to the energy of a photon (E) ($E = h\nu = hc/\lambda$).
  - Find help using $c = \lambda\nu$ and lots of problems here on ChemTeam.
  - Find help using $E = h\nu = hc/\lambda$ and lots of problems here on ChemTeam.
- Relate charge, distance, and electrostatic potential energy using Coulomb's law ($U = k\, q_1 \times q_2/r$) qualitatively.
  - Here is an interactive simulation.
  - Coulomb's law
  - Here is a review in the context of atoms with some problems.
- Describe what happens to molecules when they interact with electromagnetic radiation.
  - What happens to molecules at different wavelengths? See NO_2 in this simulation. Don't worry if this doesn't look familiar, it is just a reminder that IR, microwave, and UV light all interact with molecules differently.

Experiments that can't be explained without quantization of energy or position

Photoelectric effect
(see demo below or go to PheT)



Click to Run or Download (Needs Java!)

Atomic line spectra
(see demo below or go to PheT)



Click to Run or Download (Needs Java!)

Electron diffraction
(see demo below or go to PheT)



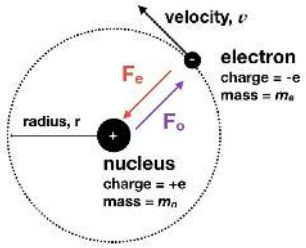
Click to Run

Double-slit experiment
(see demo or go to PheT)



Click to Run or Download (Needs Java!)

Bohr's Model of the Hydrogen Atom



The Danish scientist, Niels Bohr, introduced the first theory that quantized the energy of electrons in atoms. Although Bohr's reasoning relies on classical concepts and hence, is not a correct explanation, the reasoning is interesting, and so we examine this model for its historical significance. This is now referred to as "Old Quantum Theory", while the "New Quantum Theory" is that described by the Schrodinger equation, and that will be described a bit later. Below, the story of Bohr's model will be described. Another way to tell the story is here.

Bohr's Condition of a Stable Orbit: Bohr imagined that electrons were in circular orbit around a nucleus. He applied classical mechanics to rationalize that if the electron of charge, $-e$, were to be in a stable orbit around a nucleus of opposite charge, $+e$, then the electrostatic attractive force (F_e) between the electron and nucleus must be exactly opposed by the outward centripetal force (F_o) created by the electron's circular orbit. (We can ignore any gravitational force because it is relatively weak.)

Where the electrostatic attractive force F_e and centripetal force F_o are,

$$F_e = \frac{(+e)(-e)}{r^2} = -\frac{e^2}{r^2} \tag{1.3.1}$$

$$F_o = \frac{m_e v^2}{r} \tag{1.3.2}$$

For a stable orbit to exist $F_e + F_o = 0$, or,

$$F_o = -F_e \tag{1.3.3}$$

$$\frac{m_e v^2}{r} = \frac{e^2}{r^2} \tag{1.3.4}$$

Bohr's Calculation of the Electron's Energy: Bohr could calculate the total energy of the electron, again using classical mechanics. The total energy of a system is the sum of the kinetic energy (KE, energy of motion of the electron) and the potential energy (PE, from the electrostatic attraction, F_e and the distance, r).

$$KE = \frac{1}{2} m_e v^2 \tag{1.3.5}$$

$$PE = rF_e = r\left(-\frac{e^2}{r^2}\right) = -\frac{e^2}{r} \tag{1.3.6}$$

If total Energy (E) is equal to the sum of KE and PE,

$$E = KE + PE = \frac{1}{2} m_e v^2 - \frac{e^2}{r} \tag{1.3.7}$$

This expression can be simplified by first solving equation (4) for $m_e v^2 = \frac{e^2}{r}$ and substituting into equation 7.

$$E = \frac{1}{2}\left(\frac{e^2}{r}\right) - \frac{2}{2}\left(\frac{e^2}{r}\right) = -\frac{1}{2}\left(\frac{e^2}{r}\right) = -\frac{e^2}{2r} \tag{1.3.8}$$

Now we see that energy of the electron, E, can be calculated if we know the distance, r, at which the electron is orbiting. This is a good time to remind ourselves that we also know, from Planck's work, that $E = h\nu$. This reminds us that the electron is a wave with frequency, ν, in units of sec^{-1}. So, we could also write,

$$E = -\frac{e^2}{2r} = h\nu \tag{1.3.9}$$

Bohr's Quantization, and Equations for Radius, r, and Velocity, v: Bohr knew that electrons must have stable orbits, otherwise the electrons would fall into the nucleus. Bohr was familiar with Maxwell's theory of classical electromagnetism and knew that in a classical theory, the orbiting electron should radiate energy away and eventually collapse into the nucleus (E is given off as r decreases). He circumvented this problem by following Planck's idea underlying blackbody radiation and positing that the orbital angular momentum $p = m_e v r$ of the electron could only take on specific values. He proposed those values to be units of $\frac{h}{2\pi}$, where h is Planck's constant. Bohr's proposal was,

$$m_e v r = n\frac{h}{2\pi} \tag{1.3.10}$$

where n is the first quantum number and can have values of any integer ($n = 1, 2, 3...$). This relationship can be rearranged to find the velocity, v,

$$v = n\frac{h}{m_e r 2\pi} \tag{1.3.11}$$

This implies that only certain velocities are allowed, since only certain values of n are allowed. This expression for v can be substituted into the condition of a stable orbit (using a rearranged version of equation 4, ($m_e v^2 = \frac{e^2}{r}$) to give equation 12. Ultimately, this allows us to find how the radius, r, depends on the the quantum number, n, as shown in equation 13.

$$\frac{m_e\left(n\frac{h}{m_e r 2\pi}\right)^2}{r} = \frac{m_e n^2 h^2}{4m_e^2 r^2 \pi^2} = \frac{n^2 h^2}{4m_e r^2 \pi^2} = \frac{e^2}{r} \tag{1.3.12}$$

This expression can be rearranged to solve for r,

$$r = \frac{n^2 h^2}{4\pi^2 m_e e^2 K} \tag{1.3.13}$$

K is the Coulomb constant which is needed for unit conversion and has a value of

$K = 8.9875517923x10^9 \frac{Nm^2}{C^2}$

This expression shows Bohr's assumption that there are discrete distances where the electron can orbit, as the values or r are restricted by the integer values of n. The relationship between n and E is found by substitution of the equation for r into equation 8 or 9.

$$E = -\frac{e^2 K}{2\left(\frac{n^2 h^2}{4\pi^2 m_e e^2 K}\right)} = -\frac{e^2 K 4\pi^2 m_e e^2 K}{2n^2 h^2} = -\frac{2\pi^2 m_e e^4 2K^2}{n^2 h^2} \tag{1.3.14}$$

This expression shows that energy is quantized, as like values of v and r, the energy depends on the integer value, n.

Exercise 1.3.1

Show how you would find the Bohr radius, velocity, and energy of an electron in the first shell of a hydrogen atom.

Answer

$r = \frac{n^2 h^2}{4\pi^2 m_e e^2 K}$

$r = \frac{1^2(6.626070x10^{-34})^2}{4(3.141592654)^2(9.10938356x10^{-31})(1.602176634x10^{-19})^2(8.9875517923x10^9)}$

$r = \frac{(4.390480364x10^{-67})J^2s^2}{(8.296805693x10^{-67})kgNm^2}$

$r = 5.292x10^{-11}m$

$v = n\frac{h}{m_e r 2\pi}$

$v = 1\frac{6.626070x10^{-34}}{(9.10938356x10^{-31})(5.292x10^{-11})2(3.141592654)}$

$v = \frac{6.626070x10^{-34}Js}{3.028926207x10^{-40}kgm}$

$v = 2.19x10^6 m/s$

$E = -\frac{2\pi^2 m_e e^4 2K^2}{n^2 h^2}$

$E = -\frac{2(3.141592654)^2(9.10938356x10^{-31})(1.602176634x10^{-19})^4(8.9875517923x10^9)^2}{1^2(6.626070x10^{-34})^2}$

$E = -\frac{9.570687085x10^{-85}kgN^4m^4}{4.390480367x10^{-67}J^2s^2}$

$E = -2.1799x10^{-18}J$

Hydrogen Absorption and Emission Spectra

When a high-voltage electrical discharge is passed through a sample of hydrogen gas (H_2) at low pressure, the result is individual isolated hydrogen atoms that emit a red light. Unlike blackbody radiation, the color of the light emitted by the hydrogen atoms does not depend greatly on the temperature of the gas in the tube. When the emitted light is passed through a prism, only a few narrow lines of particular wavelengths,

called a line spectrum, are observed rather than a continuous range of wavelengths (Figure **1.3.1**). The light emitted by hydrogen atoms is red because, of its four characteristic lines, the most intense line in its spectrum is in the red portion of the visible spectrum, at 656 nm.

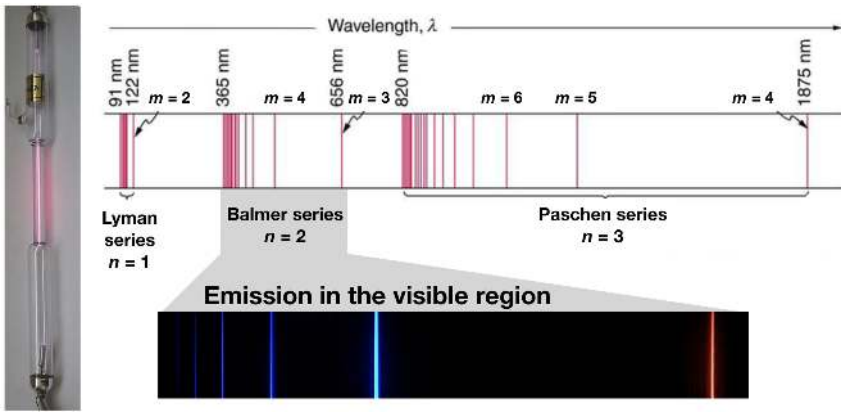


Figure* 1.3.1*: *The Emission of Light by Hydrogen Atoms. (left) A sample of excited hydrogen atoms emits a characteristic red light. (bottom) When the light emitted by a sample of excited hydrogen atoms is split into its component wavelengths by a prism, four characteristic violet, blue, green, and red emission lines can be observed, the most intense of which is at 656 nm. (top) An diagram showing extended regions of the electromagnetic spectrum and the hydrogen line spectra that are observed.*

In 1885, a Swiss mathematics teacher, Johann Balmer (1825–1898), showed that the frequencies of the lines observed in the visible region of the hydrogen line spectrum fit a simple equation that can be expressed as follows:

$$\nu = constant\left(\frac{1}{2^2} - \frac{1}{n^2}\right) \tag{1.3.15}$$

where n = 3, 4, 5, 6. As a result, these lines are known as the *Balmer series*. The Swedish physicist Johannes Rydberg (1854–1919) subsequently restated and expanded Balmer's result in the *Rydberg equation*:

$$\frac{1}{\lambda} = R_h\left(\frac{1}{n^2} - \frac{1}{m^2}\right) \tag{1.3.16}$$

where n and m are positive integers, $m > n$, and R_h the *Rydberg constant*, has a value of 1.09737 × 10^7 m^{-1}. Like Balmer's equation, Rydberg's simple equation described the wavelengths of the visible lines in the emission spectrum of hydrogen (with n = 2, m = 3, 4, 5,…). More important, Rydberg's equation also predicted the wavelengths of other series of lines that would be observed in the emission spectrum of hydrogen: one in the ultraviolet (n = 1, m = 2, 3, 4,…) and one in the infrared (n = 3, m = 4, 5, 6).

Exercise 1.3.2

Solve the Rydberg Equation for a line where $m = 3$ and $n = 1$. In what region of the electromagnetic spectrum does this appear, and which series is this?

Answer

$\frac{1}{\lambda} = R_h\left(\frac{1}{n^2} - \frac{1}{m^2}\right)$

$\frac{1}{\lambda} = 1.09737x10^7 m^{-1}\left(\frac{1}{1^2} - \frac{1}{3^2}\right)$

$\frac{1}{\lambda} = 9754400m^{-1}$

$\lambda = 1.03x10^{-7}m = 102.5nm$

This is in the Ultra-violet region.

Sources

The Bohr Theory of the Hydrogen Atom

Line Spectra and the Bohr Model

1.3: Bohr's Atom is shared under a not declared license and was authored, remixed, and/or curated by LibreTexts.

1.4: Hydrogen Atom

Atomic Spectra

When gaseous hydrogen in a glass tube is excited by a 5000-volt electrical discharge, four lines are observed in the visible part of the emission spectrum: red at 656.3 nm, blue-green at 486.1 nm, blue violet at 434.1 nm and violet at 410.2 nm:



Figure 1.4.1: Visible spectrum of atomic hydrogen.

Other series of lines have been observed in the ultraviolet and infrared regions. Rydberg (1890) found that all the lines of the atomic hydrogen spectrum could be fitted to a single formula

$$\frac{1}{\lambda} = \mathcal{R}\left(\frac{1}{n_1^2} - \frac{1}{n_2^2}\right), \quad n_1 = 1,\ 2,\ 3\ldots,\ n_2 > n_1 \tag{1.4.1}$$

where $\mathcal{R}$, known as the Rydberg constant, has the value $109,677$ cm^{-1} for hydrogen. The reciprocal of wavelength, in units of cm^{-1}, is in general use by spectroscopists. This unit is also designated *wavenumbers*, since it represents the number of wavelengths per cm. The Balmer series of spectral lines in the visible region, shown in Figure 1.4.1, correspond to the values $n_1 = 2,\ n_2 = 3,\ 4,\ 5$ and 6. The lines with $n_1 = 1$ in the ultraviolet make up the Lyman series. The line with $n_2 = 2$, designated the Lyman alpha, has the longest wavelength (lowest wavenumber) in this series, with $1/\lambda = 82.258$ cm^{-1} or $\lambda = 121.57$ nm.

Other atomic species have line spectra, which can be used as a "fingerprint" to identify the element. However, no atom other than hydrogen has a simple relation analogous to Equation 1.4.1 for its spectral frequencies. Bohr in 1913 proposed that all atomic spectral lines arise from transitions between discrete energy levels, giving a photon such that

$$\Delta E = h\nu = \frac{hc}{\lambda} \tag{1.4.2}$$

This is called the *Bohr frequency condition*. We now understand that the atomic transition energy ΔE is equal to the energy of a photon, as proposed earlier by Planck and Einstein.

The Bohr Atom

The nuclear model proposed by Rutherford in 1911 pictures the atom as a heavy, positively-charged nucleus, around which much lighter, negatively-charged electrons circulate, much like planets in the Solar system. This model is however completely untenable from the standpoint of classical electromagnetic theory, for an accelerating electron (circular motion represents an acceleration) should radiate away its energy. In fact, a hydrogen atom should exist for no longer than 5×10^{-11} sec, time enough for the electron's death spiral into the nucleus. This is one of the worst quantitative predictions in the history of physics. It has been called the Hindenberg disaster on an atomic level. (Recall that the Hindenberg, a hydrogen-filled dirigible, crashed and burned in a famous disaster in 1937.)

Bohr sought to avoid an atomic catastrophe by proposing that certain orbits of the electron around the nucleus could be exempted from classical electrodynamics and remain stable. The Bohr model was quantitatively successful for the hydrogen atom, as we shall now show.

We recall that the attraction between two opposite charges, such as the electron and proton, is given by Coulomb's law

$$F = \begin{cases} -\dfrac{e^2}{r^2} & \text{(gaussian units)} \\ -\dfrac{e^2}{4\pi\epsilon_0 r^2} & \text{(SI units)} \end{cases} \tag{1.4.3}$$

We prefer to use the Gaussian system in applications to atomic phenomena. Since the Coulomb attraction is a central force (dependent only on r), the potential energy is related by

$$F = -\frac{dV(r)}{dr} \tag{1.4.4}$$

We find therefore, for the mutual potential energy of a proton and electron,

$$V(r) = -\frac{e^2}{r} \tag{1.4.5}$$

Bohr considered an electron in a circular orbit of radius r around the proton. To remain in this orbit, the electron must be experiencing a centripetal acceleration

$$a = -\frac{v^2}{r} \tag{1.4.6}$$

where v is the speed of the electron. Using Equations 1.4.4 and 1.4.6 in Newton's second law, we find

$$\frac{e^2}{r^2} = \frac{mv^2}{r} \tag{1.4.7}$$

where m is the mass of the electron. For simplicity, we assume that the proton mass is infinite (actually $m_p \approx 1836 m_e$) so that the proton's position remains fixed. We will later correct for this approximation by introducing reduced mass. The energy of the hydrogen atom is the sum of the kinetic and potential energies:

$$E = T + V = \frac{1}{2}mv^2 - \frac{e^2}{r} \tag{1.4.8}$$

Using Equation 1.4.7, we see that

$$T = -\frac{1}{2}V \qquad \text{and} \qquad E = \frac{1}{2}V = -T \tag{1.4.9}$$

This is the form of the virial theorem for a force law varying as r^{-2}. Note that the energy of a bound atom is *negative*, since it is lower than the energy of the separated electron and proton, which is taken to be zero.

For further progress, we need some restriction on the possible values of r or v. This is where we can introduce the quantization of angular momentum $\mathbf{L} = \mathbf{r} \times \mathbf{p}$. Since $\mathbf{p}$ is perpendicular to $\mathbf{r}$, we can write simply

$$L = rp = mvr \tag{1.4.10}$$

Using Equation 1.4.9, we find also that

$$r = \frac{L^2}{me^2} \tag{1.4.11}$$

We introduce angular momentum quantization, writing

$$L = n\hbar, \qquad n = 1,\ 2... \tag{1.4.12}$$

excluding $n = 0$, since the electron would then not be in a circular orbit. The allowed orbital radii are then given by

$$r_n = n^2 a_0 \tag{1.4.13}$$

where

$$a_0 \equiv \frac{\hbar^2}{me^2} = 5.29 \times 10^{-11}\ \text{m} = 0.529 \mathring{A} \tag{1.4.14}$$

which is known as the *Bohr radius*. The corresponding energy is

$$E_n = -\frac{e^2}{2a_0 n^2} = -\frac{me^4}{2\hbar^2 n^2}, \qquad n = 1,\ 2... \tag{1.4.15}$$

Rydberg's formula (Equation 1.4.1) can now be deduced from the Bohr model. We have

$$\frac{hc}{\lambda} = E_{n_2} - E_{n_1} = \frac{2\pi^2 me^4}{h^2}\left(\frac{1}{n_1^2} - \frac{1}{n_2^2}\right) \tag{1.4.16}$$

and the Rydbeg constant can be identified as

$$\mathcal{R} = \frac{2\pi^2 me^4}{h^3 c} \approx 109,737 \text{ cm}^{-1} \tag{1.4.17}$$

The slight discrepency with the experimental value for hydrogen $(109,677)$ is due to the finite proton mass. This will be corrected later.

The Bohr model can be readily extended to hydrogenlike ions, systems in which a single electron orbits a nucleus of arbitrary atomic number Z. Thus $Z = 1$ for hydrogen, $Z = 2$ for He^+, $Z = 3$ for Li^{++}, and so on. The Coulomb potential 1.4.5 generalizes to

$$V(r) = -\frac{Ze^2}{r}, \tag{1.4.18}$$

the radius of the orbit (Equation 1.4.13) becomes

$$r_n = \frac{n^2 a_0}{Z} \tag{1.4.19}$$

and the energy Equation 1.4.15 becomes

$$E_n = -\frac{Z^2 e^2}{2a_0 n^2} \tag{1.4.20}$$

De Broglie's proposal that electrons can have wavelike properties was actually inspired by the Bohr atomic model. Since

$$L = rp = n\hbar = \frac{nh}{2\pi} \tag{1.4.21}$$

we find

$$2\pi r = \frac{nh}{p} = n\lambda \tag{1.4.22}$$

Therefore, each allowed orbit traces out an integral number of de Broglie wavelengths.

Wilson (1915) and Sommerfeld (1916) generalized Bohr's formula for the allowed orbits to

$$\oint p\, dr = nh, \qquad n = 1,\ 2... \tag{1.4.23}$$

The Sommerfeld-Wilson quantum conditions Equation 1.4.23 reduce to Bohr's results for circular orbits, but allow, in addition, elliptical orbits along which the momentum p is variable. According to Kepler's first law of planetary motion, the orbits of planets are ellipses with the Sun at one focus. Figure 1.4.2 shows the generalization of the Bohr theory for hydrogen, including the elliptical orbits. The lowest energy state $n = 1$ is still a circular orbit. But $n = 2$ allows an elliptical orbit in addition to the circular one; $n = 3$ has three possible orbits, and so on. The energy still depends on n alone, so that the elliptical orbits represent degenerate states. Atomic spectroscopy shows in fact that energy levels with $n > 1$ consist of multiple states, as implied by the splitting of atomic lines by an electric field (Stark effect) or a magnetic field (Zeeman effect). Some of these generalized orbits are drawn schematically in Figure 1.4.2.

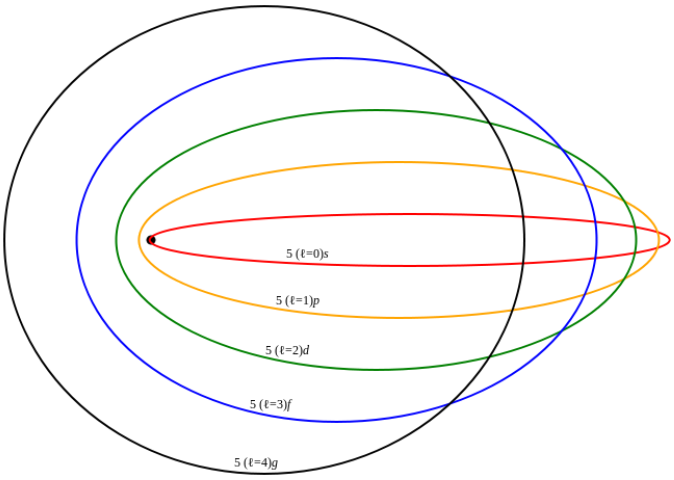


Figure 1.4.1: Elliptical orbits with the same energy and quantized angular momentum **in** Bohr-Sommerfield orbits for $n = 1,\ 2,\ 3$ (not to scale). (Public Domain; Pieter Kuiper)

The Bohr model was an important first step in the historical development of quantum mechanics. It introduced the quantization of atomic energy levels and gave quantitative agreement with the atomic hydrogen spectrum. With the Sommerfeld-Wilson generalization, it accounted as well for the degeneracy of hydrogen energy levels. Although the Bohr model was able to sidestep the atomic "Hindenberg disaster," it cannot avoid what we might call the "Heisenberg disaster." By this we mean that the assumption of well-defined electronic orbits around a nucleus is completely contrary to the basic premises of quantum mechanics. Another flaw in the Bohr picture is that the angular momenta are all too large by one unit, for example, the ground state actually has zero orbital angular momentum (rather than $\hbar$).

> *The assumption of well-defined electronic orbits around a nucleus in the Bohr atom is completely contrary to the basic premises of quantum mechanics.*

Quantum Mechanics of Hydrogenlike Atoms

In contrast to the particle in a box and the harmonic oscillator, the hydrogen atom is a real physical system that can be treated exactly by quantum mechanics. In addition to their inherent significance, these solutions suggest prototypes for atomic orbitals used in approximate treatments of complex atoms and molecules.

For an electron in the field of a nucleus of charge $+Ze$, the Schrödinger equation can be written

$$\left\{-\frac{\hbar^2}{2m}\nabla^2 - \frac{Ze^2}{r}\right\}\psi(r) = E\psi(r) \tag{1.4.24}$$

It is convenient to introduce *atomic units* in which length is measured in bohrs:

$$a_0 = \frac{\hbar^2}{me^2} = 5.29 \times 10^{-11}\ \text{m} \equiv 1\ \text{bohr} \tag{1.4.25}$$

and energy in hartrees:

$$\frac{e^2}{a_0} = 4.358 \times 10^{-18}\ \text{J} = 27.211\ \text{eV} \equiv 1\ \text{hartree} \tag{1.4.26}$$

Electron volts (**eV**) are a convenient unit for atomic energies. One **eV** is defined as the energy an electron gains when accelerated across a potential difference of **1 volt**. The ground state of the hydrogen atom has an energy of $-1/2$ **hartree** or -13.6 **eV**. Conversion to atomic units is equivalent to setting

$$\hbar = e = m = 1 \tag{1.4.27}$$

in all formulas containing these constants. Rewriting the Schrödinger equation in atomic units, we have

$$\left\{-\frac{1}{2}\nabla^2 - \frac{Z}{r}\right\}\psi(r) = E\psi(r) \tag{1.4.28}$$

Since the potential energy is spherically symmetrical (a function of r alone), it is obviously advantageous to treat this problem in spherical polar coordinates r, θ, ϕ. Expressing the Laplacian operator in these coordinates [cf. Eq (6-20)],

$$-\frac{1}{2}\left\{\frac{1}{r^2}\frac{\partial}{\partial r}r^2\frac{\partial}{\partial r}+\frac{1}{r^2\sin\theta}\frac{\partial}{\partial\theta}\sin\theta\frac{\partial}{\partial\theta}+\frac{1}{r^2\sin^2\theta}\frac{\partial^2}{\partial\phi^2}\right\} \times \psi(r,\,\theta,\,\phi)-\frac{Z}{r}\psi(r,\,\theta,\,\phi)=E\psi(r,\,\theta,\,\phi) \tag{1.4.29}$$

Equation 1.4.29 shows that the second and third terms in the Laplacian represent the angular momentum operator $\hat{L}^2$. Clearly, Equation 1.4.29 will have separable solutions of the form

$$\psi(r,\,\theta,\,\phi)=R(r)Y_{\ell m}(\theta,\,\phi) \tag{1.4.30}$$

Substituting Equation 1.4.30 into Equation 1.4.29 and using the angular momentum eigenvalue Equation Equation ???, we obtain an ordinary differential equation for the radial function $R(r)$:

$$\left\{-\frac{1}{2r^2}\frac{d}{dr}r^2\frac{d}{dr}+\frac{\ell(\ell+1)}{2r^2}-\frac{Z}{r}\right\}R(r)=ER(r) \tag{1.4.31}$$

Note that in the domain of the variable r, the angular momentum contribution $\ell(\ell+1)/2r^2$ acts as an effective addition to the potential energy. It can be identified with *centrifugal force*, which pulls the electron outward, in opposition to the Coulomb attraction. Carrying out the successive differentiations in Equation 1.4.32 and simplifying, we obtain

$$\frac{1}{2}R''(r)+\frac{1}{r}R'(r)+\left[\frac{Z}{r}-\frac{\ell(\ell+1)}{2r^2}+E\right]R(r)=0 \tag{1.4.32}$$

another second-order linear differential equation with non-constant coefficients. It is again useful to explore the asymptotic solutions to Equation 1.4.32, as $r\to\infty$. In the asymptotic approximation,

$$R''(r)-2r\,|E|\,R(r)\approx 0 \tag{1.4.33}$$

having noted that the energy E is negative for bound states. Solutions to Equation 1.4.33 are

$$R(r)\approx \text{const}\,e^{\pm\sqrt{2|E|}r} \tag{1.4.34}$$

We reject the positive exponential on physical grounds, since $R(r)\to\infty$ as $r\to\infty$, in violation of the requirement that the wavefunction must be finite everywhere. Choosing the negative exponential and setting $E=-Z^2/2$ the ground state energy in the Bohr theory (in atomic units), we obtain

$$R(r)\approx \text{const}\,e^{-Zr} \tag{1.4.35}$$

It turns out, very fortunately, that this asymptotic approximation is also an *exact* solution of the Schrödinger equation (Equation \(\ref{29}\)) with $\ell=0$, just what happened for the harmonic-oscillator problem in Chap. 5. The solutions to Equation 1.4.32, designated $R_{n\ell}(r)$, are labeled by n, known as the *principal quantum number*, as well as by the angular momentum ℓ, which is a parameter in the radial equation. The solution in Equation 1.4.35 corresponds to $R_{10}(r)$. This should be normalized according to the condition

$$\int_0^\infty [R_{10}(r)]^2\,r^2\,dr=1 \tag{1.4.36}$$

A useful definite integral is

$$\int_0^\infty r^n\,e^{-\alpha r}\,dr=\frac{n!}{\alpha^{n+1}} \tag{1.4.37}$$

The normalized radial function is thereby given by

$$R_{10}(r)=2Z^{3/2}e^{-Zr} \tag{1.4.38}$$

Since this function is nodeless, we identify it with the ground state of the hydrogenlike atom. Multipyling Equation 1.4.38 by the spherical harmonic $Y_{00}=1/\sqrt{4\pi}$, we obtain the total wavefunction (Equation 1.4.30)

$$\psi_{100}(r,\theta,\phi) = \left(\frac{Z^3}{\pi}\right)^{1/2} e^{-Zr} \tag{1.4.39}$$

This is conventionally designated as the 1*s* function $\psi_{1s}(r)$.

Integrals in spherical-polar coordinates over a spherically-symmetrical integrand (like the 1*s* orbital) can be significantly simplified. We can do the reduction

$$\int_0^\infty \int_0^\pi \int_0^{2\pi} f(r)\, r^2 \sin\theta \, dr \, d\theta \, d\phi = \int_0^\infty f(r)\, 4\pi r^2 \, dr \tag{1.4.40}$$

since integration over θ and ϕ gives 4π, the total solid angle of a sphere. The normalization of the 1*s* wavefunction can thus be written as

$$\int_0^\infty [\psi_{1s}(r)]^2 \, 4\pi r^2 \, dr = 1 \tag{1.4.41}$$

Hydrogen Atom Ground State

There are a number of different ways of representing hydrogen-atom wavefunctions graphically. We will illustrate some of these for the 1*s* ground state. In atomic units,

$$\psi_{1s}(r) = \frac{1}{\sqrt{\pi}} e^{-r} \tag{1.4.42}$$

is a decreasing exponential function of a single variable r, and is simply plotted in Figure 3.

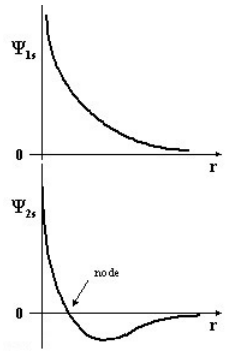


Figure **1.4.3.** Wavefunctions for 1*s* and 2*s* orbitals for atomic hydrogen. The 2*s*-wavefunction (scaled by a factor of 2) has a node at $r = 2$ bohr. Taken from voh.chem.ucla.edu/vohtar/wint.../lecture3.html

Figure **1.4.3** gives a somewhat more pictorial representation, a three-dimensional contour plot of $\psi_{1s}(r)$ as a function of x and y in the x, y-plane.

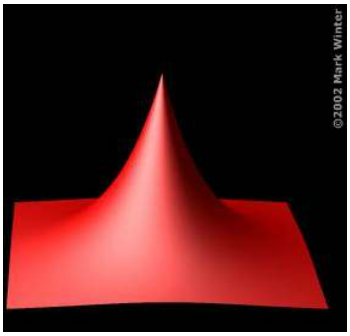


Figure **1.4.4**: Contour map of 1*s* orbital in the x-, y-plane. Taken from winter.group.shef.ac.uk/orbit...s/wave-fn.html

According to Born's interpretation of the wavefunction, the probability per unit volume of finding the electron at the point (r, θ, ϕ) is equal to the square of the normalized wavefunction

$$\rho_{1s}(r) = [\psi_{1s}(r)]^2 = \frac{1}{\pi} e^{-2r} \tag{1.4.43}$$

This is represented in Figure 5 by a scatter plot describing a possible sequence of observations of the electron position. Although results of individual measurements are not predictable, a statistical pattern does emerge after a sufficiently large number of measurements.

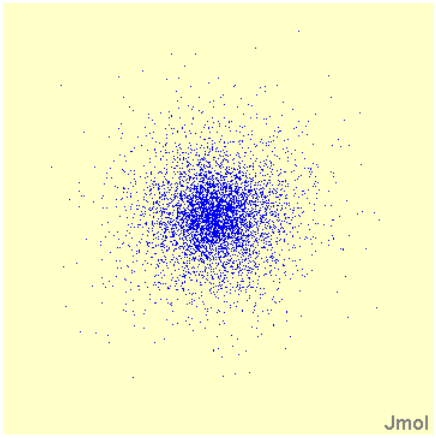


Figure **1.4.5**: Scatter plot of electron position measurements in hydrogen 1*s* orbital. Taken from winter.group.shef.ac.uk/orbit...sity-dots.html

The probability density is normalized such that

$$\int_0^\infty \rho_{1s}(r)\, 4\pi r^2\, dr = 1 \tag{1.4.44}$$

In some ways $\rho(r)$ does *not* provide the best description of the electron distribution, since the region around $r = 0$, where the wavefunction has its largest values, is a relatively small fraction of the volume accessible to the electron. Larger radii r represent larger physical regions since, in spherical polar coordinates, a value of r is associated with a shell of volume $4\pi r^2\, dr$. A more significant measure is therefore the *radial distribution function*

$$D_{1s}(r) = 4\pi r^2 [\psi_{1s}(r)]^2 \tag{1.4.45}$$

which represents the probability density within the entire shell of radius r, normalized such that

$$\int_0^\infty D_{1s}(r)\, dr = 1 \tag{1.4.46}$$

The functions $\rho_{1s}(r)$ and $D_{1s}(r)$ are both shown in Figure **1.4.6**. Remarkably, the 1*s* RDF has its maximum at $r = a_0$, equal to the radius of the first Bohr orbit

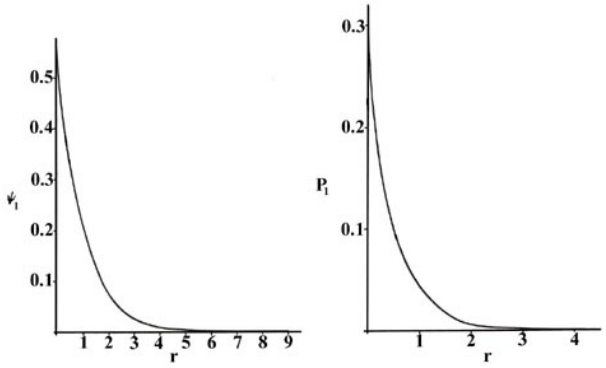


Figure **1.4.6**: The wavefunction and probability distribution as functions of r for the n = 1 level of the H atom. The functions and the radius r are in atomic units in this and succeeding figures. Image used with permisison (Bader).

Atomic Orbitals

The general solution for $R_{n\ell}(r)$ has a rather complicated form which we give without proof:

$$R_{n\ell}(r) = N_{n\ell}\,\rho^{\ell}\,L_{n+\ell}^{2\ell+1}(\rho)e^{-\rho/2} \qquad \rho \equiv \frac{2Zr}{n} \tag{1.4.47}$$

Here L_{β}^{α} is an associated Laguerre polynomial and $N_{n\ell}$, a normalizing constant. The angular momentum quantum number ℓ is by convention designated by a code: *s* for $\ell = 0$, *p* for $\ell = 1$, *d* for $\ell = 2$, *f* for $\ell = 3$, *g* for $\ell = 4$, and so on. The first four letters come from an old classification scheme for atomic spectral lines: *sharp*, *principal*, *diffuse* and *fundamental*. Although these designations have long since outlived their original significance, they remain in general use. The solutions of the hydrogenic Schrödinger equation
in spherical polar coordinates can now be written in full

$$\begin{gathered}\psi_{n\ell m}(r,\,\theta,\,\phi) = R_{n\ell}(r)Y_{\ell m}(\theta,\,\phi) \\ n = 1,\,2\ldots \qquad \ell = 0,\,1\ldots n-1 \qquad m = 0,\,\pm 1,\,\pm 2\ldots \pm \ell\end{gathered} \tag{1.4.48}$$

where $Y_{\ell m}$ are the spherical harmonics tabulated in Chap. 6. Table 1 below enumerates all the hydrogenic functions we will actually need. These are called *hydrogenic atomic orbitals*, in anticipation of their later applications to the structure of atoms and molecules.

Table 1. Real hydrogenic functions in atomic units.

$\psi_{1s} = \frac{1}{\sqrt{\pi}}e^{-r}$	(1.4.49)
$\psi_{2s} = \frac{1}{2\sqrt{2\pi}}\left(1-\frac{r}{2}\right)e^{-r/2}$	(1.4.50)
$\psi_{2p_z} = \frac{1}{4\sqrt{2\pi}}z\,e^{-r/2}$	(1.4.51)
$\psi_{2p_x},\ \psi_{2p_y}$ analogous	(1.4.52)
$\psi_{3s} = \frac{1}{81\sqrt{3\pi}}(27-18r+2r^2)e^{-r/3}$	(1.4.53)
$\psi_{3p_z} = \frac{\sqrt{2}}{81\sqrt{\pi}}(6-r)z\,e^{-r/3}$	(1.4.54)
$\psi_{3p_x},\ \psi_{3p_y}$ analogous	(1.4.55)
$\psi_{3d_{z^2}} = \frac{1}{81\sqrt{6\pi}}(3z^2-r^2)e^{-r/3}$	(1.4.56)
$\psi_{3d_{xz}} = \frac{\sqrt{2}}{81\sqrt{\pi}}zx\,e^{-r/3}$	(1.4.57)
$\psi_{3d_{yz}},\ \psi_{3d_{xy}}$ analogous	(1.4.58)
$\psi_{3d_{x^2-y^2}} = \frac{1}{81\sqrt{\pi}}(x^2-y^2)e^{-r/3}$	(1.4.59)

The energy levels for a hydrogenic system are given by

$$E_n = -\frac{Z^2}{2n^2}\ \text{hartrees} \tag{1.4.60}$$

and depends on the principal quantum number alone. Considering all the allowed values of ℓ and m, the level E_n has a degeneracy of n^2. Figure 7 shows an energy level diagram for hydrogen $(Z = 1)$. For $E \geq 0$, the energy is a continuum, since the electron is in fact a free particle. The continuum represents states of an electron and proton in interaction, but not bound into a stable atom. Figure 1.4.7 also shows some of the transitions which make up the Lyman series in the ultraviolet and the Balmer series in the visible region.

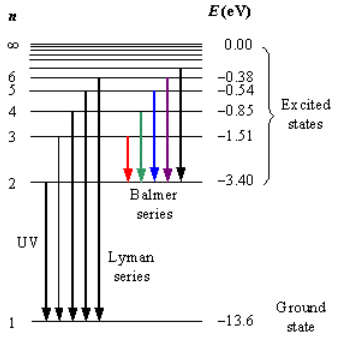


Figure 1.4.7: Energy levels of atomic hydrogen. Taken from http://eilat.sci.brooklyn.cuny.edu/c...hws/hw2d_c.htm

The ns orbitals are all spherically symmetrical, being associated with a constant angular factor, the spherical harmonic $Y_{00} = 1/\sqrt{4\pi}$. They have $n - 1$ radial nodes—spherical shells on which the wavefunction equals zero. The 1*s* ground state is nodeless and the number of nodes increases with energy, in a pattern now familiar from our study of the particle-in-a-box and harmonic oscillator. The 2*s* orbital, with its radial node at $r = 2$ bohr, is also shown in Figure 1.4.3.

p- and d-Orbitals

The lowest-energy solutions deviating from spherical symmetry are the 2*p*-orbitals. Using Equations 1.4.47, 1.4.48 and the $\ell = 1$ spherical harmonics, we find three degenerate eigenfunctions:

$$\psi_{210}(r,\ \theta,\ \phi) = \frac{1}{4\sqrt{2\pi}} r e^{-r/2} \cos\theta \tag{1.4.61}$$

and

$$\psi_{21\pm1}(r,\ \theta,\ \phi) = \mp\frac{1}{4\sqrt{2\pi}} r e^{-r/2} \sin\theta e^{\pm i\phi} \tag{1.4.62}$$

The function ψ_{210} is real and contains the factor $r\cos\theta$, which is equal to the cartesian variable z. In chemical applications, this is designated as a $2p_z$ orbital:

$$\psi_{2p_z} = \frac{1}{4\sqrt{2\pi}} z e^{-r/2} \tag{1.4.63}$$

A contour plot is shown in Figure 1.4.8. Note that this function is cylindrically-symmetrical about the z-axis with a node in the x, y-plane. The $\psi_{21\pm1}$ are complex functions and not as easy to represent graphically. Their angular dependence is that of the spherical harmonics $Y_{1\pm1}$, shown in Figure 6-4. As noted in Chap. 4, any linear combination of degenerate eigenfunctions is an equally-valid alternative eigenfunction. Making use of the Euler formulas for sine and cosine

$$\cos\phi = \frac{e^{i\phi} + e^{-i\phi}}{2} \qquad \text{and} \qquad \sin\phi = \frac{e^{i\phi} - e^{-i\phi}}{2} \tag{1.4.64}$$

and noting that the combinations $\sin\theta\cos\phi$ and $\sin\theta\sin\phi$ correspond to the cartesian variables x and y, respectively, we can define the alternative 2*p* orbitals

$$\psi_{2p_x} = \frac{1}{\sqrt{2}}(\psi_{21-1} - \psi_{211}) = \frac{1}{4\sqrt{2\pi}} x e^{-r/2} \tag{1.4.65}$$

and

$$\psi_{2p_y} = -\frac{i}{\sqrt{2}}(\psi_{21-1} + \psi_{211}) = \frac{1}{4\sqrt{2\pi}} y e^{-r/2} \tag{1.4.66}$$

Clearly, these have the same shape as the $2p_z$-orbital, but are oriented along the x- and y-axes, respectively. The threefold degeneracy of the *p*-orbitals is very clearly shown by the geometric equivalence the functions $2p_x$, $2p_y$ and $2p_z$, which is not obvious for the spherical harmonics. The functions listed in Table 1 are, in fact, the real forms for all atomic orbitals, which are more useful in chemical applications. All higher *p*-orbitals have analogous functional forms $x\,f(r)$, $y\,f(r)$ and $z\,f(r)$ and are likewise 3-fold degenerate.

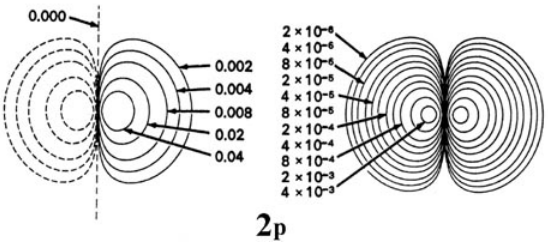


Figure 1.4.8: Contour plot of $2p_z$ orbital. (Bader).

The orbital ψ_{320} is, like ψ_{210}, a real function. It is known in chemistry as the d_{z^2}-orbital and can be expressed as a cartesian factor times a function of r:

$$\psi_{3d_{z^2}} = \psi_{320} = (3z^2 - r^2) f(r) \tag{1.4.67}$$

A contour plot is shown in Figure 1.4.9. This function is also cylindrically symmetric about the z-axis with *two* angular nodes—the conical surfaces with $3z^2 - r^2 = 0$. The remaining four 3*d* orbitals are complex functions containing the spherical harmonics $Y_{2\pm1}$ and $Y_{2\pm2}$ pictured in Figure 6-4. We can again construct real functions from linear combinations, the result being four geometrically equivalent "four-leaf clover" functions with two perpendicular planar nodes. These orbitals are designated $d_{x^2-y^2}$, d_{xy}, d_{zx} and d_{yz}. Two of them are shown in Figure 9. The d_{z^2} orbital has a different shape. However, it can be expressed in terms of two non-standard *d*-orbitals, $d_{z^2-x^2}$ and $d_{y^2-z^2}$. The latter functions, along with $d_{x^2-y^2}$ add to zero and thus constitute a linearly *dependent* set. *Two* combinations of these three functions can be chosen as independent eigenfunctions.

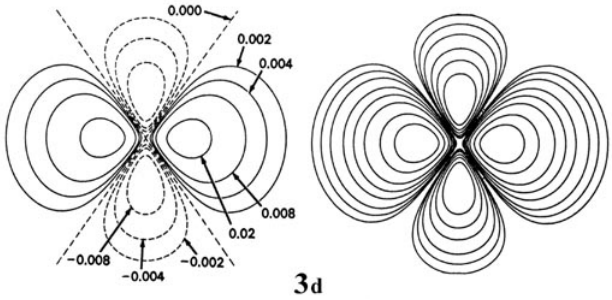


Figure 1.4.8: Contour plot of $3d_{xy}$ orbital.

Summary

The atomic orbitals listed in Table 1 are illustrated in Figure 1.4.20. Blue and red indicate, respectively, positive and negative regions of the wavefunctions (the radial nodes of the 2*s* and 3*s* orbitals are obscured). These pictures are intended as stylized representations of atomic orbitals and should *not* be interpreted as quantitatively accurate.

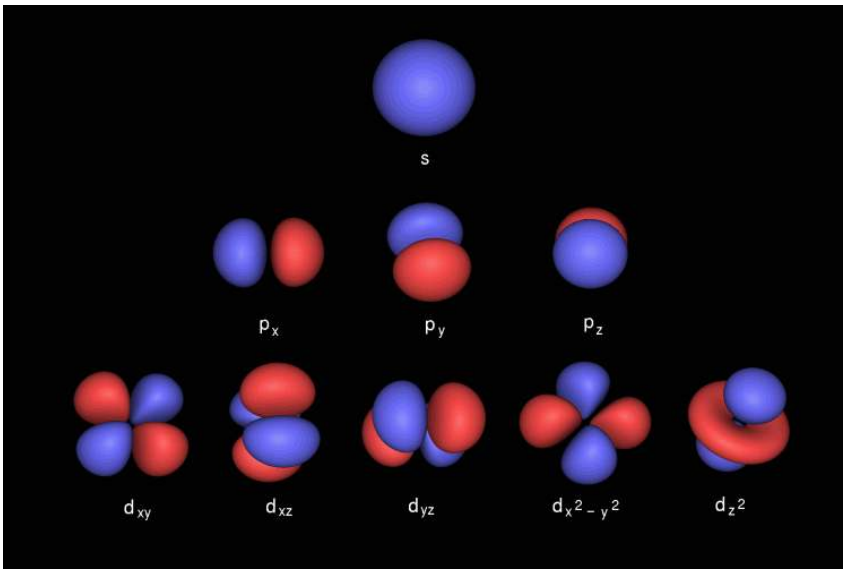


Figure 1.4.20: Hydrogenic atomic orbitals. Taken from www.chemcomp.com/journal/molorbs.htm

The electron charge distribution in an orbital $\psi_{n\ell m}(\mathbf{r})$ is given by

$$\rho(\mathbf{r}) = |\psi_{n\ell m}(\mathbf{r})|^2 \tag{1.4.68}$$

which for the *s*-orbitals is a function of r alone. The radial distribution function can be defined, even for orbitals containing angular dependence, by

$$D_{n\ell}(r) = r^2[R_{n\ell}(r)]^2 \tag{1.4.69}$$

This represents the electron density in a shell of radius r, including all values of the angular variables θ, ϕ. Figure 1.4.11 shows plots of the RDF for the first few hydrogen orbitals.

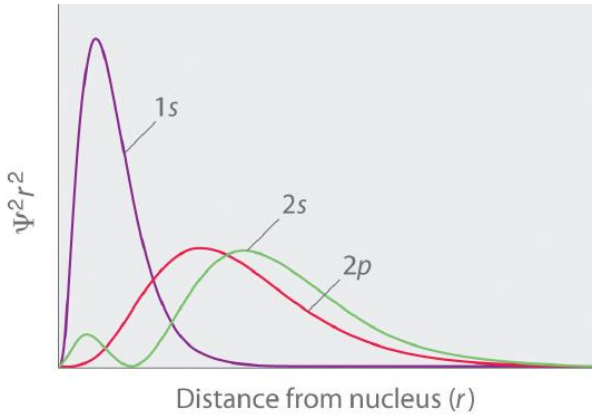


Figure 1.4.22: Some radial distribution functions.

Contributors and Attributions

Seymour Blinder (Professor Emeritus of Chemistry and Physics at the University of Michigan, Ann Arbor)

- Integrated by Daniel SantaLucia (Chemistry student at Hope College, Holland MI)

1.4: Hydrogen Atom is shared under a not declared license and was authored, remixed, and/or curated by LibreTexts.

- **Chapter 7. Hydrogen Atom** is licensed CC BY-NC-SA 4.0.

1.5: Slater Rules

Learning Objective

- To quantify the shielding effect experienced by atomic electrons.

We have previously described the concepts of electron shielding, orbital penetration and effective nuclear charge, but we did so in a qualitative manner. In this section, we explore one model for quantitatively estimating the impact of electron shielding, and then use that to calculate the effective nuclear charge experienced by an electron in an atom. The model we will use is known as Slater's Rules (J.C. Slater, *Phys Rev* **1930**, *36*, 57).

Slater's Rules

The general principle behind Slater's Rule is that the actual charge felt by an electron is equal to what you'd expect the charge to be from a certain number of protons, but minus a certain amount of charge from other electrons. Slater's rules allow you to estimate the effective nuclear charge Z_{eff} from the real number of protons in the nucleus and the effective shielding of electrons in each orbital "shell" (e.g., to compare the effective nuclear charge and shielding 3d and 4s in transition metals). Slater's rules are fairly simple and produce fairly accurate predictions of things like the electron configurations and ionization energies.

Slater's Rules

- **Step 1**: Write the electron configuration of the atom in the following form:

  (1s) (2s, 2p) (3s, 3p) (3d) (4s, 4p) (4d) (4f) (5s, 5p) . . .

- **Step 2**: Identify the electron of interest, and ignore all electrons in higher groups (to the right in the list from Step 1). These do not shield electrons in lower groups
- **Step 3**: Slater's Rules is now broken into two cases:
  - the shielding experienced by an s- or p- electron,
    - electrons within same group shield **0.35**, except the 1*s* which shield **0.30**
    - electrons within the n-1 group shield **0.85**
    - electrons within the n-2 or lower groups shield **1.00**
  - the shielding experienced by n*d* or n*f* valence electrons
    - electrons within same group shield **0.35**
    - electrons within the lower groups shield **1.00**

These rules are summarized in Figure 1.5.1 and Table 1.5.1.

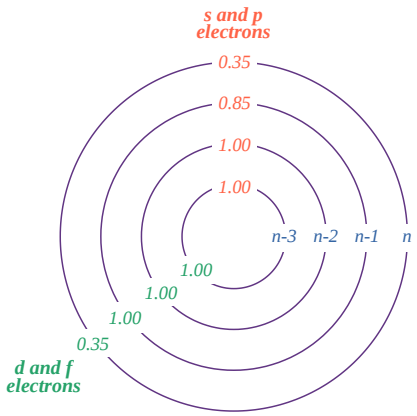


Figure 1.5.1: Graphical depiction of Slater's rules with shielding constants indicated. (CC BY-NC; Ümit Kaya)

Shielding happens when electrons in lower valence shells (or the same valence shell) provide a repulsive force to valence electrons, thereby "negating" some of the attractive force from the positive nucleus. Electrons really close to the atom (n-2 or lower) pretty

much just look like protons, so they completely negate. As electrons get closer to the electron of interest, some more complex interactions happen that reduce this shielding.

Table 1.5.1: Slater's Rules for calculating shieldings

Group	Other electrons in the same group	Electrons in group(s) with principal quantum number n and azimuthal quantum number < l	Electrons in group(s) with principal quantum number n-1	Electrons in all group(s) with principal quantum number < n-1
[1s]	0.30	-	-	-
[*n*s,*n*p]	0.35	-	0.85	1
[*n*d] or [*n*f]	0.35	1	1	1

The shielding numbers in Table 1.5.1 were derived semi-empirically (i.e., derived from experiments) as opposed to theoretical calculations. This is because quantum mechanics makes calculating shielding effects quite difficult, which is outside the scope of this Module.

Calculating *S*

Sum together the contributions as described in the appropriate rule above to obtain an estimate of the shielding constant, S, which is found by totaling the screening by **all electrons** except the one in question.

$$S = \sum n_i S_i \tag{1.5.1}$$

where

- n_i is the number of electrons in a specific shell and subshell and
- S_i is the shielding of the electrons subject to Slater's rules (Table 1.5.1)

Electrons of Nitrogen Atoms

What is the shielding constant experienced by a 2*p* electron in the nitrogen atom?

Given: Nitrogen (N)

Asked for: S, the shielding constant, for a 2*p* electron (Equation 1.5.1)

Strategy:

A. Determine the electron configuration of nitrogen, then write it in the appropriate form.
B. Use the appropriate Slater Rules (Table 1.5.1) to calculate the shielding constant for the electron.

Step A N: $1s^2\ 2s^2\ 2p^3$

N: $(1s^2)(2s^2,2p^3)$

Step B

- There are **4** other electrons in the same ns, np group @ 0.35: $(2s^2,2p^3)$.
- There are **2** electrons in the n-1 groups @ 0.85: $(1s^2)$

$$S[2p] = \underbrace{0.85(2)}_{\text{the 1s electrons}} + \underbrace{0.35(4)}_{\text{the 2s and 2p electrons}} = 3.10$$

As Table 1.5.1 indicates,

- the 1s electrons shield the other 2p electron to 0.85 "charges".
- the 2s and 2p electrons shield the other 2p electron equally at 0.35 "charges".

Electrons of Bromine Atoms

What is the shielding constant experienced by a valence *p*-electron in the bromine atom?

Answer

There are **6** other electrons in the same ns, np group.
There are **18** electrons in the n-1 groups: (3s, 3p and 3d)
There are **10** electrons in the n-2 and lower groups: (1s, 2s and 2p)

$$S = 6(0.35) + 18(0.85) + 10(1.00) = 27.4$$

Electrons of Bromine Atoms

What is the shielding constant experienced by a 3*d* electron in the bromine atom?

Given: Bromine (Br)

Asked for: S, the shielding constant, for a 3*d* electron

Strategy:

A. Determine the electron configuration of bromine, then write it in the appropriate form.
B. Use the appropriate Slater Rules (Table **1.5.1**) to calculate the shielding constant for the electron.

Step A Br: $1s^2\ 2s^2\ 2p^6\ 3s^2\ 3p^6\ 4s^2\ 3d^{10}\ 4p^5$

Br: $(1s^2)(2s^2,2p^6)(3s^2,3p^6)(3d^{10})(4s^2,4p^5)$

Step B

- There are **9** other electrons in the same ns, np group @ 0.35: $(3s^2,3p^6)$
- There are **18** other lower group elements electrons in the same nd, nf group @ 1: $(1s^2)(2s^2,2p^6)$
- Ignore the group to the right of the 3d electrons; these do not contribute to the shielding constant @ 0. $(4s^2,4p^5)$

$$S[3d] = 1.00(18) + 0.35(9) = 21.15$$

Electrons of Copper Atoms

What is the shielding constant experienced by a valence *d*-electron in the copper atom?

Answer

$S = 21.15$

Calculating Z_{eff}

One set of estimates for the effective nuclear charge (Z_{eff}) was presented in Figure 2.5.1. Previously, we qualitatively described Z_{eff} as being less than the actual nuclear charge (Z) because of the repulsive interaction between core and valence electrons. We can quantitatively represent this difference between Z and Z_{eff} as follows:

$$S = Z - Z_{eff} \tag{1.5.2}$$

Rearranging this formula to solve for Z_{eff} we obtain:

$$Z_{eff} = Z - S \tag{1.5.3}$$

We can then substitute the shielding constant obtained using Equation 1.5.3 to calculate an estimate of Z_{eff} for the corresponding atomic electron.

Example 1.5.3: The Effective Charge of p Electrons of Boron Atoms

What is the effective nuclear charge experienced by a valence *p*- electron in boron?

Given: Boron (B)

Asked for: Z_{eff} for a valence *p*- electron

Strategy:

A. Determine the electron configuration of boron and identify the electron of interest.
B. Use the appropriate Slater Rule to calculate the shielding constant for the electron.
C. Use the Periodic Table to determine the actual nuclear charge for boron.
D. Determine the effective nuclear constant.

Solution:

Step A B: $1s^2\ 2s^2\ 2p^1$. The valence p- electron in boron resides in the 2*p* subshell.

B: $(1s^2)(2s^2,2p^1)$

Step B $S[2p] = 1.00(0) + 0.85(2) + 0.35(2) = 2.40$

Step C $Z = 5$

Step D Using Equation 1.5.3, $\mathbf{Z_{eff} = 2.60}$

Exercise 1.5.3

What is the effective nuclear charge experienced by a valence d-electron in copper?

Answer

$$\mathbf{Z_{eff} = 7.85}$$

Summary

Slater's Rules can be used as a model of shielding. This permits us to quantify both the amount of shielding experienced by an electron and the resulting effective nuclear charge. Others performed better optimizations of Z_{eff} using variational Hartree-Fock methods. For example, Clementi and Raimondi published "Atomic Screening Constants from SCF Functions." J Chem Phys (1963) 38, 2686–2689.

References

- James L. Reed, "The Genius of Slater's Rules" , J. Chem. Educ., 1999, 76 (6), p 802
- David Tudela, "Slater's rules and electron configurations", J. Chem. Educ., 1993, 70 (11), p 956
- Kimberley A. Waldron, Erin M. Fehringer, Amy E. Streeb, Jennifer E. Trosky and Joshua J. Pearson, "Screening Percentages Based on Slater Effective Nuclear Charge as a Versatile Tool for Teaching Periodic Trends", J. Chem. Educ., 2001, 78 (5), p 635

Contributors and Attributions

- Brett McCollum (Mount Royal University)

1.5: Slater Rules is shared under a not declared license and was authored, remixed, and/or curated by LibreTexts.

CHAPTER OVERVIEW

2: Molecules

2.2: Molecular Shapes
2.3: The VSEPR Model
2.4: Hybrid Orbitals
2.5: Molecular Orbitals
2.5.1: Molecular Shape and Molecular Polarity
2.5.2: Prelude to Molecular Orbital Theory
2.5.3: Constructing Molecular Orbitals from Atomic Orbitals
2.5.4: Orbital Symmetry
2.5.5: Molecular Orbital Diagrams
2.5.6: π Orbitals and Diatomic Molecules
2.5.7: Orbital Filling
2.5.8: δ orbitals
2.6: The Range of Bonding
2.7: Advanced Bonding
2.7.1: Symmetry Elements and Operations
2.7.2: Point Groups
2.7.2.1: Other Groups
2.7.2.2: Groups of Low and High Symmetry
2.7.3: Ligand Group Orbitals and Generator Functions
2.7.4: Expanded Octets and Molecular Orbitals
2.8: Nuclear Magnetic Resonance (NMR)
2.8.1: The Origin of the NMR Signal
2.8.2: Chemical Equivalence
2.8.3: The 1H-NMR experiment
2.8.4: Spin-Spin Coupling
2.8.5: The Basis for Differences in Chemical Shift
Index
Glossary
Detailed Licensing

2: Molecules is shared under a not declared license and was authored, remixed, and/or curated by LibreTexts.

2.2: Molecular Shapes

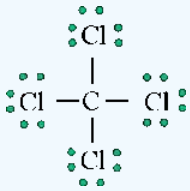
The Lewis electron-pair approach described previously can be used to predict the number and types of bonds between the atoms in a substance, and it indicates which atoms have lone pairs of electrons. This approach gives no information about the actual arrangement of atoms in space, however.

Molecular Geometry

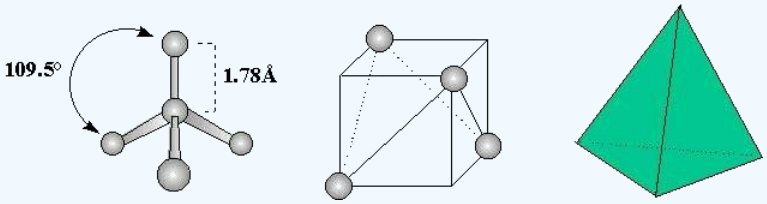
The specific three dimensional arrangement of atoms in molecules is referred to as **molecular geometry**. We also define molecular geometry as the positions of the atomic nuclei in a molecule. There are various instrumental techniques such as X-Ray crystallography and other experimental techniques which can be used to tell us where the atoms are located in a molecule. Using advanced techniques, very complicated structures for proteins, enzymes, DNA, and RNA have been determined. Molecular geometry is associated with the chemistry of vision, smell, taste, drug reactions, and enzyme controlled reactions to name a few.

Example 2.2.1: Carbon Tetrachloride

The Lewis structure of carbon tetrachloride provides information about connectivities, provides information about valence orbitals, and provides information about bond character.



However, the Lewis structure provides no information about the shape of the molecule, which is defined by *the bond angles and the bond lengths*. For carbon tetrachloride, each C-Cl bond length is 1.78Å and each Cl-C-Cl bond angle is 109.5°. Hence, carbon tetrachloride is ***tetrahedral*** in structure:



Molecular Geometries of AB_n molecules

Molecular geometry is associated with the specific orientation of bonding atoms. A careful analysis of electron distributions in orbitals will usually result in correct molecular geometry determinations. In addition, the simple writing of Lewis diagrams can also provide important clues for the determination of molecular geometry. Molecular shapes, or geometries, are critical to molecular recognition and function. Table **2.2.1** shows some examples of geometries where a central atom A is bonded to two or more X atoms. As indicated in several of the geometries below, non-bonding electrons E can strongly influence the molecular geometry of the molecule; this is discussed in more details in Section 9.2.

Table **2.2.1**:

6	5	4	3	2
AX_6  octahedral	AX_5  trigonal bipyramidal	AX_4  tetrahedral	AX_3  trigonal planar	AX_2 linear
1 lone pair of electrons				
AX_5E  square pyramidal	AX_4E  distorted tetrahedron	AX_3E  pyramidal	AX_2E  nonlinear	AXE linear
2 lone pairs of electrons				
AX_4E_2  square planar	AX_3E_2  T-shaped	AX_2E_2  bent	AXE_2 linear	

These structures can generally be predicted, when A is a nonmetal, using the "valence-shell electron-pair repulsion model (VSEPR) discussed in the next section.

Contributors and Attributions

- Mike Blaber (Florida State University)
- Robyn Rindge (Class of '98) who now works for PDI Dreamworks (look for his name in the credits of Shrek2.). Robyn drew these rotating molecules using Infini-D (MetaCreations).
- Paul Groves, chemistry teacher at South Pasadena High School and Chemmy Bear

2.2: Molecular Shapes is shared under a CC BY-NC-SA 4.0 license and was authored, remixed, and/or curated by LibreTexts.

2.3: The VSEPR Model

Learning Objectives

- To use the VSEPR model to predict molecular geometries.
- To predict whether a molecule has a dipole moment.

The Lewis electron-pair approach can be used to predict the number and types of bonds between the atoms in a substance, and it indicates which atoms have lone pairs of electrons. This approach gives no information about the actual arrangement of atoms in space, however. We continue our discussion of structure and bonding by introducing the **valence-shell electron-pair repulsion** (VSEPR) model (pronounced “vesper”), which can be used to predict the shapes of many molecules and polyatomic ions. Keep in mind, however, that the VSEPR model, like any model, is a limited representation of reality; the model provides no information about bond lengths or the presence of multiple bonds.

The VSEPR Model

The VSEPR model can predict the structure of nearly any molecule or polyatomic ion in which the central atom is a nonmetal, as well as the structures of many molecules and polyatomic ions with a central metal atom. The premise of the VSEPR theory is that electron pairs located in bonds and lone pairs repel each other and will therefore adopt the geometry that places electron pairs as far apart from each other as possible. This theory is very simplistic and does not account for the subtleties of orbital interactions that influence molecular shapes; however, the simple VSEPR counting procedure accurately predicts the three-dimensional structures of a large number of compounds, which cannot be predicted using the Lewis electron-pair approach.

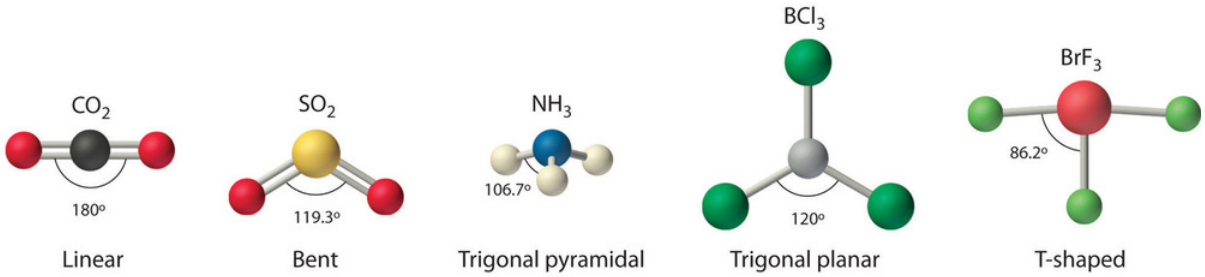


Figure **2.3.1**: Common Structures for Molecules and Polyatomic Ions That Consist of a Central Atom Bonded to Two or Three Other Atoms. (CC BY-NC-SA; anonymous)

We can use the VSEPR model to predict the geometry of most polyatomic molecules and ions by focusing only on the number of electron pairs around the *central atom*, ignoring all other valence electrons present. According to this model, valence electrons in the Lewis structure form *groups*, which may consist of a single bond, a double bond, a triple bond, a lone pair of electrons, or even a single unpaired electron, which in the VSEPR model is counted as a lone pair. Because electrons repel each other electrostatically, the most stable arrangement of electron groups (i.e., the one with the lowest energy) is the one that minimizes repulsions. Groups are positioned around the central atom in a way that produces the molecular structure with the lowest energy, as illustrated in Figures **2.3.1** and **2.3.2**.

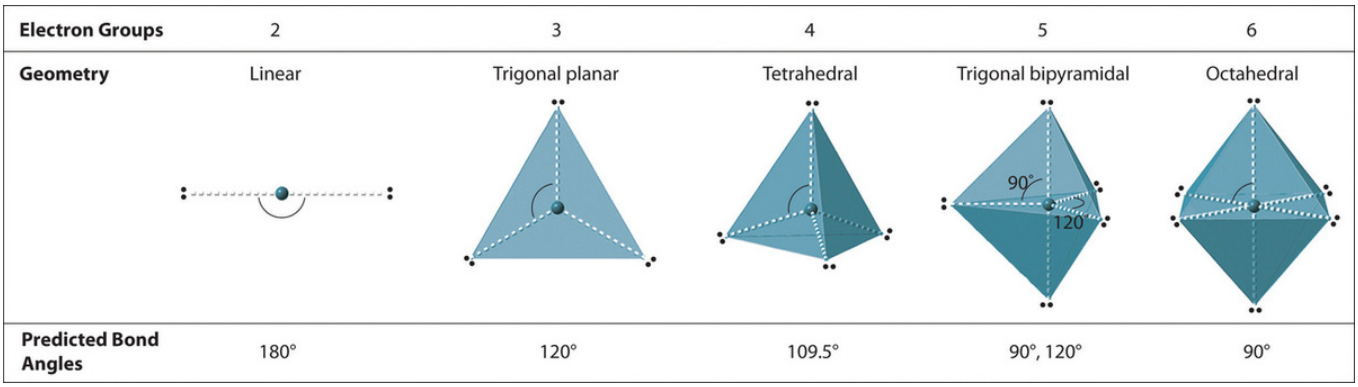


Figure **2.3.2**: Electron Geometries for Species with Two to Six Electron Groups. Groups are placed around the central atom in a way that produces a molecular structure with the lowest energy, that is, the one that minimizes repulsions. (CC BY-NC-SA; anonymous)

In the VSEPR model, the molecule or polyatomic ion is given an AX_mE_n designation, where A is the central atom, X is a bonded atom, E is a nonbonding valence electron group (usually a lone pair of electrons), and *m* and *n* are integers. Each group around the central atom is designated as a bonding pair (BP) or lone (nonbonding) pair (LP). From the BP and LP interactions we can predict both the relative positions of the atoms and the angles between the bonds, called the bond angles. Using this information, we can describe the molecular geometry, the arrangement of the *bonded atoms* in a molecule or polyatomic ion.

VESPR Produce to predict Molecular geometry

This VESPR procedure is summarized as follows:

1. Draw the Lewis electron structure of the molecule or polyatomic ion.
2. Determine the electron group arrangement around the central atom that minimizes repulsions.
3. Assign an AX_mE_n designation; then identify the LP–LP, LP–BP, or BP–BP interactions and predict deviations from ideal bond angles.
4. Describe the molecular geometry.

We will illustrate the use of this procedure with several examples, beginning with atoms with two electron groups. In our discussion we will refer to Figure **2.3.2** and Figure **2.3.3**, which summarize the common molecular geometries and idealized bond angles of molecules and ions with two to six electron groups.

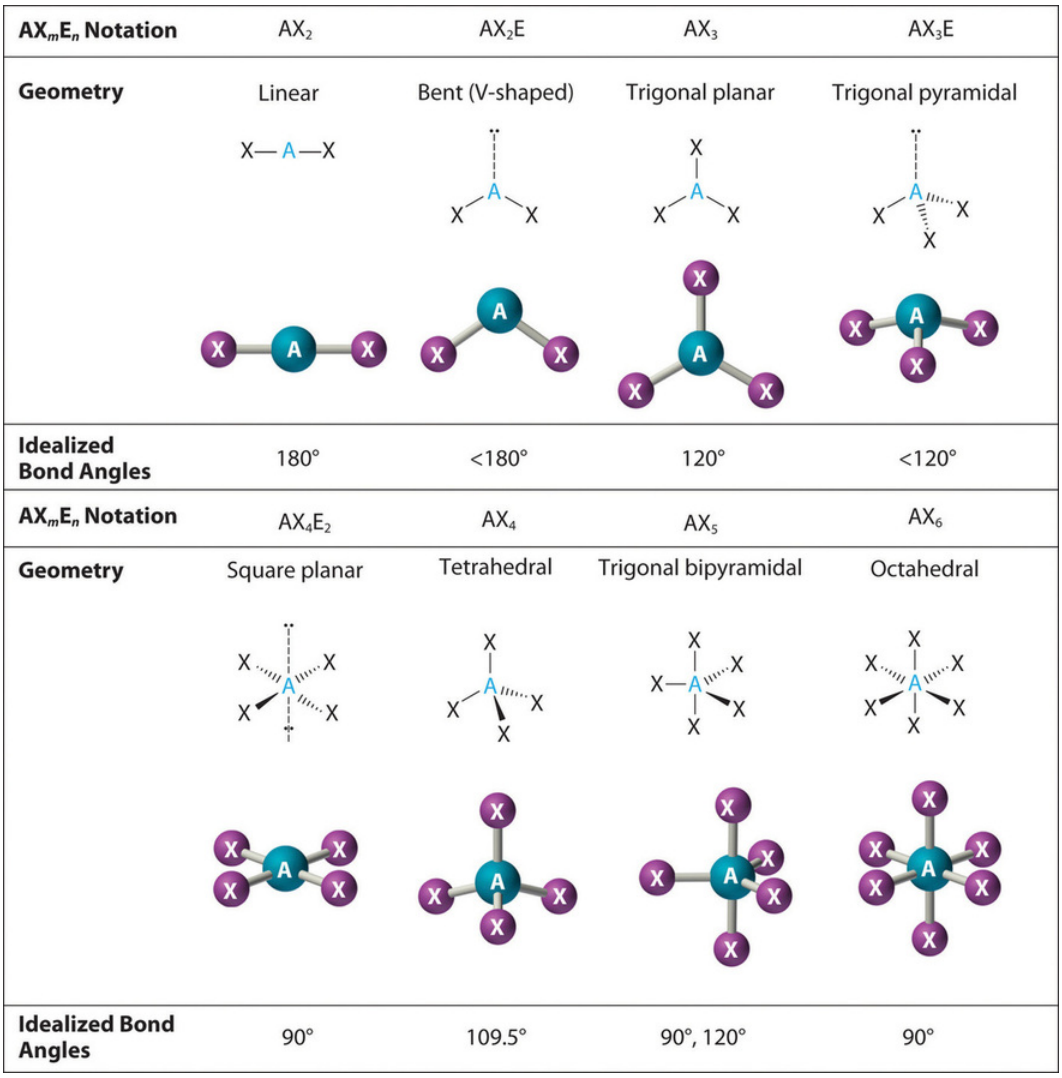


Figure **2.3.3**: Common Molecular Geometries for Species with Two to Six Electron Groups. Lone pairs are shown using a dashed line. (CC BY-NC-SA; anonymous)

Two Electron Groups

Our first example is a molecule with two bonded atoms and no lone pairs of electrons, $\boldsymbol{BeH_2}$.

AX_2 Molecules: BeH_2

1. The central atom, beryllium, contributes two valence electrons, and each hydrogen atom contributes one. The Lewis electron structure is

$$H{:}Be{:}H \quad \text{or} \quad H{-}Be{-}H$$

Lewis structure

Figure **2.3.2** that the arrangement that minimizes repulsions places the groups 180° apart. (CC BY-NC-SA; anonymous)

3. Both groups around the central atom are bonding pairs (BP). Thus BeH_2 is designated as AX_2.

4. From Figure **2.3.3** we see that with two bonding pairs, the molecular geometry that minimizes repulsions in BeH_2 is *linear*.

AX_2 Molecules: CO_2

1. The central atom, carbon, contributes four valence electrons, and each oxygen atom contributes six. The Lewis electron structure is



2. The carbon atom forms two double bonds. Each double bond is a group, so there are two electron groups around the central atom. Like BeH_2, the arrangement that minimizes repulsions places the groups 180° apart.

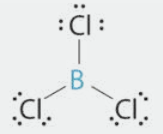
3. Once again, both groups around the central atom are bonding pairs (BP), so CO_2 is designated as AX_2.

4. VSEPR only recognizes groups around the *central* atom. Thus the lone pairs on the oxygen atoms do not influence the molecular geometry. With two bonding pairs on the central atom and no lone pairs, the molecular geometry of CO_2 is linear (Figure **2.3.3**). The structure of CO_2 is shown in Figure **2.3.1**.

Three Electron Groups

AX_3 Molecules: BCl_3

1. The central atom, boron, contributes three valence electrons, and each chlorine atom contributes seven valence electrons. The Lewis electron structure is



Lewis structure

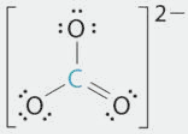
Figure **2.3.2**): (CC BY-NC-SA; anonymous)

3. All electron groups are bonding pairs (BP), so the structure is designated as AX_3.

4. From Figure **2.3.3** we see that with three bonding pairs around the central atom, the molecular geometry of BCl_3 is *trigonal planar*, as shown in Figure **2.3.2**.

AX_3 Molecules: CO_3^{2-}

1. The central atom, carbon, has four valence electrons, and each oxygen atom has six valence electrons. As you learned previously, the Lewis electron structure of one of three resonance forms is represented as

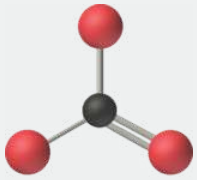


Lewis structure

Figure **2.3.2**).

3. All electron groups are bonding pairs (BP). With three bonding groups around the central atom, the structure is designated as AX_3.

4. We see from Figure **2.3.3** that the molecular geometry of CO_3^{2-} is trigonal planar with bond angles of 120°.



Molecular geometry
(trigonal planar)

In our next example we encounter the effects of lone pairs and multiple bonds on molecular geometry for the first time.

AX_2E Molecules: SO_2

1. The central atom, sulfur, has 6 valence electrons, as does each oxygen atom. With 18 valence electrons, the Lewis electron structure is shown below.

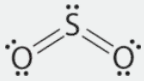


Figure **2.3.2**): (CC BY-NC-SA; anonymous)

3. There are two bonding pairs and one lone pair, so the structure is designated as AX_2E. This designation has a total of three electron pairs, two X and one E. Because a lone pair is not shared by two nuclei, it occupies more space near the central atom than a bonding pair (Figure **2.3.4**). Thus bonding pairs and lone pairs repel each other electrostatically in the order BP–BP < LP–BP < LP–LP. In SO_2, we have one BP–BP interaction and two LP–BP interactions.

4. The molecular geometry is described only by the positions of the nuclei, *not* by the positions of the lone pairs. Thus with two nuclei and one lone pair the shape is *bent*, or *V shaped*, which can be viewed as a trigonal planar arrangement with a missing vertex (Figures **2.3.2** and **2.3.3**). The O-S-O bond angle is expected to be *less than* 120° because of the extra space taken up by the lone pair.

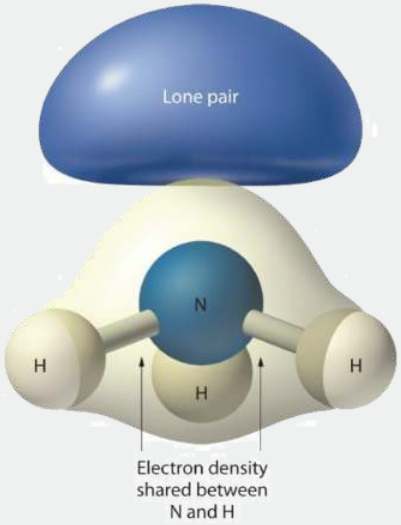
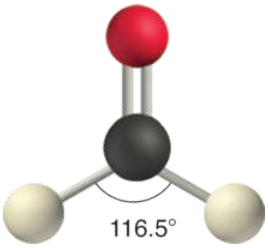


Figure **2.3.4**: The Difference in the Space Occupied by a Lone Pair of Electrons and by a Bonding Pair. (CC BY-NC-SA; anonymous)

As with SO_2, this composite model of electron distribution and negative electrostatic potential in ammonia shows that a lone pair of electrons occupies a larger region of space around the nitrogen atom than does a bonding pair of electrons that is shared with a hydrogen atom.

Like lone pairs of electrons, multiple bonds occupy more space around the central atom than a single bond, which can cause other bond angles to be somewhat smaller than expected. This is because a multiple bond has a higher electron density than a single bond, so its electrons occupy more space than those of a single bond. For example, in a molecule such as CH_2O (AX_3), whose structure is shown below, the double bond repels the single bonds more strongly than the single bonds repel each other. This causes a deviation from ideal geometry (an H–C–H bond angle of 116.5° rather than 120°).

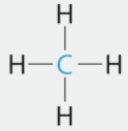


Four Electron Groups

One of the limitations of Lewis structures is that they depict molecules and ions in only two dimensions. With four electron groups, we must learn to show molecules and ions in three dimensions.

AX_4 Molecules: CH_4

1. The central atom, carbon, contributes four valence electrons, and each hydrogen atom has one valence electron, so the full Lewis electron structure is

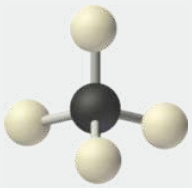


Lewis structure

2. There are four electron groups around the central atom. As shown in Figure **2.3.2**, repulsions are minimized by placing the groups in the corners of a tetrahedron with bond angles of 109.5°.

3. All electron groups are bonding pairs, so the structure is designated as AX_4.

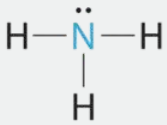
4. With four bonding pairs, the molecular geometry of methane is *tetrahedral* (Figure **2.3.3**).



Molecular geometry
(tetrahedral)

AX_3E Molecules: NH_3

1. In ammonia, the central atom, nitrogen, has five valence electrons and each hydrogen donates one valence electron, producing the Lewis electron structure



Lewis structure

2. There are four electron groups around nitrogen, three bonding pairs and one lone pair. Repulsions are minimized by directing each hydrogen atom and the lone pair to the corners of a tetrahedron.

3. With three bonding pairs and one lone pair, the structure is designated as AX_3E. This designation has a total of four electron pairs, three X and one E. We expect the LP–BP interactions to cause the bonding pair angles to deviate significantly from the angles of a perfect tetrahedron.

4. There are three nuclei and one lone pair, so the molecular geometry is *trigonal pyramidal*. In essence, this is a tetrahedron with a vertex missing (Figure **2.3.3**). However, the H–N–H bond angles are less than the ideal angle of 109.5° because of LP–BP repulsions (Figure **2.3.3** and Figure **2.3.4**).

AX_2E_2 Molecules: H_2O

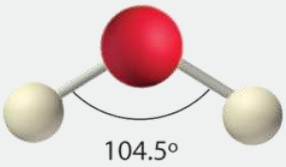
1. Oxygen has six valence electrons and each hydrogen has one valence electron, producing the Lewis electron structure



Figure **2.3.2**: (CC BY-NC-SA; anonymous)

3. With two bonding pairs and two lone pairs, the structure is designated as AX_2E_2 with a total of four electron pairs. Due to LP–LP, LP–BP, and BP–BP interactions, we expect a significant deviation from idealized tetrahedral angles.

4. With two hydrogen atoms and two lone pairs of electrons, the structure has significant lone pair interactions. There are two nuclei about the central atom, so the molecular shape is *bent*, or *V shaped*, with an H–O–H angle that is even less than the H–N–H angles in NH_3, as we would expect because of the presence of two lone pairs of electrons on the central atom rather than one. This molecular shape is essentially a tetrahedron with two missing vertices.



Five Electron Groups

In previous examples it did not matter where we placed the electron groups because all positions were equivalent. In some cases, however, the positions are not equivalent. We encounter this situation for the first time with five electron groups.

AX_5 Molecules: PCl_5

1. Phosphorus has five valence electrons and each chlorine has seven valence electrons, so the Lewis electron structure of PCl_5 is

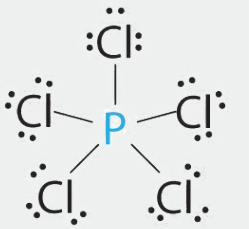
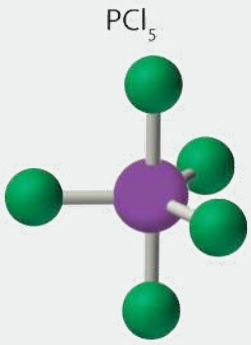


Figure **2.3.2**): (CC BY-NC-SA; anonymous)

3. All electron groups are bonding pairs, so the structure is designated as AX_5. There are no lone pair interactions.

4. The molecular geometry of PCl_5 is *trigonal bipyramidal*, as shown in Figure **2.3.3**. The molecule has three atoms in a plane in *equatorial* positions and two atoms above and below the plane in *axial* positions. The three equatorial positions are separated by 120° from one another, and the two axial positions are at 90° to the equatorial plane. The axial and equatorial positions are not chemically equivalent, as we will see in our next example.



AX_4E Molecules: SF_4

1. The sulfur atom has six valence electrons and each fluorine has seven valence electrons, so the Lewis electron structure is



Lewis structure

With an expanded valence, this species is an exception to the octet rule.

2. There are five groups around sulfur, four bonding pairs and one lone pair. With five electron groups, the lowest energy arrangement is a trigonal bipyramid, as shown in Figure **2.3.2**.

3. We designate SF_4 as AX_4E; it has a total of five electron pairs. However, because the axial and equatorial positions are not chemically equivalent, where do we place the lone pair? If we place the lone pair in the axial position, we have three LP–BP repulsions at 90°. If we place it in the equatorial position, we have two 90° LP–BP repulsions at 90°. With fewer 90° LP–BP repulsions, we can predict that the structure with the lone pair of electrons in the *equatorial position is more stable than the one with the lone pair in the axial position*. We also expect a deviation from ideal geometry because a lone pair of electrons occupies more space than a bonding pair.

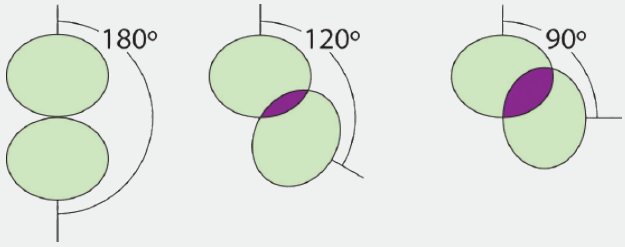
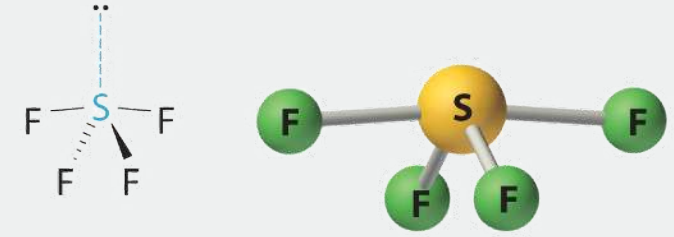


Figure **2.3.5**: Illustration of the Area Shared by Two Electron Pairs versus the Angle between Them

At 90°, the two electron pairs share a relatively large region of space, which leads to strong repulsive electron–electron interactions.

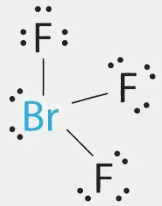
4. With four nuclei and one lone pair of electrons, the molecular structure is based on a trigonal bipyramid with a missing equatorial vertex; it is described as a *seesaw*. The F_{axial}–S–F_{axial} angle is 173° rather than 180° because of the lone pair of electrons in the equatorial plane.



Molecular geometry (seesaw)

AX_3E_2 Molecules: BrF_3

1. The bromine atom has seven valence electrons, and each fluorine has seven valence electrons, so the Lewis electron structure is



Lewis structure

Once again, we have a compound that is an exception to the octet rule.

2. There are five groups around the central atom, three bonding pairs and two lone pairs. We again direct the groups toward the vertices of a trigonal bipyramid.

3. With three bonding pairs and two lone pairs, the structural designation is AX_3E_2 with a total of five electron pairs. Because the axial and equatorial positions are not equivalent, we must decide how to arrange the groups to minimize repulsions. If we place both lone pairs in the axial positions, we have six LP–BP repulsions at 90°. If both are in the equatorial positions, we have four LP–BP repulsions at 90°. If one lone pair is axial and the other equatorial, we have one LP–LP repulsion at 90° and three LP–BP repulsions at 90°:



	Lone pairs axial (a)	Lone pairs equatorial (b)	Lone pairs axial and equatorial (c)
Interactions			
90° LP–LP	0	0	1
90° LP–BP	6	4	3

Structure (c) can be eliminated because it has a LP–LP interaction at 90°. Structure (b), with fewer LP–BP repulsions at 90° than (a), is lower in energy. However, we predict a deviation in bond angles because of the presence of the two lone pairs of electrons.

4. The three nuclei in BrF_3 determine its molecular structure, which is described as *T shaped*. This is essentially a trigonal bipyramid that is missing two equatorial vertices. The F_{axial}–Br–F_{axial} angle is 172°, less than 180° because of LP–BP repulsions (Figure **2.3.2**.1).

Because lone pairs occupy more space around the central atom than bonding pairs, electrostatic repulsions are more important for lone pairs than for bonding pairs.

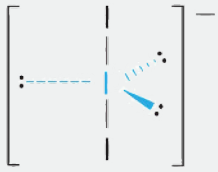
AX_2E_3 Molecules: I_3^-

1. Each iodine atom contributes seven electrons and the negative charge one, so the Lewis electron structure is



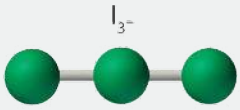
2. There are five electron groups about the central atom in I_3^-, two bonding pairs and three lone pairs. To minimize repulsions, the groups are directed to the corners of a trigonal bipyramid.

3. With two bonding pairs and three lone pairs, I_3^- has a total of five electron pairs and is designated as AX_2E_3. We must now decide how to arrange the lone pairs of electrons in a trigonal bipyramid in a way that minimizes repulsions. Placing them in the axial positions eliminates 90° LP–LP repulsions and minimizes the number of 90° LP–BP repulsions.



The three lone pairs of electrons have equivalent interactions with the three iodine atoms, so we do not expect any deviations in bonding angles.

4. With three nuclei and three lone pairs of electrons, the molecular geometry of I_3^- is linear. This can be described as a trigonal bipyramid with three equatorial vertices missing. The ion has an I–I–I angle of 180°, as expected.



Six Electron Groups

Six electron groups form an *octahedron*, a polyhedron made of identical equilateral triangles and six identical vertices (Figure **2.3.2**.)

AX_6 Molecules: SF_6

1. The central atom, sulfur, contributes six valence electrons, and each fluorine atom has seven valence electrons, so the Lewis electron structure is



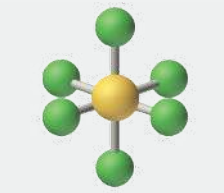
Lewis structure

With an expanded valence, this species is an exception to the octet rule.

2. There are six electron groups around the central atom, each a bonding pair. We see from Figure **2.3.2** that the geometry that minimizes repulsions is *octahedral*.

3. With only bonding pairs, SF_6 is designated as AX_6. All positions are chemically equivalent, so all electronic interactions are equivalent.

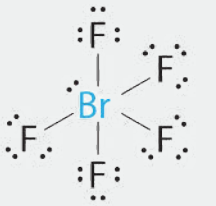
4. There are six nuclei, so the molecular geometry of SF_6 is octahedral.



Molecular geometry
(octahedral)

AX_5E Molecules: BrF_5

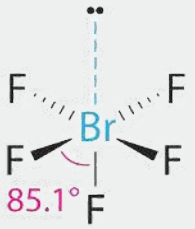
1. The central atom, bromine, has seven valence electrons, as does each fluorine, so the Lewis electron structure is



Lewis structure

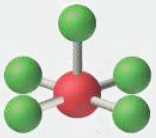
With its expanded valence, this species is an exception to the octet rule.

2. There are six electron groups around the Br, five bonding pairs and one lone pair. Placing five F atoms around Br while minimizing BP–BP and LP–BP repulsions gives the following structure:



3. With five bonding pairs and one lone pair, BrF_5 is designated as AX_5E; it has a total of six electron pairs. The BrF_5 structure has four fluorine atoms in a plane in an equatorial position and one fluorine atom and the lone pair of electrons in the axial positions. We expect all F_{axial}–Br–$F_{equatorial}$ angles to be less than 90° because of the lone pair of electrons, which occupies more space than the bonding electron pairs.

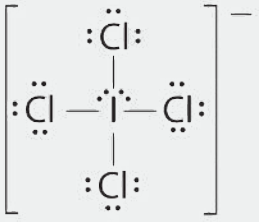
4. With five nuclei surrounding the central atom, the molecular structure is based on an octahedron with a vertex missing. This molecular structure is *square pyramidal*. The F_{axial}–B–$F_{equatorial}$ angles are 85.1°, less than 90° because of LP–BP repulsions.



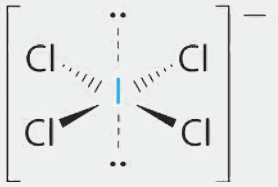
Molecular geometry
(square pyramidal)

AX_4E_2 Molecules: ICl_4^-

1. The central atom, iodine, contributes seven electrons. Each chlorine contributes seven, and there is a single negative charge. The Lewis electron structure is

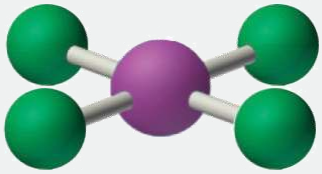


2. There are six electron groups around the central atom, four bonding pairs and two lone pairs. The structure that minimizes LP–LP, LP–BP, and BP–BP repulsions is



3. ICl_4^- is designated as AX_4E_2 and has a total of six electron pairs. Although there are lone pairs of electrons, with four bonding electron pairs in the equatorial plane and the lone pairs of electrons in the axial positions, all LP–BP repulsions are the same. Therefore, we do not expect any deviation in the Cl–I–Cl bond angles.

4. With five nuclei, the ICl4− ion forms a molecular structure that is *square planar*, an octahedron with two opposite vertices missing.



The relationship between the number of electron groups around a central atom, the number of lone pairs of electrons, and the molecular geometry is summarized in Figure **2.3.6**.

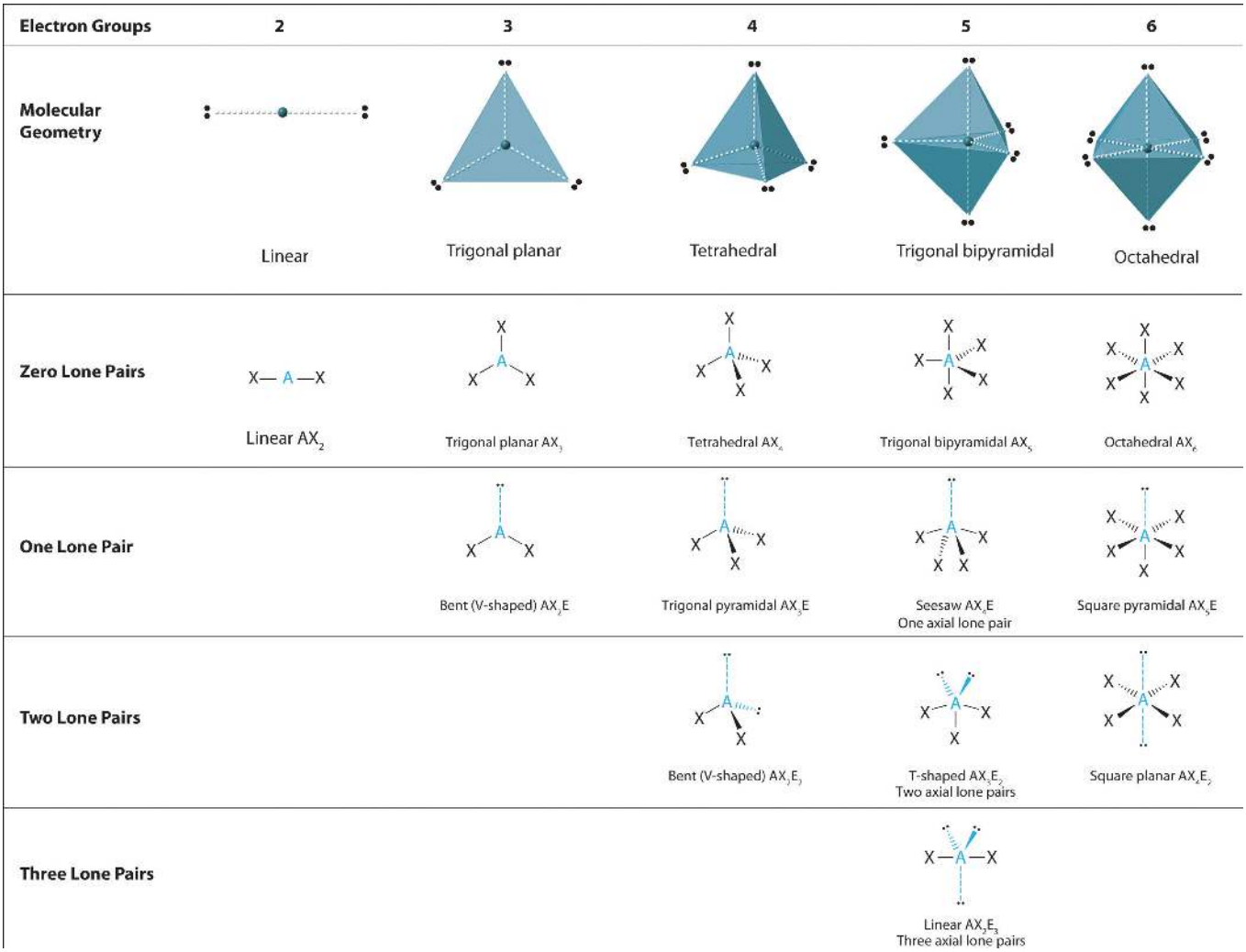


***Figure* 2.3.6:** *Overview of Molecular Geometries*

Example 2.3.1

Using the VSEPR model, predict the molecular geometry of each molecule or ion.

1. PF_5 (phosphorus pentafluoride, a catalyst used in certain organic reactions)
2. H_3O^+ (hydronium ion)

Given: two chemical species

Asked for: molecular geometry

Strategy:

A. Draw the Lewis electron structure of the molecule or polyatomic ion.
B. Determine the electron group arrangement around the central atom that minimizes repulsions.
C. Assign an AX_mE_n designation; then identify the LP–LP, LP–BP, or BP–BP interactions and predict deviations in bond angles.
D. Describe the molecular geometry.

Solution:

1. **A** The central atom, P, has five valence electrons and each fluorine has seven valence electrons, so the Lewis structure of PF_5 is

https://chem.libretexts.org/@go/page/294861

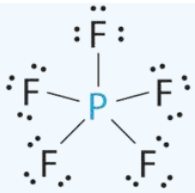


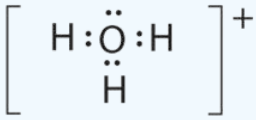
Figure **2.3.6**): (CC BY-NC-SA; anonymous)

C All electron groups are bonding pairs, so PF_5 is designated as AX_5. Notice that this gives a total of five electron pairs. With no lone pair repulsions, we do not expect any bond angles to deviate from the ideal.

D The PF_5 molecule has five nuclei and no lone pairs of electrons, so its molecular geometry is trigonal bipyramidal.



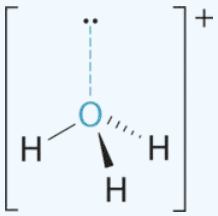
2. **A** The central atom, O, has six valence electrons, and each H atom contributes one valence electron. Subtracting one electron for the positive charge gives a total of eight valence electrons, so the Lewis electron structure is



B There are four electron groups around oxygen, three bonding pairs and one lone pair. Like NH_3, repulsions are minimized by directing each hydrogen atom and the lone pair to the corners of a tetrahedron.

C With three bonding pairs and one lone pair, the structure is designated as AX_3E and has a total of four electron pairs (three X and one E). We expect the LP–BP interactions to cause the bonding pair angles to deviate significantly from the angles of a perfect tetrahedron.

D There are three nuclei and one lone pair, so the molecular geometry is *trigonal pyramidal*, in essence a tetrahedron missing a vertex. However, the H–O–H bond angles are less than the ideal angle of 109.5° because of LP–BP repulsions:



Exercise 2.3.1

Using the VSEPR model, predict the molecular geometry of each molecule or ion.

a. XeO_3
b. PF_6^-
c. NO_2^+

Answer a

trigonal pyramidal

Answer b

octahedral

Answer c

linear

Example 2.3.2

Predict the molecular geometry of each molecule.

1. XeF_2
2. $SnCl_2$

Given: two chemical compounds

Asked for: molecular geometry

Strategy:

Use the strategy given in Example **2.3.1**.

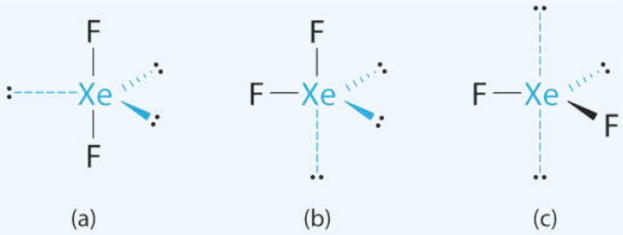
Solution:

1. **A** Xenon contributes eight electrons and each fluorine seven valence electrons, so the Lewis electron structure is



B There are five electron groups around the central atom, two bonding pairs and three lone pairs. Repulsions are minimized by placing the groups in the corners of a trigonal bipyramid.

C From B, XeF_2 is designated as AX_2E_3 and has a total of five electron pairs (two X and three E). With three lone pairs about the central atom, we can arrange the two F atoms in three possible ways: both F atoms can be axial, one can be axial and one equatorial, or both can be equatorial:

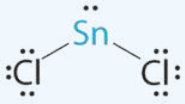


Interactions			
90 LP–LP	0	2	2

The structure with the lowest energy is the one that minimizes LP–LP repulsions. Both (b) and (c) have two 90° LP–LP interactions, whereas structure (a) has none. Thus both F atoms are in the axial positions, like the two iodine atoms around the central iodine in I_3^-. All LP–BP interactions are equivalent, so we do not expect a deviation from an ideal 180° in the F–Xe–F bond angle.

D With two nuclei about the central atom, the molecular geometry of XeF_2 is linear. It is a trigonal bipyramid with three missing equatorial vertices.

2. **A** The tin atom donates 4 valence electrons and each chlorine atom donates 7 valence electrons. With 18 valence electrons, the Lewis electron structure is



B There are three electron groups around the central atom, two bonding groups and one lone pair of electrons. To minimize repulsions the three groups are initially placed at 120° angles from each other.

C From B we designate $SnCl_2$ as AX_2E. It has a total of three electron pairs, two X and one E. Because the lone pair of electrons occupies more space than the bonding pairs, we expect a decrease in the Cl–Sn–Cl bond angle due to increased LP–BP repulsions.

D With two nuclei around the central atom and one lone pair of electrons, the molecular geometry of $SnCl_2$ is bent, like SO_2, but with a Cl–Sn–Cl bond angle of 95°. The molecular geometry can be described as a trigonal planar arrangement with one vertex missing.

Exercise 2.3.2

Predict the molecular geometry of each molecule.

a. SO_3
b. XeF_4

Answer a

trigonal planar

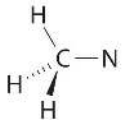
Answer b

square planar

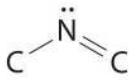
Molecules with No Single Central Atom

The VSEPR model can be used to predict the structure of somewhat more complex molecules with no single central atom by treating them as linked AX_mE_n fragments. We will demonstrate with methyl isocyanate (CH_3–N=C=O), a volatile and highly toxic molecule that is used to produce the pesticide Sevin. In 1984, large quantities of Sevin were accidentally released in Bhopal, India, when water leaked into storage tanks. The resulting highly exothermic reaction caused a rapid increase in pressure that ruptured the tanks, releasing large amounts of methyl isocyanate that killed approximately 3800 people and wholly or partially disabled about 50,000 others. In addition, there was significant damage to livestock and crops.

We can treat methyl isocyanate as linked AX_mE_n fragments beginning with the carbon atom at the left, which is connected to three H atoms and one N atom by single bonds. The four bonds around carbon mean that it must be surrounded by four bonding electron pairs in a configuration similar to AX_4. We can therefore predict the CH_3–N portion of the molecule to be roughly tetrahedral, similar to methane:



The nitrogen atom is connected to one carbon by a single bond and to the other carbon by a double bond, producing a total of three bonds, C–N=C. For nitrogen to have an octet of electrons, it must also have a lone pair:



Because multiple bonds are not shown in the VSEPR model, the nitrogen is effectively surrounded by three electron pairs. Thus according to the VSEPR model, the C–N=C fragment should be bent with an angle less than 120°.

The carbon in the –N=C=O fragment is doubly bonded to both nitrogen and oxygen, which in the VSEPR model gives carbon a total of two electron pairs. The N=C=O angle should therefore be 180°, or linear. The three fragments combine to give the following structure:

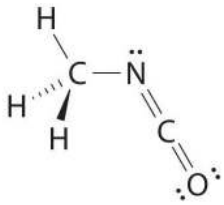


Figure **2.3.7**).

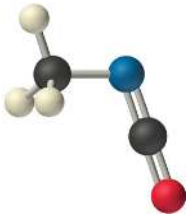


Figure **2.3.7**: The Experimentally Determined Structure of Methyl Isocyanate

Certain patterns are seen in the structures of moderately complex molecules. For example, carbon atoms with four bonds (such as the carbon on the left in methyl isocyanate) are generally tetrahedral. Similarly, the carbon atom on the right has two double bonds that are similar to those in CO_2, so its geometry, like that of CO_2, is linear. Recognizing similarities to simpler molecules will help you predict the molecular geometries of more complex molecules.

Example 2.3.3

Use the VSEPR model to predict the molecular geometry of propyne ($H_3C–C≡CH$), a gas with some anesthetic properties.

Given: chemical compound

Asked for: molecular geometry

Strategy:

Count the number of electron groups around each carbon, recognizing that in the VSEPR model, a multiple bond counts as a single group. Use Figure **2.3.3** to determine the molecular geometry around each carbon atom and then deduce the structure of the molecule as a whole.

Solution:

Because the carbon atom on the left is bonded to four other atoms, we know that it is approximately tetrahedral. The next two carbon atoms share a triple bond, and each has an additional single bond. Because a multiple bond is counted as a single bond in the VSEPR model, each carbon atom behaves as if it had two electron groups. This means that both of these carbons are linear, with C–C≡C and C≡C–H angles of 180°.

Exercise 2.3.3

Predict the geometry of allene ($H_2C=C=CH_2$), a compound with narcotic properties that is used to make more complex organic molecules.

Answer

The terminal carbon atoms are trigonal planar, the central carbon is linear, and the C–C–C angle is 180°.

Molecular Dipole Moments

You previously learned how to calculate the **dipole moments** of simple diatomic molecules. In more complex molecules with polar covalent bonds, the three-dimensional geometry and the compound's symmetry determine whether there is a net dipole moment. Mathematically, dipole moments are *vectors*; they possess both a *magnitude* and a *direction*. The dipole moment of a molecule is therefore the *vector sum* of the dipole moments of the individual bonds in the molecule. If the individual bond dipole moments cancel one another, there is no net dipole moment. Such is the case for CO_2, a linear molecule (Figure **2.3.8*a***). Each C–O bond in

CO_2 is polar, yet experiments show that the CO_2 molecule has no dipole moment. Because the two C–O bond dipoles in CO_2 are equal in magnitude and oriented at 180° to each other, they cancel. As a result, the CO_2 molecule has no *net* dipole moment even though it has a substantial separation of charge. In contrast, the H_2O molecule is not linear (Figure **2.3.8*b***); it is bent in three-dimensional space, so the dipole moments do not cancel each other. Thus a molecule such as H_2O has a net dipole moment. We expect the concentration of negative charge to be on the oxygen, the more electronegative atom, and positive charge on the two hydrogens. This charge polarization allows H_2O to hydrogen-bond to other polarized or charged species, including other water molecules.

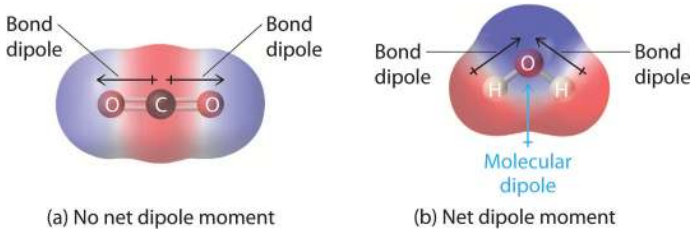


Figure **2.3.8**: How Individual Bond Dipole Moments Are Added Together to Give an Overall Molecular Dipole Moment for Two Triatomic Molecules with Different Structures. (a) In CO_2, the C–O bond dipoles are equal in magnitude but oriented in opposite directions (at 180°). Their vector sum is zero, so CO_2 therefore has no net dipole. (b) In H_2O, the O–H bond dipoles are also equal in magnitude, but they are oriented at 104.5° to each other. Hence the vector sum is not zero, and H_2O has a net dipole moment.

Other examples of molecules with polar bonds are shown in Figure **2.3.9**. In molecular geometries that are highly symmetrical (most notably tetrahedral and square planar, trigonal bipyramidal, and octahedral), individual bond dipole moments completely cancel, and there is no net dipole moment. Although a molecule like $CHCl_3$ is best described as tetrahedral, the atoms bonded to carbon are not identical. Consequently, the bond dipole moments cannot cancel one another, and the molecule has a dipole moment. Due to the arrangement of the bonds in molecules that have V-shaped, trigonal pyramidal, seesaw, T-shaped, and square pyramidal geometries, the bond dipole moments cannot cancel one another. Consequently, molecules with these geometries always have a nonzero dipole moment.

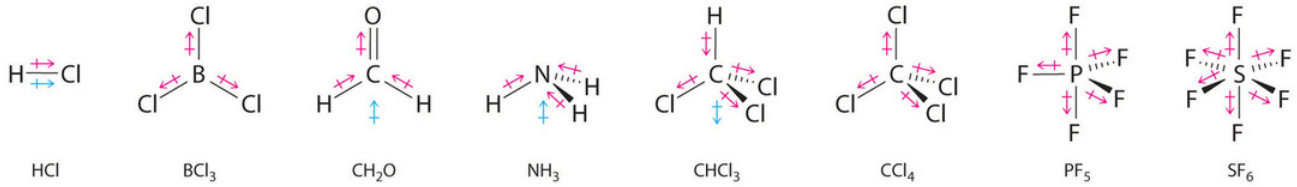


Figure **2.3.9**: Molecules with Polar Bonds. Individual bond dipole moments are indicated in red. Due to their different three-dimensional structures, some molecules with polar bonds have a net dipole moment (HCl, CH_2O, NH_3, and $CHCl_3$), indicated in blue, whereas others do not because the bond dipole moments cancel (BCl_3, CCl_4, PF_5, and SF_6).

Molecules with asymmetrical charge distributions have a net dipole moment.

Example 2.3.4

Which molecule(s) has a net dipole moment?

a. $\mathbf{H_2S}$
b. $\mathbf{NHF_2}$
c. $\mathbf{BF_3}$

Given: three chemical compounds

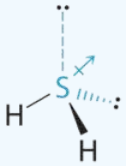
Asked for: net dipole moment

Strategy:

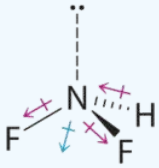
For each three-dimensional molecular geometry, predict whether the bond dipoles cancel. If they do not, then the molecule has a net dipole moment.

Solution:

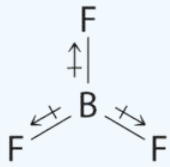
1. The total number of electrons around the central atom, S, is eight, which gives four electron pairs. Two of these electron pairs are bonding pairs and two are lone pairs, so the molecular geometry of $\mathbf{H_2S}$ is bent (Figure **2.3.6**). The bond dipoles cannot cancel one another, so the molecule has a net dipole moment.



2. Difluoroamine has a trigonal pyramidal molecular geometry. Because there is one hydrogen and two fluorines, and because of the lone pair of electrons on nitrogen, the molecule is not symmetrical, and the bond dipoles of NHF_2 cannot cancel one another. This means that NHF_2 has a net dipole moment. We expect polarization from the two fluorine atoms, the most electronegative atoms in the periodic table, to have a greater affect on the net dipole moment than polarization from the lone pair of electrons on nitrogen.



3. The molecular geometry of BF_3 is trigonal planar. Because all the B–F bonds are equal and the molecule is highly symmetrical, the dipoles cancel one another in three-dimensional space. Thus BF_3 has a net dipole moment of zero:



Exercise 2.3.4

Which molecule(s) has a net dipole moment?

- $\mathbf{CH_3Cl}$
- $\mathbf{SO_3}$
- $\mathbf{XeO_3}$

Answer

$\mathbf{CH_3Cl}$ and $\mathbf{XeO_3}$

Summary

Lewis electron structures give no information about **molecular geometry**, the arrangement of bonded atoms in a molecule or polyatomic ion, which is crucial to understanding the chemistry of a molecule. The **valence-shell electron-pair repulsion (VSEPR) model** allows us to predict which of the possible structures is actually observed in most cases. It is based on the assumption that pairs of electrons occupy space, and the lowest-energy structure is the one that minimizes electron pair–electron pair repulsions. In the VSEPR model, the molecule or polyatomic ion is given an AX_mE_n designation, where A is the central atom, X is a bonded atom, E is a nonbonding valence electron group (usually a lone pair of electrons), and m and n are integers. Each group around the central atom is designated as a bonding pair (BP) or lone (nonbonding) pair (LP). From the BP and LP interactions we can predict both the relative positions of the atoms and the angles between the bonds, called the **bond angles**. From this we can describe the **molecular geometry**. The VSEPR model can be used to predict the shapes of many molecules and polyatomic ions, but it gives no information about bond lengths and the presence of multiple bonds. A combination of VSEPR and a bonding model, such as Lewis electron structures, is necessary to understand the presence of multiple bonds.

Molecules with polar covalent bonds can have a *dipole moment*, an asymmetrical distribution of charge that results in a tendency for molecules to align themselves in an applied electric field. Any diatomic molecule with a polar covalent bond has a dipole moment, but in polyatomic molecules, the presence or absence of a net dipole moment depends on the structure. For some highly symmetrical structures, the individual bond dipole moments cancel one another, giving a dipole moment of zero.

2.3: The VSEPR Model is shared under a CC BY-NC-SA 4.0 license and was authored, remixed, and/or curated by LibreTexts.

2.4: Hybrid Orbitals

The localized **valence bond theory** uses a process called **hybridization**, in which atomic orbitals that are similar in energy but not equivalent are combined mathematically to produce sets of equivalent orbitals that are properly oriented to form bonds. These new combinations are called hybrid atomic orbitals because they are produced by combining (*hybridizing*) two or more atomic orbitals from the same atom.

Hybridization of *s* and *p* Orbitals

In BeH_2, we can generate two equivalent orbitals by combining the 2*s* orbital of beryllium and any one of the three degenerate 2*p* orbitals. By taking the sum and the difference of Be 2*s* and $2p_z$ atomic orbitals, for example, we produce two new orbitals with major and minor lobes oriented along the *z*-axes, as shown in Figure **2.4.1**.

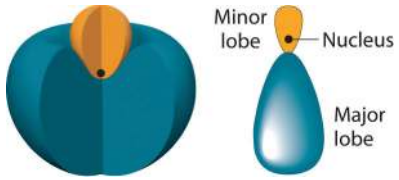


Figure **2.4.1:** The position of the atomic nucleus with respect to an sp hybrid orbital. The nucleus is actually located slightly inside the minor lobe, not at the node separating the major and minor lobes.

Because the difference A − B can also be written as A + (−B), in Figure **2.4.2** and subsequent figures we have reversed the phase(s) of the orbital being subtracted, which is the same as multiplying it by −1 and adding. This gives us Equation **2.4.2**, where the value $\frac{1}{\sqrt{2}}$ is needed mathematically to indicate that the 2*s* and 2*p* orbitals contribute equally to each hybrid orbital.

$$sp = \frac{1}{\sqrt{2}}(2s + 2p_z) \tag{2.4.1}$$

and

$$sp = \frac{1}{\sqrt{2}}(2s - 2p_z) \tag{2.4.2}$$

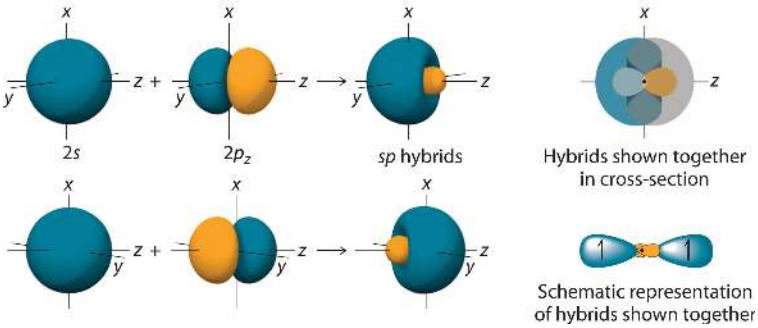


Figure **2.4.2**: The Formation of *sp* Hybrid Orbitals. Taking the sum and difference of an *ns* and an *np* atomic orbital where *n* = 2 gives two equivalent *sp* hybrid orbitals oriented at 180° to each other.

The nucleus resides just inside the minor lobe of each orbital. In this case, the new orbitals are called *sp hybrids* because they are formed from one *s* and one *p* orbital. The two new orbitals are equivalent in energy, and their energy is between the energy values associated with pure *s* and *p* orbitals, as illustrated in this diagram:

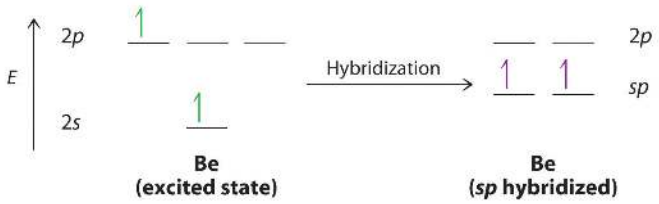


Figure **2.4.3**. each *sp* orbital on Be has the correct orientation for the major lobes to overlap with the 1*s* atomic orbital of an H atom. The formation of two energetically equivalent Be–H bonds produces a linear $\boldsymbol{BeH_2}$ molecule. Thus valence bond theory does what neither the Lewis electron structure nor the VSEPR model is able to do; it explains why the bonds in $\boldsymbol{BeH_2}$ are equivalent in energy and why $\boldsymbol{BeH_2}$ has a linear geometry.

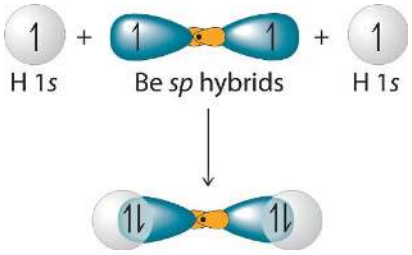


Figure **2.4.3**: Explanation of the Bonding in BeH_2 Using *sp* Hybrid Orbitals. Each singly occupied *sp* hybrid orbital on beryllium can form an electron-pair bond with the singly occupied 1*s* orbital of a hydrogen atom. Because the two *sp* hybrid orbitals are oriented at a 180° angle, the BeH_2 molecule is linear.

Because both promotion and hybridization require an input of energy, the formation of a set of singly occupied hybrid atomic orbitals is energetically uphill. The overall process of forming a compound with hybrid orbitals will be energetically favorable *only* if the amount of energy released by the formation of covalent bonds is greater than the amount of energy used to form the hybrid orbitals (Figure **2.4.4**). As we will see, some compounds are highly unstable or do not exist because the amount of energy required to form hybrid orbitals is greater than the amount of energy that would be released by the formation of additional bonds.

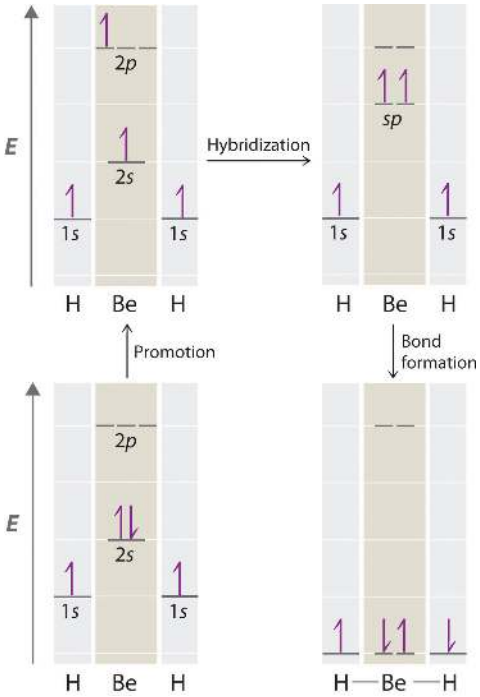


Figure **2.4.4**: A Hypothetical Stepwise Process for the Formation of BeH_2 from a Gaseous Be Atom and Two Gaseous H Atoms. The promotion of an electron from the 2*s* orbital of beryllium to one of the 2*p* orbitals is energetically uphill. The overall process of forming a BeH_2 molecule from a Be atom and two H atoms will therefore be energetically favorable *only* if the amount of energy released by the formation of the two Be–H bonds is greater than the amount of energy required for promotion and hybridization.

The concept of hybridization also explains why boron, with a $2s^22p^1$ valence electron configuration, forms three bonds with fluorine to produce BF_3, as predicted by the Lewis and VSEPR approaches. With only a single unpaired electron in its ground state,

boron should form only a single covalent bond. By the promotion of one of its 2*s* electrons to an unoccupied 2*p* orbital, however, followed by the hybridization of the three singly occupied orbitals (the 2*s* and two 2*p* orbitals), boron acquires a set of three equivalent hybrid orbitals with one electron each, as shown here:

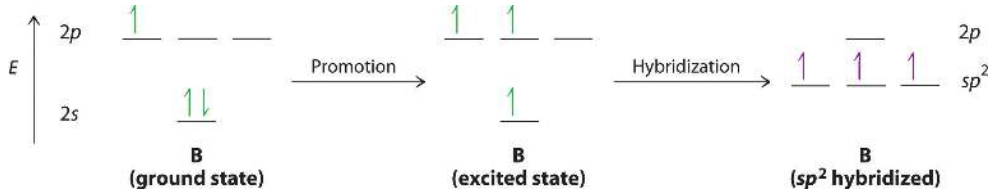


Figure **2.4.5**). Because the hybrid atomic orbitals are formed from one *s* and two *p* orbitals, boron is said to be sp^2 *hybridized* (pronounced "s-p-two" or "s-p-squared"). The singly occupied sp^2 hybrid atomic orbitals can overlap with the singly occupied orbitals on each of the three F atoms to form a trigonal planar structure with three energetically equivalent B–F bonds.

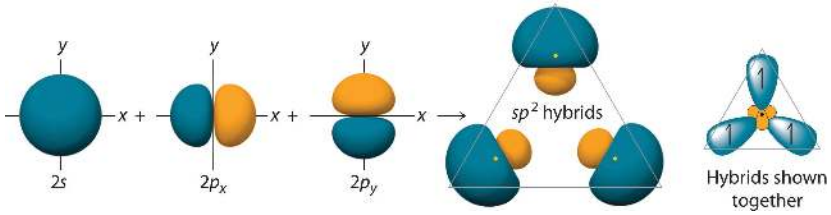


Figure **2.4.5**: Formation of sp^2 Hybrid Orbitals. Combining one *ns* and two *np* atomic orbitals gives three equivalent sp^2 hybrid orbitals in a trigonal planar arrangement; that is, oriented at 120° to one another.

Looking at the $2s^22p^2$ valence electron configuration of carbon, we might expect carbon to use its two unpaired 2*p* electrons to form compounds with only two covalent bonds. We know, however, that carbon typically forms compounds with four covalent bonds. We can explain this apparent discrepancy by the hybridization of the 2*s* orbital and the three 2*p* orbitals on carbon to give a set of four degenerate sp^3 ("s-p-three" or "s-p-cubed") hybrid orbitals, each with a single electron:

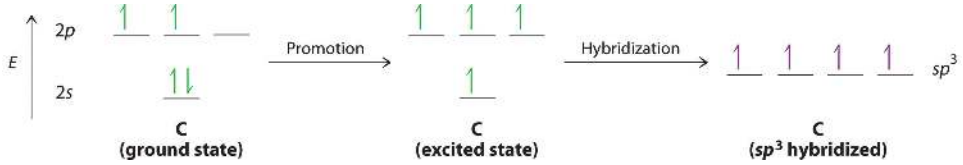


Figure **2.4.6**). Like all the hybridized orbitals discussed earlier, the sp^3 hybrid atomic orbitals are predicted to be equal in energy. Thus, methane (CH_4) is a tetrahedral molecule with four equivalent C-H bonds.

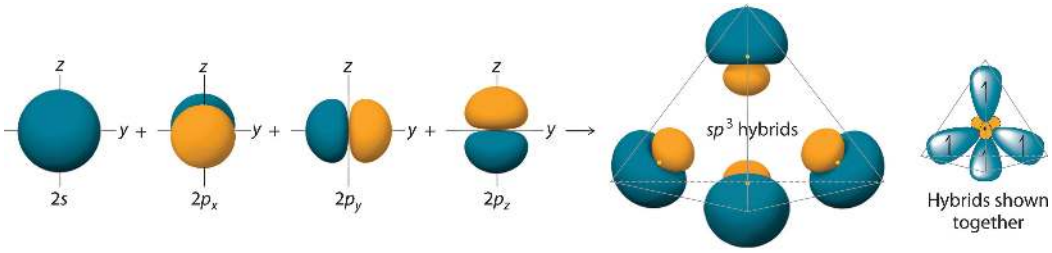
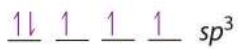


Figure **2.4.6**: Formation of sp^3 Hybrid Orbitals. Combining one *ns* and three *np* atomic orbitals results in four sp^3 hybrid orbitals oriented at 109.5° to one another in a tetrahedral arrangement.

In addition to explaining why some elements form more bonds than would be expected based on their valence electron configurations, and why the bonds formed are equal in energy, valence bond theory explains why these compounds are so stable: the amount of energy released increases with the number of bonds formed. In the case of carbon, for example, much more energy is released in the formation of four bonds than two, so compounds of carbon with four bonds tend to be more stable than those with only two. Carbon does form compounds with only two covalent bonds (such as CH_2 or CF_2), but these species are highly reactive, unstable intermediates that only form in certain chemical reactions.

> *Valence bond theory explains the number of bonds formed in a compound and the relative bond strengths.*

The bonding in molecules such as NH_3 or H_2O, which have lone pairs on the central atom, can also be described in terms of hybrid atomic orbitals. In NH_3, for example, N, with a $2s^2 2p^3$ valence electron configuration, can hybridize its 2*s* and 2*p* orbitals to produce four sp^3 hybrid orbitals. Placing five valence electrons in the four hybrid orbitals, we obtain three that are singly occupied and one with a pair of electrons:



The three singly occupied sp^3 lobes can form bonds with three H atoms, while the fourth orbital accommodates the lone pair of electrons. Similarly, H_2O has an sp^3 hybridized oxygen atom that uses two singly occupied sp^3 lobes to bond to two H atoms, and two to accommodate the two lone pairs predicted by the VSEPR model. Such descriptions explain the approximately tetrahedral distribution of electron pairs on the central atom in NH_3 and H_2O. Unfortunately, however, recent experimental evidence indicates that in NH_3 and H_2O, the hybridized orbitals are *not* entirely equivalent in energy, making this bonding model an active area of research.

Example 2.4.1

Use the VSEPR model to predict the number of electron pairs and molecular geometry in each compound and then describe the hybridization and bonding of all atoms except hydrogen.

a. H_2S
b. $CHCl_3$

Given: two chemical compounds

Asked for: number of electron pairs and molecular geometry, hybridization, and bonding

Strategy:

A. Using the VSEPR approach to determine the number of electron pairs and the molecular geometry of the molecule.
B. From the valence electron configuration of the central atom, predict the number and type of hybrid orbitals that can be produced. Fill these hybrid orbitals with the total number of valence electrons around the central atom and describe the hybridization.

Solution:

1. **A** H_2S has four electron pairs around the sulfur atom with two bonded atoms, so the VSEPR model predicts a molecular geometry that is bent, or V shaped. **B** Sulfur has a $3s^2 3p^4$ valence electron configuration with six electrons, but by hybridizing its 3*s* and 3*p* orbitals, it can produce four sp^3 hybrids. If the six valence electrons are placed in these orbitals, two have electron pairs and two are singly occupied. The two sp^3 hybrid orbitals that are singly occupied are used to form S–H bonds, whereas the other two have lone pairs of electrons. Together, the four sp^3 hybrid orbitals produce an approximately tetrahedral arrangement of electron pairs, which agrees with the molecular geometry predicted by the VSEPR model.
2. **A** The $CHCl_3$ molecule has four valence electrons around the central atom. In the VSEPR model, the carbon atom has four electron pairs, and the molecular geometry is tetrahedral. **B** Carbon has a $2s^2 2p^2$ valence electron configuration. By hybridizing its 2*s* and 2*p* orbitals, it can form four sp^3 hybridized orbitals that are equal in energy. Eight electrons around the central atom (four from C, one from H, and one from each of the three Cl atoms) fill three sp^3 hybrid orbitals to form C–Cl bonds, and one forms a C–H bond. Similarly, the Cl atoms, with seven electrons each in their 3*s* and 3*p* valence subshells, can be viewed as sp^3 hybridized. Each Cl atom uses a singly occupied sp^3 hybrid orbital to form a C–Cl bond and three hybrid orbitals to accommodate lone pairs.

Exercise 2.4.1

Use the VSEPR model to predict the number of electron pairs and molecular geometry in each compound and then describe the hybridization and bonding of all atoms except hydrogen.

a. the BF_4^- ion
b. hydrazine ($H_2N–NH_2$)

Answer a

B is sp^3 hybridized; F is also sp^3 hybridized so it can accommodate one B–F bond and three lone pairs. The molecular geometry is tetrahedral.

Answer b

Each N atom is sp^3 hybridized and uses one sp^3 hybrid orbital to form the N–N bond, two to form N–H bonds, and one to accommodate a lone pair. The molecular geometry about each N is trigonal pyramidal.

The number of hybrid orbitals used by the central atom is the same as the number of electron pairs around the central atom.

Summary

Hybridization increases the overlap of bonding orbitals and explains the molecular geometries of many species whose geometry cannot be explained using a VSEPR approach. The *localized bonding* model (called **valence bond theory**) assumes that covalent bonds are formed when atomic orbitals overlap and that the strength of a covalent bond is proportional to the amount of overlap. It also assumes that atoms use combinations of atomic orbitals (*hybrids*) to maximize the overlap with adjacent atoms. The formation of **hybrid atomic orbitals** can be viewed as occurring via **promotion** of an electron from a filled ns^2 subshell to an empty *np* valence orbital, followed by **hybridization**, the combination of the orbitals to give a new set of (usually) equivalent orbitals that are oriented properly to form bonds. The combination of an *ns* and an *np* orbital gives rise to two equivalent **sp hybrids** oriented at 180°, whereas the combination of an *ns* and two or three *np* orbitals produces three equivalent ***sp*^{2} hybrids** or four equivalent ***sp*^{3} hybrids**, respectively. The spatial orientation of the hybrid atomic orbitals is consistent with the geometries predicted using the VSEPR model.

2.4: Hybrid Orbitals is shared under a CC BY-NC-SA 4.0 license and was authored, remixed, and/or curated by LibreTexts.

SECTION OVERVIEW

2.5: Molecular Orbitals

2.5.1: Molecular Shape and Molecular Polarity

2.5.2: Prelude to Molecular Orbital Theory

2.5.3: Constructing Molecular Orbitals from Atomic Orbitals

2.5.4: Orbital Symmetry

2.5.5: Molecular Orbital Diagrams

2.5.6: π Orbitals and Diatomic Molecules

2.5.7: Orbital Filling

2.5.8: δ orbitals

2.5: Molecular Orbitals is shared under a not declared license and was authored, remixed, and/or curated by LibreTexts.

2.5.1: Molecular Shape and Molecular Polarity

Learning Objectives

- To calculate the percent ionic character of a covalent polar bond

Previously, we described the two idealized extremes of chemical bonding:

- **ionic bonding**—in which one or more electrons are transferred completely from one atom to another, and the resulting ions are held together by purely electrostatic forces—and
- **covalent bonding**, in which electrons are shared *equally* between two atoms.

Most compounds, however, have polar covalent bonds, which means that electrons are shared *unequally* between the bonded atoms. Figure 2.5.1.1 compares the electron distribution in a polar covalent bond with those in an ideally covalent and an ideally ionic bond. Recall that a lowercase Greek delta (δ) is used to indicate that a bonded atom possesses a partial positive charge, indicated by δ^+, or a partial negative charge, indicated by δ^-, and a bond between two atoms that possess partial charges is a *polar bond*.

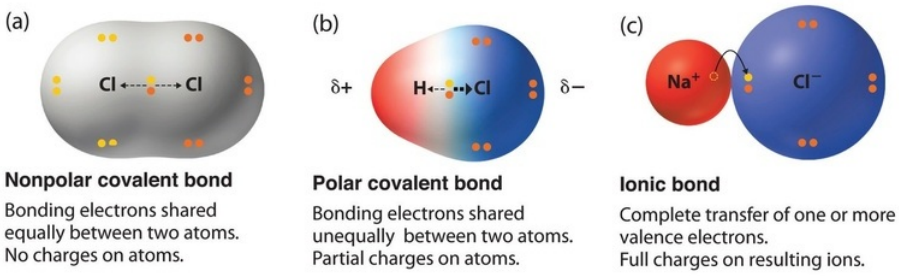


Figure 2.5.1.1: The Electron Distribution in a Nonpolar Covalent Bond, a Polar Covalent Bond, and an Ionic Bond Using Lewis Electron Structures. In a purely covalent bond (a), the bonding electrons are shared equally between the atoms. In a purely ionic bond (c), an electron has been transferred completely from one atom to the other. A polar covalent bond (b) is intermediate between the two extremes: the bonding electrons are shared unequally between the two atoms, and the electron distribution is asymmetrical with the electron density being greater around the more electronegative atom. Electron-rich (negatively charged) regions are shown in blue; electron-poor (positively charged) regions are shown in red.

Bond Polarity

The polarity of a bond—the extent to which it is polar—is determined largely by the relative electronegativities of the bonded atoms. *Electronegativity* (χ) was defined as the ability of an atom in a molecule or an ion to attract electrons to itself. Thus there is a direct correlation between electronegativity and bond polarity. A bond is *nonpolar* if the bonded atoms have equal electronegativities. If the electronegativities of the bonded atoms are not equal, however, the bond is *polarized* toward the more electronegative atom. A bond in which the electronegativity of B (χ_B) is greater than the electronegativity of A (χ_A), for example, is indicated with the partial negative charge on the more electronegative atom:

$$\underset{\delta^+}{\overset{\text{less electronegative}}{A}} - \underset{\delta^-}{\overset{\text{more electronegative}}{B}}$$

One way of estimating the ionic character of a bond—that is, the magnitude of the charge separation in a polar covalent bond—is to calculate the difference in electronegativity between the two atoms:

$$\Delta\chi = \chi_B - \chi_A.$$

To predict the polarity of the bonds in Cl_2, HCl, and NaCl, for example, we look at the electronegativities of the relevant atoms (Table A2): $\chi_{Cl} = 3.16$, $\chi_H = 2.20$, and $\chi_{Na} = 0.93$. Cl_2 must be nonpolar because the electronegativity difference ($\Delta\chi$) is zero; hence the two chlorine atoms share the bonding electrons equally. In NaCl, $\Delta\chi$ is 2.23. This high value is typical of an ionic compound ($\Delta\chi \geq \approx 1.5$) and means that the valence electron of sodium has been completely transferred to chlorine to form Na^+ and Cl^- ions. In HCl, however, $\Delta\chi$ is only 0.96. The bonding electrons are more strongly attracted to the more electronegative chlorine atom, and so the charge distribution is

$$\overset{\delta+}{H} - \overset{\delta-}{Cl}$$

Remember that electronegativities are difficult to measure precisely and different definitions produce slightly different numbers. In practice, the polarity of a bond is usually estimated rather than calculated.

> Bond polarity and ionic character increase with an increasing difference in electronegativity.

As with bond energies, the electronegativity of an atom depends to some extent on its chemical environment. It is therefore unlikely that the reported electronegativities of a chlorine atom in $\mathbf{NaCl}$, $\mathbf{Cl_2}$, $\mathbf{ClF_5}$, and $\mathbf{HClO_4}$ would be exactly the same.

Dipole Moments

The asymmetrical charge distribution in a polar substance such as $\mathbf{HCl}$ produces a dipole moment where Qr in meters (m). is abbreviated by the Greek letter mu (μ). The dipole moment is defined as the product of the partial charge Q on the bonded atoms and the distance r between the partial charges:

$$\mu = Qr \tag{2.5.1.1}$$

where Q is measured in coulombs (C) and r in meters. The unit for dipole moments is the debye (D):

$$1\ D = 3.3356 \times 10^{-30}\ C \cdot m \tag{2.5.1.2}$$

When a molecule with a dipole moment is placed in an electric field, it tends to orient itself with the electric field because of its asymmetrical charge distribution (Figure 2.5.1.2).

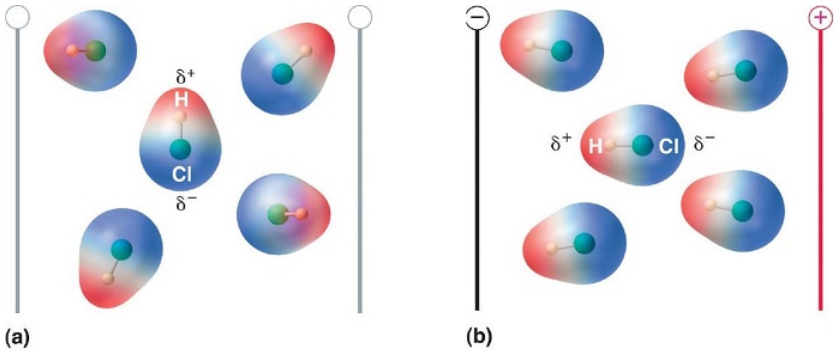


Figure 2.5.1.2: Molecules That Possess a Dipole Moment Partially Align Themselves with an Applied Electric Field In the absence of a field (a), the$\mathbf{HCl}$molecules are randomly oriented. When an electric field is applied (b), the molecules tend to align themselves with the field, such that the positive end of the molecular dipole points toward the negative terminal and vice versa.

We can measure the partial charges on the atoms in a molecule such as $\mathbf{HCl}$ using Equation 2.5.1.1. If the bonding in $\mathbf{HCl}$ were purely ionic, an electron would be transferred from H to Cl, so there would be a full +1 charge on the H atom and a full −1 charge on the Cl atom. The dipole moment of $\mathbf{HCl}$ is 1.109 D, as determined by measuring the extent of its alignment in an electric field, and the reported gas-phase H–Cl distance is 127.5 pm. Hence the charge on each atom is

$$\begin{aligned} Q &= \frac{\mu}{r} \\ &= 1.109\ \cancel{D}\left(\frac{3.3356 \times 10^{-30}\ C \cdot \cancel{m}}{1\ \cancel{D}}\right)\left(\frac{1}{127.8\ \cancel{pm}}\right)\left(\frac{1\ \cancel{pm}}{10^{-12}\ \cancel{m}}\right) \\ &= 2.901 \times 10^{-20}\ C \end{aligned}$$

By dividing this calculated value by the charge on a single electron (1.6022×10^{-19} C), we find that the electron distribution in$\mathbf{HCl}$ is asymmetric and that effectively it appears that there is a net negative charge on the $\mathbf{Cl}$ of about −0.18, effectively corresponding to about 0.18 e^-. This certainly does not mean that there is a fraction of an electron on the $\mathbf{Cl}$ atom, but that the distribution of electron probability favors the Cl atom side of the molecule by about this amount.

$$\frac{2.901 \times 10^{-20} \cancel{C}}{1.6022 \times 10^{-19} \cancel{C}} = 0.1811\ e^-$$

To form a neutral compound, the charge on the H atom must be equal but opposite. Thus the measured dipole moment of HCl indicates that the H–Cl bond has approximately 18% ionic character (0.1811 × 100), or 82% covalent character. Instead of writing HCl as

$$\overset{\delta+}{H} - \overset{\delta-}{Cl}$$

we can therefore indicate the charge separation quantitatively as

$$\overset{0.18\delta+}{H} - \overset{0.18\delta-}{Cl}$$

Our calculated results are in agreement with the electronegativity difference between hydrogen and chlorine ($\chi_H = 2.20$ and $\chi_{Cl} = 3.16$) so

$$\chi_{Cl} - \chi_H = 0.96 \tag{2.5.1.3}$$

This is a value well within the range for polar covalent bonds. We indicate the dipole moment by writing an arrow above the molecule.Mathematically, dipole moments are vectors, and they possess both a magnitude and a direction. The dipole moment of a molecule is the vector sum of the dipoles of the individual bonds. In HCl, for example, the dipole moment is indicated as follows:



The arrow shows the direction of electron flow by pointing toward the more electronegative atom.

A warning about Dipole Moment arrows

As the figure above shows, we represent dipole moments by an arrow with a length proportional to μ and pointing from the positive charge to the negative charge. However, the **opposite** convention is still widely used especially among physicists.

The charge on the atoms of many substances in the gas phase can be calculated using measured dipole moments and bond distances. Figure 2.5.1.2 shows a plot of the percent ionic character versus the difference in electronegativity of the bonded atoms for several substances. According to the graph, the bonding in species such as $NaCl_{(g)}$ and $CsF_{(g)}$ is substantially less than 100% ionic in character. As the gas condenses into a solid, however, dipole–dipole interactions between polarized species increase the charge separations. In the crystal, therefore, an electron is transferred from the metal to the nonmetal, and these substances behave like classic ionic compounds. The data in Figure 2.5.1.2 show that diatomic species with an electronegativity difference of less than 1.5 are less than 50% ionic in character, which is consistent with our earlier description of these species as containing polar covalent bonds. The use of dipole moments to determine the ionic character of a polar bond is illustrated in Example 2.5.1.1.

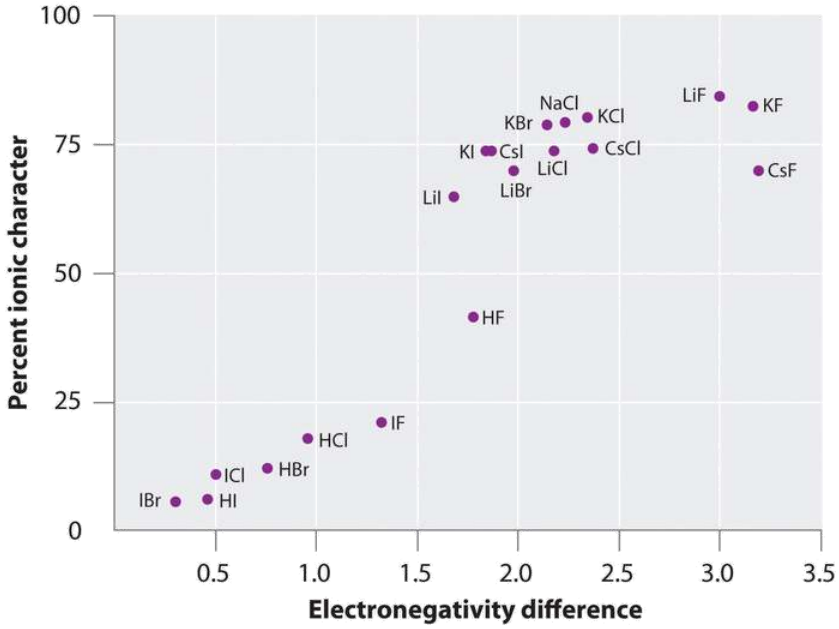


Figure 2.5.1.2: A Plot of the Percent Ionic Character of a Bond as Determined from Measured Dipole Moments versus the Difference in Electronegativity of the Bonded Atoms. In the gas phase, even CsF, which has the largest possible difference in electronegativity between atoms, is not 100% ionic. Solid CsF, however, is best viewed as 100% ionic because of the additional electrostatic interactions in the lattice.

Example 2.5.1.1: percent ionic character

In the gas phase, NaCl has a dipole moment of 9.001 D and an Na–Cl distance of 236.1 pm. Calculate the percent ionic character in NaCl.

Given: chemical species, dipole moment, and internuclear distance

Asked for: percent ionic character

Strategy:

A. Compute the charge on each atom using the information given and Equation 2.5.1.1

B. Find the percent ionic character from the ratio of the actual charge to the charge of a single electron.

Solution:

A The charge on each atom is given by

$$\begin{aligned} Q &= \frac{\mu}{r} \\ &= 9.001 \cancel{D} \left(\frac{3.3356 \times 10^{-30}\ C \cdot \cancel{m}}{1\ \cancel{D}} \right) \left(\frac{1}{236.1\ \cancel{pm}} \right) \left(\frac{1\ \cancel{pm}}{10^{-12}\ \cancel{m}} \right) \\ &= 1.272 \times 10^{-19}\ C \end{aligned}$$

Thus NaCl behaves as if it had charges of 1.272×10^{-19} C on each atom separated by 236.1 pm.

B The percent ionic character is given by the ratio of the actual charge to the charge of a single electron (the charge expected for the complete transfer of one electron):

$$\begin{aligned} \text{ionic character} &= \left(\frac{1.272 \times 10^{-19}\ \cancel{C}}{1.6022 \times 10^{-19}\ \cancel{C}} \right) (100) \\ &= 79.39\% \simeq 79\% \end{aligned}$$

Exercise 2.5.1.1

In the gas phase, silver chloride (AgCl) has a dipole moment of 6.08 D and an Ag–Cl distance of 228.1 pm. What is the percent ionic character in silver chloride?

Answer

55.5%

Summary

Bond polarity and ionic character increase with an increasing difference in electronegativity.

$$\mu = Qr$$

Compounds with **polar covalent bonds** have electrons that are shared unequally between the bonded atoms. The polarity of such a bond is determined largely by the relative electronegativites of the bonded atoms. The asymmetrical charge distribution in a polar substance produces a **dipole moment**, which is the product of the partial charges on the bonded atoms and the distance between them.

Contributors and Attributions

- Modified by Joshua Halpern (Howard University)

2.5.1: Molecular Shape and Molecular Polarity is shared under a CC BY-NC-SA 4.0 license and was authored, remixed, and/or curated by LibreTexts.

2.5.2: Prelude to Molecular Orbital Theory

Valence bond (VB) theory gave us a qualitative picture of chemical bonding, which was useful for predicting the shapes of molecules, bond strengths, etc. It fails to describe some bonding situations accurately because it ignores the wave nature of the electrons. Molecular orbital (MO) theory has the potential to be more quantitative. With it we can also get a picture of where the electrons are in the molecule, as shown in the image at the right. This can help us understand patterns of bonding and reactivity that are otherwise difficult to explain.

Although MO theory in principle gives us a way to calculate the energies and wavefunctions of electrons in molecules very precisely, usually we settle for simplified models. These models do not give very accurate orbital and bond energies, but they do explain concepts such as resonance (e.g., in the ferrocene, $C_{10}H_{10}Fe$, molecule) that are hard to represent otherwise. We can get more accurate energies from MO theory using computational methods. While MO theory is more correct than VB theory and can be very accurate in predicting the properties of molecules, it is also rather complicated even for fairly simple molecules. For example, you should be able to draw the VB pictures for CO, NH_3, and benzene, but we will find that these are increasingly challenging with MO theory.

2.5.2: Prelude to Molecular Orbital Theory is shared under a not declared license and was authored, remixed, and/or curated by LibreTexts.

- **2.1: Prelude to Molecular Orbital Theory** by Chemistry 310 is licensed CC BY-SA 4.0. Original source: https://en.wikibooks.org/wiki/Introduction_to_Inorganic_Chemistry.

2.5.3: Constructing Molecular Orbitals from Atomic Orbitals

Molecular orbital theory involves solving (approximately) the Schrödinger equation for the electrons in a molecule. To review from Chapter 1, this is a differential equation in which the first and second terms on the right represent the kinetic and potential energies:

$$E\psi = -\frac{\hbar^2}{2\mu}\nabla^2\psi + V\psi \tag{2.5.3.1}$$

While the Schrödinger equation can be solved analytically for the hydrogen atom, the potential energy function V becomes more complicated - and the equation can then only be solved numerically - when there are many (mutually repulsive) electrons in a molecule. So as a first approximation we will assume that the s, p, d, f, etc. orbitals of the atoms that make up the molecule are good solutions to the Schrödinger equation. We can then allow these wavefunctions to interfere constructively and destructively as we bring the atoms together to make bonds. In this way, we use the atomic orbitals (AO) as our basis for constructing MO's.

LCAO-MO = **linear combination of atomic orbitals.** In physics, this is called this the tight binding approximation.

We have actually seen linear combinations of atomic orbitals before when we constructed hybrid orbitals. The basic rules we developed for hybridization also apply here: orbitals are added with scalar coefficients (c) in such a way that the resulting orbitals are **orthogonal** and **normalized**. The difference is that in the MO case, the atomic orbitals come from different atoms.

The linear combination of atomic orbitals always gives back the *same number of molecular orbitals.* So if we start with two atomic orbitals (e.g., an s and a p_z orbital as shown in Fig. **2.5.3.1**), we end up with two molecular orbitals. When atomic orbitals add in phase, we get constructive interference and a lower energy orbital. When they add out of phase, we get a node and the resulting orbital has higher energy. The lower energy MOs are *bonding* and higher energy MOs are *antibonding.* Note that the antibonding orbital is raised in energy **MORE** than the bonding orbital is lowered in energy. A mnemonic for remembering this is ABIMABTBIB (a-BIM-ab-ta-bib) which stands for AntiBonding Is More AntiBonding Than Bonding Is Bonding.

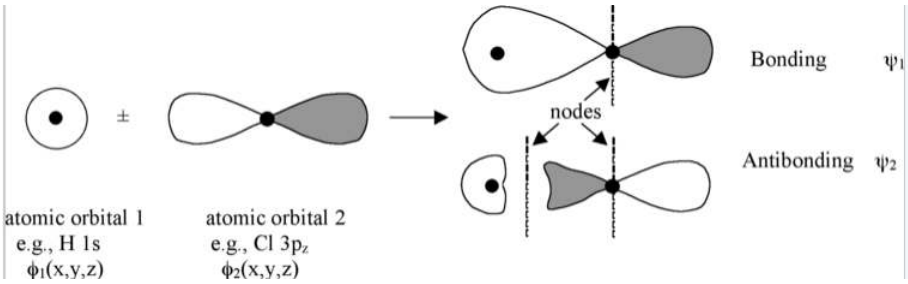


Figure* 2.5.3.1*: Sigma bonding and antibonding combinations of an s and p orbital

Molecular orbitals are also called **wavefunctions** (ψ), because they are solutions to the Schrödinger equation for the molecule. The atomic orbitals (also called basis functions) are labeled as φ's, for example, φ_{1s} and φ_{3pz} or simply as $\varphi_1$and φ_2.

In principle, we need to solve the Schrödinger equation for all the orbitals in a molecule, and then fill them up with pairs of electrons as we do for the orbitals in atoms. In practice we are really interested only in the MOs that derive from the valence orbitals of the constituent atoms, because these are the orbitals that are involved in bonding. We are especially interested in the **frontier orbitals**, i.e., the highest occupied molecular orbital (the **HOMO**) and the lowest unoccupied molecular orbital (the **LUMO**). Filled orbitals that are much lower in energy (i.e., core orbitals) do not contribute to bonding, and empty orbitals at higher energy likewise do not contribute. Those orbitals are however important in photochemistry and spectroscopy, which involve electronic transitions from occupied to empty orbitals.

As an example of the LCAO-MO approach we can construct two MO's (ψ_1 and ψ_2) of the HCl molecule from two AO's $\varphi_1$and φ_2 (Fig. 2.1.1). To make these two linear combinations, we write:

$$\Psi_1 = c_1\varphi_1 + c_2\varphi_2 \tag{2.5.3.2}$$

and

$$\Psi_2 = c_1\varphi_1 - c_2\varphi_2 \tag{2.5.3.3}$$

The coefficients c_1 and c_2 will be equal (or nearly so) when the two AOs from which they are constructed are the same, e.g., when two hydrogen 1s orbitals combine to make bonding and antibonding MOs in H_2. They will be unequal when there is an energy difference between the AOs, for example when a hydrogen 1s orbital and a chlorine 3p orbital combine to make a polar H-Cl bond.

Nodes:

The wavefunctions φ and ψ are **amplitudes** that are related to the probability of finding the electron at some point in space. They have lobes with (+) or (-) signs, which we indicate by shading or color. Wherever the wavefunction changes sign we have a node. As you can see in Fig. **2.5.3.1**, nodes in MOs result from destructive interference of (+) and (-) wavefunctions. Generally, the more nodes, the higher the energy of the orbital.

In the example above we have drawn a simplified picture of the Cl $3p_z$ orbital and the resulting MOs, leaving out the radial node. Recall that 2p orbitals have no radial nodes, 3p orbitals have one, as illustrated in Fig. **2.5.3.3**. 4p orbitals have two radial nodes, and so on. The MOs we make by combining the AOs have these nodes too.



Figure* 2.5.3.3*: Nodal structure of 2p and 3p orbitals

Normalization:

We square the wave functions to get probabilities, which are always positve or zero. So if an electron is in orbital φ_1, the probability of finding it at point xyz is the square[1] of $\varphi_1(x,y,z)$. The total probability does not change when we combine AOs to make MOs, so for the simple case of combining φ_1 and φ_2 to make $\psi_1$and ψ_2,

$$\Psi_1^2 + \Psi_2^2 = \varphi_1^2 + \varphi_2^2 \tag{2.5.3.4}$$

Overlap integral:

The spatial overlap between two atomic orbitals φ_1 and φ_2 is described by the overlap integral S,

$$S_{12} = \int \varphi_1 * \varphi_2 d\tau \tag{2.5.3.5}$$

where the integration is over all space $d\tau = dxdydz$.

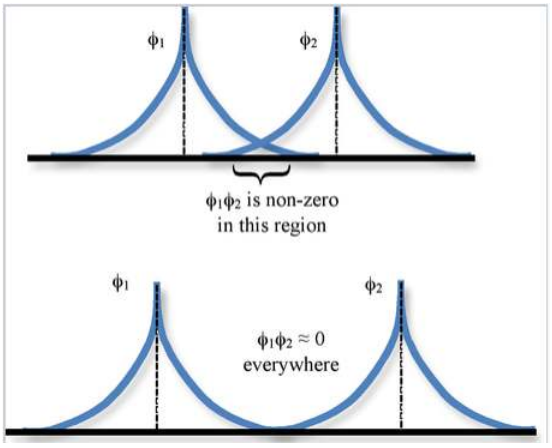


Figure* 2.5.3.4*: The wavefunctions of atomic orbitals decrease exponentially with distance. Orbital overlap is non-zero when two atoms are close together, as illustrated for 1s orbitals in the upper figure. The lower figure shows orbitals that are too far away to interact. In this case both S and β are close to zero.

Energies of bonding and antibonding MOs:

The energies of bonding and antibonding orbitals depend strongly on the distance between atoms. This is illustrated in Fig. 2.1.5 for the hydrogen molecule, H_2. At very long distances, there is essentially no difference in energy between the in-phase and out-of-

phase combinations of H 1s orbitals. As they get closer, the in-phase (bonding) combination drops in energy because electrons are shared between the two positively charged nuclei. The energy reaches a minimum at the equilibrium bond distance (0.74 Å) and then rises again as the nuclei get closer together. The antibonding combination has a node between the nuclei so its energy rises continuously as the atoms are brought together.

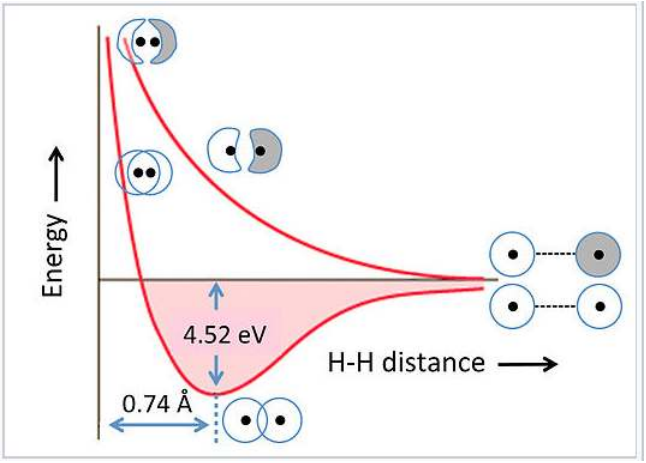


Figure* 2.5.3.5*: Energy as a function of distance for the bonding and antibonding orbitals of the H_2 molecule

At the equilibrium bond distance, the energies of the bonding and antibonding molecular orbitals (ψ_1, ψ_2) are lower and higher, respectively, than the energies of the atomic basis orbitals φ_1 and φ_2. This is shown in Fig. **2.5.3.6** for the MO's of the H_2 molecule.

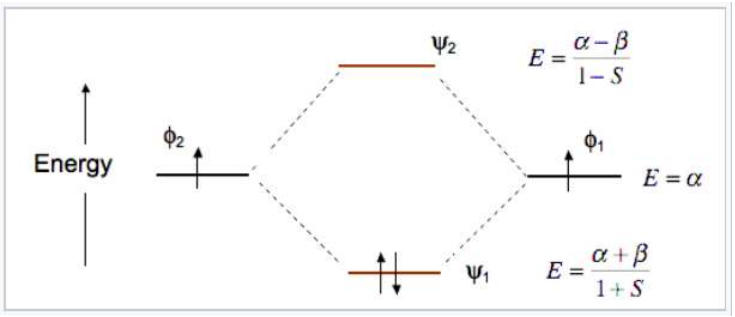


Figure* 2.5.3.6*: Molecular orbital energy diagram for the H_2 molecule

The energy of an electron in one of the atomic orbitals is α, the **Coulomb integral**.

$$\alpha = \int \varphi_1 H \varphi_1 d\tau \tag{2.5.3.6}$$

where **H** is the **Hamiltonian operator**. Essentially, α represents the *ionization energy* of an electron in atomic orbital φ_1 or φ_2.

The energy difference between an electron in the AO's and the MO's is determined by the **exchange integral β**,

$$\beta = \int \varphi_1 H \varphi_2 d\tau \tag{2.5.3.7}$$

β is an important quantity, because it tells us about the bonding energy of the molecule, and also the difference in energy between bonding and antibonding orbitals. Calculating β is not straightforward for multi-electron molecules because we cannot solve the Schrödinger equation analytically for the wavefunctions. We can however make some approximations to calculate the energies and wavefunctions numerically. In the Hückel approximation, which can be used to obtain approximate solutions for π molecular orbitals in organic molecules, we simplify the math by taking S=0 and setting H=0 for any p-orbitals that are not adjacent to each other. The extended Hückel method,[2] developed by Roald Hoffmann, and other semi-empirical methods can be used to rapidly obtain relative orbital energies, approximate wavefunctions, and degeneracies of molecular orbitals for a wide variety of molecules and extended solids. More sophisticated ab initio methods are now readily available in software packages and can be used to compute accurate orbital energies for molecules and solids.

We can get the coefficients c_1 and c_2 for the hydrogen molecule by applying the normalization criterion:

$$\Phi_1 = (\varphi_1 + \varphi_2)/(\sqrt{2(1+S)})(\text{bonding orbital}) \tag{2.5.3.8}$$

and

$$\Phi_2 = (\varphi_1 - \varphi_2)/(\sqrt{2(1-S)})(\text{antibonding orbital}) \tag{2.5.3.9}$$

In the case where S≈0, we can eliminate the 1-S terms and both coefficients become 1/√2

Note that the bonding orbital in the MO diagram of H_2 is stabilized by an energy β/1+S and the antibonding orbital is destabilized by β/1-S. That is, the antibonding orbital goes up in energy more than the bonding orbital goes down. This means that H_2 ($\psi_1^2\psi_2^0$) is energetically more stable than two H atoms, but He_2 with four electrons ($\psi_1^2\psi_2^2$) is *unstable* relative to two He atoms.

Bond order: In any MO diagram, the bond order can be calculated as ½ (# of bonding electrons - # of antibonding electrons). For H_2 the bond order is 1, and for $He_2$the bond order is zero.

Heteronuclear case (e.g., HCl) - Polar bonds

Here we introduce an electronegativity difference between the two atoms making the chemical bond. The energy of an electron in the H 1s orbital is higher (it is easier to ionize) than the electron in the chlorine $3p_z$ orbital. This results in a larger energy difference between the resulting molecular orbitals ψ_1 and ψ_2, as shown in Fig. **2.5.3.7**. The bigger the electronegativity difference between atomic orbitals (the larger Δα is) the more "φ_2 character" the bonding orbital has, i.e., the more it resembles the Cl $3p_z$ orbital in this case. This is consistent with the idea that H-Cl has a polar single bond: the two electrons reside in a bonding molecular orbital that is primarily localized on the Cl atom.

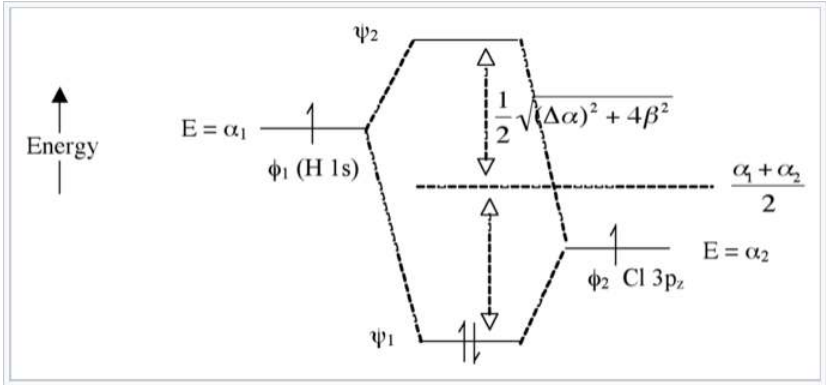


Figure* 2.5.3.7*: Molecular orbital energy diagram for the HCl molecule

The antibonding orbital (empty) has more H-character. The bond order is again 1 because there are two electrons in the bonding orbital and none in the antibonding orbital.

Extreme case - Ionic bonding (NaF): very large Δα

In this case, there is not much mixing between the AO's because their energies are far apart (Fig. **2.5.3.8**). The two bonding electrons are localized on the F atom , so we can write the molecule as Na^+F^-. Note that if we were to excite an electron from ψ_1 to ψ_2 using light, the resulting electronic configuration would be ($\psi_1^1\psi_2^1$) and we would have Na^0F^0. This is called a charge transfer transition.

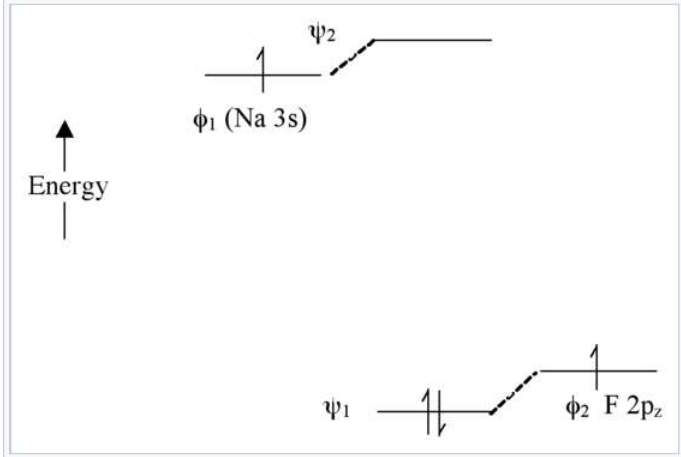


Figure* 2.5.3.8*: Molecular orbital energy diagram illustrating ionic bonding in the NaF molecule

Summary of molecular orbital theory so far:

• **Add and subtract** AO wavefunctions to make MOs. Two AOs → two MOs. More generally, the *total number of MOs equals the number of AO basis orbitals*.

• We showed the simplest case (only two basis orbitals). More accurate calculations use a much larger basis set (more AOs) and solve for the matrix of c's that gives the lowest total energy, using mathematically friendly approximations of the potential energy function that is part of the Hamiltonian operator H.

• **More nodes → higher energy** MO

• **Bond order** = ½ (# of bonding electrons - # of antibonding electrons)

• **Bond polarity** emerges in the MO picture as orbital "character."

• AOs that are **far apart in energy** do not interact much when they combine to make MOs.

2.5.3: Constructing Molecular Orbitals from Atomic Orbitals is shared under a CC BY-SA license and was authored, remixed, and/or curated by LibreTexts.

- **2.2: Constructing Molecular Orbitals from Atomic Orbitals** by Chemistry 310 is licensed CC BY-SA 4.0. Original source: https://en.wikibooks.org/wiki/Introduction_to_Inorganic_Chemistry.

2.5.4: Orbital Symmetry

The MO picture for a molecule gets complicated when many valence AOs are involved. We can simplify the problem enormously by noting (without proof here) that orbitals of different symmetry with respect to the molecule do not interact. The symmetry operations of a molecule (which can include rotations, mirror planes, inversion centers, etc.), and the symmetry classes of bonds and orbitals in molecules, can be rigorously defined according to **group theory**. Here we will take a simple approach to this problem based on our intuitive understanding of the symmetry of three-dimensional objects as illustrated in Fig. **2.5.4.1**.



Figure* 2.5.4.1*: Example of σ symmetry.

AO's must have the same **nodal symmetry** (as defined by the molecular symmetry operations), or their overlap is zero.

For example, in the HCl molecule, there is a unique symmetry axis →, which is typically defined as the Cartesian z-axis, as shown in Fig. **2.5.4.2**.

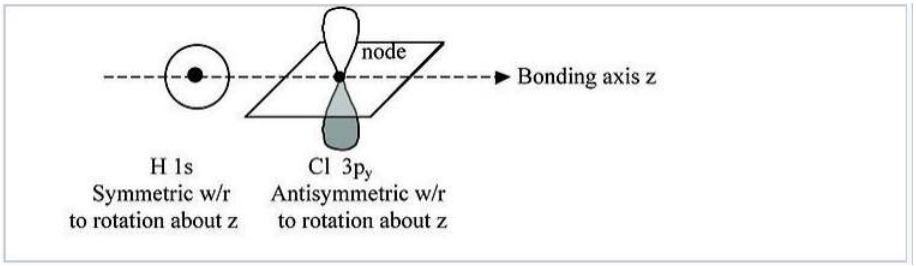


Figure* 2.5.4.2*: Orbitals of σ and π symmetry do not interact.

We can see from this figure that the H 1s orbital is unchanged by a 180° rotation about the bond axis. However, the same rotation inverts the sign of the Cl 3$p_y$wavefunction. Because these two orbitals have different symmetries, the Cl 3p_y orbital is **nonbonding** and doesn't interact with the H 1s. The same is true of the Cl 3$p_x$orbital. The p_x and p_y orbitals have π symmetry (nodal plane containing the bonding axis) and are labeled π_{nb} in the MO energy level diagram, Fig. **2.5.4.3**. In contrast, the H 1s and Cl 3p_z orbitals both have σ symmetry, which is also the symmetry of the clay pot shown in Fig. **2.5.4.1**. Because these orbitals have the same symmetry (in the point group of the molecule), they can make the bonding and antibonding combinations shown in Fig. **2.1.1**.

The MO diagram of HCl that includes all the valence orbitals of the Cl atom is shown in Fig. **2.5.4.3**. Two of the Cl valence orbitals (3p_x and 3p_y) have the wrong symmetry to interact with the H 1s orbital. The Cl 3s orbital has the same (σ) symmetry as H 1s, but it is much lower in energy so there is little orbital interaction. The energy of the Cl 3s orbital is thus affected only slightly by forming the molecule. The pairs of electrons in the π_{nb} and σ_{nb} orbitals are therefore **non-bonding**.

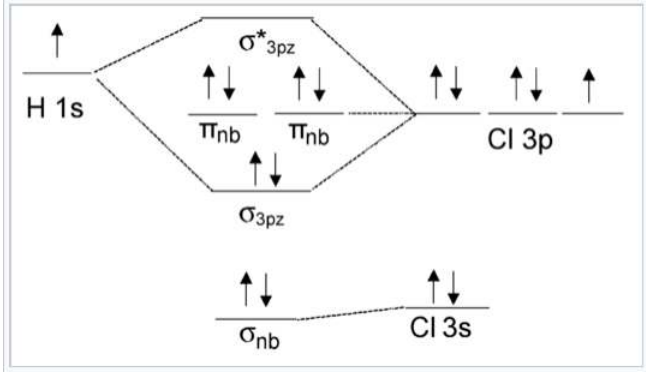


***Figure* 2.5.4.3:** Energy level diagram of the HCl molecule showing MOs derived from the valence AOs.

Note that the MO result in Fig. **2.5.4.3** (1 bond and three pairs of nonbonding electrons) is the same as we would get from valence bond theory for HCl. The nonbonding orbitals are localized on the Cl atom, just as we would surmise from the valence bond picture.

In order to differentiate it from the σ bonding orbital, the σ antibonding orbital, which is empty in this case, is designated with an asterisk.

2.5.4: Orbital Symmetry is shared under a CC BY-SA license and was authored, remixed, and/or curated by LibreTexts.

- **2.3: Orbital Symmetry** by Chemistry 310 is licensed CC BY-SA 4.0. Original source: https://en.wikibooks.org/wiki/Introduction_to_Inorganic_Chemistry.

2.5.5: Molecular Orbital Diagrams

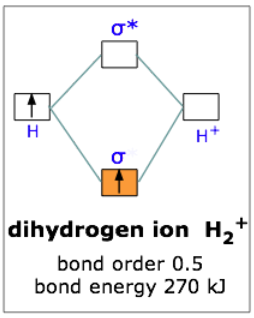
Learning Objectives

Make sure you thoroughly understand the following essential ideas

- Describe the essential difference between a *sigma* and a *pi* molecular orbital.
- Define *bond order*, and state its significance.
- Construct a "molecular orbital diagram" of the kind shown in this lesson for a simple diatomic molecule, and indicate whether the molecule or its positive and negative ions should be stable.

Molecular Orbital Diagrams

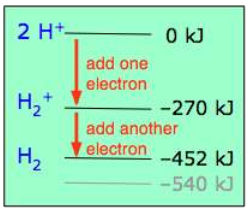
This scheme of bonding and antibonding orbitals is usually depicted by a molecular orbital diagram such as the one shown here for the **dihydrogen ion H_2^+**. Atomic valence electrons (shown in boxes on the left and right) fill the lower-energy molecular orbitals before the higher ones, just as is the case for atomic orbitals. Thus, the single electron in this simplest of all molecules goes into the bonding orbital, leaving the antibonding orbital empty.



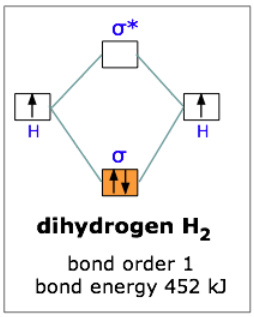
Since any orbital can hold a maximum of two electrons, the bonding orbital in $H_2^+$is only half-full. This single electron is nevertheless enough to lower the potential energy of one mole of hydrogen nuclei pairs by 270 kJ— quite enough to make them stick together and behave like a distinct molecular species. Although H_2^+ is stable in this energetic sense, it happens to be an extremely reactive molecule— so much so that it even reacts with itself, so these ions are not commonly encountered in everyday chemistry.

Dihydrogen

If one electron in the bonding orbital is conducive to bond formation, might two electrons be even better? We can arrange this by combining two hydrogen atoms-- two nuclei, and two electrons. Both electrons will enter the bonding orbital, as depicted in the Figure.



We recall that one electron lowered the potential energy of the two nuclei by 270 kJ/mole, so we might expect two electrons to produce twice this much stabilization, or 540 kJ/mole.

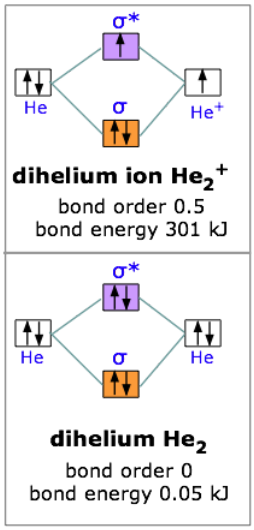


Bond order is defined as the difference between the number of electron pairs occupying bonding and nonbonding orbitals in the molecule. A bond order of unity corresponds to a conventional "single bond".

Experimentally, one finds that it takes only 452 kJ to break apart a mole of hydrogen molecules. The reason the potential energy was not lowered by the full amount is that the presence of two electrons in the same orbital gives rise to a repulsion that acts against the stabilization. This is exactly the same effect we saw in comparing the ionization energies of the hydrogen and helium atoms.

Dihelium

With two electrons we are still ahead, so let's try for three. The dihelium positive ion is a three-electron molecule. We can think of it as containing two helium nuclei and three electrons. This molecule is stable, but not as stable as dihydrogen; the energy required to break He_2^+ is 301 kJ/mole. The reason for this should be obvious; two electrons were accommodated in the bonding orbital, but the third electron must go into the next higher slot— which turns out to be the sigma antibonding orbital. The presence of an electron in this orbital, as we have seen, gives rise to a repulsive component which acts against, and partially cancels out, the attractive effect of the filled bonding orbital.



Taking our building-up process one step further, we can look at the possibilities of combining to helium atoms to form dihelium. You should now be able to predict that He_2 cannot be a stable molecule; the reason, of course, is that we now have four electrons—two in the bonding orbital, and two in the antibonding orbital. The one orbital almost exactly cancels out the effect of the other. Experimentally, the bond energy of dihelium is only .084 kJ/mol; this is not enough to hold the two atoms together in the presence of random thermal motion at ordinary temperatures, so dihelium dissociates as quickly as it is formed, and is therefore not a distinct chemical species.

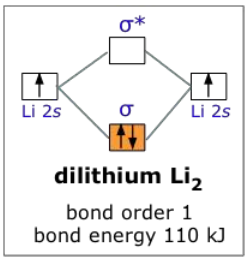
Diatomic molecules containing second-row atoms

The four simplest molecules we have examined so far involve molecular orbitals that derived from two 1*s* atomic orbitals. If we wish to extend our model to larger atoms, we will have to contend with higher atomic orbitals as well. One greatly simplifying

principle here is that only the *valence-shell* orbitals need to be considered. Inner atomic orbitals such as 1*s* are deep within the atom and well-shielded from the electric field of a neighboring nucleus, so that these orbitals largely retain their atomic character when bonds are formed.

Dilithium

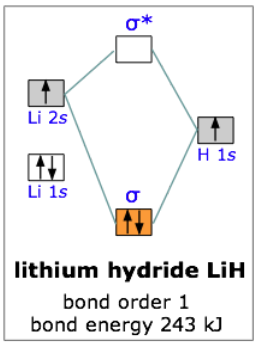
For example, when lithium, whose configuration is $1s^2 2s^1$, bonds with itself to form Li_2, we can forget about the 1*s* atomic orbitals and consider only the σ bonding and antibonding orbitals. Since there are not enough electrons to populate the antibonding orbital, the attractive forces win out and we have a stable molecule.



The bond energy of dilithium is 110 kJ/mole; notice that this value is less than half of the 270 kJ bond energy in dihydrogen, which also has two electrons in a bonding orbital. The reason, of course, is that the 2*s* orbital of Li is much farther from its nucleus than is the 1*s* orbital of H, and this is equally true for the corresponding molecular orbitals. It is a general rule, then, that the larger the parent atom, the less stable will be the corresponding diatomic molecule.

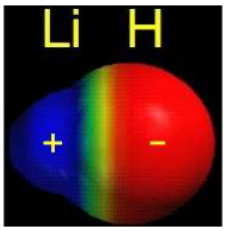
Lithium hydride

All the molecules we have considered thus far are *homonuclear*; they are made up of one kind of atom. As an example of a *heteronuclear* molecule, let's take a look at a very simple example— lithium hydride. Lithium hydride is a stable, though highly reactive molecule. The diagram shows how the molecular orbitals in lithium hydride can be related to the atomic orbitals of the parent atoms. One thing that makes this diagram look different from the ones we have seen previously is that the parent atomic orbitals have widely differing energies; the greater nuclear charge of lithium reduces the energy of its 1*s* orbital to a value well below that of the 1*s* hydrogen orbital.



There are two occupied atomic orbitals on the lithium atom, and only one on the hydrogen. With which of the lithium orbitals does the hydrogen 1*s* orbital interact? The lithium 1*s* orbital is the lowest-energy orbital on the diagram. Because this orbital is so small and retains its electrons so tightly, it does not contribute to bonding; we need consider only the 2*s* orbital of lithium which combines with the 1*s* orbital of hydrogen to form the usual pair of sigma bonding and antibonding orbitals. Of the four electrons in lithium and hydrogen, two are retained in the lithium 1*s* orbital, and the two remaining ones reside in the σ orbital that constitutes the Li–H covalent bond.

The resulting molecule is 243 kJ/mole more stable than the parent atoms. As we might expect, the bond energy of the heteronuclear molecule is very close to the average of the energies of the corresponding homonuclear molecules. Actually, it turns out that the correct way to make this comparison is to take the geometric mean, rather than the arithmetic mean, of the two bond energies. The geometric mean is simply the square root of the product of the two energies.



The geometric mean of the H_2 and Li_2 bond energies is 213 kJ/mole, so it appears that the lithium hydride molecule is 30 kJ/mole more stable than it "is supposed" to be. This is attributed to the fact that the electrons in the 2σ bonding orbital are not equally shared between the two nuclei; the orbital is skewed slightly so that the electrons are attracted somewhat more to the hydrogen atom. This *bond polarity*, which we considered in some detail near the beginning of our study of covalent bonding, arises from the greater electron-attracting power of hydrogen— a consequence of the very small size of this atom. The electrons can be at a lower potential energy if they are slightly closer to the hydrogen end of the lithium hydride molecule. It is worth pointing out, however, that the electrons are, on the average, also closer to the lithium nucleus, compared to where they would be in the 2*s* orbital of the isolated lithium atom. So it appears that everyone gains and no one loses here!

Contributors and Attributions

- Stephen Lower, Professor Emeritus (Simon Fraser U.) Chem1 Virtual Textbook

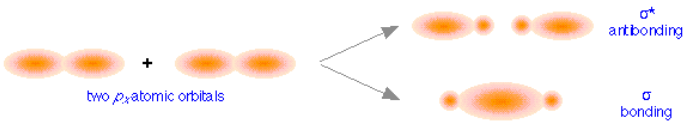
This page titled 2.5.5: Molecular Orbital Diagrams is shared under a CC BY-SA license and was authored, remixed, and/or curated by Stephen Lower via source content that was edited to the style and standards of the LibreTexts platform.

2.5.6: π Orbitals and Diatomic Molecules

π orbitals

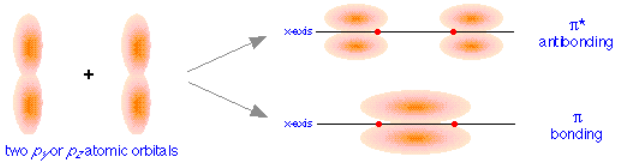
The molecules we have considered thus far are composed of atoms that have no more than four electrons each; our molecular orbitals have therefore been derived from *s*-type atomic orbitals only. If we wish to apply our model to molecules involving larger atoms, we must take a close look at the way in which *p*-type orbitals interact as well. Although two atomic *p* orbitals will be expected to split into bonding and antibonding orbitals just as before, it turns out that the extent of this splitting, and thus the relative energies of the resulting molecular orbitals, depend very much on the nature of the particular *p* orbital that is involved.

You will recall that there are three possible *p* orbitals for any value of the principal quantum number. You should also recall that *p* orbitals are not spherical like *s* orbitals, but are elongated, and thus possess definite directional properties. The three *p* orbitals correspond to the three directions of Cartesian space, and are frequently designated p_x, p_y, and p_z, to indicate the axis along which the orbital is aligned. Of course, in the free atom, where no coordinate system is defined, all directions are equivalent, and so are the *p* orbitals. But when the atom is near another atom, the electric field due to that other atom acts as a point of reference that defines a set of directions. The line of centers between the two nuclei is conventionally taken as the *x* axis. If this direction is represented horizontally on a sheet of paper, then the *y* axis is in the vertical direction and the *z* axis would be normal to the page.



These directional differences lead to the formation of two different classes of molecular orbitals. The above figure shows how two p_x atomic orbitals interact. In many ways the resulting molecular orbitals are similar to what we got when *s* atomic orbitals combined; the bonding orbital has a large electron density in the region between the two nuclei, and thus corresponds to the lower potential energy. In the out-of-phase combination, most of the electron density is away from the internuclear region, and as before, there is a surface exactly halfway between the nuclei that corresponds to zero electron density. This is clearly an *antibonding orbital*— again, in general shape, very much like the kind we saw in hydrogen and similar molecules. Like the ones derived from *s*-atomic orbitals, these molecular orbitals are σ (*sigma*) orbitals.

Sigma orbitals are cylindrically symmetric with respect to the line of centers of the nuclei; this means that if you could look down this line of centers, the electron density would be the same in all directions.



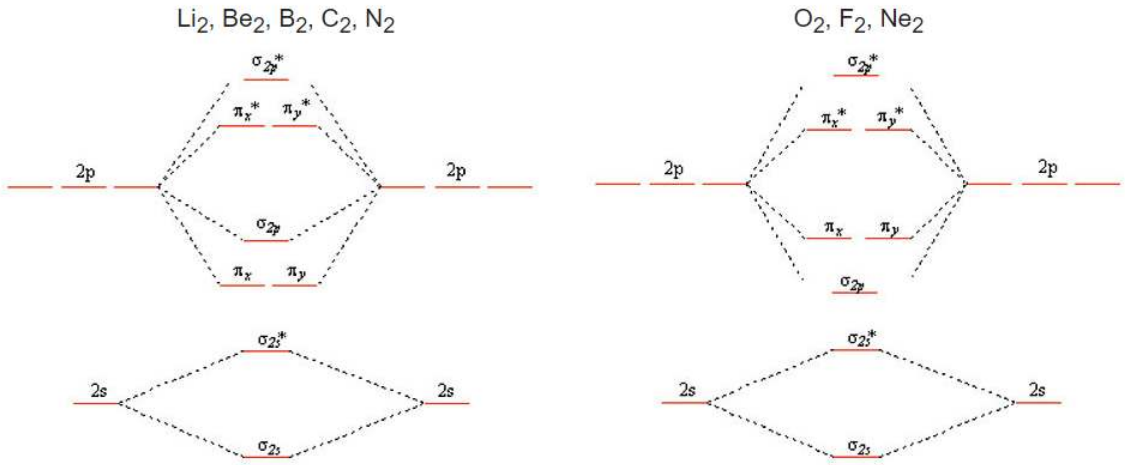
orbitals, we get the bonding and antibonding pairs that we would expect, but the resulting molecular orbitals have a different symmetry: rather than being rotationally symmetric about the line of centers, these orbitals extend in both perpendicular directions from this line of centers. Orbitals having this more complicated symmetry are called π (*pi*) orbitals. There are two of them, π_y and π_z differing only in orientation, but otherwise completely equivalent.

The different geometric properties of the π and σ orbitals causes the latter orbitals to split more than the π orbitals, so that the σ* antibonding orbital always has the highest energy. The σ bonding orbital can be either higher or lower than the π bonding orbitals, depending on the particular atom.

Second-Row Diatomics

If we combine the splitting schemes for the 2*s* and 2*p* orbitals, we can predict bond order in all of the diatomic molecules and ions composed of elements in the first complete row of the periodic table. Remember that only the *valence orbitals* of the atoms need be considered; as we saw in the cases of lithium hydride and dilithium, the inner orbitals remain tightly bound and retain their localized atomic character.

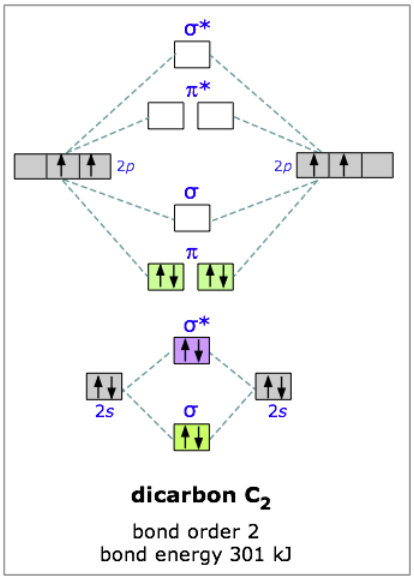
Valence bond theory fails for a number of the second row diatomics, most famously for O_2, where it predicts a diamagnetic (no unpaired electrons), doubly bonded molecule with four lone pairs. O_2 does have a double bond, but it is paramagneric (having two unpaired electrons in the ground state), a property that can be explained by the MO picture. We can construct the MO energy level diagrams for these molecules as follows:



We get the simpler diatomic MO picture on the right when the 2s and 2p AOs are well separated in energy, as they are for O, F, and Ne. The picture on the left results from mixing of the σ_{2s} and σ_{2p} MO's, which are close in energy for Li_2, Be_2, B_2, C_2, and N_2. The effect of this mixing is to push the σ_{2s}* down in energy and the σ_{2p}up, to the point where the pπ orbitals are below the σ_{2p}. Asymmetric diatomic molecules and ions such as CO, NO, and NO^+ also have the ordering of energy levels shown on the left because of sp mixing. A good animation of the molecular orbitals in the CO molecule can be found on the University of Liverpool **Structure and Bonding** website.

Dicarbon

Carbon has four outer-shell electrons, two 2*s* and two 2*p*. For two carbon atoms, we therefore have a total of eight electrons, which can be accommodated in the first four molecular orbitals. The lowest two are the 2*s*-derived bonding and antibonding pair, so the "first" four electrons make no net contribution to bonding. The other four electrons go into the pair of *pi*bonding orbitals, and there are no more electrons for the antibonding orbitals— so we would expect the dicarbon molecule to be stable, and it is. (But being extremely reactive, it is known only in the gas phase.)

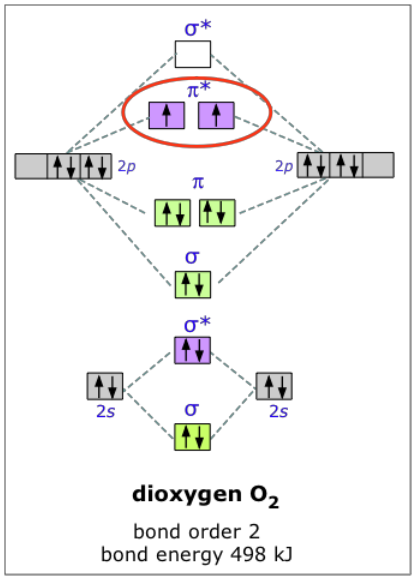


You will recall that one pair of electrons shared between two atoms constitutes a “single” chemical bond; this is Lewis’ original definition of the covalent bond. In C_2 there are two paris of electrons in the π bonding orbitals, so we have what amounts to a double bond here; in other words, the bond order in dicarbon is two.

Dioxygen

The electron configuration of oxygen is $1s^2 2s^2 2p^4$. In O_2, therefore, we need to accommodate twelve valence electrons (six from each oxygen atom) in molecular orbitals. As you can see from the diagram, this places two electrons in antibonding orbitals. Each of these electrons occupies a separate π* orbital because this leads to less electron-electron repulsion (Hund's Rule).

The bond energy of molecular oxygen is 498 kJ/mole. This is smaller than the 945 kJ bond energy of N_2— not surprising, considering that oxygen has two electrons in an antibonding orbital, compared to nitrogen’s one.



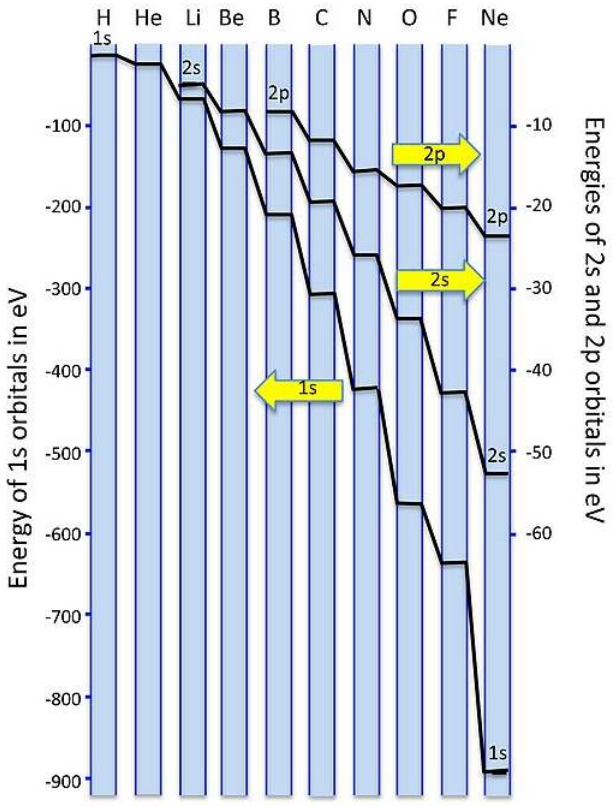
The two unpaired electrons of the dioxygen molecule give this substance an unusual and distinctive property: O_2 is *paramagnetic*. The paramagnetism of oxygen can readily be demonstrated by pouring liquid O_2 between the poles of a strong permanent magnet; the liquid stream is trapped by the field and fills up the space between the poles.

Since molecular oxygen contains two electrons in an antibonding orbital, it might be possible to make the molecule more stable by removing one of these electrons, thus increasing the ratio of bonding to antibonding electrons in the molecule. Just as we would expect, and in accord with our model, O_2^+ has a bond energy higher than that of neutral dioxygen; removing the one electron actually gives us a more stable molecule. This constitutes a very good test of our model of bonding and antibonding orbitals. In the same way, adding an electron to O_2 results in a weakening of the bond, as evidenced by the lower bond energy of O_2^-. The bond energy in this ion is not known, but the length of the bond is greater, and this is indicative of a lower bond energy. These two dioxygen ions, by the way, are highly reactive and can be observed only in the gas phase.

Why don't we get sp-orbital mixing for O_2 and F_2? The reason has to do with the energies of the orbitals, which are not drawn to scale in the simple picture above. As we move across the second row of the periodic table from Li to F, we are progressively adding protons to the nucleus. The 2s orbital, which has finite amplitude at the nucleus, "feels" the increased nuclear charge more than the 2p orbital. This means that as we progress across the periodic table (and also, as we will see later, when we move down the periodic table), the **energy difference between the s and p orbitals increases**. As the 2s and 2p energies become farther apart in energy, there is less interaction between the orbitals (i.e., less mixing).

A plot of orbital energies is shown below. Because of the very large energy difference between the 1s and 2s/2p orbitals, we plot them on different energy scales, with the 1s to the left and the 2s/2p to the right. For elements at the left side of the 2nd period (Li, Be, B) the 2s and 2p energies are only a few eV apart. The energy difference becomes very large - more than 20 electron volts - for O and F. Since single bond energies are typically about 3-4 eV, this energy difference would be very large on the scale of our MO

diagrams. For all the elements in the 2nd row of the periodic table, the 1s (core) orbitals are very low in energy compared to the 2s/2p (valence) orbitals, so we don't need to consider them in drawing our MO diagrams.



Contributors and Attributions

- Stephen Lower, Professor Emeritus (Simon Fraser U.) Chem1 Virtual Textbook

---

2.5.6: π Orbitals and Diatomic Molecules is shared under a CC BY-SA license and was authored, remixed, and/or curated by LibreTexts.

- **2.5: Diatomic Molecules** by Chemistry 310 is licensed CC BY-SA 4.0. Original source: https://en.wikibooks.org/wiki/Introduction_to_Inorganic_Chemistry.

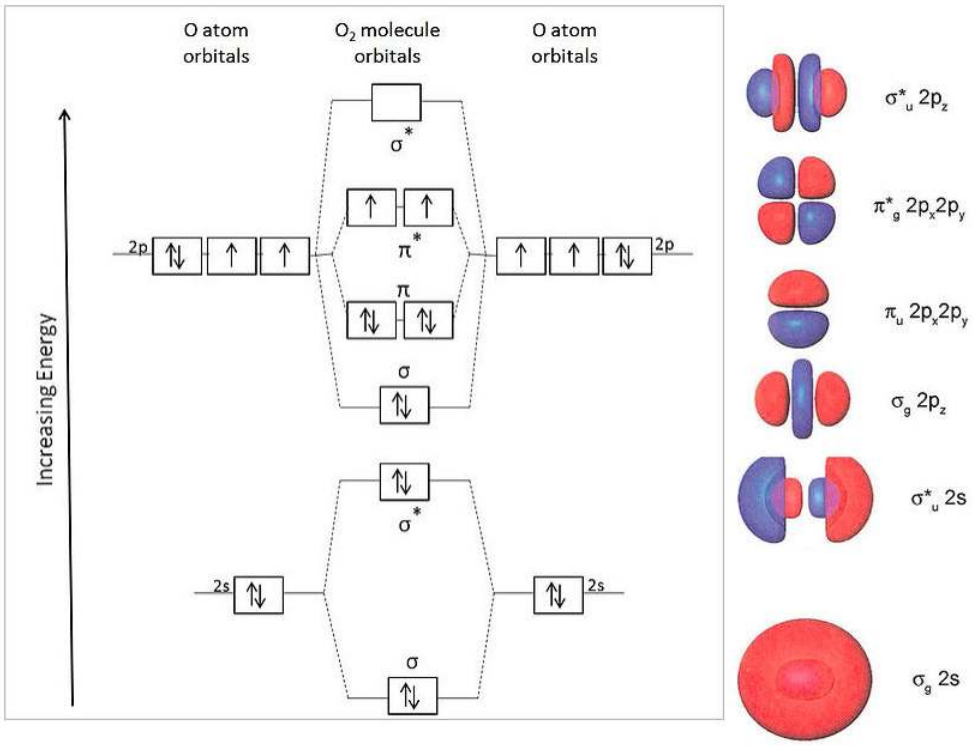
2.5.7: Orbital Filling

MO's are filled from the bottom according to the **Aufbau principle** and **Hund's rule**, as we learned for atomic orbitals.

Question: what is the quantum mechanical basis of Hund's rule?

> Consider the case of two degenerate orbitals, such as the π or π* orbitals in a second-row diatomic molecule. If these orbitals each contain one electron, their spins can be parallel (as preferred by Hund's rule) or antiparallel. The Pauli exclusion principle says that no two electrons in an orbital can have the same set of quantum numbers (n, l, m_l, m_s). That means that, in the parallel case, the Pauli principle prevents the electrons from ever visiting each other's orbitals. In the antiparallel case, they are free to come and go because they have different m_s quantum numbers. However, having two electrons in the same orbital is energetically unfavorable because like charges repel. Thus, the parallel arrangement, thanks to the Pauli principle, has lower energy.

For O_2 (12 valence electrons), we get the MO energy diagram below. The shapes of the molecular orbitals are shown at the right.



This energy ordering of MOs correctly predicts **two unpaired electrons** in the π* orbital and a net **bond order of two** (8 bonding electrons and 4 antibonding electrons). This is consistent with the experimentally observed paramagnetism of the oxygen molecule.

Other interesting predictions of the MO theory for second-row diatomics are that the C_2 molecule has a bond order of 2 and that the B_2 molecule has two unpaired electrons (both verified experimentally).

We can also predict (using the O_2, F_2, Ne_2 diagram above) that NO has a bond order of 2.5, and CO has a bond order of 3.

The symbols "g" and "u" in the orbital labels, which we only include in the case of centrosymmetric molecules, refer to their symmetry with respect to inversion. *Gerade* (g) orbitals are symmetric, meaning that inversion through the center leaves the orbital unchanged. *Ungerade* (u) means that the sign of the orbital is reversed by the inversion operation. Because g and u orbitals have different symmetries, they have zero overlap with each other. As we will see below, factoring orbitals according to g and u symmetry simplifies the task of constructing molecular orbitals in more complicated molecules, such as butadiene and benzene.

The orbital shapes shown above were computed using a *one-electron model* of the molecule, as we did for hydrogen-like AOs to get the shapes of s, p, and d-orbitals. To get accurate MO energies and diagrams for *multi-electron* molecules (i.e. all real

molecules), we must include the fact that electrons are “correlated,” i.e. that they avoid each other in molecules because of their negative charge. This problem cannot be solved analytically, and is solved approximately in numerical calculations by using density functional theory (DFT)

2.5.7: Orbital Filling is shared under a CC BY-SA license and was authored, remixed, and/or curated by LibreTexts.

- **2.6: Orbital Filling** by Chemistry 310 is licensed CC BY-SA 4.0. Original source: https://en.wikibooks.org/wiki/Introduction_to_Inorganic_Chemistry.

2.5.8: δ orbitals

Inorganic compounds use s, p, d and f orbitals to make bonding and antibonding combinations. These combinations result in **σ, π,** and **δ** bonds (and antibonds). The previous sections presented σ and π bonds. In inorganic chemistry, π bonds can be made from p- and/or d-orbitals. δ bonds are more rare and occur by face-to-face overlap of d-orbitals, as in the ion $Re_2Cl_8^{2-}$. The fact that the Cl atoms are eclipsed in this anion is evidence of δ bonding.

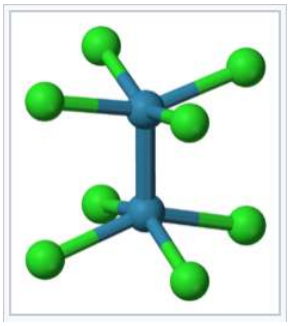
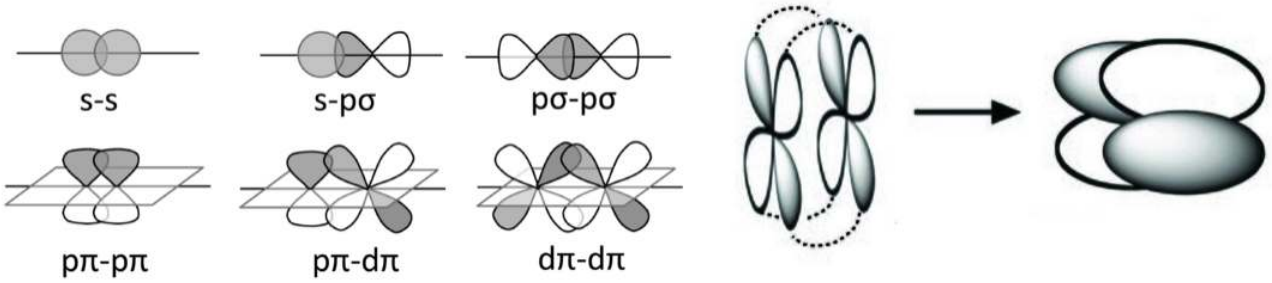


Figure* 2.5.8.1*: The octachlorodirhenate(III) anion, $[Re_2Cl_8]^{2-}$, which has a quadruple Re-Re bond.[3]

Some possible σ (top row), π (bottom row), and δ bonding combinations (right) of s, p, and d orbitals are sketched below. In each case, we can make bonding or antibonding combinations, depending on the signs of the AO wavefunctions. Because pπ-pπ bonding involves sideways overlap of p-orbitals, it is most commonly observed with second-row elements (C, N, O). π-bonded compounds of heavier elements are rare because the larger cores of the atoms prevent good π-overlap. For this reason, compounds containing C=C double bonds are very common, but those with Si=Si bonds are rare. This does not mean that there is no π-bonding in inorganic chemistry and we will further examine this in a later section. While known, δ bonds are generally quite weak compared to σ and π bonds. Compounds with metal-metal δ bonds occur in the middle of the transition series.



2.5.8: δ orbitals is shared under a CC BY-SA license and was authored, remixed, and/or curated by LibreTexts.

- **2.4: σ, π, and δ orbitals** by Chemistry 310 is licensed CC BY-SA 4.0. Original source: https://en.wikibooks.org/wiki/Introduction_to_Inorganic_Chemistry.

2.6: The Range of Bonding

In general chemistry we learned that bonding between atoms can classified as range of possible bonding between **ionic bonds** (fully charge transfer) and **covalent bonds** (fully shared electrons). When two atoms of slightly differing electronegativities come together to form a covalent bond, one atom attracts the electrons more than the other; this is called a polar covalent bond. However, simple “ionic” and “covalent” bonding are idealized concepts and most bonds exist on a two-dimensional continuum described by the van Arkel-Ketelaar Triangle (Figure **2.6.1**).

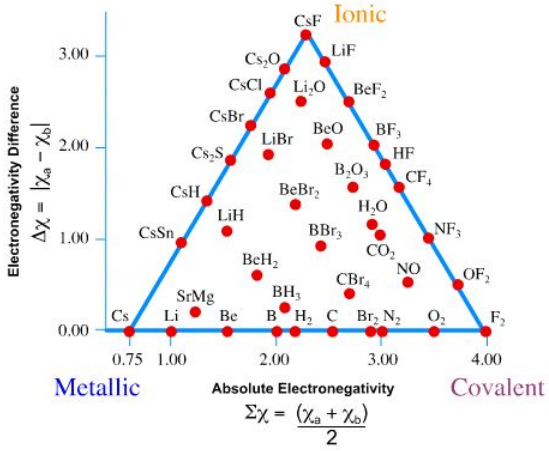


Figure **2.6.1**: van Arkel-Ketelaar Triangle plots the difference in electronegativity ($\Delta\chi$) and the average electronegativity in a bond ($\sum\chi$). the top region is where bonds are mostly ionic, the lower left region is where bonding is metallic, and the lower right region is where the bonding is covalent.

Bond triangles or **van Arkel–Ketelaar** triangles (named after Anton Eduard van Arkel and J. A. A. Ketelaar) are triangles used for showing different compounds in varying degrees of ionic, metallic and covalent bonding. In 1941 van Arkel recognized three extreme materials and associated bonding types. Using 36 main group elements, such as metals, metalloids and non-metals, he placed ionic, metallic and covalent bonds on the corners of an equilateral triangle, as well as suggested intermediate species. The bond triangle shows that chemical bonds are not just particular bonds of a specific type. Rather, bond types are interconnected and different compounds have varying degrees of different bonding character (for example, polar covalent bonds).



Video **2.6.1**: What is the van Arkel-Ketelaar Triangle of Bonding?

Using electronegativity - two compound average electronegativity on x-axis of Figure **2.6.1**.

$$\sum\chi = \frac{\chi_A + \chi_B}{2} \tag{2.6.1}$$

and electronegativity difference on y-axis,

$$\Delta\chi = |\chi_A - \chi_B| \tag{2.6.2}$$

we can rate the dominant bond between the compounds. On the right side of Figure **2.6.1** (from ionic to covalent) should be compounds with varying difference in electronegativity. The compounds with equal electronegativity, such as Cl_2 (chlorine) are placed in the covalent corner, while the ionic corner has compounds with large electronegativity difference, such as NaCl (table salt). The bottom side (from metallic to covalent) contains compounds with varying degree of directionality in the bond. At one extreme is metallic bonds with delocalized bonding and at the other are covalent bonds in which the orbitals overlap in a particular direction. The left side (from ionic to metallic) is meant for delocalized bonds with varying electronegativity difference.

The Three Extremes in bonding

In general:

- Metallic bonds have low $\Delta\chi$ **and** low average $\sum\chi$.
- Ionic bonds have moderate-to-high $\Delta\chi$ and moderate values of average $\sum\chi$.
- Covalent bonds have moderate to high average $\sum\chi$ and can exist with moderately low $\Delta\chi$.

Example 2.6.1

Use the tables of electronegativities and Figure **2.6.1** to estimate the following values

- difference in electronegativity ($\Delta\chi$)
- average electronegativity in a bond ($\sum\chi$)
- percent ionic character
- likely bond type

for the selected compounds:

a. AsH (e.g., in arsine AsH)
b. SrLi
c. KF.

Solution

a: AsH

- The electronegativity of As is 2.18
- The electronegativity of H is 2.22

Using Equations 2.6.1 and 2.6.2:

$$\begin{aligned}\sum\chi &= \frac{\chi_A + \chi_B}{2} \\ &= \frac{2.18 + 2.22}{2} \\ &= 2.2\end{aligned}$$

$$\begin{aligned}\Delta\chi &= \chi_A - \chi_B \\ &= 2.18 - 2.22 \\ &= 0.04\end{aligned}$$

- From Figure **2.6.1**, the bond is fairly nonpolar and has a low ionic character (10% or less)
- The bonding is in the middle of a covalent bond and a metallic bond

b: SrLi

- The electronegativity of Sr is 0.95
- The electronegativity of Li is 0.98

Using Equations 2.6.1 and 2.6.2:

$$\sum \chi = \frac{\chi_A + \chi_B}{2}$$
$$= \frac{0.95 + 0.98}{2}$$
$$= 0.965$$

$$\Delta\chi = \chi_A - \chi_B$$
$$= 0.98 - 0.95$$
$$= 0.025$$

- From Figure **2.6.1**, the bond is fairly nonpolar and has a low ionic character (~3% or less)
- The bonding is likely metallic.

c: **KF**

- The electronegativity of **K** is 0.82
- The electronegativity of **F** is 3.98

Using Equations **2.6.1** and **2.6.2**:

$$\sum \chi = \frac{\chi_A + \chi_B}{2}$$
$$= \frac{0.82 + 3.98}{2}$$
$$= 2.4$$

$$\Delta\chi = \chi_A - \chi_B$$
$$= |0.82 - 3.98|$$
$$= 3.16$$

- From Figure **2.6.1**, the bond is fairly polar and has a high ionic character (~75%)
- The bonding is likely ionic.

Exercise 2.6.1

Contrast the bonding of **NaCl** and silicon tetrafluoride.

Answer

NaCl is an ionic crystal structure, and an electrolyte when dissolved in water; $\Delta\chi = 1.58$, average $\sum\chi = 1.79$, while silicon tetrafluoride is covalent (molecular, non-polar gas; $\Delta\chi = 2.08$, average $\sum\chi = 2.94$.

Contributors and Attributions

- Jim Clark (Chemguide.co.uk)
- Daniel James Berger
- Wikipedia
- Ed Vitz (Kutztown University), John W. Moore (UW-Madison), Justin Shorb (Hope College), Xavier Prat-Resina (University of Minnesota Rochester), Tim Wendorff, and Adam Hahn.

This page titled 2.6: The Range of Bonding is shared under a CC BY-SA license and was authored, remixed, and/or curated by Delmar Larsen.

SECTION OVERVIEW

2.7: Advanced Bonding

2.7.1: Symmetry Elements and Operations

2.7.2: Point Groups

2.7.2.1: Other Groups

2.7.2.2: Groups of Low and High Symmetry

2.7.3: Ligand Group Orbitals and Generator Functions

2.7.4: Expanded Octets and Molecular Orbitals

2.7: Advanced Bonding is shared under a not declared license and was authored, remixed, and/or curated by LibreTexts.

2.7.1: Symmetry Elements and Operations

Introduction

The symmetry of a molecule consists of **symmetry operations** and **symmetry elements**. A symmetry operation is an operation that is performed to a molecule which leaves it indistinguishable and superimposable on the original position. Symmetry operations are performed with respect to symmetry elements (points, lines, or planes).

An example of a symmetry operation is a 180° rotation of a water molecule in which the resulting position of the molecule is indistinguishable from the original position (see Figure **2.7.1.1**). In this example, the symmetry operation is the rotation and the symmetry element is the axis of rotation.

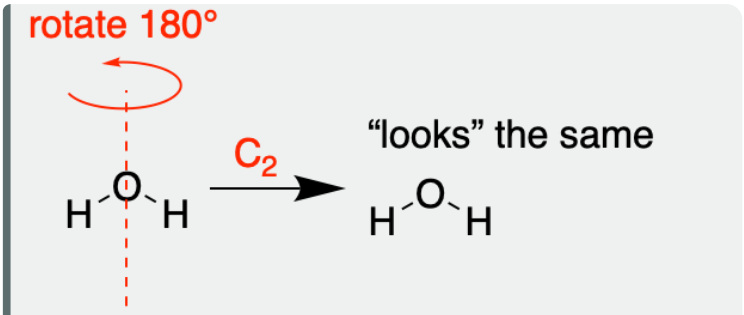


Figure 2.7.1.1: An example of a symmetry operation is a 180° rotation where the resulting position is indistinguishable from the original. A 180° rotation is called a C_2 operation; the axis of rotation is the symmetry element.

There are five types of symmetry operations: **identity**, **reflection**, **inversion**, **proper rotation**, and **improper rotation**. The symmetry elements that correspond to the five types of symmetry operations are listed in Table **2.7.1.1**.

Table **2.7.1.1***: Table of elements and operations*

Element	Operation	Symbol
Identity	identity	E
Proper rotation	rotation by (360/n)°	C_n
Reflection	reflection in a plane	σ
Inversion	inversion of a point at (x,y,z) to (-x,-y,-z)	*i*
Improper rotation	rotation by (360/n)°, followed by reflection in the plane perpendicular to the rotation axis	S_n

Symmetry Operations and Elements

Identity (E)

All molecules have the identity element. The identity operation is doing nothing to the molecule (it doesn't rotate, reflect, or invert...it just is).

Proper Rotation and Proper Axis (C_n)

A "proper" rotation is just a simple rotation operation about an axis. The symbol for any proper rotation or proper axis is $C_{(360/n)}$, where n is the degree of rotation. Thus, a 180° rotation is a C_2 rotation around a C_2 axis, and a 120° rotation is a C_3 rotation about a C_3 axis.

PRINCIPLE AXIS: The principle axis of a molecule is the highest order proper rotation axis, in other words, the largest value of n. For example, if a molecule had C_2 and C_4 axes, the C_4 is the principle axis.

Reflection and Symmetry Planes (σ)

Mirror planes are symmetry planes within the molecule. A reflection operation occurs with respect to a plane of symmetry. There are three classes of symmetry elements:

1. σ_h (horizontal): horizontal planes are perpendicular to principal axis
2. σ_v (vertical): vertical planes are parallel to the principal axis
3. σ_d (dihedral): dihedral planes are parallel to the principle axis and bisect two C_2 axes

Inversion and Inversion Center (i)

The inversion operation requires a point of symmetry (a center of symmetry within a molecule). In other words, a point at the center of the molecule that can transform (x,y,z) into (-x,-y,-z) coordinate. Structures of tetrahedron, triangles, and pentagons lack an inversion center.

Improper rotation (S_n)

Improper rotation is a combination of a rotation with respect to an axis of rotation (C_n), followed by a reflection through a plane perpendicular to that C_n axis. In short, an S_n operation is equivalent to C_n followed by σ_h.

References

1. Introduction to Molecular Symmetry by J. S Ogden
2. Inorganic Chemistry by Catherine Housecroft And Alan G. Sharpe.

2.7.1: Symmetry Elements and Operations is shared under a not declared license and was authored, remixed, and/or curated by LibreTexts.

SECTION OVERVIEW

2.7.2: Point Groups

Introduction

A **Point Group** describes all the symmetry operations that can be performed on a molecule that result in a conformation indistinguishable from the original. Point groups are used in Group Theory, the mathematical analysis of groups, to determine properties such as a molecule's molecular orbitals.

Assigning Point Groups

While a point group contains all of the symmetry operations that can be performed on a given molecule, it is not necessary to identify all of these operations to determine the molecule's overall point group. Instead, a molecule's point group can be determined by following a set of steps which analyze the presence (or absence) of particular symmetry elements.

Steps for assigning a molecule's point group:

1. Determine if the molecule has an infinite rotation axis.
2. If yes, determine if there is an inversion center. If no, find the highest order rotation axis, C_n, and continue.
3. If the molecule does not contain a rotation axis, look for either a mirror plane or an inversion center. If you find at least one rotation axis, look for multiple rotation axes where the n value is greater than 2.
4. Determine if the molecule has any C_2 axes perpendicular to the principal C_n axis. If so, then there are n such C_2 axes, and the molecule is in the D set of point groups. If not, it is in either the C or S set of point groups.
5. Determine if the molecule has a horizontal mirror plane (σ_h) perpendicular to the principal C_n axis. If so, the molecule is either in the C_{nh} or D_{nh} set of point groups.
6. Determine if the molecule has a vertical mirror plane (σ_v) containing the principal C_n axis. If so, the molecule is either in the C_{nv} or D_{nd} set of point groups. If not, and if the molecule has n perpendicular C_2 axes, then it is part of the D_n set of point groups.
7. Determine if there is an improper rotation axis, S_{2n}, collinear with the principal C_n axis. If so, the molecule is in the S_{2n} point group. The S_{2n} point group is extremely unlikely to appear in this course. If not, the molecule is in the C_n point group.

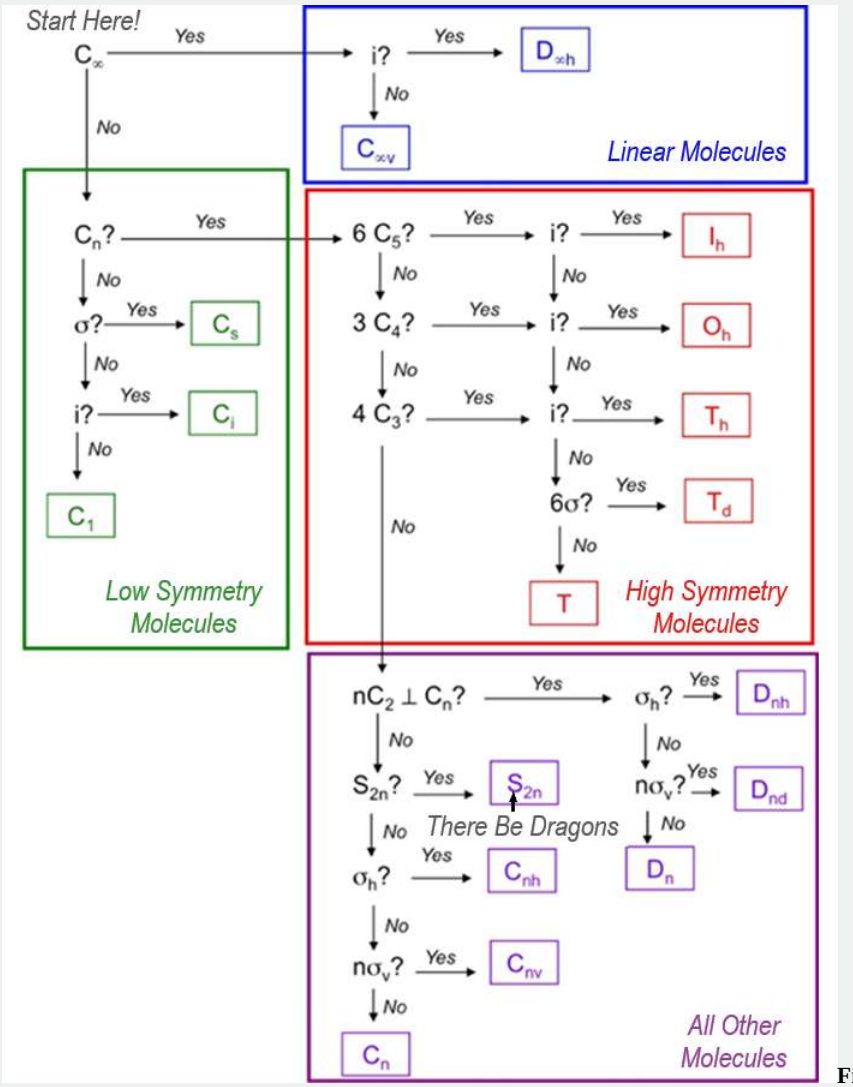


Figure 2.7.2.1: Decision tree for determining a molecule's point group (CC-BY-NC-SA; Chip Nataro)

Example 2.7.2.1

Find the point group of borane (BH3).

Answer

Solution

1. Borane does not have an infinite rotation axis.
2. Highest order rotation axis: C3
3. There are not multiple axes with n greater than 2.
4. There are 3 C_2 axes perpendicular to the principal axis
5. There is a horizontal mirror plane (σ_h)

Borane is in the D_{3h} point group.

See Also

Symmetry Challenge

2.7.2.1: Other Groups

2.7.2.2: Groups of Low and High Symmetry

2.7.2: Point Groups is shared under a not declared license and was authored, remixed, and/or curated by LibreTexts.

2.7.2.1: Other Groups

D Groups

The D set of point groups are classified as D_{nh}, D_{nd}, or D_n, where n refers to the principal axis of rotation. Overall, the D groups are characterized by the presence of n C_2 axes perpendicular to the principal C_n axis. Further classification of a molecule in the D groups depends on the presence of horizontal or vertical/dihedral mirror planes.

Group	Description	Example
D_{nh}	n perpendicular C_2 axes, and a horizontal mirror plane (σ_h)	benzene, C_6H_6 is D_{6h}
D_{nd}	n perpendicular C_2 axes, and a vertical mirror plane (σ_v)	propadiene, C_3H_4 is D_{2d}
D_n	n perpendicular C_2 axes, no mirror planes	$[Co(en)_3]^{3+}$ is D_3

C Groups

The C set of point groups are classified as C_{nh}, C_{nv}, or C_n, where n refers to the principal axis of rotation. The C set of groups are characterized by the absence of n C_2 axes perpendicular to the principal C_n axis. Further classification of a molecule in the C groups depends on the presence of horizontal or vertical/dihedral mirror planes.

Group	Description	Example
C_{nh}	horizontal mirror plane (σ_h) perpendicular to the principal C_n axis	boric acid, H_3BO_3 is C_{3h}
C_{nv}	vertical mirror plane (σ_v) containing the principal C_n axis	ammonia, NH_3 is C_{3v}
C_n	no mirror planes	$P(C_6H_5)_3$ is C_3

S Groups

The S set of point groups are classified as S_{2n}, where n refers to the principal axis of rotation. The S set of groups are characterized by the absence of n C_2 axes perpendicular to the principal C_n axis, as well as the absence of horizontal and vertical/dihedral mirror planes. However, there is an improper rotation (or a rotation-reflection) axis collinear with the principal C_n axis.

Group	Description	Example
S_{2n}	improper rotation (or a rotation-reflection) axis collinear with the principal C_n axis	12-crown-4 is S_4

2.7.2.1: Other Groups is shared under a not declared license and was authored, remixed, and/or curated by LibreTexts.

2.7.2.2: Groups of Low and High Symmetry

Low Symmetry Point Groups

Low symmetry point groups include the C_1, C_s, and C_i groups

Group	Description	Example
C_1	only the identity operation (E)	CHFClBr
C_s	only the identity operation (E) and one mirror plane	C_2H_2ClBr
C_i	only the identity operation (E) and a center of inversion (i)	$C_2H_2Cl_2Br$

High Symmetry Point Groups

High symmetry point groups include the T_d, O_h, I_h, $C_{\infty v}$, and $D_{\infty h}$ groups. The table below describes their characteristic symmetry operations. The full set of symmetry operations included in the point group is described in the corresponding character table.

Group	Description	Example
$C_{\infty v}$	linear molecule with an infinite number of rotation axes and vertical mirror planes (σ_v)	HBr
$D_{\infty h}$	linear molecule with an infinite number of rotation axes, vertical mirror planes (σ_v), perpendicular C_2 axes, a horizontal mirror plane (σ_h), and an inversion center (i)	CO_2
T_d	typically have tetrahedral geometry, with 4 C_4 axes, 3 C_2 axes, 3 S_4 axes, and 6 dihedral mirror planes (σ_d)	CH_4
O_h	typically have octahedral geometry, with 3 C_4 axes, 4 C_3 axes, and an inversion center (i) as characteristic symmetry operations	SF_6
I_h	typically have an icosahedral structure, with 6 C_5 axes as characteristic symmetry operations	$B_{12}H_{12}^{2-}$

2.7.2.2: Groups of Low and High Symmetry is shared under a not declared license and was authored, remixed, and/or curated by LibreTexts.

2.7.3: Ligand Group Orbitals and Generator Functions

So far we have examined the Molecular Orbital (MO) diagrams for diatomic molecules. These molecules can be classified in two different groups, those that contain hydrogen (and thus only have the hydrogen 1s orbital available to make MOs) and those that do not. For the second group, the general diagram developed in previous sections containing σ- and π-bonding and antibonding MOs will generally apply, although there can be subtle differences for heteronuclear diatomics that contain atoms with vastly different electroneagitivity values. The number of diatomic molecules is incredibly small compared to the number of molecules containing three or more atoms. It would be impractical to create and refer to general MO diagrams for all of the different possible combinations, so developing a method to quickly develop MO diagrams for these larger molecules is highly desirable. The method described will use group theory to do just that. For our purposes, we are only going to consider molecules that have a central atom surrounded by either hydrogen or a halide (which can be treated like hydrogen but with three lone pair). In other words, there will be no π-bonding in these molecules. While this again is a relatively small subset of all known molecules, it will provide a basis for the development and understanding of MO diagrams. As this course is not entirely dedicated to MO diagrams, it makes sense to take this limited approach. Larger molecules with π-bonding (and in some cases δ-bonding) requires advanced computational methods to develop MO diagrams.

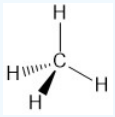
The starting point to this approach is drawing a proper three-dimensional structure of the molecule of interest. From there, the point group of the molecule must be determined. Once the symmetry of the molecule is known, the symmetry of the central atom's atomic orbitals (AOs) can be described using the appropriate symmetry labels. These are found in what is known as a character table and will be called the generator functions. The ligand group orbitals (LGOs) are then derived using a graphical approach. Combination of the generator functions and LGOs in an appropriate way gives the desired MO diagram. Using this technique, you should be able to quickly (albeit crudely) derive an MO diagram to help understand the symmetry and relative energy of the frontier orbitals, often the highest occupied molecular orbital (HOMO) and the lowest unoccupied molecular orbital (LUMO), the orbitals most responsible for chemical reactivity and spectroscopy. At this point, this approach likely seems somewhat vague at best. Rather than continue in a long narrative of the process, it is likely more effective to work through an example. This example will work through several steps that will be summarized at the end.

Step 1 - Drawing the structure and determining the hybridization of the central atom

Exercise 2.7.3.1

Using VSEPR, draw the three-dimensional structure of methane (CH_4).

Answer



Exercise 2.7.3.2

What orbitals need to be used for hybridzation of the central carbon atom?

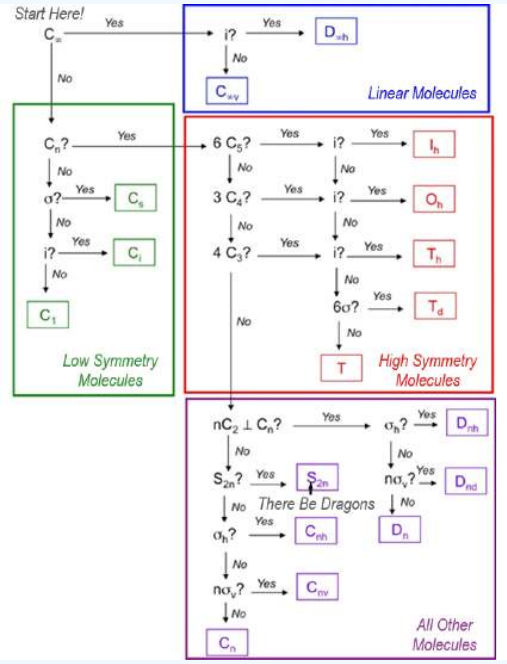
Answer

The carbon would be classified as AX_4E_0 since it is bonded to the four hydrogen atoms and has no lone pair. Based on this the carbon would have to be sp3 hybridized, which means you will need to account for the s- and all three p-orbitals on the carbon atom.

Step 2 - Determine the point group of the molecule and assign the generator functions

Exercise **2.7.3.3**

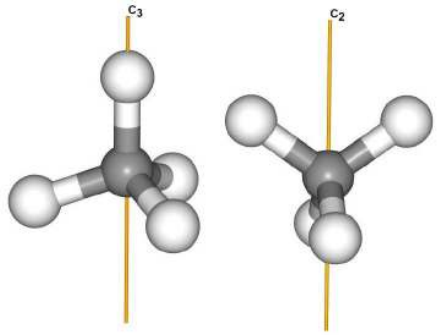
What is the point group of methane?



Answer

Methane does not have an infinite rotation axis.

There is at least one rotation axis (in fact several). The highest order rotation axis is C_3, which can be thought of as any C-H bond. While not important for this application, there are also several C_2 axes that pass between two C-H bonds.



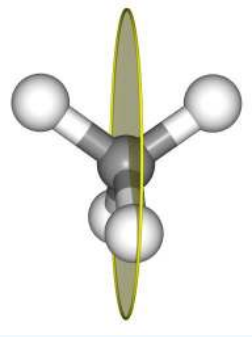
There are not 6 C_5 axes.

There are not 3 C_4 axes.

There are 4 C_3 axes as each of the C-H bonds is a C_3 axis.

There is not an inversion center (it would have to be the unique carbon atom, and none of the hydrogen atoms have another hydrogen atoms directly across from it).

There are 6 σ.



The point group of methane is T_d.

At this point we need to turn to the character table for the point group of methane. Character tables have many uses, most of which are not applicable to this course. As such, character tables have a lot of information that will will not find necessary. Shown below are two different representations for the character table for the T_d point group. The first is the full character table while the second is an abbreviated character table that will be more useful for our purposes.

T_d	E	8 C_3	3 C_2	6 S_4	6 σ_d	Linear Functions	Quadratic Functions
A_1	+1	+1	+1	+1	+1		$x^2 + y^2 + z^2$
A_2	+1	+1	+1	-1	-1		
E	+2	-1	+2	0	0		$(2z^2-x^2-y^2, x^2-y^2)$
T_1	+3	0	-1	+1	-1	(R_x, R_y, R_z)	
T_2	+3	0	-1	-1	+1	(x, y, z)	(xy, xz, yz)

Table **2.7.3.1**: Full character table for the T_d point group.

You may notice that this point group has an improper rotation (even though we did not find it when assigning the point group) and that the mirror planes are designated as σ_d. While significant and useful, there is much more information here than we need. The abbreviated character table will give us all of the information that is necessary. The table has been contracted to include on the symmetry labels (beneath T_d) and the corresponding orbitals that go with those labels. Note that some of the labels do not correspond to orbitals. The Orbitals column in the abbreviated character table corresponds to the Linear Functions column above. The (x, y, z) translates to the (p_x, p_y, p_z). The s orbital is always assigned to the row that only contains values of +1 beneath the symmetry operations. That is not significant for our purposes, but worth mentioning.

T_d	Orbitals
A_1	s
A_2	
E	
T_1	
T_2	(p_x, p_y, p_z)

Table **2.7.3.2**: Abbreviated character table for the T_d point group.

Exercise 2.7.3.4

What are the symmetry labels for the orbitals on carbon used to make methane.

Answer

s - a_1

p_x - t_2

p_y - t_2

p_z - t_2

These are now our generator functions for making the LGOs. Note that the convention is a switch to lower case when assigning symmetry to orbitals.

Step 3 - Making the LGOs

Now that we have the generator functions, we can make the LGOs. This is done pictorially essentially asking the questions "What would the hydrogen 1s orbitals have to look like in order to interact in a constructive way with the carbon orbital in question?' To do this, it is very important to define the axes of your molecule before you start considering potential interactions. Due to the high symmetry of the molecule we will slightly break from convention in order to maximize orbital interactions. In group theory, the principle axis is always assigned as the z-axis, but in this case, we will assign the axes to the C_2 axes in the molecule. To begin with, let's consider the s-orbital of carbon which is labeled a_1. The s-orbital is a sphere with the same sign for the wave function in all directions (Fig. 2.7.3.1).

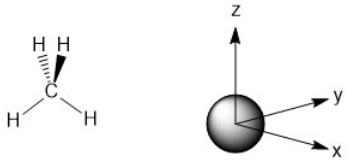


Figure 2.7.3.1: The a_1 orbital for the carbon atom in methane.

Once the axes and the orbital on carbon are drawn we want to consider what the signs for the wave functions on each hydrogen atom would have to be in order to have constructive overlap. In this case, the symmetric a_1 orbital of carbon will be able to interact with all of the hydrogen atoms in a constructive manner is they have the same sign for their wave functions (Fig. 2.7.3.2). This generates a LGO for the hydrogen atoms that has a_1 symmetry. Although it is comprised of AOs from four hydrogen atoms, we now treat this as a single orbital for all of the hydrogen atoms hence the LGO designation.

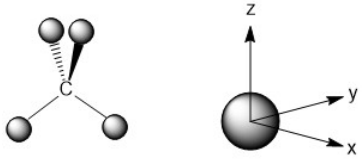


Figure 2.7.3.2: The LGO for the hydrogen atoms that has a_1 symmetry with the carbon generator function depicted on the axes.

The p-orbitals for the carbon atom all have the same symmetry label (t_2). One important consequence of this is that the orbitals are degenerate (equal in energy). While you would likely expect this for an isolated carbon atom, in compounds it is possible that the orbitals are no longer degenerate based on the shape of the molecule. The introduction of p-orbitals into our pictorial method adds one additional complication, p-orbitals are not symmetric and each lobe has a different sign for the wave function. In addition, p-orbitals also posses a nodal plane, a plane in which the probability of finding an electron is zero. In developing the LGO that matches with the p_z-orbital, these factors must be considered. For the p_z-orbital, the nodal plane is the xy plane. So, any hydrogen atoms that lie in the xy plane would be unable to interact with the carbon atom. That leads to an LGO that matches with the p_z-orbital as shown below (Fig. 2.7.3.3).

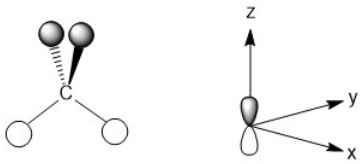


Figure **2.7.3.3**: The LGO for the hydrogen atoms that has t_2 symmetry with the carbon generator function depicted on the axes.

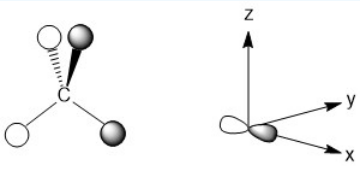
None of the hydrogen atoms are in the xy plane, so they are all capable of interacting. Notice that the change in sign of the carbon p_z-orbital impacts the way the orbitals on the hydrogen atoms are represented, but does not impact the ability of those hydrogen atoms to interact.

Exercise 2.7.3.5

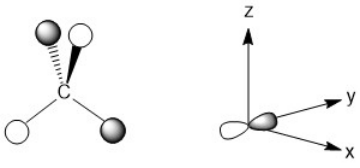
Using the remaining basis functions, sketch the rest of the LGOs for the hydrogen atoms in methane.

Answer

For the p_x-orbital, the nodal plane is the yz plane. Once again none of the hydrogen atoms are in this plane so they can all interact. The LGO is depicted below. Again, the p-orbital of carbon does not point directly at any of the hydrogen atoms, but they are still capable of interacting.



For the p_y-orbital, the nodal plane is the xz plane. Once again there are no hydrogen atoms that are unable to interact. This is a consequence of our decision to maximize the interactions possible in this highly symmetric molecule. The LGO is depicted below.



Step 4 - Constructing the MO diagram

The final step in the process is to construct the MO diagram for the molecule. Before we start constructing the MO diagram there is one final crucial question to be considered, are the atomic orbitals similar enough in energy to interact? We have actually done this to some extent already by ignoring the 1s orbital on carbon as being too low in energy to interact. Compare the energy of the valence orbitals of the atoms that are interacting and if that difference is 15 eV or less, they are close enough in energy. Like many

'rules' you have learned in chemistry, the 15 eV difference is not absolute, but is a reasonable guideline. In the case of methane, all of the orbitals are close enough in energy to interact.

Atomic Number	Element	1s	2s	2p	3s	3p	4s	4p
1	H	-13.6						
2	He	-24.5						
3	Li		-5.5					
4	Be		-9.3					
5	B		-14.0	-8.3				
6	C		-19.5	-10.7				
7	N		-25.5	-13.1				
8	O		-32.4	-15.9				
9	F		-46.4	-18.7				
10	Ne		-48.5	-21.6				
11	Na				-5.2			
12	Mg				-7.7			
13	Al				-11.3	-6.0		
14	Si				-15.0	-7.8		
15	P				-18.7	-10.0		
16	S				-20.7	-12.0		
17	Cl				-25.3	-13.7		
18	Ar				-29.3	-15.9		
19	K						-4.3	
20	Ca						-6.1	
30	Zn						-9.4	
31	Ga						-12.6	-6.0
32	Ge						-15.6	-7.6
33	As						-17.6	-9.1
34	Se						-20.8	-11.0
35	Br						-24.1	-12.5
36	Kr						-27.5	-14.3

Table **2.7.3.3**: Energy (eV) for valence orbitals of atoms from J.G. Verkade, *A Pictorial Approach to Molecular Bonding and Vibrations*, Springer-Verlag, New York, **1997**, p. 69.

Building the MO diagram is similar to how it was done for diatomic molecules (Fig. **2.7.3.4**). The central atom is placed on one side and the outer atoms, as a group, are placed on the other. The relative orbital energies are approximated based on the values in Table

2.7.3.3, in this case the hydrogen LGOs fall between the a_1 and t_2 orbitals for carbon. The hydrogen LGOs are depicted as being degenerate since they are all derived from hydrogen 1s orbitals. The molecular orbitals are drawn between the carbon and hydrogen atoms. The a_1 atomic orbital on carbon has a matching a_1 LGO from hydrogen and so these orbitals can combine to give a bonding MO and an antibonding MO. As the carbon a_1 orbital is the lowest energy AO in this system it leads to the lowest energy MO. Recall that ABIMABTBIB, so it is not surprising that the lowest energy bonding orbital would give the highest energy antibonding orbital. Again, this is a rough guideline and not always the case. Dashed lines are often added to link orbitals with the same symmetry label. This is useful, but with more complex molecules can make the diagrams difficult to read. Finally, there are orbitals with t_2 symmetry on both the carbon atom and from the hydrogen LGOs. Again, these can combine to give three degenerate bonding MOs and three degenerate antibonding MOs. The exact placement of these orbitals is not critical, however, the bonding orbitals should be lower in energy than the AO and LGOs and the antibonding should be higher. The eight valence electrons are added to the system using standard electron configuration principles (Aufbau, Paulii exclusion and Hund's rule).

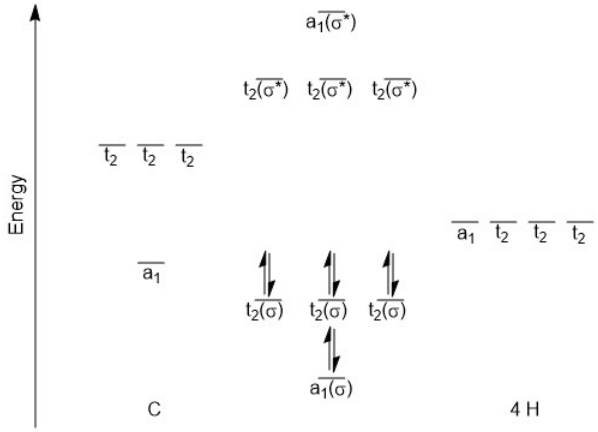


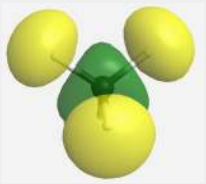
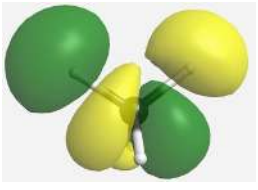
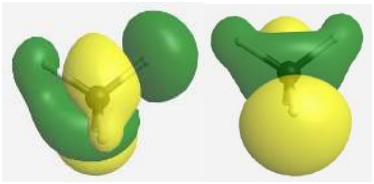
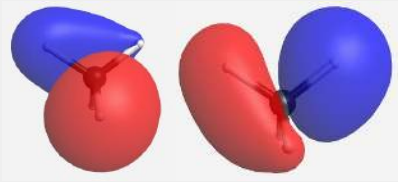
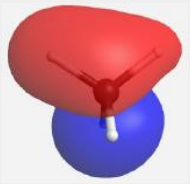
Figure **2.7.3.4**: The MO diagram for CH_4.

For this system the bond order $= \frac{8-0}{2} = 4$. Notice that while this agrees with your original structure, the MO diagram shows something very different. The lowest energy bonding MO (a_1 which is depicted in c) involves all five atoms sharing two electrons, not the carbon atom and one hydrogen atom sharing. The same would be true for the bonding t_2 orbitals, more than 2 atoms are involved. In addition it would be worth noting that the HOMO would be a t_2 orbital (remember they are degenerate so a specific one can not be distinguished) and the LUMO would be a t_2 antibonding orbital.

How did we do?

Our pictorial method is qualitative but does a reasonable job of predicting the MO diagram. A more quantitative method would be to use computational methods to derive a more accurate MO diagram for this methane. The orbitals and their energies as calculated by WebMO are presented below (Table **2.7.3.4**). Overall our MO diagram looks pretty good. We see that the bonding a_1 orbital is approximately 5 eV lower in energy than the carbon a_1 orbital. The a_1* orbital is almost 40 eV higher in energy than the a_1 LGO. This is an excellent representation of the ABIMABTBIB principle. A similar trend is noted for the t_2 orbitals in which the bonding MOs are approximately 1.7 eV lower in energy than the LGOs and the t_2* orbitals are approximately 14 eV higher in energy than the carbon 2p orbitals.

(Table 2.7.3.4). The MOs for CH_4 as calculated and displayed by WebMO. The data for CF_4 was imported into WebMO from the NIST Webbook as a computed 3-D structure and calculations were performed using B3LYP-6-31G(d). The same perspective of the molecule is used throughout.

Symmetry Label	Orbital(s)	Energy (eV)
a_1*		26.479
t_2*	 	3.649
t_2	 	-15.334
a_1		-24.545

2.7.3: Ligand Group Orbitals and Generator Functions is shared under a not declared license and was authored, remixed, and/or curated by LibreTexts.

2.7.4: Expanded Octets and Molecular Orbitals

In organic chemistry the octet rule is closer to a law; do not make more than four bonds to carbon! However, once you start dealing with atoms in the third row of the periodic table, the octet rule becomes a bit more of a guideline. Consider the common anion, hexfluorophospate, PF_6^- (Figure **2.7.4.1**), in which we draw the phosphorous atom with six bonds giving it an apparently electron count of 12.

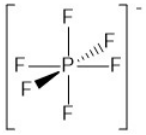


Figure 2.7.4.1. The structure of the hexafluorophosphate anion.

The bonding in these types of systems is a bit more involved and to fully appreciate it we must consider the molecular orbital diagram for such a molecule. This will be done using the same techniques as were used in the previous section, but some adjustments will need to be made as we progress from the Lewis structure to the molecular orbital diagram.

Step 1 - Drawing the structure and determining the hybridization of the central atom

Exercise 2.7.4.1

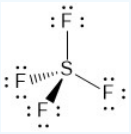
Using VSEPR, draw the three-dimensional structure of sulfur tetrafluoride (SF_4).

Answer

Sulfur has 6 valence electrons and fluorine has 7 giving a total of 34 electrons in this molecule.

To start, you would draw bonds between sulfur and each of the fluorine atoms which would use 8 of the 34 electrons.

As fluorine is more electronegative, the next step would be to give each fluorine 3 lone pair in order to fill their octets. This will use 26 of the remaining electrons. At this point you might be tempted to stop as the sulfur atom and all of the fluorine atoms have an octet.



The problem is that this structure only accounts for 32 of our 34 electrons. As fluorine is an element in the 2nd row, we will not add the missing electrons to any of the fluorine atoms. That leaves sulfur as the only option. Checking the formal charge on each of the atoms supports this placement.

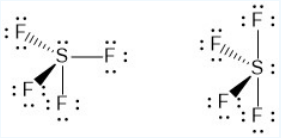
Formal Charge = number of valence electrons - (2 x number of lone pair + number of bonds)

$FC_F = 7 - (2(3) + 1) = 0$

$FC_S = 6 - (2(1) + 4) = 0$

This makes the sulfur AX_4E_1 so the structure is going to be based on AX_5E_0 which is trigonal bipyramidal.

There are two possible options for the structure, but the rules for VSEPR say that the lone pair should be as far away from other electrons as possible. In this structure that would be one of the equatorial positions and so the structure on the right (see-saw) is the correct one.



Exercise 2.7.4.2

What orbitals need to be considered for hybridization on the central sulfur atom?

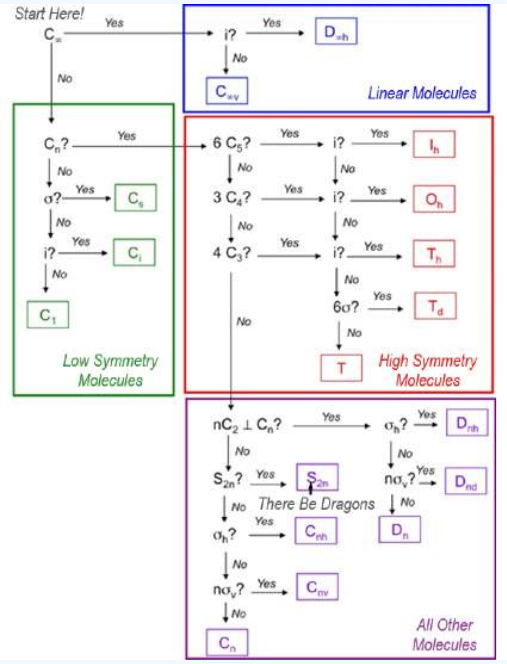
Answer

We need a total of 5 hybrid orbitals to account for the 4 fluorine atoms and the lone pair. That means we need to incorporate a d-orbital which will give sp^3d hybridization. The particular d-orbital that is used would be the d_{z^2} orbital.

Step 2 - Determine the point group of the molecule and assign the generator functions

Exercise 2.7.4.3

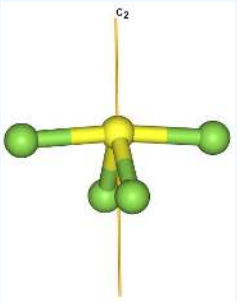
What is the point group of sulfur hexafluoride?



Answer

SF_4 does not have an infinite rotation axis.

There one rotation axis passing through the lone pair which is C_2.



There are not 6 C_5 axes.

There are not 3 C_4 axes.

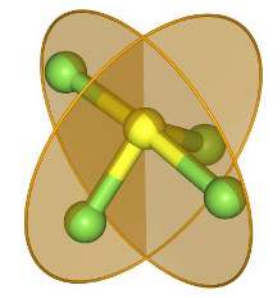
There are not 4 C_3 axes.

The are no perpendicular C_2 axes.

There is not an S_4 axis.

There is not a perpendicular mirror plane.

There are however two mirror planes.



The point group of SF_4 is C_{2v}.

Once again we need the character table for the point group of SF_4. Shown below are two different representations for the character table for the C_{2v} point group. The first is the full character table. Although we ignored it in the methane example, this does include the d-orbital needed for hybridization. In the abbreviated character table the d-orbital has just been incorporated.

C_{2v}	E	C_2	σ_v (xz)	σ_v (yz)	Linear Functions	Quadratic Functions
A_1	+1	+1	+1	+1	z	x^2, y^2, z^2
A_2	+1	+1	-1	-1	R_z	xy
B_1	+1	-1	+1	-1	x, R_y	xz
B_2	+1	-1	-1	+1	z, R_x	yz

Table **2.7.4.1**: Full character table for the C_{2v} point group.

C_{2v}	Orbitals
A_1	s, p_z, d_{z^2}
A_2	
B_1	p_x
B_2	p_y

Table **2.7.4.2**: Abbreviated character table for the C_{2v} point group.

Exercise 2.7.4.4

What are the symmetry labels for the orbitals on sulfur used to make SF_4.

Answer

s - a_1

p_x - b_1

p_y - b_2

p_z - a_1

d_{z^2} - a_1

Step 3 - Making the LGOs

Before making the LGOs, we need to assign axis labels to the molecule. While there are many ways to do this, the proper convention is to assign the principle axis to be the z-axis (Figure **2.7.4.2**).

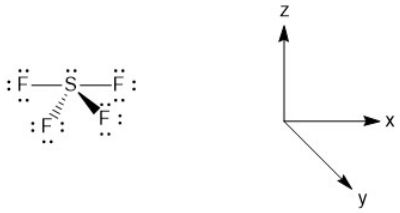


Figure 2.7.4.2. Assignment of the axes in SF_4.

As mentioned in the previous section, we can treat terminal halides using this method. To make the pictures less cluttered, the halides will be represented just as the hydrogen atoms were and we will ignore the lone pair on the fluorine atoms. Based on the assigned axes above, the LGOs can be drawn to match the orbitals on the sulfur atom (Figure **2.7.4.3**).

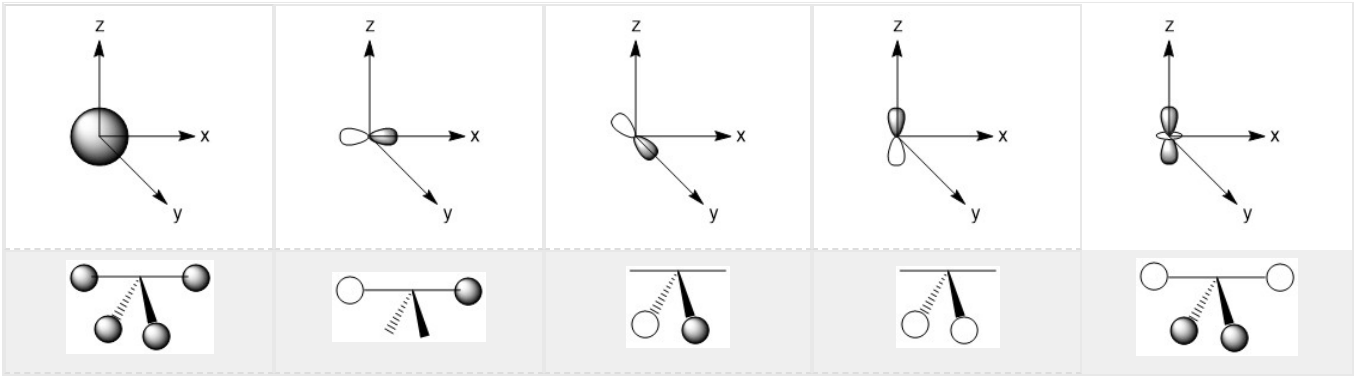


Figure 2.7.4.3. LGOs in SF_4.

Step 3a - A few new twists

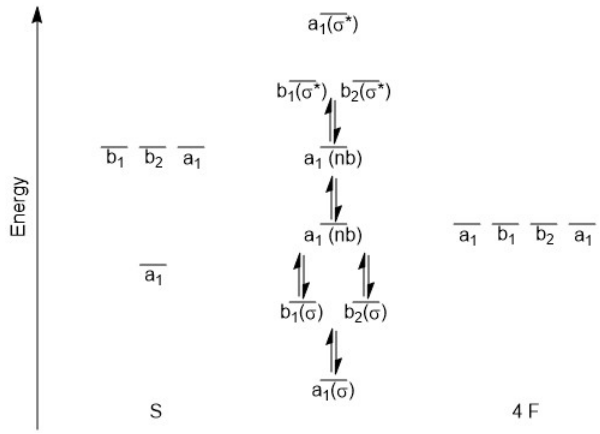
Before we go to step 4, we have a little bit of extra work to do. There are two features in this molecule that we have not dealt with before, the lone pair and the use of d-orbitals. Let's begin with the lone pair as this is something that could be encountered in molecules that do not break the octet rule. We know that this molecule has a lone pair on the sulfur atom. That lone pair has to be accounted for and must occupy one of the orbitals we considered as our basis functions. The question is, which orbital? The best option would be an orbital on the central atom that has no symmetry matched LGO. An example of this would be if all of the outer atoms in a molecule were sitting in the nodal plane of a p-orbital. We do not have that case in this example, so now we need to dig a little deeper. Our next best option is to consider all of the atomic orbitals of the central atom and ask which has the least amount of direct interaction with a LGO. The s-orbital on sulfur has interaction with all four fluorine atoms so it is not a good candidate. The p-orbitals all have interactions with two fluorine atoms, so they are slightly better options. In looking closer at the p-orbitals we see that the p_x orbital has very direct overlap with two fluorine atoms; the orbital is pointing directly at two atoms and both lobes interact. This is greater than the overlap of the p_y orbital in which the LGO does not lie directly on the y-axis. However, both lobes of the p_y orbital are interacting with the LGO. The p_z orbital is somewhat similar in that the LGO does not lie along the z-axis. However, for this orbital, only one lobe of the sulfur p_z is interacting with the LGO. So, given the options for the location of the lone pair, $p_z > p_y > p_x > s$, we must assign the p_z (a_1) orbital to be the one with the lone pair. You may have noticed that the d_{z^2} was not considered in the previous discussion. That is because the d_{z^2} orbital is not accessible energetically. It is too high in energy to participate in any meaningful bonding in this molecule. While, we draw an LGO that would match this orbital, we do not consider any possible bonding or antibonding interaction between the LGO and the d_{z^2} orbital. This is going to become very critical in the next step.

Step 4 - Constructing the MO diagram

In looking at the orbital energies from the previous section, we see that the 2s orbital of fluorine is MUCH lower in energy than the 2p of fluorine or the 3s and 3p of sulfur. It will not interact and does not need to be considered for this diagram. The 2p orbitals of fluorine fall between the 3s and 3p orbitals of sulfur. We will be bringing together a total of eight orbitals. Why only eight? Let's consider each of the combinations above (Figure **2.7.4.3**).

- Remember, we are ignoring the extra lone pairs on fluorine so that leaves a total of 12 orbitals that will not be shown in our diagram.
- The s-orbital (a_1) from sulfur and the corresponding LGO will make a bonding and antibonding set.
- The p_x orbital (b_1) orbital from sulfur and the corresponding LGO will make a bonding and antibonding set.
- The p_y orbital (b_2) orbital from sulfur and the corresponding LGO will make a bonding and antibonding set.
- The p_z orbital (a_1) has been assigned as the orbital holding the lone pair so we ignore the LGO it could interact with. Note that this does not mean that the fluorine orbitals do not contribute to this orbital, but for the purpose of constructing the MO diagram we will ignore any contribution.
- The d_{z^2} orbital (a_1) of sulfur is not energetically accessible so we do not include it, but we do consider the LGO that would interact with it.

In sketching the MO diagram, the s-orbital of sulfur is the lowest energy orbital depicted and as such will give the lowest energy bonding MO and likely the highest energy antibonding MO. We will have two a_1 orbitals that will be labeled as non-bonding (nb), one for the p_z orbital with the lone pair, and one for the LGO that would match the d_{z^2} orbital. As we are considering the orbitals to be localized on specific atoms, we will not change their energy from that of the atomic orbital from which they are derived. That leaves the b_1 and b_2 orbitals that will make a bonding and antibonding set. At first glance, you might expect these to be degenerate as they both are derived from p-orbitals on sulfur and the corresponding LGOs. However, upon examining the pictures above, (Figure **2.7.4.3**), it might be expected that the b_1 bonding orbital might be slightly lower in energy than the b_2 since there is a more direct overlap between the sulfur orbital and the LGO. For now we will treat the orbitals as being degenerate. This would lead to a MO diagram as pictured below (Figure **2.7.4.4**).



(Figure 2.7.4.4). MO diagram for SF_4.

Overall, this would give a bond order $= \frac{6-0}{2} = 3$ which is quite different from the Lewis structure. The bonding in structures of p-block elements with 'expanded' octets is not as straightforward as the Lewis structure might suggest. There are filled bonding orbitals that involve more than two atoms. There are also significant ionic contributions to what is typically drawn as covalent bonds.

How did we do?

Our MO diagram was generated using a pictorial method. Using computational methods it is possible to derive a more accurate MO diagram for this molecule. Show below are the orbitals and their energies as calculated by WebMO (Table **2.7.4.3**). Overall our MO diagram looks pretty good. We see a VERY slight difference in the energy of the b_1 and b_2 bonding orbitals. This difference is more pronounced in the antibonding orbitals. Based on the ABIMABTBIB principle, it is not surprising that we see a greater

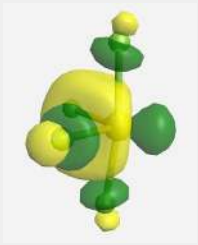
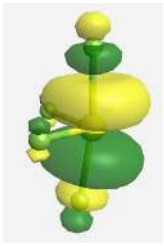
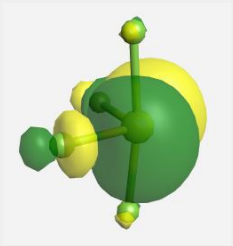
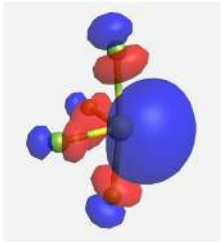
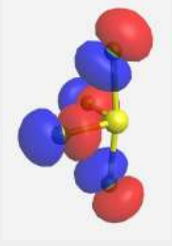
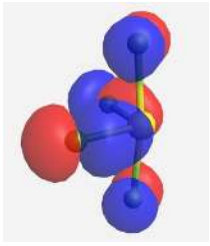
difference in the antibonding orbitals. So our approximation of the b_1 and b_2 orbitals as being degenerate is not unreasonable for the bonding MOs but not accurate for the antibonding.

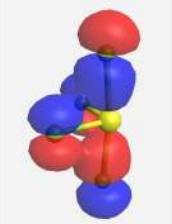
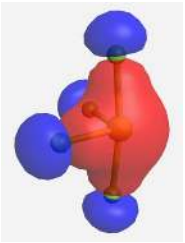
You may also notice that all of the fluorine contributions are from p-orbitals. The 2s orbital of fluorine is much too low in energy to participate in these interactions. So the only orbital involved in bonding with the sulfur would be the p-orbital pointing directly at the sulfur atom. This justifies our treatment of the fluorine as being hydrogen-like. Again, we are ignoring any possible π-bonding interactions in this molecule.

We also estimated that the a_1 (nb) would not change in energy much from the atomic orbitals they were derived from. The energy for the a_1 (nb) derived from the sulfur p_z is -12.049 eV which compares very favorably to the value of -12.0 eV for the 3p orbital of sulfur found in the previous page. For the a_1 (nb) LGO, the energy was calculated to be -17.853 eV which is slightly higher than the -18.7 eV listed for the 2p orbitals of fluorine. Again, while not completely accurate, our pictorial method did a fairly reasonable job of generating the MO diagram.

(Table 2.7.4.3). The MOs for SF_4 (ignoring the lone pairs) as calculated and displayed by WebMO. The data for SF_4 was imported

into WebMO from the NIST Webbook as a computed 3-D structure and calculations were performed using B3LYP-6-31G(d).

Orbital	Label	Energy (eV)
	a_1*	0.517
	b_1*	-1.950
	b_2*	-4.083
	a_1 (nb)	-12.049
	a_1 (nb)	-17.853
	b_2	-18.559

	b_1	-18.697
	a_1	-20.655

2.7.4: Expanded Octets and Molecular Orbitals is shared under a not declared license and was authored, remixed, and/or curated by LibreTexts.

SECTION OVERVIEW

2.8: Nuclear Magnetic Resonance (NMR)

2.8.1: The Origin of the NMR Signal

2.8.2: Chemical Equivalence

2.8.3: The 1H-NMR experiment

2.8.4: Spin-Spin Coupling

2.8.5: The Basis for Differences in Chemical Shift

2.8: Nuclear Magnetic Resonance (NMR) is shared under a not declared license and was authored, remixed, and/or curated by LibreTexts.

2.8.1: The Origin of the NMR Signal

The Magnetic Moment

Nuclear magnetic resonance spectroscopy is an incredibly powerful tool for inorganic chemists because it allows us to analyze the connectivity of atoms in molecules. The basis for NMR is the observation that many atomic nuclei generate their own magnetic field, or magnetic moment, as they spin about their axes. Not all nuclei have a magnetic moment. Fortunately for inorganic chemists, though, hydrogen (^{1}H), the ^{13}C isotope of carbon, the ^{19}F isotope of fluorine, and the ^{31}P isotope of phosphorus all have magnetic moments and therefore can be observed by NMR – they are, in other words, NMR-active. Other nuclei - such as the common ^{12}C and ^{16}O isotopes of carbon and oxygen - do not have magnetic moments, and cannot be directly observed by NMR. Still other nuclei such as the hydrogen isotope deuterium (^{2}H) and nitrogen (^{14}N) have magnetic moments and are NMR-active, but the nature of their magnetic moments is such that analysis of these nuclei by NMR is more complex.

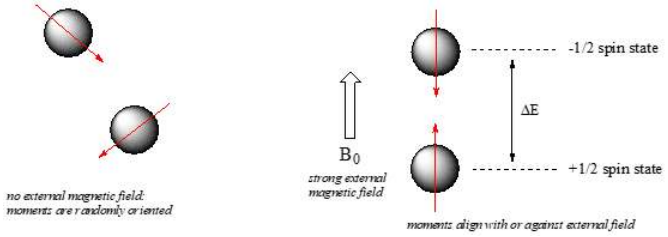
In practice it is ^{1}H and ^{13}C nuclei that are most commonly observed by NMR spectroscopy. The fundamentals of interpreting ^{1}H NMR are covered in organic chemistry and as such will not be a focus of this course. However, the principles behind ^{1}H NMR apply to other nuclei, so ^{1}H NMR will be used in much of the discussion. The terms 'proton' and 'hydrogen' are used interchangeably when discussing because the ^{1}H nucleus is just a single proton.

Table **2.8.1.1**: Some examples of magnetic and nonmagnetic nuclei relevant to inorganic chemistry.

Magnetic Nuclei	Nonmagnetic Nuclei
^{1}H	^{12}C
^{2}H	^{16}O
^{13}C	^{32}S
^{14}N	^{35}Cl
^{19}F	
^{31}P	

Spin States and the Magnetic Transition

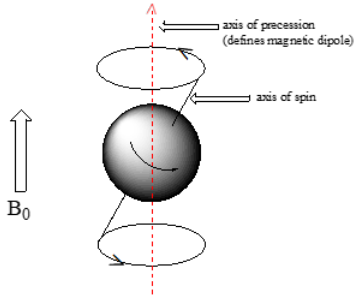
When a sample of an inorganic compound is sitting in a flask on a laboratory bench, the magnetic moments of all of its nuclei are randomly oriented. However, when the same sample is placed within the field of a very strong superconducting magnet (this field is referred to by NMR spectroscopists as the applied field, abbreviated B_0) each nucleus will assume one of two possible quantum spin states. In the +½ spin state, the magnetic moment is aligned with the direction of B_0, while in the -½ spin state it is aligned opposed to the direction of B_0.



The +½ spin state is slightly lower in energy than the -½ state, and the energy gap between them, which we will call ΔE, depends upon the strength of B_0: a stronger applied field results in a larger ΔE. For a large population of inorganic molecules in an applied field, slightly more than half of the protons will occupy the lower energy +½ spin state, while slightly less than half will occupy the higher energy -½ spin state. It is this population difference (between the two spin states) that is exploited by NMR, and the difference increases with the strength of the applied magnetic field.

At this point, we need to look a little more closely at how a nucleus spins in an applied magnetic field. You may have see a toy spinning top. When a top slows down a little and the spin axis is no longer completely vertical, it begins to exhibit precessional

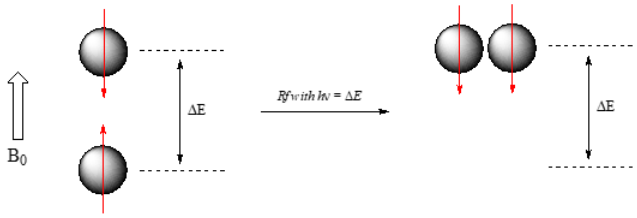
motion, as the spin axis rotates slowly around the vertical. In the same way, a nucleus spinning in an applied magnetic field also exhibits precessional motion about a vertical axis. It is this axis (which is either parallel or antiparallel to B_0) that defines the proton's magnetic moment.



Watch the first minute or so of this video of spinning tops: look for the precessional motion

The frequency of precession (also called the Larmour frequency, abbreviated ν_L) is simply the number of times per second that the nucleus precesses in a complete circle. The precessional frequency increases with the strength of B_0.

If a nucleus that is precessing in an applied magnetic field is exposed to electromagnetic radiation of a frequency νthat matches its precessional frequency ν_L, we have a condition called resonance. In the resonance condition, a nucleus in the lower-energy +½ spin state (aligned with B_0) will transition (flip) to the higher energy –½ spin state (opposed to B_0). In doing so, it will absorb radiation at this resonance frequency n - and this frequency corresponds to ΔE, the energy difference between the two spin states. With the strong magnetic fields generated by the superconducting magnets used in modern NMR instruments, the resonance frequency for protons falls within the radio-wave range, anywhere from 100 MHz to 800 MHz depending on the strength of the magnet.



Recall that photons of electromagnetic radiation of a given frequency correspond to energy (E) given by $E = h\nu$, where h is Plank's constant and ν is the frequency in waves per second, or Hz. Now, we know that in NMR, the energy gap ΔE between the +½ and -½ spin states of a proton in a strong magnetic field corresponds to the energy associated with radiation in the radio frequency (Rf) region of the spectrum. By detecting the frequency of radiation that is absorbed, we can gain information about the chemical environment of the nucleus.

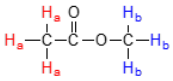
Contributors

- Organic Chemistry With a Biological Emphasis by Tim Soderberg (University of Minnesota, Morris)

This page titled 2.8.1: The Origin of the NMR Signal is shared under a CC BY-NC-SA 4.0 license and was authored, remixed, and/or curated by Tim Soderberg.

2.8.2: Chemical Equivalence

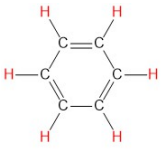
The frequency of radiation absorbed by a proton (or any other nucleus) during a spin transition in an NMR experiment is called its 'resonance frequency'. If all nuclei in all inorganic molecules had the same resonance frequency, NMR spectroscopy but would not be terribly useful for chemists. Fortunately for us, however, resonance frequencies are not uniform for different nuclei in a molecule - rather, the resonance frequency varies according to the electronic environment that a given nucleus inhabits. In methyl acetate, for example, there are two distinct ‘sets’ of protons.



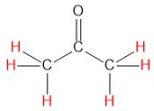
methyl acetate

The three methyl acetate protons labeled H_a above have a different resonance frequency compared to the three H_b protons, because the two sets of protons are in non-identical electronic environments: the H_a protons are on a carbon next to a carbonyl (C=O) carbon, while the H_b protons or on a carbon next to the an oxygen. In the terminology of NMR, all three H_a protons are chemically equivalent to each other, as are all three H_b protons. The H_a protons are, however, chemically nonequivalent to the H_b protons. As a consequence, the resonance frequency of the H_a protons is different from that of the H_b protons. For now, do not worry about why the different electronic environment gives rise to different resonance frequencies - we will get to that soon.

The ability to recognize chemical equivalancy and nonequivalency among atoms in a molecule will be central to understanding NMR. Each of the molecules below contains only one set of chemically equivalent protons: all six protons on benzene, for example, are equivalent to each other and have the same resonance frequency in an NMR experiment. Notice that any description of the bonding and position of one proton in benzene applies to all five other protons as well.

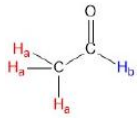


benzene



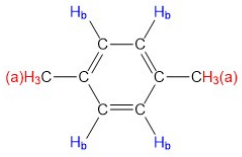
acetone

Acetaldehyde contains two sets of chemically equivalent protons, just like our previous example of methyl acetate, and again in each case the resonance frequency of the H_a protons will be different from that of the H_b proton. A description of the bonding and position of the H_b proton does not apply to the three H_a protons: H_b is bonded to an sp^2-hybridized carbonyl carbon while the H_a protons are bonded to an sp^3-hybridized methyl carbon.

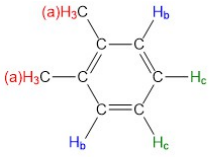


acetaldehyde

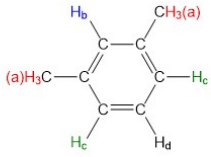
Note that while all four aromatic protons in 1,4-dimethylbenzene are chemically equivalent, its constitutional isomer 1,2 dimethylbenzene has two sets of aromatic protons in addition to the six methyl ($\boldsymbol{H_a}$) protons. The 1,3-substituted isomer, on the other hand, has three sets of aromatic protons.



1,4-dimethylbenzene



1,2-dimethylbenzene



1,3-dimethylbenzene

In 1,2-dimethylbenzene, both H_b protons are adjacent to a methyl substituent, while both H_c protons are two carbons away. In 1,3-dimethylbenzene, H_b is situated between two methyl groups, the two H_c protons are one carbon away from a methyl group, and H_d is two carbons away from a methyl group.

As you have probably already realized, chemical equivalence or non-equivalence in NMR is closely related to symmetry. Different planes of symmetry in the three isomers of dimethylbenzene lead to different patterns of equivalence.

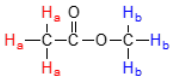
Contributors

- Organic Chemistry With a Biological Emphasis by Tim Soderberg (University of Minnesota, Morris)

This page titled 2.8.2: Chemical Equivalence is shared under a CC BY-NC-SA 4.0 license and was authored, remixed, and/or curated by Tim Soderberg.

2.8.3: The 1H-NMR experiment

In an NMR experiment, a sample compound (we'll again use methyl acetate as our example) is placed inside a very strong applied magnetic field (B_0) generated by a superconducting magnet in the instrument.

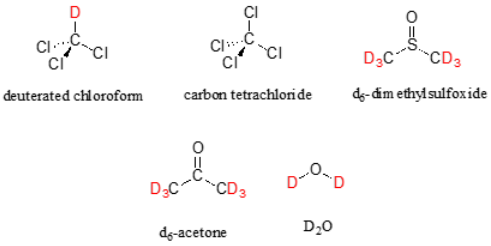


methyl acetate

At first, the magnetic moments of (slightly more than) half of the protons in the sample are aligned with B_0, and half are aligned against B_0. Then, the sample is exposed to a range of radio frequencies. Out of all of the frequencies which hit the sample, only two - the resonance frequencies for H_a and H_b - are absorbed, causing those protons which are aligned with B_0 to 'spin flip' so that they align themselves against B_0. When the 'flipped' protons flip back down to their ground state, they emit energy, again in the form of radio-frequency radiation. The NMR instrument detects and records the frequency and intensity of this radiation, making using of a mathematical technique known as a 'Fourier Transform'.

In most cases, a sample being analyzed by NMR is in solution. If we use a common laboratory solvent (diethyl ether, acetone, dichloromethane, ethanol, water, etc.) to dissolve our NMR sample, however, we run into a problem – there many more solvent protons in solution than there are sample protons, so the signals from the sample protons will be overwhelmed. To get around this problem, we use special NMR solvents in which all protons have been replaced by deuterium. Deuterium is NMR-active, but its resonance frequency is far outside of the range in which protons absorb, so it is `invisible` in ^{1}H-NMR. Some common NMR solvents are shown below.

Common NMR solvents



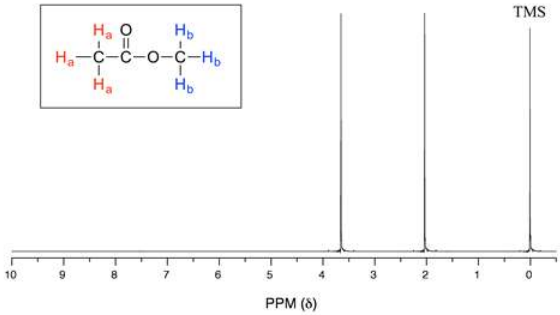
deuterated chloroform | carbon tetrachloride | d_6-dimethylsulfoxide

d_6-acetone | D_2O

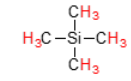
Note that this is not necessarily a problem when looking at nuclei such as ^{31}P. Very few solvents contain phosphorus so there is no chance for the phosphorus signals to be overwhelmed by signals from the solvent. However, most spectra are still obtained in deuterated solvents because the instruments often rely on a deutrerium signal to fine tune the signal and a proton spectrum is often obtained along with spectra for other nuclei.

It should also be noted that when conducting an NMR experiment, the operator chooses which nucleus is being observed. As mentioned previously, the resonance frequency of deuterium is significantly different than that of protons. One could choose to observe a proton spectrum of a sample or the deuterium spectrum of the same sample, but not both at the same time. There are some very specialized experiments that do allow the observation of two different nuclei in the same experiment, but that is beyond the score of this course. If the ^{31}P spectrum of a sample is obtained, the presence of protons in the solvent will not have an impact on the spectrum. This does not mean that different nuclei (e.g. phosphorus and proton) do not influence each other as we will see when we discuss coupling.

Let's look at an actual ^{1}H-NMR spectrum for methyl acetate. The vertical axis corresponds to intensity of absorbance, the horizontal axis to frequency. However, you will notice right away that a) there is no y-axis line or units drawn in the figure, and b) the x-axis units are not Hz, which you would expect for a frequency scale. Both of these mysteries will become clear very soon.



We see three absorbance signals: two of these correspond to H_a and H_b (don't worry yet which is which), while the peak at the far right of the spectrum corresponds to the 12 chemically equivalent protons in tetramethylsilane (TMS), a standard reference compound that was added to our sample.



tetramethylsilane (TMS)

First, let's talk about the x-axis. The 'ppm' label stands for 'parts per million', and simply tells us that the two sets of equivalent protons in our methyl acetate sample have resonance frequencies about 2.0 and 3.6 parts per million higher than the resonance frequency of the TMS protons, which we are using as our reference standard. This is referred to as their chemical shift.

The reason for using a relative value (chemical shift expressed in ppm) rather than the actual resonance frequency (expressed in Hz) is that every NMR instrument will have a different magnetic field strength, so the actual value of resonance frequencies expressed in Hz will be different on different instruments - remember that ΔE for the magnetic transition of a nucleus depends upon the strength of the externally applied magnetic field. However, the resonance frequency values relative to the TMS standard will always be the same, regardless of the strength of the applied field. For example, if the resonance frequency for the TMS protons in a given NMR instrument is exactly 300 MHz (300 million Hz), then a chemical shift of 2.0 ppm corresponds to an actual resonance frequency of 300,000,600 Hz (2 parts per million of 300 million is 600). In another instrument (with a stronger magnet) where the resonance frequency for TMS protons is 400 MHz, a chemical shift of 2.0 ppm corresponds to a resonance frequency of 400,000,800 Hz.

A frequently used symbolic designation for chemical shift in ppm is the lower-case Greek letter δ. Most protons in organic compounds have chemical shift values between 0 and 10 ppm relative to TMS, although values below 0 ppm and up to 12 ppm and above are occasionally observed. By convention, the left-hand side of an NMR spectrum (higher chemical shift) is called downfield, and the right-hand direction is called upfield.

In modern research-grade NMR instruments, it is no longer necessary to actually add TMS to the sample: the computer simply calculates where the TMS signal should be, based on resonance frequencies of the solvent. So, from now on you will not see a TMS peak on NMR spectra - but the 0 ppm point on the x-axis will always be defined as the resonance frequency of TMS protons.

A Chemical Shift Analogy

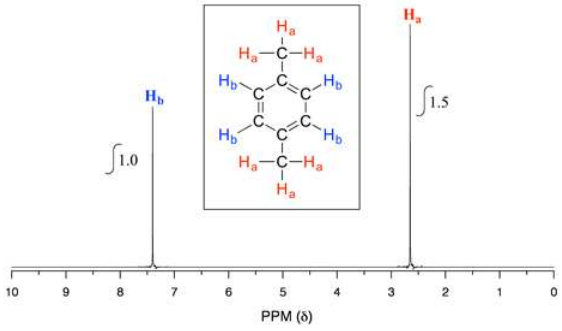
If you are having trouble understanding the concept of chemical shift and why it is used in NMR, try this analogy: imagine that you have a job where you travel frequently to various planets, each of which has a different gravitational field strength. Although your body mass remains constant, your measured weight is variable - the same scale may show that you weigh 60 kg on one planet, and 75 kg on another. You want to be able to keep track your body mass in a meaningful, reproducible way, so you choose an object to use as a standard: a heavy iron bar, for example. You record the weight of the iron bar and yourself on your home planet, and find that the iron bar weighs 50 kg and you weigh 60 kg. You are 20

percent (or pph, parts per hundred) heavier than the bar. The next day you travel (with the iron bar in your suitcase) to another planet and find that the bar weighs 62.5 kg, and you weigh 75 kg. Although your measured weight is different, you are still 20% heavier than the bar: you have a 'weight shift' of 20 pph relative to the iron bar, no matter what planet you are on.

We have already pointed out that, on our spectrum of methyl acetate, there is there is no y-axis scale indicated. With y-axis data it is relative values, rather than absolute values, that are important in NMR. The computer in an NMR instrument can be instructed to mathematically integrate the area under a signal or group of signals. The signal integration process is very useful, because in ^{1}H-NMR spectroscopy the area under a signal is proportional to the number of protons to which the signal corresponds. When we instruct the computer to integrate the areas under the H_a and H_b signals in our methyl acetate spectrum, we find that they have approximately the same area. This makes sense, because each signal corresponds to a set of three equivalent protons.

Be careful not to assume that you can correlate apparent peak height to number of protons - depending on the spectrum, relative peak heights will not always be the same as relative peak areas, and it is the relative areas that are meaningful. Because it is difficult to compare relative peak area by eye, we rely on the instrument's computer to do the calculations. Note also that in the spectrum above the signal for TMS represents 12 protons and yet is appears to be similar to the signals for the methyl acetate. The intensity of the signals is also dependent on the concentration of the species in solution. Without careful sample preparation, it is extremely unlikely that the concentration of TMS is the same as that of the methyl acetate meaning that there can not be a direct comparison of their signals.

Take a look next at the spectrum of 1,4-dimethylbenzene:



As we discussed earlier, this molecule has two sets of equivalent protons: the six methyl H_a protons and the four aromatic H_b protons. When we instruct the instrument to integrate the areas under the two signals, we find that the area under the peak at 2.6 ppm is 1.5 times greater than the area under the peak at 7.4 ppm. The ratio 1.5 to 1 is of course the same as the ratio 6 to 4. This integration information (along with the actual chemical shift values, which we'll discuss soon) tells us that the peak at 7.4 ppm must correspond to H_b, and the peak at 2.6 ppm to H_a.

Contributors

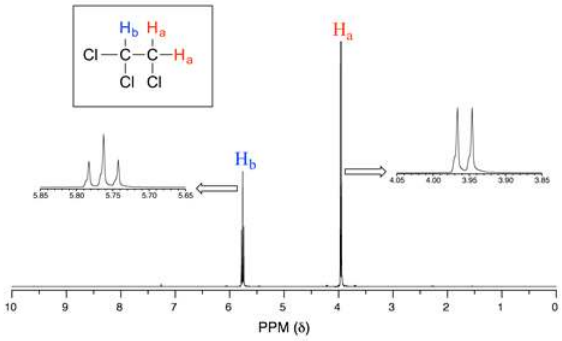
- Organic Chemistry With a Biological Emphasis by Tim Soderberg (University of Minnesota, Morris)

This page titled 2.8.3: The 1H-NMR experiment is shared under a CC BY-NC-SA 4.0 license and was authored, remixed, and/or curated by Tim Soderberg.

2.8.4: Spin-Spin Coupling

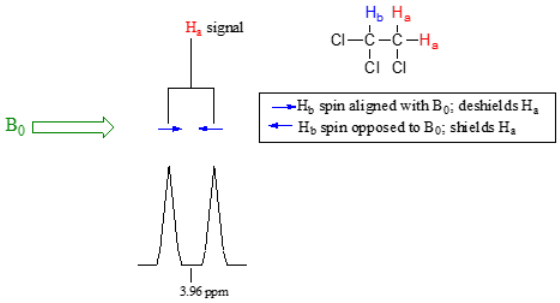
The ^{1}H-NMR spectra that we have seen so far (of methyl acetate and 1,4-dimethylbenzene) are somewhat unusual in the sense that in both of these molecules, each set of protons generates a single NMR signal. In fact, the ^{1}H-NMR spectra of most molecules contain signals that are 'split' into two or more sub-peaks. Rather than being a complication, however, this splitting behavior is actually very useful because it provides us with more information about our sample molecule.

Consider the spectrum for 1,1,2-trichloroethane. In this and in many spectra to follow, we show enlargements of individual signals so that the signal splitting patterns are recognizable.



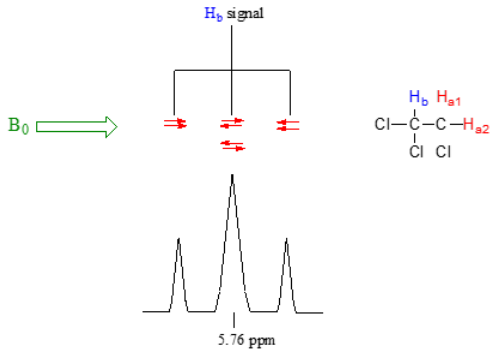
The signal at 3.96 ppm, corresponding to the two H_a protons, is split into two subpeaks of equal height (and area) – this is referred to as a doublet. The H_b signal at 5.76 ppm, on the other hand, is split into three sub-peaks, with the middle peak higher than the two outside peaks - if we were to integrate each subpeak, we would see that the area under the middle peak is twice that of each of the outside peaks. This is called a triplet.

The source of signal splitting is a phenomenon called spin-spin coupling, a term that describes the magnetic interactions between neighboring, non-equivalent NMR-active nuclei. (The terms 'splitting' and 'coupling' are often used interchangeably when discussing NMR.) In our 1,1,2 trichloromethane example, the H_a and H_b protons are spin-coupled to each other. Here's how it works, looking first at the H_a signal: in addition to being shielded by nearby valence electrons, each of the H_a protons is also influenced by the small magnetic field generated by H_b next door (remember, each spinning proton is like a tiny magnet). The magnetic moment of H_b will be aligned with B_0 in slightly more than half of the molecules in the sample, while in the remaining molecules it will be opposed to B_0. The B_{eff} 'felt' by H_a is a slightly weaker if H_b is aligned against B_0, or slightly stronger if H_b is aligned with B_0. In other words, in half of the molecules H_a is shielded by H_b (thus the NMR signal is shifted slightly upfield) and in the other half H_a is deshielded by H_b (and the NMR signal shifted slightly downfield). What would otherwise be a single H_a peak has been split into two sub-peaks (a doublet), one upfield and one downfield of the original signal. These ideas an be illustrated by a splitting diagram, as shown below.



Now, let's think about the H_b signal. The magnetic environment experienced by H_b is influenced by the fields of both neighboring H_a protons, which we will call H_{a1} and H_{a2}. There are four possibilities here, each of which is equally probable. First, the magnetic fields of both H_{a1} and H_{a2} could be aligned with B_0, which would deshield H_b, shifting its NMR signal slightly downfield. Second, both the H_{a1} and H_{a2} magnetic fields could be aligned opposed to B_0, which would shield H_b, shifting its resonance signal slightly upfield. Third and fourth, H_{a1} could be with B_0 and H_{a2} opposed, or H_{a1} opposed to B_0 and H_{a2} with B_0. In each of the last two

cases, the shielding effect of one H_a proton would cancel the deshielding effect of the other, and the chemical shift of H_b would be unchanged.



So in the end, the signal for H_b is a triplet, with the middle peak twice as large as the two outer peaks because there are two ways that H_{a1} and H_{a2} can cancel each other out.

While this coupling most often occurs between the same nuclei as seen in the proton spectrum above, nuclei of different atoms will couple if they are in close enough proximity. For example, if the ^{13}C NMR spectrum of 1,1,2-trichloroethane were obtained, there would be two signals. Since the carbon atoms are not equivalent, they would couple each other. In practice this is not typically a concern due to the low natural abundance of ^{13}C. The carbon signals would also couple with the protons making for a very complex signal. As many molecules contain multiple protons, we often seek to eliminate this complication. In this case, the $^{13}C\{^1H\}$ NMR spectrum would be obtained. The $\{^1H\}$ indicates proton decoupling which means irradiating the sample with a frequency such that the protons become 'invisible' and no coupling to them is seen. Running decoupled spectra is very common for non-hydrogen nuclei.

Video tutorials: proton NMR spectroscopy

Video of an actual NMR experiment

Contributors

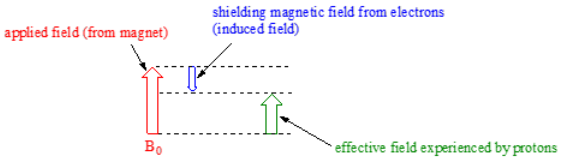
- Organic Chemistry With a Biological Emphasis by Tim Soderberg (University of Minnesota, Morris)

This page titled 2.8.4: Spin-Spin Coupling is shared under a CC BY-NC-SA 4.0 license and was authored, remixed, and/or curated by Tim Soderberg.

2.8.5: The Basis for Differences in Chemical Shift

We come now to the question of why nonequivalent protons have different resonance frequencies and thus different chemical shifts. The chemical shift of a given proton is determined primarily by interactions with the nearby electrons. The most important thing to understand is that when electrons are subjected to an external magnetic field, they form their own small induced magnetic fields in opposition to the external field.

Consider the methane molecule (CH_4) in which the four equivalent protons have a chemical shift of 0.23 ppm. The valence electrons around the methyl carbon, when subjected to B_0, generate their own very small induced magnetic field that opposes B_0. This induced field, to a small but significant degree, shields the nearby protons from experiencing the full force of B_0, an effect known as local diamagnetic shielding. In other words, the methane protons do not quite experience the full force of B_0 - what they experience is called B_{eff}, or the effective field, which is slightly weaker than B_0 due to the influence of the nearby electrons.



Because B_{eff} is slightly weaker than B_0, the resonance frequency (and thus the chemical shift) of the methane proton is slightly lower than what it would be if it did not have electrons nearby and was feeling the full force of B_0. (You should note that the figure above is not to scale: the applied field is generated by a superconducting magnet and is extremely strong, while the opposing induced field from the electrons is comparatively very small.)

Now consider methyl fluoride, CH_3F, in which the protons have a chemical shift of 4.26 ppm, significantly higher than that of methane. This is caused by something called the deshielding effect. Recall that fluorine is very electronegative: it pulls electrons towards itself, effectively decreasing the electron density around each of the protons. For the protons, being in a lower electron density environment means less diamagnetic shielding, which in turn means a greater overall exposure to B_0, a stronger B_{eff}, and a higher resonance frequency. Put another way, the fluorine, by pulling electron density away from the protons, is deshielding them, leaving them more exposed to B_0. As the electronegativity of the substituent increases, so does the extent of deshielding, and so does the chemical shift. This is evident when we look at the chemical shifts of methane and three halomethane compounds (remember that electronegativity increases as we move up a column in the periodic table, so fluorine is the most electronegative and bromine the least).

CH_4	CH_3Br	CH_3Cl	CH_3F
0.23 ppm	2.68 ppm	3.05 ppm	4.26 ppm

Table 2.4.4.1. ^{1}H NMR chemical shifts for CH_3X compounds.

To a large extent, then, we can predict trends in chemical shift by considering how much deshielding is taking place near a proton.

The chemical shift of trichloromethane (common name chloroform) is, as expected, higher than that of dichloromethane, which is in turn higher than that of chloromethane.

CH_4	CH_3Cl	CH_2Cl_2	$CHCl_3$
0.23 ppm	3.05 ppm	5.30 ppm	7.26 ppm

Table 2.4.4.2. ^{1}H NMR chemical shifts for $CH_{4-n}Cl_n$ compounds.

The deshielding effect of an electronegative substituent diminishes significantly with increasing distance.

Contributors

- Organic Chemistry With a Biological Emphasis by Tim Soderberg (University of Minnesota, Morris)

This page titled 2.8.5: The Basis for Differences in Chemical Shift is shared under a CC BY-NC-SA 4.0 license and was authored, remixed, and/or curated by Tim Soderberg.

CHAPTER OVERVIEW

Back Matter

Index

Glossary

Detailed Licensing

Index

A

achiral
5.5.3: Stereoisomers - Optical Isomerism in Transition Metal Complexes
acidity
4.3: Acidity of the Hexaaqua Ions
active site
6.2: Introduction to Amino Acids and Proteins
ambidentate ligands
5.5.4: Structural Isomers - Linkage Isomerism in Transition Metal Complexes
amino acids
6.2: Introduction to Amino Acids and Proteins
ammine ligands
5.8: Ligand Exchange Reactions (Thermodynamics)
antibonding
2.5.5: Molecular Orbital Diagrams
aqua ligands
5.8: Ligand Exchange Reactions (Thermodynamics)
Associative Substitution
6.4: Associative Ligand Substitution

B

base peak
1.1: Mass Spectrometry
bent
2.3: The VSEPR Model
Berry pseudorotation
6.4: Associative Ligand Substitution
Bicapped square antiprism geometry
5.3: Coordination Numbers and Geometry
birefringence
3.14: Structures Related to NaCl and NiAs
Bohr Atom
1.2: Rutherford's Atom
Bohr model
1.2: Rutherford's Atom
bond angle
2.3: The VSEPR Model
bond order
2.5.5: Molecular Orbital Diagrams
bond polarity
2.5.1: Molecular Shape and Molecular Polarity
bonding molecular orbital
2.5.5: Molecular Orbital Diagrams
Bragg equation
3.9: X-ray Crystallography

C

Capped octahedron
5.3: Coordination Numbers and Geometry
Capped trigonal prism
5.3: Coordination Numbers and Geometry
chelate effect
5.8: Ligand Exchange Reactions (Thermodynamics)
Chemical Equivalence
2.8.2: Chemical Equivalence
chemical shift
2.8.5: The Basis for Differences in Chemical Shift
chiral
5.5.3: Stereoisomers - Optical Isomerism in Transition Metal Complexes
chiral center
5.5.3: Stereoisomers - Optical Isomerism in Transition Metal Complexes
Cis isomers
5.5.2: Structural Isomers - Geometric Isomerism in Transition Metal Complexes
complex ion
4.2: Lewis Acids and Bases
4.3: Acidity of the Hexaaqua Ions
compression
5.6.5: Jahn-Teller Distortions
conservative forces
1.2: Rutherford's Atom
coordinate compound
5.5.3: Stereoisomers - Optical Isomerism in Transition Metal Complexes
coordinate covalent bond
4.2: Lewis Acids and Bases
coordination complex
5.6.2: Colors of Coordination Complexes
coordination complexes
5.6.2: Colors of Coordination Complexes
Coordination Compounds
5.1: Introduction to Coordination Chemistry
coordination number
5.3: Coordination Numbers and Geometry
Coulombic force
1.2: Rutherford's Atom
crystal field splitting
5.6.3: Crystal Field Stabilization Energy
crystal field stabilization energy
5.6.3: Crystal Field Stabilization Energy
crystal field theory
5.6: Crystal Field Theory
5.6.2: Colors of Coordination Complexes
5.6.3: Crystal Field Stabilization Energy
6.5: Dissociative Ligand Substitution
Cube
5.3: Coordination Numbers and Geometry
Cube geometry
5.3: Coordination Numbers and Geometry
cuboctahedron geometry
5.3: Coordination Numbers and Geometry

D

Debye (unit)
2.5.1: Molecular Shape and Molecular Polarity
diamagnetic
2.5.5: Molecular Orbital Diagrams
diamagnetic anisotropy
2.8.5: The Basis for Differences in Chemical Shift
diamagnetic deshielding
2.8.5: The Basis for Differences in Chemical Shift
diamagnetic shielding
2.8.5: The Basis for Differences in Chemical Shift
dipole moment
2.3: The VSEPR Model
2.5.1: Molecular Shape and Molecular Polarity
Dissocative Substitution
6.5: Dissociative Ligand Substitution
dissociation
6.5: Dissociative Ligand Substitution
dissociation constant
4.2: Lewis Acids and Bases
Dissociative Ligand Substitution
6.5: Dissociative Ligand Substitution
Dodecahedron
5.3: Coordination Numbers and Geometry
Dodecahedron Geometry
5.3: Coordination Numbers and Geometry
Drago and Wayland's EC Model
4.5: Quantitative Measures of Hardness and Softness

E

electromagnetic spectrum
5.6.2: Colors of Coordination Complexes
electron ionization
1.1: Mass Spectrometry
electronegativity (Mulliken)
4.5: Quantitative Measures of Hardness and Softness
Electronic Configurations
5.6.5: Jahn-Teller Distortions
Electrospray Ionization
1.1: Mass Spectrometry
elongation
5.6.5: Jahn-Teller Distortions
enzymes
6.2: Introduction to Amino Acids and Proteins

F

fluorite (structure)
3.15: Tetrahedral Structures
formation constant
4.2: Lewis Acids and Bases
Formation Constants
5.8: Ligand Exchange Reactions (Thermodynamics)

G

geometric isomers
5.5.2: Structural Isomers - Geometric Isomerism in Transition Metal Complexes

H

Hexaaqua Ions
4.3: Acidity of the Hexaaqua Ions
Hexagonal bipyramid
5.3: Coordination Numbers and Geometry
Hexagonal bipyramid geometry
5.3: Coordination Numbers and Geometry
Hexagonal planar Geometry
5.3: Coordination Numbers and Geometry
high spin
5.6.3: Crystal Field Stabilization Energy
5.6.5: Jahn-Teller Distortions
hybrid orbital
2.4: Hybrid Orbitals
hybridization
2.4: Hybrid Orbitals
hydrate isomer
5.5.1: Structural Isomers - Ionization Isomerism in Transition Metal Complexes

hydration
5.6.3: Crystal Field Stabilization Energy

I

ionic radius
4.3: Acidity of the Hexaaqua Ions
ionization isomerism
5.5.1: Structural Isomers - Ionization Isomerism in Transition Metal Complexes
isomerism
5.5.4: Structural Isomers - Linkage Isomerism in Transition Metal Complexes
isomers
5.5: Isomers
5.5.2: Structural Isomers - Geometric Isomerism in Transition Metal Complexes

K

Kapustinskii equation
3.23: Kapustinskii Equation

L

Lancashire
5.3: Coordination Numbers and Geometry
5.6.5: Jahn-Teller Distortions
Lenz's Law
5.6.7: Magnetism
Lewis acid
4.2: Lewis Acids and Bases
Lewis base
4.2: Lewis Acids and Bases
ligand
4.2: Lewis Acids and Bases
6.4: Associative Ligand Substitution
6.5: Dissociative Ligand Substitution
Ligand Exchange Reactions
5.8: Ligand Exchange Reactions (Thermodynamics)
linear
2.3: The VSEPR Model
low spin
5.6.3: Crystal Field Stabilization Energy
5.6.5: Jahn-Teller Distortions

M

M+1 peak (mass spec)
1.1: Mass Spectrometry
M+2 peak (mass spec)
1.1: Mass Spectrometry
Magnetic Moment
2.8.1: The Origin of the NMR Signal
magnetic moments
5.6.6: Magnetic Moments of Transition Metals
magnetic permeability
5.6.7: Magnetism
magnetism
5.6.7: Magnetism
mass spectrometry
1.1: Mass Spectrometry
McLafferty rearrangement
1.1: Mass Spectrometry
metallic bonding
2.6: The Range of Bonding
miller indicies
3.10: Miller Indices (hkl)
Mirror Image Method
5.5.3: Stereoisomers - Optical Isomerism in Transition Metal Complexes
molecular geometry
2.2: Molecular Shapes
molecular ion peak
1.1: Mass Spectrometry
molecular ions
1.1: Mass Spectrometry
molecular orbital
2.5.5: Molecular Orbital Diagrams
Molecular orbital diagram
2.5.5: Molecular Orbital Diagrams

N

NMR
2.8.1: The Origin of the NMR Signal
2.8.2: Chemical Equivalence
2.8.3: The 1H-NMR experiment
2.8.4: Spin-Spin Coupling
2.8.5: The Basis for Differences in Chemical Shift

O

octahedral
2.3: The VSEPR Model
5.3: Coordination Numbers and Geometry
Octahedral Preference
5.6.3: Crystal Field Stabilization Energy
Octahedral Site Preference Energy
5.6.3: Crystal Field Stabilization Energy
Optical Isomers
5.5.3: Stereoisomers - Optical Isomerism in Transition Metal Complexes
optical isomers (complex ions)
5.5.3: Stereoisomers - Optical Isomerism in Transition Metal Complexes
organometallic
6.4: Associative Ligand Substitution

P

paramagnetic
2.5.5: Molecular Orbital Diagrams
parent peak
1.1: Mass Spectrometry
Pearson's absolute hardness
4.5: Quantitative Measures of Hardness and Softness
Pentagonal Bipyramid
5.3: Coordination Numbers and Geometry
Peptide bond
6.2: Introduction to Amino Acids and Proteins
Plane of Symmetry Method
5.5.3: Stereoisomers - Optical Isomerism in Transition Metal Complexes
polar covalent bond
2.5.1: Molecular Shape and Molecular Polarity
polarimeter
5.5.3: Stereoisomers - Optical Isomerism in Transition Metal Complexes
Polarimetry
5.5.3: Stereoisomers - Optical Isomerism in Transition Metal Complexes
Pourbaix diagrams
6.3.6: Pourbaix Diagrams
proteins
6.2: Introduction to Amino Acids and Proteins
proteomics
1.1: Mass Spectrometry

R

radical cation
1.1: Mass Spectrometry
radius
4.3: Acidity of the Hexaaqua Ions
rate law
6.4: Associative Ligand Substitution
reaction kinetics
6.4: Associative Ligand Substitution
6.5: Dissociative Ligand Substitution

S

seesaw
2.3: The VSEPR Model
soft ionization
1.1: Mass Spectrometry
solvents
2.8.3: The 1H-NMR experiment
sp hybrid orbital
2.4: Hybrid Orbitals
sp2 hybrid orbital
2.4: Hybrid Orbitals
sp3 hybrid orbital
2.4: Hybrid Orbitals
sp3d hybrid orbital
2.4: Hybrid Orbitals
sp3d2 hybrid orbital
2.4: Hybrid Orbitals
spectrochemical series
5.6.2: Colors of Coordination Complexes
spectroscopy
2.8.1: The Origin of the NMR Signal
2.8.2: Chemical Equivalence
2.8.3: The 1H-NMR experiment
2.8.4: Spin-Spin Coupling
2.8.5: The Basis for Differences in Chemical Shift
spin pairing energy
5.6.3: Crystal Field Stabilization Energy
Square antiprism
5.3: Coordination Numbers and Geometry
Square antiprism geometry
5.3: Coordination Numbers and Geometry
Square Planar Geometry
5.3: Coordination Numbers and Geometry
Square pyramid Geometry
5.3: Coordination Numbers and Geometry
square pyramidal
2.3: The VSEPR Model
Stability Constants
5.8: Ligand Exchange Reactions (Thermodynamics)
steady state approximation
6.5: Dissociative Ligand Substitution
stereochemistry
6.4: Associative Ligand Substitution
6.5: Dissociative Ligand Substitution
stereoisomers
5.5: Isomers
structural isomers
5.5: Isomers
5.5.4: Structural Isomers - Linkage Isomerism in Transition Metal Complexes

substitution
6.4: Associative Ligand Substitution
substrate
6.2: Introduction to Amino Acids and Proteins
symmetry elements
2.7.1: Symmetry Elements and Operations
symmetry operations
2.7.1: Symmetry Elements and Operations

T

tetrahedral
2.2: Molecular Shapes
2.3: The VSEPR Model
tetrahedral geometry
5.3: Coordination Numbers and Geometry
thermodynamics
5.8: Ligand Exchange Reactions (Thermodynamics)
Trans Isomers
5.5.2: Structural Isomers - Geometric Isomerism in Transition Metal Complexes
Transition Metal Complexes
5.5.1: Structural Isomers - Ionization Isomerism in Transition Metal Complexes
5.5.2: Structural Isomers - Geometric Isomerism in Transition Metal Complexes
5.5.4: Structural Isomers - Linkage Isomerism in Transition Metal Complexes
Trigonal Bipyramid Geometry
5.3: Coordination Numbers and Geometry
trigonal bipyramidal
2.3: The VSEPR Model
trigonal planar
2.3: The VSEPR Model
Trigonal planar Geometry
5.3: Coordination Numbers and Geometry
Trigonal prism Geometry
5.3: Coordination Numbers and Geometry
Trigonal pyramid Geometry
5.3: Coordination Numbers and Geometry
trigonal pyramidal
2.3: The VSEPR Model

U

Unsaturated Intermediate
6.5: Dissociative Ligand Substitution

V

valence bond theory
2.4: Hybrid Orbitals
valence shell electron pair repulsion theory
2.3: The VSEPR Model
VSEPR
2.3: The VSEPR Model

Glossary

Sample Word 1 | Sample Definition 1

Detailed Licensing

Overview

Title: CHEM 211: Foundational Inorganic Chemistry (Nataro)

Webpages: 121

Applicable Restrictions: Noncommercial

All licenses found:

- Undeclared: 60.3% (73 pages)
- CC BY-SA 4.0: 25.6% (31 pages)
- CC BY-NC-SA 4.0: 11.6% (14 pages)
- CC BY-NC 4.0: 1.7% (2 pages)
- CC BY 4.0: 0.8% (1 page)

By Page

- CHEM 211: Foundational Inorganic Chemistry (Nataro) - *Undeclared*
  - Front Matter - *Undeclared*
    - TitlePage - *Undeclared*
    - InfoPage - *Undeclared*
    - Table of Contents - *Undeclared*
    - Licensing - *Undeclared*
  - 1: Atoms - *Undeclared*
    - 1.1: Mass Spectrometry - *CC BY-NC-SA 4.0*
    - 1.2: Rutherford's Atom - *Undeclared*
    - 1.3: Bohr's Atom - *Undeclared*
    - 1.4: Hydrogen Atom - *Undeclared*
    - 1.5: Slater Rules - *Undeclared*
  - 2: Molecules - *Undeclared*
    - 2.2: Molecular Shapes - *CC BY-NC-SA 4.0*
    - 2.3: The VSEPR Model - *CC BY-NC-SA 4.0*
    - 2.4: Hybrid Orbitals - *CC BY-NC-SA 4.0*
    - 2.5: Molecular Orbitals - *Undeclared*
      - 2.5.1: Molecular Shape and Molecular Polarity - *CC BY-NC-SA 4.0*
      - 2.5.2: Prelude to Molecular Orbital Theory - *Undeclared*
      - 2.5.3: Constructing Molecular Orbitals from Atomic Orbitals - *CC BY-SA 4.0*
      - 2.5.4: Orbital Symmetry - *CC BY-SA 4.0*
      - 2.5.5: Molecular Orbital Diagrams - *CC BY-SA 4.0*
      - 2.5.6: π Orbitals and Diatomic Molecules - *CC BY-SA 4.0*
      - 2.5.7: Orbital Filling - *CC BY-SA 4.0*
      - 2.5.8: δ orbitals - *CC BY-SA 4.0*
    - 2.6: The Range of Bonding - *CC BY-SA 4.0*
    - 2.7: Advanced Bonding - *Undeclared*
      - 2.7.1: Symmetry Elements and Operations - *Undeclared*
      - 2.7.2: Point Groups - *Undeclared*
        - 2.7.2.1: Other Groups - *Undeclared*
        - 2.7.2.2: Groups of Low and High Symmetry - *Undeclared*
      - 2.7.3: Ligand Group Orbitals and Generator Functions - *Undeclared*
      - 2.7.4: Expanded Octets and Molecular Orbitals - *Undeclared*
    - 2.8: Nuclear Magnetic Resonance (NMR) - *Undeclared*
      - 2.8.1: The Origin of the NMR Signal - *CC BY-NC-SA 4.0*
      - 2.8.2: Chemical Equivalence - *CC BY-NC-SA 4.0*
      - 2.8.3: The 1H-NMR experiment - *CC BY-NC-SA 4.0*
      - 2.8.4: Spin-Spin Coupling - *CC BY-NC-SA 4.0*
      - 2.8.5: The Basis for Differences in Chemical Shift - *CC BY-NC-SA 4.0*
    - Back Matter - *Undeclared*
      - Index - *Undeclared*
      - Glossary - *Undeclared*
      - Detailed Licensing - *Undeclared*
  - 3: Solid state - *Undeclared*
    - 3.1: Prelude to Metals and Alloys - *Undeclared*
    - 3.2: Unit Cells and Crystal Structures - *CC BY-SA 4.0*
    - 3.3: Crystal Structures of Metals - *CC BY-SA 4.0*
    - 3.4: Conduction in Metals - *CC BY-SA 4.0*
    - 3.5: Atomic Orbitals and Magnetism - *CC BY-SA 4.0*

- 3.6: Ferro-, Ferri- and Antiferromagnetism - *CC BY-SA 4.0*
- 3.7: Hard and Soft Magnets - *CC BY-SA 4.0*
- 3.8: Defects in Metallic Crystals - *CC BY-SA 4.0*
- 3.9: X-ray Crystallography - *Undeclared*
- 3.10: Miller Indices (hkl) - *Undeclared*
- 3.11: Powder X-ray Diffraction - *Undeclared*
- 3.12: Prelude to Ionic and Covalent Solids - Structures - *Undeclared*
- 3.13: Close-packing and Interstitial Sites - *CC BY-SA 4.0*
- 3.14: Structures Related to NaCl and NiAs - *CC BY-SA 4.0*
- 3.15: Tetrahedral Structures - *CC BY-SA 4.0*
- 3.16: Layered Structures and Intercalation Reactions - *CC BY-SA 4.0*
- 3.17: Ionic Radii and Radius Ratios - *CC BY-SA 4.0*
- 3.18: Structure Maps - *CC BY-SA 4.0*
- 3.19: Energetics of Crystalline Solids- The Ionic Model - *CC BY-SA 4.0*
- 3.20: Born-Haber Cycles for NaCl and Silver Halides - *CC BY-SA 4.0*
- 3.21: Lattice Energies and Solubility - *CC BY-SA 4.0*
- 3.22: Spinel, Perovskite, and Rutile Structures - *CC BY-SA 4.0*
- 3.23: Kapustinskii Equation - *CC BY-SA 4.0*

4: Acid-Base Theories - *Undeclared*

- 4.1: Bronsted-Lowry acids and bases - *Undeclared*
- 4.2: Lewis Acids and Bases - *CC BY 4.0*
- 4.3: Acidity of the Hexaaqua Ions - *CC BY-NC 4.0*
- 4.4: Hard-soft Acids and Bases - *Undeclared*
- 4.5: Quantitative Measures of Hardness and Softness - *Undeclared*

5: Coordination Chemistry - *Undeclared*

- 5.1: Introduction to Coordination Chemistry - *Undeclared*
- 5.2: Ligands and Nomenclature - *Undeclared*
- 5.3: Coordination Numbers and Geometry - *Undeclared*
- 5.4: Bonding with d-orbitals - *CC BY-SA 4.0*
- 5.5: Isomers - *Undeclared*
  - 5.5.1: Structural Isomers - Ionization Isomerism in Transition Metal Complexes - *Undeclared*
  - 5.5.2: Structural Isomers - Geometric Isomerism in Transition Metal Complexes - *Undeclared*
  - 5.5.3: Stereoisomers - Optical Isomerism in Transition Metal Complexes - *Undeclared*
  - 5.5.4: Structural Isomers - Linkage Isomerism in Transition Metal Complexes - *Undeclared*
- 5.6: Crystal Field Theory - *Undeclared*
  - 5.6.1: Crystal Field Theory - *CC BY-NC-SA 4.0*
  - 5.6.2: Colors of Coordination Complexes - *Undeclared*
  - 5.6.3: Crystal Field Stabilization Energy - *Undeclared*
  - 5.6.4: Factors That Affect the Magnitude of Δo - *Undeclared*
  - 5.6.5: Jahn-Teller Distortions - *Undeclared*
  - 5.6.6: Magnetic Moments of Transition Metals - *Undeclared*
  - 5.6.7: Magnetism - *Undeclared*
  - 5.6.8: Thermodynamics and Structural Consequences of d-Orbital Splitting - *CC BY-NC-SA 4.0*
- 5.7: Ligand Field Theory - *Undeclared*
- 5.8: Ligand Exchange Reactions (Thermodynamics) - *CC BY-NC 4.0*
- 5.9: Electronic Spectra of Coordination Compounds - *Undeclared*

6: Bioinorganic Chemistry - *Undeclared*

- 6.1: Biological Significance of Iron, Zinc, Copper, Molybdenum, Cobalt, Chromium, Vanadium, and Nickel - *Undeclared*
- 6.2: Introduction to Amino Acids and Proteins - *CC BY-NC-SA 4.0*
- 6.3: Redox Reactions - *Undeclared*
  - 6.3.1: Introduction to Redox Reactions - *CC BY-SA 4.0*
  - 6.3.2: Balancing Redox Reactions - *CC BY-SA 4.0*
  - 6.3.3: Electrochemical Potentials - *CC BY-SA 4.0*
  - 6.3.4: Prelude to Redox Stability and Redox Reactions - *Undeclared*
  - 6.3.5: Latimer and Frost Diagrams - *CC BY-SA 4.0*
  - 6.3.6: Pourbaix Diagrams - *CC BY-SA 4.0*
- 6.4: Associative Ligand Substitution - *Undeclared*
- 6.5: Dissociative Ligand Substitution - *Undeclared*
- 6.6: Biological Significance of Iron, Zinc, Copper, Molybdenum, Cobalt, Chromium, Vanadium, and Nickel - *Undeclared*
- 6.7: Ferrodoxins, Hydrogenases, and Nitrogenases - Metal-Sulfide Proteins - *Undeclared*
  - 6.7.1: Iron-sulfur Proteins and Models - *Undeclared*
  - 6.7.2: Iron-sulfur Proteins and Models (Part 2) - *Undeclared*
  - 6.7.3: Iron-sulfur Proteins and Models (Part 3) - *Undeclared*

- 6.7.4: Iron-sulfur Proteins and Models (Part 4) - *Undeclared*
- 6.8: Overview of Hemoglobin and Myoglobin - *Undeclared*
  - 6.8.1: Myoglobin, Hemoglobin, and their Ligands - *CC BY-NC-SA 4.0*
  - 6.8.2: Oxygen Transport by the Proteins Myoglobin and Hemoglobin - *Undeclared*
- Back Matter - *Undeclared*
  - Index - *Undeclared*
  - Glossary - *Undeclared*
  - Glossary - *Undeclared*
  - Detailed Licensing - *Undeclared*

CHAPTER OVERVIEW

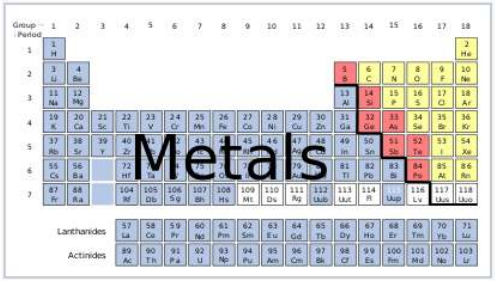
3: Solid state

3.1: Prelude to Metals and Alloys
3.2: Unit Cells and Crystal Structures
3.3: Crystal Structures of Metals
3.4: Conduction in Metals
3.5: Atomic Orbitals and Magnetism
3.6: Ferro-, Ferri- and Antiferromagnetism
3.7: Hard and Soft Magnets
3.8: Defects in Metallic Crystals
3.9: X-ray Crystallography
3.10: Miller Indices (hkl)
3.11: Powder X-ray Diffraction
3.12: Prelude to Ionic and Covalent Solids - Structures
3.13: Close-packing and Interstitial Sites
3.14: Structures Related to NaCl and NiAs
3.15: Tetrahedral Structures
3.16: Layered Structures and Intercalation Reactions
3.17: Ionic Radii and Radius Ratios
3.18: Structure Maps
3.19: Energetics of Crystalline Solids- The Ionic Model
3.20: Born-Haber Cycles for NaCl and Silver Halides
3.21: Lattice Energies and Solubility
3.22: Spinel, Perovskite, and Rutile Structures
3.23: Kapustinskii Equation

3: Solid state is shared under a not declared license and was authored, remixed, and/or curated by LibreTexts.

3.1: Prelude to Metals and Alloys

In the chemistry of molecular compounds, we are accustomed to the idea that properties depend strongly on structure. For example we can rationalize the polarity of the water molecule based on its shape. We also know that two molecules with the same composition (e.g., ethanol and dimethyl ether) have very different properties based on the bonding arrangements of atoms. It should come as no surprise that the properties of extended solids are also connected to their structures, and so to understand what they do we should begin with their crystal structures. Most of the metals in the periodic table have relatively simple structures and so this is a good place to begin.



Over 2/3 of the elements in the periodic table exist in their pure form as metals. All elemental metals (except the three - Cs, Ga, Hg - that are liquid) are crystalline solids at room temperature, and most have one of three simple crystal structures.

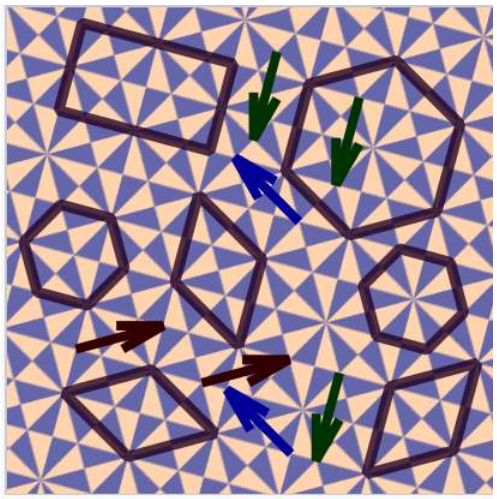
3.1: Prelude to Metals and Alloys is shared under a not declared license and was authored, remixed, and/or curated by LibreTexts.

- **6.1: Prelude to Metals and Alloys** by Chemistry 310 is licensed CC BY-SA 4.0. Original source: https://en.wikibooks.org/wiki/Introduction_to_Inorganic_Chemistry.

3.2: Unit Cells and Crystal Structures

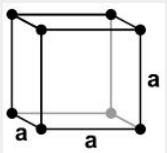
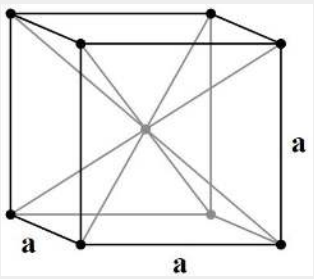
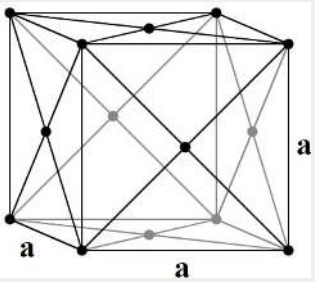
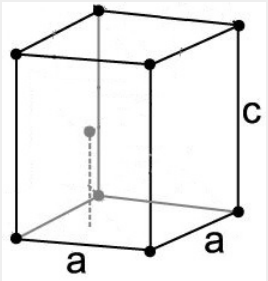
Crystals can be thought of as repeating patterns, much like wallpaper or bathroom tiles, but in three dimensions. The fundamental repeating unit of the crystal is called the **unit cell**. It is a three dimensional shape that can be repeated over and over by unit translations to fill space (and leave minimal gaps) in the structure. Some possible unit cells are shown in the tiling pattern at the right, along with arrows that indicate **unit translation vectors**. In three dimensions, the hexagonal or rhombic unit cells of this pattern would be replaced by three dimensional boxes that would stack together to fill all space. As shown in the figure, the origin of the unit cell is arbitrary. The same set of boxes will fill all space no matter where we define the origin of the lattice. We will see that pure metals typically have very simple crystal structures with cubic or hexagonal unit cells. However the crystal structures of alloys can be quite complicated.

When considering the crystal structures of metals and alloys, it is not sufficient to think of each atom and its neighboring ligands as an isolated system. Instead, think of the entire metallic crystal as a network of atoms connected by a sea of shared valence electrons. The **electrons are delocalized** because there are **not enough of them** to fill each "bond" between atoms with an electron pair. For example, in the crystal structures of s-block and p-block metals, each atom has either 8 or 12 nearest neighbors, but the maximum number of s + p electrons is 8. Thus, there are not enough to put two electrons between each pair of atoms. Transition metals can also use their d-orbitals in bonding, but again there are never enough electrons to completely fill all the "bonds."



Possible unit cells in a periodic tile pattern. The arrows connect translationally equivalent points (lattice points) in the pattern.

The atoms in a metal lattice arrange themselves in a certain pattern which can be represented as a 3D box structure known as the **unit cell** which repeats across the entire metal.

Simple Cubic	Body Centered Cubic	Face Centered Cubic	Hexagonal Close Packed
			
1 atom/cell	2 atoms/cell	4 atoms/cell	2 atoms/cell

Metal atoms can be approximated as spheres, and therefore are not 100 % efficient in packing, the same way a stack of cannonballs has some empty spaces between the balls. Different unit cells have different packing efficiencies. The number of atoms that is

included in the unit cell only includes the fractions of atoms *inside* of the box. Atoms on the corners of the unit cell count as ⅛ of an atom, atoms on a face count as ½, an atom in the center counts as a full atom. Using this, let's calculate the number of atoms in a simple cubic unit cell, a face centered cubic (fcc) unit cell, and a body centered cubic (bcc) unit cell.

Simple Cubic:

8 corner atoms × ⅛ = 1 atom/cell. The packing in this structure is not efficient (52%) and so this structure type is very rare for metals.

Body Centered Cubic, bcc:

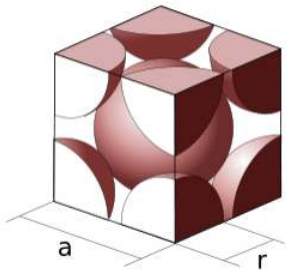
(8 corner atoms × ⅛) + (1 center atom × 1)= 2 atoms/cell. The packing is more efficient (68%) and the structure is a common one for alkali metals and early transition metals. Alloys such as brass (CuZn) also adopt these structures.

Face Centered Cubic, fcc (also called Cubic Close Packed, ccp):

(8 corner atoms × ⅛)+ (6 face atoms × ½)= 4 atoms/cell. This structure, along with its hexagonal relative (hcp), has the most efficient packing (74%). Many metals adopt either the fcc or hcp structure.

Hexagonal Close Packed, hcp:

Like the fcc structure, the packing density of hcp is 74%.

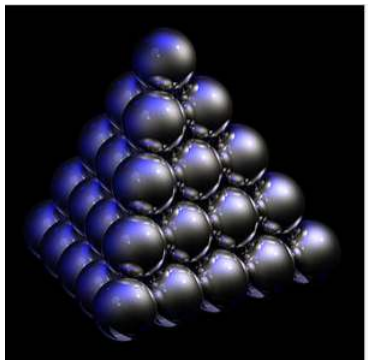


The unit cell of a bcc metal contains two atoms.

Calculating the packing fraction. The packing fractions of the crystal structures shown above can be calculated by dividing the volume of the atoms in the cell by the volume of the cell itself. The volume of the atoms in the cell is equal to the number of atoms/cell times the volume of a sphere, $(4/3)\pi r^3$. The volume of the cubic cells is found by cubing the side length. As an example, let's calculate the packing efficiency of a simple cubic unit cell. As we saw earlier in the section, a simple cubic unit cell contains one atom. The side length of the simple cubic unit cell is 2r, since the centers of each atom occupy the corners of the unit cell.

$$\text{Packing efficiency} = \frac{(1\ atom) \times (\frac{4}{3})\pi r^3}{(2r)^3} = 0.523 \tag{3.2.1}$$

The same method can be applied to bcc and fcc structures.



Face-centered cubic stack of cannonballs.

3.2: Unit Cells and Crystal Structures is shared under a CC BY-SA license and was authored, remixed, and/or curated by LibreTexts.

- **6.2: Unit Cells and Crystal Structures** by Chemistry 310 is licensed CC BY-SA 4.0. Original source: https://en.wikibooks.org/wiki/Introduction_to_Inorganic_Chemistry.

3.3: Crystal Structures of Metals

Crystal structures

Most metals and alloys crystallize in one of three very common structures: body-centered cubic (bcc), hexagonal close packed (hcp), or cubic close packed (ccp, also called face centered cubic, fcc). In all three structures the coordination number of the metal atoms (i.e., the number of equidistant nearest neighbors) is rather high: 8 for bcc, and 12 for hcp and ccp. We can contrast this with the low coordination numbers (i.e., low valences - like 2 for O, 3 for N, or 4 for C) found in nonmetals. Atoms in metallic crystals have a tendency to pack in dense arrangments that fill space efficiently.

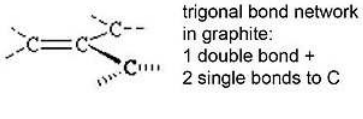
Periodic trends in structure and metallic behavior

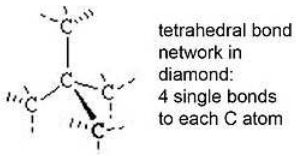
Remember where we find the metallic elements in the periodic table - everywhere except the upper right corner. This means that as we go down a group in the p-block (let's say, group IVA, the carbon group, or group VA, the nitrogen group), the properties of the elements gradually change from nonmetals to metalloids to metals. The carbon group nicely illustrates the transition. Starting at the top, the element carbon has two stable allotropes - graphite and diamond. In each one, the valence of carbon atoms is exactly satisfied by making four electron pair bonds to neighboring atoms. In graphite, each carbon has three nearest neighbors, and so there are two single bonds and one double bond. In diamond, there are four nearest neighbors situated at the vertices of a tetrahedron, and so there is a single bond to each one.

The two elements right under carbon (silicon and germanium) in the periodic table also have the diamond structure (recall that these elements cannot make double bonds to themselves easily, so there is no graphite allotrope for Si or Ge). While diamond is a good insulator, both silicon and germanium are semiconductors (i.e., metalloids). Mechanically, they are hard like diamond. Like carbon, each atom of Si and Ge satisfies its valence of four by making single bonds to four nearest neighbors.

The next element under germanium is tin (Sn). Tin has two allotropes, one with the diamond structure, and one with a slightly distorted bcc structure. The latter has metallic properties (metallic luster, malleability), and conductivity about 10^9 times higher than Si. Finally, lead (Pb), the element under Sn, has the ccp structure, and also is metallic. Note the trends in coordination number and conducting properties:

Element	Structure	Coord. no.	Conductivity
C	graphite, diamond	3, 4	semimetal, insulator
Si	diamond	4	semiconductor
Ge	diamond	4	semiconductor
Sn	diamond, distorted bcc	4, 8	semiconductor, metal
Pb	ccp	12	metal





The elements C, Si, and Ge obey the octet rule, and we can easily identify the electron pair bonds in their structures. Sn and Pb, on the other hand, adopt structures with high coordination numbers. They *do not have enough valence electrons* to make electron pair bonds to each neighbor (this is a common feature of metals). What happens in this case is that the valence electrons become "smeared out" or delocalized over all the atoms in the crystal. It is best to think of the bonding in metals as a crystalline arrangement of positively charged cores with a "sea" of shared valence electrons gluing the structure together. Because the electrons are not localized in any particular bond between atoms, they can move in an electric field, which is why metals conduct electricity well. Another way to describe the bonding in metals is nondirectional. That is, an atom's nearest neighbors surround it in every direction, rather than in a few particular directions (like at the corners of a tetrahedron, as we found for diamond). Nonmetals

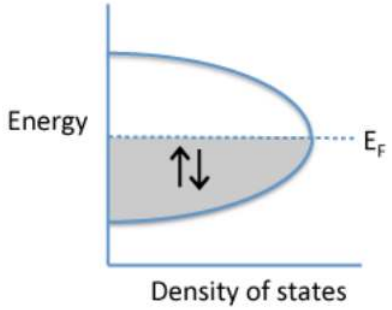
(insulators and semiconductors), on the other hand, have directional bonding. Because the bonding is non-directional and coordination numbers are high, it is relatively easy to deform the coordination sphere (i.e., break or stretch bonds) than it is in the case of a nonmetal. This is why elements like Pb are much more malleable than C, Si, or Ge.

3.3: Crystal Structures of Metals is shared under a CC BY-SA license and was authored, remixed, and/or curated by LibreTexts.

- **6.4: Crystal Structures of Metals** by Chemistry 310 is licensed CC BY-SA 4.0. Original source: https://en.wikibooks.org/wiki/Introduction_to_Inorganic_Chemistry.

3.4: Conduction in Metals

In metals, the valence electrons are in molecular orbitals that extend over the entire crystal lattice. Metals are almost always crystalline and the individual crystal grains are typically micron size. This means that the spatial extent of the orbitals is *very large* compared to the size of the atoms or the unit cell. The diagram shows a generic plot of electron energy vs. density of states for a metal such as Na, Cu, or Ag. In these cases, there are N orbitals for N electrons, and each orbital can accommodate two electrons. Therefore the Fermi level, which corresponds to the energy of the highest occupied MO at zero temperature, is somewhere in the middle of the band of orbitals. The energy level spacing between orbitals is very small compared to the thermal energy kT, so we can think of the orbitals as forming a continuous band.



Classically, if the electrons in this band were free to be thermally excited, we would expect them to have a specific heat of 3R per mole of electrons. However, experimentally we observe that C_p is only about 0.02 R per mole. This suggests that *only about 1%* of the electrons in the metal can be thermally excited at room temperature. However, essentially *all* of the valence electrons are free to move in the crystal and contribute to electrical conduction. To understand this apparent paradox, we need to recall that the electrons exist in *quantized energy levels.*

Because of quantization, electrons in metals have a Fermi-Dirac distribution of energies. In this distribution, most of the electrons are spin-paired, although the individual electrons in these pairs can be quite far apart since the orbitals extend over the entire crystal. A relatively small number of electrons at the top of the Fermi sea are unpaired by thermal excitation. This is the origin of the Pauli paramagnetism of metals.

How fast are electrons traveling in a typical metal? Because of the bell shape of the E vs. DOS curve, most of the electrons have $E \approx E_F$. At the midpoint energy (E_F) of the band, the MO's have one node for every two atoms. We can calculate the de Broglie wavelength as twice the distance between nodes and thus:

$\lambda = \mathbf{4a}$ at the midpoint of the band.

where **a** is the interatomic spacing. Since a typical value of **a** is about 2 Å, we obtain the **de Broglie wavelength λ ≈ 8 Å**.

Using the de Broglie relation p = h/λ, we can write:

$$\mathbf{p = \frac{h}{\lambda} = m_e v_F} \tag{3.4.1}$$

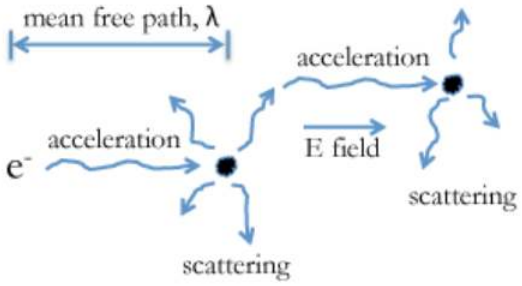
where $\mathbf{m_e}$ is the mass of the electron and $\mathbf{v_F}$ is the velocity of electrons with energy E_F.

Solving for $V_F = \frac{h}{m_e \lambda}$ we obtain $\mathbf{v_F = \frac{(6.62\times10^{-34} Js)}{(9.1\times10^{-31} kg)(8\times10^{-10} m)} = 1.0 \times 10^6 m/s}$

Experimental values of v_F are 1.07 x 10^6 and 1.39 x 10^6 m/s for Na and Ag, respectively, so our approximations are pretty good.

How fast are electrons moving in metals? Really, really fast!! **1,000,000 meters per second!** This is about 1/300 the speed of light, and about 3000 times the speed of sound in air (3 x 10^2 m/s).

However, the **drift velocity** of electrons in metals - the speed at which electrons move in applied electric field - is quite slow, on the order of 0.0001 m/s, or .01 cm/s. You can easily outrun an electron drifting in a metal, even if you have been drinking all night and have been personally reduced to a very slow crawl.



In order to understand the great disparity between the Fermi velocity and the drift velocity of electrons in metals, we need to consider a picture for the scattering of electrons, and their acceleration in an electric field, as shown at the left. If we apply a voltage across a metal (e.g., a metal wire), the electrons are subjected to an electric field **E**, which is the voltage divided by the length of the wire. This electric field exerts a force on the electron, causing it to accelerate. However, the electron is frequently scattered, mostly by phonons (lattice vibrations). Each time the electron is scattered its acceleration starts all over again. The time between scattering events is **τ** and the distance the electrons travel between scattering events is the **mean free path**, **λ**. (Note that this is NOT the same λ as the de Broglie wavelength, they just unfortunately have the same symbol!)

We can write the force on the electron as:

$$\mathbf{F = eE = m_e a = \frac{m_e v_{drift}}{\tau}} \tag{3.4.2}$$

In this equation, **a** is the acceleration in the electric field, $\mathbf{m_e}$ is the mass, and v_{drift} is the **drift velocity** of the electron.

Experimentally, the mean free path is typically obtained by measuring the scattering time. For an electron in Cu metal at 300 K, the scattering time τ is about 2 x 10^{-14} s. From this we can calculate the mean free path as:

$$\mathbf{\lambda = v_{avg}\tau \approx v_F\tau = (1 \times 10^6 m/s)(2 \times 10^{-14}) = 40nm} \tag{3.4.3}$$

The mean free path (40 nm = 400 Å) is quite long compared to the interatomic spacing (2 Å). To put it in perspective, if the interatomic spacing were scaled to the length of a football (0.3 m), the mean free path would be over half the length of the football field (60 m). Thus an electron travels a fairly long way between scattering events and scarcely notices the atomic structure of the metal in which it is traveling.

To summarize, electrons are traveling in metals at the Fermi velocity v_F, which is very, very fast (10^6 m/s), but the flux of electrons is the same in all directions. That is, they are *going nowhere fast*. In an electric field, a very small but directional *drift velocity* is superimposed on this fast random motion of valence electrons.

From F = ma, we obtain the acceleration (a) as:We can calculate the drift velocity of electrons as the acceleration in the electric field times the scattering time:

$$\mathbf{a = \frac{F}{m_e} = \frac{eE}{m_e}} \tag{3.4.4}$$

And thus,

$$\mathbf{v_{drift} = a\tau = \frac{eE\tau}{m_e}} \tag{3.4.5}$$

If we divide both sides of this equation by the magnitude of the electric field (**E**), we obtain the **mobility (μ)**:

$$\mathbf{\mu = \frac{v_{drift}}{E} = \frac{e\tau}{m_e}} \tag{3.4.6}$$

μ has units of velocity/field = cm/s / V/cm = cm^2/Vs

An important consequence of the calculation of v_{drift} is **Ohm's Law**, V = iR. From the equations above, we can see that the drift velocity increases linearly with the applied electric field. The drift velocity (cm/s) is proportional to the current (i, coul/s), and the electric field (E, V/cm) is proportional to the voltage (V):

$$\textbf{Current (i)} = \textbf{nev}_{\textbf{drift}} \times \textbf{area} \tag{3.4.7}$$

$$\textbf{Voltage (V)} = \textbf{E} \times \textbf{length} \tag{3.4.8}$$

Here **n** is the density of valence electrons (#/cm^3) and **e** is the charge of the electron (coul). Combining these equations with our equation for v_{drift} we obtain:

$$V = i(\frac{m_e}{ne^2\tau})\frac{(}{length}area) = iR \tag{3.4.9}$$

Thus, V = iR, where R is the combination of the two terms in parentheses. The first of these is the **resistivity**, ρ, and the second is a geometrical factor.

The **conductivity (σ)** of a metal, which is the inverse of ρ, is proportional to μ, which in turn is proportional to τ (and λ):

$$\sigma = \textbf{ne}\mu = \frac{\textbf{ne}^2\tau}{\textbf{m}_\textbf{e}} \tag{3.4.10}$$

We can use this equation to work out the conductivity of a specific metal (Cu), for which n = 8.5 x 10^{22} cm^{-3} and τ = 2 x 10^{-14} s. Putting in the numbers for m_e and e, we obtain σ = 7 x 10^5 Ω^{-1} cm^{-1} for Cu, in good agreement with the measured value (6 x 10^5 $\Omega^{-1}cm^{-1}$).

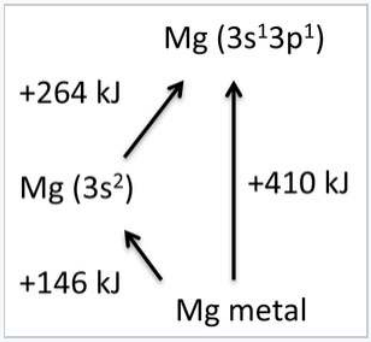
3.4: Conduction in Metals is shared under a CC BY-SA license and was authored, remixed, and/or curated by LibreTexts.

- **6.6: Conduction in Metals** by Chemistry 310 is licensed CC BY-SA 4.0. Original source: https://en.wikibooks.org/wiki/Introduction_to_Inorganic_Chemistry.

3.5: Atomic Orbitals and Magnetism

The MO picture we developed in Section 6.4 helps us rationalize the electrical conductivity of Na ($3s^1$), but what about Mg, which (as an atom in the gas phase) has a $3s^2$ electronic configuration? The two valence electrons are spin-paired in atomic Mg, as they are in the helium atom ($1s^2$). When the 3s orbitals of Mg combine to form a band, we would expect the band to be completely filled, since Mg has two electrons per orbital. By this reasoning, solid Mg should be an insulator. But Mg has all the properties of a metal: high electrical and thermal conductivity, metallic luster, malleability, etc. In this case the 3s and 3p bands are sufficiently broad (because of strong orbital overlap between Mg atoms) that they form a continuous band. This band, which contains a total of four orbitals (one 3s and three 3p) per atom, is only partially filled by the two valence electrons.

Another way to think about this is to consider the **hybridization** of the 3s and 3p electrons in Mg. Hybridization requires promotion from the $3s^23p^0$ ground state of an Mg atom to a $3s^13p^1$ excited state. The **promotion energy** (+264 kJ/mol) is more than offset by the **bonding energy** (-410 kJ/mol), the energy released when gaseous atoms in the excited state condense to form the metallic solid. The heat of vaporization, or the cohesive energy of a metal, is the difference between the bonding energy and the promotion energy. Experimentally, we can measure the vaporization energy (+146 kJ/mol) and the promotion energy and use them to calculate the bonding energy. From this we learn that each s or p electron is worth about 200 kJ/mol in bonding energy. The concepts of promotion energy and bonding energy are very useful in rationalizing periodic trends in the bond strengths and magnetic properties of metals, which are described below.

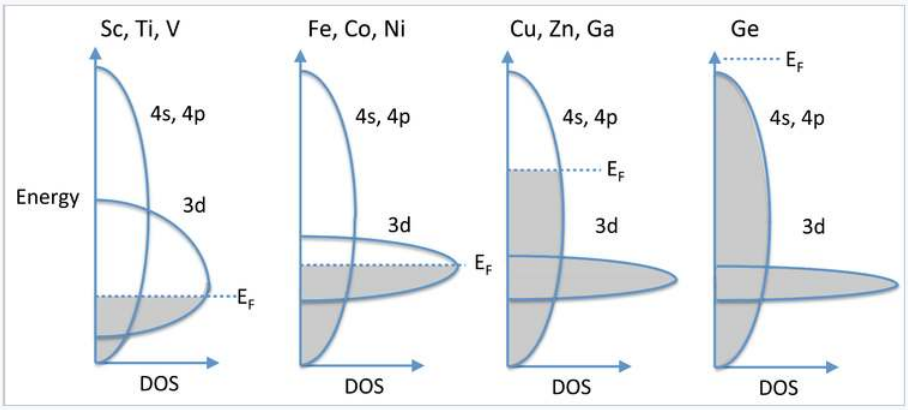


The cohesive energy of Mg metal is the difference between the bonding and promotion energies. The ground state of a gas phase Mg atom is $[Ar]3s^2$, but it can be promoted to the $[Ar]3s^13p^1$ state, which is 264 kJ/mol above the ground state. Mg uses two electrons per atom to make bonds, and the sublimation energy of the metal is 146 kJ/mol.

Filling of the 3d and 4s,4p bands

In the 3d series, we see magnetic behavior for elements and alloys between Cr and Ni. Past Ni, the elements (Cu, Zn, Ga,...) are no longer magnetic and they are very good electrical conductors, implying that their valence electrons are highly delocalized. We can understand this behavior by considering the overlap of 4s, 4p, and 3d orbitals, all of which are close in energy. The 4s and 4p have strong overlap and form a broad, continuous band. On the other hand, the 3d electrons are contracted and form a relatively narrow band. Progressing from the early 3d elements (Sc, Ti, V), we begin to fill the 3d orbitals, which are not yet so contracted that they cannot contribute to bonding. Thus, the valence electrons in Sc, Ti, and V are all spin-paired, except for a small number near the Fermi level that give rise to a weak Pauli paramagnetism. Moving across the 3d series to the magnetic elements (Fe, Co, Ni), the d-orbitals are now so contracted that their electrons unpair and we see cooperative ordering of spins (ferromagnetism and antiferromagnetism). Referring to the band diagram at the right, the 3d band is only partially filled and the Fermi level cuts through it. For Cu, Zn, and Ga, the 3d orbitals are even more contracted and the 3d band is thus more narrow, but now it is completely filled and the Fermi level is in the 4s,4p band. The strong orbital overlap in these bands results in spin pairing and a high degree of

electron delocalization. Consequently, metals in this part of the periodic table (Cu, Ag) are diamagnetic and are among the best electrical conductors at room temperature. Finally, at Ge, the 4s,4p band is completely filled and the solid is a semiconductor.



Progressive filling of the 3d and 4s,4p bands going across the periodic table from Sc to Ge.

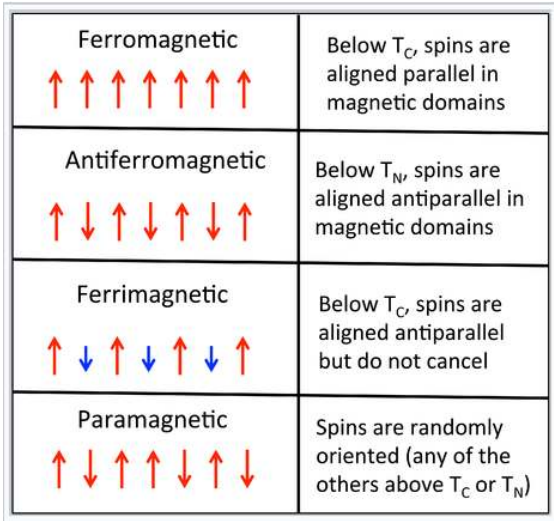
Materials are classified as diamagnetic if they contain no unpaired electrons. Diamagnetic substances are very weakly repelled from an inhomogeneous magnetic field. Molecules or ions that have unpaired spins are paramagnetic and are attracted to a magnet, i.e., they move towards the high field region of an inhomogeneous field. This attractive force results from the alignment of spins with the field, but in the case of paramagnetism each molecule acts independently. In metals, alloys, oxides, and other solid state compounds, the unpaired spins interact strongly with each other and can order spontaneously, resulting in the cooperative magnetic phenomena described below.

3.5: Atomic Orbitals and Magnetism is shared under a CC BY-SA license and was authored, remixed, and/or curated by LibreTexts.

- **6.7: Atomic Orbitals and Magnetism** by Chemistry 310 is licensed CC BY-SA 4.0. Original source: https://en.wikibooks.org/wiki/Introduction_to_Inorganic_Chemistry.

3.6: Ferro-, Ferri- and Antiferromagnetism

The magnetism of metals and other materials are determined by the orbital and spin motions of the unpaired electrons and the way in which unpaired electrons align with each other. All magnetic substances are **paramagnetic** at sufficiently high temperature, where the thermal energy (kT) exceeds the interaction energy between spins on neighboring atoms. Below a certain critical temperature, spins can adopt different kinds of ordered arrangements.



A pictorial description of the ordering of spins in ferromagnetism, antiferromagnetism, ferrimagnetism, and paramagnetism

Let's begin by considering an individual atom in the bcc structure of iron metal. Fe is in group VIIIb of the periodic table, so it has eight valence electrons. The atom is promoted to the $4s^1 3d^7$ state in order to make bonds. A localized picture of the d-electrons for an individual iron atom might look like this:



Since each unpaired electron has a spin moment of 1/2, the total spin angular momentum, **S**, for this atom is:

$S = 3\frac{1}{2} = \frac{3}{2}$ (in units of h/2π)

We can think of each Fe atom in the solid as a little bar magnet with a spin-only moment **S** of 3/2. The spin moments of neigboring atoms can align in parallel (↑ ↑), antiparallel (↑ ↓), or random fashion. In bcc Fe, the tendency is to align parallel because of the positive sign of the exchange interaction. This results in **ferromagnetic** ordering, in which all the spins within a magnetic domain (typically hundreds of unit cells in width) have the same orientation, as shown in the figure at the right. Conversely, a negative exchange interaction between neighboring atoms in bcc Cr results in **antiferromagnetic** ordering. A third arrangement, **ferrimagnetic** ordering, results from an antiparallel alignment of spins on neighboring atoms when the magnetic moments of the neighbors are unequal. In this case, the spin moments do not cancel and there is a net magnetization. The ordering mechanism is like that of an antiferromagnetic solid, but the magnetic properties resemble those of a ferromagnet. Ferrimagnetic ordering is most common in metal oxides.

Magnetization and susceptibility

The **magnetic susceptibility**, **χ**, of a solid depends on the ordering of spins. Paramagnetic, ferromagnetic, antiferromagnetic, and ferrimagnetic solids all have $\chi > 0$, but the magnitude of their susceptibility varies with the kind of ordering and with temperature. We will see these kinds of magnetic ordering primarily among the **3d** and **4f** elements and their alloys and compounds. For example, Fe, Co, Ni, $Nd_2Fe_{14}B$, $SmCo_5$, and YCo_5 are all ferromagnets, Cr and MnO are antiferromagnets, and Fe_3O_4 and $CoFe_2O_4$ are ferrimagnets. Diamagnetic compounds have a weak *negative* susceptibility ($\chi < 0$).

Definitions

- H = applied magnetic field (units: Henry (H))
- B = induced magnetic field in a material (units: Tesla (T))
- M = magnetization, which represents the magnetic moments within a material in the presence of an external field H.

Magnetic susceptibility $\chi = M/H$

Usually, χ is given in *molar* units in the *cgs system*:

χ_M = molar susceptibility (units: cm^3/mol)

Typical values of χ_M:

Compound	Type of Magnetism	χ at 300K (cm^3/mol)
SiO_2	Diamagnetic	-3×10^{-4}
Pt metal	Pauli paramagnetic	$+2 \times 10^{-4}$
$Gd_2(SO_4)_3 \cdot 8H_2O$	Paramagnetic	$+5 \times 10^{-2}$
Ni-Fe alloy	Ferromagnetic	$+10^4 - 10^6$

To correlate χ with the number of unpaired electrons in a compound, we first correct for the small diamagnetic contribution of the core electrons:

$$\chi^{corr} = \chi^{obs} - \chi^{diamagnetic\ cores} \tag{3.6.1}$$

Susceptibility of paramagnets

For a paramagnetic substance,

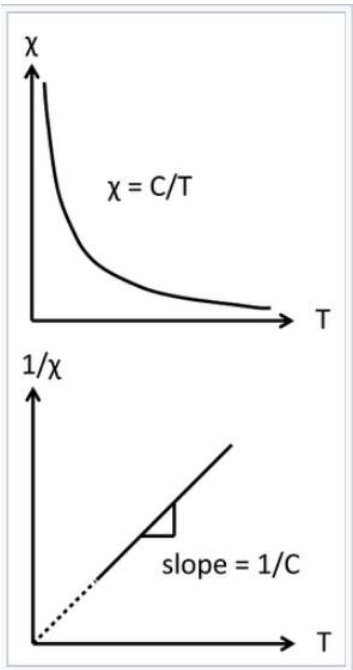
$$\chi_M^{corr} = \frac{C}{T} \tag{3.6.2}$$

The inverse relationship between the magnetic susceptibility and T, the absolute temperature, is called **Curie's Law**, and the proportionality constant C is the **Curie constant**:

$$C = \frac{N_A}{3k_B}\mu_{eff}^2 \tag{3.6.3}$$

Note that C is not a "constant" in the usual sense, because it depends on μ_{eff}, the **effective magnetic moment** of the molecule or ion, which in turn depends on its number of unpaired electrons:

$$\mu_{eff} = \sqrt{n(n+2)}\mu_B \tag{3.6.4}$$



Curie law behavior of a paramagnet. A plot of 1/χ vs. absolute temperature is a straight line, with a slope of 1/C and an intercept of zero.

Here μ_B is the Bohr magneton, a physical constant defined as $\mu_B = eh/4\pi m_e = 9.274 \times 10^{-21}$ erg/gauss (in cgs units).

In cgs units, we can combine physical constants,

$$\frac{N_A}{3k_B}\mu_B^2 = .125 \tag{3.6.5}$$

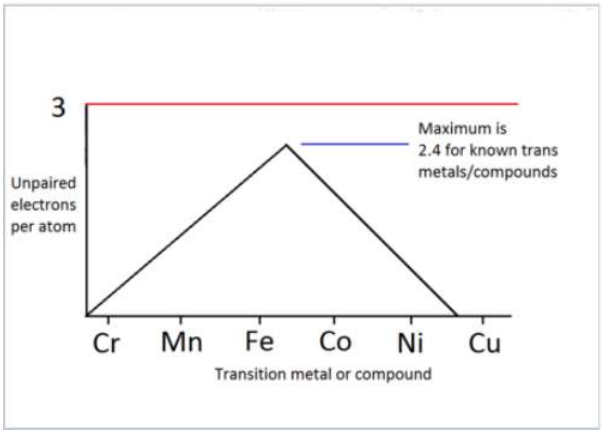
Combining these equations, we obtain

$$\chi_M^{corr} = \frac{.125}{T}\left(\frac{\mu_{eff}}{\mu_B}\right)^2 \tag{3.6.6}$$

These equations relate the molar susceptibility, a bulk quantity that can be measured with a magnetometer, to μ_{eff}, a quantity that can be calculated from the number of unpaired electrons, n. Two important points to note about this formula are:

- The magnetic susceptibility is inversely proportional to the absolute temperature, with a proportionality constant C (Curie's Law)

- So far we are talking only about paramagnetic substances, where there is no interaction between neighboring atoms.



Number of unpaired electrons per atom, determined from Curie constants of transition metals and their 1:1 alloys.

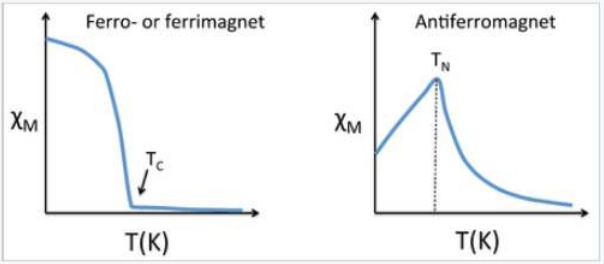
Returning to the isolated Fe atom with its three unpaired electrons, we can measure the Curie constant for iron metal (above the temperature of its transition to a paramagnetic solid) and compare it to the calculation of μ_{eff}. Since n = 3, we calculate:

$$\mu_{eff} = \sqrt{(3)(5)}\mu_B = 3.87\mu_B \tag{3.6.7}$$

The plot at the right shows the number of unpaired electrons per atom, calculated from measured Curie constants, for the magnetic elements and 1:1 alloys in the 3d series. The plot peaks at a value of 2.4 spins per atom, slightly lower than we calculated for an isolated iron atom. This reflects that fact that there is some pairing of d-electrons, i.e., that they do contribute somewhat to bonding in this part of the periodic table.

Susceptibility of ferro-, ferri-, and antiferromagnets

Below a certain critical temperature, the spins of a solid paramagnetic substance order and the susceptibility deviates from simple Curie-law behavior. Because the ordering depends on the short-range exchange interaction, this critical temperature varies widely. Metals and alloys in the 3d series tend to have high critical temperatures because the atoms are directly bonded to each other and the interaction is strong. For example, Fe and Co have critical temperatures (also called the Curie temperature, T_c, for ferromagnetic substances) of 1043 and 1400 K, respectively. The Curie temperature is determined by the strength of the magnetic exchange interaction and by the number of unpaired electrons per atom. The number of unpaired electrons peaks between Fe and Co as the d-band is filled, and the exchange interaction is stronger for Co than for Fe. In contrast to ferromagnetic metals and alloys, paramagnetic salts of transition metal ions typically have critical temperatures below 1K because the magnetic ions are not directly bonded to each other and thus their spins are very weakly coupled in the solid state. For example, in gadolinium sulfate, the paramagnetic Gd^{3+} ions are isolated from each other by SO_4^{2-} ions.

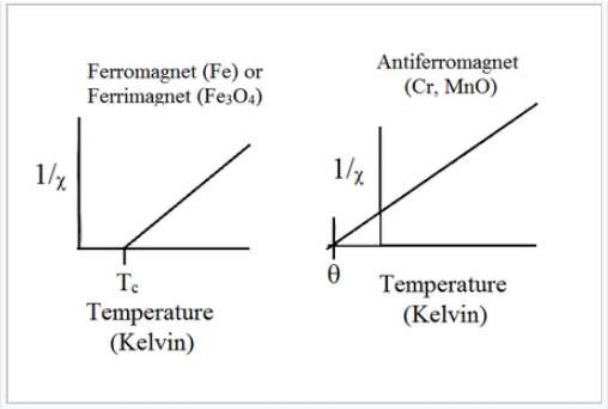


Magnetic susceptibility vs temperature (Kelvin) for ferrimagnetic, ferromagnetic, and antiferromagnetic materials

Above the critical temperature T_C, **ferromagnetic** compounds become paramagnetic and obey the **Curie-Weiss law:**

$$\chi = \frac{C}{T - T_c} \tag{3.6.8}$$

This is similar to the Curie law, except that the plot of $1/\chi$ vs. T is shifted to a positive intercept T_C on the temperature axis. This reflects the fact that ferromagnetic materials (in their paramagnetic state) have a greater tendency for their spins to align in a magnetic field than an ordinary paramagnet in which the spins do not interact with each other. Ferrimagnets follow the same kind of ordering behavior. Typical plots of χ vs. T and $1/\chi$ vs. T for ferro-/ferrimagnets are shown above and below.



Plots of $1/\chi$ vs. T for ferromagnets, ferrimagnets, and antiferromagnets.

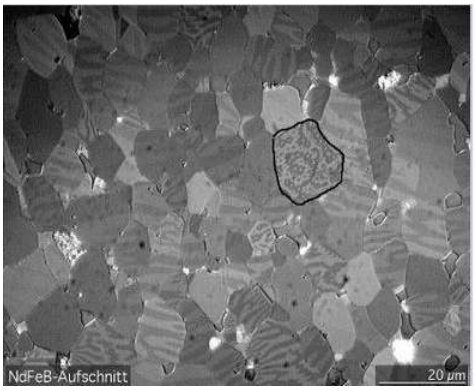
Antiferromagnetic solids are also paramagnetic above a critical temperature, which is called the Néel temperature, T_N. For antiferromagnets, χ reaches a maximum at T_N and is smaller at higher temperature (where the paramagnetic spins are further disordered by thermal energy) and at lower temperature (where the spins pair up). Typically, antiferromagnets retain some positive susceptibility even at very low temperature because of canting of their paired spins. However the maximum value of χ is much lower for an antiferromagnet than it is for a ferro- or ferrimagnet. The Curie-Weiss law is also modified for an antiferromagnet, reflecting the tendency of spins (in the paramagnetic state above T_N) to resist parallel ordering. A plot of $1/\chi$ vs. T intercepts the temperature axis at a negative temperature, $-\theta$, and the Curie-Weiss law becomes:

$$\chi = \frac{C}{T+\theta} \tag{3.6.9}$$

Ordering of spins below T_C

Below T_C, the spins align spontaneously in ferro- and ferrimagnets. Complex magnetization behavior is observed that depends on the history of the sample. For example, if a ferromagnetic material is cooled in the absence of an applied magnetic field, it forms a mosaic structure of magnetic domains that each have internally aligned spins. However, neighboring domains tend to align the opposite way in order to minimize the total energy of the system. This is illustrated in the figure at the left for a Nd-Fe-B magnet. The sample consists of 5-10 μm wide crystal grains that can be easily distinguished by the sharp boundaries in the image. Within

each grain are a series of lighter and darker stripes (imaged by using the optical Kerr effect) that are ferromagnetic domains with opposite orientations. Averaged over the whole sample, these domains have random orientation so the net magnetization is zero.



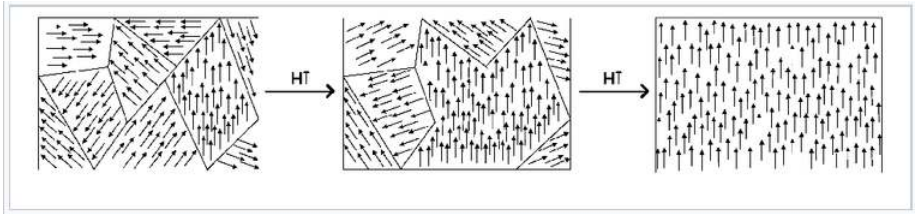
Microcrystalline grains within a piece of $Nd_2Fe_{14}B$ (the alloy used in neodymium magnets) with magnetic domains made visible with a Kerr microscope. The domains are the light and dark stripes visible within each grain.

When a sample like this one is magnetized (i.e., exposed to a strong magnetic field), the domain walls move and the favorably aligned domains grow at the expense of those with the opposite orientation. This transformation can be seen in real time in the Kerr microscope. The domain walls are typically hundreds of atoms wide, so movement of a domain wall involves a cooperative tilting of spin orientation (analogous to "the wave" in a sports stadium) and is a relatively low energy process.



The movement of domain walls in a grain of silicon steel is driven in this movie by increasing the external magnetic field in the "downward" direction, and is imaged using a Kerr microscope. White areas are domains with their magnetization directed up, dark areas - which eventually comprise the entire grain - are domains with their magnetization directed down.

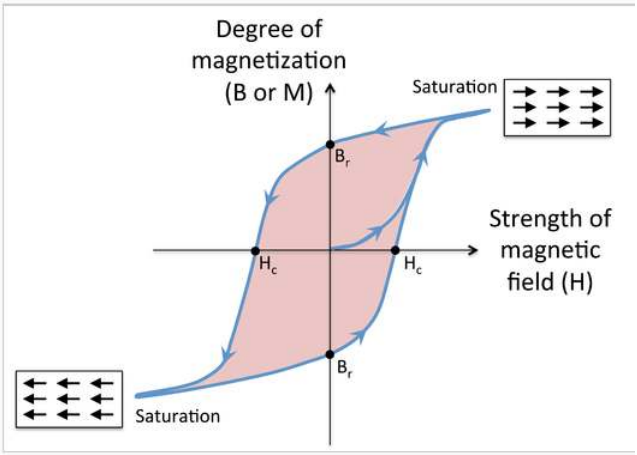
The process of magnetization moves the solid away from its lowest energy state (random domain orientation), so magnetization involves input of energy. When the external magnetic field is removed, the domain walls relax somewhat, but the solid (especially in the case of a "hard" magnet) can retain much of its magnetization. If you have ever magnetized a nail or a paper clip by using a permanent magnet, what you were doing was moving the walls of the magnetic domains inside the ferromagnet. The object thereafter retains the "memory" of its magnetization. However, annealing a permanent magnet destroys the magnetization by returning the system to its lowest energy state in which all the magnetic domains cancel each other.



Rotation of orientation and increase in size of magnetic domains in response to an externally applied magnetic field.

Magnetic hysteresis. Cycling a ferro- or ferrimagnetic material in a magnetic field results in hysteresis in the magnetization of the material, as shown in the figure at the left. At the beginning, the magnetization is zero, but it begins to rise rapidly as the magnetic field is applied. At high field, the magnetic domains are aligned and the magnetization is said to be saturated. When the field is removed, a certain **remanent magnetization** (indicated as the point $\mathbf{B_r}$ on the graph) is retained, i.e., the material is magnetized. Applying a field in the opposite direction begins to orient the magnetic domains in the other direction, and at a field $\mathbf{H_c}$ (the **coercive field**), the magnetization of the sample is reduced to zero. Eventually the material reaches saturation in the opposite direction, and when the field is removed again, it has remanent magnetization Br, but in the opposite direction. As the field continues to reverse, the magnet follows the hysteresis loop as indicated by the arrows. The area of colored region inside the loop is

proportional to the magnetic work done in each cycle. When the field cycles rapidly (for example, in the core of a transformer, or in read-write cycles of a magnetic disk) this work is turned into heat.



Magnetization of a ferro- or ferrimagnet vs. applied magnetic field H. Starting at the origin, the upward curve is the initial magnetization curve. The downward curve after saturation, along with the lower return curve, form the main loop. The intercepts Hc and Br are the coercivity and remanent magnetization.

3.6: Ferro-, Ferri- and Antiferromagnetism is shared under a CC BY-SA license and was authored, remixed, and/or curated by LibreTexts.

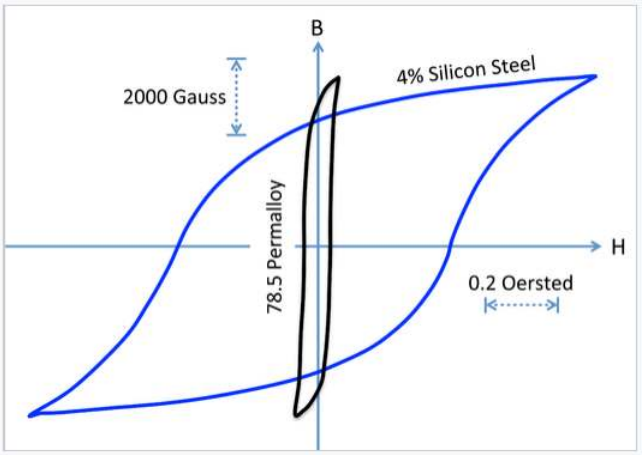
- **6.8: Ferro-, Ferri- and Antiferromagnetism** by Chemistry 310 is licensed CC BY-SA 4.0. Original source: https://en.wikibooks.org/wiki/Introduction_to_Inorganic_Chemistry.

3.7: Hard and Soft Magnets

Whether a ferro- or ferrimagnetic material is a **hard** or a **soft magnet** depends on the strength of the magnetic field needed to align the magnetic domains. This property is characterized by $\mathbf{H_c}$, the coercivity. Hard magnets have a high coercivity (H_c), and thus retain their magnetization in the absence of an applied field, whereas soft magnets have low values.

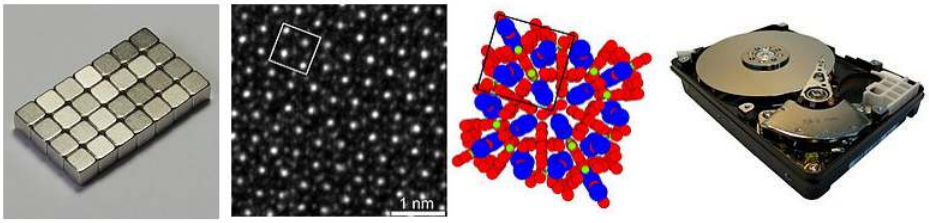
The figure at the right compares hysteresis loops for hard and soft magnets. Recall that the energy dissipated in magnetizing and demagnetizing the material is proportional to the area of the hysteresis loop. We can see that soft magnets, while they can achieve a high value of B_{sat}, dissipate relatively little energy in the loop. This makes **soft magnets** preferable for use in **transformer cores**, where the field is switched rapidly. **Permalloy**, an alloy consisting of about 20% Fe and 80% Ni, is a soft magnet that has very high magnetic permeability μ (i.e., a large maximum slope of the B vs. H curve) and a very narrow hysteresis loop.

Some materials, such as iron metal, can exist as either hard or soft magnets. Whether bcc iron is a hard or soft magnet depends on the crystal grain size. When crystal grains in iron are sub-micron size, and comparable to the size of the magnetic domains, then the magnetic domains are pinned by crystal grain boundaries. When the magnetic domains are pinned a stronger coercive magnetic field needs to be applied to cause them to re-align. When iron is annealed, the crystal grains grow and the magnetic domains become more free to align with applied magnetic fields. This decreases the coercive field and the material becomes a soft magnet.



Hysteresis loops comparing a hard magnet (iron-silicon steel) to a soft magnet (permalloy) on the same scale. H_c for permallloy is 0.05 Oe, about 10 times lower than that of the hard magnet. The remanent magnetizations of the two materials are comparable.

Hard magnets such as CrO_2, γ-Fe_2O_3, and cobalt ferrite ($CoFe_2O_4$) are used in magnetic recording media, where the high coercivity allows them to retain the magnetization state (read as a logical 0 or 1) of a magnetic bit over long periods of time. Hard magnets are also used in disk drives, refrigerator magnets, electric motors and other applications. Drive motors for hybrid and electric vehicles such as the Toyota Prius use the hard magnet $Nd_2Fe_{14}B$ (also used to make strong refrigerator magnets) and require 1 kilogram (2.2 pounds) of neodymium.[6]. A high-resolution transmission electron microscope image of $Nd_2Fe_{14}B$ is shown below and compared to the crystal structure with the unit cell marked.

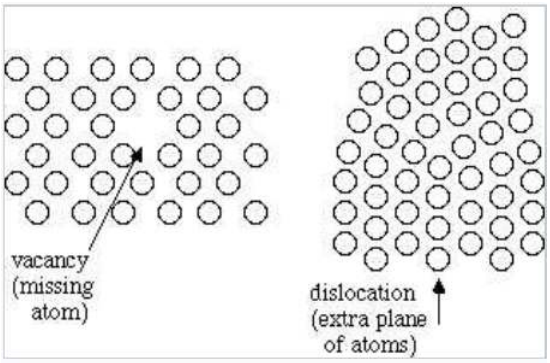


3.7: Hard and Soft Magnets is shared under a CC BY-SA license and was authored, remixed, and/or curated by LibreTexts.

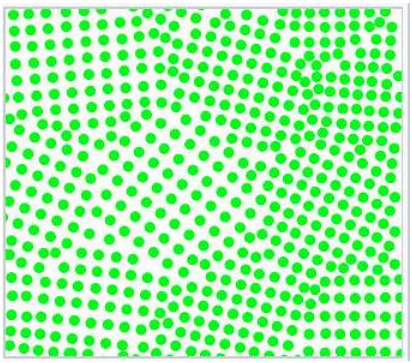
- **6.9: Hard and Soft Magnets** by Chemistry 310 is licensed CC BY-SA 4.0. Original source: https://en.wikibooks.org/wiki/Introduction_to_Inorganic_Chemistry.

3.8: Defects in Metallic Crystals

“Crystals are like people, it is the defects in them which tend to make them interesting!” - *Colin Humphreys.*



Metals, by virtue of their non-directional bonding, are more energetically tolerant of **defects** than are covalent network or ionic solids. Because there is no strong preference for one atomic position over another, the energy of a metallic crystal is not greatly impaired by the vacancy of a single atom or by the dislocation of a group of atoms. These kinds of "mistakes" in the packing of metal atoms within crystals are collectively called defects. The deformability of metals is the direct result of defects in the crystal structure. Defects in metals such as Al and Fe are responsible for the three orders of magnitude difference between the yield stress of annealed polycrystalline samples (i.e., normal articles of commerce) and perfect single crystals.



Grains and grain boundaries in a polycrystalline material

3.8: Defects in Metallic Crystals is shared under a CC BY-SA license and was authored, remixed, and/or curated by LibreTexts.

- **7.1: Defects in Metallic Crystals** by Chemistry 310 is licensed CC BY-SA 4.0. Original source: https://en.wikibooks.org/wiki/Introduction_to_Inorganic_Chemistry.

3.9: X-ray Crystallography

X-ray Crystallography is a scientific method used to determine the arrangement of atoms of a crystalline solid in three dimensional space. This technique takes advantage of the interatomic spacing of most crystalline solids by employing them as a diffraction gradient for x-ray light, which has wavelengths on the order of 1 angstrom (10^{-8} cm).

Introduction

In 1895, Wilhelm Rontgen discovered X-rays. The nature of X-rays, whether they were particles or electromagnetic radiation, was a topic of debate until 1912. If the wave idea was correct, researchers knew that the wavelength of this light would need to be on the order of 1 Angstrom (Å) (10^{-8} cm). Diffraction and measurement of such small wavelengths would require a gradient with spacing on the same order of magnitude as the light.

In 1912, Max von Laue, at the University of Munich in Germany, postulated that atoms in a crystal lattice had a regular, periodic structure with interatomic distances on the order of 1 Å. Without having any evidence to support his claim on the periodic arrangements of atoms in a lattice, he further postulated that the crystalline structure can be used to diffract X-rays, much like a gradient in an infrared spectrometer can diffract infrared light. His postulate was based on the following assumptions: the atomic lattice of a crystal is periodic, X-rays are electromagnetic radiation, and the interatomic distance of a crystal are on the same order of magnitude as X-ray light. Laue's predictions were confirmed when two researchers: Friedrich and Knipping, successfully photographed the diffraction pattern associated with the X-ray radiation of crystalline $CuSO_4$ • 5 H_2O. The science of X-ray crystallography was born.

The arrangement of the atoms needs to be in an ordered, periodic structure in order for them to diffract the X-ray beams. A series of mathematical calculations is then used to produce a diffraction pattern that is characteristic to the particular arrangement of atoms in that crystal. X-ray crystallography remains to this day the primary tool used by researchers in characterizing the structure and bonding of organometallic compounds.

Diffraction

Diffraction is a phenomena that occurs when light encounters an obstacle. The waves of light can either bend around the obstacle, or in the case of a slit, can travel through the slits. The resulting diffraction pattern will show areas of constructive interference, where two waves interact in phase, and destructive interference, where two waves interact out of phase. Calculation of the phase difference can be explained by examining Figure 1 below.

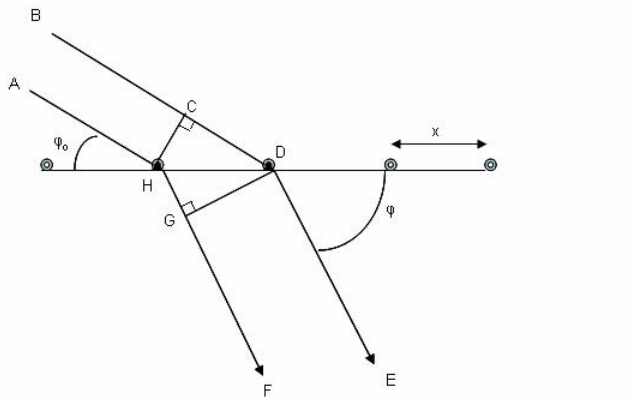


Figure 1: Scattering of light by a diffraction gratting

In the figure below, two parallel waves, BD and AH are striking a gradient at an angle θ_o. The incident wave BD travels farther than AH by a distance of CD before reaching the gradient. The scattered wave (depicted below the gradient) HF, travels father than the scattered wave DE by a distance of HG. So the total path difference between path AHGF and BCDE is CD - HG. To observe a wave of high intensity (one created through constructive interference), the difference CD - HG must equal to an integer number of

wavelengths to be observed at the angle psi, $CD - HG = n\lambda$, where λ is the wavelength of the light. Applying some basic trigonometric properties, the following two equations can be shown about the lines:

$$CD = x\cos(\theta o) \tag{3.9.1}$$

and

$$HG = x\cos(\theta) \tag{3.9.2}$$

where x is the distance between the points where the diffraction repeats. Combining the two equations,

$$x(\cos\theta_o - \cos\theta) = n\lambda \tag{3.9.3}$$

Bragg's Law

Diffraction of an X-ray beam, occurs when the light interacts with the electron cloud surrounding the atoms of the crystalline solid. Due to the periodic crystalline structure of a solid, it is possible to describe it as a series of planes with an equal interplaner distance. As an X-ray's beam hits the surface of the crystal at an angle, θ, some of the light will be diffracted at that same angle away from the solid (Figure 2). The remainder of the light will travel into the crystal and some of that light will interact with the second plane of atoms. Some of the light will be diffracted at an angle θ, and the remainder will travel deeper into the solid. This process will repeat for the many planes in the crystal. The X-ray beams travel different pathlengths before hitting the various planes of the crystal, so after diffraction, the beams will interact constructively only if the path length difference is equal to an integer number of wavelengths (just like in the normal diffraction case above). In the figure below, the difference in path lengths of the beam striking the first plane and the beam striking the second plane is equal to BG + GF. So, the two diffracted beams will constructively interfere (be in phase) only if $BG + GF = n\lambda$. Basic trigonometry will tell us that the two segments are equal to one another with the interplaner distance times the sine of the angle θ. So we get:

$$BG = BC = d\sin\theta \tag{3.9.4}$$

Thus,

$$2d\sin\theta = n\lambda \tag{3.9.5}$$

This equation is known as Bragg's Law, discovered in 1912. {C}{C}Bragg's Law relates the distance between two planes in a crystal and the angle of reflection to the X-ray wavelength. The X-rays that are diffracted off the crystal have to be in-phase in order to signal. Only certain angles that satisfy the following condition will register:

$$\sin\theta = \frac{n\lambda}{2d} \tag{3.9.6}$$

For historical reasons, the resulting diffraction spectrum is represented as intensity vs. 2θ.

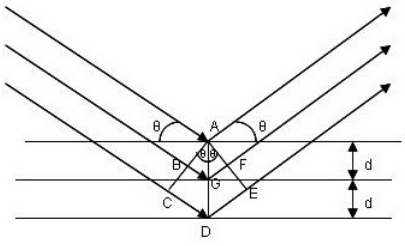


Figure 2: Incident X-ray strikes a set of planes (with an interplaner distance of d) at an angle of θ

Instrument Components

The main components of an X-ray instrument are similar to those of many optical spectroscopic instruments. These include a source, a device to select and restrict the wavelengths used for measurement, a holder for the sample, a detector, and a signal converter and readout. However, for X-ray diffraction; only a source, sample holder, and signal converter/readout are required.

The Source

X-ray tubes provides a means for generating X-ray radiation in most analytical instruments. An evacuated tube houses a tungsten filament which acts as a cathode opposite to a much larger, water cooled anode made of copper with a metal plate on it. The metal plate can be made of any of the following metals: chromium, tungsten, copper, rhodium, silver, cobalt, and iron. A high voltage is passed through the filament and high energy electrons are produced. The machine needs some way of controlling the intensity and wavelength of the resulting light. The intensity of the light can be controlled by adjusting the amount of current passing through the filament; essentially acting as a temperature control. The wavelength of the light is controlled by setting the proper accelerating voltage of the electrons. The voltage placed across the system will determine the energy of the electrons traveling towards the anode. X-rays are produced when the electrons hit the target metal. Because the energy of light is inversely proportional to wavelength ($E = hc = h(1/\lambda)$), controlling the energy, controls the wavelength of the X-ray beam.

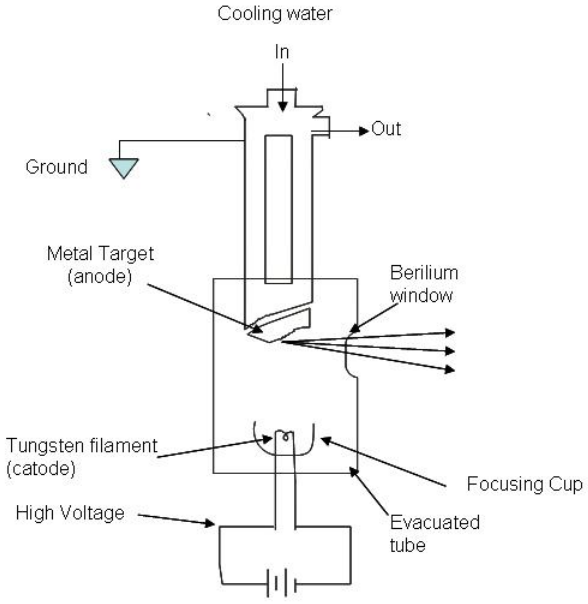


Figure 3: X-ray tube schematic

X-ray Filter

Monochromators and filters are used to produce monochromatic X-ray light. This narrow wavelength range is essential for diffraction calculations. For instance, a zirconium filter can be used to cut out unwanted wavelengths from a molybdenum metal target (see figure 4). The molybdenum target will produce X-rays with two wavelengths. A zirconium filter can be used to absorb the unwanted emission with wavelength $K\beta$, while allowing the desired wavelength, K_α to pass through.

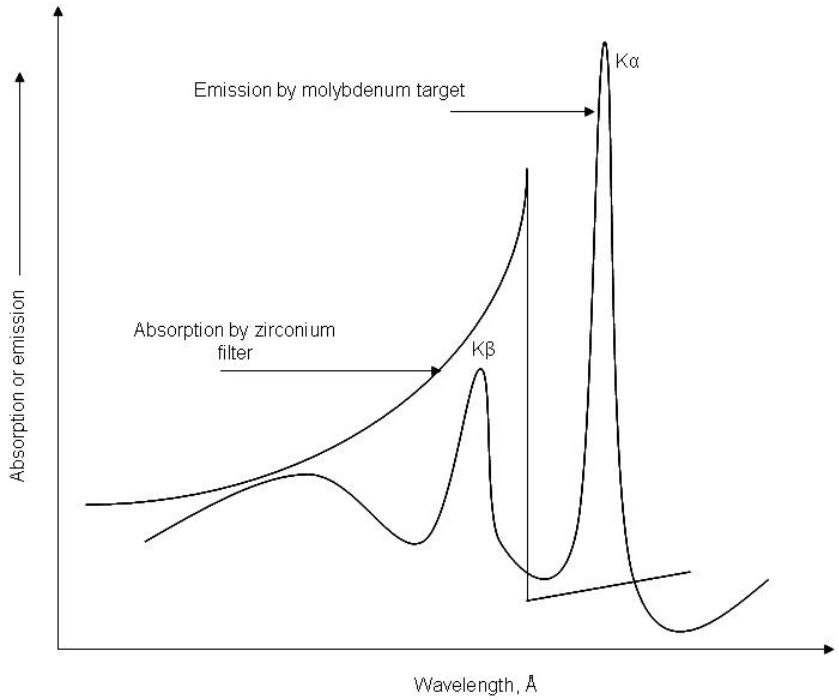


Figure 4: Monochromatic light produce by absorption of unwanted emissions.

Signal Converter

In x-ray diffraction, the detector is a transducer that counts the number of photons that collide into it. This photon counter gives a digital readout in number of photons per unit time.

References

1. Skoog, D . A.; Holler, F. J.; Stanley R. C.; Principles of Instrumental Analysis; Thomson Brooks/Cole: Belmont CA, 2007.
2. Sands, D. E.; Introduction to Crystallography; Dover Publications, Inc.; New York, 1975
3. Drenth, Jan. Principles of Protein x-ray Crystallography, 3rd edition. 2007, Springer Science + Business Media, LLC. pg. 14.
4. Rhodes, Gale. Crystallography Made Crystal Clear, 3rd edition. 2006, Elsevier Inc. pg. 33, 55 - 57.
5. Actual experimentation done of APS Kinase D63N *Penicillium Chrysogenum*.

Contributors and Attributions

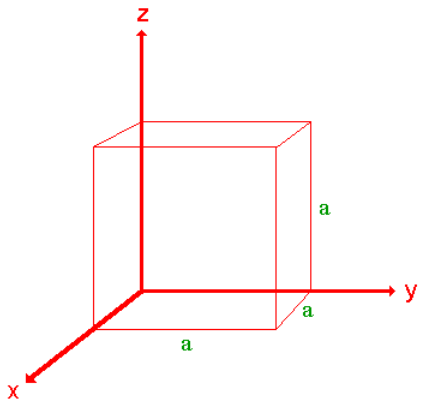
- Roman Kazantsev (UC Davis) and Michelle Towles (UC Davis)

3.9: X-ray Crystallography is shared under a not declared license and was authored, remixed, and/or curated by LibreTexts.

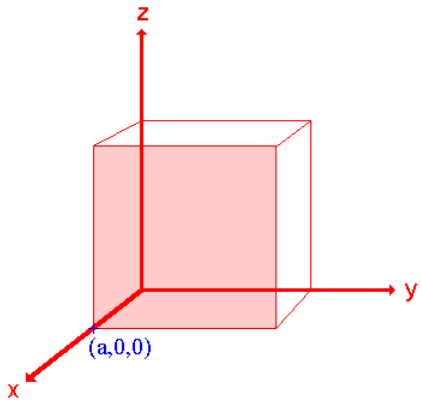
3.10: Miller Indices (hkl)

The orientation of a surface or a crystal plane may be defined by considering how the plane (or indeed any parallel plane) intersects the main crystallographic axes of the solid. The application of a set of rules leads to the assignment of the Miller Indices (*hkl*), which are a set of numbers which quantify the intercepts and thus may be used to uniquely identify the plane or surface.

The following treatment of the procedure used to assign the Miller Indices is a simplified one and only a **cubic** crystal system (one having a cubic unit cell with dimensions a x a x a) will be considered.



The procedure is most easily illustrated using an example so we will first consider the following surface/plane:



Step 1: *Identify the intercepts on the* x- , y- *and* z- *axes.*

In this case the intercept on the x-axis is at x = a (at the point (a,0,0)), but the surface is parallel to the y- and z-axes - strictly therefore there is no intercept on these two axes but we shall consider the intercept to be at infinity (∞) for the special case where the plane is parallel to an axis. The intercepts on the x- , y- and z-axes are thus **a , ∞ , ∞**.

Step 2: Specify the intercepts in fractional co-ordinates

Co-ordinates are converted to fractional co-ordinates by dividing by the respective cell-dimension - for example, a point (x,y,z) in a unit cell of dimensions a x b x c has fractional co-ordinates of (x/a , y/b , z/c). In the case of a cubic unit cell each co-ordinate will simply be divided by the cubic cell constant, a. This gives

Fractional Intercepts = **a/a , ∞/a, ∞/a** i.e. **1 , ∞ , ∞**.

Step 3: Take the reciprocals of the fractional intercepts

This final manipulation generates the Miller Indices which (by convention) should then be specified without being separated by any commas or other symbols. The Miller Indices are also enclosed within standard brackets (….) when one is specifying a unique

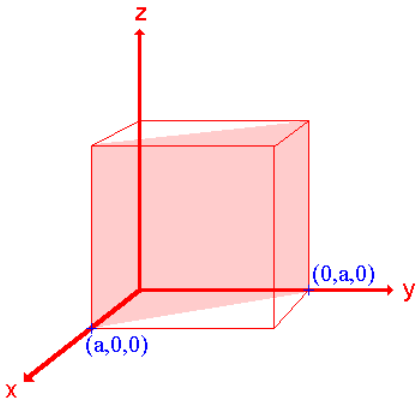
surface such as that being considered here.

The reciprocals of 1 and ∞ are 1 and 0 respectively, thus yielding Miller Indices **(100)**.

So the surface/plane illustrated is the (100) plane of the cubic crystal.

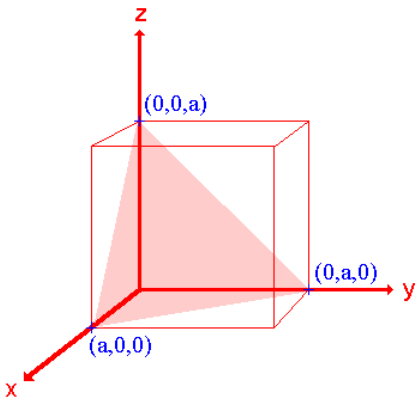
Other Examples

1. The (110) surface



Assignment
Intercepts: a , a , ∞
Fractional intercepts: 1 , 1 , ∞
Miller Indices: **(110)**

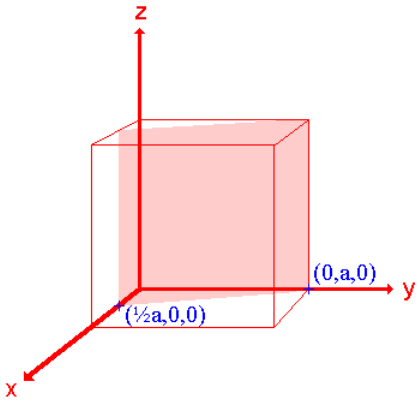
2. The (111) surface



Assignment
Intercepts: a , a , a
Fractional intercepts: 1 , 1 , 1
Miller Indices: **(111)**

The (100), (110) and (111) surfaces considered above are the so-called low index surfaces of a cubic crystal system (the "low" refers to the Miller indices being small numbers - 0 or 1 in this case). These surfaces have a particular importance but there an infinite number of other planes that may be defined using Miller index notation. We shall just look at one more …

3. The (210) surface



Assignment
Intercepts: ½ a , a , ∞
Fractional intercepts: ½ , 1 , ∞
Miller Indices: **(210)**

Further notes:

i. in some instances the Miller indices are best multiplied or divided through by a common number in order to simplify them by, for example, removing a common factor. This operation of multiplication simply generates a parallel plane which is at a different distance from the origin of the particular unit cell being considered. e.g. (200) is transformed to (100) by dividing through by 2 .
ii. if any of the intercepts are at negative values on the axes then the negative sign will carry through into the Miller indices; in such cases the negative sign is actually denoted by overstriking the relevant number. e.g. (00-1) is instead denoted by (00$\bar{1}$)
iii. in the *hcp* crystal system there are four principal axes; this leads to four Miller Indices e.g. you may see articles referring to an *hcp* (0001) surface. It is worth noting, however, that the intercepts on the first three axes are necessarily related and not completely independent; consequently the values of the first three Miller indices are also linked by a simple mathematical relationship.

Contributors and Attributions

- Roger Nix (Queen Mary, University of London)

This page titled 3.10: Miller Indices (hkl) is shared under a not declared license and was authored, remixed, and/or curated by Roger Nix.

3.11: Powder X-ray Diffraction

When an X-ray is shined on a crystal, it diffracts in a pattern characteristic of the structure. In powder X-ray diffraction, the diffraction pattern is obtained from a powder of the material, rather than an individual crystal. Powder diffraction is often easier and more convenient than single crystal diffraction since it does not require individual crystals be made. Powder X-ray diffraction (XRD) also obtains a diffraction pattern for the bulk material of a crystalline solid, rather than of a single crystal, which doesn't necessarily represent the overall material. A diffraction pattern plots intensity against the angle of the detector, 2θ.

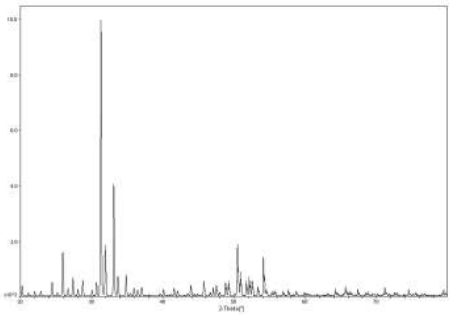
Introduction

Since most materials have unique diffraction patterns, compounds can be identified by using a database of diffraction patterns. The purity of a sample can also be determined from its diffraction pattern, as well as the composition of any impurities present. A diffraction pattern can also be used to determine and refine the lattice parameters of a crystal structure. A theoretical structure can also be refined using a method known as **Rietveld refinement**. The particle size of the powder can also be determined by using the Scherrer formula, which relates the particle size to the peak width. The Scherrer fomula is

$$t = \frac{0.9\lambda}{\sqrt{B_M^2 - B_s^2}\cos\theta} \tag{3.11.1}$$

with

- λ is the x-ray wavelength,
- B_M is the observed peak width,
- B_S is the peak width of a crystalline standard, and
- θ is the angle of diffraction.



To the left is an example XRD pattern for $Ba_{24}Ge_{100}$. The x axis is 2θ and the y axis is the intensity.

References

1. Dann, S.E. *Reactions and Characterization of SOLIDS.* Royal Society of Chemistry, USA (2002).
2. Skoog, D.A.; Holler, F.J.; Crouch, S.R. *Principles of Instrumental Analysis*. Sixth Edition, Thomson Brooks/Cole, USA (2007).

Contributors and Attributions

- Jason Grebenkemper

3.11: Powder X-ray Diffraction is shared under a not declared license and was authored, remixed, and/or curated by LibreTexts.

3.12: Prelude to Ionic and Covalent Solids - Structures

As we noted in our discussion of metal and alloy structures, there is an intimate connection between the structures and the physical properties of materials. As we "graduate" from simple metal structures based on sphere packings to more complex structures, we find that this is still true. In this section we will try to systematize the structures of inorganic solids - metal oxides, halides, sulfides, and related compounds - and develop some rules for which structures to expect based on electronegativity differences, hard-soft acid-base rules, and other periodic trends. We will see that many of these structures are related to the sphere packings that we learned about previously.



The morphology of twinned crystals of iron pyrite (FeS_2) is related to the underlying cubic symmetry of the unit cell. Like NaCl, the pyrite crystal structure can be thought of as a face-centered cubic array of anions (S_2^{2-}) with cations (Fe^{2+}) occupying all the octahedral holes.

Inorganic solids often have simple crystal structures, and some of these structures are adopted by large families of ionic or covalent compounds. Examples of the most common structures include NaCl, CsCl, NiAs, zincblende, wurtzite, fluorite, perovskite, rutile, and spinel. We will develop these structures systematically from the close packed and non-close packed lattices. Some layered structures, such as $CdCl_2$ and CdI_2, can be thought of as relatives of simple ionic lattices with some atoms "missing."

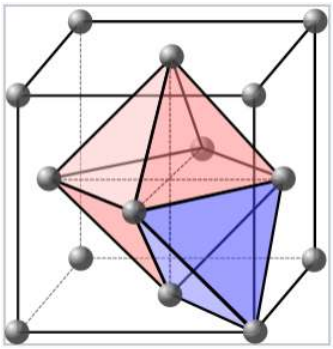
3.12: Prelude to Ionic and Covalent Solids - Structures is shared under a not declared license and was authored, remixed, and/or curated by LibreTexts.

- **8.1: Prelude to Ionic and Covalent Solids - Structures** by Chemistry 310 is licensed CC BY-SA 4.0. Original source: https://en.wikibooks.org/wiki/Introduction_to_Inorganic_Chemistry.

3.13: Close-packing and Interstitial Sites

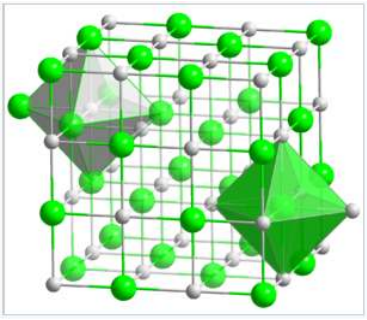
Many common inorganic crystals have structures that are related to cubic close packed (face-centered cubic) or hexagonal close packed sphere packings. These packing lattices contain two types of sites or "holes" that the interstitial atoms fill, and the coordination geometry of these sites is either **tetrahedral** or **octahedral**. An interstitial atom filling a tetrahedral hole is coordinated to four packing atoms, and an atom filling an octahedral hole is coordinated to six packing atoms. In both the hexagonal close packed and cubic close packed lattices, there is one octahedral hole and two tetrahedral holes per packing atom.

Question: Would anions or cations be better as packing atoms?
We might expect that anions, which are often larger than cations, would be better suited to the positions of packing atoms. While this is often true, there are many examples of structures in which cations are the packing atoms, and others in which the distinction is arbitrary. The NaCl structure is a good example of the latter.



One octahedral and one tetrahedral site in a face-centered cubic unit cell. Each cell contains four packing atoms (gray), four octahedral sites (pink), and eight tetrahedral sites (blue).

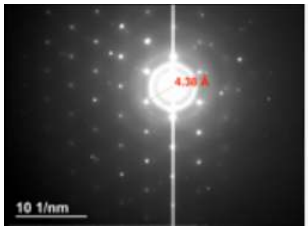
In the NaCl structure, shown on the right, the green spheres are the Cl^- ions and the gray spheres are the Na^+ ions. The octahedral holes in a face-centered cubic lattice can be found at fractional coordinates (1/2 1/2 1/2), (1/2 0 0), (0 1/2 0), and (0 0 1/2). There are four of these holes per cell, and they are filled by the chloride ions. The packing atoms (Na^+) have coordinates (0 0 0), (0 1/2 1/2), (1/2 1/2 0), and (1/2 0 1/2). Note that each of the Na^+ positions is related to a Cl^- position by a translation of (1/2 0 0). Another way of stating this is that the structure consists of **two interpenetrating fcc lattices**, which are related to each other by a translation of half the unit cell along any of the three Cartesian axes. We could have equivalently placed the Cl ions at the fcc lattice points and the Na ions in the octahedral holes by simply translating the origin of the unit cell by (1/2 0 0). Thus the distinction between packing and interstitial atoms in this case is arbitrary.



Crystal structure of NaCl. Both the Na^+ and Cl^- ions are octahedrally coordinated.

NaCl is interesting in that it is a three-dimensional checkerboard, and thus there are no NaCl "molecules" that exist in the structure. When this structure was originally solved (in 1913 by using X-ray diffraction) by W. L. Bragg, his interpretation met resistance by chemists who thought that precise integer stoichiometries were a consequence of the valency of atoms in molecules. The German chemist Pfeiffer noted in 1915 that ‘the ordinary notion of valency didn’t seem to apply’, and fourteen years later, the influential chemist Armstrong still found Bragg’s proposed structure of sodium chloride ‘more than repugnant to the common sense, not

chemical cricket'! Nevertheless, Bragg and his father, W. H. Bragg, persevered and used the then-new technique of X-ray diffraction to determine the structures of a number of other compounds, including diamond, zincblende, calcium fluoride, and other alkali halides. These experiments gave chemists their first real look at the atomic structure of solids, and laid the groundwork for X-ray diffraction experiments that later elucidated the structures of DNA, proteins, and many other compounds. For their work on X-ray diffraction the Braggs received the Nobel prize in Physics in 1915.

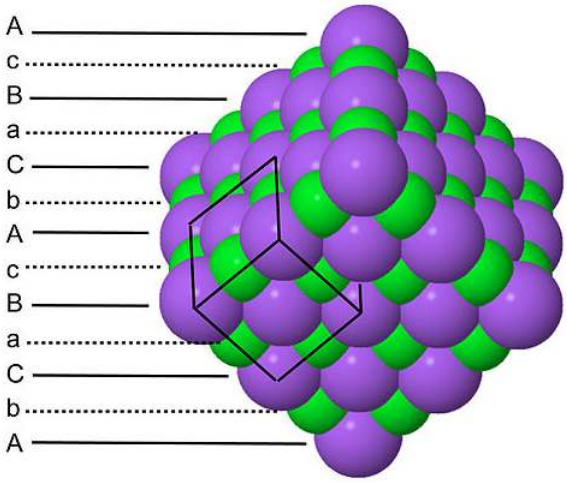


The lattice dimensions and positions of atoms in crystals such as NaCl are inferred from diffraction patterns.

Since each type of atom in the NaCl structure forms a face-centered cubic lattice, there are four Na and four Cl atoms per NaCl unit cell. It is because of this ratio that NaCl has a 1:1 stoichiometry. The shaded green and gray bipyramidal structures in the NaCl lattice show that the Na^+ ions are coordinated to six Cl^- ions, and vice versa. The NaCl structure can be alternatively drawn as a stacking of close-packed layer planes, AcBaCbAcBa... along the body diagonal of the unit cell. Here the uppercase letters represent the packing atoms, and the lower case letters are the interstitial atoms. This layered packing is illustrated below:

NaCl structure

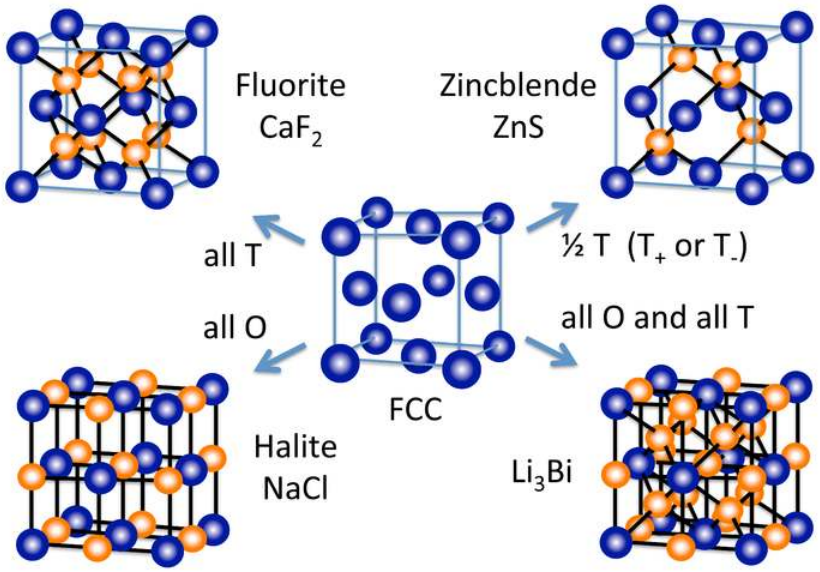
- ---------- A
- - - -c- - - -
- ---------- B
- - - -a- - - -
- ---------- C
- - - -b- - - -
- ---------- A
- - - -c- - - -
- ---------- B
- - - -a- - - -
- ---------- C
- - - -b- - - -
- ---------- A



Note that both the packing atoms and interstitials are stacked in the sequence A-B-C-A-B-C..., in keeping with the fact that each forms a cubic close-packed lattice.

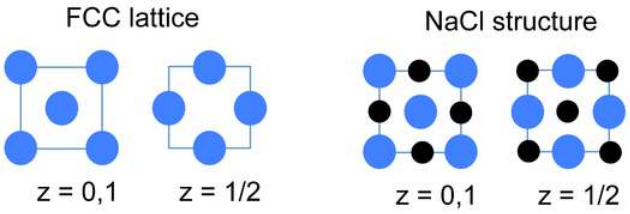
The NaCl structure is fairly common among ionic compounds:

- Alkali Halides (except CsCl, CsBr, and CsI)
- Transition Metal Monoxides (TiO, VO,..., NiO)
- Alkali Earth Oxides and Sulfides (MgO, CaO, BaS... except BeO and MgTe)
- Carbides and Nitrides (TiC, TiN, ZrC, NbC) -these are very stable refractory, interstitial alloys (metallic)



A number of other inorganic crystal structures are formed (at least conceptually) by filling octahedral and/or tetrahedral holes in close-packed lattices. The figure at the right shows some of the most common structures (fluorite, halite, zincblende) as well as a rather rare one (Li_3Bi) that derive from the fcc lattice. From the hcp lattice, we can make the NiAs and wurzite structures, which are the hexagonal relatives of NaCl and zincblende, respectively.

An alternative and very convenient way to represent inorganic crystal structures (especially complex structures such as Li_3Bi) is to draw the unit cell in slices along one of the unit cell axes. This kind of representation is shown at the left for the fcc lattice and the NaCl structure. Since all atoms in these structures have z-coordinates of either 0 or 1/2, only those sections need to be drawn in order to describe the contents of the unit cell. It is a useful exercise to draw some of the fcc compound structures (above) in sections.



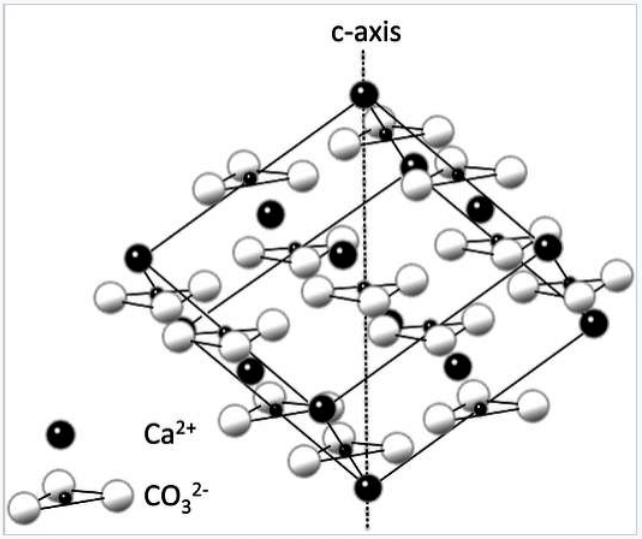
3.13: Close-packing and Interstitial Sites is shared under a CC BY-SA license and was authored, remixed, and/or curated by LibreTexts.

- **8.2: Close-packing and Interstitial Sites** by Chemistry 310 is licensed CC BY-SA 4.0. Original source: https://en.wikibooks.org/wiki/Introduction_to_Inorganic_Chemistry.

3.14: Structures Related to NaCl and NiAs

There are a number of compounds that have structures similar to that of NaCl, but have a lower symmetry (usually imposed by the geometry of the anion) than NaCl itself. These compounds include:

- FeS_2 (pyrite, "fools gold"): S_2^{2-} (disulfide) and Fe^{2+}
- CaC_2 (a salt-like carbide): Ca^{2+} and linear C_2^{2-} anions
- $CaCO_3$ (calcite, limestone, marble): Ca^{2+} and triangular CO_3^{2-}.



The rhombohedral unit cell of the calcite crystal structure. The hexagonal c-axis is shown.

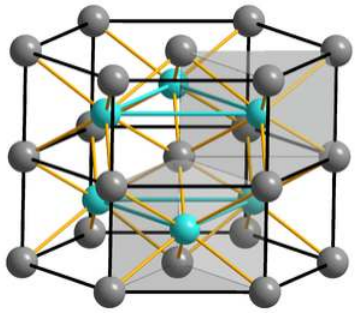
The **calcite** ($CaCO_3$) crystal structure is shown above. Triangular CO_3^{2-} ions fill octahedral holes between the Ca^{2+} ions (black spheres) in a distorted NaCl lattice. As in NaCl, each ion is coordinated by six of the other kind. From this image we can see why the $CaCO_3$ structure has a lower symmetry than that of NaCl. The fourfold rotation symmetry of the NaCl unit cell is lost when the spherical Cl^- ions are replaced by triangular CO_3^{2-} ions. Because of this symmetry lowering, transparent crystals calcite are birefringent, as illustrated below.



Calcite crystals are birefringent, meaning that their refractive indices are different along the two principal crystal directions. This gives rise to the phenomenon of double refraction.

NiAs structure

The NaCl structure can be described a face-centered cubic lattice with all of the octahedral holes filled. What if we start with a hexagonal-close packed lattice rather than a face-centered cubic lattice?



Nickel arsenide crystal structure. The Ni_6As trigonal prisms are shaded gray. One octahedron of six As atoms surrounding a Ni atom is shown in the center of the figure.

This is the structure adopted by **NiAs** and many other transition metal sulfides, phosphides, and arsenides. The cations are shown in gray while the anions are light blue in the figure at the right. The cations are in octahedral coordination, so each cation is coordinated to six anions. The anions are also coordinated to six cations, but they occupy trigonal prismatic sites. In terms of layer stacking, the NiAs structure is AcBcAcBc..., where the A and B sites (the hcp lattice) are occupied by the As atoms, and the c sites, which are eclipsed along the layer stacking axis, are occupied by Ni. Unlike the NaCl structure, where the anion and cation sites are interchangeable, NiAs has unique anion and cation sites. The layer stacking sequence for NiAs is shown below:

- ---------- A
- - - -c- - - -
- ---------- B
- - - -c- - - -
- ---------- A
- - - -c- - - -
- ---------- B
- - - -c- - - -

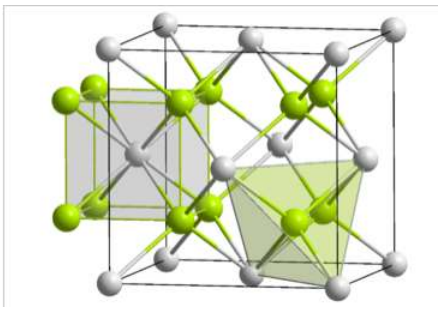
The NiAs structure cannot be adopted by ionic compounds because of the eclipsing cations, because the cation-cation repulsions would be internally destabilizing for an ionic compound. This structure is mainly adopted by covalent and polar covalent MX compounds, typically with "soft" X anions (S, Se, P, As,....) and low-valent transition metal cations. For example, some compounds with the NiAs structure are: MS, MSe, MTe (M=Ti, V, Fe, Co, Ni). Often these are nonstoichiometric or complex stoichiometries with ordered vacancies (Cr_7S_8, Fe_7S_8).

3.14: Structures Related to NaCl and NiAs is shared under a CC BY-SA license and was authored, remixed, and/or curated by LibreTexts.

- **8.3: Structures Related to NaCl and NiAs** by Chemistry 310 is licensed CC BY-SA 4.0. Original source: https://en.wikibooks.org/wiki/Introduction_to_Inorganic_Chemistry.

3.15: Tetrahedral Structures

In ccp and hcp lattices, there are two tetrahedral holes per packing atom. A stoichiometry of either M_2X or MX_2 gives a structure that fills all tetrahedral sites, while an MX structure fills only half of the sites. An example of an MX_2 structure is **fluorite**, CaF_2, whose structure is shown in the figure at the left. The packing atom in fluorite is Ca^{2+} and the structure is composed of three interpenetrating fcc lattices. It should be noted that the Ca^{2+} ion (gray spheres) as a packing atom defies our "rule" that anions are larger than cations and therefore must be the packing atoms. The fluorite structure is common for ionic MX_2 (MgF_2, ZrO_2, etc.) and M_2X compounds (Li_2O). In contrast, the hcp relative of the fluorite structure is quite rare because of unfavorable close contacts between like-charged ions.



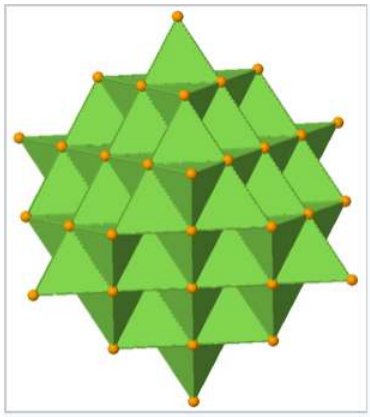
The fluorite (CaF_2) crystal structure showing the coordination environments of the Ca and F atoms

In terms of geometry, Ca^{2+} is in cubic coordination with eight F^- neighbors, and the fluoride ions are tetrahedrally coordinated by four Ca^{2+} ions. The 8:4 coordination geometry is consistent with the 1:2 Ca:F stoichiometry; in all crystal structures the ratio of the coordination numbers is the inverse of the stoichiometric ratio. The three interpenetrating fcc lattices have Ca at 0,0,0 , 1/2,1/2,0 , etc....F at 1/4,1/4,1/4 , 3/4,3/4,1/4 , etc... and F at 3/4,3/4,3/4 , 1/4,1/4/3/4 , etc.

Looking more closely at the tetrahedral sites in fluorite, we see that they fall into two distinct groups: T_+ and T_-. If a tetrahedron is oriented with a vertex pointing upwards along the stacking axis, the site is T_+. Likewise, a tetrahedron with a vertex oriented downward is T_-. The alternation of T_+ and T_- sites allows for efficient packing of ions in the structure. The layer stacking sequence in this structure (including fluoride ions in the T_+ and T_- sites) is:

- ---------- A
- - - -b- - - T_+
- - - -a- - - T_-
- ---------- B
- - - -c- - - T_+
- - - -b- - - T_-
- ---------- C
- - - -a- - - T_+
- - - -c- - - T_-
- ---------- A
- - - -b- - - T_+

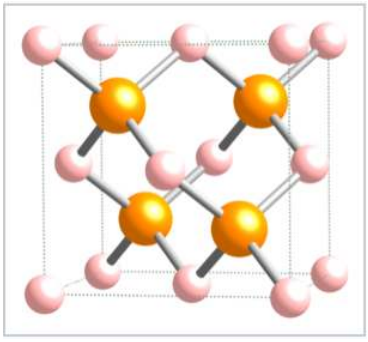
- - - -a- - - T_-



Polyhedral view of the fluorite crystal structure, showing T_+ and T_- Ca_4F tetrahedra. The Ca^{2+} ions are stacked ABCABC... along the body diagonal of the unit cell, which is the vertical direction in this image.

Tetrahedrally bonded compounds with a 1:1 stoichiometry (MX compounds) have only **half** of the tetrahedral sites (either the T_+ or T_- sites) filled. In this case, both the M and the X atoms are tetrahedrally coordinated. The **zincblende** and **wurtzite** structures of ZnS are 1:1 tetrahedral structures based on fcc and hcp lattices, respectively. Both structures are favored by p-block compounds that follow the octet rule, and these compounds are usually semiconductors or insulators. The zincblende structure, shown below, can be thought of as two interpenetrating fcc lattices, one of anions and one of cations, offset from each other by a translation of 1/4 along the body diagonal of the unit cell. Examples of compounds with the zincblende structure include CuCl, CuI, ZnSe, HgS, BeS, CdTe, AlP, GaP, SnSb, CSi, and diamond. Additionally, the compound $CuInSe_2$ is zincblende in an ordered, doubled unit cell (the chalcopyrite structure). The solid solution compounds $CuIn_{1-x}Ga_xSe_2$ with this structure are among the most widely studied materials for use in efficient thin film photovoltaic cells. Using ZnS as a representative of zincblende, the coordination of both Zn and S atoms is tetrahedral. The layer sequence, which is AbBcCaAbBcC..., results in non-planar, six-membered ZnS rings which allows for a relatively long distance between opposite atoms in the ring. The sequence of close-packed layers in zincblende, filling only the T_+ sites and leaving the T_- sites empty, is shown below:

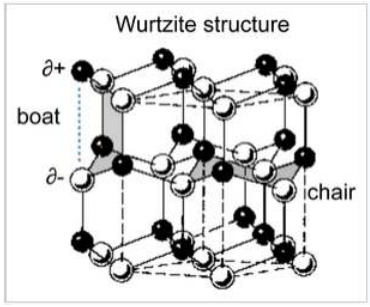
- ---------- A
- - - -b- - - T_+
- - - - - - T_-
- ---------- B
- - - -c- - - T_+
- - - - - - T_-
- ---------- C
- - - -a- - - T_+
- - - - - - T_-



The zincblende unit cell

The wurtzite structure is a close relative of zinc blende, based on filling half the tetrahedral holes in the hcp lattice. Like zincblende, wurtzite contains planes of fused six-membered rings in the chair conformation. Unlike zincblende, however, the rings joining these planes contain non-planar, six-membered rings. The structure aligns the anions so that they are directly above the cations in the structure, a less favorable situation sterically but a more favorable one in terms of electrostatics. As a result, the wurtzite structure tends to favor more polar or ionic compounds (e.g., ZnO, $NH_4^+F^-$) than the zincblende structure. As with zincblende, both ions are in tetrahedral (4:4) coordination and there are typically eight valence electrons in the MX compound. Examples of compounds with this structure include: BeO, ZnO, MnS, CdSe, MgTe, AlN, and NH_4F. The layered structure of wurtzite is AbBaAbB and the layer sequence with T_+ sites filled is illustrated below:

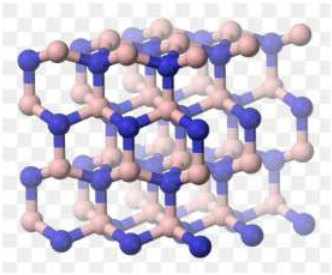
- ---------- A
- - - -b- - - T_+
- - - - - - - T_-
- ---------- B
- - - -a- - - T_+
- - - - - - - T_-
- ---------- A
- - - -b- - - T_+
- - - - - - - T_-
- ---------- B



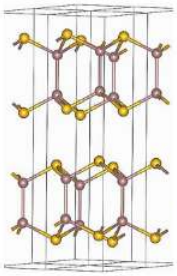
The chair and boat conformations of six-membered ZnS rings in the wurtzite structure.

An interesting consequence of the layer stacking in the wurtzite structure is that the crystals are polar. When cleaved along the c-axis (the stacking axis), crystals of ZnO, ZnS, and GaN have one negatively charged face and an opposite positively charged face. An applied electric field interacts with the crystal dipole, resulting in compression or elongation of the lattice along this direction. For this reason crystals of compounds in the wurtzite structure are typically piezoelectric (increasing the pressure on the material generates a voltage in the material).

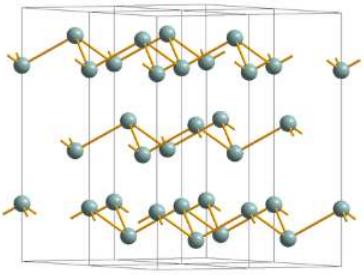
Some compounds are diamorphic and can have either the zincblende or wurtzite structure. Examples of these compounds that have intermediate polarities include CdS and ZnS. SiO_2 exists in polymorphs (crystobalite and tridymite) that resemble zincblende and wurtzite with O atoms midway between each of the Si atoms. The zincblende and wurtzite structures have efficient packing arrangements for tetrahedrally bonded networks and are commonly found in compounds that have tetrahedral bonding. Water, for example, has a tetrahedral hydrogen bonding network and is wurtzite-type. The undistorted wurtzite and zinc blende structures are typically found for AX compounds with eight valence electrons, which follow the octet rule. AX compounds with nine or ten electrons such as GaSe and GaAs crystallize in distorted variants of the wurtzite structure. In GaSe, the extra electrons form lone pairs and this creates layers in the structure, as can be seen in the figure below. To the right of GaSe, the structures of As, Sb, and SbAs show an ever further breakdown of the structure into layers as more valence electrons are added.



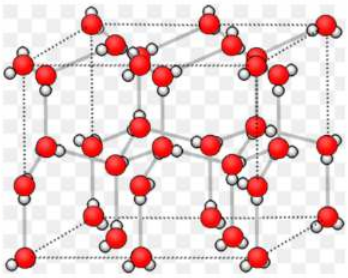
Wurtzite crystal structure



GaSe crystal structure



Crystal structure of Sb, SbAs, and gray As



Crystal structure of hexagonal ice

Hexagonal ice is the most stable polymorph of ice, which is obtained upon freezing at 1 atmosphere pressure. This polymorph (ice-I) has a hcp wurtzite-type structure. Looking at the structure shown at the right, we see that there are irregular arrangements of the O-H---O bonds. In the structure, hydrogen bonding enforces the tetrahedral coordination of each water molecule, resulting in a relatively open structure that is less dense than liquid water. For this reason, ice floats in water.

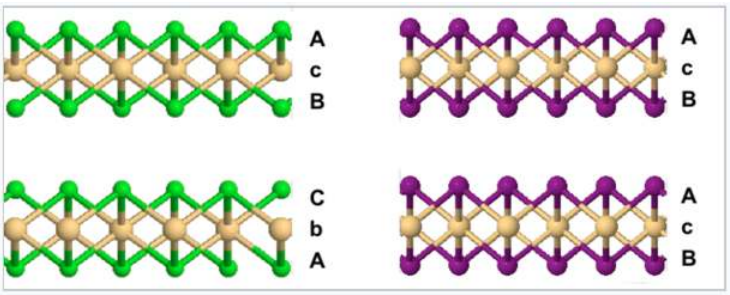
3.15: Tetrahedral Structures is shared under a CC BY-SA license and was authored, remixed, and/or curated by LibreTexts.

- **8.4: Tetrahedral Structures** by Chemistry 310 is licensed CC BY-SA 4.0. Original source: https://en.wikibooks.org/wiki/Introduction_to_Inorganic_Chemistry.

3.16: Layered Structures and Intercalation Reactions

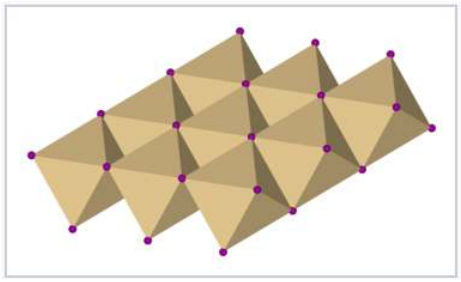
Layered structures are characterized by strong (and typically covalent) bonding between atoms in two dimensions and weaker bonding in the third. A broad range of compounds including metal halides, oxides, sulfides, selenides, borides, nitrides, carbides, and allotropes of some pure elements (B, C, P, As) exist in layered forms. Structurally, the simplest of these structures (for example binary metal halides and sulfides) can be described as having some fraction of the octahedral and/or tetrahedral sites are filled in the fcc and hcp lattices. For example, the $CdCl_2$ structure is formed by filling all the octahedral sites in alternate layers of the fcc lattice, and the CdI_2 structure is the relative of this structure in the hcp lattice.

In the **$CdCl_2$ structure**, the stacking sequence of anion layers is ABCABC...
In the **CdI_2 structure**, the anion stacking sequence is ABAB..., and all the cations are eclipsed along the stacking axis.



Comparison of the $CdCl_2$ (left) and CdI_2 (right) crystal structures

These are examples of **6-3 structures**, because the cations are coordinated by an octahedron of six anions, and the anions are coordinated by three cations to make a trigonal pyramid (like NH_3). Another way to describe these structures is to say that the MX_6 octahedra each share six edges in the MX_2 sheets.



Polyhedral drawing of one layer of the $CdCl_2$ or CdI_2 structure showing edge-sharing MX_6 octahedra

Because these structures place the packing atoms (the anions) in direct van der Waals contact, they are most stable for relatively **covalent** compounds. Otherwise, the electrostatic repulsion between contacting anions would destabilize the structure energetically. More ionic MX_2 compounds tend to adopt the fluorite (CaF_2) or rutile (TiO_2) structures, which are not layered.

Despite the fact that these two structure types are the same at the level of nearest and next-nearest neighbor ions, the CdI_2 structure is much more common than the $CdCl_2$ structure.

$CdCl_2$ structure:

MCl_2 (M = Mg, Mn, Fe, Co, Ni, Zn, Cd)

$NiBr_2$, NiI_2, $ZnBr_2$, ZnI_2

CdI_2 structure:

MCl_2 (M = Ti, V)

MBr_2 (M = Mg, Fe, Co, Cd)

MI_2 (M = Mg, Ca, Ti, V, Mn, Fe, Co, Cd, Ge, Pb, Th)

$M(OH)_2$ (M = Mg, Ca, Mn, Fe, Co, Ni, Cd)

MS_2 (M = Ti, Zr, Sn, Ta, Pt)

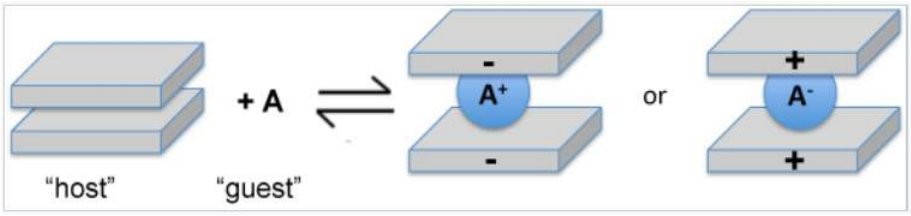
MSe_2 (M = Ti, Zr, Sn, V, Pt)

MTe_2 (M = Ti, Co, Ni, Rh, Pd, Pt)

Physically, layered compounds are **soft** and **slippery**, because the layer planes slide past each other easily. For example, graphite, MoS_2, and talc (a silicate) are layered compounds that are used widely as **lubricants** and lubricant additives.

An important reaction of layered compounds is **intercalation**. In intercalation reactions, guest molecules and ions enter the galleries that separate the sheets, usually with expansion of the lattice along the stacking axis. This reaction is typically reversible if it does not perturb the bonding within the sheets. Often the **driving force for intercalation is a redox reaction**, i.e., electron transfer between the host and guest. For example, lithium metal reacts with TiS_2, MoS_2, and graphite to produce $LiTiS_2$, Li_xMoS_2 ($x < 1$), and LiC_6. In these compounds, lithium is ionized to Li^+ and the sheets are negatively charged. Oxidizing agents such as Br_2, $FeCl_3$, and AsF_5 also react with graphite. In the resulting intercalation compounds, the sheets are positively charged and the intercalated species are anionic.

Intercalation reactions are especially important for electrochemical energy storage in **secondary batteries**, such as **lithium ion** batteries, **nickel-metal hydride** batteries, and **nickel-cadmium** batteries. The reversible nature of the intercalation reaction allows the electrodes to be charged and discharged up to several thousand times without losing their mechanical integrity. In lithium ion batteries, the negative electrode material is typically graphite, which is intercalated by lithium to make LiC_6. Several different oxides and phosphates containing redox active transition metal ions (Mn, Fe, Co, Ni) are used as the positive electrode materials.



Oxidative or reductive intercalation involves the placement of anions or cations between sheets.

Lithium ion batteries based on CoO_2 were first described in 1980[1] by John B. Goodenough's research group at Oxford. In batteries based on CoO_2, which has the CdI_2 structure, the positive electrode half-reaction is:

$$\mathrm{LiCoO_2 \leftrightharpoons Li_{1-x}CoO_2 + x\,Li^+ + xe^-} \tag{3.16.1}$$

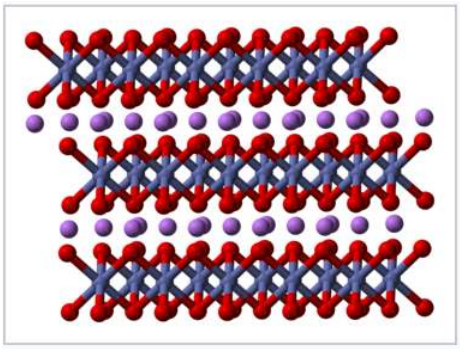
The negative electrode half reaction is:

$$\mathrm{x\,Li^+ + xe^- + x\,C_6 \leftrightharpoons x\,LiC_6} \tag{3.16.2}$$

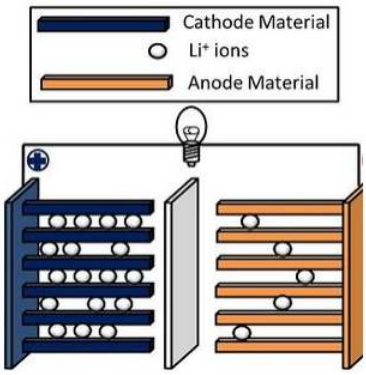
The battery is fully charged when the positive electrode is in the CoO_2 form and the negative electrode is in the LiC_6 form. Discharge involves the motion of Li^+ ions through the electrolyte, forming Li_xCoO_2 and graphite at the two electrodes.



Blue plaque erected by the Royal Society of Chemistry commemorating the development of cathode materials for the lithium-ion battery



Crystal structure of $LiCoO_2$[2]



The lithium ion battery is a "rocking chair" battery, so named because charging and discharging involve moving Li^+ ions from one side to the other. CoO_2 is one example of a positive electrode material that has been used in lithium ion batteries. It has a high energy density, but batteries based on CoO_2 have poor thermal stability. Safer materials include lithium iron phosphate ($LiFePO_4$), and $LiMO_2$ (M = a mixture of Co, Mn, and Ni). These batteries are used widely in laptop computers, portable electronics, cellular telephones, cordless tools, and electric and hybrid vehicles.

A similar intercalation reaction occurs in nickel-cadmium batteries and nickel-metal hydride batteries, except in this case the reaction involves the movement of protons in and out of the $Ni(OH)_2$ lattice, which has the CdI_2 structure:

$$\mathrm{NiO(OH) + H_2O + e^- \longrightarrow Ni(OH)_2 + OH^-} \tag{3.16.3}$$

There are many layered compounds that cannot be intercalated by redox reactions, typically because some other stable product is formed. For example, the reaction of layered CdI_2 with Li produces LiI (NaCl structure) and Cd metal.

3.16: Layered Structures and Intercalation Reactions is shared under a CC BY-SA license and was authored, remixed, and/or curated by LibreTexts.

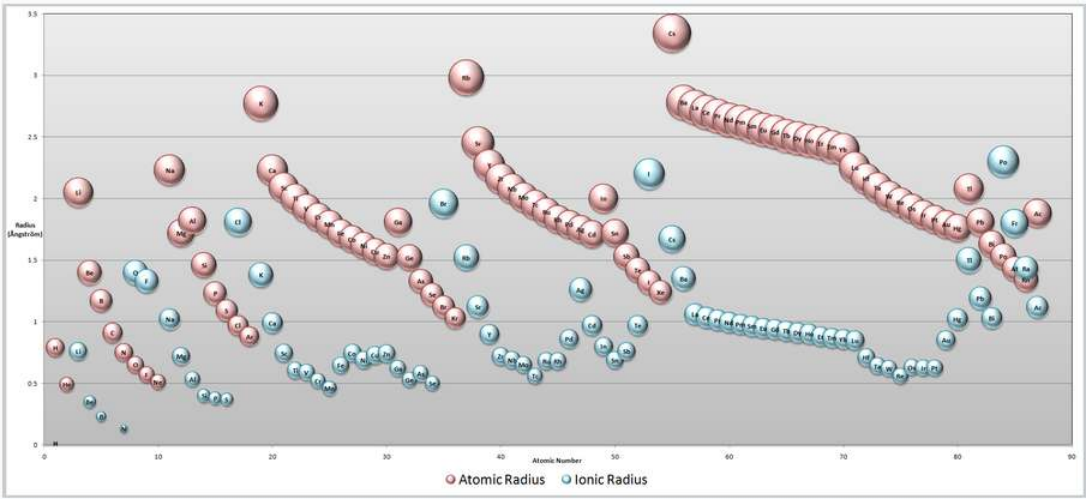
- **8.5: Layered Structures and Intercalation Reactions** by Chemistry 310 is licensed CC BY-SA 4.0. Original source: https://en.wikibooks.org/wiki/Introduction_to_Inorganic_Chemistry.

3.17: Ionic Radii and Radius Ratios

Atoms in crystals are held together by electrostatic forces, van der Waals interactions, and covalent bonding. It follows that arrangements of atoms that can maximize the strength of these attractive interactions should be most favorable and lead to the most commonly observed crystal structures.

Radius ratio rules

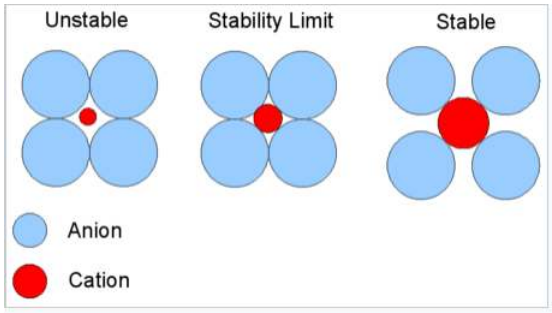
Early crystallographers had trouble solving the structures of inorganic solids using X-ray diffraction because some of the mathematical tools for analyzing the data had not yet been developed. Once a trial structure was proposed, it was relatively easy to calculate the diffraction pattern, but it was difficult to go the other way (from the diffraction pattern to the structure) if nothing was known *a priori* about the arrangement of atoms in the unit cell. It was (and still is!) important to develop some guidelines for guessing the coordination numbers and bonding geometries of atoms in crystals. The first such rules were proposed by Linus Pauling, who considered how one might pack together oppositely charged spheres of different radii. Pauling proposed from geometric considerations that the quality of the "fit" depended on the **radius ratio** of the anion and the cation.



Atomic and Ionic Radii. Note that cations are always smaller than the neutral atom (pink) of the same element, whereas anions are larger. Going from left to right across any row of the periodic table, neutral atoms and cations contract in size because of increasing nuclear charge. (click for larger image)

The basic idea of radius ratio rules is illustrated at the right. We consider that the anion is the packing atom in the crystal and the smaller cation fills interstitial sites ("holes"). Cations will find arrangements in which they can contact the largest number of anions. If the cation can touch all of its nearest neighbor anions, as shown at the right for a small cation in contact with larger anions, then the fit is good. If the cation is too small for a given site, that coordination number will be unstable and it will prefer a

lower coordination structure. The table below gives the ranges of cation/anion radius ratios that give the best fit for a given coordination geometry.



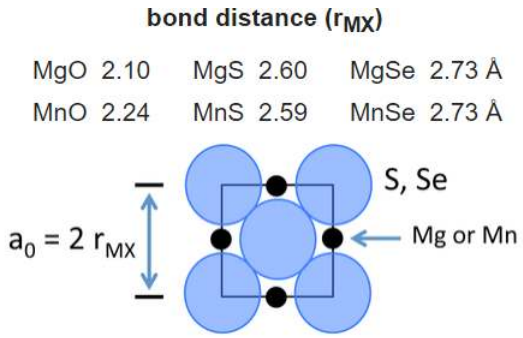
Critical Radius Ratio. This diagram is for coordination number six: 4 anions in the plane are shown, 1 is above the plane and 1 is below. The stability limit is at $r_C/r_A = 0.414$

Coordination number	Geometry	$\rho = r_{cation}/r_{anion}$
2	linear	0 - 0.155
3	triangular	0.155 - 0.225
4	tetrahedral	0.225 - 0.414
4	square planar	0.414 - 0.732
6	octahedral	0.414 - 0.732
8	cubic	0.732 - 1.0
12	cuboctahedral	1.0

There are unfortunately several challenges with using this idea to predict crystal structures:

- We don't know the radii of individual ions
- Atoms in crystals are not really ions - there is a varying degree of covalency depending electronegativity differences
- Bond distances (and therefore ionic radii) depend on bond strength and coordination number (remember Pauling's rule D(n) = D(1) - 0.6 log n)
- Ionic radii depend on oxidation state (higher charge => smaller cation size, larger anion size)

We can build up a table of ionic radii by assuming that the bond length is the sum of the radii ($r_+ + r_-$) if the ions are in contact in the crystal. Consider for example the compounds MgX and MnX, where X = O, S, Se. All of these compounds crystallize in the NaCl structure:



For the two larger anions (S^{2-} and Se^{2-}), the unit cell dimensions are the same for both cations. This suggests that the anions are in contact in these structures. From geometric considerations, the anion radius in this case is given by:

Extra close brace or missing open brace

and thus the radii of the S^{2-} and Se^{2-} ions are 1.84 and 1.93 Å, respectively. Once the sizes of these anions are fixed, we can obtain a self-consistent set of cation and anion radii from the lattice constants of many MX compounds.

How well does this model work? Let's consider the structures of tetravalent metal oxides (MO_2), using Pauling radii and the predictions of the radius ratio model:

Oxide MO_2	Radius ratio	Predicted coord. no.	Observed coord no. (structure)
CO_2	~0.1	2	2 (linear molecule)
SiO_2	0.32	4	4 (various tetrahedral structures)
GeO_2	0.43	4	4 (silica-like structures)
"	0.54	6	6 (rutile)
TiO_2	0.59	6	6 (rutile)
ZrO_2	0.68	6	7 (baddleyite)
"	0.77	8	8 (fluorite)
ThO_2	0.95	8	8 (fluorite)

Note that cations have different radii depending on their coordination numbers, and thus different radius ratios are calculated for Ge^{4+} with coordination numbers 4 and 6, and for Zr^{4+} with coordination numbers 6 and 8.

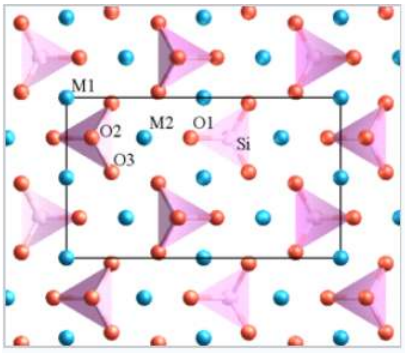
For this series of oxides, the model appears to work quite well. The correct coordination number is predicted in all cases, and borderline cases such as GeO_2 and ZrO_2 are found in structures with different coordination numbers. The model also correctly predicts the structures of BeF_2 (SiO_2 type), MgF_2 (rutile), and CaF_2 (fluorite).

What about the alkali halides NaCl, KBr, LiI, CsF, etc.? All of them have the NaCl structure except for CsCl, CsBr, and CsI, which have the CsCl (8-8) structure. In this case the radius ratio model fails rather badly. The Li^+ salts LiBr and LiI are predicted to have tetrahedral structures, and KF is predicted to have an 8-8 structure like CsCl. We can try adjusting the radii (e.g., making the cations larger and anions smaller), but the best we can do with the alkali halides is predict about half of their structures correctly. Since the alkali halides are clearly ionic compounds, this failure suggests that there is something very wrong with the radius ratio model, and its success with MO_2 compounds was coincidental.

In addition to the radius ratio rule, Linus Pauling developed other useful rules that are helpful in rationalizing and also predicting the structures of inorganic compounds. Pauling's rules[1] state that:

- Stable structures are **locally electroneutral**. For example, in the structure of the double perovskite Sr_2FeMoO_6, MO_6 (M = Fe^{2+}, Mo^{6+}) octahedra share all their vertices, and Sr^{2+} ions fill the cubooctahedral cavities that are flanked by eight MO_6 octahedra.[2] Each O^{2-} ion is coordinated to one Fe^{2+} and one Mo^{6+} ion in order to achieve local electroneutrality, and thus the FeO_6 and MoO_6 octahedra alternate in the structure.
- **Cation-cation repulsion** should be minimized. Anion polyhedra can share vertices (as in the perovskite structure) without any energetic penalty. Shared polyhedral edges, and especially shared faces, cause cation-cation repulsion and should be avoided. For example, in rutile, the most stable polymorph of TiO_2, the TiO_6 octahedra share vertices and two opposite edges, forming ribbons in the structure. In anatase TiO_2, each octahedron shares four edges so the anatase polymorph is less thermodynamically stable.

- **Highly charged cations** in anion polyhedra tend not to share edges or even vertices, especially when the coordination number is low. For example, in orthosilicates such as olivine (M_2SiO_4), there are isolated SiO_4^{4-} tetrahedra.



Structure of olivine. M (Mg or Fe) = blue spheres, Si = pink tetrahedra, O = red spheres.

As we will soon see, all of Pauling's rules are justified on the basis of lattice energy considerations. In ionic compounds, the arrangement of atoms that maximizes anion-cation interactions while minimizing cation-cation and anion-anion contacts is energetically the best.

3.17: Ionic Radii and Radius Ratios is shared under a CC BY-SA license and was authored, remixed, and/or curated by LibreTexts.

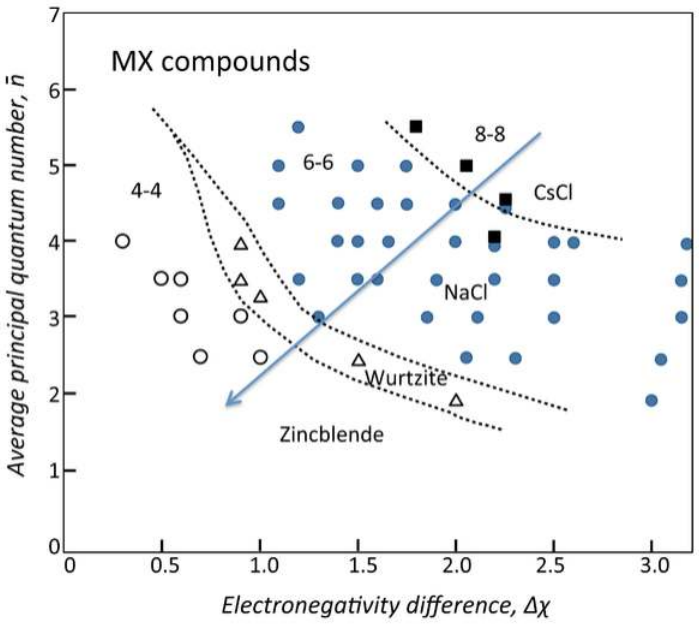
- **9.1: Ionic Radii and Radius Ratios** by Chemistry 310 is licensed CC BY-SA 4.0. Original source: https://en.wikibooks.org/wiki/Introduction_to_Inorganic_Chemistry.

3.18: Structure Maps

Structure maps, which plot structures against properties such electronegativity, are more consistent than radius ratio rules in correctly predicting coordination numbers and crystal structures. One of the early examples of this approach was published by Mooser and Pearson in 1959.[3]

A **Mooser-Pearson diagram** maps crystal structures according to the average principal quantum numbers of the atoms and their electronegativity difference. The basic ideas behind such a plot are:

- The greater the electronegativity difference, the more ionic is the compound. Higher ionicity results in higher coordination numbers because anions like to surround cations (and vice versa).
- Higher principal quantum numbers result in less s-p hybridization, less directional bonding, and therefore higher coordination number. We saw this trend before with the structures of elements in group IV: descending the group the coordination number increases progressively from 3-4 (carbon) to 12 (Pb).



The lines in the Mooser-Pearson diagram separate MX compounds with CsCl, NaCl, and tetrahedral (wurtzite and zincblende) structures. Note that wurtzite has higher ionicity than zincblende in the plot, consistent with our discussion of the "boat" and "chair" ring structures in Chapter 8. Diamorphic compounds tend to fall on the boundaries. On the whole, the Mooser-Pearson diagram makes far fewer errors in predicting structures than the radius ratio rule. There are similar diagrams for MX_2 structures, in which the order of ionicity is CaF_2 (8:4 coordination) > rutile (6:3) > silica structures (4:2).

3.18: Structure Maps is shared under a CC BY-SA license and was authored, remixed, and/or curated by LibreTexts.

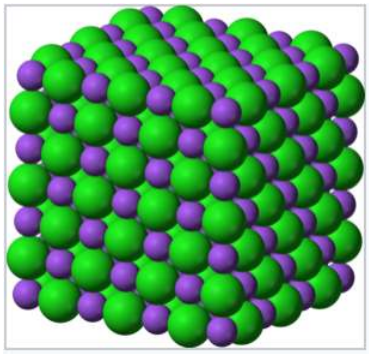
- **9.2: Structure Maps** by Chemistry 310 is licensed CC BY-SA 4.0. Original source: https://en.wikibooks.org/wiki/Introduction_to_Inorganic_Chemistry.

3.19: Energetics of Crystalline Solids- The Ionic Model

Many ionic compounds have simple structures. Because the forces holding the atoms together are primarily electrostatic, we can calculate the cohesive energy of the crystal lattice with good accuracy. Interesting questions to ask about these lattice energy calculations are:

- How accurate are lattice energy calculations?
- What do they teach us about the chemical bonds in ionic crystals?
- Can we use lattice energies to predict properties such as solubility, stability, and reactivity?
- Can we use lattice energies to predict the crystal structures of ionic compounds?

Let's start by looking at the forces that hold ionic lattices together. There are mainly two kinds of force that determine the energy of an ionic bond.



The NaCl crystal structure is the archetype for calculating lattice energies and computing enthalpies of formation from Born-Haber cycles.

1) **Electrostatic Force** of attraction and repulsion (Coulomb's Law): Two ions with charges z_+ and z_-, separated by a distance r, experience a force F:

$$\mathbf{F} = -\frac{e^2}{4\pi\varepsilon_0}\frac{z_+z_-}{r^2} \tag{3.19.1}$$

where

e = 1.6022×10^{-19} C

4 π ε_0 = 1.112×10^{-10} C²/(J m)

This force is attractive for ions of opposite charge.

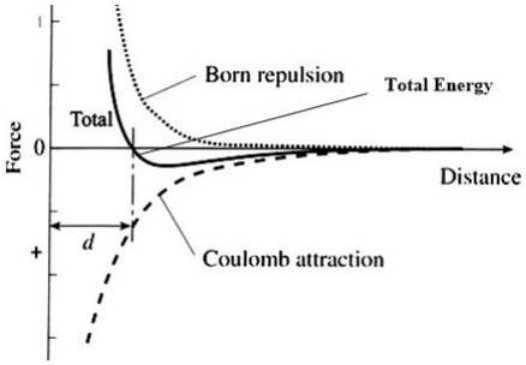
The electrostatic potential energy, E_{elec}, is then given by

$$\mathbf{E}_{elec}\int_{\infty}^{r} F(r)dr = \frac{e^2}{4\pi\varepsilon_0}\frac{z_+z_-}{r} \tag{3.19.2}$$

The sign of E_{elec} is negative for the attractive interaction between a cation and an anion. That is, the closer oppositely charged ions approach each other, the lower the potential energy.

2) **Closed-shell repulsion**. When electrons in the closed shells of one ion overlap with those of another ion, there is a repulsive force comes from the Pauli exclusion principle. A third electron cannot enter an orbital that already contains two electrons. This force is short range, and is typically modeled as falling off exponentially or with a high power of the distance r between atoms. For example, in the Born approximation, B is a constant and ρ is a number with units of length, which is usually empirically determined from compressibility data. A typical value of ρ is 0.345 Å.

$$\mathbf{E}_{repulsion} = Bexp(\frac{-r}{\rho}) \tag{3.19.3}$$



The energy of the ionic bond between two atoms is then calculated as the combination of net electrostatic and the closed-shell repulsion energies, as shown in the figure at the right. Note that for the moment we are ignoring the attractive van der Waals energy between ions, which we will explain below. For a pair of ions, the equilibrium distance between ions is determined by the minimum in the total energy curve. At this distance, the net force on each ion is zero.

Electrostatic energy of a crystal lattice

We can use these equations to calculate the lattice energy of a crystal by summing up the interactions between all pairs of ions. Because the closed-shell repulsion force is short range, this term is typically calculated only for interactions between neighboring ions. However, the Coulomb force is long range, and must be calculated over the entire crystal. This problem was first solved in 1918 by Erwin Madelung, a German physicist.[4]

Consider an ion in the NaCl structure labeled "O" in the diagram at the right. We can see that the nearest neighbor interactions (+ -) with ions labeled "1" are attractive, the next nearest neighbor interactions (- - and + +) are repulsive, and so on. In the NaCl structure, counting from the ion in the center of the unit cell, there are 6 nearest neighbors (on the faces of the cube), 12 next nearest neighbors (on the edges of the cube), 8 in the next shell (at the vertices of the cube), and so on. Their distances from ion "0" increase progressively: r_o, $\sqrt{2}\ r_o$, $\sqrt{3}\ r_o$, and so on, where r_o is the nearest neighbor distance.

We can now write the electrostatic energy at ion "O" as:

$$\mathbf{E}_{elec} = -6\frac{e^2}{4\pi\varepsilon_0}\frac{z_+z_-}{r_o} + 12\frac{e^2}{4\pi\varepsilon_0}\frac{z_+z_-}{\sqrt{2}r_o} - 8\frac{e^2}{4\pi\varepsilon_0}\frac{z_+z_-}{\sqrt{3}r_o} + \ldots \tag{3.19.4}$$

Factoring out constants and the nearest-neighbor bond distance r_o we obtain:

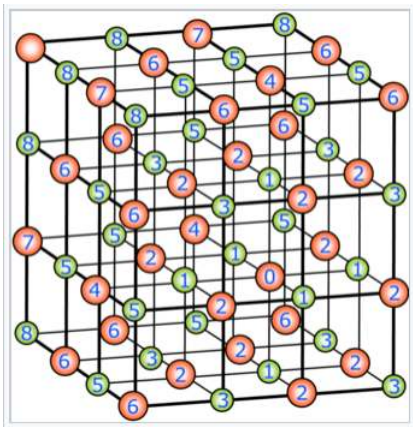
$$\mathbf{E}_{elec} = \frac{e^2}{4\pi\varepsilon_0}\frac{z_+z_-}{r_o}\left(6 - \frac{12}{\sqrt{2}} + \frac{8}{\sqrt{3}} - \frac{6}{\sqrt{4}} + \ldots\right) \tag{3.19.5}$$

Where the sum in parentheses, which is unitless, slowly converges to a value of A = 1.74756. Generalizing this formula for any three-dimensional ionic crystal we get a function:

$$\mathbf{E}_{elec} = \frac{e^2}{4\pi\varepsilon_0}\frac{z_+z_-}{r_o}NA \tag{3.19.6}$$

where N is Avogadro's number (because we are calculating energy per mole of ions) and A is called the *Madelung constant*. The **Madelung constant** depends only on the geometrical arrangement of the ions and so it varies between different types of crystal

structures, but within a given structure type it does not change. Thus MgO and NaCl have the same Madelung constant because they both have the NaCl structure. We will see more about the Madelung constant in an upcoming section.



The Madelung constant is calculated by summing up electrostatic interactions with ion labeled 0 in the expanding spheres method. Each number designates the order in which it is summed. For example, ions labeled 1 represent the six nearest neighbors (attractive interaction), ions labeled 2 are the 12 next nearest neighbors (repulsive interaction) and so on. Note that if the sum is carried out over shells 1-2-3..., it converges very slowly, but there are mathematical methods for summing it which give a rapidly converging series.

Total lattice energy of a crystal

Having in hand a formula for the electrostatic energy, we can now add in the closed-shell repulsion term to obtain an equation that gives us the total lattice energy.

$$E_L = \frac{e^2}{4\pi\varepsilon_0}\frac{z_+z_-}{r_o}NA + NBexp(\frac{-r}{\rho}) \tag{3.19.7}$$

At the equilibrium bond distance, the forces on all the ions are zero, and we can use this fact to eliminate the constant B:

$$[\frac{dE}{dr}]_{r=r_o} = 0 \tag{3.19.8}$$

Expressed this way, E_L is a negative number (because z_+ and z_- have opposite signs). It represents the energy change for forming one mole of solid salt from one mole of the gaseous ions, separated initially at an infinite distance.



Lithium fluoride (shown here as a large single crystal in a beaker of water) is the only alkali halide that is not freely soluble in water. The lattice energy of LiF is the most negative of the alkali fluorides because Li^+ and F^- are both small ions and E_L is proportional to $1/r_0$.

3.19: Energetics of Crystalline Solids- The Ionic Model is shared under a CC BY-SA license and was authored, remixed, and/or curated by LibreTexts.

- **9.3: Energetics of Crystalline Solids- The Ionic Model** by Chemistry 310 is licensed CC BY-SA 4.0. Original source: https://en.wikibooks.org/wiki/Introduction_to_Inorganic_Chemistry.

3.20: Born-Haber Cycles for NaCl and Silver Halides

Now that we have an equation for the lattice energy of an ionic crystal, we can ask the question of how accurate it is. Remember, we made several approximations in arriving at this formula. We assumed that the lattice was completely ionic, we ignored the van der Waals attractive energy of the ions, and we assumed that there was no covalent contribution to the bonding.

Let's consider the lattice energy of table salt (NaCl)

$$Na^+_{(g)} + Cl^-_{(g)} \longrightarrow NaCl_{(s)}$$

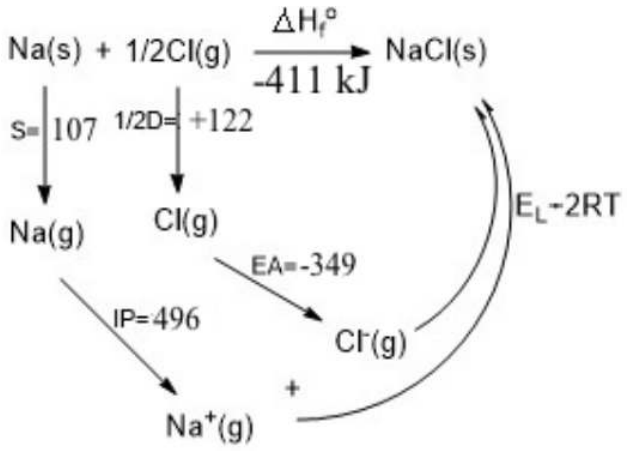
To calculate the lattice energy, we lump together the physical constants:

$$E_L(\frac{kJ}{mol}) = (1389.3)\frac{Aq_1q_2}{r_o}(1 - \frac{.345}{r_o}) \tag{3.20.1}$$

where r_o is expressed in Å. Now we can calculate the lattice energy for NaCl using r_o = 2.814 Å, as:

$$E_L = -(1389.3)\frac{1.7476}{2.814}(1 - \frac{.345}{2.814}) = -766.5\frac{kJ}{mol} \tag{3.20.2}$$

We can alternatively construct a **Born-Haber cycle** for the formation of NaCl from the elements and calculate the lattice energy as the "missing" term in the cycle.



S= Sublimation energy of Na(s)

IP= Ionization potential of Na(g)

D= Bond dissocation energy of Cl_2(g)

EA= Electron affinity of Cl(g)

E_L=Lattice energy of NaCl

R= Gas constant

T= Absolute temperature

From **Hess' Law:** $\Delta H_f = s + \frac{1}{2}D + IP + EA + E_L - 2RT = -396\frac{kJ}{mol}$

Here we have to subtract 2RT to convert our cycle of energies to a cycle of enthalpies, because we are compressing two moles of gas in making NaCl(s) and PΔV = ΔnRT, where Δn = -2.

Experimentally ΔH_f for NaCl is **-411 kJ/mol**

Because all the other numbers in the cycle are known accurately, the error in our calculation is only about 15 kJ (about 2% of E_L). The result is promising because we neglected the van der Waals term.

But....how did we get away with neglecting the van der Waals term?

This is because we used **energy minimization** to obtain the repulsion energy in the Born-Mayer equation. If we underestimate the attractive energy of the crystal lattice, the energy minimization criterion ensures that the repulsion energy is underestimated as well. The two errors partially compensate, so the overall error in the calculation is small.

We can do better by explicitly including the short-range van der Waals attractive energy between ions. The table below shows results of more detailed lattice energy calculations for ionic fluorides in which the van der Waals term is explicitly included. The errors in this case are only about 1% of E_L.

Compound	Calculated Lattice Energy (kJ/mol)	Experimental E_L from Born-Haber Cycle
MgF_2 (rutile structure)	-2,920	-2,908
CaF_2 (fluorite structure)	-2,586	-2,611
BaF_2 (fluorite structure)	-2,326	-2,368

Silver Halides

It is interesting to repeat this exercise for the silver halides, which have either the NaCl structure (AgF, AgCl, AgBr) or zincblende structure (AgI).

Silver Halide	Calculated	Cycle	Difference (kJ/mol)
AgF	-920	-954	34
AgCl	-833	-908	75
AgBr	-816	-900	84
AgI	-778	-883	105

Looking at the table, we see that the error is small for AgF and becomes progressively larger for the heavier silver halides. However we are still obtaining answers within about 12% error even for AgI. Should we interpret the good agreement with values calculated from the ionic model to mean that these compounds are ionic? Clearly, this description is inappropriate for AgI, where the electronegativity difference $\Delta\chi$ is only 0.6 (compare this value to 0.4 for a C-H bond, which we typically view as non-polar).



A drop of siver nitrate solution, when added to a dilute hydrochloric acid solution, results in the immediate formation of a white silver chloride precipitate. This reaction is used as a qualitative test for the presence of halide ions in solutions. The covalent bonding contribution to the lattice energies of AgCl, AgBr, and AgI makes these salts sparingly soluble in water.

Again, we can interpret the fortuitous agreement between the calculated and experimentally obtained energies in terms of compensating errors. Our lattice energy calculation *overestimates* the ionic contribution in the case of the heavier silver halides, but *underestimates* the covalent contribution. Of these compounds, only AgF is soluble in water and should be thought of as an ionic compound. The others are progressively more insoluble in water (K_{sp} is 10^{-10}, 10^{-13}, and 10^{-16} for AgCl, AgBr, and AgI), reflecting increasing covalency as $\Delta\chi$ decreases.

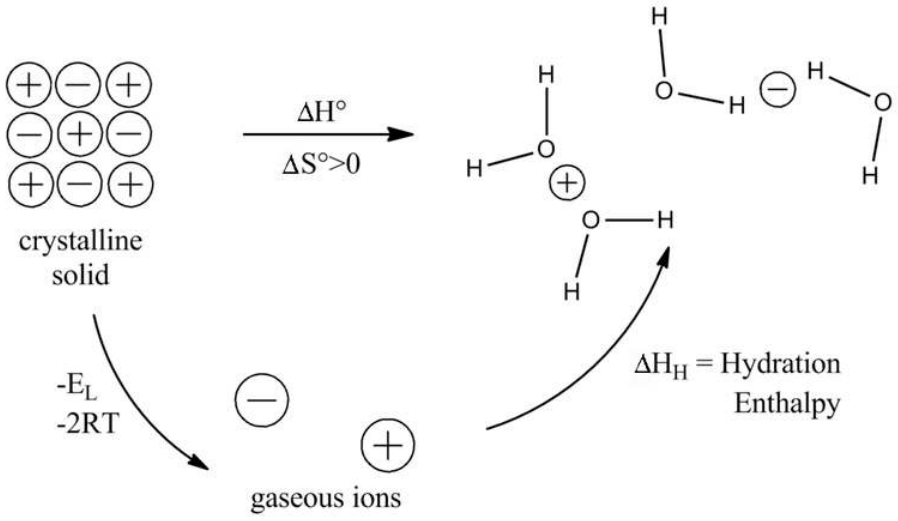
The moral of the story is that simple lattice energy calculations based on the ionic model work well, but *they do not necessarily imply that the compounds are ionic*!

3.20: Born-Haber Cycles for NaCl and Silver Halides is shared under a CC BY-SA license and was authored, remixed, and/or curated by LibreTexts.

- **9.4: Born-Haber Cycles for NaCl and Silver Halides** by Chemistry 310 is licensed CC BY-SA 4.0. Original source: https://en.wikibooks.org/wiki/Introduction_to_Inorganic_Chemistry.

3.21: Lattice Energies and Solubility

Lattice energies can also help predict compound solubilities. Let's consider a Born-Haber cycle for dissolving a salt in water. We can imagine this as the sum of two processes: (1) the vaporization of the salt to produce gaseous ions, characterized by the lattice enthalpy, and (2) the hydration of those ions to produce the solution. The enthalpy change for the overall process is the sum of those two steps. We know that the entropy change for dissolution of a solid is positive, so the solubility depends on the enthalpy change for the overall process.



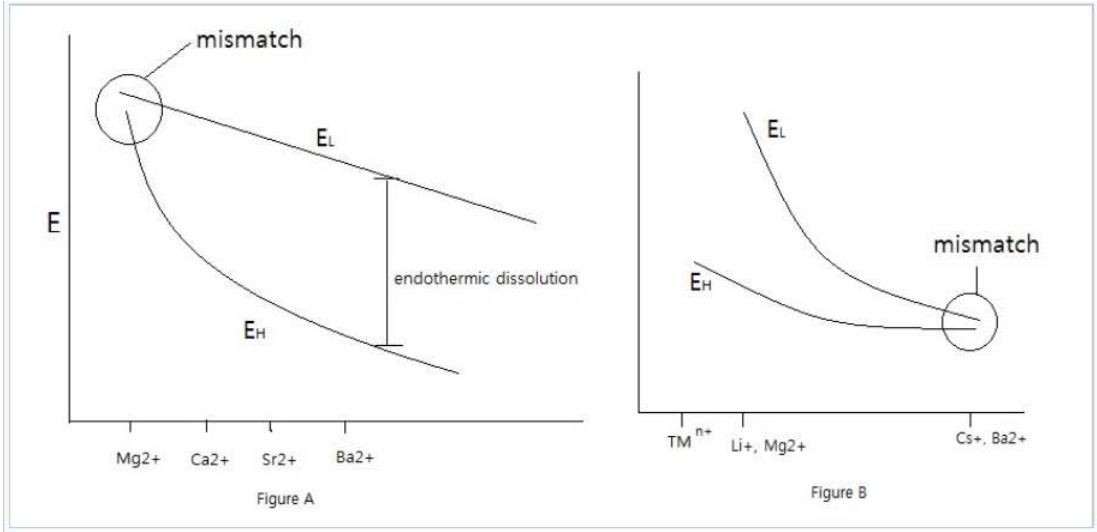
Here we need to consider the trends in both the lattice energy E_L and the hydration energy E_H. The lattice energy depends on the sum of the anion and cation radii ($r_+ + r_-$), whereas the hydration energy has separate anion and cation terms. Generally the solvation of small ions (typically cations) dominates the hydration energy because of the $1/r^2$ dependence.

$$E_L \alpha \frac{1}{r_+ + r_-} \tag{3.21.1}$$

$$E_H \alpha \frac{1}{r_+^2} + \frac{1}{r_-^2} \tag{3.21.2}$$

For salts that contain large anions, E_L doesn't change much as r_+ changes. That is because the anion dominates the $r_+ + r_-$ term in the denominator of the formula for E_L. On the other hand, E_H changes substantially with r_+, especially for small cations.

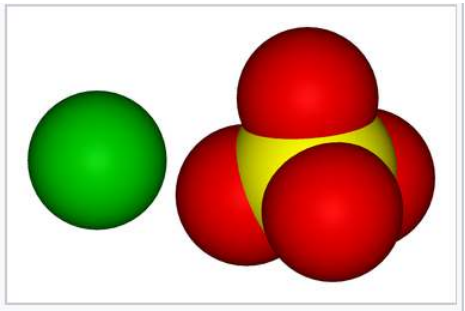
As a result, sulfate salts of small divalent cations, such as $MgSO_4$ (epsom salts), are soluble, whereas the lower hydration energy of Ba^{2+} in $BaSO_4$ makes that salt insoluble ($K_{sp} = 10^{-10}$).



Left: E_L diagram for sulfate salts. The large SO_4^{2-} ion is size-mismatched to small cations such as Mg^{2+}, which have large hydration energies, resulting soluble salts. With larger cations such as Ba^{2+}, which have lower E_H, the lattice energy exceeds the solvation enthalpy and the salts are insoluble.. Right: In the case of small anions such as F^- and OH^-, the lattice energy dominates with small cations such as transition metal ions (TM^{n+}), Mg^{2+}, and Li^+. Anion-cation size mismatch occurs with larger cations, such as Cs^+ and Ba^{2+}, which make soluble fluoride salts.

For small anions, E_L is more sensitive to r_+, whereas E_H does not depend on r_+ as strongly. For fluorides and hydroxides, LiF is slightly soluble whereas CsF is very soluble, and $Mg(OH)_2$ is insoluble whereas $Ba(OH)_2$ is very soluble.

Putting both trends together, we see that **low solubility** is most often encountered when the **anion and cation match well in their sizes**, especially when one or both are **multiply charged**.



Space-filling models showing the van der Waals surfaces of Ba^{2+} and SO_4^{2-}. The similarity in size of the two ions contributes to the low solubility of $BaSO_4$ in water.

Combining all our conclusions about solubility, we note the following trends:

1) Increasing **size mismatch** between the anion and cation leads to greater solubility, so CsF and LiI are the most soluble alkali halides.

2) Increasing **covalency** leads to lower solubility in the salts (due to larger E_L. For example, AgF, AgCl, AgBr, and AgI exhibit progressively lower solubility because of increasing covalency.

AgF > AgCl > AgBr > AgI

3) Increasing the **charge on the anion** lowers the solubility because the increase in E_L is large relative to the increase in E_H.

4) Small, polyvalent cations (having large E_H) make **soluble salts with large, univalent anions** such as I^-, NO_3^-, ClO_4^-, PF_6^-, and acetate.

Examples: Salts of transition metal and lanthanide ions

- Ln^{3+}: Nitrate salts are soluble, but oxides and hydroxides are insoluble.
- Fe^{3+}: Perchlorate is soluble, but sulfate is insoluble.

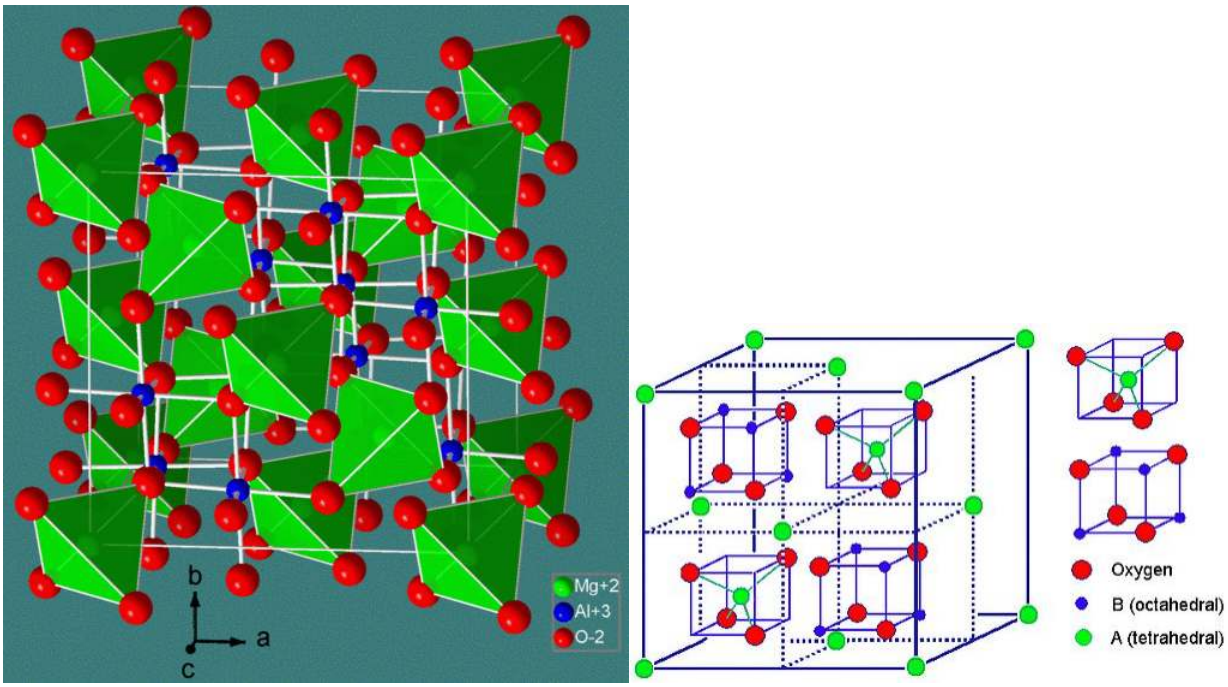
5) Multiple charged anions such as O^{2-}, S^{2-}, PO_4^{3-}, and SO_4^{2-} make insoluble salts with most M^{2+}, M^{3+}, and M^{4+} metals.

3.21: Lattice Energies and Solubility is shared under a CC BY-SA license and was authored, remixed, and/or curated by LibreTexts.

- **9.12: Lattice Energies and Solubility** by Chemistry 310 is licensed CC BY-SA 4.0. Original source: https://en.wikibooks.org/wiki/Introduction_to_Inorganic_Chemistry.

3.22: Spinel, Perovskite, and Rutile Structures

There are three more structures, which are derived from close-packed lattices, that are particularly important because of the material properties of their compounds. These are the **spinel** structure, on which ferrites and other magnetic oxides are based, the **perovskite** structure, which is adopted by ferroelectric and superconducting oxides, and the **rutile** structure, which is a common binary 6:3 structure adopted by oxides and fluorides.



The **spinel structure** is formulated MM'_2X_4, where M and M' are tetrahedrally and octahedrally coordinated cations, respectively, and X is an anion (typically O or F). The structure is named after the mineral $MgAl_2O_4$, and oxide spinels have the general formula AB_2O_4.

In the **normal spinel** structure, there is a close-packed array of anions. The A-site cations fill 1/8 of the tetrahedral holes and the B-site cations fill 1/2 of the octahedral holes. A polyhedral view of the normal spinel unit cell is shown at the left, and a simplified view (with the contents of the back half of the cell removed for clarity) is shown above. Each unit cell contains eight formula units and has a composition $A_8B_{16}O_{32}$.

Inverse spinels have a closely related structure (with the same large unit cell) in which the A-site ions and half of the B-site ions switch places. Inverse spinels are thus formulated $B(AB)O_4$, where the AB ions in parentheses occupy octahedral sites, and the other B ions are on tetrahedral sites. There are also mixed spinels, which are intermediate between the **normal** and **inverse** spinel structure.

Some spinel and inverse spinel AB combinations are:

$A^{2+}B^{3+}$, e.g., $MgAl_2O_4$ (normal spinel)

$A^{4+}B^{2+}$, e.g., $Pb_3O_4 = Pb^{II}(Pb^{II}Pb^{IV})O_4$ (inverse spinel)

$A^{6+}B^{+}$, e.g., Na_2WO_4 (normal spinel)

Many magnetic oxides, such as Fe_3O_4 and $CoFe_2O_4$, are spinels.

Normal vs. inverse spinel structure

For transition metal oxide spinels, the choice of the normal vs. inverse spinel structure is driven primarily by the **crystal field stabilization energy** (CFSE) of ions in the tetrahedral and octahedral sites. For spinels that contain 3d elements such as Cr, Mn, Fe,

Co, and Ni, the electron configuration is typically **high spin** because O^{2-} is a **weak field ligand**. We will learn more about these terms in the next section.

Ferrites are compounds of general formula $\mathbf{M^{II}Fe_2O_4}$. We can see that magnetite is one example of a ferrite (with M = Fe). Other divalent metals (M = Mg, Mn, Co, Ni, Zn) also form ferrites. Ferrites can be normal or inverse spinels, or mixed spinels, depending on the CFSE of the M^{II} ion. Based on their CFSE, Fe^{2+}, Co^{2+}, and Ni^{2+} all have a strong preference for the octahedral site, so those compounds are all inverse spinels. $ZnFe_2O_4$ is a normal spinel because the small Zn^{2+} ion (d^{10}) fits more easily into the tetrahedral site than Fe^{3+} (d^5), and both ions have zero CFSE. $MgFe_2O_4$ and $MnFe_2O_4$, in which all ions have zero CFSE and no site preference, are mixed spinels. **Chromite** spinels, $\mathbf{M^{II}Cr_2O_4}$, are always **normal spinels** because the d^3 Cr^{3+} ion has a strong preference for the octahedral site.

Examples of normal and inverse spinel structures:

> $\mathbf{MgAl_2O_4}$ is a **normal spinel** since both Mg^{2+} and Al^{3+} are non-transition metal ions and thus CFSE = 0. The more highly charged Al^{3+} ion prefers the octahedral site, where it is surrounded by six negatively charged oxygen atoms.
>
> $\mathbf{Mn_3O_4}$ is a **normal spinel** since the Mn^{2+} ion is a high spin d^5 system with zero CFSE. The two Mn^{3+} ions are high spin d^4 with higher CFSE on the octahedral sites ($3/5\ \Delta_O$) than on the tetrahedral site ($2/5\ \Delta_t \sim 1/5\ \Delta_O$).
>
> $\mathbf{Fe_3O_4}$ is an **inverse spinel** since the Fe^{3+} ion is a high spin d^5 system with zero CFSE. Fe^{2+} is a high spin d^6 system with more CFSE on an octahedral site than on a tetrahedral one.
>
> $\mathbf{NiFe_2O_4}$ is again an **inverse spinel** since Ni^{2+} (a d^8 ion) prefers the octahedral site and the CFSE of Fe^{3+} (a d^5 ion) is zero.
>
> $\mathbf{FeCr_2O_4}$ is a **normal spinel** since Fe^{2+} is high spin d^6 ion with $CFSE = [4(\frac{2}{5}) - 2(\frac{3}{5})]\Delta_o = \frac{2}{5}\Delta_o$ on an octahedral site, and Cr^{3+} is a d^3 ion with CFSE = $3(2/5)\ \Delta_O = 6/5\ \Delta_O$. Hence it is more energetically favorable for Cr^{3+} to occupy both of the octahedral sites.
>
> $\mathbf{Co_3O_4}$ is a **normal spinel**. Even in the presence of weak field oxo ligands, Co^{3+} is a low spin d^6 ion with very high CFSE on the octahedral sites, because of the high charge and small size of the Co^{3+} ion. Hence the Co^{3+} ions occupy both octahedral sites, and Co^{2+} occupies the tetrahedral site.

Magnetism of ferrite spinels

Ferrite spinels are of technological interest because of their magnetic ordering, which can be ferrimagnetic or antiferromagnetic depending on the structure (normal or inverse) and the nature of the metal ions. Fe_3O_4, $CoFe_2O_4$, and $NiFe_2O_4$ are all inverse spinels and are ferrimagnets. The latter two compounds are used in magnetic recording media and as deflection magnets, respectively.

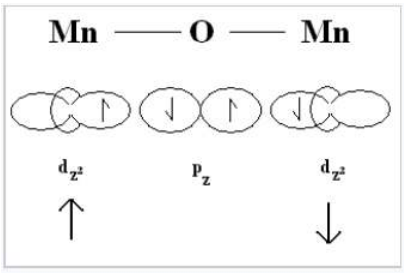
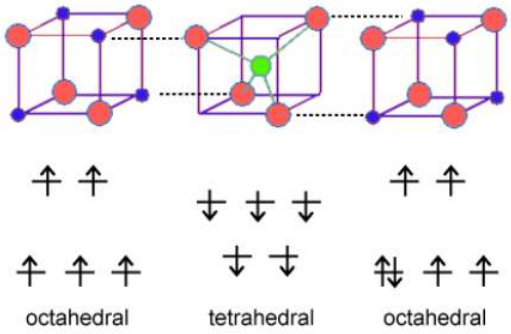


Illustration of antiferromagnetic superexchange between two transition metal cations through a shared oxygen atom.

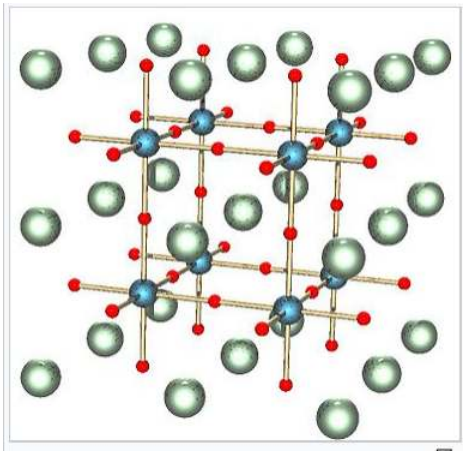
In order to understand the magnetism of ferrites, we need to think about how the unpaired spins of metal ions are coupled in oxides. If an oxide ion is shared by two metal ions, it can mediate the coupling of spins by superexchange as shown at the right. The coupling can be antiferromagnetic, as shown, or ferromagnetic, depending on the orbital filling and the symmetry of the orbitals involved. The **Goodenough-Kanamori rules** predict the local magnetic ordering (ferromagnetic vs. antiferromagnetic) that results from superexchange coupling of the electron spins of transition metal ions. For ferrites, the strongest coupling is between ions on neighboring **tetrahedral and octahedral sites**, and the ordering of spins between these two sites is reliably **antiferromagnetic**.



Because all the tetrahedral and octahedral sites in a spinel or inverse spinel crystal are coupled together identically, it works out that ions on the tetrahedral sites will all have one orientation (e.g., spin down) and ions on all the octahedral sites will have the opposite orientation (e.g., spin up). If the number of spins on the two sites is the same, then the solid will be antiferromagnetic. However, if the **number of spins is unequal** (as in the case of Fe_3O_4, $CoFe_2O_4$, and $NiFe_2O_4$) then the solid will be **ferrimagnetic**. This is illustrated above for Fe_3O_4. The spins on the Fe^{3+} sites cancel, because half of them are up and half are down. However, the four unpaired electrons on the Fe^{2+} ions are all aligned the same way in the crystal, so the compound is ferrimagnetic.

Perovskites are **ternary oxides** of general formula **ABO_3**. More generally, the perovskite formula is ABX_3, where the anion X can be **O, N, or halogen**. The A ions are typically large ions such as Sr^{2+}, Ba^{2+}, Rb^{+}, or a lanthanide 3+ ion, and the B ions are smaller transition metal ions such as Ti^{4+}, Nb^{5+}, Ru^{4+}, etc. The mineral after which the structure is named has the formula $CaTiO_3$.

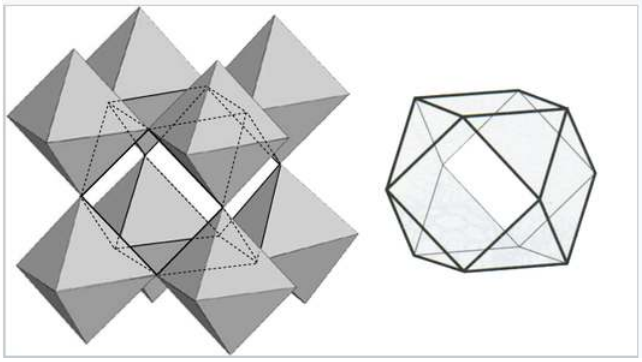
The perovskite structure has simple cubic symmetry, but is related to the fcc lattice in the sense that the A site cations and the three O atoms comprise a fcc lattice. The B-site cations fill 1/4 of the octahedral holes and are surrounded by six oxide anions.



ABX_3 perovskite structure. A, B, and X are white, blue, and red, respectively.

The coordination of the A ions in perovsite and the arrangement of BO_6 octahedra is best understood by looking at the ReO_3 structure, which is the same structure but with the A-site cations removed. In the polyhedral representation of the structure shown at the right, it can be seen that the octahedra share all their vertices but do not share any octahedral edges. This makes the ReO_3 and perovskite structures flexible, like three-dimensional wine racks, in that the octahedra can **rotate and tilt cooperatively**. Eight such

octahedra surround a large **cuboctahedral cavity**, which is the site of the A ions in the perovskite structure. Cations in these sites are coordinated by 12 oxide ions, as expected from the relationship between the perovskite and fcc lattices.



Polyhedral representation of the ReO_3 structure showing the large cuboctahedral cavity that is surrounded by 12 oxygen atoms

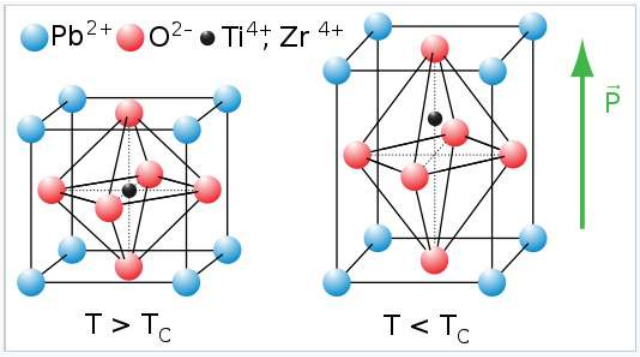
Because the A-site is empty in the ReO_3 structure, compounds with that structure can be reversibly **intercalated** by small ions such as **Li^+ or H^+**, which then occupy sites in the cuboctahedral cavity. For example, smart windows that darken in bright sunlight contain the **electrochromic** material WO_3, which has the ReO_3 structure. In the sunlight, a photovoltaic cell drives the reductive intercalation of WO_3 according to the reaction:

$$x\,H^+ + xe^- + WO_3 \leftrightharpoons H_xWO_3 \qquad (3.22.1)$$

WO_3 is a light yellow compound containing d^0 W(VI). In contrast, H_xWO_3, which is mixed-valent W(V)-W(VI) = d^1-d^0, has a deep blue color. Such coloration is typical of mixed-valence transition metal complexes because their d-electrons can be excited to delocalized conduction band levels by red light. Because the electrochemical intercalation-deintercalation process is powered by a solar cell, the tint of the windows can adjust automatically to the level of sunlight.

Ferroelectric perovskites

The flexibility of the network of corner-sharing BO_6 octahedra is also very important in ferroelectric oxides that have the perovskite structure. In some perovsites with small B-site cations, such as Ti^{4+} and Nb^{5+}, the cation is too small to fit symmetrically in the BO_6 octahedron. The octahedron distorts, allowing the cation to move off-center. These distortions can be **tetragonal** (as in the example shown at the right), **rhombohedral**, or **orthorhombic**, depending on whether the cation moves towards a vertex, face, or edge of the BO_6 octahedron. Moving the cation off-center in the octahedron creates an **electric dipole**. In ferroelectrics, these dipoles align in neighboring unit cells through cooperative rotation and tilting of octahedra. The crystal thus acquires a net electrical polarization.



Tetragonal distortion of the perovskite unit cell in the ferroelectric oxide PZT, $PbTi_xZr_{1-x}$

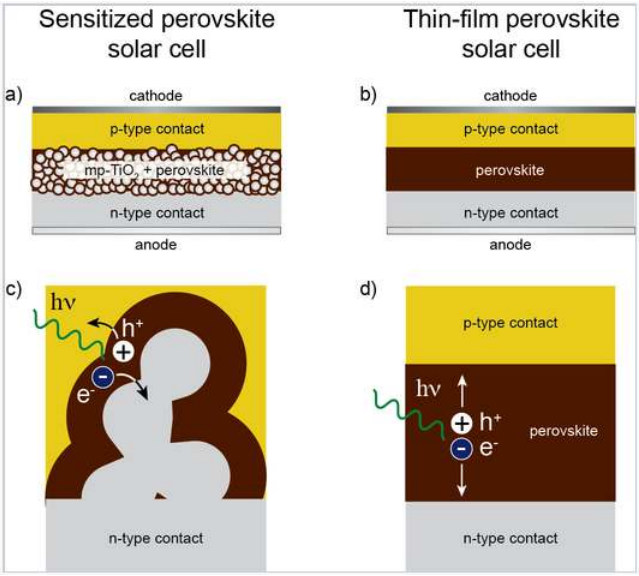
Ferroelectricity behaves analogously to **ferromagnetism**, except that the polarization is electrical rather than magnetic. In both cases, there is a **critical temperature (T_c)** above which the **spontaneous polarization** of the crystal disappears. Below T_c, the

electric polarization of a ferroelectric can be switched with a coercive field, and hysteresis loop of polarization vs. field resembles that of a ferromagnet. Above T_c, the crystal is **paraelectric** and has a high dielectric permittivity.

Ferroelectric and paraelectric oxides (along with piezoelectrics and pyroelectrics) have a wide variety of applications as switches, actuators, transducers, and dielectrics for capacitors. **Ferroelectric capacitors** are important in memory devices (FRAM) and in the tuning circuits of cellular telephones. **Multiferroics**, which are materials that are simultaneously ferroelectric and ferromagnetic, are rare and are being now intensively researched because of their potential applications in electrically adressable magnetic memory.

Halide perovskites (ABX_3, X = Cl, Br, I) can be made by combining salts of monovalent A ions ($A^+ = Cs^+$, NH_4^+, RNH_3^+) and divalent metal salts such as $PbCl_2$ or PbI_2. These compounds have sparked recent interest as light absorbers for **thin film solar cells** that produce electricity from sunlight. Lead and tin halide perovskites can be grown as thin films from solution precursors or by thermal evaporation at relatively low temperatures. In some lead halide perovskites, the mobility of electrons and holes is very high, comparable to that of more expensive III-V semiconductors such as GaAs, which must be grown as very pure single crystals at high temperatures for use in solar cells. Because of their high carrier mobility, some lead halide perovskites are also electroluminescent and are of interest as inexpensive materials for light-emitting diodes (LEDs).

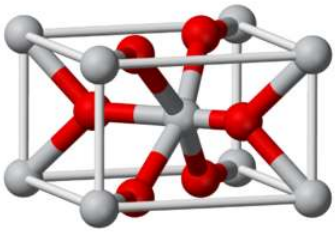
Tin and lead halide perovskites were first studied in the 1990s as materials for thin film electronics,[4] and more recently as light absorbers in dye-sensitized solar cells. Soon after the results on dye-sensitized perovskite cells were reported, it was discovered that halide perovskites could also be used in thin film solid state solar cells. The structures of these solar cells are shown schematically at the right. The highest reported solar power conversion efficiencies of perovskite solar cells have jumped from 3.8% in 2009 [5] to 10.2% in 2012[6] and a certified 20.1% in 2014.[7]. The highest performing cells to date contain divalent lead in the perovskite B cation site and a mixture of methylammonium and formamidinium ions in the perovskite A cation site.



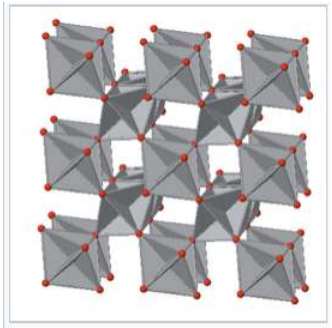
a) Solar cell architecture in which a lead halide perovskite absorber coats a layer of nanocrystalline anatase TiO_2. b) Thin-film solar cell, with a layer of lead halide perovskite sandwiched between two selective contacts. c) Charge generation and extraction in the sensitized architecture and d) in the thin-film architecture.

Despite their very impressive efficiency, perovskite solar cells are stable for relatively short periods of time and are sensitive to air and moisture. Current research is focused on understanding the degradation mechanisms of these solar cells and improving their stability under operating conditions.

The **rutile structure** is an important MX_2 (X = O, F) structure. It is a 6:3 structure, in which the cations are octahedrally coordinated by anions, and as such is intermediate in polarity between the CaF_2 (8:4) and SiO_2 (4:2) structures. The mineral rutile is one of the polymorphs of TiO_2, the others (anatase and brookite) also being 6:3 structures.



The rutile structure can be described as a distorted version of the NiAs structure with half the cations removed. Recall that compounds with the NiAs structure were typically metallic because the metal ions are eclipsed along the stacking axis and thus are in relatively close contact. In rutile, the MO_6 **octahedra share edges** along the tetragonal c-axis, and so some rutile oxides, such as **NbO_2, RuO_2 and IrO_2,** are also **metallic** because of **d-orbital overlap** along that axis. These compounds are important as electrolyzer catalysts and catalyst supports because they combine high catalytic activity with good electronic conductivity.



View down the tetragonal c-axis of the rutile lattice, showing edge-sharing MO_6 octahedra.

Rutile TiO_2, because of its high refractive index, is the base pigment for white paint. It is a wide bandgap semiconductor that has also been extensively researched as an electrode for water splitting solar cells and as a photocatalyst (primarily as the anatase polymorph) for degradation of pollutants in air and water. Self-cleaning glass exploits the photocatalytic properties of a thin film of TiO_2 to remove oily substances from the glass surface and improve the wetting properties of the glass.

3.22: Spinel, Perovskite, and Rutile Structures is shared under a CC BY-SA license and was authored, remixed, and/or curated by LibreTexts.

- **8.7: Spinel, Perovskite, and Rutile Structures** by Chemistry 310 is licensed CC BY-SA 4.0. Original source: https://en.wikibooks.org/wiki/Introduction_to_Inorganic_Chemistry.

3.23: Kapustinskii Equation

From the discussion above, it is clear that the lattice energy, E_L, of an ionic crystal can be calculated with reasonable accuracy if the structure is known. But how can we calculate E_L for a new or hypothetical compound of unknown structure? Recall that the reduced Madelung constant is about the same for different crystal structures. Russian chemist A. F. Kapustinskii recognized this fact and devised a formula that allows one to calculate E_L for any compound if we know the univalent radii of the constituent ions. [5]

The Madelung constant, A, is proportional to the number of ions (n) in formula unit, so dividing by the n gives similar values as shown in the table below:

A/n ~ invariant

Structure	A/n
NaCl	0.874
CsCl	0.882
Rutile	0.803
Fluorite	0.800

Kapustinskii noticed that the difference in ionic radii between M^+ and M^{2+} (the monovalent vs. divalent radius) largely compensates for the differences in A/n between monovalent (NaCl, CsCl) and divalent (rutile, CaF_2) structures. He thus arrived at a lattice energy formula using an average Madelung constant, corrected to monovalent radii. In the **Kapustinskii formula**, the lattice energy (kJ/mol) is given by:

$$E_L = \frac{1213.8 z_+ z_- n}{r_+ + r_-}\left(1 - \frac{0.345}{r_+ + r_-}\right) \tag{3.23.1}$$

Here the sum of the monovalent radii is used in place of r_o, the bond distance in the Born-Mayer equation. The beauty of this formula is that it requires no knowledge of the structure of the compound. Therefore it can be used, in combination with Born-Haber cycles, to predict the stability of unknown compounds. As we show below, this is a broadly useful tool in guiding syntheses and predicting the reactivity of inorganic solids.

3.23: Kapustinskii Equation is shared under a CC BY-SA license and was authored, remixed, and/or curated by LibreTexts.

- **9.5: Kapustinskii Equation** by Chemistry 310 is licensed CC BY-SA 4.0. Original source: https://en.wikibooks.org/wiki/Introduction_to_Inorganic_Chemistry.

CHAPTER OVERVIEW

4: Acid-Base Theories

4.1: Bronsted-Lowry acids and bases

4.2: Lewis Acids and Bases

4.3: Acidity of the Hexaaqua Ions

4.4: Hard-soft Acids and Bases

4.5: Quantitative Measures of Hardness and Softness

4: Acid-Base Theories is shared under a not declared license and was authored, remixed, and/or curated by LibreTexts.

4.1: Bronsted-Lowry acids and bases

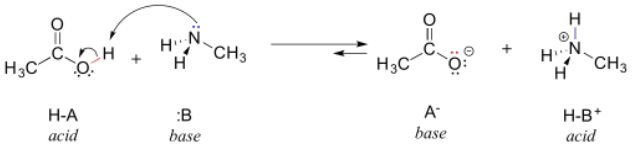
We'll begin our discussion of acid-base chemistry with a couple of essential definitions. The first of these was proposed in 1923 by the Danish chemist Johannes Brønsted and the English chemist Thomas Lowry, and has come to be known as the **Brønsted-Lowry definition of acidity and basicity**. An acid, by the Brønsted-Lowry definition, is a species which acts as a proton donor (i.e., it gives away an H^+), while a base is a proton (H^+) acceptor. One of the most familiar examples of a Brønsted-Lowry acid-base reaction is between hydrochloric acid and hydroxide ion:



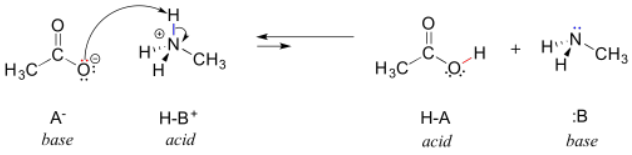
In this reaction, a proton is transferred from HCl (the acid, or proton *donor*) to hydroxide ion (the base, or proton *acceptor*). As we learned in the previous chapter, curved arrows depict the movement of electrons in this bond-breaking and bond-forming process.

After a Brønsted-Lowry acid donates a proton, what remains is called the **conjugate base**. Chloride ion is thus the conjugate base of hydrochloric acid. Conversely, when a Brønsted-Lowry base accepts a proton it is converted into its **conjugate acid** form: water is thus the conjugate acid of hydroxide ion.

Here is an organic acid-base reaction between acetic acid and methylamine:

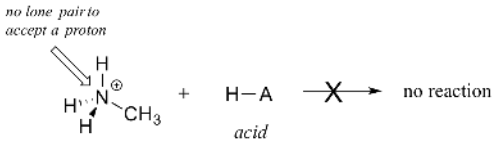


In the reverse of this reaction, acetate ion is the base and methylammonium ion (protonated methylamine) is the acid.



For now, let's just consider one common property of bases: *in order to act as a base, a molecule must have a reactive pair of electrons*. In all of the acid-base reactions we'll see in this chapter, the basic species has an atom with a lone pair of electrons. When methylamine acts as a base, for example, the lone pair of electrons on the nitrogen atom is used to form a new bond to a proton. A negative charge often (but not always!) indicates that a structure (in this case, an anion) is likely to act as a base.

Clearly, methylammonium ion cannot act as a base – it does not have a reactive pair of electrons with which to accept a proton.



In summary,

- A Brønsted-Lowry acid is a proton (hydrogen ion) donor.
- A Brønsted-Lowry base is a proton (hydrogen ion) acceptor.

When a Brønsted acid HA dissociates in water, it increases the concentration of hydrogen ions in the solution, H^+; conversely, Brønsted bases dissociate by taking a proton from the solvent (water) to generate OH^-.

- *Acid dissociation*

$$HA_{(aq)} \rightleftharpoons A^-_{(aq)} + H^+_{(aq)} \tag{4.1.1}$$

- *Acid Ionization Constant:*

$$K_a = \frac{[A^-][H^+]}{[HA]} \tag{4.1.2}$$

- *Base dissociation:*

$$B_{(aq)} + H_2O_{(l)} \rightleftharpoons HB^+_{(aq)} + OH^-_{(aq)} \tag{4.1.3}$$

- Base Ionization Constant

$$K_b = \frac{[HB^+][OH^-]}{[B]} \tag{4.1.4}$$

The determination of a substance as a Brønsted-Lowry acid or base can only be done by observing the reaction. In the case of the H_2O it is a base in the first case and an acid in the second case.

Water does not need to be involved in a Bronsted-Lowry reaction. In general, for an acid HA and a base Z, we have

$$HA + Z \rightleftharpoons A^- + HZ^+ \tag{4.1.5}$$

- A Donates H to form HZ^+.
- Z Accepts H from A which forms HZ^+
- A^- becomes conjugate base of HA and in the reverse reaction it accepts a H from HZ to recreate HA in order to remain in equilibrium
- HZ^+ becomes a conjugate acid of Z and in the reverse reaction it donates a H to A^- recreating Z in order to remain in equilibrium

4.1: Bronsted-Lowry acids and bases is shared under a not declared license and was authored, remixed, and/or curated by LibreTexts.

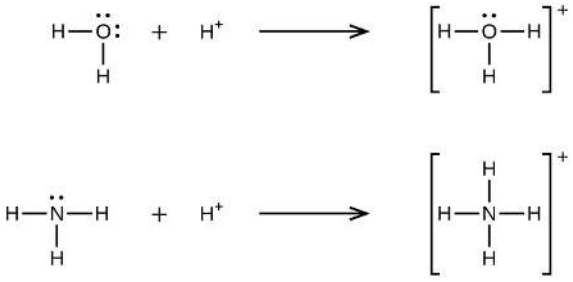
4.2: Lewis Acids and Bases

Learning Objectives

- Explain the Lewis model of acid-base chemistry
- Write equations for the formation of adducts and complex ions
- Perform equilibrium calculations involving formation constants

In 1923, G. N. Lewis proposed a generalized definition of acid-base behavior in which acids and bases are identified by their ability to accept or to donate a pair of electrons and form a coordinate covalent bond.

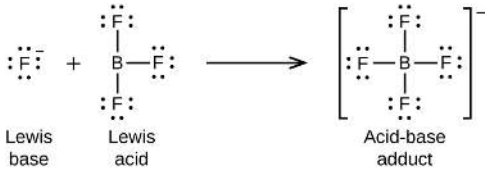
A coordinate covalent bond (or dative bond) occurs when one of the atoms in the bond provides both bonding electrons. For example, a coordinate covalent bond occurs when a water molecule combines with a hydrogen ion to form a hydronium ion. A coordinate covalent bond also results when an ammonia molecule combines with a hydrogen ion to form an ammonium ion. Both of these equations are shown here.



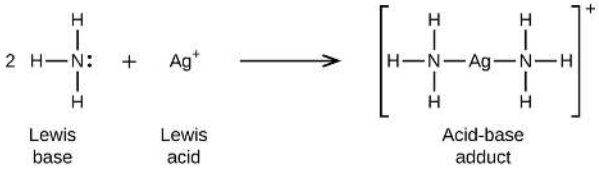
- A Lewis acid is any species (molecule or ion) that can *accept* a pair of electrons, and a Lewis base is any species (molecule or ion) that can *donate* a pair of electrons.

A Lewis acid-base reaction occurs when a base donates a pair of electrons to an acid. A **Lewis acid-base adduct**, a compound that contains a coordinate covalent bond between the Lewis acid and the Lewis base, is formed. The following equations illustrate the general application of the Lewis concept.

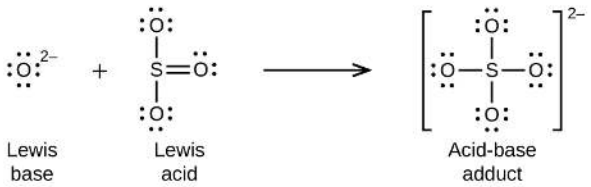
The boron atom in boron trifluoride, BF_3, has only six electrons in its valence shell. Being short of the preferred octet, BF_3 is a very good Lewis acid and reacts with many Lewis bases; a fluoride ion is the Lewis base in this reaction, donating one of its lone pairs:



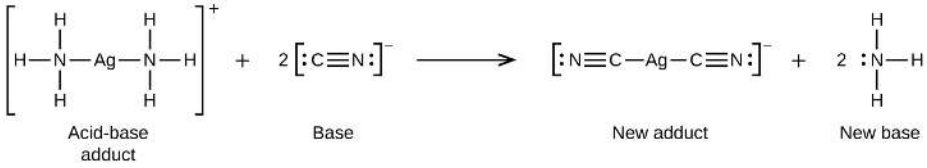
In the following reaction, each of two ammonia molecules, Lewis bases, donates a pair of electrons to a silver ion, the Lewis acid:

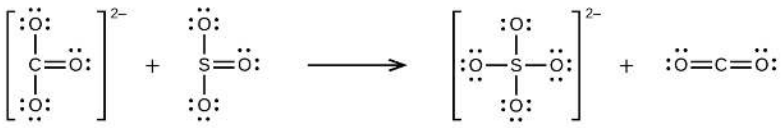


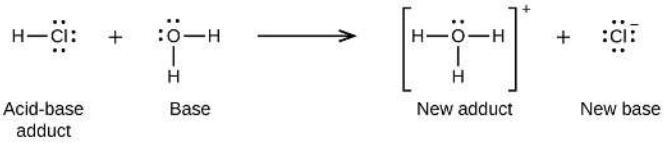
Nonmetal oxides act as Lewis acids and react with oxide ions, Lewis bases, to form oxyanions:



Many Lewis acid-base reactions are displacement reactions in which one Lewis base displaces another Lewis base from an acid-base adduct, or in which one Lewis acid displaces another Lewis acid:

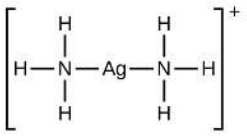






The last displacement reaction shows how the reaction of a Brønsted-Lowry acid with a base fits into the Lewis concept. A Brønsted-Lowry acid such as HCl is an acid-base adduct according to the Lewis concept, and proton transfer occurs because a more stable acid-base adduct is formed. Thus, although the definitions of acids and bases in the two theories are quite different, the theories overlap considerably.

Many slightly soluble ionic solids dissolve when the concentration of the metal ion in solution is decreased through the formation of complex (polyatomic) ions in a Lewis acid-base reaction. For example, silver chloride dissolves in a solution of ammonia because the silver ion reacts with ammonia to form the complex ion $[Ag(NH_3)_2]^+$. The Lewis structure of the $[Ag(NH_3)_2]^+$ ion is:



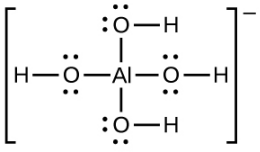
The equations for the dissolution of AgCl in a solution of NH_3 are:

$$\mathrm{AgCl}(s) \longrightarrow \mathrm{Ag^+}(aq) + \mathrm{Cl^-}(aq) \tag{4.2.1}$$

$$\mathrm{Ag^+}(aq) + 2\,\mathrm{NH_3}(aq) \longrightarrow [\mathrm{Ag(NH_3)_2}]^+(aq) \tag{4.2.2}$$

$$\text{Net: } \mathrm{AgCl}(s) + 2\,\mathrm{NH_3}(aq) \longrightarrow [\mathrm{Ag(NH_3)_2}]^+(aq) + \mathrm{Cl^-}(aq) \tag{4.2.3}$$

Aluminum hydroxide dissolves in a solution of sodium hydroxide or another strong base because of the formation of the complex ion $\mathrm{Al(OH)_4^-}$. The Lewis structure of the $\mathrm{Al(OH)_4^-}$ ion is:



The equations for the dissolution are:

$$[Al(OH)_3](s) \longrightarrow Al^{3+}(aq) + 3\,OH^-(aq) \tag{4.2.4}$$

$$Al^{3+}(aq) + 4\,OH^-(aq) \longrightarrow [Al(OH)_4]^-(aq) \tag{4.2.5}$$

$$\text{Net: } [Al(OH)_3](s) + OH^-(aq) \longrightarrow [Al(OH)_4]^-(aq) \tag{4.2.6}$$

Mercury(II) sulfide dissolves in a solution of sodium sulfide because HgS reacts with the S^{2-} ion:

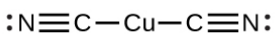
$$HgS(s) \longrightarrow Hg^{2+}(aq) + S^{2-}(aq) \tag{4.2.7}$$

$$Hg^{2+}(aq) + 2\,S^{2-}(aq) \longrightarrow [HgS_2]^{2-}(aq) \tag{4.2.8}$$

$$\text{Net: } HgS(s) + S^{2-}(aq) \longrightarrow [HgS_2]^{2-}(aq) \tag{4.2.9}$$

A complex ion consists of a central atom, typically a transition metal cation, surrounded by ions, or molecules called ligands. These ligands can be neutral molecules like H_2O or NH_3, or ions such as CN^- or OH^-. Often, the ligands act as Lewis bases, donating a pair of electrons to the central atom. The ligands aggregate themselves around the central atom, creating a new ion with a charge equal to the sum of the charges and, most often, a transitional metal ion. This more complex arrangement is why the resulting ion is called a *complex ion*. The complex ion formed in these reactions cannot be predicted; it must be determined experimentally. The types of bonds formed in complex ions are called coordinate covalent bonds, as electrons from the ligands are being shared with the central atom. Because of this, complex ions are sometimes referred to as coordination complexes. This will be studied further in upcoming chapters.

The equilibrium constant for the reaction of the components of a complex ion to form the complex ion in solution is called a formation constant (K_f) (sometimes called a stability constant). For example, the complex ion $[Cu(CN)_2]^-$ is shown here:



It forms by the reaction:

$$Cu^+(aq) + 2\,CN^-(aq) \rightleftharpoons [Cu(CN)_2]^-(aq) \tag{4.2.10}$$

At equilibrium:

$$K_f = Q = \frac{[Cu(CN)2-]}{[Cu+][CN-]^2} \tag{4.2.11}$$

The inverse of the formation constant is the dissociation constant (K_d), the equilibrium constant for the *decomposition* of a complex ion into its components in solution. We will work with dissociation constants further in the exercises for this section. Table E4 and Table **4.2.1** are tables of formation constants. In general, the larger the formation constant, the more stable the complex; however, as in the case of K_{sp} values, the stoichiometry of the compound must be considered.

Table **4.2.1**: Common Complex Ions by Decreasing Formation Constants

Substance	K_f at 25 °C
$[Cd(CN)_4]^{2-}$	3×10^{18}
$[Ag(NH_3)_2]^+$	1.7×10^7
$[AlF_6]^{3-}$	7×10^{19}

As an example of dissolution by complex ion formation, let us consider what happens when we add aqueous ammonia to a mixture of silver chloride and water. Silver chloride dissolves slightly in water, giving a small concentration of Ag^+ ($[Ag^+] = 1.3 \times 10^{-5}\ M$):

$$AgCl(s) \rightleftharpoons Ag^+(aq) + Cl^-(aq) \tag{4.2.12}$$

However, if NH_3 is present in the water, the complex ion, $[Ag(NH_3)_2]^+$, can form according to the equation:

$$Ag^+(aq) + 2\,NH_3(aq) \rightleftharpoons [Ag(NH_3)_2]^+(aq) \tag{4.2.13}$$

with

$$K_f = \frac{[Ag(NH3)2+]}{[Ag+][NH3]^2} = 1.7 \times 10^7 \tag{4.2.14}$$

The large size of this formation constant indicates that most of the free silver ions produced by the dissolution of AgCl combine with NH_3 to form $[Ag(NH_3)_2]^+$. As a consequence, the concentration of silver ions, $[Ag^+]$, is reduced, and the reaction quotient for the dissolution of silver chloride, $[Ag^+][Cl^-]$, falls below the solubility product of AgCl:

$$Q = [Ag^+][Cl^-] < K_{sp} \tag{4.2.15}$$

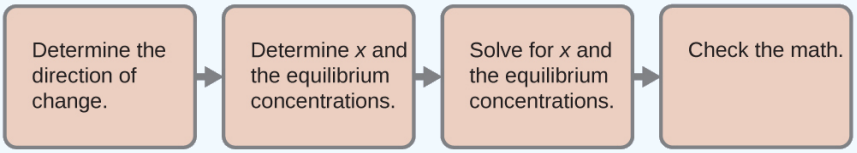
More silver chloride then dissolves. If the concentration of ammonia is great enough, all of the silver chloride dissolves.

Example 4.2.1: Dissociation of a Complex Ion

Calculate the concentration of the silver ion in a solution that initially is 0.10 *M* with respect to $[Ag(NH_3)_2]^+$.

Solution

We use the familiar path to solve this problem:



1. *Determine the direction of change.* The complex ion $[Ag(NH_3)_2]^+$ is in equilibrium with its components, as represented by the equation:

$$Ag^+(aq) + 2\,NH_3(aq) \rightleftharpoons [Ag(NH_3)_2]^+(aq) \tag{4.2.16}$$

We write the equilibrium as a formation reaction because Table **4.2.1** lists formation constants for complex ions. Before equilibrium, the reaction quotient is larger than the equilibrium constant (K_f = 1.7 x 10^7), and $Q = \frac{0.10}{0 \times 0} = \infty$ (it is infinitely large), so the reaction shifts to the left to reach equilibrium.

This page titled 4.2: Lewis Acids and Bases is shared under a CC BY license and was authored, remixed, and/or curated by OpenStax.

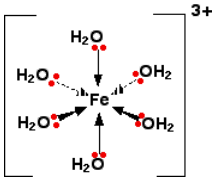
- **15.2: Lewis Acids and Bases** by OpenStax is licensed CC BY 4.0. Original source: https://openstax.org/details/books/chemistry-2e.

4.3: Acidity of the Hexaaqua Ions

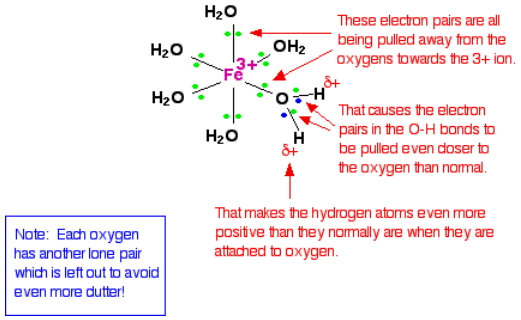
This page explains why complex ions of the type $[M(H_2O)_6]^{n+}$ are acidic.

The Charge Distribution within Complex Ion

The pH of solutions containing hexaaqua ions vary a lot from one metal to another (assuming you are comparing solutions of equal concentrations). However, the underlying explanation is the same for all of them. We'll take the hexaaquairon(III) ion, $[Fe(H_2O)_6]^{3+}$ as typical. The structure of the ion is:



Each of the six water molecules are attached to the central iron(III) ion via a coordinate bond using one of the lone pairs on the oxygen. We'll choose one of these water molecules at random (it doesn't make any difference which one!), and look at the bonding in a bit more detail - showing all the bonds around the oxygen. Imagine for the moment that the 3+ charge is located entirely on the iron.



When the lone pairs on the oxygen atoms form coordinate bonds with the iron, there is obviously a movement of electrons towards the iron. That has an effect on the electrons in the O-H bonds. These electrons, in turn, get pulled towards the oxygen even more than usual. That leaves the hydrogen nuclei more exposed than normal. The overall effect is that each of the hydrogen atoms is more positive than it is in ordinary water molecules. The 3+ charge is no longer located entirely on the iron but spread out over the whole ion - much of it on the hydrogen atoms.

The effect of dissolving this ion in water

The hydrogen atoms attached to the water ligands are sufficiently positive that they can be pulled off in a reaction involving water molecules in the solution. The first stage of this process is:

$$Fe(H_2O)_6^{3+} + H_2O \rightleftharpoons Fe(H_2O)_5(OH)^{2+} + H_3O^+ \tag{4.3.1}$$

The complex ion is acting as an (Arrhenius) acid by donating a hydrogen ion to water molecules in the solution. The water is, of course, acting as a (Arrhenius) base by accepting the hydrogen ion. Because of the confusing presence of water from two different sources (the ligands and the solution), it is easier to simplify Equation 4.3.1:

$$[Fe(H_2O)_6]^{3+}(aq) \rightleftharpoons [Fe(H_2O)_5(OH)]^{2+}(aq) + H^+(aq) \tag{4.3.2}$$

However, if you write it like this, remember that the hydrogen ion is not just falling off the complex ion. It is being pulled off by a water molecule in the solution. Whenever you write "$H^+(aq)$" what you really mean is a hydroxonium ion, H_3O^+.

The hexaaquairon(III) ion is quite strongly acidic giving solutions with a pH around 1.5, depending on concentration. You can get further loss of hydrogen ions as well, from a second and a third water molecule since the complex ion is a polyprotic acid.

Losing a second hydrogen ion:

$$[Fe(H_2O)_5(OH)]^{2+}(aq) \rightleftharpoons [Fe(H_2O)_4(OH)_2]^{+}(aq) + H^{+}(aq) \quad (4.3.3)$$

and a third one:

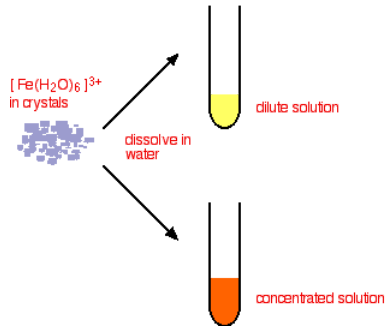
$$[\,Fe(H_2O)_4(OH)_2]^{+}(aq) \rightleftharpoons [\,Fe(H_2O)_3(OH)_4](s) + H^{+}(aq) \quad (4.3.4)$$

This time you end up with a neutral complex and because it has no charge, it does not dissolve to any extent in water, and a precipitate is formed.

In practice

What do you actually get in solution if you dissolve an iron(III) salt in water? In fact you get a mixture of all the complexes that you have seen in the equations above. These reactions are all equilibrium, so everything will be present. The proportions depend on how concentrated the solution is.

The color of the solution is very variable and depends in part on the concentration of the solution. Dilute solutions containing iron(III) ions can be pale yellow. More concentrated ones are much more orange, and may even produce some orange precipitate. None of these colors represents the true color of the $[Fe(H_2O)_6]^{3+}$ ion - which is a very pale lilac color and is only really easy to see in solids containing the ion.

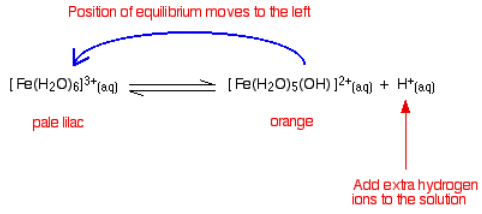


Looking at the equilibrium showing the loss of the first hydrogen ion:

$$\underbrace{Fe(H_2O)_6^{3+}}_{\text{pale lilac}} + H_2O \rightleftharpoons \underbrace{Fe(H_2O)_5(OH)^{2+}}_{\text{orange}} + H_3O^{+} \quad (4.3.5)$$

The color of the new complex ion on the right-hand side is so strong that it completely masks the color of the hexaaqua ion. In concentrated solutions, the equilibrium position will be even further to the right-hand side (Le Chatelier's Principle), and so the color darkens. You will also get significant loss of other hydrogen ions (Equation 4.3.3 and 4.3.4) leading to some formation of the neutral complex and thus some precipitate.

The position of this equilibrium can be shifted by adding extra hydrogen ions from a concentrated acid (e.g., by adding concentrated nitric acid to a solution of iron(III) nitrate). The new hydrogen ions push the position of the equilibrium to the left so that you can see the color of the hexaaqua ion. This is slightly easier to follow if you write the simplified version of the equilibrium (Equation 4.3.2).



3+ Ions are More Acidic than 2+ ions

Solutions containing 3+ hexaaqua ions tend to have pH in the range from 1 to 3. Solutions containing 2+ ions have higher pH - typically around 5 - 6, although they can go down to about 3. Remember that the reason that these ions are acidic is because of

the pull of the electrons towards the positive central ion. An ion with 3+ charges on it is going to pull the electrons more strongly than one with only 2+ charges.

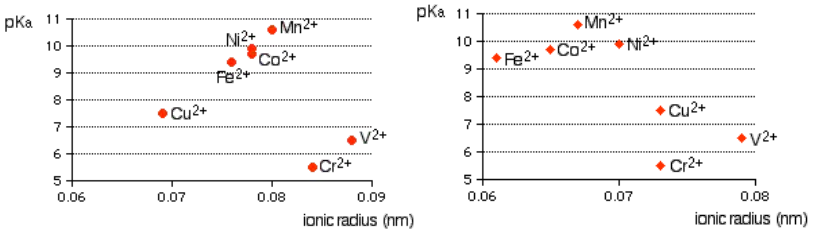
In 3+ ions, the electrons in the O-H bonds will be pulled further away from the hydrogen atoms than in 2+ ions. That means that the hydrogen atoms in the water ligands will have a greater positive charge in a 3+ ion, and so will be more attracted to water molecules in the solution. If they are more attracted, they will be more readily lost - and so the 3+ ions are more acidic.

The Effect of ionic radius on acidity

If you have ions of the same charge, it seems reasonable that the smaller the volume this charge is packed into, the greater the distorting effect on the electrons in the O-H bonds. Ions with the same charge but in a smaller volume (a higher charge density) would be expected to be more acidic. You would therefore expect to find that the smaller the radius of the metal ion, the stronger the acid. Unfortunately, it's not that simple!

Almost every data source that you refer to quotes different values for ionic radii. This is because the radius of a metal ion varies depending on what negative ion it is associated with. We are interested in what happens when the metal ion is bonded to water ligands. Whatever values we take are unlikely to represent the real situation. In the graphs which follow, values for ionic radii from two common sources were used so that you can see the difference it makes to the argument.

If it is true that the smaller the ionic radius, the stronger the acidity of the hexaaqua ion, you would expect some sort of regular increase in pK_a (showing weaker acids) as ionic radius increases. The following graphs plot pK_a against ionic radii for the 2+ ions of the elements in the first transition series from vanadium to copper. The first graph plots pK_a against ionic radii taken from Chemistry Data Book by Stark and Wallace.



There is a trend for several of the ions, but it is completely broken by vanadium and chromium. The second graph uses ionic radii taken from the Nuffield Advanced Science Book of Data.

There probably is a relationship between ionic radius and acid strength. The problem is that there are other more important effects operating as well (quite apart from differences in charge) that can completely swamp the effect of the changes in ionic radius. You have to look in far more detail at the bonding in the hexaaqua ions and the product ions.

Contributors and Attributions

- Jim Clark (Chemguide.co.uk)

This page titled 4.3: Acidity of the Hexaaqua Ions is shared under a CC BY-NC 4.0 license and was authored, remixed, and/or curated by Jim Clark.

4.4: Hard-soft Acids and Bases

The Hard Soft Acid Base Principle is a Conceptual Tool for Thinking About Patterns of Lewis acid base Reactivity

The explanation of the trends in metal distribution, halide salt solubility, and preferred metal coordination patterns is rooted in Arland, Chatt, and Davies' observation that *Lewis acids and bases could be classified into two groups based on their propensity to form stable compounds with one another* (*e.g.* acids in a class tend to form more stable adducts with bases in the same class than they did with bases in the other).[1] Arland, Chatt, and Davies somewhat boringly termed these groups class a and class b but today they are known by Ralph Pearson's name for them. Pearson called the class a acids and bases hard and class b acids and bases soft. These terms reflect how "soft" these substance's electron clouds are towards distortion or, in other words, their polarizability (Figure **4.4.1**). Pearson terms acids and bases which are relatively polarizable **soft** and those which are difficult to polarize **hard.**

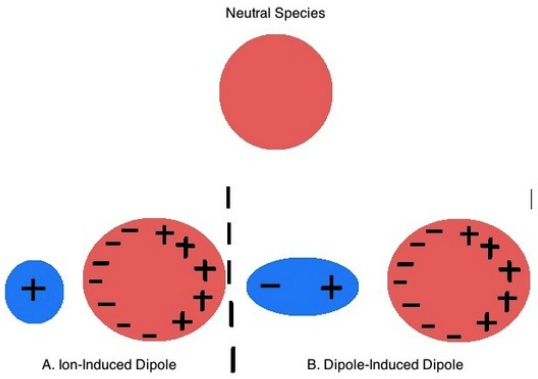


Figure **4.4.1**: Polarizability refers to the ease with which a substance's electron cloud may be distorted under the action of an electric field. An fragment's polarizability determines the degree to which its electron cloud is distorted by A.) an Ion and B.) a polar molecule to induce a dipole moment. The figure is taken from (and the caption expanded from) Cox, Kelly and Dana Reusser "Polarizability" in https://chem.libretexts.org/Bookshelves/Physical_and_Theoretical_Chemistry_Textbook_Maps/Supplemental_Modules_(Physical_and_Theoretical_Chemistry)/Physical_Properties_of_Matter/Atomic_and_Molecular_Properties/Intermolecular_Forces/Specific_Interactions/Polarizability

Recognizing Hard and Soft Acids and Bases

Hard acids and bases come in two varieties:

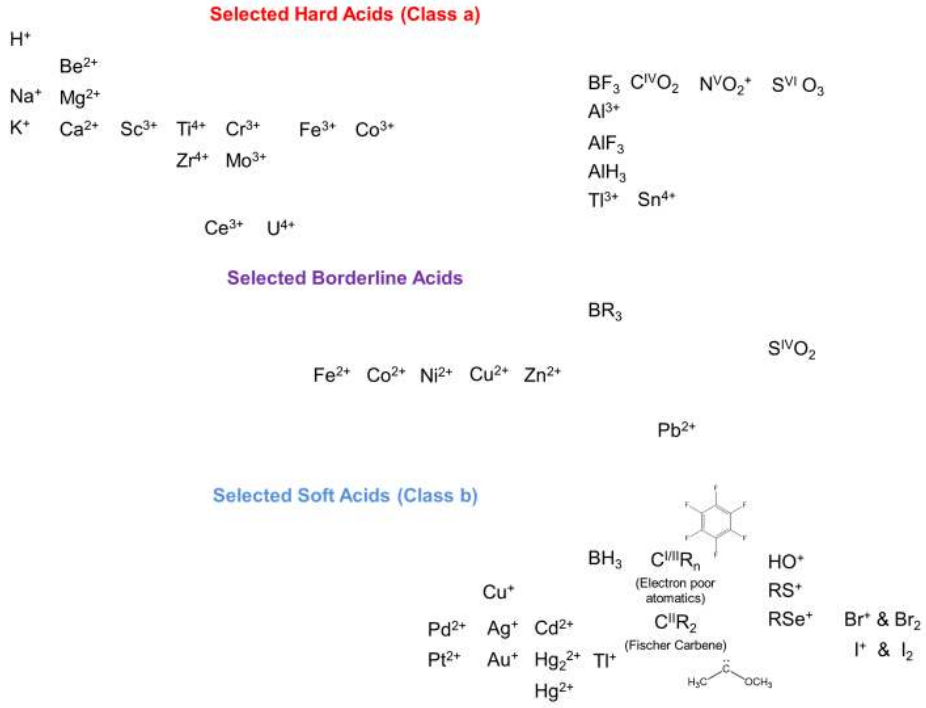
1. hard acid and base sites which possess few valence electrons and for which polarization therefore involves distorting core electrons, which are difficult to distort because they are close to the nucleus and experience a high nuclear charge. The most common examples of such substances are Lewis acids hard acids towards the left of the periodic table.
2. hard acids and base sites with a high charge density (highly charged relative to size) and/or which are electron deficient. In these cases polarization involves distorting electrons that already experience strong unshielded electrostatic interactions.

Soft acids and bases also come in two varieties

1. soft acids and bases which posses many valence electrons and so are more readily polarized. In consequence, all other tings being equal, soft acids and bases are more likely to be found towards the middle or right of the periodic table.
2. soft acids and bases with little charge density and/or which are relatively electron rich.

Note that the hard-soft classification should not be thought of as if all hard acids and bases are equally hard and all soft acids and bases equally soft. There is a graduation in hardness and softness and a number of intermediate acids and bases which do not fit

neatly in either category. With this caveat in mind, representative **hard, soft, and borderline acids** are given below. Notice how they illustrate the trends just outlined.



As expected, hard acids tend to be found towards the left side of the periodic table and involve higher oxidation states and/or electron donating substituents while soft acids are more common to the right of the periodic table and involve lower oxidation states and/or electron donating substituents.

Illustrative hard, soft, and borderline bases are given below. Again, notice how these substances illustrate the general trends.

Selected Hard Bases (Class a)

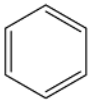
Nitrogen bases	Oxygen bases		small halides
NH_2^-	OH^-	CO_3^{2-}	F^-
NH_3	H_2O	RCO_2^-	Cl^-
RNH_2	ROH	NO_3^-	
NH_2NH_2	ROR	PO_4^{3-}	
		SO_4^{2-}	

Selected Borderline Bases

electron-poor Nitrogen bases		low oxidation state element oxyanions	intermediate halides
N_3^-		NO_2^-	
NO_2^-			
SCN^-		SO_3^{2-}	Br^-
N_2			

Selected Soft Bases (Class b)

Carbon bases	P and As bases	Sulfur bases	large halides & pseudohalides
R^-	PR_3	RS^-	H^-
CO	$P(OR)_3$	RSH	I^-
CN^-	AsR_3	RSR	
RNC		SCN^-	
$R_2C{=}CR_2$ (alkenes)			



(electron-rich aromatics)

Qualitative Estimation of the Relative Hardness and Softness of Lewis Acids and Bases

As can be seen from the examples above, **hard acids are relatively electron-poor and hard bases electron-rich** since they have comparatively

- small frontier orbitals, reflective of their relatively small atom/ion/fragment sizes
- high (for acids) or low (for bases) oxidation states on the base atom, reflected in a large positive formal charge (for acids) or negative formal charge (for bases)
- low polarizability, due to loss or gain of substantial numbers of electrons, or the localization of
  - positive charge on an electropositive element or an atom bearing electron-withdrawing substituents
  - negative charge on an electronegative element or an atom bearing electron-donating substituents

In contrast to hard acids and bases **soft acids are relatively electron-rich and soft bases larger and more electron poor** since they have comparatively

- large frontier orbitals, reflective of their relatively large atom/ion/fragment sizes
- low oxidation states, often resulting in small or nonexistent atomic charges
- high polarizability, as might be expected of species in which electron-electron repulsions are lower and electrons are spread over a large volume. Sometimes this is indicated by
  - positive charge on an electronegative element or an atom bearing electron-donating substituents
  - negative charge on an electropositive element or an atom bearing electron-withdrawing substituents

Exercise 4.4.1

Rank the acid or bases in each set in increasing order of expected hardness?

(a) Cr^{2+} and Cr^{3+}

(b) H^+, Cs^+, and Tl^+

(c) SCN^- (acting as a base at N) and SCN^- (acting as a base at S)

(d) AlF_3, AlH_3, $AlMe_3$

(e) The side chains of the following proteinogenic amino acids

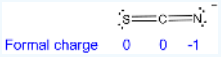


Answer

(a) $Cr^{2+} < Cr^{3+}$ All other things being equal, hardness increases with oxidation state.

(b) $Tl^+ < Cs^+ < H^+$ The order reflects Cs^+ and Tl^+'s larger size relative to H^+ (which doesn't possess any electrons that can be polarized anyway) and that Tl^+ still possesses two valence electrons while Cs^+ possesses none.

(c) SCN^- (acting as a base at S) < SCN^- (acting as a base at N) The order reflects that N is more elctronegative than S and possesses a more negative formal charge of -1.



(d) $AlH_3 < AlMe_3$, AlF_3 The hardness increases as the substituents on the Lewis acid Al center become less electron donating and more electron withdrawing (and, incidentally, harder bases) as their electronegativity increases in the order $H^- < CH_3^- < F^-$. Note that the order of electron donating ability for H^- and CH_3^- is the opposite observed for carbocations, for which hyperconjugation plays a larger role.

(e) Sec < Cys < Ser The hardness increases as the electronegativity of the Lewis base chalcogen increases on going from a selenol to a thiol to an alcohol.

The Hard-Soft Acid-Base Principle (HSAB Principle)

The **Hard-Soft acid-base principle (HSAB Principle) explains patterns in Lewis acid-base reactivity in terms of a *like reacts with like preference***. Both thermodynamically and kinetically hard acids prefer hard bases and soft acids soft bases. Specifically,

- Thermodynamically, hard acids form stronger acid-base complexes with hard bases while soft acids form stronger complexes with soft bases.
- Kinetically, hard acids/electrophiles react more quickly with hard bases/nucleophiles while soft acids/electrophiles react more quickly with soft bases/neucleophiles

Applications of the HSAB principle include

1. Predicting the equilibrium or speed of *Lewis acid-base metathesis and displacement reactions.* In a Lewis acid-base *metathesis reaction* the acids and bases swap partners

$$A_1{:}B_1 + A_2{:}B_2 \underset{}{\overset{k_1,\ K_{eq}}{\rightleftharpoons}} A_1B_2 + A_2{:}B_1 \tag{4.4.1}$$

For example, the equilibrium position of the metathesis reaction between TlF and K_2S favors the products:

$$2TlF + K_2S \rightleftharpoons Tl_2S + 2KF$$

(4.4.2)

consistent with the HSAB's hard-hard and soft-soft preference.

$$\underset{\text{soft hard}}{2\,Tl^{+}F^{-}} + \underset{\text{hard soft}}{(K^{+})_2S^{2-}} \rightleftharpoons \underset{\text{soft soft}}{(Tl^{+})_2\,S^{2-}} + \underset{\text{hard hard}}{2\,K^{+}F^{-}}$$

(4.4.3)

The HSAB principle also allows for prediction of the position of displacement reactions, in which a Lewis acid or base forms an adduct using a base or acid from an existing Lewis acid-base complex. In these reactions, the displacement of acid or base from the reactant complex to may be thought of as a sort of metathesis reaction, one in which in the unbound acid or base switches places with one in the complex. For example, the reaction between HI and methylmercury cation

$$HI + HgSCH_3^{+} \rightleftharpoons CH_3SHgI + H^{+}$$

(4.4.4)

involves displacement of an iodide from HI to give CH_3HgI. The position of the equilibrium favors CH_3HgI since both CH_3Hg^{+} and I^{-} are both soft, while H^{+} is a hard acid.

$$\underset{\text{hard-soft}}{H\text{-}I} + \underset{\text{soft}}{CH_3Hg^{+}} \rightleftharpoons \underset{\text{soft -soft}}{CH_3Hg\text{-}I} + \underset{\text{hard}}{H^{+}}$$

(4.4.5)

Exercise 4.4.2

Predict the position of equilibrium for the following reaction.

$$Fe_2O_3 + 3Ag_2S \rightleftharpoons Fe_2S_3 + 3Ag_2O$$

Answer

The equilibrium will favor the reactants (K<1) since the hard-hard and soft-soft interactions in the reactants are more stable than the hard-soft interactions in the products.

$$\underset{\text{hard hard}}{(Fe^{3+})_2\,(O^{2-})_3} + \underset{\text{soft soft}}{3\,(Ag^{+})_2S^{2-}} \rightleftharpoons \underset{\text{hard soft}}{(Fe^{3+})_2\,(S^{2-})_3} + \underset{\text{soft hard}}{3\,(Ag^{+})_2O^{2-}}$$

Exercise 4.4.3

Predict whether K for the following equilibria will be <<1, ~1, or >>1.

a. $2HF + (CH_3Hg)_2S \rightleftharpoons 2CH_3HgF + H_2S$

b. $Ag(NH_3)_2^{+} + 2PH_3 \rightleftharpoons Ag(PH_3)_2^{+} + 2NH_3$

c. $Ag(PH_3)_2^{+} + 2H_3B-SH_2 \rightleftharpoons 2H_3B-PH_3 + Ag(SH_2)_2^{+}$

d. $H_3B-NH_3 + F_3B-SH_2 \rightleftharpoons H_3B-SH_2 + F_3B-NH_3$

Answer

a. K< < 1 since the reactant adducts are hard-hard and soft-soft while the products involve hard-soft interactions

b. K>>1 since the reactant complex, diamine silver(I) is a complex of a hard base, NH_3, with the soft acid, Ag^+, while the product is a complex of the same soft acid with the soft base phosphine.

c. K~1 since all the adducts amongst the reactants and products involve soft acids and bases

d. K>>1 since BH_3 is a softer acid than BF_3 so it will form a stronger complex with the softer base H_2S while the harder BF_3 forms a stronger complex with the harder base NH_3.

2. Predicting the relative strengths of a given set of *Lewis acids or bases towards a particular substrate*. Consider, for example, the relative strengths of a BH_3, BMe_3, and BF_3 towards group 15 hydrides like NH_3, PH_3, and AsH_3. Of the boranes listed, the hardest acid BF_3 is the strongest acid towards the hard base NH_3 while BH_3 is the strongest towards AsH_3.[†]

Exercise 4.4.4

Which acid will form the most stable complex with CO - BH_3, BF_3, or BMe_3?

Answer

BH_3. Since CO forms complexes primarily through its carbon lone pair it is a soft base and so will form the strongest complex with the softest Lewis acid.

The Theoretical Interpretation of the Hard Soft Acid-Base Principle is that hard-hard preferences reflect superior electrostatic stabilization while soft-soft preferences reflect superior covalent stabilization.

The hard-hard and soft-soft preferences in Lewis acid-base interactions reflect that

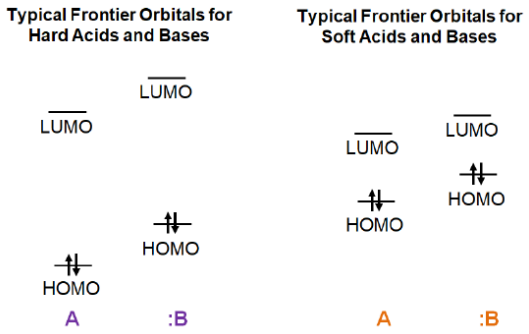
- The lone pair of a hard base is strongly stabilized electrostatically by a hard acid
- The lone pair of a soft base is strongly stabilized by forming a covalent bond with a soft acid
- The lone pair of a hard or soft base is comparatively weakly stabilized by an acid opposite to it in hardness or softness since the overall electrostatic and covalent stabilization of the adduct is comparatively weak.

To see why this is the case it is helpful to divide the contributions to the interaction energy between an acid and a base as follows:

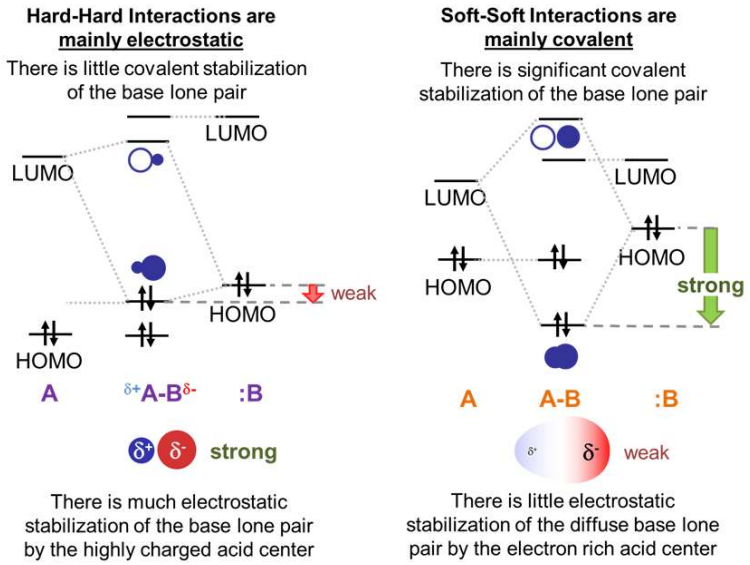
$$\text{Interaction Energy} = \underbrace{\text{Electrostatic attractions and repulsions of partial atomic charges}}_{\text{Ionic term}} + \underbrace{\text{Interactions between filled orbitals on one fragment and unfilled orbitals on the other}}_{\text{Covalent term}} + \underbrace{\text{Electrostatic repulsions between filled orbitals on the two fragments}}_{\text{Steric term}} \tag{4.4.6}$$

Of the three contributions to the interaction energy, only the ionic and covalent terms directly relate to the hardness of the interacting acid and base. One approach to thinking about how hardness influences the ionic and covalent contributions is to consider the frontier orbitals involved in the acid-base interaction. This is sometimes done through the use of the Salem-Klopman equation,[1,*] although in the treatment which follows a more qualitative approach will be employed.

Both hard acids and bases will have comparatively low energy HOMO levels and high energy LUMO levels, with a correspondingly high HOMO-LUMO gap. In contrast, soft acids and bases will have comparatively high-energy HOMO levels and low-energy LUMO levels, giving a comparatively smaller HOMO-LUMO gap.



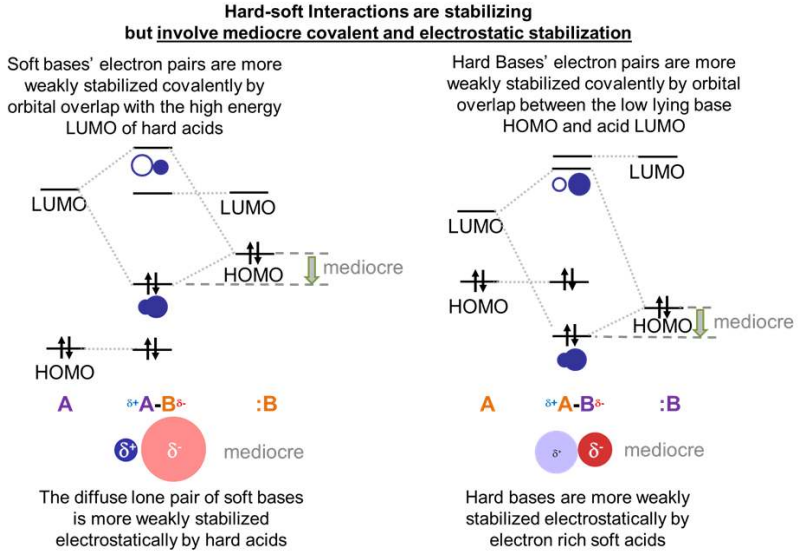
Given this, consider the frontier orbital interactions involved in the formation of an acid-base complex for the possible cases, as illustrated schematically below.



The large gap in energy between hard bases' highly stabilized HOMO lone pairs and the high energy LUMO of hard acids ensures that in **hard acid-hard base adducts the dominant stabilizing interaction will involve electrostatic attraction between the base lone pair and the electropositive Lewis acid center**. Fortunately, since the electron clouds in hard bases are relatively dense and electron rich while hard Lewis acids are highly charged and small these electrostatic interactions are strong.

In contrast, in **soft acid-soft base adducts the dominant stabilizing interaction will be covalent.** This is because the small gap in energy between a soft base HOMO and soft acid LUMO enables the formation of a well-stabilized bonding orbital with significant electron density between the acid and base.

The orbitals interactions between hard acids and soft bases and soft acids and hard bases are intermediate between the hard acid-hard base and soft acid-soft base cases.



This means that the adducts are stable relative to free acid and base – just not as well stabilized as in the hard acid and hard base case. In the case of hard acids and soft bases the hard acids are less able to stabilize the soft bases' relatively diffuse electron pair electrostatically and there isn't as much covalent stabilization as in adducts of soft acids and bases due to hard acid's high energy.

References

1. Ahrland, S.; Chatt, J.; Davies, N. R., The relative affinities of ligand atoms for acceptor molecules and ions. Quarterly Reviews, Chemical Society 1958, 12 (3), 265-276.

2. Pearson, R. G., Hard and Soft Acids and Bases. Journal of the American Chemical Society 1963, 85 (22), 3533-3539.

3. Fleming, I., Molecular orbitals and organic chemical reactions. Reference ed.; Wiley: Hoboken, N.J., 2010.

Notes

* Despite the fruitfulness of this observation, in general it is important to reduce the potential for observer bias by checking observations like these against compounds reported in the chemical literature and databases like the Inorganic Crystal Structure and Cambridge Crystallographic Databases.

** These are very soluble in water, to the point where some solutions are perhaps better described as solutions of water in the halide.

† This can be predicted based on the relative hardness of BF_3, BR_3, and BH_3 in the list of hard and soft acids. However, for those of you who may be confused as to why H is considered a better electron donor for the purposes of softening a Lewis acid center while alkyl groups are better electron donors for the purposes of stabilizing carbocations in organic chemistry, the dominant effect is the lower electronegativity of H relative to carbon (in CH_3). The effect of electron donation due to hyperconjugation isn't as great for thermodynamically stable bases like BX_3/BR_3.

†† For more on the Salem-Klopman equation see Fleming, I., Molecular orbitals and organic chemical reactions. Reference ed.; Wiley: Hoboken, N.J., 2010; pp. 138-143.

Contributors and Attributions

Stephen M. Contakes (Westmont College)

4.4: Hard-soft Acids and Bases is shared under a not declared license and was authored, remixed, and/or curated by LibreTexts.

4.5: Quantitative Measures of Hardness and Softness

Pearson Absolute Hardness is a useful metric of hardness based on orbital energies

The recognition that hard acids and bases possess a large HOMO-LUMO gap suggests that the gap size itself might serve as a useful index of hardness. The basis for this idea may be found by considering Pearson's definition of absolute hardness, η.[1] **Pearson's absolute hardness, η**, is half the second derivative of a species energy with respect to changes in total number of electrons, N_{e^-}

$$Pearson's\ absolute\ hardness = \eta = \frac{1}{2}\frac{d^2E}{dN_{e^-}^2} \tag{4.5.1}$$

$$(in\ \ eV)$$

and, since acid and bases' hardness and softness are inversely related, Pearson's absolute softness, σ, is just the inverse of hardness

$$Pearson's\ \ softness = \frac{1}{\eta} \tag{4.5.2}$$

Of these, Pearson's absolute hardness is related to the **Mulliken definition of electronegativity** as the first derivative of a species energy with respect to changes in total number of electrons.

$$Mulliken\ electronegativity = \chi = \frac{dE}{dN_{e^-}} \tag{4.5.3}$$

$$(in\ \ eV)$$

Operationally, both the Pearson hardness and Mulliken electronegativity are approximated in terms of the energies associated with unit changes in the number of electrons – *i.e.* in terms of ionization energies and electronegativities. Specifically,

$$Pearson's\ absolute\ hardness = \eta \approx \frac{IE - EA}{2} \tag{4.5.4}$$

$$Mulliken\ \ electronegativity = \chi \approx \frac{IE + EA}{2} \tag{4.5.5}$$

$$where\ \ IE\ \ and\ \ EA\ \ are\ \ in\ \ eV$$

The connection between Pearson's absolute hardness/softness and the HOMO-LUMO gap then follows from Koopman's theorem, in which the ionization energy (IE) is just the opposite of the HOMO energy.

$$IE = -E_{HOMO} \tag{4.5.6}$$

Similarly, the electron affinity (EA), defined as the opposite of the energy released on absorption of an electron, may be taken as an approximation of the LUMO energy.

$$E_{LUMO} \approx -EA \tag{4.5.7}$$

So Pearson's absolute hardness is just half the HOMO-LUMO gap (band gap) size in electron volts

$$Pearson's\ absolute\ hardness, \eta \approx \frac{E_{LUMO} - E_{HOMO}}{2} \tag{4.5.8}$$

$$where\ all\ values\ are\ given\ in\ eV$$

and the Mulliken electronegativity is just the average of the HOMO and LUMO energies (~Fermi energy):

$$Mulliken\ electronegativity, \chi \approx -\frac{E_{LUMO} + E_{HOMO}}{2} \tag{4.5.9}$$

$$where\ all\ values\ are\ given\ in\ eV$$

The relationships between the Pearson absolute hardness, Mulliken electronegativity, and HOMO and LUMO energies are depicted schematically for the group 1A monocations in Figure **4.5.1**.

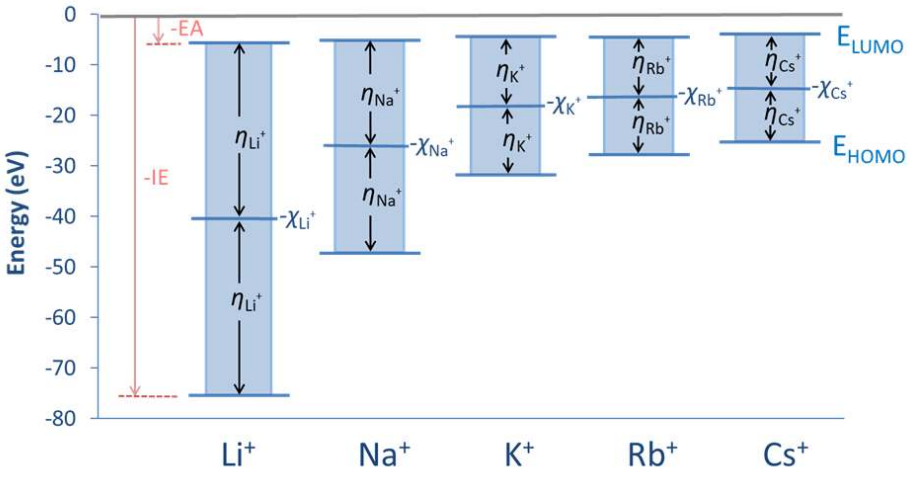


Figure **4.5.1**. Relationships between Pearson absolute hardness, Mulliken electronegativity, and HOMO and LUMO energies for the group 1A monocations.

Values of the Pearson hardness and Mulliken electronegativity for several acids and bases are given in Table **4.5.1**. The values in the table confirm the expected trends, showing an increase in hardness with size (down a group), with increasing charge, and as substituent electronegativity increases for a series of isolobal ions.

Table **4.5.1**: Pearson Absolute Hardness and Related Parameters for Selected Acids and Bases.[2] Taken from Pearson, R. G., Absolute electronegativity and hardness: application to inorganic chemistry. Inorganic Chemistry 1988, 27 (4), 734-740.

Species	Ionization Energy, IE or I (eV)	Electron Affinity, EA or A (eV)	Mulliken Electronegativity, χ (eV)	Pearson Absolute Hardness, η (eV)
Selected Acids				
Group 1A monocations				
Li^+	75.64	5.39	40.52	35.12
Na^+	47.29	5.14	26.21	21.08
K^+	31.63	4.34	17.99	13.64
Rb^+	27.28	4.18	15.77	11.55
Cs^+	25.1	3.89	14.5	10.6

Group 11 monocations				
Cu^{+}	20.29	7.73	14.01	6.28
Ag^{+}	21.49	7.58	14.53	6.96
Au^{+}	20.5	9.23	14.9	5.6
Isoelectronic Row 3 Metal Cations				
Na^{+}	47.29	5.14	26.21	21.08
Mg^{2+}	80.14	15.04	47.59	32.55
Al^{3+}	119.99	28.45	74.22	45.77
Changes with Transition Metal Ion Charge				
Fe^{2+}	30.65	16.18	23.42	7.24
Fe^{3+}	54.8	30.65	42.73	12.08
Co^{2+}	33.50	17.06	25.28	8.22
Co^{3+}	51.3	22	42.4	8.9

		.5		
Boron trihalides				
BF_3	15.81	-3.5	6.2	9.7
BCl_3	11.60	0.33	5.97	5.64
BBr_3	10.51	0.82	5.67	4.85
CO_2	13.8	-3.8	5.0	8.8
CS_2	10.08	0.62	5.35	5.56
Selected Bases				
Group 17 monoanions (taken to be identical to the free atom values; for arguments as to why this is reasonable see Pearson, R. G., Inorg. Chem. 1988, 27 (4), 734-740.)				
F^-	17.42	3.40	10.41	7.01
Cl^-	13.01	3.62	8.31	4.70
Br^-	11.84	3.36	7.60	4.24
I^-	10.45	3.06	6.76	3.70
Group 15 hydrides				
NH_3	10.7	-5	2.6	8.2

		.6		
PH_3	10.0	-1.9	4.1	6.0
Trimethylpnictides				
NMe_3	7.8	-4.8	1.5	6.3
PMe_3	8.6	-3.1	2.8	5.9
$AsMe_3$	8.7	-2.7	3.0	5.7
Group 16 hydrides				
H_2O	12.6	-6.4	3.1	9.5
H_2S	10.5	-2.1	4.2	6.2
Phosphorous trihalides				
PF_3	12.3	-1.0	5.7	6.7
$PC1_3$	10.2	0.8	5.5	4.7
PBr_3	9.9	1.6	5.6	4.2

Drago-Wayland Acid-Base Parameters allow for estimation of the electrostatic and covalent contributions to the enthalpy of formation of a Lewis acid-base adduct.

Although Pearson hardness values are a useful metric of acid and bases' hardness, they cannot easily be used to estimate the Lewis acid-base interaction energy. This is not the case for the EC model developed by Drago and Wayland.[3] In the **Drago and Wayland's EC Model** the enthalpy of formation of an acid base adduct, AB,

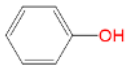
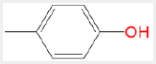
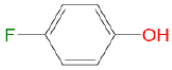
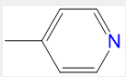
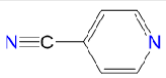
$$A + B \rightleftharpoons AB \qquad \Delta H_{AB\ adduct} \tag{4.5.10}$$

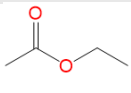
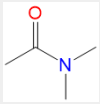
from the acid (A) and base (B) can be calculated as the sum of products of electrostatic (E) and covalent (C) factors that reflect the propensity of the acid and base to engage in strong electrostatic and covalent interactions with one another:

$$-\Delta H_{AB\ adduct} = E_A E_B + C_A C_B \tag{4.5.11}$$

where E_A and C_A are the electrostatic and covalent parameters for the acid and E_B and C_B the electrostatic and covalent parameters for the base given in units of $kcal^{½}$ $mol^{-½}$. E and C parameters for selected acids and bases are given in Table **4.5.2**.

Table **4.5.2**: E and C Parameters for selected Lewis acids and bases according to the ECW model.[4,5] Taken from Vogel, G. C.; Drago, R. S., The ECW Model. *Journal of Chemical Education* 1996, 73 (8), 701 and Drago, R. S. A modern approach to acid-base chemistry. *Journal of Chemical Education* 1974, 51 (5), 300 (for BF_3).

Species	E (kcal^{½} mol$^{-½}$)	C (kcal^{½} mol$^{-½}$)	W (kcal mol^{-1})	C/E
Acids				
I_2	0.5†	2†	0	4
ICl	2.92	1.66	0	0.57
H_2O	1.31	0.78	0	0.59
SO_2	0.51	1.56	0	3.1
$HCCl_3$ (chloroform)	1.56	0.44	0	0.28
$(CH_3)_3COH$	1.07	0.69	0	0.65
$(CF_3)_3COH$	3.06	1.88	-0.87	0.61
	2.27	1.07	0	0.47
	2.23	1.03	0	0.46
	2.30	1.11	0	0.48
	1.38	0.68	0	0.49
BF_3	1.62	9.88		6.10
$B(CH_3)_3$	2.90	3.60	0	1.2
$Al(CH_3)_3$	8.66	3.68	0	0.43
$Ga(C_2H_5)_3$	6.95	1.48	0	0.21
$In(CH_3)_3$	6.60	2.15	0	0.33
$Zn[N(Si(CH_3)_3)]_2$	2.75	2.32	0	0.84
$Cd[N(Si(CH_3)_3)]_2$	2.50	1.83	0	0.73
Bases				
NH_3	2.31	2.04		0.88
CH_3NH_2	2.16	3.13		1.4
$(CH_3)_2NH$	1.80	4.21		2.3
$(CH_3)_3N$	1.21	5.61		4.6
	1.78	3.54		2.0
	1.81	3.73		2.0
	1.53	2.94		1.9

Species	E ($kcal^{½}\ mol^{-½}$)	C ($kcal^{½}\ mol^{-½}$)	W ($kcal\ mol^{-1}$)	C/E
CH_3CN	1.64	0.71		0.43
$ClCH_2CN$	1.67	0.33		0.20
$CH_3C(O)CH_3$	1.74	1.26		0.72
$(C_2H_5)_2O$	1.80	1.63		0.91
	1.64	2.18		1.3
 (EtOAc)	1.63	0.95		0.58
	2.35†	1.31		0.56
$(CH_3)_2S$	0.25	3.75		15
$(CH_3CH_2)_2S$	0.24	3.92†		15
	0.26	4.07		16
$(CH_3)_2Se$	0.05	4.24		83
$(CH_3)_2SO$	2.4	1.47		0.61
$(CH_3)_3P$	0.25	5.81		24
$(CH_3O)_3P$	0.13	4.83		37
$(C_6H_5)_3PO$	2.59	1.67		0.64
$(C_6H_5)_3PS$	0.35	3.65		10
C_6H_6	0.70	0.45		0.64

† These values were fixed to parameterize the rest of the E and C parameters.

Trends in the relative values of C and E for the acids and bases in Table **4.5.2** are very roughly consistent with the trends in hardness and softness outlined earlier. However, the parameters suggest that some trends in hardness reflect changes in species ability to engage in ionic interactions while others reflect changes in species ability to engage in strong covalent interactions. For example, C_B for the dimethylchalcogenides increases steadily from 1.5 to 4.25 $kcal^{½}\ mol^{-½}$ on going from Me_2O to Me_2Se while E_B decreases from 1.68 to 0.05 $kcal^{½}\ mol^{-½}$, suggesting that electrostatic and covalent factors are both involved in a decreases in base hardness down group 16. However, in the case of phosphines and amines it appears that electrostatic factors are primarily responsible for the decrease in hardness down group 15. On going from Me_3N to Me_3P, C_B only increases slighly from 5.61 to 5.81 $kcal^{½}\ mol^{-½}$while E_B decreases from 1.21 to 0.25 $kcal^{½}\ mol^{-½}$- *i.e.* to 20% of the Me_3N value.

However, some species tend to have very high values for both E and C, reflecting their ability to engage in strong electrostatic and covalent interactions while others have small values for both, reflecting their relative stability as free species in solution.

As can be seen by comparing the acids and bases listed in the absolute hardness table (Table **4.5.1**) and the EC parameters table (Table **4.5.2**) The EC model has primarily been applied to organic and main group organometallic acids and bases. However, a variety of extensions have been proposed that enable its wider applicability.

Since the simple EC model only includes electrostatic and covalent considerations and thus ignores steric, lattice energy, and other contributions to the interaction energy. Thus it is only useful for analyzing the interaction energies of sterically unhindered adducts in which solvation energy and other contributions to the overall interaction energy are insignificant. However, additional refinements of the model attempt to extend its usefulness by accomodating various factors, such as

- *Steric strain.* Specifically, Hancock and Martell[6] introduced a D parameter to account for any additional steric strain introduced on adduct formation,* giving

$$-\Delta H_{AB\ adduct} = E_A E_B + C_A C_B - D_A D_B \tag{4.5.12}$$

- *Charge transfer on adduct formation.* As discussed in section 6.4.2 the formation of a Lewis acid base complex results in a net transfer of electron density from the electron donor (base) to the acceptor (acid). Drago and Wong[7] extended the EC model to include that charge transfer by adding what they called receptance factors that account for the acid's ability to receive electron density (R_A) and transference factors that account for the base's ability to donate electron density (T_B), giving

$$-\Delta H_{AB\ adduct} = E_A E_B + C_A C_B + R_A T_B \tag{4.5.13}$$

  This extension of the EC model is called the **electrostatic-covalent-transfer or ECT model**. Notably, it has been applied successfully to adducts involving ions, for which the R_AT_B term can account for as much as 31% of the interaction energy.

- *Any constant energy term, such as the energy needed to cleave a dimer in order to make the Lewis acid (e.g. $Al_2Cl_6 \rightarrow 2AlCl_3$).* Drago and Vogel[4] extended the EC model to accommodate these constant energy terms, which they designated W. The resulting model is called the **ECW model** for which

$$-\Delta H_{AB\ adduct} = E_A E_B + C_A C_B + W \tag{4.5.14}$$

$$where\ \ W = W_A + W_B$$

A simple application of EC and extended EC models is that they allow the enthalpy of adduct formation to be calculated. These enthalpy calculations based on the EC model are consistent with the superior interaction energy of hard-hard and soft-soft interactions compared to hard-soft ones. Consider, for example, the transfer of I_2 between BF_3 and $InMe_3$. H_3N-BF_3 and H_3N-$InMe_3$.

$$H_3N - BF_3 + InMe_3 \rightleftharpoons BF_3 + H_3N - InMe_3 \tag{4.5.15}$$

Since H_3N is a hard base and BF_3 and $InMe_3$ harder and softer acids, respectively, the equilibrium us expected to favor the reactant, H_3N-BF_3. Assuming the equilbrium is enthalpically driven this qualitative analysis is consistent with the expected endothermic enthalpy of the reaction, as may be seen from the calculated enthalpies of adduct formation for both H_3N-BF_3 and H_3N-$InMe_3$.

For H_3N-BF_3:

$$-\Delta H_{H_3N-BF_3} = E_{BF_3} E_{NH_3} + C_{BF_3} C_{NH_3} \tag{4.5.16}$$

$$-\Delta H_{H_3N-BF_3} = (1.62)(2.31) + (9.88)(2.04) \tag{4.5.17}$$

$$-\Delta H_{H_3N-BF_3} = 3.74\ kcal/mol + 20.1\ kcal/mol = 23.8\ kcal/mol \tag{4.5.18}$$

$$\Delta H_{H_3N-BF_3} = -23.8\ kcal/mol \tag{4.5.19}$$

For H_3N-$InMe_3$:

$$-\Delta H_{H_3N-InMe_3} = E_{InMe_3} E_{NH_3} + C_{InMe_3} C_{NH_3} \tag{4.5.20}$$

$$-\Delta H_{H_3N-InMe_3} = (6.6)(2.31) + (2.15)(2.04) \tag{4.5.21}$$

$$-\Delta H_{H_3N-InMe_3} = 15.25\ kcal/mol + 4.39\ kcal/mol = 19.63\ kcal/mol \tag{4.5.22}$$

$$\Delta H_{H_3N-InMe_3} = -19.63\ kcal/mol \tag{4.5.23}$$

So H_3N-BF_3 is enthalpically favored by -4.2 kcal/mol [=-23.8 kcal/mol - (-19.63 kcal/mol) according to Hess' Law].

In addition to their utility for estimating enthalpies of Lewis acid-base complex formation, EC and related models serve as a useful tool for estimating the relative importance of ionic, covalent, and steric factors in complex formation. Specifically,

- The relative contributions of ionic and covalent factors can be calculated directly as from the E and C terms. This can provide insight into why some complexes are more stable than others. Such calculations reveal that the hard-hard adduct H_3N-BF_3 is favored over the hard-soft adduct H_3N-$InMe_3$ because of the strong covalent interaction holding together H_3N-BF_3. The covalent term accounts for 84% of energy of the H_3N-BF_3 interaction and is largely lost on formation of H_3N-$InMe_3$, for which it contributes only 22% of the interaction energy. When the electrostatic term is accounted for it can be seen that the formation of H_3N-$InMe_3$ from H_3N-BF_3 is disfavored since it would result in a loss of 15.7 kcal/mol of covalent stabilization that would be incompletely compensated for by a gain of 11.5 kcal/mol of electrostatic stabilization.
- The role of other contributions to the bonding in a Lewis acid-base complex may be estimated from the discrepancy between experimental and EC model calculated stabilization energies. This is because the EC parameters assume sigma bonding and so any deviation between the calculated and experimental enthalpies of complex formation can be attributed to non-sigma contributions.
    - This is done explicitly in extensions of the EC model. For instance, in the case of the Hancock and Martell, ECT, and ECW extensions of the EC model the contribution of the steric, charge transfer, and constant energy factors (like dimer dissociation) are directly computed in the model.
    - Comparisons of the difference between the energies calculated using ordinary EC parameters and the observed enthalpies has also been used as an estimate of the
        - steric strain energy in strained adducts, which exhibit a less exothermic heat of adduct formation than expected
        - π-backbonding energy in adducts which are capable of such interactions and exhibit a more exothermic heat of formation than expected.[8-10]
    - For examples see (a) Drago, R. S., The interpretation of reactivity in chemical and biological systems with the E and C model. Coordination Chemistry Reviews 1980, 33 (3), 251-277; (b) Drago, R. S.; Bilgrien, C. J., Inductive transfer and coordination of ligands in metal—metal bonded systems. Polyhedron 1988, 7 (16), 1453-1468; (c) Drago, R. S., The question of a synergistic metal-metal interaction leading to .pi.-back-bond stabilization in dirhodium tetrabutyrate adducts. Inorganic Chemistry 1982, 21 (4), 1697-1698.
- The role of electrostatic, covalent, and other contributions to the spectroscopic behavior of Lewis acid-base complexes can be assessed similarly using specialized versions of the ECW or ECT model that allow for calculation of changes in spectroscopic parameters on adduct formation - *e.g.* OH stretching frequencies. Details are beyond the scope of this text but may be found in the original literature;[11] for example Drago, R. S.; Vogel, G. C. *JACS* 1992, 114 (24), 9527-9532; Vogel, G. C.; Drago, R. S., *J. Chem. Educ.* 1996, 73 (8), 701; Drago, R. S.; Wong, N. M., *J. Chem. Educ.* 1996, 73 (2), 123.).

Pearson Softness Parameters have been proposed as a means of calculating the equilibrium constant for formation of a Lewis acid-base adduct, although they are more commonly used to estimate metal toxicity

Pearson also proposed a softness parameter that can be used to estimate the thermodynamics of Lewis acid base complex formation, this time in the form fo the equilibrium constant for

$$A + B \overset{K}{\rightleftharpoons} AB \tag{4.5.24}$$

for which Pearson proposed

$$logK = S_A S_B + \sigma_a \sigma_B \tag{4.5.25}$$

where S_A and S_B are acid and base parameters related to the strength of the acid-base interaction and σ_A and σ_B are acid and base parameters related to softness. This approach hasn't found as wide acceptance in studies of chemical reactivity as the Drago-Wayland and absolute hardness parameters. However, because the toxicity of metal ions' sometimes depends on their propensity to bind soft Lewis bases in living systems, the softness parameter's which Pearson and Mawby subsequently proposed based on the relative energies of metal flourine and metal iodine bonds[12] has been widely used as a tool for predicting metal ion toxicity.[13]

References

1. Pearson, R. G., Absolute electronegativity and absolute hardness of Lewis acids and bases. *Journal of the American Chemical Society* 1985, 107 (24), 6801-6806.

2. Pearson, R. G., Absolute electronegativity and hardness: application to inorganic chemistry. *Inorganic Chemistry* 1988, 27 (4), 734-740.

3. Drago, R. S.; Wayland, B. B., A Double-Scale Equation for Correlating Enthalpies of Lewis Acid-Base Interactions. *Journal of the American Chemical Society* 1965, 87 (16), 3571-3577.

4. Vogel, G. C.; Drago, R. S., The ECW Model. *Journal of Chemical Education* 1996, 73 (8), 701.

5. Drago, R. S. A modern approach to acid-base chemistry. *Journal of Chemical Education* 1974, 51 (5), 300

6. Hancock, R. D.; Martell, A. E., Hard and Soft Acid-Base Behavior in Aqueous Solution: Steric Effects Make Some Metal Ions Hard: A Quantitative Scale of Hardness-Softness for Acids and Bases. *Journal of Chemical Education* 1996, 73 (7), 654.

7. Drago, R. S.; Wong, N. M., The Role of Electron-Density Transfer and Electronegativity in Understanding Chemical Reactivity and Bonding. *Journal of Chemical Education* 1996, 73 (2), 123.

8. Drago, R. S., The interpretation of reactivity in chemical and biological systems with the E and C model. Coordination Chemistry Reviews 1980, 33 (3), 251-277.

9. Drago, R. S.; Bilgrien, C. J., Inductive transfer and coordination of ligands in metal—metal bonded systems. Polyhedron 1988, 7 (16), 1453-1468.

10. Drago, R. S., The question of a synergistic metal-metal interaction leading to .pi.-back-bond stabilization in dirhodium tetrabutyrate adducts. Inorganic Chemistry 1982, 21 (4), 1697-1698.

11. Drago, R. S.; Vogel, G. C., Interpretation of spectroscopic changes upon adduct formation and their use to determine electrostatic and covalent (E and C) parameters. *Journal of the American Chemical Society* 1992, 114 (24), 9527-9532.

12. Pearson, R. G.; Mawby, R. J. The Nature of Metal-Halogen Bonds in Gutmann, V. *Halogen Chemistry, vol. 3.* Academic Press: London, 1967, pp. 55-84.

13. Kinraide, T. B. Improved Scales for Metal Ion Softness and Toxicity *Environmental Toxicology and Chemistry* 2009, 28 (3), 525-533.

Notes

* More precisely, the D parameters account for the difference in steric strain in the adduct relative to a water adduct of the Lewis acid.

Contributors

Stephen Contakes (Westmont College, USA)

4.5: Quantitative Measures of Hardness and Softness is shared under a not declared license and was authored, remixed, and/or curated by LibreTexts.

CHAPTER OVERVIEW

5: Coordination Chemistry

5.1: Introduction to Coordination Chemistry
5.2: Ligands and Nomenclature
5.3: Coordination Numbers and Geometry
5.4: Bonding with d-orbitals
5.5: Isomers
5.5.1: Structural Isomers - Ionization Isomerism in Transition Metal Complexes
5.5.2: Structural Isomers - Geometric Isomerism in Transition Metal Complexes
5.5.3: Stereoisomers - Optical Isomerism in Transition Metal Complexes
5.5.4: Structural Isomers - Linkage Isomerism in Transition Metal Complexes
5.6: Crystal Field Theory
5.6.1: Crystal Field Theory
5.6.2: Colors of Coordination Complexes
5.6.3: Crystal Field Stabilization Energy
5.6.4: Factors That Affect the Magnitude of Δo
5.6.5: Jahn-Teller Distortions
5.6.6: Magnetic Moments of Transition Metals
5.6.7: Magnetism
5.6.8: Thermodynamics and Structural Consequences of d-Orbital Splitting
5.7: Ligand Field Theory
5.8: Ligand Exchange Reactions (Thermodynamics)
5.9: Electronic Spectra of Coordination Compounds

5: Coordination Chemistry is shared under a not declared license and was authored, remixed, and/or curated by LibreTexts.

5.1: Introduction to Coordination Chemistry

Coordination chemistry is the study of the compounds that form between metals and **ligands**, where a ligand is any molecule or ion that binds to the metal. A metal **complex** is the unit containing the metal bound to its ligands. For example, $[PtCl_2(NH_3)_2]$ is the neutral metal complex where the Pt(II) metal is bound to two Cl ligands and two NH_3 ligands. If a complex is charged, it is called a **complex ion** (ex. $[Pt(NH_3)_4]^{+2}$ is a complex cation). A complex ion is stabilized by formation of a **coordination compound** with ions of opposite charge (ex. $[Pt(NH_3)_4]Cl_2$). It is convention to write the formula of a complex or complex ion inside of square brackets, while counterions are written outside of the brackets. In this convention, it is understood that ligands inside the brackets are bound directly to the metal, in the metal's *first coordination sphere* (a.k.a inner coordination sphere). Ions written outside of the brackets are assumed to be in the *second coordination sphere*, and they are not directly bound to the metal.

- Neutral Complex: $[CoCl_3(NH_3)_3]$
- Complex Cation: $[Co(NH_3)_6]^{3+}$
- Complex Anion: $[CoCl_4(NH_3)_2]^-$
- Coordination Compound: $K_4[Fe(CN)_6]$

A common metal complex is $[Ag(NH_3)_2]^+$ formed when Ag^+ ions are mixed with neutral ammonia molecules.

$$Ag^+ + 2NH_3 \rightarrow [Ag(NH_3)_2]^+ \tag{5.1.1}$$

A complex $[Ag(S_2O_3)_2]^{3-}$ is formed between silver ions and negative thiosulfate ions:

$$Ag^+ + 2S_2O_3^{2-} \rightarrow [Ag(S_2O_3)_2]^{3-} \tag{5.1.2}$$

How did the study of coordination compounds started?

The coordination chemistry was pioneered by Nobel Prize winner Alfred Werner (1866-1919). He received the Nobel Prize in 1913 for his coordination theory of transition metal-amine complexes. At the start of the 20th century, inorganic chemistry was not a prominant field until Werner studied the metal-amine complexes of cobalt. Werner recognized the existence of several forms of cobalt-ammonia chloride. These compounds have different color and other characteristics. The chemical formula has three chloride ions per mole, but the number of chloride ions that precipitate with Ag^+ ions per formula was not always three. He thought only **ionized chloride ions** will form precipitate with silver ion. In the following table, the number below the **Ionized Cl^-** is the number of ionized chloride ions per formula. To distinguish ionized chloride from the coordinated chloride, Werner formulated the **Complex formula** and explained structure of the cobalt complexes.

Table 5.1.1 : Proposed Structure of Cobalt Ammonia Complexes from Number of Ionized Chloride

Solid	Color	Ionized Cl^-	Complex formula
$CoCl_3 6NH_3$	Yellow	3	$[Co(NH_3)_6]Cl_3$
$CoCl_3 5NH_3$	Purple	2	$[Co(NH_3)_5Cl]Cl_2$
$CoCl_3 4NH_3$	Green	1	*trans*-$[Co(NH_3)_4Cl_2]Cl$
$CoCl_3 4NH_3$	Violet	1	*cis*-$[Co(NH_3)_4Cl_2]Cl$

The structures of the complexes were proposed based on a coordination number of 6. The six ligands can be ammonia or chloride. Two different structures were proposed for the last two compounds, the *trans*- compound has two chloride ions on opposite vertices of an octahedral, whereas the the two chloride ions are adjacent to each other in the *cis*- compound. The *cis*- and *trans*- compounds are known as geometric isomers. Isomers will be the focus of a later section.

Classification of ligands

The discussion of the cobalt complexes above suggests that there are two types of chlorides in the $[Co(NH_3)_5Cl]Cl_2$ and *cis*-/*trans*-$[Co(NH_3)_4Cl_2]Cl$ complexes. In comparing the formula and the amounts of ionized Cl^- listed in Table **5.1.1**, the outer sphere chlorides must be the ionizable ones. The reason the inner sphere ligands are not ionizable is because there is significant covalent

character in the bond with the cobalt. Even though we call these inner sphere ligands chloride (or more properly chloro) ligands, they are not Cl^-, but rather better thought of as being Co-Cl.

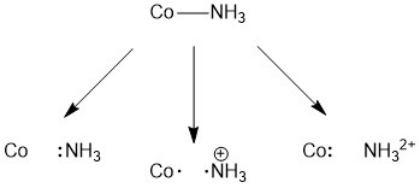
In order to account for this difference, we will use the Covalent Bond Classification (CBC) method for thinking about ligands. In this system, ligands are classified as either being X-type (one-electron donors) or L-type (two-electron donors). In order to determine if a ligand is an X-type or L-type ligand, perform a thought experiment in which you remove the ligand from the metal as a neutral atom or molecule.

Example 5.1.1

Consider the complex cation, $[Co(NH_3)_5Cl]^{2+}$. What types of ligands are NH_3 and Cl?

NH_3

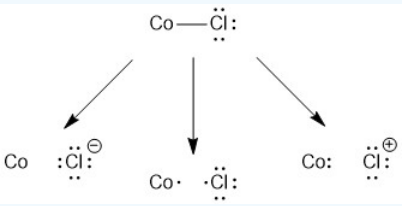
There are three possible ways you could think of breaking the Co-N bond. One could consider homolytic cleavage (one electron goes with Co and one with N) or heterolytic cleavage (one atom takes both electrons). The homolytic cleavage option is shown in the middle results in the formation of NH_3^+. Our goal is to remove the ligand as a neutral species, so this is not the correct option. If both electrons in the bond go with the nitrogen, there is no charge on the outgoing ligand. When considering the two heterolytic cleavage options, the pair of electrons can either go with the nitrogen (left) or Co (right). Only one of these options (the one on the left) results in the formation of the neutral NH_3 molecule. As such, NH_3 is a two-electron donor and therefore a L-type ligand.



It is important to note two things before we move on to our consideration of chloride. First, even though there are four bonds to the nitrogen atom in the initial Co-NH_3, we do not put a positive charge on the nitrogen. While the nitrogen atom bound to cobalt is certainly less electron rich than the nitrogen atom in an uncoordinated ammonia molecule, if we think back on our discussion of the acidity of hexaaqua species, the charge is difficult to localize and so we ignore it. This will be true for all metal complexes. Second, no charge is shown on any of the cobalt species as accounting for charge on the ligand will likely be more straightforward.

Cl

Similar to our treatment of NH_3, there are three ways to consider removing the chloride. In this case, both heterolytic cleavage options (left and right) result in a charged chlorine species so these are not the correct option. However homolytic cleavage (center) of the Co-Cl bond results in a neutral chlorine atom. So the chloride ligand is a X-type ligand.



Why do we need to classify the different ligand types? Doing so is going to help us in determining the valence of the metal. Valence is somewhat similar to oxidation state, but there are subtle differences. The main difference is that valence accounts for both the overall charge on the complex and the number of X-type ligands in the complex. The emphasis with valence is once again on the idea that the metal needs to provide electrons to make covalent bonds to some ligands. To determine the valence of a metal use the following equation:

valence - number of X-type ligands = overall charge on the complex

Example 5.1.2

Determine the valence of cobalt in $[Co(NH_3)_5Cl]^{2+}$.

Previously we determined that the cobalt in this complex has one X-type ligand, the chloride. The complex has an overall +2 charge. Based on the equation above, the valence of the cobalt would be +3 or Co(III).

Had you followed traditional oxidation state rules, you should have arrived at the same conclusion. These rules would have treated the chloride as Cl^- and accounted for the remainder of the charge by oxidizing the cobalt. While a subtle difference, the results of experiments in which Ag^+ is added to $[Co(NH_3)_5Cl]^{2+}$ clearly indicate that the chloride is not ionizable and therefore should not be treated as Cl^-. While similar, the idea of valence emphasizes the covalent nature of the Co-Cl bond.

Exercise 5.1.1

Determine the valence of cobalt in $[Co(NH_3)_4Cl_2]Cl$.

Answer

While the amounts have changed, the NH_3 ligands are still L-type and the Cl ligands are X-type.

The valence on cobalt is (valence - 2 = +1) or Co(III) just like in the previous example.

Contributors and Attributions

- Chung (Peter) Chieh (Professor Emeritus, Chemistry @ University of Waterloo)

5.1: Introduction to Coordination Chemistry is shared under a not declared license and was authored, remixed, and/or curated by LibreTexts.

5.2: Ligands and Nomenclature

Ligand Denticity

Ligands can also be classified based on whether they bind to the metal center through a single site on the ligand or whether they bind at multiple sites. Ligands which bind through only a single site are called **monodentate** at the Latin word for tooth; in contrast those those which bind through multiple sites are called **chelating** after the Greek $\chi\alpha\lambda\epsilon$ for “claw”. These relationships are summarized in Figure **5.2.1**.

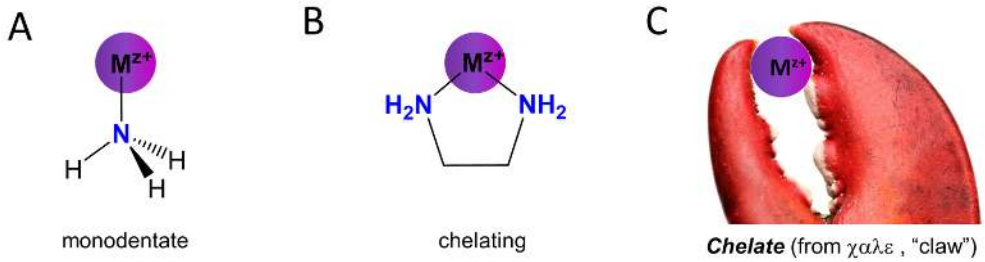


Figure 5.2.1. (A) Ammonia is monodentate ligand while (B) ethylene diamine is a chelating ligand owing to its capacity to bind metals via its two amine functional groups. (C) Chelating ligands act like a Lobster claw in attaching to the metal via multiple sites. The lobster claw image is adapted from https://www.clipart.email/download/1127636.html. Otherwise this work by Stephen Contakes is licensed under a Creative Commons Attribution 4.0 International License.

Following naturally from the classification of non-chelating ligands as monodentate, chelating ligands are further classified according to the number of sites which they can use to bind a metal center. This number of binding sites is called the denticity and ligands are referred to as monodentate (non chelating), bidentate, tridentate, etc. based on the number of sites available. Ligands with two binding sites have a denticity of two and are said to be bidentate; those with three are tridentate, four tetradentate, and so on. To illustrate this classification system examples of chelating ligands classified according to denticity are given in Figure **5.2.2**.

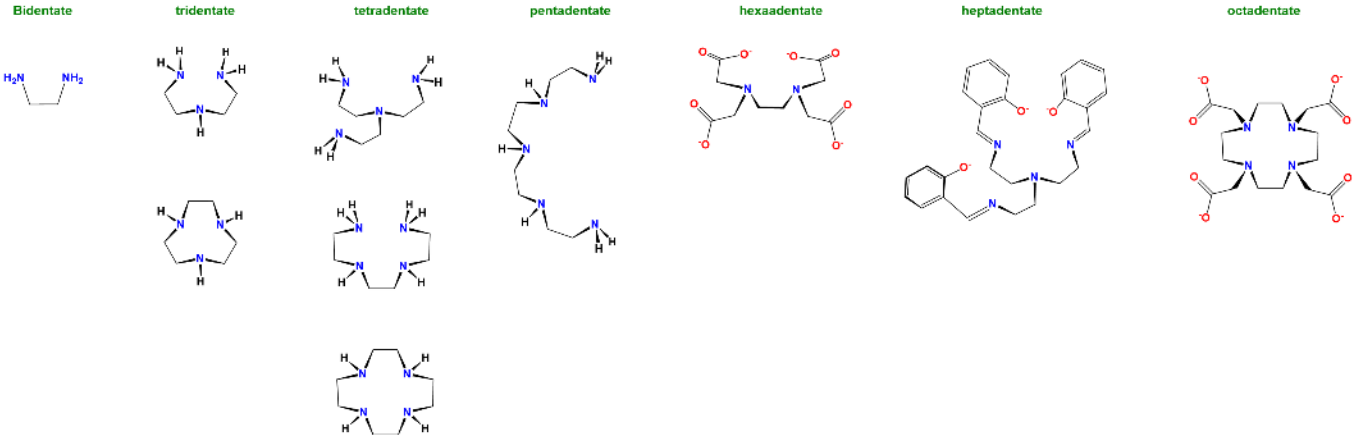


Figure 5.2.2. A selection of chelating ligands classified according to denticity. this work by Stephen Contakes is licensed under a Creative Commons Attribution 4.0 International License.

The classification of several of the ligands in Figure **5.2.2** requires a bit of explanation, specifically as to why the denticity of the carboxylate-containing ligands is less than the total number of lone-pair bearing oxygen and nitrogen atoms present. This is because only one of the carboxylate oxygen atoms is counted. Only one is counted because in most cases only one oxygen binds to a metal at any given time. When that oxygen is bound the other oxygen faces away from the metal, as depicted for the iron complex shown in Figure **5.2.3A**. Because only one oxygen per carboxylate *typically* binds only one is counted when assigning a ligand's denticity.

Although only one carboxylate oxygen usually binds to a metal it is still possible to bind a metal using both oxygen atoms. As shown in Figure **5.2.3B** complexes in which both carboxylates bind to a metal are known, and in fact are common in the active sites

of some enzymes. It is just that the binding of both oxygen atoms gives a strained four-membered ring that is usually unstable.

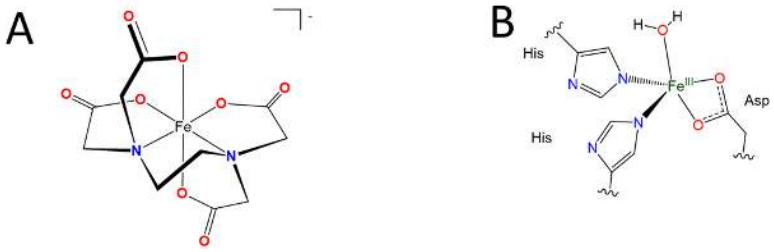


Figure 5.2.3. (A) Only one oxygen per carboxylate counts towards the denticity of EDTA since on binding the other oxygen generally points away from the metal center, as in the structure of $Fe(EDTA)^-$. This does not mean that both oxygens of a carboxylate can *never* both bind to metal centers in a complex. (B) Structures in which both oxygens of a carboxylate side chain bind to a metal are sometimes found in the active sites of some of the nonheme iron enzymes your body uses to break down amino acids. this work by Stephen Contakes is licensed under a Creative Commons Attribution 4.0 International License.

As was the case for carboxylate groups above, sometimes the classification of a group's denticity is based on experimental knowledge of their common binding modes. Carboxylates might commonly act as monodentate ligands but dithiocarbamates more commonly bind metals through both sulfur atoms (Figure **5.2.4**) and are classified as bidentate.

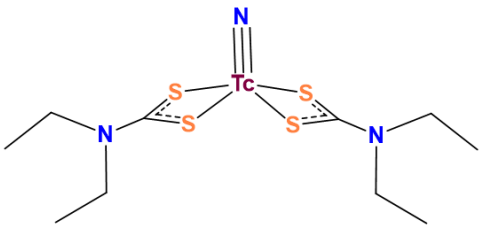
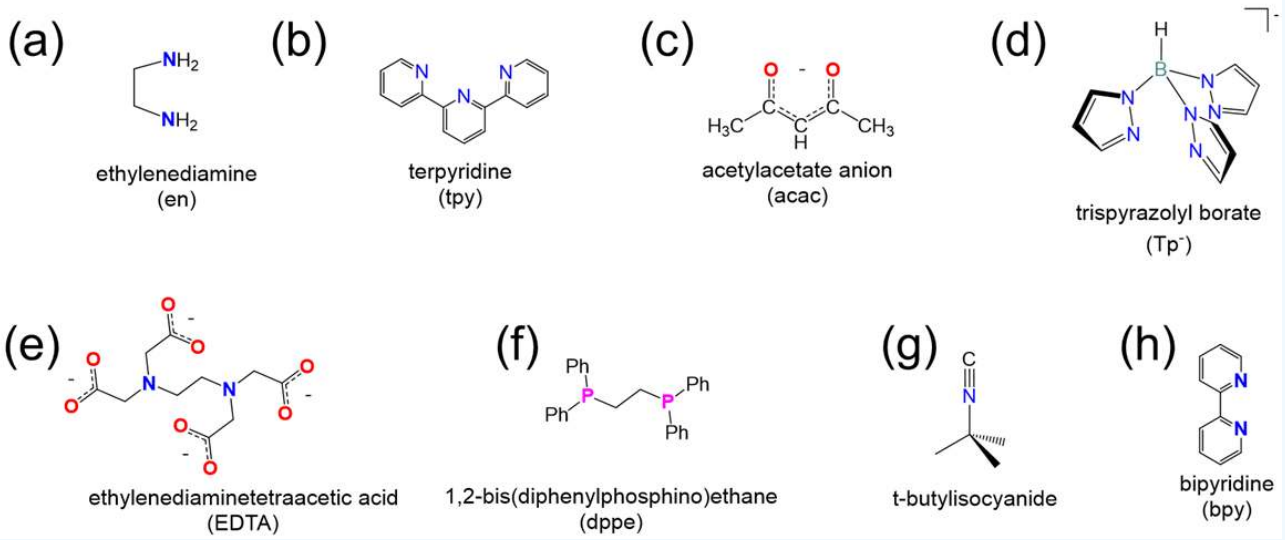


Figure 5.2.4. As in this complex, dithiocarbamates commonly bind metals through both sulfur atoms. Consequently, dithiocarbamates are classified as bidentate. this work by Stephen Contakes is licensed under a Creative Commons Attribution 4.0 International License.

Because of these factors it is technically more correct to say that carboxylates *usually act as* monodentate ligands and dithiocarbamates bidentate ones than it is to say that carboxylates *are* monodentate ligands and dithiocarbamates bidentate ones. So in other words the ligand classifications presented here are just represent common binding modes.

Exercise 5.2.1

Determine the denticity of each ligand in the list below and classify them as monodentate, tridentate, etc.



Answer

(a) bidentate

(b) tridentate

(c) bidentate

(d) tridentate (only the lower N on each ring has a lone pair that can be used to bind the metal)

(e) hexadentate (remember that each carboxylate only counts as one point of attachment)

(f) bidentate

(g) monodentate (through the lone pair on the isocyanide C)

(h) bidentate

This experimentally-based classification of dithiocarbamates as bidentate and carboxylates as monodentate can be confusing to a beginner. Fortunately, such experimentally based classifications are embedded in the lists of common monodentate ligands are given in Table **5.2.1** and common chelating ligands in Table **5.2.2**.

A perusal of the ligands in Table **5.2.1** reveals that several can bind to a metal in multiple ways. For example, thiocyanate, SCN^- can bind metal's through its S or N atoms. Such ligands are called **ambidentate ligands**. When naming an ambidentate ligand the atom through which it attaches to the metal is commonly specified after the ligand name using the italicized element symbol or, more formally a κ followed by the italicized element symbol.

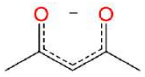
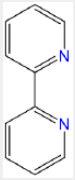
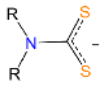
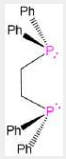
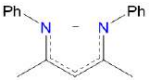
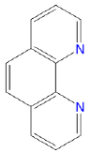
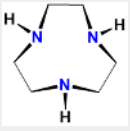
Table 5.2.1. Common monodentate ligands. Most chemists still prefer common names over the IUPAC ones.

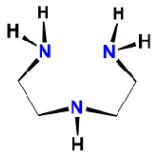
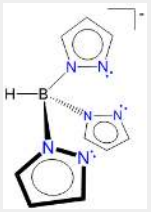
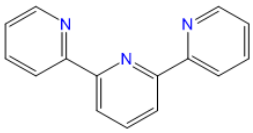
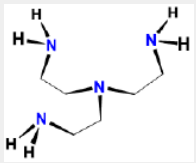
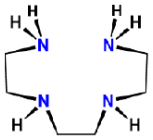
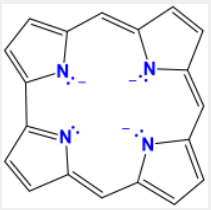
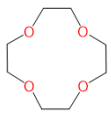
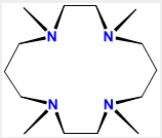
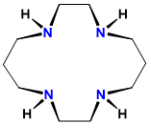
Ligand	Ligand Type	Common name	IUPAC name
H	X	hydrido	hydrido
F	X	fluoro	fluorido
Cl	X	chloro	chloridо
Br	X	bromo	bromido
I	X	iodo	iodido
M-CN	X	cyano	cyanido or cyanido-*κC* or cyanido-*C*
RNC	L	alkyl or aryl isocyanide	alkyl or aryl isocyanide
N_3	X	azido	azido
M-SCN	X	thiocyanato	thiocyanato-*κS* or thiocyanato-*S*
M-NCS	X	isothiocyanato	thiocyanato-*κN* or thiocyanato-*N*
CH_3CO_2	X	acetato	ethanoato
N	X_3	nitrido	nitrido
NH	X_2	imido	azanediido
NH_2	X	amido	azanido
NH_3	L	ammine	ammine
RNH_2, R_2NH, R_3N	L	alkylamine, dialkylamine, trialkalyamine (*e.g.* methylamine for CH_3NH_2)	alkylamine, dialkylamine, trialkalyamine (*e.g.* methylamine for CH_3NH_2)
 piperidine, abbreviated pip	L	piperidine	piperidine
 pyridine, abbreviated py	L	pyridine	pyridine
CH_3CN acetonitrile, abbreviated MeCN	L	acetonitrile	acetonitrile
P	X_3	phosphido	phosphido
PH_3	L	phosphine	phosphane
PR_3	L	trialkylphosphine (*e.g.* trimethylphosphine for Me_3P)	trialkylphosphane (*e.g.* trimethylphosphane for Me_3P)
PAr_3	L	triarylphosphine (*e.g.* triphenylphosphine for Ph_3P)	triarylphosphine (*e.g.* triphenylphosphane for Ph_3P)
O	X_2	oxo	oxido

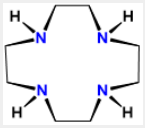
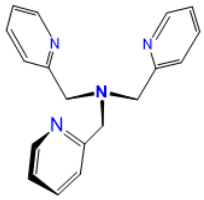
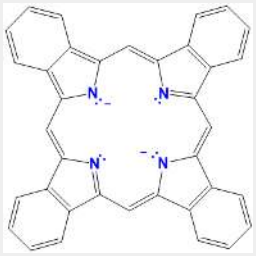
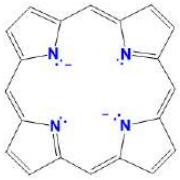
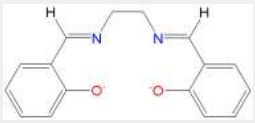
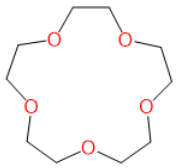
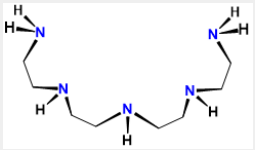
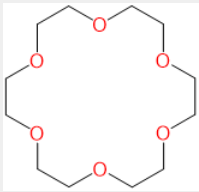
OH	X	hydroxo	hydroxido
H_2O	L	aqua	aqua
S	X_2	sulfo	sulfo
HS	X	hydrosulfido	hydrosulfido
RS	X	alkanethiolate (*e.g.* ethanthiolate for EtS^-)	thioalkanoate
NO	X	nitrosyl	nitrosyl
CO	L	carbonyl	carbonyl
CS	L	thiocarbonyl	thiocarbonyl
M-NO_2	L	nitro or nitrito-*N*	nitrito-κ*N* or nitrito-*N*
M-ONO	X	nitrito or nitrito-*O*	nitrito-κ*O* or nitrito-*O*

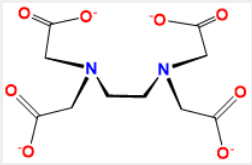
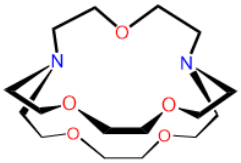
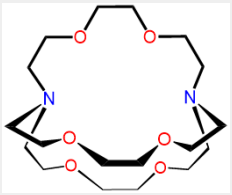
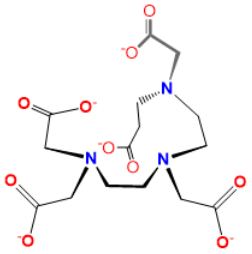
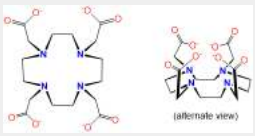
Table 5.2.2. Common chelating ligands organized by denticity. Most chemists use the common names and abbreviations to describe

these ligands.

Common Ligand name	IUPAC ligand name	abbreviation (if applicable)	Ligand Type	structure or representative/parent structure (shown in the ionization state in which they bind to a metal)
bidentate ligands				
acetylacetonato	2,4-pentanediono	acac	LX	
2,2'-bipyridine	2,2'-bipyridine	bpy or bipy	L_2	
dialkyldithiocarbamato	dialkylcarbamodithiolato	$R_2NCS_2^-$ or dtc	LX	
diphenylphosphinoethane or 1,2-(diphenylphosphino)ethane	Ethane-1,2-diylbis(diphenylphosphane)	dppe	L_2	
ethylenediamine	Ethane-1,2-diamine	en	L_2	
ethylenedithiolato	Ethane-1,2-dithiolato	$C_2H_2S_2^{2-}$	X_2	
nacnac	*N*,*N*'-diphenyl-2,4-pentanediiminato	nacnac	LX	
oxalato	oxalato	ox	X_2	
1,10-phenanthroline or *o*-phenanthroline	1,10-phenanthroline	phen or *o*-phen	L_2	
tridentate ligands				
triazacyclononane	1,3,7-triazacyclononane	tacn	L_3	

diethylenetriamine	1,4,7-triazaheptane	dien	L_3	
pyrazoylborato (scorpionate)	hydrotris(pyrazo-1-yl)borato	Tp	L_2X	
terpyridine or 2,2';6',2"-terpyridine	$1^2,2^2:2^6,3^2$-terpyridine or 2,6-bis(2-pyridyl)pyridine, tripyridyl, 2,2′:6′,2″-terpyridine	tpy or terpy	L_3	
tetradentate ligands				
β, *β*', *β*"-triaminotriethylamine	*β*, *β*', *β*"-tris(2-aminoethyl)amine	tren	L_4	
triethylenetetramine	1,4,7,10-tetraazadecane	trien	L_4	
corroles	variable and generally not used	cor or Cor	L_2X_2	
12-crown-4	1,4,7,10-tetraoxacyclododecane	12-crown-4	L_4	
tetramethylcyclam	1,4,8,11-tetramethyl-1,4,8,11-tetraazacyclotetradecane	TMC or cyclam	L_4	
cyclam	1,4,8,11-tetraazacyclotetradecane	cyclam	L_4	

cyclen	1,4,7,10-tetraazacyclododecane	cyclen	L_4	
tris(2-pyridylmethyl)amine	1-pyridin-2-yl-*N*,*N*-bis(pyridin-2-ylmethyl)methanamine	tpa or TPA	L_4	
phthalocyanines	variable and generally not used	variable, usually a modified Pc	L_2X_2	
porphyrins	variable and generally not used	variable, usually a modified por, Por, or P (e.g. TPP = tetraphenylporphyrin)	L_2X_2	
salen	2,2'-ethylenebis(nitrilomethylidene)diphenoxido	salen	L_2X_2	
pentadentate ligands				
15-crown-5	1,4,7,10,13-Pentaoxacyclopentadecane	15-crown-5	L_5	
tetraethylenepentamine	1,4,7,10,13-pentaazatridecane	tepa or TEPA	L_5	
hexadentate ligands				
18-crown-6	1,4,7,10,13,16-hexaoxacyclooctadecane	18-crown-6	L_6	

2,1,1-cryptand	4,7,13,18-Tetraoxa-1,10-diazabicyclo[8 .5.5]icosane	2,1,1-crypt or [2.1.1]-cryptand kryptofix 211 and variations thereof	L_6	
ethylenediaminetetraaceto	2,2′,2″,2‴-(Ethane-1,2-diyldinitrilo)tetraaceto	EDTA, edta, Y^{4-}	L_2X_4	
heptadentate ligands				
2,2,1-cryptand	4,7,13,16,21-pentaoxa-1,10-diazabicyclo[8 .8.5]icosane	2,2,1-crypt or [2.2.1]-cryptand kryptofix 221 and variations thereof	L_7	
octadentate ligands				
2,2,2-cryptand	4,7,13,16,21,24-Hexaoxa-1,10-diazabicyclo[8.8.8]hexacosan	2,2,2-crypt or [2.2.2]-cryptand kryptofix 222 and variations thereof	L_8	
pentetato acid or diethylenetriaminepentaacetato or DTPA	2-[bis[2-[bis(carboxylatomethyl)amino]ethyl]amino]acetato	DTPA	L_3X_5	
DOTA or tetraxetan	1,4,7,10-Tetraazacyclododecane-1,4,7,10-tetraacetic acid	Dota, DOTA	L_4X_4	

Rules for Naming Coordination Compounds

There are well-established rules for both naming and writing the formulae of coordination compounds. The purpose of these rules is to facilitate clear and precise communication among chemists. As with all such rules some are more burdensome than others to employ and some serve more crucial roles in the communication process while others are more peripheral.

Coordination Complexes are named as the ligand derivatives of a metal

A variety of systems have been used for naming coordination compounds since the development of the discipline in the time of Alfred Werner. In this section the most common approaches as they are currently used by practicing chemists will be described. Those who need a more thorough and accurate acquaintance with the full IUPAC nomenclature rules are encouraged to consult the IUPAC brief guide to inorganic nomenclature followed by complete guidelines, commonly known as the IUPAC red book. The

systems for naming coordination compounds used at present are additive, meaning that they consider coordination compounds as comprised of a central metal to which are added ligands. To specify the structure and bonding in this metal-ligand complex then involves

1. When there are several different ways of attaching the metal and ligands, specifying the structural or stereoisomer

2. systematically listing the ligands in a way that, as necessary, conveys information about how they are linked to the metal and their stereochemistry

3. providing the identity of the metal and its valence, or if the valence is unclear, at least the overall charge on the complex

4. specifying any counterions present

Since the stereochemistry of coordination compounds forms is the subject subsequent sections, in this section it will be addressed by simply giving the prefixes that designate stereochemistry as if they were self-evident. Do not worry about these for now. They will make sense after you have learned more about stereochemistry in the next sections. At that time, you can go back over the examples in this section to solidify your understanding of how to name coordination compounds.

Before going into these rules it is worth pointing out a few things.

1. It is easiest to learn these rules by starting with one or two of the rules, learning how to apply them, and then adding additional rules one at a time.

2. The rules also assume some familiarity with common coordination geometries and patterns of isomerism in metal complexes. Again, we will learn more about these in a later section. For now it is safe to assume

- complexes in which the metal has a coordination number of six are octahedral
- complexes in which the metal has a coordination number of five are trigonal bipyramidal
- complexes in which Pt^{II} , Pd^{II} , or Rh^{I}, or Ir^{I} have a coordination number of four are square planar
- other complexes in which the metal has a coordination number of four are tetrahedral

Like all assumptions these don't always work in real life but they should be good enough for now.

Rule 1: If ions are present, name the cation first, followed by the anion.

Examples:

$K_2[Pt^{II}Cl_4]$: potassium tetrachloroplatinate(2- or II)

$[Co^{III}(NH_3)_6](NO_3)_3$: hexaamminecobalt(3+ or III) nitrate

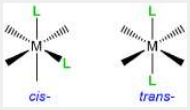
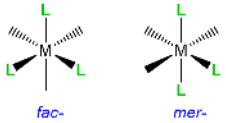
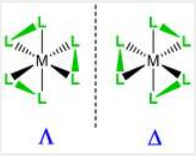
$[Co^{III}(NH_3)_6][Cr^{III}(C_2O_4)_3]$: hexaamminecobalt(3+ or III) tris(oxalato)chromate(3- or III)

You may notice two unusual features in these name. First, there are two numbers in parentheses. Second, in a few places the name of the metal seems to have changed to end in -ate. Both of these will be addressed in later rules.

Rule 2: When multiple isomers are possible, designate the particular isomer in italics at the front of the name of each complex

When a complex might exist as one of two stereosisomers prefixes are commonly used to designate which isomer is present. The most common cases are listed in Table **5.2.3**.

Table5.2.3. Prefixes used to specify isomerism about a metal center when naming and writing coordination compounds' formulae.

Type of isomerism	Graphical reminder	Prefixes
Geometric, *cis-* , *trans-*		*cis-* or *trans-*
Geometric, *fac- /mer-*		*fac-* or *mer-*
Enantiomers, **Λ-**, **Δ-**		**Λ-** or **Δ-**

Examples of how isomerism about a metal center is designated are given in Figure **5.2.5**.

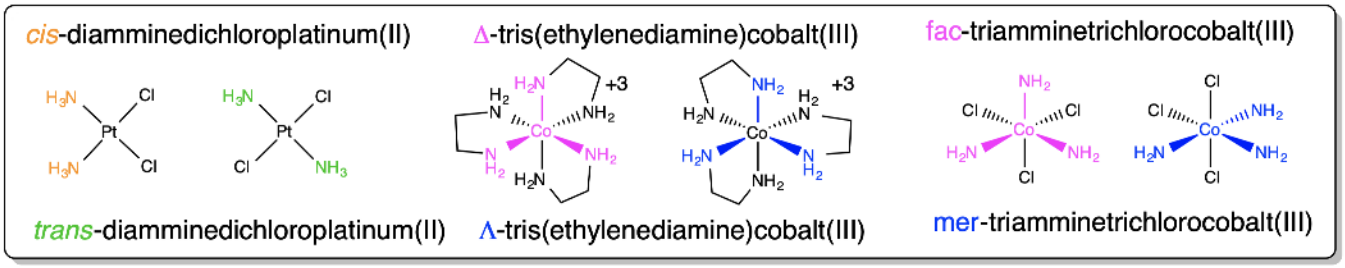


Figure 5.2.5. Application of nomenclature rules for stereosimerism about a metal.[1]

There are a number of other cases where it might be advisable to specify the stereochemistry of a complex. These cases involve specifying

- the coordination geometry about a metal center (octahedral, trigonal prismatic, tetrahedral, square planar, etc.)
- the geometry cannot be unambigouously described by a single *cis/trans* or *fac/mer* relaionship of ligands

These cases may also be handled by using a designator to specify the coordination geometry and, as necessary, giving the position of ligated atoms in terms of designated numbered positions for that geometry. See the IUPAC red book for details as such cases fall outside the scope of this course.

Rule 3: Specify the identity, number, and as appropriate, isomerism of the ligands present in alphabetical order by ligand name.

Before specifying the metal, the ligands are written as prefixes of the metal.

In specifying the ligands several rules are followed.

1. The ligands are written in alphabetical order by the ligand name only; symbols are not considered and prefixes do not count in determining alphabetical order.

   Example: In the name of the complex ion $[Co(NH)_3Cl]^{2+}$, pentamminechlorocobalt(II), the ammine ligand is named before the chloro ligand because the order is alphabetical by the ligand name by virtue of which ammine comes before chloro.

2. Prefixes are used to indicate the number of each ligand present. Specifically, *di-*, *tri-*, *tetra-* , *penta-*, *hexa-*, *etc.* prefixes are used to indicate multiple ligands of the same type EXCEPT when the ligand is polydentate or its name already has a *di-*, *tri-*, *tetra-* etc. In that case *bis-*,*tris-*, *tetrakis-*, etc. are used instead. These prefix rules are summarized in Table **5.2.3**.

Table 5.2.3. Prefixes used to specify the number of a given ligand present.

Number of identical ligands	prefix used when the ligand name is simple	prefix used when the ligand is polydentate or its name already has a *di-*, *tri-*, *tetra-* etc.
2	di-	bis-
3	tri-	tris-
4	tetra-	tetrakis-
5	penta-	pentakis-
6	hexa-	hexakis-
7	hepta-	heptakis-
8	octa-	octakis-
9	nona-	nonakis-
10	deca-	decakis-

An example of the application of the prefix rule is given in Figure **5.2.6**.

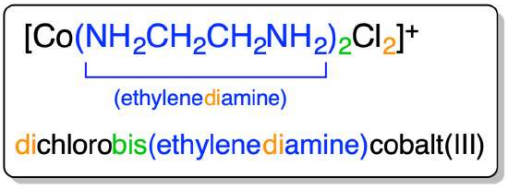


Figure 5.2.6. Example of the use of prefixes to specify the number of ligands of each type in a complex.[1]

3. Ligand names are based on their charge

- L-type ligand names are the same as the names of their neutral compounds with two caveats

  i. names that involve spaces should either be put in parentheses or the spaces should be eliminated (preferred)

  Example: cis-dichlorobis(**dimethyl sulfoxide**)platinum(II) or *cis*-dichlorobis(**dimethylsulfoxide**)platinum(II)

  ii. A few ligands are given common names.

  - H_2O = aqua
  - NH_3 = ammine (notice that there ate two n's)
  - CO = carbonyl
  - CS = thiocarbonyl
  - NO = nitrosyl

- For X-type ligands, the ending is typically changed to end in an -"o"

  Examples: Cl = chloro, NH_2 = amido, N_3 = azido

  Caveat: some X-type ligands have common names that may also be used

  Examples:

  I = iodo or iodino

  CN = cyano or cyanido

  O = oxo or oxido

The IUPAC and common names of many ligands are given in Tables **5.2.1**. and **5.2.2**.

4. When an ambidentate ligand is present the atom through which it is bound to the metal is indicated by giving either its element symbol or a κ and its element symbol in italics after the ligand name

   Example:

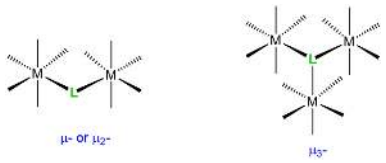
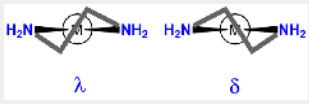
   M-SCN is thiocyanato-*S* or thiocyanato-κ*S*

   M-NCS = thiocyanato-*N or* thiocyanato-κ*N*

   The use of κ and an element symbol to indicate how a ligand and metal are linked is called a **k-term**. More complex k-terms might also involve specifying the atoms by number, though their use is outside the scope of this text.

5. As appropriate, additional information about the way a ligand is bound to the metal center and/or its stereochemistry is specified using a prefix. The prefixes to provide linkage and stereochemistry for ligands are given in Table**5.2.4**.

Table5.2.4. Prefixes used to specify ligands' isomerism when naming and writing coordination compounds' formulae. Some of these types of isomerism will be discussed in later pages.

Type of isomerism	Graphical reminder	Prefixes
when a multidentate ligand binds through less than the full number of atoms		κ^n where n is the number of attached atoms; used when the attached atoms are not directly connected by a chemical bond. The metal-ligand bonding usually involves σ-type coordination.
bridging ligands		μ_n where n is the number of atoms bridged. The number n is usually omitted when n =2.
chelating ligand ring twist		λ- or δ-

A example showing how the nomenclature rule is applied to a ligand that can have two coordination modes is given in Figure **5.2.7**.

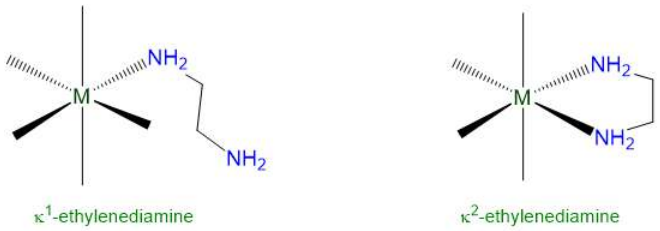


Figure 5.2.7. Use of the κ notation to specify the number of attached groups in a multidentate ligand.

6. If desired, parentheses *may* be used to delineate a ligand name to make it easier to identify in the name. This can be particularly helpful when the name contains a lot of information to keep track of. An example is given in Figure **5.2.8**.

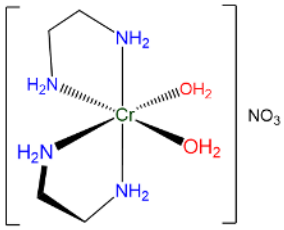


Figure 5.2.8. When naming the complex shown *cis*-diaquabis(ethylenediamine)chromium(III) nitrate is easier to read than *cis*-diaquabisethylenediaminechromium(III) nitrate.

Rule 4: Specify the identity of the metal

- In neutral and cationic complexes the metal's name is used directly

  - *e.g.* as in hexammineruthenium(III) for $[Ru(NH_3)_6]^{3+}$

- In anionic complexes, *-ate* replaces *-ium*, *-en*, or *–ese* or adds to the metal name.

  e.g. as in hexachloromanganate(IV) for $[MnCl_6]^{2-}$

- In anionic complexes of some metals a Latin-derived name is used instead of the element's English name. These names are given in Table **5.2.5**.

  Table 5.2.5. Latin terms for Select Metal Ions. Redrawn from this page describing the nomenclature of coordination complexes.

Transition Metal	Latin
Copper	Cuprate
Gold	Aurate
Iron	Ferrate
Lead	Plumbate
Silver	Argentate
Tin	Stannate

An example of the application of the metal naming rules is given in Figure \sf{\PageIndex{9}}\).

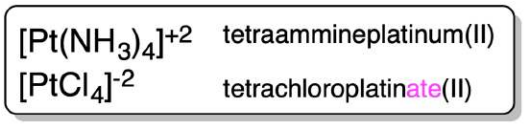


Figure 5.2.9. Example of the application of the metal specification rules to a cationic and anionic platinum complexes.[1]

Rule 5: Specify the valence of the metal.

Two different systems are used to specify the valence of the metal.

1. In the **Stock system** the metal's valence is indicated in Roman numerals after the metal name.

   Examples:

   $[CoCl(NH_3)_5]Cl_2$ = pentamminechlorocobalt(III) chloride

   $[PtBr_2(bpy)]$ = bipyridinedibromoplatinium(II)

   $K[Ag(SCN)_2]$ = potassium di-*S*-thiocyanatoargentate(I)

2. In the **Ewing-Bassett system** the charge on the complex is specified in Arabic numerals after the complex name. This provides a way of specifying a complex even when the valence of the metal isn't known and, in cases where it is known, the value of the metal's valence may be inferred from the complex ion's charge.

   $[CoCl(NH_3)_5]Cl_2$ = pentamminechlorocobalt(2+) chloride

   $[PtBr_2(bpy)]$ = bipyridinedibromoplatinium(0)

   $K[Ag(SCN)_2]$ = potassium di-*S*-thiocyanatoargentate(1-)

Exercise 5.2.2. Assigning metal valence in a complex

In order to name a complex in the Stock system it is necessary to assign a valence to the metal.

For this reason it is important to be able to assign the valence of a metal in a complex. Remember the relationship

valence - number of X-type ligands = total charge on the complex

Assign the valence of the metal in the following real and hypothetical complexes.

a. $K_3[Fe(CN)_6]$
b. $K_2[PtCl_4]$
c. [MnCl(por)]
d. $[Ru(bpy)_3]Cl_2$
e. $[PdCl_2(dppe)]$

Answer for $K_3[Fe(CN)_6]$.

This contains $[Fe(CN)_6]^{3-}$; so valence - 6 (for 6 CN^-) = -3 (the complexes' charge) so valence = +3 or Fe^{3+}.

Answer for $K_2[PtCl_4]$.

This contains $[PtCl_4]^{2-}$; so valence - 4 (for 4 Cl) = -2 (the complexes' charge) so valence = +2 or Pt^{2+}.

Answer for [MnCl(por)].

valence - 2 (for por a which is L_2X_2; see table 9.2.2) - 1 (for Cl) = 0 (the complexes' charge) so valence = +3 or Mn^{3+}.

Answer $[Ru(bpy)_3]Cl_2$.

This contains $[Ru(bpy)_3]^{2+}$; so valence - 0 (for bpy which is L_2) = +2 (the complexes' charge) so valence = +2 or Ru^{2+}.

Answer $[PdCl_2(dppe)]$.

valence - 2 (for 2 Cl) - 0 (for dppe which is L_2) = 0 (the complexes' charge) so valence = +2 or Pd^{2+}.

Exercise 5.2.3: Simple Nomenclature Problems.

Name the following compounds in both the Stock and Ewing-Bassett systems:

a. $[Ru(NH_3)_6](NO_3)_3$
b. $K_2[PtCl_4]$
c. $K[Ag(CN)_2]$
d. $Cs[CuBrCl_2F]$
e. $[Cu(acac)_2]$
f. $K_4[Fe(CN)_6]$
g. *trans*-$[Cu(en)_2(NO_2)_2]$ (the N is bound to Cu)
h. cis-$IrCl_2(CO)(PPh_3)$ (ignore stereochemistry)
i. $IrCl(PPh_3)$

Answer

	Complex	Stock system name	Ewing-Bassett System name
a	$[Ru(NH_3)_6](NO_3)_3$	hexammineruthenium(III) nitrate	hexammineruthenium(3+) nitrate
b	$K_2[PtCl_4]$	potassium tetrachloroplatinate(II)	potassium tetrachloroplatinate(2-)
c	$K[Ag(CN)_2]$	potassium dicyanoargentate(I)	potassium dicyanoargentate(1-)
d	$Cs_2[CuBrCl_2F]$	cesium bromodichloroflourocuprate(II)	cesium bromodichloroflourocuprate(2-)
e	$[Cu(acac)_2]$	bis(acetylacetonato)copper(II)	bis(acetylacetonato)copper(0)
f	$K_4[Fe(CN)_6]$	potassium hexacyanoferrate(II) or potassium hexacyanidoferrrate(II)	potassium hexacyanoferrate(4-) or potassium hexacyanidoferrrate(4-)
g	*trans*-$[Cu(en)_2(NO_2)_2]$ (the N is bound to Cu)	bis(ethylenediamine)bisnitrocopper(II) or bis(ethylenediamine)bis(nitrito-κN)copper(II)	bis(ethylenediamine)bisnitrocopper(0) or bis(ethylenediamine)bis(nitrito-κN)copper(0)
h	*cis*-$IrCl_2(CO)(PPh_3)$	*cis*-dichlorocarbonyltriphenylphosphineiridium(I) or *cis*-dichloro(carbonyl)(triphenylphosphine)iridium(I)	*cis*-dichlorocarbonyltriphenylphosphineiridium(0) or *cis*-dichloro(carbonyl)(triphenylphosphine)iridium(0)
i	$IrCl(PPh_3)$	chlorotris(triphenylphosphine)iridium(I)	chlorotris(triphenylphosphine)iridium(0)

Exercise 5.2.8

Draw structural formulae for the following compounds and ions. You may assume that

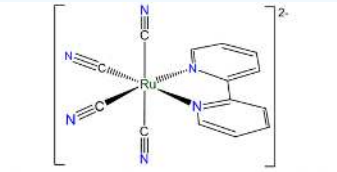
- complexes in which the metal has a coordination number of six are octahedral
- complexes in which the metal has a coordination number of five are trigonal bipyramidal

- complexes in which Pt^{II} , Pd^{II} , or Rh^{I}, or Ir^{I} have a coordination number of four are square planar
- other complexes in which the metal has a coordination number of four will be tetrahedral

a. (2,2'-bipyridine)tetracyanoruthenium(2-)
b. sodium tetrachloroalumnate (note that since Al is a main group metal with a generally fixed oxidation state no oxidation state is given)
c. carbonylhydridotris(triphenylphosphine)rhodium(I) (the ligands in this complex occupy sterically preferred positions)
d. bromotrichlorocobaltate(III)
e. sodium tris(oxalato)cobalt(III)
f. *fac*-(1,10-phenanthroline)tricarbonylchlororhenium(I)
g. *mer*-triaquatrichlorochromium(III)
h. *trans*-dichlorobis(ethylenediamine)platinum(IV)

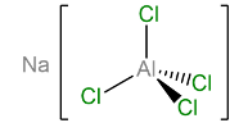
Answers

a



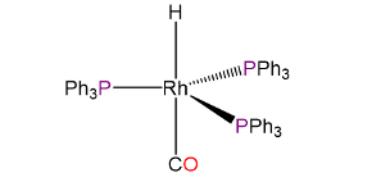
(2,2'-bipyridine)tetracyanoruthenium(2-)

b



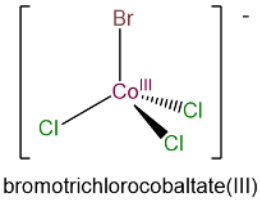
Sodium tetrachloroalumnate

c



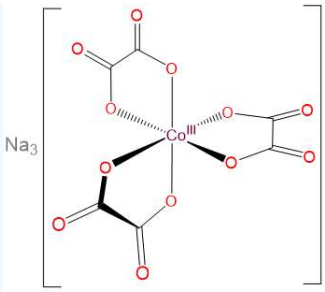
carbonylhydridotris(triphenylphosphine)rhodium(I)

d



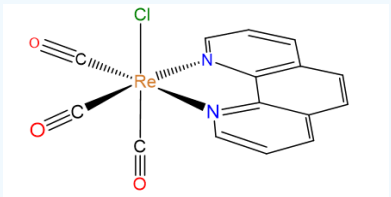
bromotrichlorocobaltate(III)

e



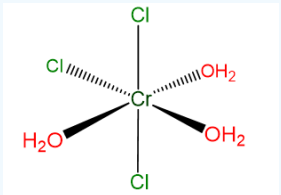
sodium tris(oxalato)cobalt(III)
Λ-enantiomer shown

f



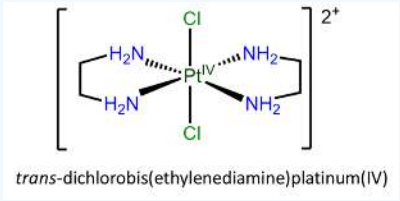
fac-(1,10-phenanthroline)tricarbonylchlororhenium(I)

g



mer-triaquatrichlorochromium(III)

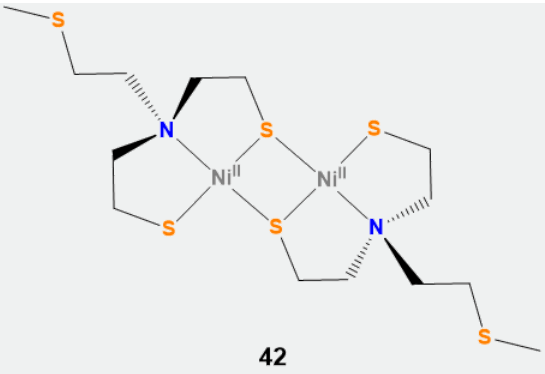
h



trans-dichlorobis(ethylenediamine)platinum(IV)

Note 5.2.1: Sometimes the most helpful name to give a compound is 42.

Even though the IUPAC nomenclature rules permit specification of even the most complex structures, it is often much easier and more effective to supply a numbered structure that can be referred to instead of the IUPAC name. Consider bis{[(μμ-2-mercaptoethyl)(2-mercaptoethyl)-methylthioethylaminato (2-)]Nickel(II)}. Which is easier, to expect readers and hearers to work out the structure from that name or to just refer them to compound **42** in Figure **5.2.10**.



42

Figure 5.2.10. Structure of bis{[(μ-2-mercaptoethyl)(2-mercaptoethyl)-methylthioethylaminato (2-)]Nickel(II)}. The authors of the synthesis of this compound in *Inorganic syntheses*[2] may have had to figure out an IUPAC name for this compound but if you have this scheme in your paper and your instructor is OK with it you can just call it **42**.

References

1. Haas, K. Naming Transition Metal Complexes. https://chem.libretexts.org/Courses/Saint_Mary's_College%2C_Notre_Dame%2C_IN/CHEM_342%3A_Bio-inorganic_Chemistry/Readings/Week_2%3A_Introduction_to_Metal-Ligand_Interactions_and_Biomolecules/2.1_Transition_metal_complexes/2.1.6%3A_Naming_Transition_Metal_Complexes

2. The structure and name is taken from Choudhury, S. B.; Allan, C. B.; Maroney, M.; Wodward, A. D.; Lucas, C. R. *Inorg. Synth.* **1998**, *32*, 98-107.

Contributors and Attributions

Stephen Contakes, Westmont College, to whom comments, corrections, and criticisms should be addressed.

with some examples taken from Naming Transition Metal Complexes by Kathryn Haas.

Consistent with the policy for original artwork made as part of this project, all unlabeled drawings of chemical structures are by Stephen Contakes and licensed under a Creative Commons Attribution 4.0 International License.

5.2: Ligands and Nomenclature is shared under a not declared license and was authored, remixed, and/or curated by LibreTexts.

5.3: Coordination Numbers and Geometry

The total number of points of attachment to the central element is termed the **coordination number** and this can vary from 2 to as many as 16, but is usually 6. In simple terms, the coordination number of a complex is influenced by the relative sizes of the metal ion and the ligands and by electronic factors, such as charge which is dependent on the electronic configuration of the metal ion.

Introduction

Based on the radius ratio, it can be seen that the bigger the charge on the central ion, the more attraction there will be for negatively charged ligands, however at the same time, the bigger the charge the smaller the ion becomes which then limits the number of groups able to coordinate. It is important to recognize that every geometry has a specific coordination number, but every complex wish a specific coordination number will have a choice of several possible geometries (i.e., there is not a one-to-one correspondance between coordination number and geometry).

Coordination Number 2

This arrangement is not very common for first row transition metal ion complexes and some of the best known examples are for Silver(I). In this case we have a low charge and an ion at the right hand side of the d-block indicating smaller size

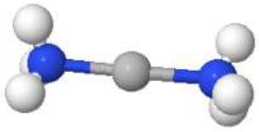


Figure 1: The linear $[Ag(NH_3)_2]^+$ ion

Coordination Number 3

Once again, this is not very common for first row transition metal ions. Examples with three different geometries have been identified:

- **Trigonal planar Geometry**: Well known for main group species like CO_3^{2-} etc., this geometry has the four atoms in a plane with the bond angles between the ligands at 120 degrees.

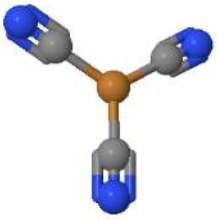


Figure 2: The Trigonal planar $[Cu(CN)_3]^{2-}$ system

- **Trigonal pyramid Geometry**: More common with main group ions.
- **T-shaped**: The first example of a rare T-shaped molecule was found in 1977.

Coordination Number 4

Two different geometries are possible. The tetrahedron is the more common while the square planar is found almost exclusively with metal ions having a d^8 electronic configuration.

- **Tetrahedral Geometry**:

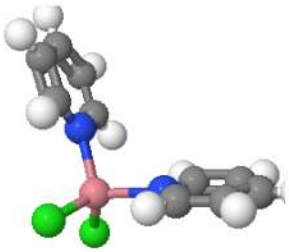


Figure 3: $[CoCl_2pyr_2]$

- **Square Planar Geometry:** This is fairly common with Rh(I), Ir(I), Pd(II) and Pt(II) compounds.

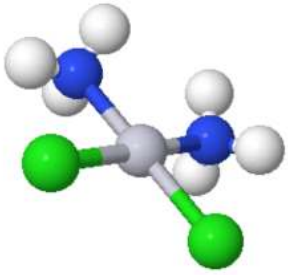


Figure 4: cisplatin - cis-$[PtCl_2(NH_3)_2]$

Coordination Number 5

- **Square pyramid Geometry:** Oxovanadium salts (Vanadyl, VO^{2+}) often show square pyramidal geometry, for example, $[VO(acac)_2]$. Note that the Vanadium(IV) can be considered coordinatively unsaturated and addition of pyridine leads to the formation of an octahedral complex.
- **Trigonal Bipyramid Geometry:** The structure of $[Cr(en)_3][Ni(CN)_5] \cdot 1.5\ H_2O$ was reported in 1968 to be a remarkable example of a complex exhibiting both types of geometry in the same crystal. The reaction of cyanide ion with Ni^{2+} proceeds via several steps:

$$Ni^{2+} + 2CN^- \rightarrow Ni(CN)_2 \tag{5.3.1}$$

$$Ni(CN)_2 + 2CN^- \rightarrow \underset{\text{orange-red}}{[Ni(CN)_4]^{2-}} \tag{5.3.2}$$

$$[Ni(CN)_4]^{2-} + CN^- \rightarrow \underset{\text{deep red}}{[Ni(CN)_5]^{3-}} \tag{5.3.3}$$

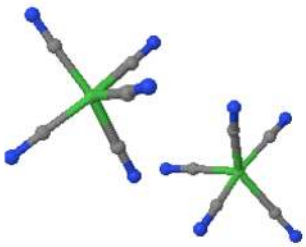


Figure 5: $[Ni(CN)_5]^{3-}$

Coordination Number 6

- **Hexagonal planar Geometry**: Unknown for first row transition metal ions, although the arrangement of six groups in a plane is found in some higher coordination number geometries.
- **Trigonal prism Geometry**: Most trigonal prismatic compounds have three bidentate ligands such as dithiolates or oxalates and few are known for first row transition metal ions.

- **Octahedral (Oh):** The most common geometry found for first row transition metal ions, including all aqua ions. In some cases distortions are observed and these can sometimes be explained in terms of the Jahn-Teller Theorem which we will discuss later.

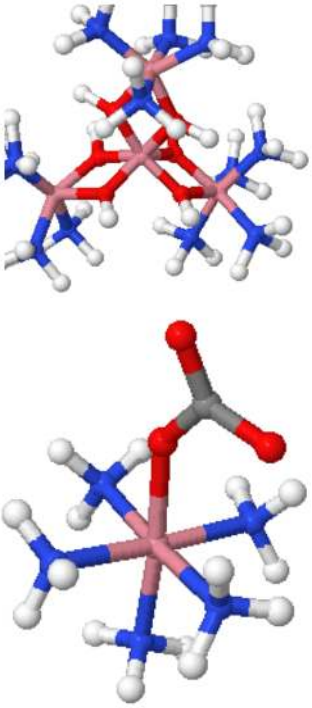


Figure 6: $[Co(en)_3]Cl_3$(left) and $[CoCO_3(NH_3)_5]^+$ (right)

Coordination Number 7

Not very common for 1st row complexes and the energy difference between the structures seems small and distortions occur so that prediction of the closest "idealized" shape is generally difficult. Three geometries are possible:

- **Capped octahedron (C_{3v}) Geometry**

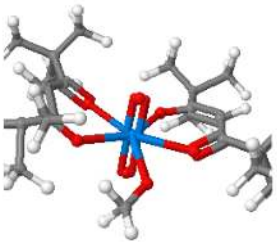


Figure 7: $K_3[NbOF_6]$

- **Capped trigonal prism (C_{2v})**
- **Pentagonal Bipyramid (D_{5h})**

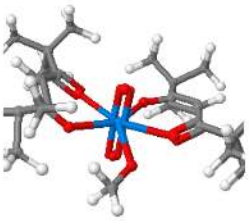


Figure 8: bis-[(tert-butylacac)$_2$(DMSO)di-oxoUranium]

Coordination Number 8

- **Dodecahedron (D_{2d}) Geometry**
- **Cube (O_h) Geometry**
- **Square antiprism (D_{4d}) Geometry**
- **Hexagonal bipyramid (D_{6h}) Geometry**

Coordination Number 9

- **Three-face centered trigonal prism (D_{3h}) Geometry**

Coordination Number 10

- **Bicapped square antiprism (D_{4d}) Geometry**

Coordination Number 11

- **All-faced capped trigonal prism (D_{3h}) Geometry: This is not a common stereochemistry.**

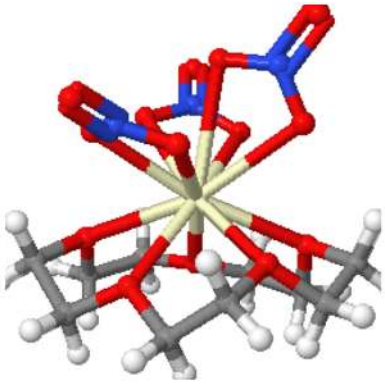


***Figure 9**: aqua-(12-crown-4)-tris(nitrato-O,O')-cerium(III) (12-crown-4) solvate and (15-crown-5)-tris(nitrato-O,O')-cerium(III) the Cerium ion is 11 coordinate.*

Coordination Number 12

- **cuboctahedron (O_h) Geometry**

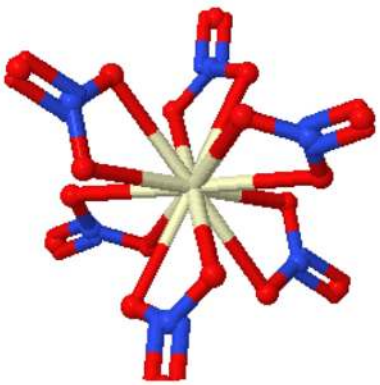


Figure 10: Ceric ammonium nitrate -$(NH_4)_2Ce(NO_3)_6$

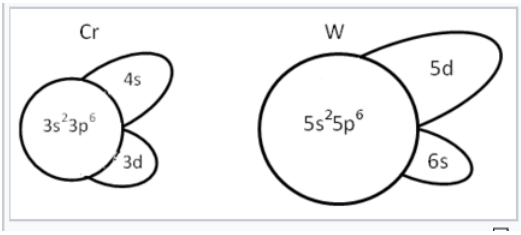
Contributors and Attributions

- Prof. Robert J. Lancashire (The Department of Chemistry, University of the West Indies)

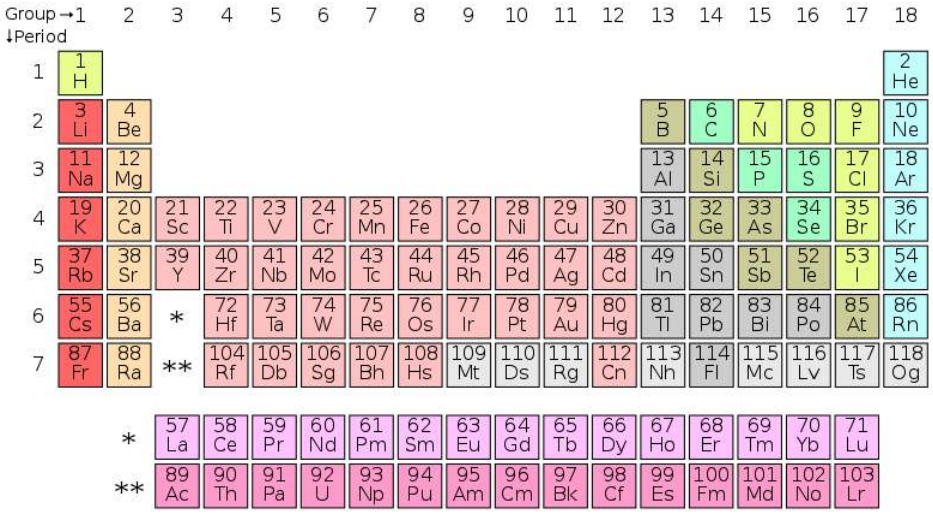
5.3: Coordination Numbers and Geometry is shared under a not declared license and was authored, remixed, and/or curated by LibreTexts.

5.4: Bonding with d-orbitals

While electrons in s and p orbitals tend to form strong bonds, d-electron bonds can be strong or weak. There are two important periodic trends that are related to orbital size and orbital overlap. As we move *across the periodic table* (Sc - Ti - V - Cr - Fe), the *d orbitals contract* because of increasing nuclear charge. Moving *down the periodic table* (V - Nb - Ta), the *d orbitals expand* because of the increase in principal quantum number. These trends explain the distinct behavior of the 3d elements relative to those in the 4d and 5d series. In the 3d series, the contraction of orbitals affects the ability of the d electrons to contribute to bonding. Past V in the first row of the transition metals, the 3d electrons become much less effective in bonding because they overlap weakly with their neighbors. Weak overlap of 3d orbitals gives narrow d-bands and results in the emergence of magnetic properties as discussed below.

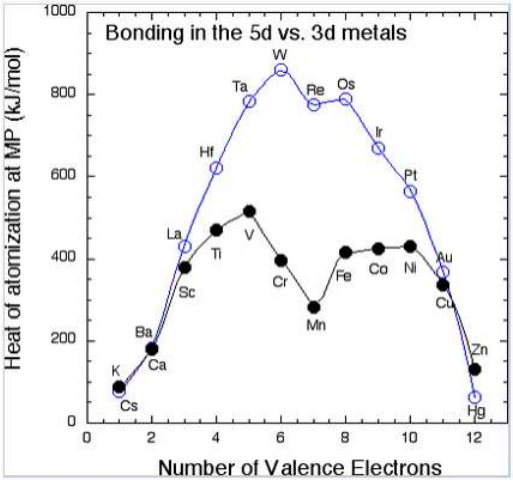


Schematic representation of the sizes of different orbitals of Cr and W. In the first transition series, shielding of the 3d orbitals is poor. Therefore the 4s and 4p orbitals are more effective in bonding than the 3d. In the third transition series, the situation is reversed. The increased nuclear charge is felt most strongly by the 6s, which takes on the character of an inert electron pair. The 5d orbitals are well shielded by the complete n=4 shell so they have good orbital overlap with neighboring atoms.



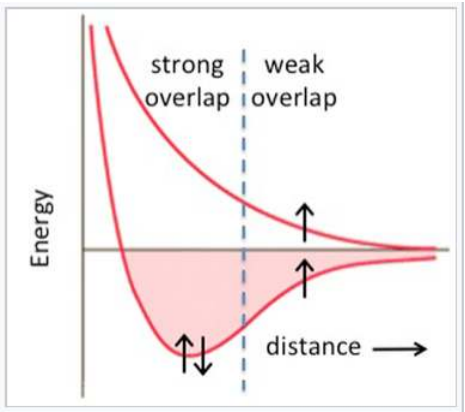
In the **4d and 5d series**, a plot of cohesive energy vs. number of valence electrons (below left) has a "volcano" shape that is peaked at the elements Mo and W ($5s^1 4d^5$ and $6s^1 5d^5$, respectively). The number of bonding electrons, and therefore the bonding energy, increases steadily going from Rb to Mo in the 4d series, and from Cs to W in the 5d series. Mo and W have the most bonding energy because they can use all six of their valence electrons in bonding without promotion. Elements past Mo and W have more d electrons, but some of them are spin paired and so some promotion energy is needed to prepare these electrons for bonding. For example, Pt metal must be promoted from the $6s^1 5d^9$ atomic ground state to $6s^1 5d^7 6p^2$ in order to make six bonds per atom, and the energy cost of promoting electrons from the 5d to the 6p orbitals is reflected in the net bonding energy. Because of their strong

bonding energy, elements in the middle of the 4d and 5d series have very high melting points. We do not see magnetism in the 4d or 5d metals or their alloys because orbital overlap is strong and the bonding energy exceeds the electron pairing energy.



The heat of vaporization (the cohesive energy) of metals in the 3d and 5d series, measured at the melting point of the metal.

The **3d elements** (Sc through Zn) are distinctly different from the 4d and 5d elements in their bonding (and consequently in their magnetic properties). In the 3d series, we see the expected increase in cohesive energy going from Ca ($4s^2$) to Sc ($4s^23d^1$) to Ti ($4s^23d^2$) to V ($4s^23d^3$), but then something very odd happens. The 3d series has a "crater" in the cohesive energy plot where there was a peak in the 5d series. The cohesive energy actually *decreases* going from V to Mn, even though the number of valence electrons is increasing. We can explain this effect by remembering that the 3d orbitals are progressively contracting as more protons are added to the nucleus. For elements beyond V, the orbital overlap is so poor that the 3d electrons are no longer effective in bonding, and the valence electrons begin to unpair. At this point the elements become **magnetic**. Depending on the way the spins order, metals and alloys in this part of the periodic table can be ferromagnetic (spins on neighboring atoms aligned parallel, as in the case of Fe or Ni) or antiferromagnetic (spins on neighboring atoms antiparallel, as in the case of Mn). We have seen the trade-off between orbital overlap and magnetism before (in Chapter 5) in the context of paramagnetic transition metal complexes. It is worth recalling that this behavior is predicted in the energy vs. distance diagram of the hydrogen atom (from Chapter 2). At short interatomic distances (or with strong overlap between atomic orbitals), the spins of the electrons pair and a bond is formed. Unpairing the electrons becomes favorable at larger interatomic distances where the overlap between orbitals is poor.



With strong overlap between orbitals of neighboring atoms, the bonding energy exceeds the pairing energy and electrons spin-pair. With weaker overlap, bonding is weak and spins unpair, resulting in magnetic behavior.

Interestingly, many alloys of the **4f elements** (the lanthanides) are also magnetic because the 4f orbitals, like the 3d orbitals, are poorly shielded from the nuclear charge and are ineffective in bonding. Strong permanent magnets often contain alloys of Nd, Sm, or Y, usually with magnetic 3d elements such as Fe and Co.

Because the 4f orbitals are contracted and not very effective in bonding, other physical properties of the lanthanides can also be affected. For example, it has been proposed that oxides of the 4f elements have weak surface interactions with polar molecules such as water because of f-orbital contraction. Experimentally, CeO_2, Er_2O_3, and Ho_2O_3 are observed to be hydrophobic, whereas main group and early transition metal oxides (e.g., Al_2O_3, SiO_2, TiO_2) are quite hydrophilic.[1]

5.4: Bonding with d-orbitals is shared under a CC BY-SA license and was authored, remixed, and/or curated by LibreTexts.

- **6.7: Atomic Orbitals and Magnetism** by Chemistry 310 is licensed CC BY-SA 4.0. Original source: https://en.wikibooks.org/wiki/Introduction_to_Inorganic_Chemistry.

SECTION OVERVIEW

5.5: Isomers

There are several types of this isomerism frequently encountered in coordination chemistry and the following represents some of them. Isomers that contain the same number of atoms of each kind but differ in which atoms are bonded to one another are called structural isomers, which differ in structure or bond type. For inorganic complexes, there are three types of structural isomers: *ionization*, *coordination*, and *linkage* and two types of stereoisomers: *geometric and optical*.

Structural isomers, as their name implies, differ in their structure or bonding, which are separate from **stereoisomers** that differ in the spatial arrangement of the ligands are attached, but still have the bonding properties. The different chemical formulas in structural isomers are caused either by a difference in what ligands are bonded to the central atoms or how the individual ligands are bonded to the central atoms. When determining a structural isomer, you look at: (1) the ligands that are bonded to the central metal, and (2) which atom of the ligands attach to the central metal. Below is a quick look at the different types of structural isomers. The highlighted ions are the ions that switch or change somehow to make the type of structural isomer it is.

5.5.1: Structural Isomers - Ionization Isomerism in Transition Metal Complexes

5.5.2: Structural Isomers - Geometric Isomerism in Transition Metal Complexes

5.5.3: Stereoisomers - Optical Isomerism in Transition Metal Complexes

5.5.4: Structural Isomers - Linkage Isomerism in Transition Metal Complexes

---

5.5: Isomers is shared under a not declared license and was authored, remixed, and/or curated by LibreTexts.

5.5.1: Structural Isomers - Ionization Isomerism in Transition Metal Complexes

Coordination isomerism is a form of structural isomerism in which the composition of the complex ion varies. In a coordination isomer the total ratio of ligand to metal remains the same, but the ligands attached to a specific metal ion change. Ionization isomers can be thought of as occurring because of the formation of different ions in solution.

Introduction

Ionization isomers are identical except for a ligand has exchanged places with an anion or neutral molecule that was originally outside the coordination complex. The central ion and the other ligands are identical. For example, an octahedral isomer will have five ligands that are identical, but the sixth will differ. The non-matching ligand in one compound will be outside of the coordination sphere of the other compound. Because the anion or molecule outside the coordination sphere is different, the chemical properties of these isomers is different.

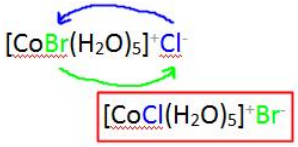


Figure **5.5.1.1**: Two Ionization isomers. The two isomers differ only which ligands are actually bound to the center metal. These two isomers are called pentaaqua**bromo**cobaltate(II) **chloride** and pentaaqua**chloro**cobaltate(II) **bromide**.

The difference between the ionization isomers can be view within the context of the ions generated when each are dissolved in solution.

For example, when pentaaquabromocobaltate(II)chloride is dissolved in water, Cl^- ions are generated:

$$CoBr(H_2O)_5Cl(s) \rightarrow CoBr(H_2O)_5^+(aq) + Cl^+(aq) \tag{5.5.1.1}$$

whereas when pentaaquachlorocobaltate(II)bromide is dissolved, Br^- ions are generated:

$$CoCl(H_2O)_5Br(s) \rightarrow CoCl(H_2O)_5^+(aq) + Br^+(aq). \tag{5.5.1.2}$$

Note

If one dissolved $[PtBr(NH_3)_3]NO_2$ and $[Pt(NO_2)(NH_3)_3]Br$ into solution, then two different set of ions will be general.

- Dissolving $[Pt(NO_2)(NH_3)_3]Br$ in aqueous solution would have the following reaction

$$[PtBr(NH_3)_3]NO_2(s) \rightarrow [PtBr(NH_3)_3]^+(aq) + NO_2^-(aq) \tag{5.5.1.3}$$

- Dissolving of $[Pt(NO_2)(NH_3)_3]Br$ in aqueous solution would be

$$[Pt(NO_2)(NH_3)_3]Br(s) \rightarrow [Pt(NO_2)(NH_3)_3]^+(aq) + Br^-(aq) \tag{5.5.1.4}$$

Notice that these two ionization isomers differ in that one ion is directly attached to the central metal, but the other is not.

Equations 5.5.1.3 and 5.5.1.4 are valid under the assumption that the platinum-ligand bonds of the complexes are do not break and allow other ligands (e.g., water) to bind.

Example 5.5.1.1

Are $[Cr(NH_3)_5(OSO_3)]Br$ and $[Cr(NH_3)_5Br]SO_4$ coordination isomers?

Solution

First, we need confirm that each compound has the same number of atoms of the respective elements (this requires viewing both cations and anions of each compound).

Element	number of atoms in $[Cr(NH_3)_5(OSO_3)]Br$	number of atoms in $[Cr(NH_3)_5Br]SO_4$
Cr	1	1
N	5	5
H	15	15
O	4	4
S	1	1
Br	1	1

Now, let's look at what these two compounds look like (Figure **5.5.1.2**). The sulfate group is a ligand with a dative bond to the chromium atom and the bromine atom is a counter ion (\ce{[Cr(NH3)5(OSO3)]Br}\). For $[Cr(NH_3)_5Br]SO_4$, this is the the reverse.

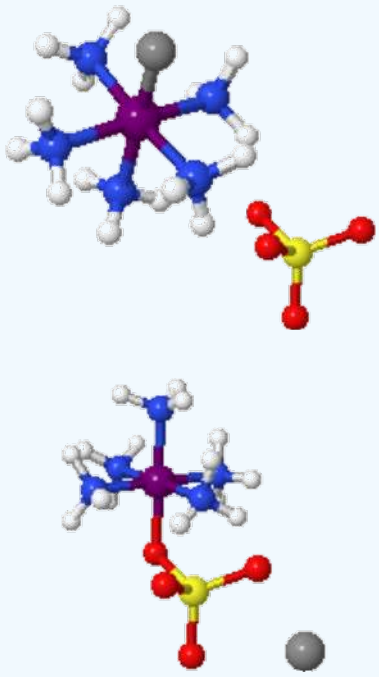


Figure **5.5.1.2**: $[Cr(NH_3)_5(OSO_3)]Br$ (left) and $[Cr(NH_3)_5Br]SO_4$ (right) are coordination isomers.

Yes, $[Cr(NH_3)_5(OSO_3)]Br$ and $[Cr(NH_3)_5Br]SO_4$ are coordination isomers.

Exercise 5.5.1.1

Are $[Co(NH_3)_5(SO_4)]Br$ and $[Co(NH_3)_5Br]SO_4$ ionization isomers?

Answer

In the first isomer, SO_4 is attached to the Cobalt and is part of the complex ion (the cation), with Br as the anion. In the second isomer, Br is attached to the cobalt as part of the complex and SO_4 is acting as the anion.

A hydrate isomer is a specific kind of ionization isomer where a water molecule is one of the molecules that exchanges places.

Solvate or Hydrate Isomerization: A Special kind of Ionization Isomer

A very similar type of isomerism results from replacement of a coordinated group by a solvent molecule (*Solvate Isomerism*). In the case of water, this is called *Hydrate Isomerism*. The best known example of this occurs for chromium chloride "$CrCl_3.6H_2O$" which may contain 4, 5, or 6 coordinated water molecules.

- $[CrCl_2(H_2O)_4]Cl \cdot 2H_2O$: bright-green colored
- $[CrCl(H_2O)_5]Cl_2 \cdot H_2O$: grey-green colored
- $[Cr(H_2O)_6]Cl_3$: violet colored

These isomers have very different chemical properties and on reaction with $AgNO_3$ to test for Cl^- ions, would find 1, 2, and 3 Cl^- ions in solution respectively.

Contributors and Attributions

- Prof. Robert J. Lancashire (The Department of Chemistry, University of the West Indies)

5.5.1: Structural Isomers - Ionization Isomerism in Transition Metal Complexes is shared under a not declared license and was authored, remixed, and/or curated by LibreTexts.

5.5.2: Structural Isomers - Geometric Isomerism in Transition Metal Complexes

Geometric Isomers are isomers that differ in the arrangement of the ligands around the metal or the central atom. In other words, these isomers differ from each other based on where the ligands are placed in the coordinate compound. This will be much easier to understand as examples will be considered. There are 2 main types of geometric isomers:

- Cis-Trans Isomers (referencing the spatial arrangement of two species)
- Mer-Fac Isomers (referencing the spatial arrangement of three species)

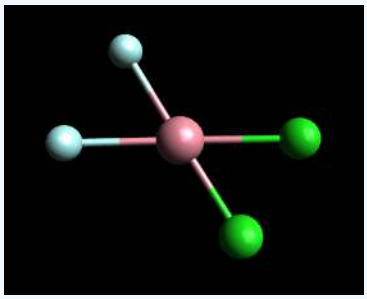
Cis-Trans Isomers

Cis-Trans Isomers are isomers that differ in the arrangement of two ligands in square planar and octahedral geometry. Cis isomers are isomers where the two ligands are 90 degrees apart from one another in relation to the central molecule. This is because Cis isomers have a bond angle of 90^o, between two same atoms. Trans isomers, on the other hand, are isomers where the two ligands are on opposite sides in a molecule because trans isomers have a bond angle of 180^o, between the two same atoms. When naming cis or trans isomers, the name begins either with cis or trans, whichever applies, followed by a hyphen and then the name of a molecule. For example a cis isomer of $CoCl_2F_2$ would be called cis-$CoCl_2F_2$. Finally, the last thing to keep in mind when examining cis and trans isomers is that **only square planar and octahedral** geometries can have cis or trans isomers. Examples of both isomers are provided below.

Example 5.5.2.1: cis Isomer

$CoCl_2F_2$:

(Color scheme: pink=cobalt, blue=fluorine, green=chlorine)



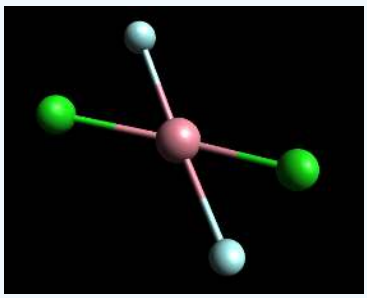
This above is an example of the molecule cis-$CoCl_2F_2$ or cis-dichlorodifluorocobalt (IV). The molecule pictured above is a cis isomer because both fluorine and chlorine ligands, respectively, are on the same side of the molecule. Additionally, one can approximate that the bond angle between each of the chlorine atoms and between each of the fluorine atoms is 90^o.

Isomer

$CoCl_2F_2$:

(Color scheme: pink=cobalt, blue=fluorine, green=chlorine)

(Note, the differences in the length of the bond between the two pictures are not intentional and have nothing to do with cis-trans isomerism)

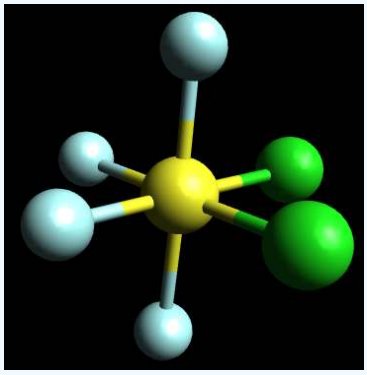


This above is an example of the molecule trans-$CoCl_2F_2$ or trans-dichlorodifluorocobalt (IV).

We know the above molecule is a trans isomer because the two same chlorine atoms and the two same fluorine atoms are opposite each other. Furthermore, the bond angle between the two chlorine atoms and between the two fluorine atoms is 180^o. The above examples were all for square planar geometry but as the examples below illustrate, cis-trans isomerism can also occur in octahedral geometry. Both the molecules below are isomers of the molecule SCl_2F_4 (color scheme: yellow=sulfur, blue=fluorine, green=chlorine).

Example 5.5.2.3: Octahedral cis Isomer

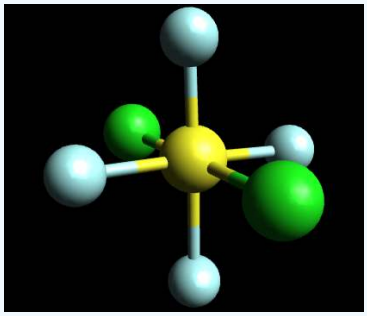
SCl_2F_4:



We know this isomer above is a cis isomer because both the chlorine ligands are on the same side and the bond angle between the chlorine atoms appears to be 90^o.

Example 5.5.2.4: Octahedral trans Isomer

SCl_2F_4:



The isomer above is a trans isomer because the chlorine ligands are on opposite sides and the bond angle between the chlorine atoms is 180^o. All other isomers are essentially just rotations of these two isomers. Once again when trying to find cis and trans isomers look at the arrangement of the ligands. If two same ligands are on the same side, it is a cis isomer and if the ligands are on opposite sides, it is a trans isomer. Another way to tell the isomers apart is the bond angles: cis isomers have a 90^o bond angle whereas trans isomers have a 180^o bond angle.

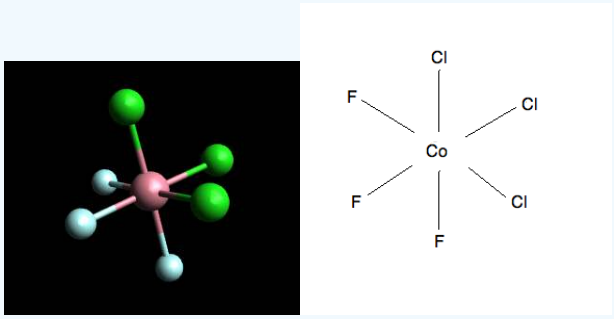
Mer-Fac Isomers

Mer-Fac isomers are easier to notice than cis-trans isomers in the sense that they only exist in octahedral geometry. Just like cis-trans isomers, mer-fac isomers are determined based on whether or not the ligands exist on the same side. Instead of dealing with 2 ligands, mer-fac isomers deal with 3 ligands. If the 3 ligands are all on the same side, the isomer is called a fac-isomer. Another way to identify fac isomers is to look at the bond angle between the ligands because fac isomers have a 90^o bond angle between each of the 3 atoms. The mer isomer on the other hand is where only 2 of the 3 ligands are on the same side. In mer isomers, there exists a 90^o-90^o-180^o bond angle between the 3 same ligands. In terms of nomenclature, mer-fac isomers follow the same rule as

cis-trans isomers where you put the isomer type, followed by a hyphen, followed by the molecular formula. Examples have been provided below.

Example 5.5.2.5: fac Isomer

Below is an example of the fac isomer, fac-$CoCl_3F_3$:

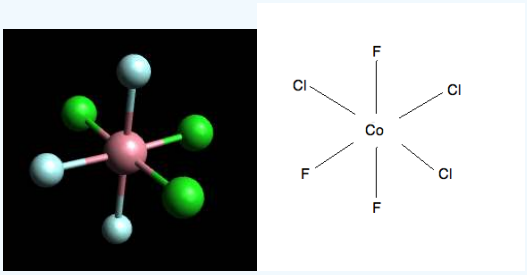


(note the color scheme: pink=cobalt, green=chlorine, blue=fluorine)

Through the 2d version, it is easier to see how the ligands are all on the same side. Nonetheless, in the 3D version, one can observe that the bond angle between the 3 same ligands is 90^o, thus making this isomer a fac-isomer.

Example 5.5.2.6: mer Isomer

Below is an example of the mer isomer, mer-$CoCl_3F_3$:



(note the color scheme: pink=cobalt, green=chlorine, blue=fluorine)

Its hard to tell in the 3D version but in the 2D version, one can easily tell how the same ligands are not on the same side. Additionally, one can approximate that the bond angle between the three chlorine atoms and between the three fluorine atoms is 90^o-90^o-180^o, thus making the above molecule a mer isomer.

Contributors and Attributions

Prof. Robert J. Lancashire (The Department of Chemistry, University of the West Indies)

5.5.2: Structural Isomers - Geometric Isomerism in Transition Metal Complexes is shared under a not declared license and was authored, remixed, and/or curated by LibreTexts.

5.5.3: Stereoisomers - Optical Isomerism in Transition Metal Complexes

Optical activity refers to whether or not a compound has optical isomers. A coordinate compound that is optically active **has** optical isomers and a coordinate compound that is not optically active does **not have** optical isomers. As we will discuss later, optical isomers have the unique property of rotating light. When light is shot through a polarimeter, optical isomers can rotate the light so it comes out in a different direction on the other end. Armed with the knowledge of symmetry and mirror images, optical isomers should not be very difficult. There are two ways optical isomers can be determined: using mirror images or using planes of symmetry.

Optical isomers do not exhibit symmetry and do not have identical mirror images. Let's go through a quick review of symmetry and mirror images. A *mirror image* of an object is that object flipped or the way the object would look in front of a mirror. For example, the mirror image of your left hand would be your right hand. Symmetry on the other hand refers to when an object looks exactly the same when sliced in a certain direction with a plane. For example imagine the shape of a square. No matter in what direction it is sliced, the two resulting images will be the same.

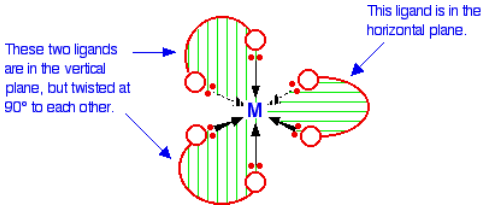
Method 1: The "Mirror Image Method"

The mirror images method uses a mirror image of the molecule to determined whether optical isomers exist or not. If the mirror image **can** be rotated in such a way that it looks identical to the original molecule, then the molecule is said to be superimposable and has no optical isomers. On the other hand, if the mirror image **cannot** be rotated in any way such that it looks identical to the original molecule, then the molecule is said to be non-superimposable and the molecule has optical isomers. Once again, if the mirror image is superimposable, then no optical isomers but if the mirror image is non-superimposable, then optical isomers exist.

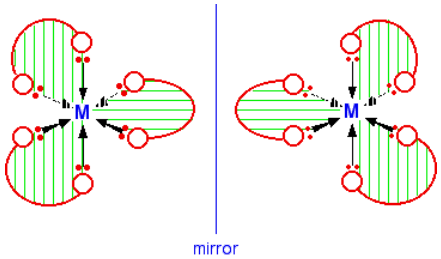
Definition: Non-superimposable

Non-superimposable means the structure cannot be rotated in a way that one can be put on top of another. This means that no matter how the structure is rotated, it cannot be put on top of another with all points matching. An example of this is your hands. Both left and right hands are identical, but they cannot be put on top of each other with all points matching.

The examples you are most likely to need occur in octahedral complexes which contain bidentate ligands - ions like $[Ni(NH_2CH_2CH_2NH_2)_3]^{2+}$ or $[Cr(C_2O_4)_3]^{3-}$. The diagram below shows a simplified view of one of these ions. Essentially, they all have the same shape - all that differs is the nature of the "headphones".



A substance with *no plane of symmetry is going to have optical isomers* - one of which is the mirror image of the other. One of the isomers will rotate the plane of polarization of plane polarised light clockwise; the other rotates it counter-clockwise. In this case, the two isomers are:



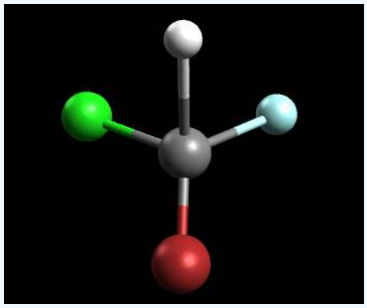
You may be able to see that there is no way of rotating the second isomer in space so that it looks exactly the same as the first one. As long as you draw the isomers carefully, with the second one a true reflection of the first, the two structures will be different.

Method 2: The "Plane of Symmetry Method"

The plane of symmetry method uses symmetry, as it's name indicates, to identify optical isomers. In this method, one tries to see if such a plane exists which when cut through the coordinate compound produces two exact images. In other words, one looks for the existence of a plane of symmetry within the coordinate compound. If a plane of symmetry exists, then no optical isomers exist. On the other hand, if there is no plane of symmetry, the coordinate compound has optical isomers. Furthermore, if a plane of symmetry exists around the central atom, then that molecule is called **achiral** but if a plane of symmetry does not exist around the central molecule, then that molecule has chiral center.

Example 5.5.3.1: CHBrClF

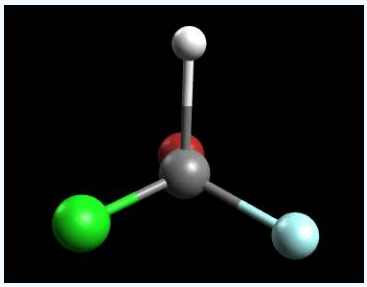
Consider the tetrahedral molecule, CHBrClF (note the color scheme: grey=carbon, white=hydrogen, green=chlorine, blue=fluorine, red=bromine)



Is this molecule optically active? In other words, does this molecule have optical isomers?

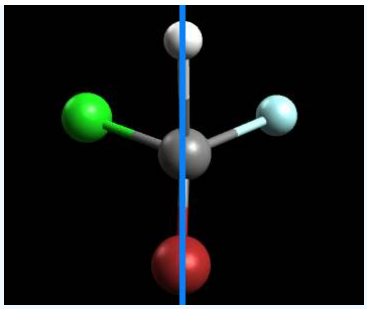
Solution

First take the Mirror-image method. The mirror image of the molecule is:



Note that this mirror image is not superimposable. In other words, the mirror image above cannot be rotated in any such way that it looks identical to the original molecule. Remember, if the mirror image is not superimposable, then optical isomers exist. Thus we know that this molecule has optical isomers.

Let's try approaching this problem using the symmetry method. If we take the original molecule and draw an axis or plane of symmetry down the middle, this is what we get:



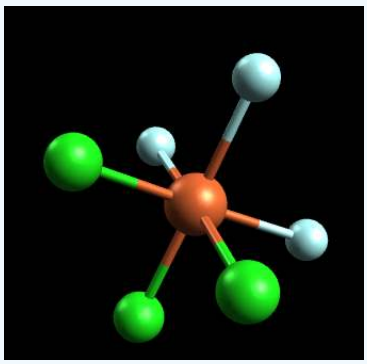
Since the left side is not identical to the right, this molecule does not have a symmetrical center and thus can be called chiral.Additionally, because it does not have a symmetrical center, we can conclude that this molecule has optical isomers. In general, when dealing with a tetrahedral molecule that has 4 different ligands, optical isomers will exist most of the time.

No matter which method you use, the answer will end up being the same.

Optical isomers because they have no plane of symmetry. In the organic case, for tetrahedral complexes, this is fairly easy to recognize the possibility of this by looking for a center atom with **four** different things attached to it. Unfortunately, this is not quite so easy with more complicated geometries!

Example 5.5.3.1: fac−$FeCl_3F_3$

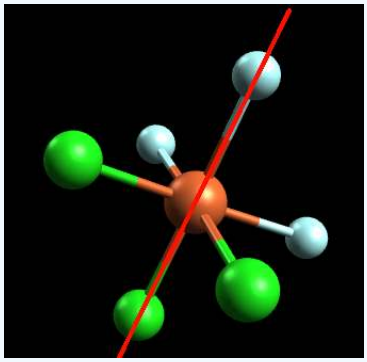
This time we will be analyzing the octahedral compound fac-$FeCl_3F_3$. Is this molecule optically active?



(note the color scheme: orange=iron, blue=fluorine, green=chlorine):

Solution

If we try to attempt this problem using the mirror image method, we notice that the mirror image is essentially identical to the original molecule. In other words, the mirror image can be placed on top of the original molecule and is thus superimposable. Since the mirror image is superimposable, this molecule does not have any optical isomers. Let's attempt this same problem using the symmetry method. If we draw an axis or plane of symmetry, this is what we get:



Since the left side is identical to the right side, this molecule has a symmetrical center and is an achiral molecule. Thus, it has no optical isomers.

What is a Polarimeter?

A polarimeter is a scientific instrument used to measure the angle of rotation caused by passing polarized light through an optically active substance. Some chemical substances are optically active, and polarized (uni-directional) light will rotate either to the left (counter-clockwise) or right (clockwise) when passed through these substances. The amount by which the light is rotated is known as the *angle of rotation*. The angle of rotation is basically known as observed angle.

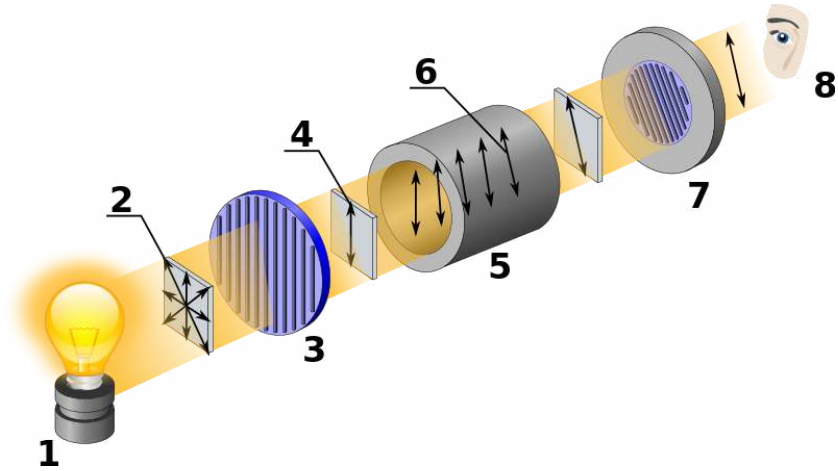


Figure **5.5.3.1**: Schematic of a polarimeter showing the principles behind it's operation. Unpolarized light is passed through a polarizing filter before traveling through a sample. The degree of rotation of polarization is determined by a second, rotatable filter. (CC AS 3.0; Kaidor).

The polarimeter is made up of a polarizer (#3 on Figure **5.5.3.1**) and an analyzer (#7 on Figure **5.5.3.1**). The polarizer allows only those light waves which move in a single plane. This causes the light to become plane polarized. When the analyzer is also placed in a similar position it allows the light waves coming from the polarizer to pass through it. When it is rotated through the right angle no waves can pass through the right angle and the field appears to be dark. If now a glass tube containing an optically active solution is placed between the polarizer and analyzer the light now rotates through the plane of polarization through a certain angle, the analyzer will have to be rotated in same angle.

Nomenclature of Optical Isomers

Various methods have been used to denote the absolute configuration of optical isomers such as R or S, Λ or Δ, or C and A. The IUPAC rules suggest that for general octahedral complexes C/A scheme is convenient to use and that for bis and tris bidentate complexes the absolute configuration be designated Λ (left-handed) and Δ (right-handed).

Priorities are assigned for mononuclear coordination systems based on the standard sequence rules developed for enantiomeric carbon compounds by Cahn, Ingold and Prelog (CIP rules). These rules use the coordinating atom to arrange the ligands into a priority order such that the highest atomic number gives the highest priority number (smallest CIP number). For example the hypothetical complex [Co Cl Br I NH_3 NO_2 SCN]$^{2-}$ would assign the I- as 1, Br as 2, Cl as 3, SCN as 4, NO_2 as 5 and NH_3 as 6.

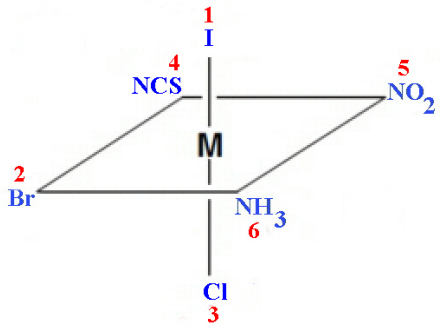


Figure* 5.5.3.2*: *Here is one isomer where the I and Cl, and Br and NO_2 were found to be trans- to each other.*

The reference axis for an octahedral center is that axis containing the ligating atom of CIP priority 1 and the trans ligating atom of lowest possible priority (highest numerical value). The atoms in the coordination plane perpendicular to the reference axis are viewed from the ligand having that highest priority (CIP priority 1) and the clockwise and anticlockwise sequences of priority numbers are compared. The structure is assigned the symbol C or A, according to whether the clockwise (C) or anticlockwise (A) sequence is lower at the first point of difference. In the example shown below this would be C (Figure **5.5.3.3**).

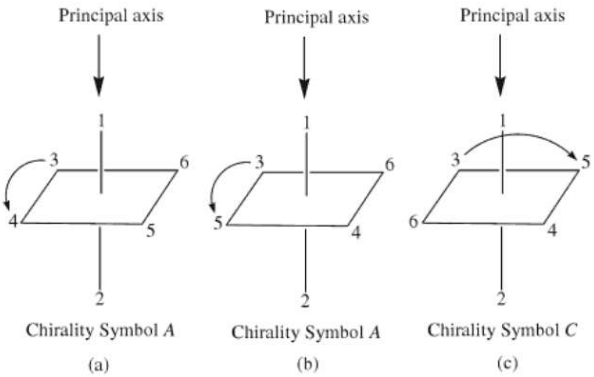


***Figure* 5.5.3.3.** Reference axes for assigning group priority.

Isomers with bidentate ligands

Bidentate ligands bind very tightly to a metal because they form two bonds with it, rather than just one. We will investigate this further in a later section. The spatial relationship between the metal and the two atoms connected to it from the same ligand forms a plane. If more than one bidentate ligand is connected to the metal, the relative orientation of one plane to another creates the possibility of mirror images. A complex containing three bidentate ligands can take on the shape of a left-handed propeller or a right-handed propeller.

These shapes are alternatively described as a left-handed screw and a right handed screw. If you can picture turning the shape so that it screws into the page behind it, which direction would you turn the screwdriver? If you would twist the screwdriver clockwise, then you have a right handed screw. If you would twist the screwdriver counter-clockwise, then you have a left handed screw. The two optical isomers of $[Co(en)_3]^{3+}$ have identical chemical properties and just denoting their absolute configuration does NOT give any information regarding the direction in which they rotate plane-polarised light. This can ONLY be determined from measurement and then the isomers are further distinguished by using the prefixes (-) and (+) depending on whether they rotate left or right.

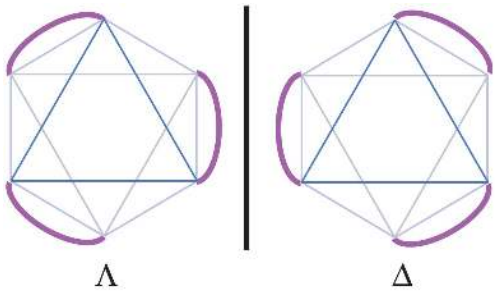


Figure **5.5.3.3**: left-handed Λ isomer (left) and right-handed Δ isomer (right)

To add to the confusion, when measured at the sodium D line (589 nm), the tris(1,2-diaminoethane)M(III) complexes (M= Rh(III) and Co(III)) with **IDENTICAL** absolute configuration, rotate plane polarized light in **OPPOSITE** directions! The left-handed (Λ)-$[Co(en)_3]^{3+}$ isomer gives a rotation to the right and therefore corresponds to the (+) isomer. Since the successful resolution of an entirely inorganic ion (containing no C atoms) (hexol) only a handful of truly inorganic complexes have been isolated as their optical isomers e.g. $(NH_4)_2Pt(S_5)_3.2H_2O$.

For tetrahedral complexes, R and S would be used in a similar method to tetrahedral Carbon species and although it is predicted that tetrahedral complexes with 4 different ligands should be able to give rise to optical isomers, in general they are too labile and can not be isolated.

Contributors and Attributions

- Prof. Robert J. Lancashire (The Department of Chemistry, University of the West Indies)
- Jim Clark (Chemguide.co.uk)

5.5.3: Stereoisomers - Optical Isomerism in Transition Metal Complexes is shared under a not declared license and was authored, remixed, and/or curated by LibreTexts.

5.5.4: Structural Isomers - Linkage Isomerism in Transition Metal Complexes

Linkage isomerism occurs with *ambidentate* ligands that are capable of coordinating in more than one way. The best known cases involve the monodentate ligands: SCN^{-}/NCS^{-} and NO_2^{-}/ONO^{-}. The only difference is what **atoms the molecular ligands bind to the central ion**. The ligand(s) must have more than one donor atom, but bind to ion in only one place. For example, the (NO_2^-) ion is a ligand can bind to the central atom through the nitrogen or the oxygen atom, but cannot bind to the central atom with both oxygen and nitrogen at once, in which case it would be called a *polydentate* rather than an *ambidentate* ligand.

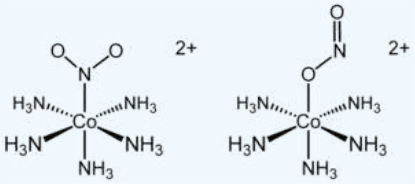


Figure 5.5.4.1: Linkage Isomerism in the NO_2 ligand. This occurs when a particular ligand is capable of coordinating to a metal in two different and distinct ways.

The names used to specify the changed ligands are changed as well. For example, the (NO_2^-) ion is called *nitro* when it binds with the N atom and is called *nitrito* when it binds with the O atom.

Example 5.5.4.1: Nitro- vs. Nitrito- Linkage Isomers

The cationic cobalt complex $[Co(NH_3)_5(NO_2)]Cl_2$ exists in two separable linkage isomers of the complex ion: $[Co(NH_3)_5(NO_2)]^{2+}$.



(left) The nitro isomer (Co-NO_2) and (right) the nitrito isomer (Co-ONO)

When donation is from nitrogen to a metal center, the complex is known as a *nitro-* complex and when donation is from one oxygen to a metal center, the complex is known as a *nitrito-* complex.

- $[Co(ONO)(NH_3)_5]Cl$: the *nitrito* isomer -O attached
- $[Co(NO_2)(NH_3)_5]Cl$: the *nitro* isomer - N attached.

The formula of the complex is unchanged, but the properties of the complex may differ.

Another example of an ambidentate ligans is thiocyanate, SCN^-, which can attach at either the sulfur atom or the nitrogen atom. Such compounds give rise to linkage isomerism. Polyfunctional ligands can bond to a metal center through different ligand atoms to form various isomers. Other ligands that give rise to linkage isomers include selenocyanate, $SeCN^-$ – isoselenocyanate, $NCSe^-$ and sulfite, SO_3^{2-}.

Exercise 5.5.4.1

Sketch the linkage isomers of $[FeCl_5(SCN)]^{3-}$.

Answer

In the first isomer, the ligand bonds to the metal through the nitrogen atom. In the second isomer, the ligand bonds to the metal through the sulfur atom. It's easier to see it:



Contributors and Attributions

- Prof. Robert J. Lancashire (The Department of Chemistry, University of the West Indies)

5.5.4: Structural Isomers - Linkage Isomerism in Transition Metal Complexes is shared under a not declared license and was authored, remixed, and/or curated by LibreTexts.

SECTION OVERVIEW

5.6: Crystal Field Theory

One of the most striking characteristics of transition-metal complexes is the wide range of colors they exhibit. Crystal field theory (CFT) is a bonding model that explains many important properties of transition-metal complexes, including their colors, magnetism, structures, stability, and reactivity. The central assumption of CFT is that metal–ligand interactions are purely electrostatic in nature.

5.6.1: Crystal Field Theory

5.6.2: Colors of Coordination Complexes

5.6.3: Crystal Field Stabilization Energy

5.6.4: Factors That Affect the Magnitude of Δo

5.6.5: Jahn-Teller Distortions

5.6.6: Magnetic Moments of Transition Metals

5.6.7: Magnetism

5.6.8: Thermodynamics and Structural Consequences of d-Orbital Splitting

Template:HideTOC

5.6: Crystal Field Theory is shared under a not declared license and was authored, remixed, and/or curated by LibreTexts.

5.6.1: Crystal Field Theory

Crystal field theory (CFT) describes the breaking of orbital degeneracy in transition metal complexes due to the presence of ligands. CFT qualitatively describes the strength of the metal-ligand bonds. Based on the strength of the metal-ligand bonds, the energy of the system is altered. This may lead to a change in magnetic properties as well as color. This theory was developed by Hans Bethe and John Hasbrouck van Vleck.

Basic Concept

In Crystal Field Theory, it is assumed that the ions are **simple point charges** (a simplification). When applied to alkali metal ions containing a symmetric sphere of charge, calculations of bond energies are generally quite successful. The approach taken uses classical potential energy equations that take into account the attractive and repulsive interactions between charged particles (that is, Coulomb's Law interactions).

$$E \propto \frac{q_1 q_2}{r} \tag{5.6.1.1}$$

with

- E the bond energy between the charges and
- q_1 and q_2 are the charges of the interacting ions and
- r is the distance separating them.

This approach leads to the correct prediction that large cations of low charge, such as K^+ and Na^+, should form few coordination compounds. For transition metal cations that contain varying numbers of d electrons in orbitals that are NOT spherically symmetric, however, the situation is quite different. The shape and occupation of these d-orbitals then becomes important in an accurate description of the bond energy and properties of the transition metal compound.

Description of *d*-Orbitals

To understand CFT, one must understand the description of the lobes:

- d_{xy}: lobes lie in-between the x and the y axes.
- d_{xz}: lobes lie in-between the x and the z axes.
- d_{yz}: lobes lie in-between the y and the z axes.
- $d_{x^2-y^2}$: lobes lie on the x and y axes.
- d_{z^2}: there are two lobes on the z axes and there is a donut shape ring that lies on the xy plane around the other two lobes.

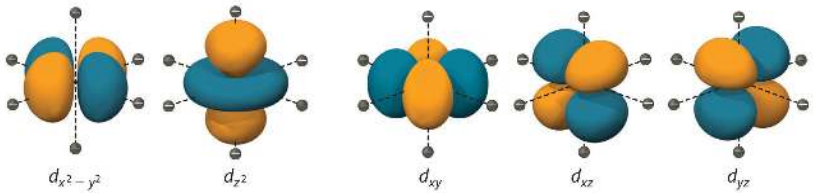


Figure 5.6.1.1: Spatial arrangement of ligands in the an octahedral ligand field with respect to the five d-orbitals.

Octahedral Complexes

When examining a single transition metal ion, the five d-orbitals have the same energy (Figure 5.6.1.2). When ligands approach the metal ion, some experience more opposition from the d-orbital electrons than others based on the geometric structure of the molecule. Since ligands approach from different directions, not all d-orbitals interact directly. These interactions, however, create a splitting due to the electrostatic environment.

For example, consider a molecule with octahedral geometry. Ligands approach the metal ion along the x, y, and z axes. Therefore, the electrons in the d_{z^2} and $d_{x^2-y^2}$ orbitals (which lie along these axes) experience greater repulsion. It requires more energy to have an electron in these orbitals than it would to put an electron in one of the other orbitals. This causes a splitting in the energy levels of the d-orbitals. This is known as **crystal field splitting**. For octahedral complexes, crystal field splitting is denoted by Δ_o (or Δ_{oct}). Any orbital that has a lobe on the axes moves to a higher energy level. The energies of the d_{z^2} and $d_{x^2-y^2}$ orbitals increase due to greater interactions with the ligands. The d_{xy}, d_{xz}, and d_{yz} orbitals decrease in energy with respect to the normal energy level and become more stable. This means that in an octahedral, the energy levels of e_g are higher (by $0.6\Delta_o$) while t_{2g} are lower (by $0.4\Delta_o$). It should be noted that the labels t_{2g} and e_g come from group theory and the octahedral point group. The energy difference between the t_{2g} and e_g orbitals dictates the energy that the complex will absorb causing electrons to move from one level to the next. For transition metal complexes, the absorbed energy is typically in the visible part of the spectrum and thus this will determine the color of the complex. Whether the complex is paramagnetic or diamagnetic will be determined by the spin state. If there are unpaired electrons, the complex is paramagnetic; if all electrons are paired, the complex is diamagnetic.

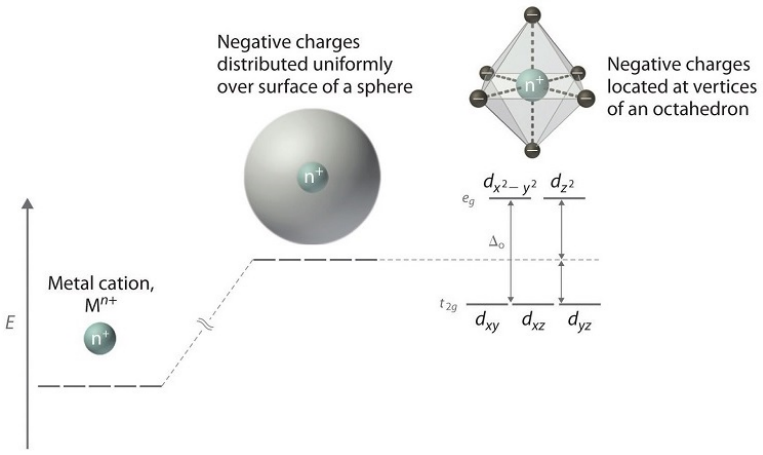


Figure **5.6.1.2**: (a) Distributing a charge of −6 uniformly over a spherical surface surrounding a metal ion causes the energy of all five d orbitals to increase due to electrostatic repulsions, but the five d orbitals remain degenerate. Placing a charge of −1 at each vertex of an octahedron causes the d orbitals to split into two groups with different energies: the $d_{x^2-y^2}$ and d_{z^2} orbitals increase in energy, while the, d_{xy}, d_{xz}, and d_{yz} orbitals decrease in energy. The average energy of the five d orbitals is the same as for a spherical distribution of a −6 charge, however. Attractive electrostatic interactions between the negatively charged ligands and the positively charged metal ion (far right) cause all five d orbitals to decrease in energy but does not affect the splittings of the orbitals. (b) The two e_g orbitals (left) point directly at the six negatively charged ligands, which increases their energy compared with a spherical distribution of negative charge. In contrast, the three t_{2g} orbitals (right) point between the negatively charged ligands, which decreases their energy compared with a spherical distribution of charge.

Electrons in Orbitals

According to the Aufbau principle, electrons are filled from lower to higher energy orbitals (Figure **5.6.1.3**). For the octahedral case above, this corresponds to the d_{xy}, d_{xz}, and d_{yz} orbitals. Following Hund's rule, electrons are filled in order to have the highest number of unpaired electrons. For example, if one had a d^3 complex, there would be three unpaired electrons. If one were to add an electron, however, it has the ability to fill a higher energy orbital (d_{z^2} or $d_{x^2-y^2}$) or pair with an electron residing in the d_{xy}, d_{xz}, or d_{yz} orbitals. This pairing of the electrons requires energy (spin pairing energy). If the pairing energy is less than the crystal field splitting energy, Δ_o, then the next electron will go into the d_{xy}, d_{xz}, or d_{yz} orbitals due to stability. This situation allows for the least amount of unpaired electrons, and is known as low spin. If the pairing energy is greater than Δ_o, then the next electron will go into the d_{z^2} or $d_{x^2-y^2}$ orbitals as an unpaired electron. This situation allows for the most number of unpaired electrons, and is known as high spin. Ligands that cause a transition metal to have a small crystal field splitting, which leads to high spin, are called weak-field ligands. Ligands that produce a large crystal field splitting, which leads to low spin, are called *strong field ligands*.

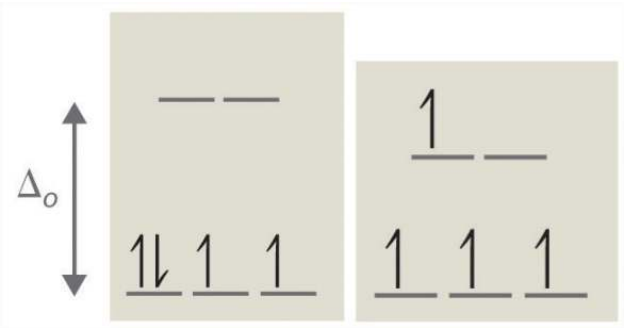


Figure **5.6.1.3**: Low Spin, Strong Field (Δ_o > P) High Spin, Weak Field (Δ_o < P)Splitting for a d^4 complex under a strong field (left) and a weak field (right). The strong field is a low spin complex, while the weak field is a high spin complex.

As mentioned above, CFT is based primarily on symmetry of ligands around a central metal/ion and how this anisotropic (properties depending on direction) ligand field affects the metal's atomic orbitals; the energies of which may increase, decrease or not be affected at all. Once the ligands' electrons interact with the electrons of the d-orbitals, the electrostatic interactions cause the energy levels of the d-orbital to fluctuate depending on the orientation and the nature of the ligands. For example, the valence and the strength of the ligands determine splitting; the higher the valence or the stronger the ligand, the larger the splitting. Ligands are classified as strong or weak based on the spectrochemical series:

$$I < Br < Cl < \underline{S}CN < F < OH < ox < \underline{O}NO < H_2O < SC\underline{N} < EDTA < NH_3 < en < \underline{N}O_2 < CN$$

Note that SCN and NO_2 ligands are represented twice in the above spectrochemical series since there are two different Lewis base sites (e.g., free electron pairs to share) on each ligand (e.g., for the SCN ligand, the electron pair on the sulfur or the nitrogen can form the bond to a metal). The specific atom that binds in such ligands is underlined.

Tetrahedral Complexes

In a tetrahedral complex, there are four ligands attached to the central metal. The d orbitals also split into two different energy levels. The top three consist of the d_{xy}, d_{xz}, and d_{yz} orbitals. The bottom two consist of the $d_{x^2-y^2}$ and d_{z^2} orbitals. The reason for this is due to poor orbital overlap between the metal and the ligand orbitals. The orbitals are directed on the axes, while the ligands are not.

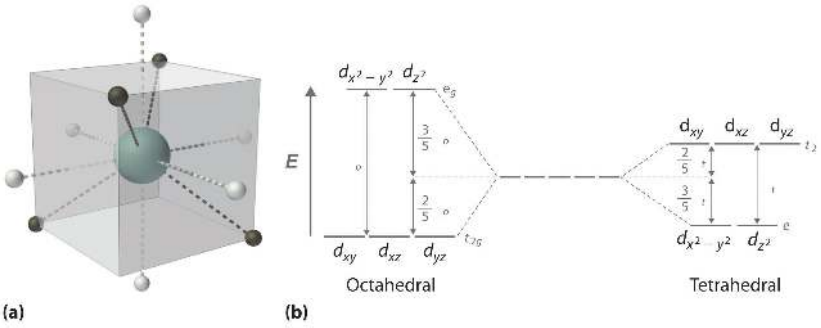


Figure **5.6.1.5**: (a) Tetraheral ligand field surrounding a central transition metal (blue sphere). (b) Splitting of the degenerate d-orbitals (without a ligand field) due to an octahedral ligand field (left diagram) and the tetrahedral field (right diagram).

The difference in the splitting energy is tetrahedral splitting constant (Δ_t), which less than (Δ_o) for the same ligands:

$$\Delta_t = 0.44\,\Delta_o \tag{5.6.1.2}$$

Consequentially, Δ_t is typically smaller than the spin pairing energy, so tetrahedral complexes are usually **high spin**. As seen with octahedral compounds, the labels for the groups of orbitals, t_2 and e in this case, come from group theory and the tetrahedral point group.

Square Planar Complexes

In a square planar, there are four ligands as well. However, the difference is that the electrons of the ligands are only attracted to the ***xy*** plane. Any orbital in the xy plane has a higher energy level (Figure **5.6.1.6**). There are four different energy levels for the square planar (from the highest energy level to the lowest energy level): $d_{x^2-y^2}$, d_{xy}, d_{z^2}, and both d_{xz} and d_{yz}.

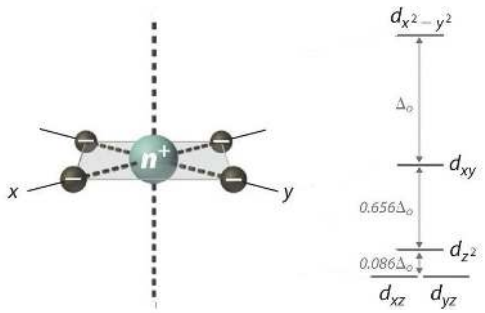


Figure **5.6.1.6**: Splitting of the degenerate d-orbitals (without a ligand field) due to an square planar ligand field.

The splitting energy (from highest orbital to lowest orbital) is Δ_{sp} and tends to be larger then Δ_o

$$\Delta_{sp} = 1.74\,\Delta_o \tag{5.6.1.3}$$

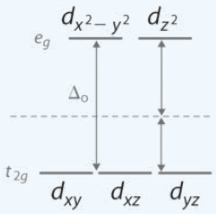
Moreover, Δ_{sp} is also larger than the pairing energy, so the square planar complexes are usually **low spin** complexes.

Exercise 5.6.1.1

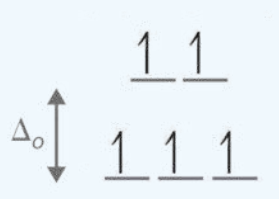
For the complex ion $[Fe(Cl)_6]^{3-}$ determine the number of d-electrons for Fe, sketch the d-orbital energy levels and the distribution of d electrons among them, list the number of lone electrons, and label whether the complex is paramagnetic or diamagnetic.

Answer

Step 1: Determine the valence of Fe. Here it is Fe(III). Based on its electron configuration, Fe(III) has **5 d-electrons**. Step 2: Determine the geometry of the ion. Here it is an octahedral which means the energy splitting should look like:



Step 3: Decide whether the ligand induces is a strong or weak field spin by looking at the spectrochemical series. Cl^- is a weak field ligand (i.e., it induces high spin complexes). Therefore, electrons will likely fill all orbitals before being paired.



Step four: Count the number of lone electrons. Here, there are **5 electrons**. Step five: The five unpaired electrons means this complex ion is **paramagnetic** (and strongly so).

Exercise 5.6.1.2

A *tetrahedral* complex absorbs at 545 nm. Estimate the octahedral crystal field splitting (Δ_o) for an octahedral compound of the same metal with the same ligands? What would be the color of the complex?

Answer

$$\Delta_t = \frac{hc}{\lambda} \tag{5.6.1.4}$$

$$\Delta_t = \frac{(6.626 \times 10^{-34} J \cdot s)(3 \times 10^8 m/s)}{545 \times 10^{-9} m} = 3.65 \times 10^{-19}\ J \tag{5.6.1.5}$$

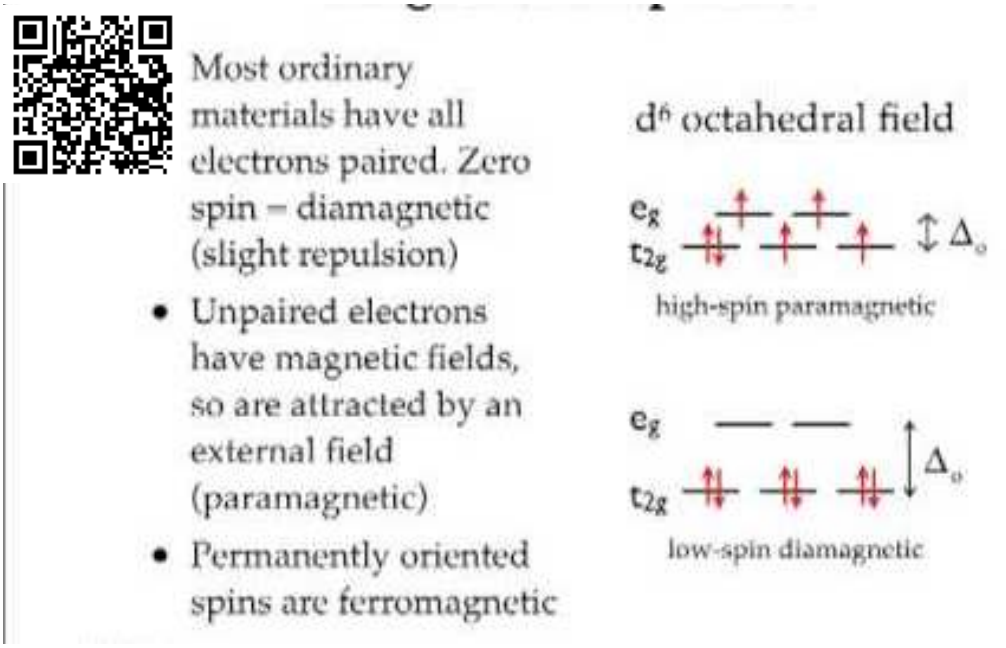
However, the *tetrahedral* splitting (Δ_t) is ~4/9 that of the *octahedral* splitting (Δ_o).

$$\Delta_t = 0.44\Delta_o \tag{5.6.1.6}$$

$$\Delta_o = \frac{\Delta_t}{0.44} = \frac{3.65 \times 10^{-19} J}{0.44} = 8.30 \times 10^{-18} J \tag{5.6.1.7}$$

This is the energy needed to promote *one* electron in *one* complex. Often the crystal field splitting is given per mole, which requires this number to be multiplied by Avogadro's Number (6.022×10^{23}).

This complex appears red, since it absorbs in the complementary green color (determined via the color wheel).



Video:

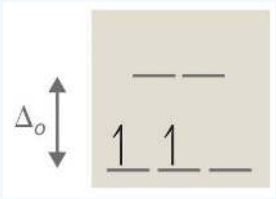
Exercise 5.6.1.3

For each of the following, sketch the d-orbital energy levels and the distribution of d electrons among them, state the geometry, list the number of d-electrons, list the number of lone electrons, and label whether they are paramagnetic or dimagnetic:

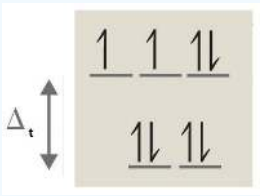
1. $[Ti(H_2O)_6]^{2+}$
2. $[NiCl_4]^{2-}$
3. $[CoF_6]^{3-}$ (also state whether this is low or high spin)
4. $[Co(NH_3)_6]^{3+}$ (also state whether this is low or high spin)

Answer

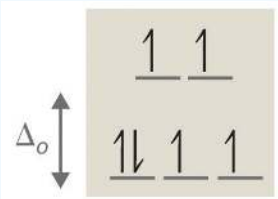
1. octahedral, 2, 2, paramagnetic



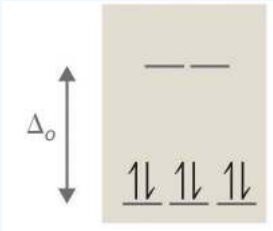
2. tetrahedral, 8, 2, paramagnetic (see Octahedral vs. Tetrahedral Geometries)



3. octahedral, 6, 4, paramagnetic, high spin



4. octahedral, 6, 0, diamagnetic, low spin



Contributors and Attributions

- Asadullah Awan (UCD), Hong Truong (UCD)
- Prof. Robert J. Lancashire (The Department of Chemistry, University of the West Indies)

5.6.1: Crystal Field Theory is shared under a CC BY-NC-SA 4.0 license and was authored, remixed, and/or curated by LibreTexts.

5.6.2: Colors of Coordination Complexes

The color for a coordination complex can be predicted using the Crystal Field Theory (CFT). Knowing the color can have a number of useful applications, such as the creation of pigments for dyes in the textile industry. The tendency for coordination complexes to display such a wide array of colors is merely coincidental; their absorption energies happen to fall within range of the visible light spectrum. Chemists and physicists often study the color of a substance not to understand its sheer appearance, but because color is an indicator of a chemical's physical proprieties on the atomic level.

The Electromagnetic Spectrum

The electromagnetic spectrum (EM) spectrum is made up of photons of different wavelengths. Photons, unique in displaying the properties of both waves and particles, create visible light and colors in a small portion of the EM spectrum. This visible light portion has wavelengths in approximately the 400-700 nanometer range (a nanometer, “nm,” is 10^{-9} meters). Each specific wavelength corresponds to a different color (Figure **5.6.2.1**), and when all the wavelengths are present, it appears as white light.

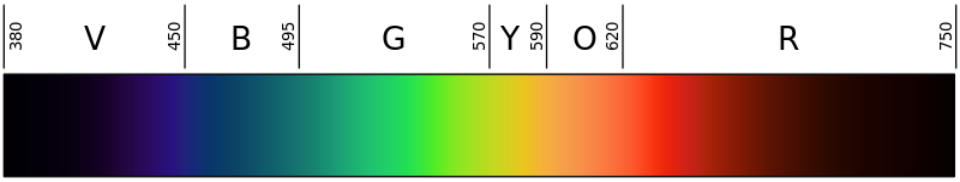


Figure **5.6.2.1**: A linear representation of the visible light spectrum. (Public Domain; Gringer via Wikipedia)

The wavelength and frequency of a wave are inversely proportional: as one increases, the other decreases; this is a consequence of all light traveling at the same speed.

$$\lambda = \nu^{-1} \tag{5.6.2.1}$$

Because of this relationship, blue light has a much higher frequency and more energy than red light. In general, photons to the right of the EM spectrum have increasingly higher energy than photons to the left.

Perceiving Color

Color is perceived in two ways, through additive mixing, where different colors are made by combining different colors of light, and through subtractive mixing, where different wavelengths of light are taken out so that the light is no longer pure white. For colors of coordination complexes, subtractive mixing is considered. As shown in Figure **5.6.2.2**, the idea behind subtractive mixing is that white light (which is made from all the colors mixed together) interacts with an object. The object absorbs some of the light, and then reflects or transmits (or both, depending on the object) the rest of the light, which contacts the eye. The object is perceived as whichever color is not absorbed. In Figure **5.6.2.2**, white light (simplified as green, red, and blue bands) is shone through a solution. The solution absorbs the red and green wavelengths; however, the blue light is reflected and passes through, so the solution appears blue. This procedure takes place whenever an object displays visible color. If none of the light is absorbed, and all is reflected back off, the object appears white; if all of the light is absorbed, and there is none left to reflect or transmit through, the object appears black.

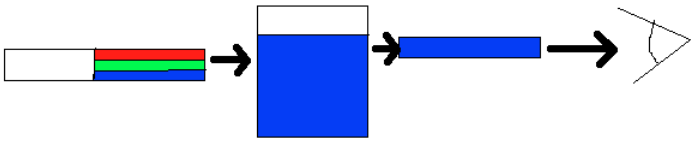


Figure **5.6.2.2**: Subtractive mixing

Colors of Coordination Complexes: Crystal Field Splitting

When ligands attach to a transition metal to form a coordination complex, electrons in the d orbital split into high energy and low energy orbitals. The difference in energy of the two levels is denoted as Δ, and it is a characteristic a property both of the metal and the ligands. This is illustrated in Figure **5.6.2.3**; the "o" subscript on the Δ indicates that the complex has octahedral geometry.

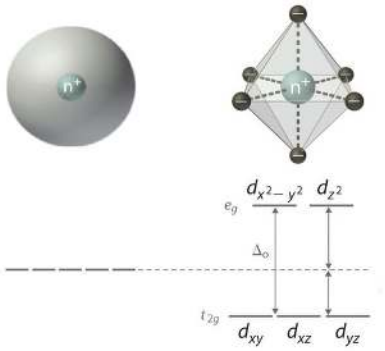


Figure **5.6.2.3**: d-Orbitals Splitting in an octahedral ligand field. (CC BY-SA-NC; anonymous by request)

If Δ_o is large, and much energy is required to promote electrons into the high energy orbitals, the electrons will instead pair in the lower energy orbitals, resulting in a "low spin" complex (Figure **5.6.2.4*A***); however, if Δ_o is small, and it takes little energy to occupy the higher orbitals, the electrons will do so, and remain unpaired (until there are more than five electrons), resulting in a “high spin” complex (Figure **5.6.2.4*B***). Different ligands are associated with either high or low spin —a "strong field" ligand results in a large Δ_o and a low spin configuration, while a "weak field" ligand results in a small Δ_o and a high spin configuration. For more details, see the Crystal Field Theory (CFT) page.

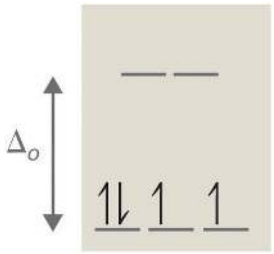


Figure **5.6.2.4*A***: Low Spin, Strong Field ($\Delta_o > P$). (CC BY-SA-NC; anonymous by request)

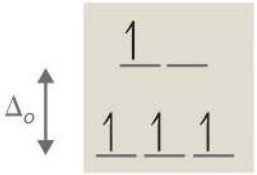


Figure **5.6.2.4*B***: High Spin, Weak Field ($\Delta_o < P$). (CC BY-SA-NC; anonymous by request)

A photon equal to the energy difference Δ_o can be absorbed, promoting an electron to the higher energy level. As certain wavelengths are absorbed in this process, subtractive color mixing occurs and the coordination complex solution becomes colored. If the ions have a noble gas configuration, and have no unpaired electrons, the solutions appear colorless; in reality, they still have a measured energy and absorb certain wavelengths of light, but these wavelengths are not in the visible portion of the EM spectrum and no color is perceived by the eye.

In general, a larger Δ_o indicates that higher energy photons are absorbed, and the solution appears further to the left on the EM spectrum shown in Figure **5.6.2.1**. This relationship is described in the equation

$$\Delta_o = hc/\lambda \tag{5.6.2.2}$$

where h and c are constants, and λ is the wavelength of light absorbed.

Using a color wheel can be useful for determining what color a solution will appear based on what wavelengths it absorbs (Figure **5.6.2.6**). If a complex absorbs a particular color, it will have the appearance of whatever color is directly opposite it on the wheel. For example, if a complex is known to absorb photons in the orange range, it can be concluded that the solution will look blue. This concept can be used in reverse to determine Δ for a complex from the color of its solution.

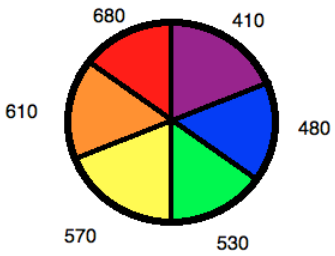


Figure **5.6.2.5**

Relating the Colors of Coordination Complexes to the Spectrochemical Series

According to the Crystal Field Theory, ligands that have smaller Δ) values are considered "weak field" and will absorb lower-energy light with longer λ values (ie a "red shift"). Ligands that have larger Δ) values are considered "strong field" and will absorb higher-energy light with shorter λ values (ie a "blue shift"). This relates to the colors seen in a coordination complex. Weaker-field ligands induce the absorption of longer wavelength (lower frequency=lower energy) light than stronger-field ligands since their respective Δ_o values are **smaller** than the electron pairing energy.

The energy difference, Δ_o, determines the color of the coordination complex. According to the **spectrochemical series**, the high spin ligands are considered "weak field," and absorb longer wavelengths of light (weak Δ_o), while complexes with low spin ligands absorb light of greater frequency (high Δ_o). The color seen is the complementary color of the color associated with the absorbed wavelength. To predict which possible colors and their corresponding wavelengths are absorbed, the spectrochemical series can be used:

(Strong field/large Δ_0/low spin) (weak field/ small Δ_0/high spin)

CO, NO, CN>$\underline{N}O_2$>en>py≈NH_3>EDTA>SC$\underline{N}$>H_2O>ON$\underline{O}$>ox>OH>F>$\underline{S}$CN>Cl>Br>I

Exercise 5.6.2.1

If a solution with a dissolved octahedral complex appears yellow to the eye, what wavelength of light does it absorb? Is this complex expected to be low spin or high spin?

Answer

A solution that looks yellow absorbs light that is violet, which is roughly 410 nm from the color wheel. Since it absorbs high energy, the electrons must be raised to a higher level, and Δ_o is high, so the complex is likely to be low spin

Exercise 5.6.2.2

An octahedral metal complex absorbs light with wavelength 535 nm. What is the crystal field splitting Δ_o for the complex? What color is it to the eye?

Answer

To solve this question, we need to use the equation

$$\Delta_o = \frac{hc}{\lambda}$$

with

h is Planck's constant and is $6.625 \times 10^{-34} J \cdot s$ and c is the speed of light and is $2.998 \times 10^8 \, m/s$.

Note: the fact that the complex is octahedral makes no impact when solving this problem. Although the splitting is different for complexes of different structures, the mechanics of solving the problem are identical.

It is also important to remember that 1 nm is equal to 1×10^{-9} meters. With all this information, the final equation looks like this:

$$\Delta_o = \frac{(6.625 \times 10^{-34}\, J \cdot s)(2.998 \times 10^{8}\, m/s)}{(535 nm)\left(\frac{1\, m}{1 \times 10^{9}\, nm}\right)} = 3.712\, J/molecule$$

It is not necessary to use any equations to solve the second part of the problem. Light that is 535 nm is green, and because green light is absorbed, the complex appears red (refer to Figures **5.6.2.1** and **5.6.2.6** for this information).

Exercise 5.6.2.3

There are two solutions, one orange and one blue. Both solutions are known to be made up of a cobalt complex; however, one has chloride ions as ligands, while the other has ammonia ligands. Which solution is expected to be orange?

Answer

In order to solve this problem, it is necessary to know the relative strengths of the ligands involved. A sample ligand strength list is given here, but see Crystal Field Splitting for a more complete list:

$$CN > en > NH_3 > H_2O > F > SCN > Cl$$

From this information, it is clear that NH_3 is a stronger ligand than Cl, which means that the complex involving NH_3 has a greater Δ, and the complex will be low spin. Because of the larger Δ, the electrons absorb higher energy photons, and the solution will have the appearance of a lower energy color. Since orange light is less energetic than blue light, the NH_3 containing solution is predicted to be orange

References

1. Cox, P. A. Instant Notes Inorganic Chemistry. Second ed. Grand Rapids: Garland, Incorporated, 2004.
2. Nassau, Kurt. The Physics and Chemistry of Color : The Fifteen Causes of Color. Second ed. New York: Wiley-Interscience, 2001.
3. Petrucci, Ralph H., William S. Harwood, and Geoff E. Herring. General Chemistry : Principles and Modern Applications. Ninth ed. Upper Saddle River: Prentice Hall PTR, 2006.
4. Petrucci, Ralph H., Carey Bissonnette, F. Geoffrey Herring, Jeffrey D. Madura. General Chemistry: Principles and Modern Applications. Tenth Ed. Upper Saddle River: Pearson Education, Inc. 2011.

Contributors and Attributions

- Deyu Wang (UCD)

5.6.2: Colors of Coordination Complexes is shared under a not declared license and was authored, remixed, and/or curated by LibreTexts.

5.6.3: Crystal Field Stabilization Energy

A consequence of Crystal Field Theory is that the distribution of electrons in the d orbitals may lead to net stabilization (decrease in energy) of some complexes depending on the specific ligand field geometry and metal d-electron configurations. It is a simple matter to calculate this stabilization since all that is needed is the electron configuration and knowledge of the splitting patterns.

Definition: Crystal Field Stabilization Energy

The Crystal Field Stabilization Energy is defined as the energy of the electron configuration in the ligand field minus the energy of the electronic configuration in the isotropic field.

$$CFSE = \Delta E = E_{\text{ligand field}} - E_{\text{isotropic field}} \tag{5.6.3.1}$$

The CSFE will depend on multiple factors including:

- Geometry (which changes the d-orbital splitting patterns)
- Number of d-electrons
- Spin Pairing Energy
- Ligand character (via Spectrochemical Series)

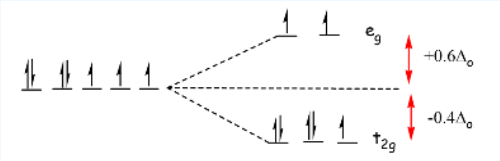
For an octahedral complex, an electron in the more stable t_{2g} subset is treated as contributing $-2/5\Delta_o$ whereas an electron in the higher energy e_g subset contributes to a destabilization of $+3/5\Delta_o$. The final answer is then expressed as a multiple of the crystal field splitting parameter Δ_o. If any electrons are paired within a single orbital, then the term P is used to represent the spin pairing energy.

Example 5.6.3.1: CFSE for a high Spin d^7 complex

What is the Crystal Field Stabilization Energy for a high spin d^7 octahedral complex?

Solution

The splitting pattern and electron configuration for both isotropic and octahedral ligand fields are compared below.



The energy of the isotropic field ($E_{\text{isotropic field}}$) is

$$E_{\text{isotropic field}} = 7 \times 0 + 2P = 2P$$

The energy of the octahedral ligand field $E_{\text{ligand field}}$ is

$$E_{\text{ligand field}} = (5 \times -2/5\Delta_o) + (2 \times 3/5\Delta_o) + 2P = -4/5\Delta_o + 2P$$

So via Equation 5.6.3.1, the CFSE is

$$\begin{aligned} CFSE &= E_{\text{ligand field}} - E_{\text{isotropic field}} \\ &= (-4/5\Delta_o + 2P) - 2P \\ &= -4/5\Delta_o \end{aligned}$$

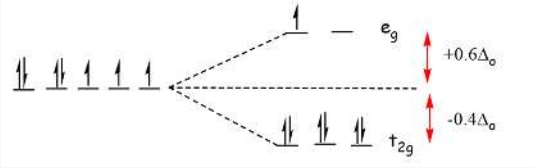
Notice that the Spin pairing Energy falls out in this case (and will when calculating the CFSE of high spin complexes) since the number of paired electrons in the ligand field is the same as that in isotropic field of the free metal ion.

Exercise 5.6.3.1

What is the Crystal Field Stabilization Energy for a low spin d^7 octahedral complex?

Answer

The splitting pattern and electron configuration for both isotropic and octahedral ligand fields are compared below.



The energy of the isotropic field is the same as calculated for the high spin configuration in Example 1:

$$E_{\text{isotropic field}} = 7 \times 0 + 2P = 2P$$

The energy of the octahedral ligand\) field $E_{\text{ligand field}}$ is

$$\begin{aligned} E_{\text{ligand field}} &= (6 \times -2/5\Delta_o) + (1 \times 3/5\Delta_o) + 3P \\ &= -9/5\Delta_o + 3P \end{aligned}$$

So via Equation 5.6.3.1, the CFSE is

$$\begin{aligned} CFSE &= E_{\text{ligand field}} - E_{\text{isotropic field}} \\ &= (-9/5\Delta_o + 3P) - 2P \\ &= -9/5\Delta_o + P \end{aligned}$$

Adding in the pairing energy since it will require extra energy to pair up one extra group of electrons. This appears more a more stable configuration than the high spin d^7 configuration in Example 5.6.3.1, but we have then to take into consideration the Pairing energy P to know definitely, which varies between $200-400\ kJ\ mol^{-1}$ depending on the metal.

Table 5.6.3.1: Crystal Field Stabilization Energies (CFSE) for high and low spin octahedral complexes

Total d-electrons	Isotropic Field	Octahedral Complex				Crystal Field Stabilization Energy	
		High Spin		Low Spin			
	$E_{\text{isotropic field}}$	Configuration	$E_{\text{ligand field}}$	Configuration	$E_{\text{ligand field}}$	High Spin	Low Spin
d^0	0	$t_{2g}0e_g0$	0	$t_{2g}^0e_g^0$	0	0	0
d^1	0	$t_{2g}1e_g0$	-2/5 Δ_o	$t_{2g}^1e_g^0$	-2/5 Δ_o	-2/5 Δ_o	-2/5 Δ_o
d^2	0	$t_{2g}2e_g0$	-4/5 Δ_o	$t_{2g}^2e_g^0$	-4/5 Δ_o	-4/5 Δ_o	-4/5 Δ_o
d^3	0	$t_{2g}3e_g0$	-6/5 Δ_o	$t_{2g}^3e_g^0$	-6/5 Δ_o	-6/5 Δ_o	-6/5 Δ_o
d^4	0	$t_{2g}3e_g1$	-3/5 Δ_o	$t_{2g}^4e_g^0$	-8/5 Δ_o + P	-3/5 Δ_o	-8/5 Δ_o + P
d^5	0	$t_{2g}3e_g2$	0 Δ_o	$t_{2g}^5e_g^0$	-10/5 Δ_o + 2P	0 Δ_o	-10/5 Δ_o + 2P
d^6	P	$t_{2g}4e_g2$	-2/5 Δ_o + P	$t_{2g}^6e_g^0$	-12/5 Δ_o + 3P	-2/5 Δ_o	-12/5 Δ_o + P
d^7	2P	$t_{2g}5e_g2$	-4/5 Δ_o + 2P	$t_{2g}^6e_g^1$	-9/5 Δ_o + 3P	-4/5 Δ_o	-9/5 Δ_o + P
d^8	3P	$t_{2g}6e_g2$	-6/5 Δ_o + 3P	$t_{2g}^6e_g^2$	-6/5 Δ_o + 3P	-6/5 Δ_o	-6/5 Δ_o
d^9	4P	$t_{2g}6e_g3$	-3/5 Δ_o + 4P	$t_{2g}^6e_g^3$	-3/5 Δ_o + 4P	-3/5 Δ_o	-3/5 Δ_o
d^{10}	5P	$t_{2g}6e_g4$	0 Δ_o + 5P	$t_{2g}^6e_g^4$	0 Δ_o + 5P	0	0

P is the spin pairing energy and represents the energy required to pair up electrons within the same orbital. For a given metal ion P (pairing energy) is constant, but it does not vary with ligand and oxidation state of the metal ion).

Octahedral Preference

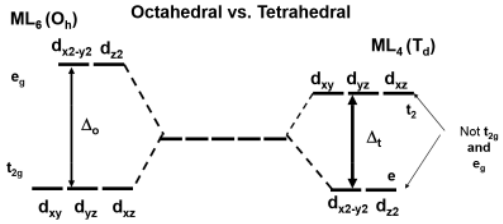
Similar CFSE values can be constructed for non-octahedral ligand field geometries once the knowledge of the d-orbital splitting is known and the electron configuration within those orbitals known, e.g., the tetrahedral complexes in Table **5.6.3.2**. These energies geoemtries can then be contrasted to the octahedral CFSE to calculate a thermodynamic preference (Enthalpy-wise) for a metal-ligand combination to favor the octahedral geometry. This is quantified via a Octahedral Site Preference Energy defined below.

Definition: Octahedral Site Preference Energies

The Octahedral Site Preference Energy (OSPE) is defined as the difference of CFSE energies for a non-octahedral complex and the octahedral complex. For comparing the preference of forming an octahedral ligand field vs. a tetrahedral ligand field, the OSPE is thus:

$$OSPE = CFSE_{(oct)} - CFSE_{(tet)} \tag{5.6.3.2}$$

The OSPE quantifies the preference of a complex to exhibit an octahedral geometry vs. a tetrahedral geometry.



Note: the conversion between Δ_o and Δ_t used for these calculations is:

$$\Delta_t \approx \frac{4}{9}\Delta_o \tag{5.6.3.3}$$

which is applicable for comparing octahedral and tetrahedral complexes that involve same ligands only.

Table 5.6.3.2: Octahedral Site Preference Energies (OSPE)

Total d-electrons	**CFSE(Octahedral)**		**CFSE(Tetrahedral)**		**OSPE (for high spin complexes)****
	High Spin	Low Spin	Configuration	**Always High Spin***	
d^0	0 Δ_o	0 Δ_o	e^0	0 Δ_t	0 Δ_o
d^1	-2/5 Δ_o	-2/5 Δ_o	e^1	-3/5 Δ_t	-6/45 Δ_o
d^2	-4/5 Δ_o	-4/5 Δ_o	e^2	-6/5 Δ_t	-12/45 Δ_o
d^3	-6/5 Δ_o	-6/5 Δ_o	$e^2t_2^1$	-4/5 Δ_t	-38/45 Δ_o
d^4	-3/5 Δ_o	-8/5 Δ_o + P	$e^2t_2^2$	-2/5 Δ_t	-19/45 Δ_o
d^5	0 Δ_o	-10/5 Δ_o + 2P	$e^2t_2^3$	0 Δ_t	0 Δ_o
d^6	-2/5 Δ_o	-12/5 Δ_o + P	$e^3t_2^3$	-3/5 Δ_t	-6/45 Δ_o
d^7	-4/5 Δ_o	-9/5 Δ_o + P	$e^4t_2^3$	-6/5 Δ_t	-12/45 Δ_o
d^8	-6/5 Δ_o	-6/5 Δ_o	$e^4t_2^4$	-4/5 Δ_t	-38/45 Δ_o
d^9	-3/5 Δ_o	-3/5 Δ_o	$e^4t_2^5$	-2/5 Δ_t	-19/45 Δ_o
d^{10}	0	0	$e^4t_2^6$	0 Δ_t	0 Δ_o

P is the spin pairing energy and represents the energy required to pair up electrons within the same orbital.

> Tetrahedral complexes are always high spin since the splitting is appreciably smaller than P (Equation 5.6.3.3).

After conversion with Equation 5.6.3.3. The data in Tables 5.6.3.1 and 5.6.3.2 are represented graphically by the curves in Figure 5.6.3.1 below for the high spin complexes only. The low spin complexes require knowledge of P to graph.

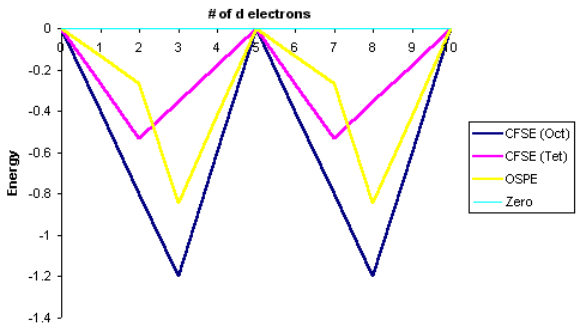


***Figure* 5.6.3.1:** *Crystal Field Stabilization Energies for both octahedral fields ($CFSE_{oct}$) and tetrahedral fields ($CFSE_{tet}$). Octahedral Site Preference Energies (OSPE) are in yellow. This is for high spin complexes.*

From a simple inspection of Figure 5.6.3.1, the following observations can be made:

- The OSPE is *small* in d^1, d^2, d^5, d^6, d^7 complexes and other factors influence the stability of the complexes including steric factors
- The OSPE is *large* in d^3 and d^8 complexes which strongly favor octahedral geometries

Applications

The "double-humped" curve in Figure 5.6.3.1 is found for various properties of the first-row transition metals, including Hydration and Lattice energies of the M(II) ions, ionic radii as well as the stability of M(II) complexes. This suggests that these properties are somehow related to Crystal Field effects.

In the case of Hydration Energies describing the complexation of water ligands to a bare metal ion:

$$M^{2+}(g) + H_2O \rightarrow [M(OH_2)_6]^{2+}(aq) \tag{5.6.3.4}$$

Table 5.6.3.3 and Figure 5.6.3.1 shows this type of curve. Note that in any series of this type not all the data are available since a number of ions are not very stable in the M(II) state.

Table 5.6.3.3: Hydration energies of M^{2+} ions

M	ΔH°/kJmol^{-1}	M	ΔH°/kJmol^{-1}
Ca	-2469	Fe	-2840
Sc	no stable 2+ ion	Co	-2910
Ti	-2729	Ni	-2993
>V	-2777	Cu	-2996
Cr	-2792	Zn	-2928
Mn	-2733		

Graphically the data in Table 2 can be represented by:

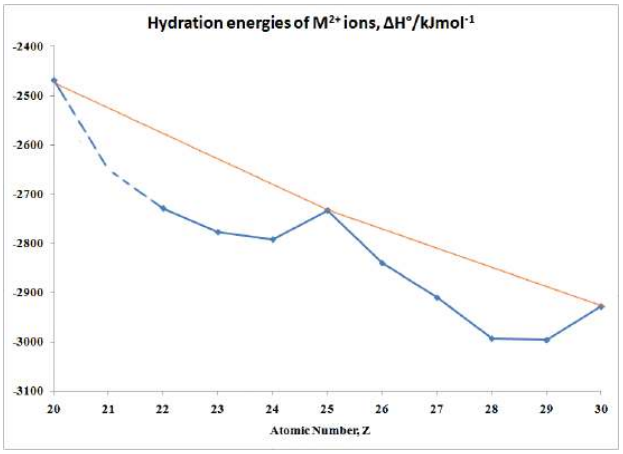


Figure* 5.6.3.2*: hydration energies of M^{2+} ions

Contributors and Attributions

- Prof. Robert J. Lancashire (The Department of Chemistry, University of the West Indies)

5.6.3: Crystal Field Stabilization Energy is shared under a not declared license and was authored, remixed, and/or curated by LibreTexts.

5.6.4: Factors That Affect the Magnitude of Δo

The magnitude of Δ_o dictates whether a complex with four, five, six, or seven d electrons is high spin or low spin, which affects its magnetic properties, structure, and reactivity. Large values of Δ_o (i.e., $\Delta_o > P$) yield a low-spin complex, whereas small values of Δ_o (i.e., $\Delta_o < P$) produce a high-spin complex. The magnitude of Δ_o depends on three factors: the valence of the metal, the principal quantum number of the metal (and thus its location in the periodic table), and the nature of the ligand(s). Values of Δ_o for some representative transition-metal complexes are given in Table **5.6.4.1**.

Table **5.6.4.1**: Crystal Field Splitting Energies for Some Octahedral (Δ_o)* and Tetrahedral (Δ_t) Transition-Metal Complexes

Octahedral Complexes	Δ_o (cm^{-1})	Octahedral Complexes	Δ_o (cm^{-1})	Tetrahedral Complexes	Δ_t (cm^{-1})
$[Ti(H_2O)_6]^{3+}$	20,300	$[Fe(CN)_6]^{4-}$	32,800	VCl_4	9010
$[V(H_2O)_6]^{2+}$	12,600	$[Fe(CN)_6]^{3-}$	35,000	$[CoCl_4]^{2-}$	3300
$[V(H_2O)_6]^{3+}$	18,900	$[CoF_6]^{3-}$	13,000	$[CoBr_4]^{2-}$	2900
$[CrCl_6]^{3-}$	13,000	$[Co(H_2O)_6]^{2+}$	9300	$[CoI_4]^{2-}$	2700
$[Cr(H_2O)_6]^{2+}$	13,900	$[Co(H_2O)_6]^{3+}$	27,000		
$[Cr(H_2O)_6]^{3+}$	17,400	$[Co(NH_3)_6]^{3+}$	22,900		
$[Cr(NH_3)_6]^{3+}$	21,500	$[Co(CN)_6]^{3-}$	34,800		
$[Cr(CN)_6]^{3-}$	26,600	$[Ni(H_2O)_6]^{2+}$	8500		
$Cr(CO)_6$	34,150	$[Ni(NH_3)_6]^{2+}$	10,800		
$[MnCl_6]^{4-}$	7500	$[RhCl_6]^{3-}$	20,400		
$[Mn(H_2O)_6]^{2+}$	8500	$[Rh(H_2O)_6]^{3+}$	27,000		
$[MnCl_6]^{3-}$	20,000	$[Rh(NH_3)_6]^{3+}$	34,000		
$[Mn(H_2O)_6]^{3+}$	21,000	$[Rh(CN)_6]^{3-}$	45,500		
$[Fe(H_2O)_6]^{2+}$	10,400	$[IrCl_6]^{3-}$	25,000		
$[Fe(H_2O)_6]^{3+}$	14,300	$[Ir(NH_3)_6]^{3+}$	41,000		

*Energies obtained by spectroscopic measurements are often given in units of wave numbers (cm^{-1}); the wave number is the reciprocal of the wavelength of the corresponding electromagnetic radiation expressed in centimeters: 1 cm^{-1} = 11.96 J/mol.

Source of data: Duward F. Shriver, Peter W. Atkins, and Cooper H. Langford, Inorganic Chemistry, 2nd ed. (New York: W. H. Freeman and Company, 1994).

Factor 1: Valence of the Metal

Increasing the valence of a metal ion has two effects: the radius of the metal decreases, and ligands are more strongly attracted to it. Both factors decrease the metal–ligand distance, which in turn causes the ligands to interact more strongly with the d-orbitals. Consequently, the magnitude of Δ_o increases as the valence of the metal increases. Typically, Δ_o for a M(III) is about 50% greater than for the M(II) of the same metal; for example, for $[V(H_2O)_6]^{2+}$, Δ_o = 11,800 cm^{-1}; for $[V(H_2O)_6]^{3+}$, Δ_o = 17,850 cm^{-1}.

Factor 2: Principal Quantum Number of the Metal

For a series of complexes of metals from the same group in the periodic table with the same charge and the same ligands, the magnitude of Δ_o increases with increasing principal quantum number: Δ_o (3d) < Δ_o (4d) < Δ_o (5d). The data for hexaammine complexes of the trivalent Group 9 metals illustrate this point:

$$[Co(NH_3)_6]^{3+}: \Delta_o = 22{,}900\ cm^{-1}$$

$$[Rh(NH_3)_6]^{3+}: \Delta_o = 34{,}100\ cm^{-1}$$

$$[Ir(NH_3)_6]^{3+}: \Delta_o = 40{,}000\ cm^{-1}$$

The increase in Δ_o with increasing principal quantum number is due to the larger radius of valence orbitals down a column. In addition, repulsive ligand–ligand interactions are most important for smaller metal ions. Relatively speaking, this results in shorter M–L distances and stronger d orbital–ligand interactions.

Factor 3: The Nature of the Ligands

Experimentally, it is found that the Δ_o observed for a series of complexes of the same metal ion depends strongly on the nature of the ligands. For a series of chemically similar ligands, the magnitude of Δ_o decreases as the size of the donor atom increases. For example, Δ_o values for halide complexes generally decrease in the order F > Cl > Br > I because smaller, more localized charges, such as we see for F, interact more strongly with the d-orbitals of the metal. In addition, a small neutral ligand with a highly localized lone pair, such as NH_3, results in significantly larger Δ_o values than might be expected. Because the lone pair points directly at the metal ion, the electron density along the M–L axis is greater than for a spherical anion such as F. The experimentally observed order of the crystal field splitting energies produced by different ligands is called the spectrochemical series which was presented in a previous section.

5.6.4: Factors That Affect the Magnitude of Δo is shared under a not declared license and was authored, remixed, and/or curated by LibreTexts.

5.6.5: Jahn-Teller Distortions

The Jahn-Teller effect is a geometric distortion of a non-linear molecular system that reduces its symmetry and energy. This distortion is typically observed among octahedral complexes where the two axial bonds can be shorter or longer than those of the equatorial bonds. This effect can also be observed in tetrahedral compounds. This effect is dependent on the electronic state of the system.

Introduction

In 1937, Hermann Jahn and Edward Teller postulated a theorem stating that "stability and degeneracy are not possible simultaneously unless the molecule is a linear one," in regards to its electronic state.[1] This leads to a break in degeneracy which stabilizes the molecule and by consequence, reduces its symmetry. Since 1937, the theorem has been revised which Housecroft and Sharpe have eloquently phrased as "any non-linear molecular system in a degenerate electronic state will be unstable and will undergo distortion to form a system of lower symmetry and lower energy, thereby removing the degeneracy."[2] This is most commonly observed with transition metal octahedral complexes, however, it can be observed in tetrahedral compounds as well.

For a given octahedral complex, the five d atomic orbitals are split into two degenerate sets when constructing a molecular orbital diagram. These are represented by the sets' symmetry labels: t_{2g} (d_{xz}, d_{yz}, d_{xy}) and e_g (d_{z^2} and $d_{x^2-y^2}$). When a molecule possesses a degenerate electronic ground state, it will distort to remove the degeneracy and form a lower energy (and by consequence, lower symmetry) system. The octahedral complex will either elongate or compress the z ligand bonds as shown in Figure 5.6.5.1 below:

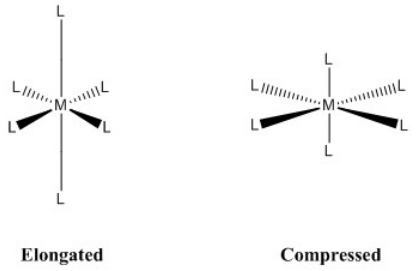


Figure 5.6.5.1: Jahn-Teller distortions for an octahedral complex.

When an octahedral complex exhibits elongation, the axial bonds are longer than the equatorial bonds. For a compression, it is the reverse; the equatorial bonds are longer than the axial bonds. Elongation and compression effects are dictated by the amount of overlap between the metal and ligand orbitals. Thus, this distortion varies greatly depending on the type of metal and ligands. In general, the stronger the metal-ligand orbital interactions are, the greater the chance for a Jahn-Teller effect to be observed.

Elongation

Elongation Jahn-Teller distortions occur when the degeneracy is broken by the stabilization (lowering in energy) of the d orbitals with a z component, while the orbitals without a z component are destabilized (higher in energy) as shown in Figure 5.6.5.2 below:

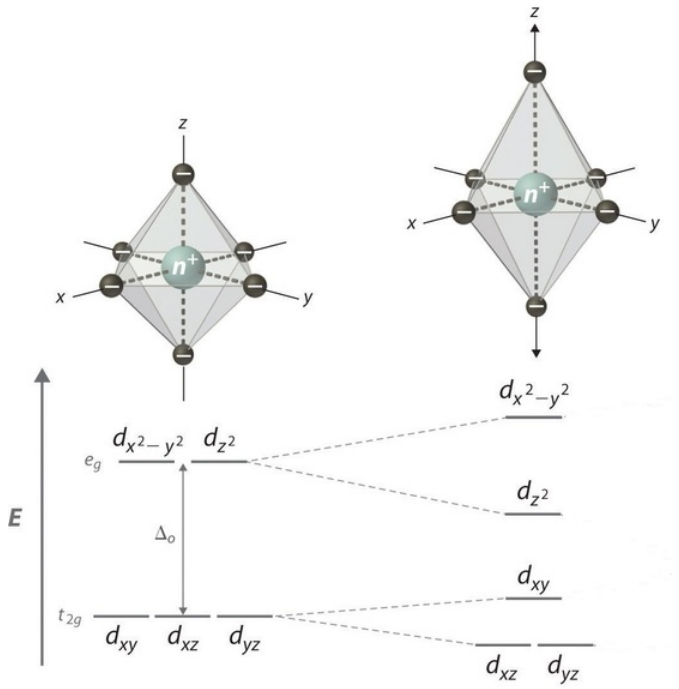


Figure **5.6.5.2**: Illustration of tetragonal distortion (elongation) for an octahedral complex.

This is due to the d_{xy} and $d_{x^2-y^2}$ orbitals having greater overlap with the ligand orbitals, resulting in the orbitals being higher in energy. Since the $d_{x^2-y^2}$ orbital is antibonding, it is expected to increase in energy due to elongation. The d_{xy} orbital is still nonbonding, but is destabilized due to the interactions. Jahn-Teller elongations are well-documented for copper(II) octahedral compounds. A classic example is that of copper(II) fluoride as shown in Figure **5.6.5.3**.

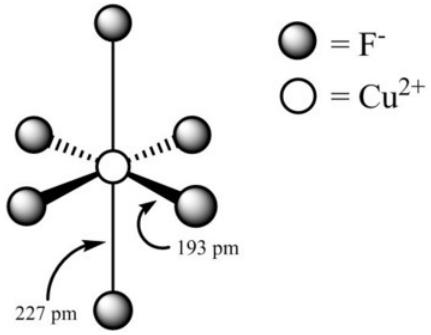


Figure **5.6.5.3**: Structure of octahedral copper(II) fluoride.[3]

Notice that the two axial bonds are both elongated and the four shorter equatorial bonds are the same length as each other. According the theorem, the orbital degeneracy is eliminated by distortion, making the molecule more stable based on the model presented in Figure **5.6.5.2**.

Compression

Compression Jahn-Teller distortions occur when the degeneracy is broken by the stabilization (lowering in energy) of the d orbitals *without* a *z* component, while the orbitals with a *z* component are destabilized (higher in energy) as shown in Figure **5.6.5.4** below:

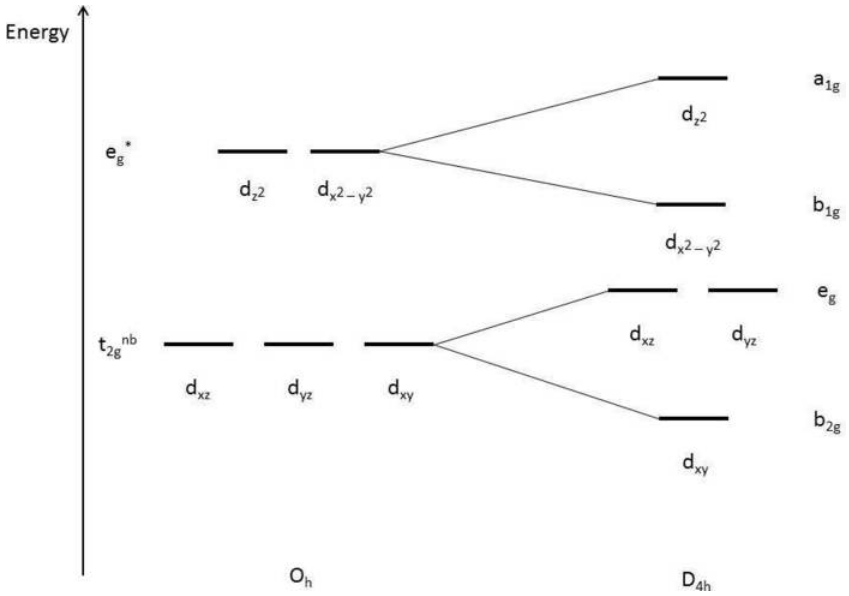


Figure **5.6.5.4**: Illustration of tetragonal distortion (compression) for an octahedral complex.

This is due to the *z*-component d orbitals having greater overlap with the ligand orbitals, resulting in the orbitals being higher in energy. Since the d_{z^2} orbital is antibonding, it is expected to increase in energy due to compression. The d_{xz} and d_{yz} orbitals are still nonbonding, but are destabilized due to the interactions.

Electronic Configurations

For Jahn-Teller effects to occur in transition metals there must be degeneracy in either the t_{2g} or e_g orbitals. The electronic states of octahedral complexes depend on the number of d-electrons and the splitting energy, **Δ**. When **Δ** is large and is greater than the energy required to pair electrons, electrons pair in t_{2g} before occupying e_g. On the other hand, when ***Delta*** small and is less than the pairing energy, electrons will occupy e_g before pairing in t_{2g}. The **Δ** of an octahedral complex is dictated by the chemical environment (ligand identity), and the identity and charge of the metal ion. If there electron configurations for any d-electron count is different depending on **Δ**, the configuration with more paired electrons is called low spin while the one with more unpaired electrons is called high spin.

The electron configurations diagrams for d1 through d10 with large and small ***δ*** are illustrated in the figures below. Notice that the electron configurations for d^1, d^2, d^3, d^8, d^9, and d^{10} are the same no matter what the magnitude of **Δ**. Low spin and high spin configurations exist only for the electron counts d^4, d^5, d^6, and d^7.

Large Δ

Figure **5.6.5.5** (below) shows the various electronic configurations for octahedral complexes with large **Δ**, including the low-spin configurations of d^4, d^5, d^6, and d^7:

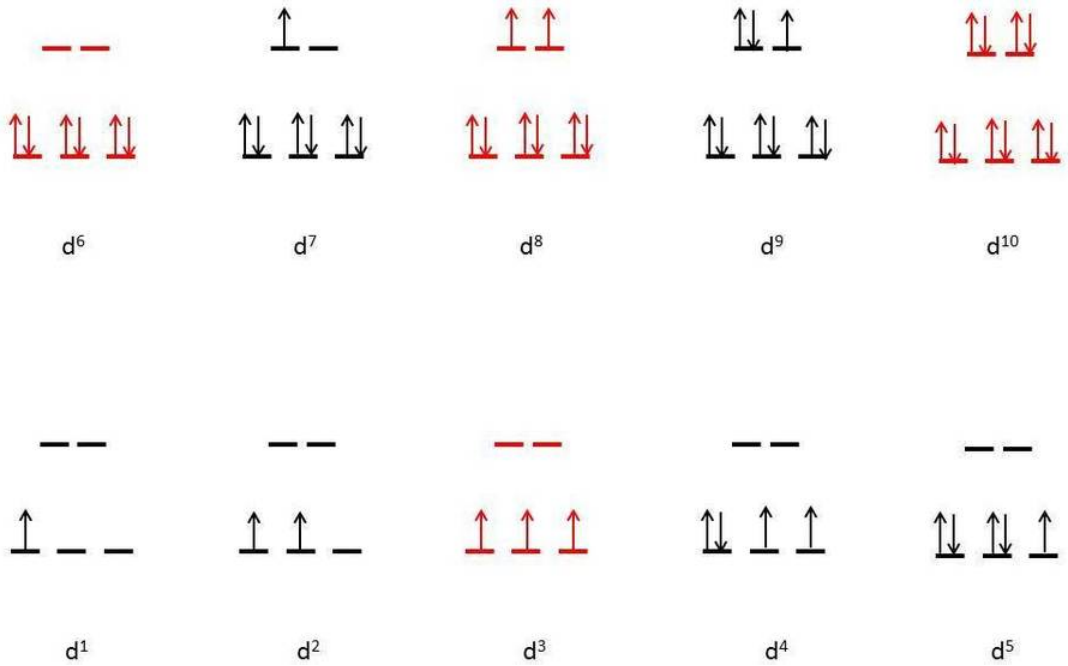


Figure 5.6.5.5: Electron configuration diagram of octahedral complexes (red indicates no degeneracies possible, thus no Jahn-Teller effects).

The figure illustrates the electron configurations in the case of large **Δ**. The electron configurations highlighted in red (d^3, low spin d^6, d^8, and d^{10}) **do not** exhibit Jahn-Teller distortions. On the other hand d^1, d^2, low spin d^4, low spin d^5, low spin d^7, and d^9, would be expected to exhibit Jhan-Teller distortion. These electronic configurations correspond to a variety of transition metals. Some common examples include Cr^{3+}, Co^{3+}, and Ni^{2+}.

Small Δ

Figure 5.6.5.6 (below) shows the various electronic configurations for octahedral complexes with small **Δ**, including the high-spin configurations of d^4, d^5, d^6, and d^7::

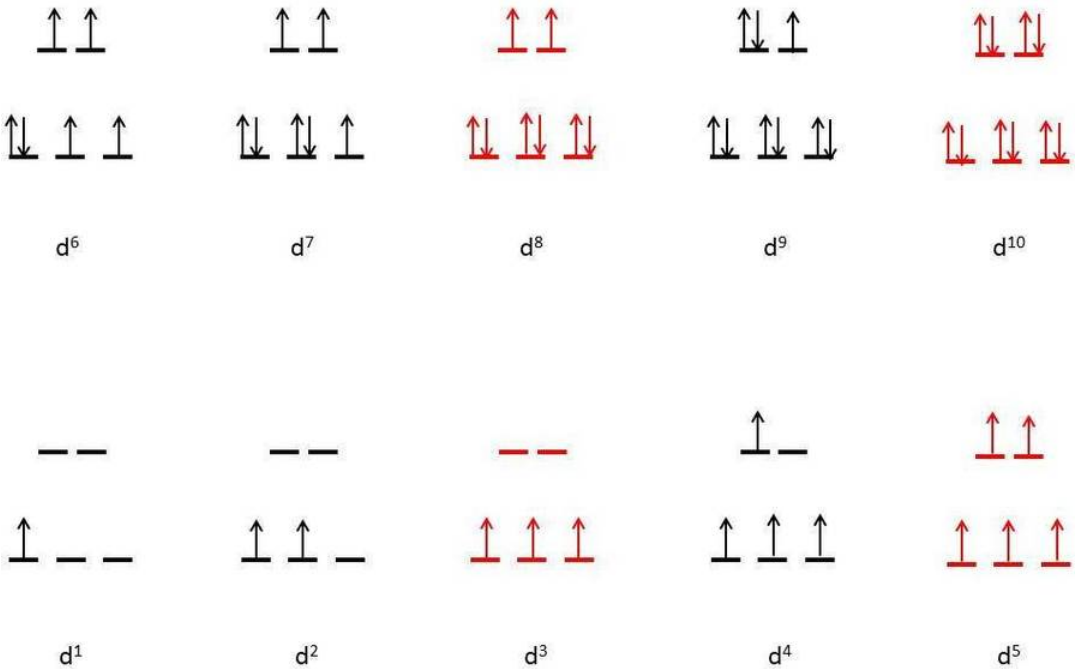


Figure 5.6.5.6: High spin octahedral coordination diagram (red indicates no degeneracies possible, thus no Jahn-Teller effects).

The figure illustrates the electron configurations in the case of small Δ. The electron configurations highlighted in red (d^3, high spin d^5, d^8, and d^{10}) **do not** exhibit Jahn-Teller distortions. In general, degenerate electronic states occupying the e_g orbital set tend to show stronger Jahn-Teller effects. This is primarily caused by the occupation of these high energy orbitals. Since the system is more stable with a lower energy configuration, the degeneracy of the e_g set is broken, the symmetry is reduced, and occupations at lower energy orbitals occur.

Spectroscopic Observation

Jahn-Teller distortions can be observed using a variety of spectroscopic techniques. In UV-VIS absorption spectroscopy, distortion causes splitting of bands in the spectrum due to a reduction in symmetry (O_h to D_{4h}). Consider a hypothetical molecule with octahedral symmetry showing a single absorption band. If the molecule were to undergo Jahn-Teller distortion, the number of bands would increase as shown in Figure **5.6.5.7** below:

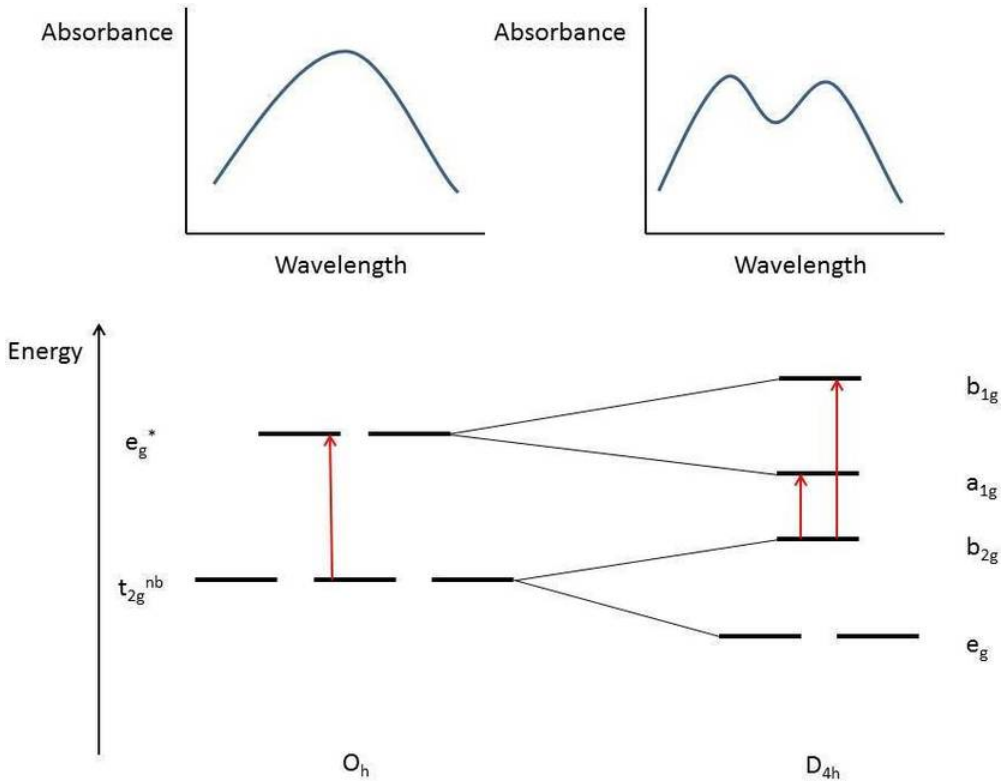


Figure **5.6.5.7**: Hypothetical absorption spectra of an octahedral molecule (left) and the same molecule with Jahn-Teller elongation (right). The red arrows indicate electronic transitions.

A similar phenomenon can be seen with IR and Raman vibrational spectroscopy. The number of vibrational modes for a molecule can be calculated using the 3n - 6 rule (or 3n - 5 for linear geometry) rule. If a molecule exhibits an O_h symmetry point group, it will have fewer bands than that of a Jahn-Teller distorted molecule with D_{4h} symmetry. Thus, one could observe Jahn-Teller effects through either IR or Raman techniques. This effect can also be observed in EPR experiments as long as there is at least one unpaired electron.

Table **5.6.5.1**: Examples of Jahn-Teller distorted complexes

$CuBr_2$	4 Br at 240 pm 2 Br at 318 pm
$CuCl_2$	4 Cl at 230 pm 2 Cl at 295 pm
$CuCl_2.2H_2O$	2 O at 193 pm 2 Cl at 228 pm 2 Cl at 295 pm
$CsCuCl_3$	4 Cl at 230 pm 2 Cl at 265 pm
CuF_2	4 F at 193 pm 2 F at 227 pm
$CuSO_4.4NH_3.H_2O$	4 N at 205 pm 1 O at 259 pm 1 O at 337 pm
K_2CuF_4	4 F at 191 pm 2 F at 237 pm
$KCuAlF_6$	2 F at 188 pm 4 F at 220 pm
CrF_2	4 F at 200 pm 2 F at 243 pm
$KCrF_3$	4 F at 214 pm 2 F at 200 pm
MnF_3	2 F at 209 pm 2 F at 191 pm 2 F at 179 pm

The Jahn-Teller Theorem predicts that distortions should occur for *any degenerate state*, including degeneracy of the t_{2g} level, however distortions in bond lengths are much more distinctive when the degenerate electrons are in the e_g level.

References

1. Jahn, H. A.; Teller, E. *Proc. R. Soc. London A*, **1937**, *161*, 220-235. DOI: 10.1098/rspa.1937.0142
2. Housecroft, C.; Sharpe, A. G. *Inorganic Chemistry*. Prentice Hall, 3rd Ed., 2008, p. 644. ISBN: 978-0-13-175553-6
3. Billy, C.; Haendler, H. A. *J. Am. Chem. Soc.*, **1957**, *79*, 1049–1051. DOI: 10.1021/ja01562a011

References

- Janes, R.; Moore, E. A. *Metal-ligand bonding*. The Open University, 2004, p. 23. ISBN 0-85404-979-7
- P.T.Miller, P.G.Lenhert and M.D.Joesten, *Inorg. Chem.*, 11, 2221, 1972.
- J.S.Wood, C.P.Keijzers and R.O.Day, *Acta Crystallogr., Sect.C (Cr. Str. Comm.)*, 40, 404, 1984.
- M.D.Joesten, M.S.Hussain and P.G.Lenhert, *Inorg. Chem.*, 9, 151, 1970.

Practice Questions

1. Why do d^3 complexes not show Jahn-Teller distortions?
2. Does the spin system (high spin v. low spin) of a molecule play a role in Jahn-Teller effects?
3. What spectroscopic method would one utilize in order to observe Jahn-Teller distortions in a diamagnetic molecule?
4. What spectroscopic method(s) would one utilize in order to observe Jahn-Teller distortions in a paramagnetic molecule?
5. Why are Jahn-Teller effects most prevalent in inorganic (transition metal) compounds?

Answers

1. Complexes with d^3 electron configurations do not show Jahn-Teller distortions because there is no ground state degeneracy.
2. Yes. Examining the d^5 electron configuration, one finds that the high spin scenario contains all singly occupied d orbitals (no degeneracy). However, the low spin d^5 electron configuration shows degeneracy, which then leads to possible Jahn-Teller effects.
3. UV-VIS absorption spectroscopy is one of the most common techniques for observing these effects. In general, it is independent of magnetism (diamagnetic v. paramagnetic). Thus, one would see the effect in the spectrum of UV-VIS absorption analysis. Note that EPR requires at least one unpaired electron, and therefore not EPR active.
4. Inorganic, specifically transition metal, complexes are most prevalent in showing Jahn-Teller distortions due to the availability of d orbitals. The most common geometry that the Jahn-Teller effect is observed is in octahedral complexes (see **Figures 2, 4, 5** and **6** above) due to the splitting of d orbitals into two degenerate sets. Due to stabilization, the degeneracies are removed, making a lower symmetry and lower energy molecule.

5. In addition to UV-VIS absorption, one can also employ EPR spectroscopy if a molecule possesses and unpaired electron.

Contributors and Attributions

- Kamran Ghiassi (UC Davis)
- Prof. Robert J. Lancashire (The Department of Chemistry, University of the West Indies)

5.6.5: Jahn-Teller Distortions is shared under a not declared license and was authored, remixed, and/or curated by LibreTexts.

- **Jahn-Teller Distortions** is licensed CC BY-NC-SA 4.0.

5.6.6: Magnetic Moments of Transition Metals

Magnetic moments are often used in conjunction with electronic spectra to gain information about the valence and stereochemistry of the central metal atom in coordination complexes. A common laboratory procedure for the determination of the magnetic moment for a complex is the Gouy method which involves weighing a sample of the complex in the presence and absence of a magnetic field and observing the difference in weight. A template is provided for the calculations involved.

For first row transition metal ions in the free ion state, i.e. isolated ions in a vacuum, all 5 of the 3d orbitals are degenerate.

A simple crystal field theory approach to the bonding in these ions assumes that when they form octahedral complexes, the energy of the d orbitals are no longer degenerate but are split such that two orbitals, the d_{x2-y2} and the d_{z2} (e_g subset) are at higher energy than the d_{xy}, d_{xz}, d_{yz} orbitals (the t_{2g} subset).

For octahedral ions with between 4 and 7 d electrons, this gives rise to 2 possible arrangements called either high spin/weak field or low spin/strong field respectively. The energy gap is dependent on the position of the coordinated ligands in the SPECTROCHEMICAL SERIES.

Note

A good starting point is to assume that all Co(III), d^6 complexes are octahedral and LOW spin, i.e. t_{2g}^6.

In tetrahedral complexes, the energy levels of the orbitals are again split, such that the energy of two orbitals, the $d_{x^2-y^2}$ and the d_{z^2} (e subset) are now at lower energy (more favored) than the remaining three d_{xy}, d_{xz}, d_{yz} (the t_2 subset) which are destabilized.

> *Tetrahedral complexes are ALL high spin since the difference between the 2 subsets of energies of the orbitals is much smaller than is found in octahedral complexes.*

The usual relationship quoted between them is:

$$\Delta_{tet} \approx \frac{4}{9}\Delta_{oct} \tag{5.6.6.1}$$

Square planar complexes are less common than tetrahedral and d^8 e.g. Ni(II), Pd(II), Pt(II), etc, have a strong propensity to form square planar complexes. As with octahedral complexes, the energy gap between the d_{xy} and $d_{x^2-y^2}$ is Δ_{oct} and these are considered strong field / low spin hence they are all diamagnetic, μ=0 Bohr Magneton (B.M.)

The formula used to calculate the spin-only magnetic moment can be written in two forms; the first based on the number of unpaired electrons, n, and the second based on the electron spin quantum number, S. Since for each unpaired electron, $n = 1$ and $S = 1/2$ then the two formulae are related and the answer obtained must be identical.

$$\mu_{so} = \sqrt{n(n+2)} \tag{5.6.6.2}$$

$$\mu_{so} = \sqrt{4S(S+1)} \tag{5.6.6.3}$$

Comparison of calculated spin-only magnetic moments with experimental data for some octahedral complexes

Metal	Config	μ_{so} / B.M.	μ_{obs} / B.M.
Ti(III)	d^1 (t_{2g}^1)	√3 = 1.73	1.6-1.7
V(III)	d^2 (t_{2g}^2)	√8 = 2.83	2.7-2.9
Cr(III)	d^3 (t_{2g}^3)	√15 = 3.88	3.7-3.9
Cr(II)	d^4 high spin (t_{2g}^3 e_g^1)	√24 = 4.90	4.7-4.9
Cr(II)	d^4 low spin (t_{2g}^4)	√8 = 2.83	3.2-3.3
Mn(II)/ Fe(III)	d^5 high spin (t_{2g}^3 e_g^2)	√35 = 5.92	5.6-6.1
Mn(II)/ Fe(III)	d^5 low spin (t_{2g}^5)	√3 = 1.73	1.8-2.1
Fe(II)	d^6 high spin (t_{2g}^4 e_g^2)	√24 = 4.90	5.1-5.7
Co(III)	d^6 low spin (t_{2g}^6)	0	0
Co(II)	d^7 high spin (t_{2g}^5 e_g^2)	√15 = 3.88	4.3-5.2
Co(II)	d^7 low spin (t_{2g}^6 e_g^1)	√3 = 1.73	1.8
Ni(II)	d^8 (t_{2g}^6 e_g^2)	√8 = 2.83	2.9-3.3
Cu(II)	d^9 (t_{2g}^6 e_g^3)	√3 = 1.73	1.7-2.2

Comparison of calculated spin-only magnetic moments with experimental data for some tetrahedral complexes

Ion	Config	μ_{so} / B.M.	μ_{obs} / B.M.
Cr(V)	d^1 (e^1)	√3 = 1.73	1.7-1.8
Cr(IV) / Mn(V)	d_2 (e^2)	√8 = 2.83	2.6 - 2.8
Fe(V)	d^3 (e^2 t_2^1)	√15 = 3.88	3.6-3.7
-	d^4 (e^2 t_2^2)	√24 = 4.90	-
Mn(II)	d^5 (e^2 t_2^3)	√35 = 5.92	5.9-6.2
Fe(II)	d^6 (e^3 t_2^3)	√24 = 4.90	5.3-5.5
Co(II)	d^7 (e^4 t_2^3)	√15 = 3.88	4.2-4.8
Ni(II)	d^8 (e^4 t_2^4)	√8 = 2.83	3.7-4.0
Cu(II)	d^9 (e^4 t_2^5)	√3 = 1.73	-

Contributors and Attributions

- Prof. Robert J. Lancashire (The Department of Chemistry, University of the West Indies)

5.6.6: Magnetic Moments of Transition Metals is shared under a not declared license and was authored, remixed, and/or curated by LibreTexts.

5.6.7: Magnetism

Movement of an electrical charge (which is the basis of electric currents) generates a magnetic field in a material. Magnetism is therefore a characteristic property of all materials that contain electrically charged particles and for most purposes can be considered to be entirely of electronic origin.

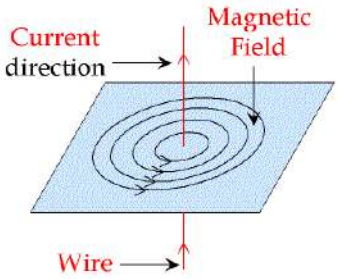


Figure 5.6.7.1: The Right Hand Rule for an induced magnetic field

In an atom, the magnetic field is due to the coupled spin and orbital magnetic moments associated with the motion of electrons. The spin magnetic moment is due to the precession of the electrons about their own axes whereas the orbital magnetic moment is due to the motion of electrons around the nucleus. The resultant combination of the spin and orbital magnetic moments of the constituent atoms of a material gives rise to the observed magnetic properties.

Historically, magnetism has been recognized for thousands of years. An account, that is probably apochryphal, tells of a shepherd called Magnes in Crete who around 900 B.C discovered the naturally occurring magnet lodestone (a form of the the spinel magnetite, Fe_3O_4) in a region later named Magnesia. Supposedly while he was walking over a deposit, the lodestone pulled the nails out of his sandals and the metal tip from his staff.

The Classical Theory of Magnetism

The classical theory of magnetism was well developed before quantum mechanics. Lenz's Law states that when a substance is placed within a magnetic field, $\boldsymbol{H}$, the field within the substance, $\boldsymbol{B}$, differs from $\boldsymbol{H}$ by the induced field, $\boldsymbol{4\pi I}$, which is proportional to the intensity of magnetization, $\boldsymbol{I}$. That is;

$$\boldsymbol{B = H + 4\pi I} \tag{5.6.7.1}$$

where $\boldsymbol{B}$ is the magnetic field within the substance and $\boldsymbol{H}$ is the applied magnetic field and $\boldsymbol{I}$ is the intensity of magnetization

Lenz's Law (1834)

Lenz's Law can also be written as

$$\frac{\boldsymbol{B}}{\boldsymbol{H}} = 1 + \frac{\boldsymbol{4\pi I}}{\boldsymbol{H}} \tag{5.6.7.2}$$

or

$$\frac{\boldsymbol{B}}{\boldsymbol{H}} = 1 + \boldsymbol{4\pi\kappa} \tag{5.6.7.3}$$

where

- $\boldsymbol{B/H}$ is called the magnetic permeability of the material and
- $\boldsymbol{\kappa}$ is the magnetic susceptibility per unit volume, (I/H)

By definition, $\boldsymbol{\kappa}$ in a vacuum is zero, so under those conditions the equation would reduce to $\boldsymbol{B = H}$. It is usually more convenient to measure mass than volume and the mass susceptibility, $\boldsymbol{\chi_g}$, is related to the volume susceptibility, $\boldsymbol{\kappa}$, through the density.

$$\boldsymbol{\chi_g = \frac{\kappa}{\rho}} \tag{5.6.7.4}$$

where ρ is the density.

Finally to get our measured quantity on a basis that can be related to atomic properties, we convert to molar susceptibility

$$\chi_m = \chi_g \times RMM \tag{5.6.7.5}$$

Since this value includes the underlying diamagnetism of paired electrons, it is necessary to correct for the diamagnetic portion of χ_m to get a corrected paramagnetic susceptibility.

$$\chi'_m = \chi_m + \chi_{dia} \tag{5.6.7.6}$$

Examples of these corrections are tabulated below.

Table **5.6.7.1**: Table of Diamagnetic Corrections (Pascal's constants, 10^{-6} c.g.s. units)

Ion	DC	Ion	DC
Na^+	6.8	Co^{2+}	12.8
K^+	14.9	Co^{3+}	12.8
NH_4^+	13.3	Ni^{2+}	12.8
Hg^{2+}	40	VO^{2+}	12.5
Fe^{2+}	12.8	Mn^{3+}	12.5
Fe^{3+}	12.8	Cr^{3+}	12.5
Cu^{2+}	12.8	Cl^-	23.4
Br^-	34.6	SO_4^{2-}	40.1
I^-	50.6	OH^-	12
NO_3^-	18.9	$C_2O_4^{2-}$	34
ClO_4^-	32	OAc^-	31.5
IO_4^-	51.9	pyr	49.2
CN^-	13	Me-pyr	60
NCS^-	26.2	$Acac^-$	62.5
H_2O	13	en	46.3
$EDTA^{4-}$	~150	urea	33.4

these can be converted to S.I units of $m^3\ mol^{-1}$ by multiplying by $4\ \pi \times 10^{-7}$

There are numerous methods for measuring magnetic susceptibilities, including, the **Gouy, Evans and Faraday methods**. These all depend on measuring the force exerted upon a sample when it is placed in a magnetic field. The more paramagnetic the sample, the more strongly it will be drawn toward the more intense part of the field.

Determination of Magnetic Susceptibility

- **The Gouy Method:** The underlying theory of the Gouy method is described here and a form for calculating the magnetic moment from the collected data is available as well.
- **The Evans method:** The Evans balance measures the change in current required to keep a pair of suspended magnets in place or balanced after the interaction of the magnetic field with the sample. The Evans balance differs from that of the Gouy in that, in the former the permanent magnets are suspended and the position of the sample is kept constant while in the latter the position of the magnet is constant and the sample is suspended between the magnets.

Orbital contribution to magnetic moments

From a quantum mechanics viewpoint, the magnetic moment is dependent on both spin and orbital angular momentum contributions. The spin-only formula used last year was given as:

$$\mu_{s.o.} = \sqrt{4S(S+1)} \tag{5.6.7.7}$$

and this can be modified to include the orbital angular momentum

$$\mu_{S+L} = \sqrt{4S(S+1) + L(L+1)} \tag{5.6.7.8}$$

An orbital angular momentum contribution is expected when the ground term is triply degenerate (i.e. a triplet state). These show temperature dependence as well.

In order for an electron to contribute to the orbital angular momentum the orbital in which it resides must be able to transform into an exactly identical and degenerate orbital by a simple rotation (it is the rotation of the electrons that induces the orbital contribution). For example, in an octahedral complex the degenerate t_{2g} set of orbitals (d_{xz},d_{yx},d_{yz}) can be interconverted by a 90^o rotation. However the orbitals in the e_g subset (d_{z^2},$d_{x^2-y^2}$) cannot be interconverted by rotation about any axis as the orbital shapes are different; therefore an electron in the e_g set does not contribute to the orbital angular momentum and is said to be quenched. In the free ion case the electrons can be transformed between any of the orbitals as they are all degenerate, but there will still be partial orbital quenching as the orbitals are not identical.

Electrons in the t_{2g} set do not always contribute to the orbital angular moment. For example in the d^3, t_{2g}^3 case, an electron in the d_{xz} orbital cannot by rotation be placed in the d_{yz} orbital as the orbital already has an electron of the same spin. This process is also called quenching.

Tetrahedral complexes can be treated in a similar way with the exception that we fill the e orbitals first, and the electrons in these do not contribute to the orbital angular momentum. The tables in the links below give a list of all d^1 to d^9 configurations including high and low spin complexes and a statement of whether or not a direct orbital contribution is expected.

- Octahedral complexes
- Tetrahedral complexes

Contributors and Attributions

- Prof. Robert J. Lancashire (The Department of Chemistry, University of the West Indies)

5.6.7: Magnetism is shared under a not declared license and was authored, remixed, and/or curated by LibreTexts.

5.6.8: Thermodynamics and Structural Consequences of d-Orbital Splitting

The energy level splitting of the d-orbitals due to their interaction with the ligands in a complex has important structural and thermodynamic effects on the chemistry of transition-metal complexes. Although these two types of effects are interrelated, they are considered separately here.

Structural Effects

There are two major kinds of structural effects: effects on the ionic radii of metal ions with regular octahedral or tetrahedral geometries, and structural distortions observed for specific electron configurations.

Ionic Radii

Figure 5.6.8.1 is a plot of the ionic radii of the divalent fourth-period metal ions versus atomic number. The dashed line represents the behavior predicted based on the effects of screening and variation in effective nuclear charge (Z_{eff}), assuming a spherical distribution of the 3d electrons. Because these radii are based on the structures of octahedral complexes and Cr^{2+} and Cu^{2+} do not form truly octahedral complexes, the points for these ions are shown as open circles.

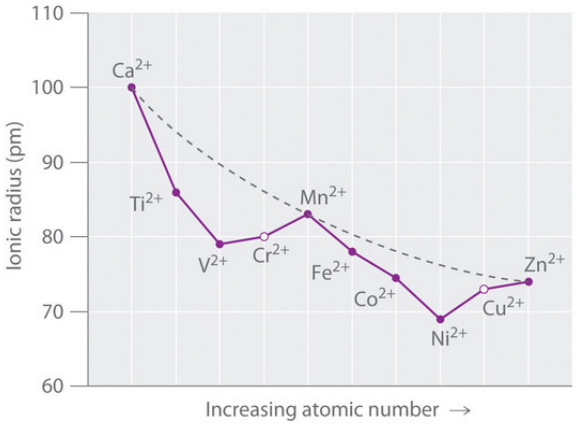


Figure 5.6.8.1: The Effect of d-Orbital Splittings on the Radii of the Divalent Ions of the Fourth-Period Metals. Only $Ca^{2+}(d^0)$, Mn^{2+} (high-spin d^5), and Zn^{2+} (d^{10}) lie on the smooth dashed curve. All other divalent ions fall below this curve because they have asymmetrical distributions of d electrons. To explain why an asymmetrical distribution of d electrons makes a metal ion smaller than expected, consider the Ti^{2+} ion, which has a d^2 configuration with both electrons in the t_{2g} orbitals. Because the t_{2g} orbitals are directed between the ligands, the two d-electrons are unable to shield the ligands from the nuclear charge. Consequently, the ligands experience a higher effective nuclear charge than predicted, the metal–ligand distance is unusually short, and the ionic radius is smaller than expected. If instead the two electrons were distributed uniformly over all five d orbitals, they would be much more effective at screening the ligands from the nuclear charge, making the metal–ligand distances longer and giving the metal a larger ionic radius.

A similar effect is observed for the V^{2+} ion, which has a d^3 configuration. Because the three electrons in the t_{2g} orbitals provide essentially no shielding of the ligands from the metal, the ligands experience the full increase of +1 in nuclear charge that occurs from Ti^{2+} to V^{2+}. Consequently, the observed ionic radius of the V^{2+} ion is significantly smaller than that of the Ti^{2+} ion.

Skipping the Cr^{2+} ion for the moment, consider the d^5 Mn^{2+} ion. Because the nuclear charge increases by +2 from V^{2+} to Mn^{2+}, Mn^{2+} might be expected to be smaller than V^{2+}. The two electrons added from V^{2+} to Mn^{2+} occupy the e_g orbitals, however, which are oriented directly toward the six ligands. Because these electrons are localized directly between the metal ion and the ligands, they are effective at screening the ligands from the increased nuclear charge. As a result, the ionic radius actually increases significantly from V^{2+} to Mn^{2+}, despite the higher nuclear charge of the latter.

The same effects are observed in the second half of the first-row transition metals. In the Fe^{2+}, Co^{2+}, and Ni^{2+} ions, the extra electrons are added successively to the t_{2g} orbitals, resulting in increasingly poor shielding of the ligands from the nuclei and in abnormally small ionic radii. Skipping over Cu^{2+}, adding the last two electrons causes a significant increase in the ionic radius of Zn^{2+}, despite its greater nuclear charge.

The Jahn–Teller Effect

Because simple octahedral complexes are not observed for the Cr^{2+} and Cu^{2+} ions, only estimated values for their radii are shown in Figure **5.6.8.1**. Since both Cr^{2+} and Cu^{2+} ions have electron configurations with an odd number of electrons in the e_g orbitals. Because the single electron (in the case of Cr^{2+}) or the third electron (in the case of Cu^{2+}) can occupy either one of two degenerate e_g orbitals, both systems have degenerate ground states. The Jahn–Teller theorem states that such non-linear systems are not stable; they undergo a distortion that makes the complex less symmetrical and splits the degenerate states, which decreases the energy of the system. The distortion and resulting decrease in energy are collectively referred to as the Jahn–Teller effect. Neither the nature of the distortion nor its magnitude is specified, and in fact, they are difficult to predict. In principle, Jahn–Teller distortions are possible for many transition-metal ions; in practice, however, they are observed only for systems with an odd number of electrons in the e_g orbitals, such as the Cr^{2+} and Cu^{2+} ions.

Consider an octahedral Cu^{2+} complex, $[Cu(H_2O)_6]^{2+}$, which is elongated along the z axis. As indicated in Figure **5.6.8.2**, this kind of distortion splits both the e_g and t_{2g} sets of orbitals. Because the axial ligands interact most strongly with the d_{z^2} orbital, the splitting of the e_g set (δ_1) is significantly larger than the splitting of the t_{2g} set (δ_2), but both δ_1 and δ_2 are much, much smaller than the Δ_o. This splitting does not change the centerpoint of the energy within each set, so a Jahn–Teller distortion results in no net change in energy for a filled or half-filled set of orbitals. If, however, the e_g set contains one electron (as in the d^4 ions, Cr^{2+} and Mn^{3+}) or three electrons (as in the d^9 ion, Cu^{2+}), the distortion decreases the energy of the system. For Cu^{2+}, for example, the change in energy after distortion is $2(-\delta_1/2) + 1(\delta_1/2) = -\delta_1/2$. For Cu^{2+} complexes, the observed distortion is always an elongation along the z axis by as much as 50 pm; in fact, many Cu^{2+} complexes are distorted to the extent that they are effectively square planar. In contrast, the distortion observed for most Cr^{2+} complexes is a compression along the z axis. In both cases, however, the net effect is the same: the distorted system is more stable than the undistorted system.

Jahn–Teller distortions are most important for d^9 and high-spin d^4 complexes; the distorted system is more stable than the undistorted one.

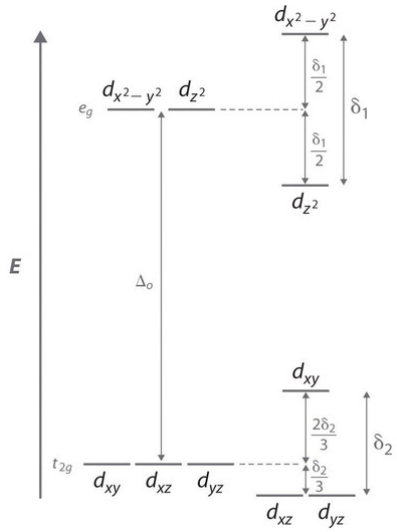


Figure **5.6.8.2**: The Jahn–Teller Effect

Increasing the axial metal–ligand distances in an octahedral d^9 complex is an example of a Jahn–Teller distortion, which causes the degenerate pair of e_g orbitals to split in energy by an amount δ_1; δ_1 and δ_2 are much smaller than Δ_o. As a result, the distorted system is more stable (lower in energy) than the undistorted complex by $\delta_1/2$.

Thermodynamic Effects

As previously noted, crystal field splitting energies (CFSEs) can be as large as several hundred kilojoules per mole, which is the same magnitude as the strength of many chemical bonds or the energy change in most chemical reactions. Consequently, CFSEs are important factors in determining the magnitude of hydration energies, lattice energies, and other thermodynamic properties of the transition metals.

Hydration Energies

The hydration energy of a metal ion is defined as the change in enthalpy for the following reaction:

$$M^{2+}_{(g)} + H_2O_{(l)} \rightarrow M^{2+}_{(aq)} \tag{5.6.8.1}$$

Although hydration energies cannot be measured directly, they can be calculated from experimentally measured quantities using thermochemical cycles. In Figure **5.6.8.3*a***, a plot of the hydration energies of the fourth-period metal dications versus atomic number forms a curve with two valleys. Note the relationship between the plot in Figure **5.6.8.3*a*** and the plot of ionic radii in Figure **5.6.8.1** the overall shapes are essentially identical, and only the three cations with spherically symmetrical distributions of d electrons (Ca^{2+}, Mn^{2+}, and Zn^{2+}) lie on the dashed lines. In Figure **5.6.8.3*a***, the dashed line corresponds to hydration energies calculated based solely on electrostatic interactions. Subtracting the CFSE values for the $[M(H_2O)_6]^{2+}$ ions from the experimentally determined hydration energies gives the points shown as open circles, which lie very near the calculated curve. Therefore, CFSEs are primarily responsible for the differences between the measured and calculated values of hydration energies.

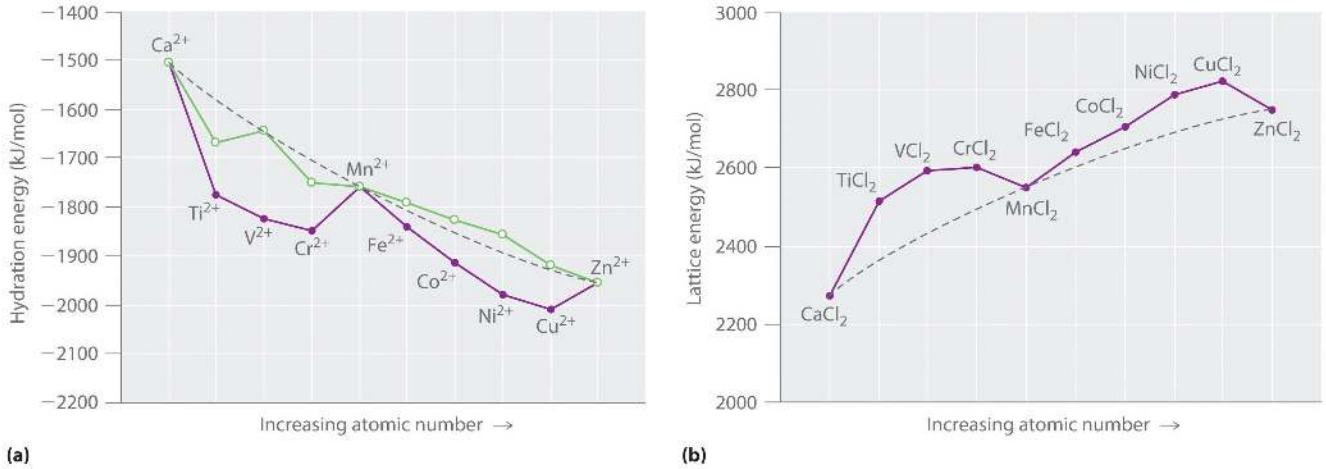


Figure **5.6.8.3**: Thermochemical Effects of d-Orbital Splittings. (a) A plot of the hydration energies of the divalent fourth-period metal ions versus atomic number (solid circles) shows large deviations from the smooth curve calculated, assuming a spherical distribution of d electrons (dashed line). Correcting for CFSE gives the points shown as open circles, which, except for Ti^{2+} and Cr^{2+}, are close to the calculated values. The apparent deviations for these ions are caused by the fact that solutions of the Ti^{2+} ion in water are not stable, and Cr^{2+} does not form truly octahedral complexes. (b) A plot of the lattice energies for the fourth-period metal dichlorides versus atomic number shows similar deviations from the smooth curve calculated, assuming a spherical distribution of d electrons (dashed lines), again illustrating the importance of CFSEs.

Lattice Energies

Values of the lattice energies for the fourth-period metal dichlorides are plotted against atomic number in part (b) of Figure **5.6.8.3**. Recall that the lattice energy is defined as the negative of the enthalpy change for the reaction below. Like hydration energies, lattice energies are determined indirectly from a thermochemical cycle.

$$M^{2+}(g) + 2Cl^-(g) \rightarrow MCl_2(s) \tag{5.6.8.2}$$

The shape of the lattice-energy curve is essentially the mirror image of the hydration-energy curve in part (a) of Figure **5.6.8.3**, with only Ca^{2+}, Mn^{2+}, and Zn^{2+} lying on the smooth curve. It is not surprising that the explanation for the deviations from the curve is exactly the same as for the hydration energy data: all the transition-metal dichlorides, except $MnCl_2$ and $ZnCl_2$, are more stable than expected due to CFSE.

Summary

Distorting an octahedral complex by moving opposite ligands away from the metal produces a tetragonal or square planar arrangement, in which interactions with equatorial ligands become stronger. Because none of the d orbitals points directly at the ligands in a tetrahedral complex, these complexes have smaller values of the crystal field splitting energy Δ_t. The crystal field stabilization energy (CFSE) is the additional stabilization of a complex due to placing electrons in the lower-energy set of d orbitals. CFSE explains the unusual curves seen in plots of ionic radii, hydration energies, and lattice energies versus atomic

number. The Jahn–Teller theorem states that a non-linear molecule with a spatially degenerate electronic ground state undergoes a geometrical distortion to remove the degeneracy and lower the overall energy of the system.

5.6.8: Thermodynamics and Structural Consequences of d-Orbital Splitting is shared under a CC BY-NC-SA 4.0 license and was authored, remixed, and/or curated by LibreTexts.

5.7: Ligand Field Theory

Ligand Field Theory (LFT) can be considered an extension of Crystal Field Theory such that all levels of covalent interactions can be incorporated into the model. LFT describes the bonding, orbital arrangement, and other characteristics of coordination complexes. It represents an application of molecular orbital theory to transition metal complexes. A transition metal has nine valence atomic orbitals: five nd, one (n+1)s, and three (n+1)p orbitals. These orbitals are of appropriate energy to form bonding interaction with ligands. The LFT analysis is highly dependent on the geometry of the complex, but will begin by examining octahedral complexes.

Treatment of the bonding in LFT is generally done using molecular orbital theory. A qualitative approach using generator functions and LGOs can be applied to these compounds just as we did previously. For the purpose of this discussion, we will consider the octahedral complex ion $[Co(NH_3)_6]^{3+}$. There are several assumptions that we must make in this approach.

1. The 4s, 4p and 3d orbitals are of the correct energy to interact with the nitrogen donor atoms of the NH_3 ligands.
2. As the NH_3 ligands are L-type ligands and will not participate in any π-bonding with the cobalt, we can treat the nitrogen atoms as though they were hydrogen atoms. This means our MO diagram will not account for any N-H bonding. As there are 18 N-H bonds in the complex, it certainly simplifies matters by choosing to ignore this.

Step 1 - Drawing the structure and determining the hybridization of the central atom

The geometry of the complex has already been specified and the structure of the complex is depicted below (Figure 5.7.1).

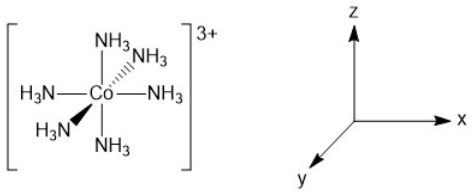


Figure 5.7.1. Structure and assigned axes for $[Co(NH_3)_6]^{3+}$.

Exercise 5.7.1

Using rules for VSEPR, what orbitals need to be used for hybridization of the central cobalt atom? Be as specific as possible about the orbitals.

Answer

The cobalt would be treated as AX_6E_0 and so would be sp^3d^2 hybridized.

The orbitals involved would be the 4s, 4p and two of the 3d orbitals. For the 3d orbitals, we can decide which ones to involve based on the assigned axes. As we are making σ-bonds, the orbitals involved must be pointing at the incoming ligands. In this geometry that means we much use the d_{z^2} and $d_{x^2-y^2}$ orbitals.

Step 2 - Determine the point group of the complex and assign the generator functions

The molecule is octahedral and so the point group is O_h. The O_h character table is rather robust and so only the abbreviated version will appear here.

O_h	Orbitals
A_{1g}	s
A_{2g}	
E_g	d_{z^2}, $d_{x^2-y^2}$
T_{1g}	
T_{2g}	d_{xy}, d_{yz}, d_{xz}
A_{1u}	
A_{2u}	
E_u	
T_{1u}	p_x. p_y, p_z
T_{2u}	

Exercise 5.7.2

What are the symmetry labels for the cobalt orbitals used to make $[Co(NH_3)_6]^{3+}$?.

Answer

- s - a_{1g}
- p_x - t_{1u}
- p_y - t1u
- p_z - t_{1u}
- d_{z^2} - e_g
- $d_{x^2-y^2}$ - e_g

Step 3 - Making the LGOs

As we have done previously, we will consider all of the potential interactions between the metal orbitals and ligand orbitals using a pictorial method. Based on the axes assigned above, the matching LGOs can be drawn as shown (Figure 5.7.2).

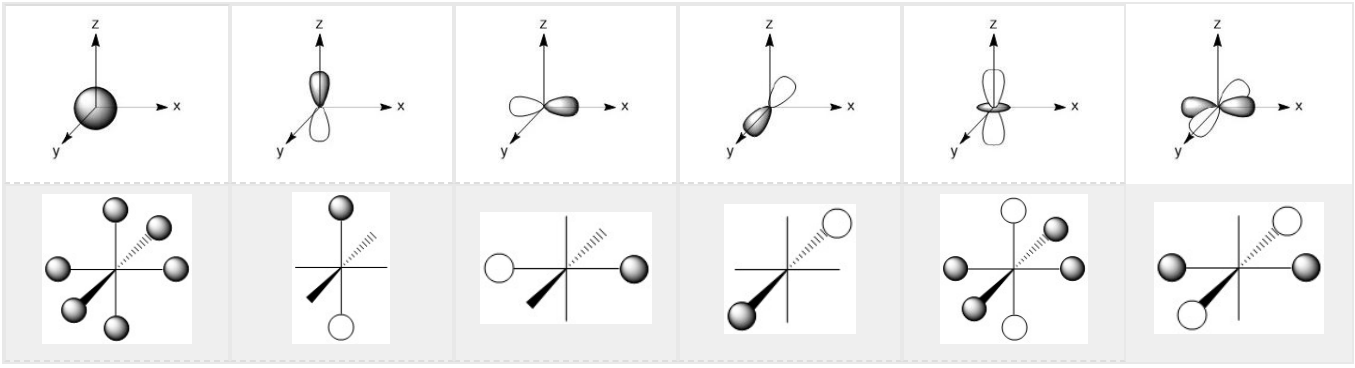


Figure 5.7.2. LGOs $[Co(NH_3)_6]^{3+}$.

Step 4 - Constructing the MO diagram

Previously when we were building MO diagrams we would start by looking at the orbital energies. In this case, doing this is a little more complicated. One complication is that the ligand is NH_3 and so we can not just use the orbital energy for nitrogen. Another complication is that the orbital energies for transition metals in various valence states are not as readily available. However, we can make some reasonable approximations. From WebMO, the orbital energies for Co(III) are 3d (-12.12 eV), 4s (-8.10 eV), and 4p (-5.290 eV). The lone pair in NH_3 would be the HOMO and from WebMO the energy of this orbital was calculated to be -13.702 eV. The general trend here is that the ligand orbitals are lower in energy than the metal orbitals. Once again we match the symmetry labels and if there is a match on the metal and the LGOs, we make bonding and antibonding orbitals. The t_{2g} orbitals on the metal do not have a match among the LGOs and so they will make non-bonding orbitals that do not change in energy much from the original metal d-orbitals. The rest of the metal orbitals have a match with the LGOs and so we get the diagram below (Figure **5.7.3**).

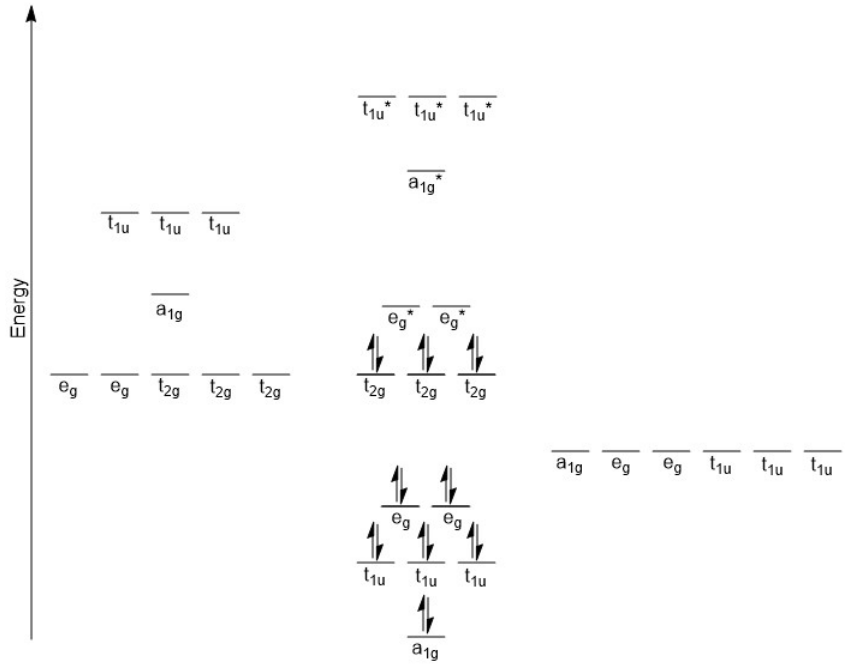


Figure 5.7.3. MO diagram for $[Co(NH_3)_6]^{3+}$.

This diagram likely raises a number of questions. One likely question would be the ordering of the bonding MOs. The e_g orbitals on the cobalt are the lowest energy, and yet they make the highest energy bonding MOs. Recall from our previous discussion that d-orbitals are not terribly good at forming bonding interactions. The s- and p-orbitals are much better at interacting with the incoming ligands and as such, give rise to lower energy bonding MOs. The a_{1g} orbital is based on the 4s orbital of cobalt which is lower in energy than the 4p orbitals which are t_{1u}. Somewhat similar logic can be applied to the antibonding orbitals. Since the e_g orbitals are not very good at forming bonding interactions, their antibonding interactions (e_g*) will not be quite as high in energy. The ordering of the a_{1g}* and t_{1u}* orbitals is a bit more difficult to rationalize. However, when considering the electron configuration of a cobalt atom ([Ar] $4s^2$ $3d^7$), the 4p orbitals are unoccupied. In fact, it may have seemed a bit odd to even consider these orbitals in the hybridization. They are certainly higher in energy and as the t_{1u}* orbitals are more localized on the cobalt, this could cause them to be higher in energy than the a_{1g}* orbital.

Another subtle point is that the d-orbital splitting that was previously discussed is found in this diagram. The MOs are labeled as t_{2g} and e_g*. The e_g* is slightly different than what we saw in the discussion on crystal field theory. However, these orbitals are closer in energy to the metal d-orbitals and as such are mostly metal d-orbital in character. It is common practice to refer to the t_{2g} and e_g* orbitals show in this diagram as the metal d-orbitals but realize there is antibonding character to the e_g* orbitals. In addition, this compound is drawn as being Low Spin, with the t_{2g} completely occupied and the e_g* unoccupied. Just building the

MO diagram there is no way to make that distinction. Looking at the spectrochemical series we see that NH_3 is towards the strong field end of the series so a Low Spin configuration is not unreasonable.

How did we do?

The calculations are a bit more involved for this complex. There are a total of 51 MOs for this complex cation, 18 from the 18 hydrogen atoms, 24 from the six nitrogen atoms and 9 from the cobalt. Pictorially, the 18 lowest energy MOs are mostly N-H in nature and will be ignored for this discussion. As there are multiple degenerate levels in the MO diagram, one representative orbital will be shown. The energy for the cobalt orbitals was calculated to be -13.180 eV (3d), -9.210 eV (4s) and -5.290 eV (4p). The energy of the HOMO for NH_3 was calculated to be -13.684 eV. This supports the idea that the orbitals from the ligands are lower in energy that those of the metal.

a_{1g}	t_{1u}	e_g	t_{2g}	e_g^*	a_{1g}^*	t_{1u}^*
						
-15.2 eV	-13.9 eV	-13.8 eV	-13.2 eV	-12.5 eV	20.7 eV	24.795 eV

Overall this isn't a bad match to our pictorial method. Overall the pictures help to visualize the orbitals and the energies do make sense with our rough approximations. The a_{1g}, t_{1u} and e_g orbitals are all lower in energy than the HOMO of NH_3. The t_{2g} orbitals are very similar to the energy of the 3d orbitals of cobalt. The e_g* orbitals are slightly higher in energy than the t_{2g} orbitals. The energy difference from this very rough calculation corresponds to an absorption of light with a wavelength of 1700 nm. While well outside the visible range and much larger than the actual value of approximately 470 nm displayed by the yellow $[Co(NH_3)_6]^{3+}$, this is a rough estimate made from fairly low level calculations.

Why did we choose NH_3?

The choice of NH_3 might seem a bit odd at first. Certainly a halide even with three lone pair would have been easier to deal with than NH_3. The choice of NH_3 was not by chance. The NH_3 ligand is purely σ-donating to the cobalt through the lone pair on the nitrogen atom. There are no other lone pair that could be donated to the cobalt to form and kind of π-bonding interaction. Although you may not think of halides as making π-bonds, the lone pair on the halides are capable of interacting in a π-bonding manner with an atom capable of accepting electrons. And it just so happens that the t_{2g} orbitals of a transition metal are of the proper symmetry and energy to interact with ligands capable of donating electrons to give a π-bonding interaction. While we would still draw a single bond (M-Cl) and not a double bond (M=Cl), we should appreciate that there is possibly some π-bonding interaction occurring in a M-Cl bond. In fact, all of the weak field ligands are capable of this sort of interaction to some extent.

An explanation for strong field ligands is also based on π-bonding arguments. However, in the case of strong field ligands, it is the metal that is providing the electrons in the π-bonding interaction. This interaction is a bit tougher to deal with. Unlike say the halide ligands, we never draw lone pair on metals. This means it is not always readily apparent that there are electrons on the metal available for π-bonding. However, as long as the metal does not have a d^0 configuration, we can consider that there are electrons in the t_{2g} orbitals that could be used for π-bonding. Even harder to visualize is how is the ligand going to be accepting these electrons. As we saw for weak field ligands, the key is that the ligand must have an orbital of the right symmetry and energy to be able to interact with a metal t_{2g} orbital. These orbitals are not readily apparent for many ligands. Consider the CO ligand which is called a carbonyl ligand (similar to an organic carbonyl, $R_2C{=}O$ but there are no groups on the carbon atom and so we draw a C≡O). The π-bonding interaction between the carbonyl and the metal involves the π* orbital of CO Figure **5.7.4**. Consider first the CO portion depicted. The orbitals are not drawn along the C-O bond axis. This tells us that we are dealing with some type of π-orbital. In the top half of the picture, the orbital is blue on the carbon atom and white on the oxygen atom. And these lobes point away from each other. The combination of the direction and the sign change indicate that this is a π* orbital. In addition (although it is a bit subtle in this picture), the lobes on the carbon atom are larger than the lobes on the oxygen atom. Antibonding orbitals are more localized on the LEAST electronegative atom where as bonding orbitals are localized on the more electronegative atom. This π* orbital of CO has the right symmetry and energy to give a boding interaction with a metal d-orbital. But way, we said this was a π* orbital. It

is...with respect to the carbon-oxygen bond. However, the interaction is bonding (as noted by the interaction of lobes with the same sign) with respect to the metal-carbon bond. In general, strong field ligands will share this ability to act as π-acceptors.

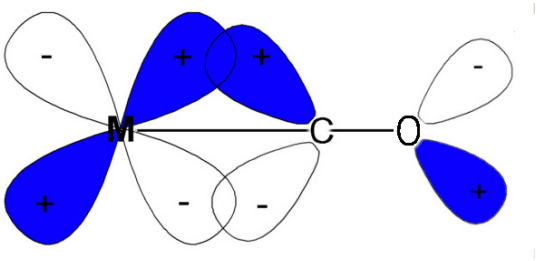


Figure 5.7.4. π interaction between a metal and a carbonyl ligand.

How does this impact our diagram for the metal d-orbitals? In both cases we consider the ligands to be interacting with the t_{2g} orbitals of the metal. In the case of a weak field ligand, the filled orbitals of the π-donating ligand are at a lower energy than the t_{2g} orbitals. The ligand orbitals and the t_{2g} orbitals interact to give π-bonding and π-antibonding orbitals. The π-antibonding orbitals will be more localized on the metal and they will get pushed up in energy relative to the starting t_{2g} orbitals. This will make them closer in energy to the e_g orbitals and therefore decrease Δ_o. With strong field ligands, the metal t_{2g} orbitals are lower in energy than the π-accepting orbitals of the ligands. These orbitals interact to give π-bonding and π-antibonding (with respect to the M-L) orbitals. The π-bonding orbital will go down in energy and be more metal in character. The moves it further away from the e_g orbitals and thus increases Δ_o. These interactions are illustrated below Figure 5.7.5).

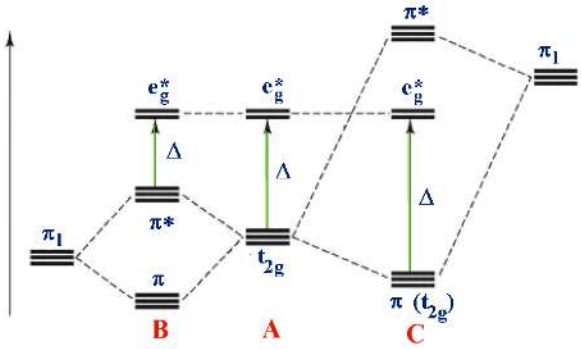


Figure 5.7.5. π interactions between a metal and its ligands (B: $[M(II)I_6]^{4-}$; A: $[M(II)(H_2O)_6]^{2+}$; C: $[M(II)(CN)_6]^{4-}$).

Contributors and Attributions

- Prof. Robert J. Lancashire (The Department of Chemistry, University of the West Indies)

5.7: Ligand Field Theory is shared under a not declared license and was authored, remixed, and/or curated by LibreTexts.

5.8: Ligand Exchange Reactions (Thermodynamics)

Replacing aqua ligands with ammine ligands

If you add ammonia solution to a solution containing hexaaquacopper(II) ions, $[Cu(H_2O)_6]^{2+}$, four of the water molecules are eventually replaced by ammonia molecules to give $[Cu(NH_3)_4(H_2O)_2]^{2+}$. This can be written as an equilibrium reaction to show the overall effect:

$$[Cu(H_2O)_6]^{2+} + 4\,NH_3 \rightleftharpoons [Cu(NH_3)_4(H_2O)_2]^{2+} + 4\,H_2O \tag{5.8.1}$$

In fact, the water molecules get replaced one at a time, and so this is made up of a series of part-reactions:

$$[Cu(H_2O)_6]^{2+} + NH_3 \rightleftharpoons [Cu(NH_3)(H_2O)_5]^{2+} + H_2O \tag{5.8.2}$$

$$[Cu(NH_3)(H_2O)_5]^{2+} + NH_3 \rightleftharpoons [Cu(NH_3)_2(H_2O)_4]^{2+} + H_2O \tag{5.8.3}$$

$$[Cu(NH_3)_2(H_2O)_4]^{2+} + NH_3 \rightleftharpoons [Cu(NH_3)_3(H_2O)_3]^{2+} + H_2O \tag{5.8.4}$$

$$[Cu(NH_3)_3(H_2O)_3]^{2+} + NH_3 \rightleftharpoons [Cu(NH_3)_4(H_2O)_2]^{2+} + H_2O \tag{5.8.5}$$

Although this can look a bit daunting at first sight, all that is happening is that first you have one, then two, then three, then four water molecules in total replaced by four ammine ligands.

Individual stability constants

Let's take a closer look at the first of these equilibria (Equation 5.8.2). Like any other equilibrium, this one has an equilibrium constant, K_c - except that in this case, we call it a stability constant. Because this is the first water molecule to be replaced, we call it K_1 and is given by this expression:

$$K_1 = \frac{[[Cu(NH_3)(H_2O)_5]^{2+}]}{[[Cu(H_2O)_6]^{2+}][NH_3]} \tag{5.8.6}$$

There are two points of possible confusion here - one minor, one more important!

- First, the square brackets have changed their meaning! Square brackets are often used to keep everything in a complex ion together and tidy. Here, they have reverted to their other use, which implies concentrations in mol dm^{-3}.
- In order to avoid complete confusion, the square brackets keeping the complexes together have been removed entirely.
- More importantly, if you compare the equilibrium constant expression with the equation, you will see that the water on the right-hand side hasn't been included. That is normal practice with these expressions.
- Because everything is dissolved in water, the water is present as a huge excess. Generating a little bit more during the reaction is going to make no effective difference to the total concentration of the water in terms of moles of water per dm^3.
- The concentration of the water is approximately constant. The equilibrium constant is defined so that you avoid having an extra unnecessary constant in the expression.

With that out of the way, let's go back to where we were - but introduce a value for K_1:

$$[Cu(H_2O)_6]^{2+} + NH_3 \rightleftharpoons [Cu(NH_3)(H_2O)_5]^{2+} + H_2O$$

$$K_1 = \frac{[Cu(NH_3)(H_2O)_5^{2+}]}{[Cu(H_2O)_6^{2+}]\,[NH_3]} = 1.78 \times 10^4\ mol^{-1}\ dm^3$$

The value of the equilibrium constant is fairly large, suggesting that there is a strong tendency to form the ion containing an ammonia molecule. A high value of a stability constant shows that the ion is easily formed. Each of the other equilibria above also has its own stability constant, K_2, K_3 and K_4. For example, K_2 is given by:

$$[Cu(NH_3)(H_2O)_5]^{2+} + NH_3 \rightleftharpoons [Cu(NH_3)_2(H_2O)_4]^{2+} + H_2O$$

$$K_2 = \frac{[Cu(NH_3)_2(H_2O)_4^{2+}]}{[Cu(NH_3)(H_2O)_5^{2+}]\,[NH_3]} = 4.07 \times 10^3 \ mol^{-1}\ dm^3$$

The ion with two ammonias is even more stable than the ion with one ammonia. You could keep plugging away at this and come up with the following table of stability constants:

ion	K_n	value (mol^{-1} dm^3)	log K_n
$[Cu(NH_3)(H_2O)_5]^{2+}$	K_1	1.78×10^4	4.25
$[Cu(NH_3)_2(H_2O)_4]^{2+}$	K_2	4.07×10^3	3.61
$[Cu(NH_3)_3(H_2O)_3]^{2+}$	K_3	9.55×10^2	2.98
$[Cu(NH_3)_4(H_2O)_2]^{2+}$	K_4	1.74×10^2	2.24

You will often find these values quoted as log K_1 or whatever. All this does is tidy the numbers up so that you can see the patterns more easily. The ions keep on getting more stable as you replace up to 4 water molecules, but notice that the equilibrium constants are gradually getting smaller as you replace more and more water ligands. This is common with individual stability constants.

Overall Formation constants

The overall stability constant is simply the equilibrium constant for the total reaction:

$$[Cu(H_2O)_6]^{2+} + 4NH_3 \rightleftharpoons [Cu(NH_3)_4(H_2O)_2]^{2+} + 4H_2O$$

It is given by this expression:

$$\text{overall } K_{stab} = \frac{[Cu(NH_3)_4(H_2O)_2^{2+}]}{[Cu(H_2O)_6^{2+}]\,[NH_3]^4} = 1.20 \times 10^{13} \ mol^{-4}\ dm^{12}$$

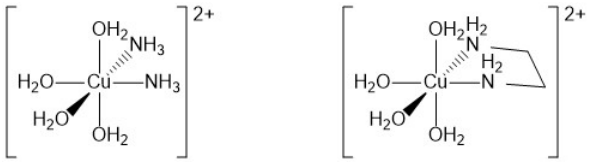
You can see that overall this is a very large equilibrium constant, implying a high tendency for the ammonia ligands to replace the water ligands. The "log" value is 13.1. This overall value is found by multiplying together all the individual values of K_1, K_2 and so on. To find out why that works, write down expressions for all the individual values (the first two are done for you above), and then multiply those expressions together. You will find that all the terms for the intermediate ions cancel out to leave you with the expression for the overall stability constant.

Summary

Whether you are looking at the replacement of individual water molecules or an overall reaction producing the final complex ion, a stability constant is simply the equilibrium constant for the reaction you are looking at. The **larger** the value of the stability constant, the further the reaction lies to the **right**. That implies that complex ions with large stability constants are more stable than ones with smaller ones.

Stability constants and entropy - the chelate effect

The chelate effect is an effect which happens when you replace water (or other simple ligands) around the central metal ion by multidentate ligands like 1,2-diaminoethane (en) or EDTA. Compare what happens if you replace two water ligands around a $[Cu(H_2O)_6]^{2+}$ ion with either 2 ammonia ligands or one en ligand.



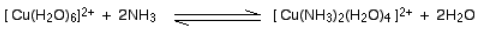
Chelates are much more stable than complex ions formed from simple monodentate ligands. The overall stability constants for the two ions are:

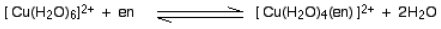
ion	log K
$[Cu(NH_3)_2(H_2O)_4]^{2+}$	7.86
$[Cu(H_2O)_4(en)]^{2+}$	10.6

The reaction with the 1,2-diaminoethane could eventually go on to produce a complex ion $[Cu(en)_3]^{2+}$. The overall stability constant for this (as log K) is 18.7. Another copper-based chelate comes from the reaction with EDTA. This also has a high stability constant - log K is 18.8. However many examples you take, you always find that a chelated complex is more stable than one with only monodentate ligands. This is known as the chelate effect.

The reason for the chelate effect

If you compare the two equilibria below, the one with the en has the higher equilibrium (stability) constant (for values, see above).





The enthalpy changes of the two reactions are fairly similar. You might expect this because in each case you are breaking two bonds between copper and oxygen atoms and replacing them by two bonds between copper and nitrogen atoms. However, when considering the reverse reaction there is a bit of a difference in enthalpy. If one Cu-N bond breaks, the NH_3 ligand can be replaced by a water ligand. However, for en to leave, both Cu-N bonds to the ligand must be broken. If only one Cu-N bond to en is broken, the unbound nitrogen atom remains in close proximity to the copper atom, making it very likely that it will just reform the Cu-N bond.

Another factor in the chelate effect is the difference has to do with the entropy change during each reaction.

Entropy is most easily thought of as a measure of disorder. Any change which increases the amount of disorder increases the tendency of a reaction to happen.

If you look again at the two equiilbria, you might notice that the en equilibrium does lead to an increase in the entropy. There are only two species on the left-hand side of the equation, but three on the right.

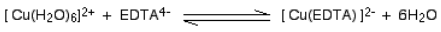


You can obviously get more entropy out of three species than out of only two. Compare that with the other equilibrium. In this case, there is no change in the total number of species before and after reaction, and so no useful contribution to an increase in

entropy.



In the case of the complex with EDTA, the increase in entropy is very pronounced.



Here, we are increasing the number of species present from two on the left-hand side to seven on the right. You can get a major amount of increase in disorder by making this change.

Reversing this last change is going to be far more difficult in entropy terms. You would have to move from a highly disordered state to a much more ordered one. That isn't so likely to happen, and so the copper-EDTA complex is very stable.

Summary

Complexes involving multidentate ligands are more stable than those with only monodentate ligands. The underlying reason for this is that each multidentate ligand displaces more than one water molecule. This leads to an increase in the number of species present in the system, and therefore an increase in entropy. An increase in entropy makes the formation of the chelated complex more favorable.

Contributors and Attributions

- Jim Clark (Chemguide.co.uk)

This page titled 5.8: Ligand Exchange Reactions (Thermodynamics) is shared under a CC BY-NC 4.0 license and was authored, remixed, and/or curated by Jim Clark.

5.9: Electronic Spectra of Coordination Compounds

Term Splitting for Octahedral d^2 metal complexes

At first glance, one might think that there is only one possible transition for the d-electrons in an octahedral compound with a d^2 configuration when it absorbs light. That transition would be one of the electrons in a t_{2g} orbital raising in energy to one of the e_g orbitals. One example of this is shown below (Figure **5.9.1**). This might lead you to think there is only one band (peak) in the visible absorption spectrum for d^2 complexes, but that is not the case. In order to explain the additional bands, there would have to be other possible transitions. Perhaps you might think that since the electrons in the t_{2g} orbitals are equal in energy either of them could move to the e_g. Similarly, the e_g orbitals are degenerate, so the electron could go to either of those orbitals. That could give multiple transitions, but they would all be the same energy as the one depicted.

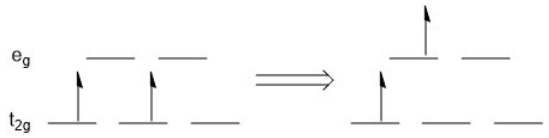


Figure 5.9.1. A possible transition for an electron in the t_{2g} orbital of a d^2 system.

What other transitions would be possible? The state shown above depicts the ground state electron configuration of a d^2 system. Remember back to general chemistry, the ground state follows Hund's rule in that the electrons are spread out and have the same spin. There are multiple possible excited states and these do not have to abide by Hund's rule, but they still must follow the Pauli exclusion principle. Several possible excited state configurations are shown below (Figure **5.9.2**).

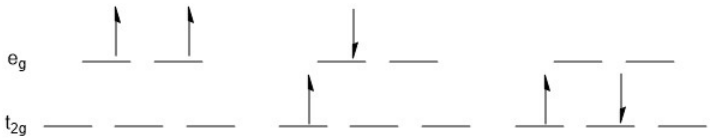


Figure 5.9.2. Additional possible excited states for a d^2 system.

To help keep track of all of the possible transitions, we use Term Symbols. Term Symbols are a method of accounting for electron-electron interactions in an atom. They are derived from the quantum numbers, in particular the values of m_l and m_s, associated with the electrons of interest. These term symbols take the form $^{2S+1}L_J$, where S represents the total spin angular momentum, L specifies the total orbital angular momentum, and J refers to the total angular momentum. How do we get these term symbols? The value of S comes from the sum of the m_s values for the electrons under consideration. As has typically been the case since general chemistry, the first electron we place is spin up or $+\frac{1}{2}$. So for the ground state shown in (Figure **5.9.1**) the value of S would be +1. The value of 2S+1 is called the multiplicity and in this example the multiplicity would equal three. This is referred to as a triplet or triplet state. The value of L comes from the sum of the m_l values. In the case above we are looking at d-orbitals. The possible m_l values are +2, +1, 0, -1 and -2. Standard practice is to begin filling the orbital with the highest value of m_l working to the lowest value. So for the ground state d^2 system, one electron would have a m_l or +2 and the other would be +1 giving a total of +3 as the value for L. However, L is not represented by this value, but rather a letter. This system is very similar to that used for the naming of atomic orbitals; an atomic orbital with an l value of 0 is an s-orbital while a term symbol with a L value of 0 would be an S term. This follows the same order as we learned for atomic orbitals, but it is very easy to get L values greater than 3, so after S, P, D, F the order proceeds G, H, K, I, etc. So far, this would make our ground state term for the d^2 system a ^3F term. The final value in the term symbol is J (which is why the letter J was skipped in the list above). This value comes from combinations of L and S.

The term symbols just described are known as free ion terms. This means we would be thinking about a d^2 metal ion in the gas phase. Things change a bit when you consider a metal with ligands. We move from the free ion terms to symbols that come from group theory. We also now have to deal with a wide range of ligands from weak field to strong field. As the ligands impact the separation of the t_{2g} and e_g orbitals, they should have an impact on the absorption of the complex. Doing much more with Term symbols is beyond the scope of this course. However, they do appear in the discussion below so it is important you have some appreciation of their source.

Selection Rules

In most cases the ligand field strength is in between the very weak and very strong case, and thus, we could expect very complicated spectra. Fortunately, nature does not make things quite as complicated, because not all possible electron transitions are quantum-mechanically allowed. The allowed transitions are defined by two rules: The spin selection rule and the Laporte rule.

The spin selection rule states that only transitions are allowed in which the total spin quantum number S does not change. Another way to say this is that only transitions between states with the same multiplicity are allowed. For example, it would be allowed to excite an electron from a triplet term to another triplet term, but not from a triplet term to a doublet or singlet term.

The Laporte rule state that transitions are only allowed when there is a change of parity. To fully appreciate this, we must define the terms gerade (symmetric with respect to inversion) and ungerade (not symmetric with respect to inversion). In thinking about this in terms of atomic orbitals, s-orbitals are completely spherical and as such are gerade. While it might take a little more to visualize it, d-orbitals are also gerade. On the other hand, p-orbitals, with the lobes having different signs are ungerade. This means that transitions between d-orbitals should not be allowed by the Laporte rule. However, in an octahedral geometry, it is possible that some terms may have a change in parity. So overall, a transition from a gerade (g) to an ungerade (u)-term and vice versa is possible, but not a transition from a g-term to another g-term, or the transition from a u-term to another u-term. For example the transition from a T_{2g} to a T_{1u} term would be allowed, but not the transition from a T_{2g} to a T_{1g} term.

Tanabe-Sugano diagram of a d^2 octahedral complex

In order to provide a somewhat quantitative way of representing the possible transitions for electrons in an octahedral compound, Tanabe-Sugano diagrams were developed (Figure **5.9.3**). The y-axis is energy divide by B, the Racah parameter. The Racah parameter is a quantum-mechanical energy unit for the electromagnetic interactions between the electrons. It is chosen because it provides “handy” numbers. Also on the y-axis one can find the free ion terms. The ground state is the lowest energy term. The x-axis is a measurement of the ligand field strength also given in terms of the Racah parameter. At 0, there are no ligands so we use the free ion terms. As the values on the x-axis increase so does the ligand field strength so weak-field ligands are towards the origin and strong field ligands are further away.

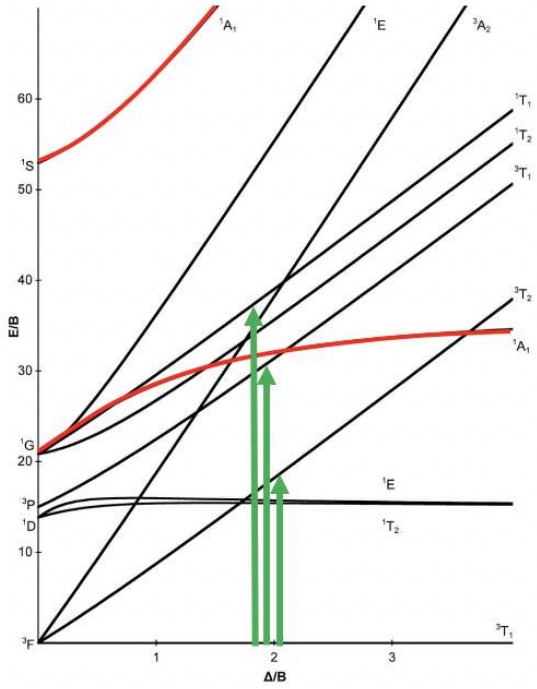


Figure 5.9.3. Tanabe-Sugano diagram for d^2 octahedral complexes.

You can see that some lines coming from the free ion terms in the diagram are bent, and some are straight. Bending of lines occurs when two terms interact with each other because they are close in energy and have the same symmetry. This is again an analogy to

orbitals. Like orbitals interact when they have the same symmetry and similar energy, terms interact when they have the same symmetry and the same energy. The closer the terms come to the point where they cross, the stronger their interactions, because their energies become more and more similar. The interactions lead to the fact that the terms bend away from each other, leading to bent curves. This means that curves for two terms of the same symmetry type will bend away in a Tanabe-Sugano diagram and never cross. For example the terms for the two $^1A_{1g}$ terms (in red above) bend away from each other and do not cross.

Next, let us think about which electron transitions would be allowed under the consideration of the spin selection and the Laporte rule. We notice that in the symmetry labels the "g" for gerade has been omitted. This is a common simplification made in the literature but all the terms shown are "g" terms. What does this mean for the allowance of electron transitions? It suggests that no electron transition should be allowed, and that would imply that the complex could not absorb light. The Laporte selection rule however does not hold strictly. It only says that the probability of the electron-transition is reduced, however, not forbidden. This means that an absorption band that disobeys the Laporte rule will have lower intensity compared to one that follows the Laporte rule, but it still can be observed. The spin-selection rule, however, holds strictly, and transitions between terms of different spin multiplicity are strictly forbidden, meaning that they have near zero probability to occur. Overall, we can therefore excite an electron from the $^3T_1$ ground state to other triplet terms, namely the $^3T_2$, $^3T_1$ and the $^3A_2$ terms.

Tanabe-Sugano diagram of d^3 octahedral complexes

Now, let us have a look at the Tanabe-Sugano diagram for a d^3 system in an octahedral ligand field (Figure **5.9.4**). What is the ground term? We can see the term designation on the horizontal line reads "$^4A_2$", therefore this term is the ground term. How many electron transitions from the ground state should we expect? To answer this question we need to count the number of other quartet terms. There is the $^4T_2$, the $^4T_1$, and the $^4T_1$. Thus, there are overall three electron transitions possible.

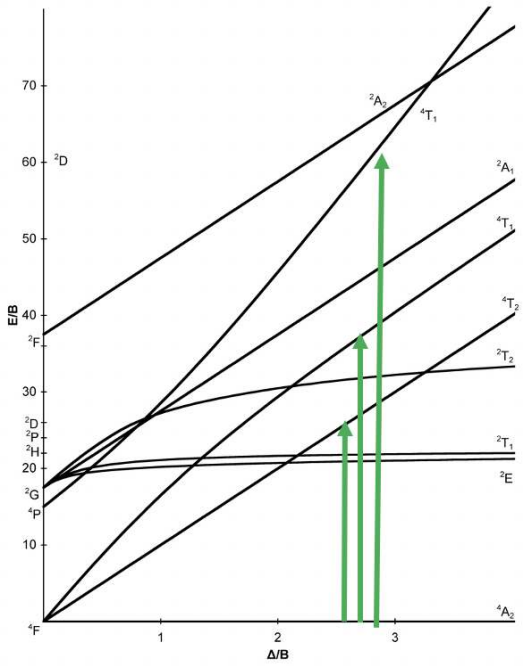


Figure 5.9.4. Tanabe-Sugano diagram for d^3 octahedral complexes.

Tanabe-Sugano diagram of d^4 octahedral complexes

Now let us look at the Tanabe-Sugano diagram for d^4 octahedral complexes (Figure **5.9.5**). You can see that this diagram is separated into two parts separated by a vertical line. The line indicates the ligand field strength at which the complex changes from a low sping complex to a high spin complex. At lower ligand field strengths, the ground term is a ^5E term. At higher field strength the ground term is a ^3T term. For a high spin complex there is only one allowed transition because there is only one other quintet term, namely the $^5T_2$ term. For the low spin complex, there are four transitions because there are four other triplet terms.

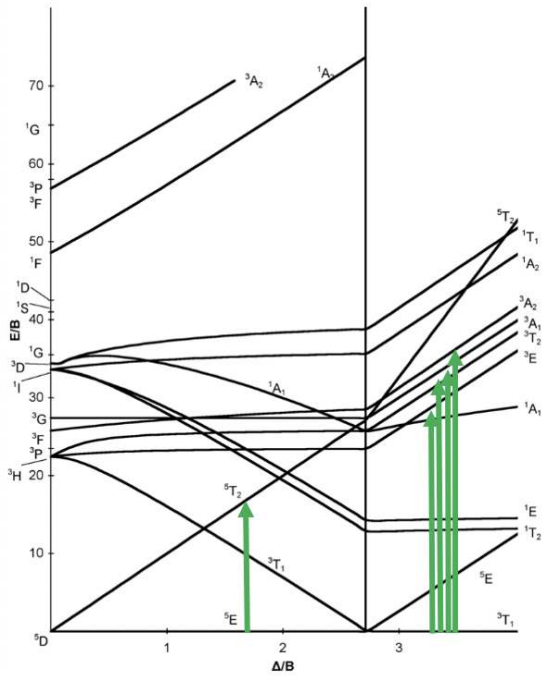


Figure 5.9.5. Tanabe-Sugano diagram for d^4 octahedral complexes.

Tananbe-Sugano diagram of d^5 octahedral complexes

The Tanabe-Sugano diagram for d^5 octahedral complexes is divided into two parts separated by a vertical line (Figure **5.9.6**). The left part reflects that high spin and the right part the low spin complex. The high spin ground state is a sextet term, and the low spin ground state is a doublet term. For the high-spin complex there are no other sextet terms, meaning that there is no electron transition possible. Hence, high-spin octahedral d^5-complexes are nearly colorless. An example for that is the hexaaqua manganese (2+) complex. A solution of this complex is near colorless, only very slightly pinkish. The slight color is because spin-forbidden transitions can occur albeit at a very low probability. For a d^5-low spin complex there are three additional doublet states, and thus there are three electron transitions possible.

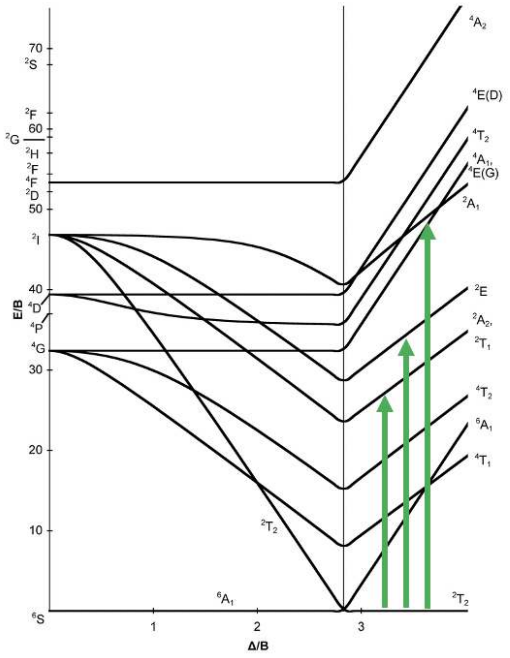


Figure 5.9.6. Tanabe-Sugano diagram for d^5 octahedral complexes.

Tanabe-Sugano diagram of d^6 octahedral complexes

The next diagram is the one for the d^6 electron configuration (Figure **5.9.7**). Again, the diagram is separated into parts for high and low spin complexes. There are dotted lines in the diagram. They indicate the terms that have a different spin multiplicity than the ground term. This way we can more easily see how many electron transitions are allowed. The ground term for the high-spin complex is the quintet $^5T_2$ term. The ground term for the low spin complex is a $^1A_1$ term. There is only transition allowed for the high-spin comples because the ^5E term is the only other quintet term. There are two transitions possible for the low-spin case because there are two additional singlet terms, namely the $^1T_1$ and the $^1T_2$.

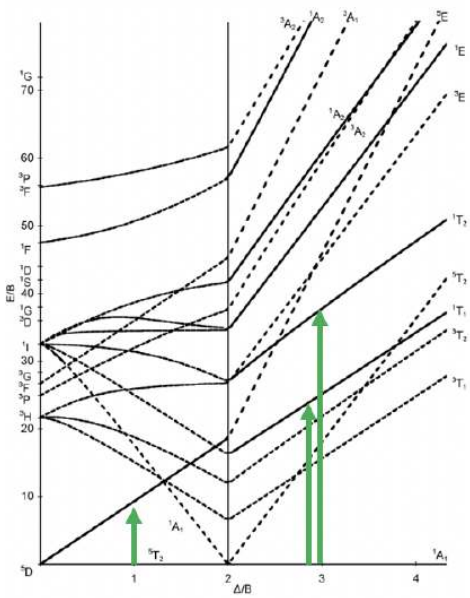


Figure 5.9.7. Tanabe-Sugano diagram for d^6 octahedral complexes.

Tanabe-Sugano diagram of d^7 octahedral complexes

Next, is the Tanabe-Sugano diagram for d^7 octahedral complexes (Figure **5.9.8**). In this case, the high spin complex has a $^4T_1$ ground term, and the low spin complex has a ^2E ground term. There are two other quartet terms, and two other doublet terms, hence there are two electrons transitions for the high-spin complex, and two for the low spin complex.

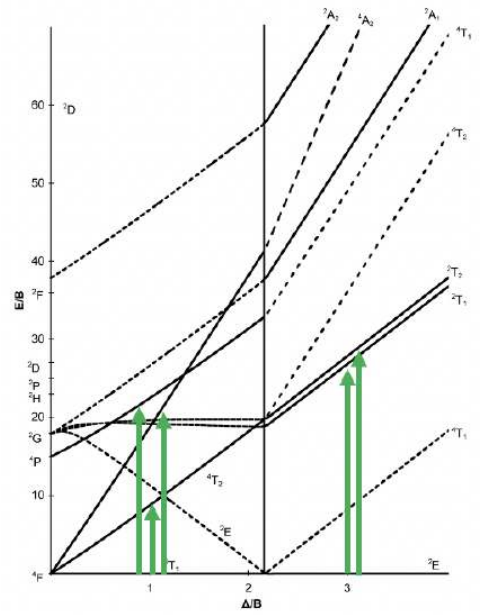


Figure 5.9.8. Tanabe-Sugano diagram for d^7 octahedral complexes.

Tanabe-Sugano diagram of d^8 octahedral complexes

Finally, we will examine the Tanabe-Sugano diagram for octahedral complexes with d^8 electron configuration (Figure **5.9.9**). For this electron configuration, there are no high and low spin complexes possible, therefore, the Tanabe-Sugano diagram is no longer divided into two parts. There is a single ground term of the type $^3A_2$. There are three other triplet states, namely the $^3T_2$ and two $^3T_1$ terms. Therefore, there are three electron transitions possible.

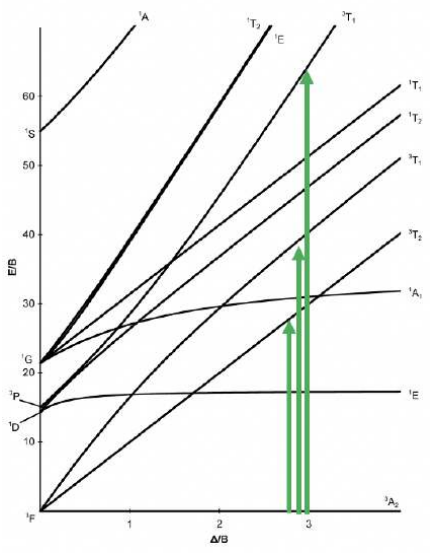


Figure 5.9.9. Tanabe-Sugano diagram for d^8 octahedral complexes.

You might wonder where are the Tanabe-Sugano diagrams for d^1, d^9, and d^{10}? For d^1 there are no electron-electron interactions, thus a simple orbital picture is sufficient. The ^2D term splits into T_{2g} and E_g terms, and there is only one electron transition possible. The d^9 electron configuration is the "hole-analog" of the d^1 electron configuration. It has also just one ^2D term which splits into a T_{2g} and an E_g term in the octahedral ligand field. Therefore, also in this case there is only one electron transition from the T_{2g} into the E_g term possible. In the case of d^{10} the orbitals are filled, and there is only the ^1S term which does not split in an octahedral ligand field. Therefore, there are no electron transitions in this case.

Finally, it should be mentioned that it is also possible to construct Tanabe-Sugano diagrams for other shapes such as the tetrahedral shape, but we will not discuss these further here.

Charge Transfer Transitions

Zn^{2+}		d^{10} ion	white
$[Cu(MeCN)_4]^+$	Cu(I)	d^{10} ion	colourless
$[Cu(phen)_2]^+$	Cu(I)	d^{10} ion	dark orange
TiF_4		d^0 ion	white
$TiCl_4$		d^0 ion	white
$TiBr_4$		d^0 ion	orange
TiI_4		d^0 ion	dark brown
$[MnO_4]^-$	Mn(VII)	d^0 ion	extremely purple
$[Cr_2O_7]^-$	Cr(VI)	d^0 ion	bright orange

Figure 8.2.19 d-d transitions

We are still not done with our electronic spectra. Thus, far we have only considered transitions of d-electrons between d-orbitals, and their terms. They are called d-d transitions. However, there are also so-called charge transfer transitions possible, that are not d-d transitions. We can easily see that there must be other transitions but d-d transitions when we look at the color of d^{10} and d^0 ions. For those, the are no d-d transitions possible. Therefore, they all should be colorless. However, that is not always true. Some of these ions are indeed colorless, but some are not. For example, Zn^{2+}, a d^{10} ion are always colorless in complexes, but not Cu(I) which is also d^{10}. While tetrakis(acetonitrile)copper (+) is colorless, bis(phenanthrene) copper(+) is dark orange. Similar is true for d0 ions. While TiF_4 and $TiCl_4$ are colorless, $TiBr_4$ is orange, and TiI_4 is brown. Some d^0 species are even extremely colorful, for example permanganate with Mn^{7+} which is extremely purple, and dichromate with Cr(VI) which is bright orange.

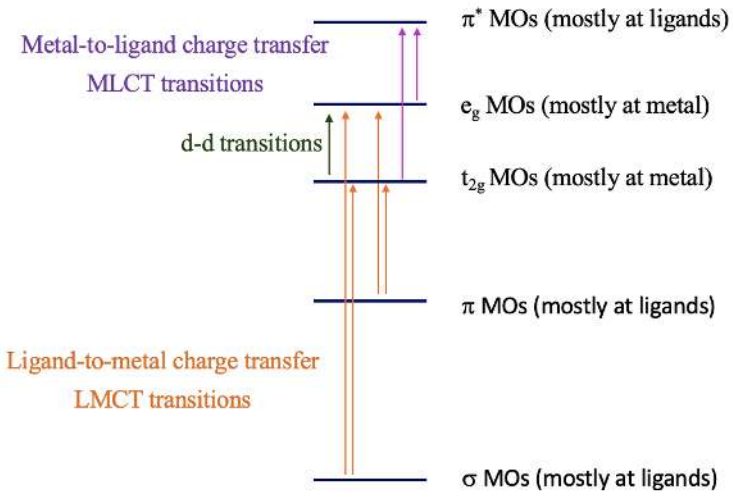


Figure 8.2.20 Charge-transfer transitions

The explanation of these phenomena are charge-transfer transitions. There are two types of charge-transfer transitions, the ligand-to-metal (LCMT) and the metal-to-ligand (MLCT) charge transfer transitions. For the ligand-to-metal transitions, electrons from bonding σ and π-orbitals get excited into metal d-orbitals in the ligand field, for example the t_{2g} and the e_g orbitals in an octahedral complex. If the energy difference between the σ/π-orbitals and the d-orbitals is small enough, then this electron-transition is associated with the absorption of visible light. The transition is called a ligand-to-metal transition because the ligand σ/π-orbitals

are mostly located at the ligands, while the metal-d-orbitals in a ligand field are mostly located at the metal. Vice versa, the metal-to-ligand transition involves the transition of an electron from metal d-orbitals in a ligand field to ligand π*-orbitals. This essentially moves electron density from the metal to the ligand, hance the name ligand-to-metal-charge transfer transition. If the energy-difference between the ligand π* and the metal orbitals is small enough, then the absorption occurs in the visible range. Charge-transfer transitions are usually both spin- and Laporte allowed, hence if they occur the color is often very intense. How can we distinguish between d-d and charge transfer transitions? Charge transfer transitions often change in energy as the solvent polarity is varied (solvatochromic) as there is a change in polarity of the complex associated with the charge transfer transition. This can be used to distinguish between d-d transitions and charge-transfer bands.

LMCT Transitions

Can we predict when the energy windows between the bonding molecular orbitals and the metal d-orbitals are small enough so that LMCT transitions in the visible can take place? Generally, it would be desirable if the energy of the metal orbitals was as low as possible and the energy of the bonding ligand orbitals are as high as possible. The energy of metal d-orbitals decreases with increasing positive charge at the metal because the effective nuclear charge on the metal increases. This means that very high oxidation states favor an LMCT transition. The d-orbitals should have few or no electrons, so that electrons can be promoted into the orbitals, and orbital energy increase due to electron-electron repulsion is minimized. Examples are Mn(VII), Cr(VI), and Ti(IV). The energy of MOs from bonding ligand orbitals increases when the ligand orbitals have high energy this is typically the case for π-donor ligand with negative charge.

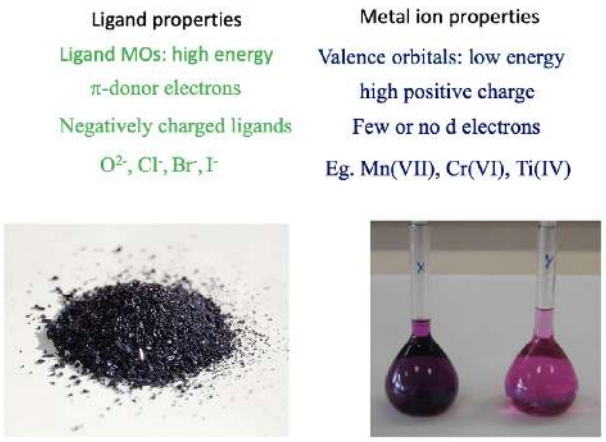


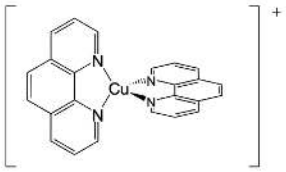
Figure 8.2.21 The properties of the metal ion and ligands in MnO_4^- (Attribution: Pradana Aumars / CC (https://commons.wikimedia.org/wiki/F...entrations.jpg))

Examples of ligands are oxo- and halo ligands. This explains for example the LMCT transitions in permanganate. The Mn is in the very high oxidation state +7, and the ligands are are oxo-ligands wich are π-donors with a 2- negative charge. The transitions are both Laporte and spin-allowed leading to very high intensity of light absorption, and thus color.

MLCT Transitions

What are favorable metal ion and ligand properties for a metal-to-ligand transition, then? In this case we would like to keep the energy of the metal orbitals as high as possible so that the energy difference between a metal d-orbital and a π*-orbital is minimized. This is accomplished when the positive charge at the metal ion is small, and there are many d-electrons that can repel each other, thereby increasing orbital energies, for examples Cu(I).

Metal ion properties	Ligand properties
low metal ion charge	π-acceptor ligand with low-lying π* orbitals
many electrons	
Cu(I), d^{10} ion	1,10-phenanthroline, CN^-, CO, SCN^-



$[Cu(phen)_2]^+$, dark orange

Figure 8.2.22 bis(phenanthroline) copper(+)

The ligand should be a π-acceptor with low-lying π*-orbitals, for example phenanthroline, CN^-, SCN^-, and CO. For instance, the bis(phenanthroline) copper(+) is dark-orange and has a MCLT absorption band a 458 nm. Also, the MLCT transfer is both spin and Laporte-allowed.

It should be mentioned that some complexes allow for both metal-to-ligand and ligand to metal transitions. For example, in the $Cr(CO)_6$ complex the σ-orbitals are high enough and the π*-orbitals are low enough in energy to allow for light absorption in the visible range. Finally, also intraligand bands are possible when the ligand is a chromophore.

Dr. Kai Landskron (Lehigh University). If you like this textbook, please consider to make a donation to support the author's research at Lehigh University: Click Here to Donate.

Tags recommended by the template: article:topic

This page titled 5.9: Electronic Spectra of Coordination Compounds is shared under a not declared license and was authored, remixed, and/or curated by Kai Landskron.

CHAPTER OVERVIEW

6: Bioinorganic Chemistry

6.1: Biological Significance of Iron, Zinc, Copper, Molybdenum, Cobalt, Chromium, Vanadium, and Nickel

6.2: Introduction to Amino Acids and Proteins

6.3: Redox Reactions

6.3.1: Introduction to Redox Reactions

6.3.2: Balancing Redox Reactions

6.3.3: Electrochemical Potentials

6.3.4: Prelude to Redox Stability and Redox Reactions

6.3.5: Latimer and Frost Diagrams

6.3.6: Pourbaix Diagrams

6.4: Associative Ligand Substitution

6.5: Dissociative Ligand Substitution

6.6: Biological Significance of Iron, Zinc, Copper, Molybdenum, Cobalt, Chromium, Vanadium, and Nickel

6.7: Ferrodoxins, Hydrogenases, and Nitrogenases - Metal-Sulfide Proteins

6.7.1: Iron-sulfur Proteins and Models

6.7.2: Iron-sulfur Proteins and Models (Part 2)

6.7.3: Iron-sulfur Proteins and Models (Part 3)

6.7.4: Iron-sulfur Proteins and Models (Part 4)

6.8: Overview of Hemoglobin and Myoglobin

6.8.1: Myoglobin, Hemoglobin, and their Ligands

6.8.2: Oxygen Transport by the Proteins Myoglobin and Hemoglobin

---

6: Bioinorganic Chemistry is shared under a not declared license and was authored, remixed, and/or curated by LibreTexts.

6.1: Biological Significance of Iron, Zinc, Copper, Molybdenum, Cobalt, Chromium, Vanadium, and Nickel

The transition metals are among the least abundant metal ions in sea water from which contemporary organisms are thought to have evolved (Table 1.1).[1-5] For many of the metals, the concentration in human blood plasma greatly exceeds that in sea water. Such data indicate the importance of mechanisms for accumulation, storage, and transport of transition metals and zinc in living organisms.

Table 1.1: Concentrations of transition metals and zinc in sea water and human plasma.a*Data from References 1 - 5 and 12

Element	Sea Water (M) x 10^8	Human Plasma (M) x 10^8
Fe	0.005 - 2	2230
Zn	8.0	1720
Cu	1.0	1650
Mo	10.0	1000
Co	0.7	0.0025
Cr	0.4	5.5
V	4.0	17.7
Mn	0.7	10.9
Ni	0.5	4.4

The metals are generally found either bound directly to proteins, found in cofactors, or part of clusters that are in turn bound by a protein. The ligands usually contain O, N, S, or C donor atoms. Proteins with transition metals are most commonly associated with the catalysis involving the intramolecular or intermolecular rearrangement of electrons. Although the redox properties of the metals are important in many of the reactions, in others the metal appears to contribute to the structure of the active state, e.g., zinc in the Cu-Zn dismutases and some of the iron in the photosynthetic reaction center. Sometimes equivalent reactions are catalyzed by proteins with different metal centers; the metal binding sites and proteins have evolved separately for each type of metal center.

Iron is the most common transition metal in biology.[6,7] Its use has created a dependence that has survived the appearance of dioxygen in the atmosphere ca. 2.5 billion years ago, and the concomitant conversion of ferrous ion to ferric ion and insoluble rust. All plants, animals, and bacteria use iron, except for a lactobacillus that appears to maintain high concentrations of manganese instead of iron. The processes and reactions in which iron participates are crucial to the survival of terrestrial organisms, and include ribonucleotide reduction (DNA synthesis), energy production (respiration), energy conversion (photosynthesis), nitrogen reduction, oxygen transport (respiration, muscle contraction), and oxygenation (e.g., steroid synthesis, solubilization and detoxification of aromatic compounds). Among the transition metals used in living organisms, iron is the most abundant in the environment. Whether this fact alone explains the biological predominance of iron or whether specific features of iron chemistry contribute is not clear.

Many of the other transition metals participate in reactions equivalent to those involving iron, and can sometimes substitute for iron, albeit less effectively, in natural Fe-proteins. Additional biological reactions are unique to nonferrous transition metals.

Zinc is relatively abundant in biological materials.[8,9] The major location of zinc in the body is metallothionein, which also binds copper, chromium, mercury, and other metals. Among the other well-characterized zinc proteins are the Cu-Zn superoxide dismutases (other forms have Fe or Mn), carbonic anhydrase (an abundant protein in red blood cells responsible for maintaining the pH of the blood), alcohol dehydrogenase, and a variety of hydrolases involved in the metabolism of sugars, proteins, and nucleic acids. Zinc is a common element in nucleic-acid polymerases and transcription factors, where its role is considered to be structural rather than catalytic. Interestingly, zinc enhances the stereoselectivity of the polymerization of nucleotides under reaction conditions designed to simulate the environment for prebiotic reactions. Recently a group of nucleic-acid binding proteins, with a

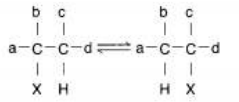
repeated sequence containing the amino acids cysteine and histidine, were shown to bind as many as eleven zinc atoms necessary for protein function (transcribing DNA to RNA).[10] Zinc plays a structural role, forming the peptide into multiple domains or "zinc fingers" by means of coordination to cysteine and histidine. A survey of the sequences of many nucleic-acid binding proteins shows that many of them have the common motif required to form zinc fingers. Other zinc-finger proteins called steroid receptors bind both steroids such as progesterone and the progesterone gene DNA . Much of the zinc in animals and plants has no known function, but it may be maintaining the structures of proteins that activate and deactivate genes.[11]

Copper and iron proteins participate in many of the same biological reactions:

1. reversible binding of dioxygen, e.g., hemocyanin (Cu), hemerythrin (Fe), and hemoglobin (Fe);
2. activation of dioxygen, e.g., dopamine hydroxylase (Cu) (important in the synthesis of the hormone epinephrine), tyrosinases (Cu), and catechol dioxygenases (Fe);
3. electron transfer, e.g., plastocyanins (Cu), ferredoxins, and c-type cytochromes (Fe);
4. dismutation of superoxide by Cu or Fe as the redox-active metal (superoxide dismutases).

The two metal ions also function in concert in proteins such as cytochrome oxidase, which catalyzes the transfer of four electrons to dioxygen to form water during respiration. Whether any types of biological reactions are unique to copper proteins is not clear. However, use of stored iron is reduced by copper deficiency, which suggests that iron metabolism may depend on copper proteins, such as the serum protein ceruloplasmin, which can function as a ferroxidase, and the cellular protein ascorbic acid oxidase, which also is a ferrireductase.

Cobalt is found in vitamin B_{12} , its only apparent biological site.[12] The vitamin is a cyano complex, but a methyl or methylene group replaces CN in native enzymes. Vitamin-B_{12} deficiency causes the severe disease of pernicious anemia in humans, which indicates the critical role of cobalt. The most common type of reaction in which cobalamin enzymes participate results in the reciprocal exchange of hydrogen atoms if they are on adjacent carbon atoms, yet not with hydrogen in solvent water:



(An important exception is the ribonucleotide reductase from some bacteria and lower plants, which converts ribonucleotides to the DNA precursors, deoxyribonucleotides, a reaction in which a sugar -OH is replaced by -H. Note that ribonucleotide reductases catalyzing the same reaction in higher organisms and viruses are proteins with an oxo-bridged dimeric iron center.) The cobalt in vitamin B_{12} is coordinated to five N atoms, four contributed by a tetrapyrrole (corrin); the sixth ligand is C, provided either by C5 of deoxyadenosine in enzymes such as methylmalonyl-CoA mutase (fatty acid metabolism) or by a methyl group in the enzyme that synthesizes the amino acid methionine in bacteria.

Nickel is a component of a hydrolase (urease), of hydrogenase, of CO dehydrogenase, and of S-methyl CoM reductase, which catalyzes the terminal step in methane production by methanogenic bacteria. All the Ni-proteins known to date are from plants or bacteria.[13,14] However, about 50 years elapsed between the crystallization of jack-bean urease in 1925 and the identification of the nickel component in the plant protein. Thus it is premature to exclude the possibility of Ni-proteins in animals. Despite the small number of characterized Ni-proteins, it is clear that many different environments exist, from apparently direct coordination to protein ligands (urease) to the tetrapyrrole F430 in methylreductase and the multiple metal sites of Ni and Fe-S in a hydrogenase from the bacterium *Desulfovibrio gigas*. Specific environments for nickel are also indicated for nucleic acids (or nucleic acid-binding proteins), since nickel activates the gene for hydrogenase.[15]

Manganese plays a critical role in oxygen evolution catalyzed by the proteins of the photosynthetic reaction center. The superoxide dismutase of bacteria and mitochondria, as well as pyruvate carboxylase in mammals, are also manganese proteins.[16,17] How the multiple manganese atoms of the photosynthetic reaction center participate in the removal of four electrons and protons from water is the subject of intense investigation by spectroscopists, synthetic inorganic chemists, and molecular biologists.[17]

Vanadium and chromium have several features in common, from a bioinorganic viewpoint.[18a] First, both metals are present in only small amounts in most organisms. Second, the biological roles of each remain largely unknown.[18] Finally, each has served as a probe to characterize the sites of other metals, such as iron and zinc. Vanadium is required for normal health, and could act *in vivo* either as a metal cation or as a phosphate analogue, depending on the oxidation state, V(lV) or V(V), respectively. Vanadium in a

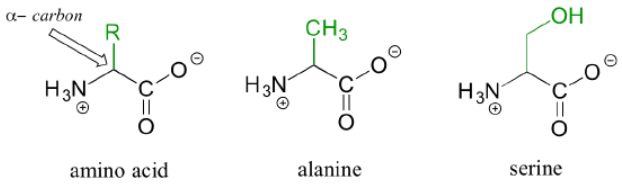
sea squirt (tunicate), a primitive vertebrate, is concentrated in blood cells, apparently as the major cellular transition metal, but whether it participates in the transport of dioxygen (as iron and copper do) is not known. In proteins, vanadium is a cofactor in an algal bromoperoxidase and in certain prokaryotic nitrogenases. Chromium imbalance affects sugar metabolism and has been associated with the glucose tolerance factor in animals. But little is known about the structure of the factor or of any other specific chromium complexes from plants, animals, or bacteria.

Molybdenum proteins catalyze the reduction of nitrogen and nitrate, as well as the oxidation of aldehydes, purines, and sulfite.[19] Few Mo-proteins are known compared to those involving other transition metals. Nitrogenases, which also contain iron, have been the focus of intense investigations by bioinorganic chemists and biologists; the iron is found in a cluster with molybdenum (the iron-molybdenum cofactor, or FeMoCo) and in an iron-sulfur center (Chapter 7). Interestingly, certain bacteria (*Azotobacter*) have alternative nitrogenases, which are produced when molybdenum is deficient and which contain vanadium and iron or only iron. All other known Mo-proteins are also Fe-proteins with iron centers, such as tetrapyrroles (heme and chlorins), Fe-sulfur clusters, and, apparently, non-heme/non-sulfur iron. Some Mo-proteins contain additional cofactors such as the Havins, e.g., in xanthine oxidase and aldehyde oxidase. The number of redox centers in some Mo-proteins exceeds the number of electrons transferred; reasons for this are unknown currently.

6.1: Biological Significance of Iron, Zinc, Copper, Molybdenum, Cobalt, Chromium, Vanadium, and Nickel is shared under a not declared license and was authored, remixed, and/or curated by LibreTexts.

6.2: Introduction to Amino Acids and Proteins

Proteins are polymers of **amino acids**, linked by amide groups known as **peptide bond**s. An amino acid can be thought of as having two components: a 'backbone', or 'main chain', composed of an ammonium group (H_3N^+-C), an 'alpha-carbon' bonded to the nitrogen atom, a carboxylate (COO^-), and a variable 'side chain' (in green below) bonded to the alpha-carbon (Figure **6.2.1**).



(Figure 6.2.1). Structures of amino acids.

There are twenty different side chains in naturally occurring amino acids, and it is the identity of the side chain that determines the identity of the amino acid: for example, if the side chain is a $-CH_3$ group, the amino acid is alanine, and if the side chain is a $-CH_2OH$ group, the amino acid is serine. Many amino acid side chains contain a functional group (the side chain of serine, for example, contains a primary alcohol), while others, like alanine, lack a functional group, and contain only a simple hydrocarbon group.

The two 'hooks' on an amino acid monomer are the ammonium and carboxylate groups. Proteins (polymers of ~50 amino acids or more) and peptides (shorter polymers) are formed when the amino group of one amino acid monomer reacts with the carboxylate carbon of another amino acid to form an amide linkage, which in protein terminology is a **peptide bond**. Which amino acids are linked, and in what order - the protein **sequence** - is what distinguishes one protein from another. This sequence is coded for by an organism's DNA. Protein sequences are written in the ammonium terminal (N-terminal) to carboxylate terminal (C-terminal) direction, with either three-letter or single-letter abbreviations for the amino acids. Below is a four amino acid peptide with the sequence "cysteine - histidine - glutamate - methionine". Using the single-letter code, the sequence is abbreviated CHEM (Figure **6.2.2**).

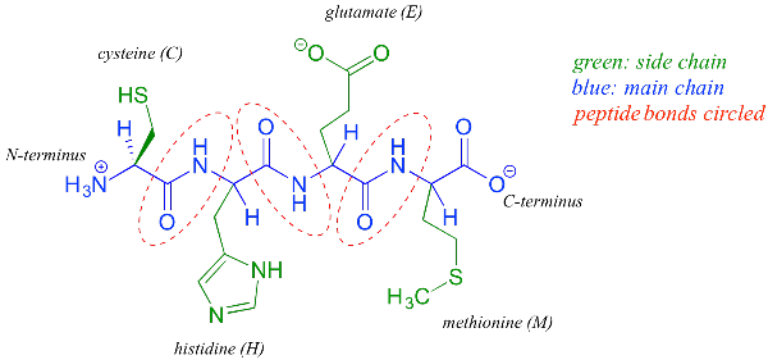


Figure 6.2.2. The CHEM peptide.

When an amino acid is incorporated into a protein it loses a molecule of water and what remains is called a **residue** of the original amino acid. Thus we might refer to the 'glutamate residue' at position 3 of the CHEM peptide above.

Once a protein polymer is constructed, it in many cases folds up very specifically into a three-dimensional structure, which often includes one or more 'binding pockets' in which other molecules can be bound. It is this shape of this folded structure, and the precise arrangement of the functional groups within the structure (especially in the area of the binding pocket) that determines the function of the protein.

Enzymes are proteins which catalyze biochemical reactions. One or more reacting molecules - often called **substrates** - become bound in the **active site** pocket of an enzyme, where the actual reaction takes place. **Receptors** are proteins that bind specifically to

one or more molecules - referred to as **ligands** - to initiate a biochemical process. For example, we saw in the introduction to this chapter that the TrpVI receptor in mammalian tissues binds capsaicin (from hot chili peppers) in its binding pocket and initiates a heat/pain signal which is sent to the brain.

Contributors and Attributions

- Organic Chemistry With a Biological Emphasis by Tim Soderberg (University of Minnesota, Morris)

This page titled 6.2: Introduction to Amino Acids and Proteins is shared under a CC BY-NC-SA 4.0 license and was authored, remixed, and/or curated by Tim Soderberg.

6.3: Redox Reactions

6.3: Redox Reactions is shared under a not declared license and was authored, remixed, and/or curated by LibreTexts.

SECTION OVERVIEW

6.3.1: Introduction to Redox Reactions

6.3.1: Introduction to Redox Reactions is shared under a CC BY-SA license and was authored, remixed, and/or curated by LibreTexts.

6.3.2: Balancing Redox Reactions

In studying redox chemistry, it is important to remember balancing electrochemical reactions. Simple redox reactions (for example, $H_2 + I_2 \rightarrow 2\ HI$) can be balanced by inspection, but for more complex reactions it is helpful to have a systematic method. There are many different methods for doing this. The focus in this section will be on the **ion-electron method** allows one to balance redox reactions regardless of their complexity and allows for identification of the species changing valence states in the reaction. We illustrate this method with two examples.

Example 1:
I^- is oxidized to **IO_3^-** by **MnO_4^-**, which is reduced to **Mn^{2+}**.

How can this reaction be balanced? In the ion-electron method we follow a series of four steps:

Step 1A: Write out the (unbalanced) reaction and identify the elements that are undergoing redox.

$\mathbf{Mn}O_4^- + \mathbf{I}^- \rightarrow \mathbf{I}O_3^- + \mathbf{Mn}^{2+}$ (The elements undergoing redox are **Mn** and **I**)

Step 1B: Separate the reaction into two **half reactions**, balancing the element undergoing redox in each.

$\mathbf{Mn}O_4^- \rightarrow \mathbf{Mn}^{2+}$
$\mathbf{I}^- \rightarrow \mathbf{I}O_3^-$

Step 2A: Balance the **oxygen** atoms by adding water to one side of each half reaction.

$Mn\mathbf{O_4}^- \rightarrow Mn^{2+} + \mathbf{4}H_2\mathbf{O}$
$\mathbf{3}H_2\mathbf{O} + I^- \rightarrow I\mathbf{O_3}^-$

Step 2B: Balance the **hydrogen** atoms by adding H^+ ions.

$\mathbf{8H^+} + MnO_4^- \rightarrow Mn^{2+} + \mathbf{4H_2}O$

The left side has a net charge of **+7** and the right side has a net charge of **+2**

$\mathbf{3H_2}O + I^- \rightarrow IO_3^- + \mathbf{6H^+}$

The left side has a net charge of **-1** and the right side has a net charge of **+5**

Step 2C: Balance the overall charge by adding **electrons**

$8H^+ + \mathbf{5e}^- + MnO_4^- \rightarrow Mn^{2+} + 4H_2O$

The left side has a charge of **+2** while the right side has a charge of **+2**. They are balanced.

$3H_2O + I^- \rightarrow IO_3^- + 6H^+ + \mathbf{6e}^-$

The left side has a charge of **-1** while the right side has a charge of **-1**. They are balanced.
Note: We did not need to explicitly determine the oxidation states of Mn or I to arrive at the correct number of electrons in each half reaction.

Step 3: Combine the half reactions so that there are equal numbers of electrons on the left and right sides

6 $(8H^+ + \mathbf{5e}^- + MnO_4^- \rightarrow Mn^{2+} + 4H_2O)$
5 $(3H_2O + I^- \rightarrow IO_3^- + 6H^+ + \mathbf{6e}^-)$

$48H^+ + \mathbf{30e}^- + 15H_2O + 6MnO_4^- + 5I^- \rightarrow 5IO_3^- + 6Mn^{2+} + 24H_2O + \mathbf{30e}^- + 30H^+$
Cancel the **H^+**, **electrons**, and **water**:

~~$48H^+$~~ + ~~$30e^-$~~ + ~~$15H_2O$~~ + $6MnO_4^-$ + $5I^-$ → $5IO_3^-$ + $6Mn^{2+}$ + ~~$24H_2O$~~ + ~~$30e^-$~~ + ~~$30H^+$~~

The overall balanced reaction is therefore:
$18H^+ + 6MnO_4^- + 5I^- \rightarrow 5IO_3^- + 6Mn^{2+} + 9H_2O$

Check your work by making sure that all **elements** and **charges** are balanced.

Step 4: If the reaction occurs under basic conditions, we add **OH^-** to each side to cancel **H^+**
$18H^+$ + **$18OH^-$** + $6MnO_4^-$ + $5I^-$ → $5IO_3^-$ + $6Mn^{2+}$ + **$9H_2O$** + **$18OH^-$**

The **$18H^+$** + **$18OH^-$** will become **$18H_2O$** so the overall balanced reaction is:

$9H_2O + 6MnO_4^- + 5I^- \rightarrow 5IO_3^- + 6Mn^{2+} + 18OH^-$

Again, it is a good idea to check and make sure that all of the elements are balanced, and that the charge is the same on both sides. If this is not the case, you need to find the error in one of the earlier steps.

Example 2:
Redox reaction of **$S_2O_3^{2-}$** and **H_2O_2**
$S_2O_3^{2-}$ + **H_2O_2** → **$S_4O_6^{2-}$** + **H_2O**

Which elements are undergoing redox? **S** and **O**

Step 1: Write out half reactions, balancing the element undergoing redox

$2S_2O_3^{2-} \rightarrow S_4O_6^{2-}$
$H_2O_2 \rightarrow 2H_2O$

Step 2A: Balance oxygen (already balanced)

Step 2B: Balance hydrogen:

$2S_2O_3^{2-} \rightarrow S_4O_6^{2-}$
$H_2O_2 + 2H^+ \rightarrow 2H_2O$

Step 2C: Balance charge by adding electrons:

$2S_2O_3^{2-} \rightarrow S_4O_6^{2-} + 2e^-$
$H_2O_2 + 2H^+ + 2e^- \rightarrow 2H_2O$

Step 3: Combine the half reactions so that there are equal numbers of electrons on the left and right sides (already equal)
Overall balanced reaction:

$2S_2O_3^{2-} + H_2O_2 + 2H^+ \rightarrow S_4O_6^{2-} + 2H_2O$

Note that again, we did not need to know the valence states of S or O in the reactants and products in order to balance the reaction. In this case, assigning the valence states is a bit complex, because $S_4O_6^{2-}$ contains sulfur in more than one valence state.

6.3.2: Balancing Redox Reactions is shared under a CC BY-SA license and was authored, remixed, and/or curated by LibreTexts.

- **4.2: Balancing Redox Reactions** by Chemistry 310 is licensed CC BY-SA 4.0. Original source: https://en.wikibooks.org/wiki/Introduction_to_Inorganic_Chemistry.

6.3.3: Electrochemical Potentials

In electrochemical cells, or in redox reactions that happen in solution, the thermodynamic driving force can be measured as the **cell potential**. Chemical reactions are spontaneous in the direction of -ΔG, which is also the direction in which the cell potential (defined as $E_{cathode}$ - E_{anode}) is positive. A cell operating in the **spontaneous** direction (for example, a battery that is discharging) is called a **galvanic cell**. A cell that is being driven in the **non-spontaneous** direction is called an **electrolytic cell**. For example, let us consider the reaction of hydrogen and oxygen to make water:

$$2\,H_{2\,(g)} + O_{2\,(g)} = 2\,H_2O_{(l)} \tag{6.3.3.1}$$

Thermodynamically, this reaction is spontaneous in the direction shown and has an overall standard free energy change (ΔG°) of -237 kJ per mole of water produced.

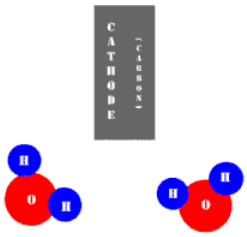
When this reaction occurs electrochemically in the spontaneous direction (e.g., in a hydrogen-air fuel cell), the two half cell reactions that occur are:

Anode: $H_{2\,(g)} \longrightarrow 2\,H^+_{(aq)} + 2\,e^-$

Cathode: $O_{2\,(g)} + 4\,H^+_{(aq)} + 4\,e^- \longrightarrow 2\,H_2O_{(l)}$

Here the anode is the negative electrode and the cathode is the positive electrode; under conditions of very low current density (where there are minimal resistive losses and kinetic overpotentials), the potential difference we would measure between the two electrodes would be 1.229 V.

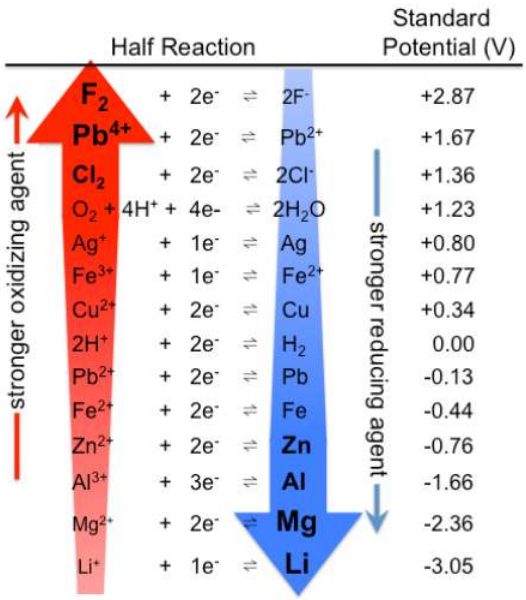
In an **electrolytic cell**, this reaction is run in reverse. That is, we put in electrical energy to split water into hydrogen and oxygen molecules. In this case, the half reactions (and their standard potentials) reverse. O_2(g) bubbles form at the anode and H_2(g) is formed at the cathode. Now the **anode** is the **positive** electrode and the **cathode** is **negative**. Electrons are extracted from the substance at the anode (water) and pumped into the solution at the cathode to make hydrogen. An animation of the cathode half reaction is shown below.



In both galvanic and electrolytic cells, **oxidation** occurs at the **anode** and **reduction** occurs at the **cathode**.

Half-cell potentials

As noted above, the equilibrium voltage of an electrochemical cell is proportional to the free energy change of the reaction. Because electrochemical reactions can be broken up into two half-reactions, it follows that the potentials of half reactions (like free energies) can be added and subtracted to give an overall value for the reaction. If we take the **standard hydrogen electrode** as our reference, i.e., if we assign it a value of zero volts, we can measure all the other half cells against it and thus obtain the voltage of each one. This allows us to rank redox couples according to their **standard reduction potentials** (or more simply their **standard potentials**), as shown in the table below.



Note that when we construct an electrochemical cell and calculate the voltage, we simply take the difference between the half cell potentials and do not worry about the number of electrons in the reaction. For example, for the displacement reaction in which silver ions are reduced by copper metal, the reaction is:

$$2\,Ag^{+}{}_{(aq)} + Cu_{(s)} = 2\,Ag_{(s)} + Cu^{2+}{}_{(aq)}$$

The two half-cell reactions are:

$$Ag^{+}_{(aq)} + e^{-} = Ag_{(s)} \quad +0.80V$$

$$Cu^{2+}_{(aq)} + 2e^{-} = Cu_{(s)} \quad +0.34V$$

and the standard potential $E^{o} = +0.80 - 0.34V = +0.46V$

The reason we don't need to multiply the Ag potential by 2 is that E^{o} is a measure of the free energy change **per electron**. Dividing the free energy change by the number of electrons (see below) makes E^{o} an **intensive property** (like pressure, temperature, etc.).

Relationship between E and ΔG. For systems that are in equilibrium, $\Delta G^{o} = -nFE^{o}_{cell}$, where n is number of moles of electrons per mole of products and F is the Faraday constant, ~96485 C/mol. Here the ^{o} symbol indicates that the substances involved in the reaction are in their standard states. For example, for the water electrolysis reaction, the standard states would be pure liquid water, H^{+} at 1M concentration (or more precisely, at unit activity), and O_2 and H_2(g) at 1 atmosphere pressure.

More generally (at any concentration or pressure), $\Delta G = -nFE$, where

$$E = E^{o} - \frac{RT}{nF} * lnQ \tag{6.3.3.2}$$

,

or at 298 K

$$E = E^{o} - \frac{0.0592}{n} * \log Q \tag{6.3.3.3}$$

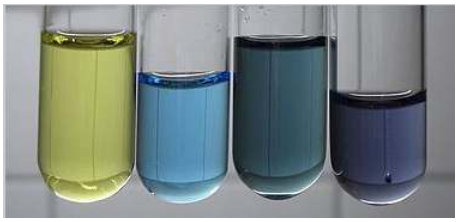
where Q is the concentration ratio of products over reactants, raised to the powers of their coefficients in the reaction. This equation (in either form) is called the Nernst equation. The second term in the equation, when multiplied by -nF, is RT*lnQ. This is the free energy difference between ΔG and ΔG°. We can think of this as an entropic term that takes into account the positive entropy change of dilution, or the negative entropy change of concentrating a reactant or product, relative to its standard state.

6.3.3: Electrochemical Potentials is shared under a CC BY-SA license and was authored, remixed, and/or curated by LibreTexts.

- **4.3: Electrochemical Potentials** by Chemistry 310 is licensed CC BY-SA 4.0. Original source: https://en.wikibooks.org/wiki/Introduction_to_Inorganic_Chemistry.

6.3.4: Prelude to Redox Stability and Redox Reactions

In redox reactions, one element or compound is reduced (gains electrons) and another is oxidized (loses electrons). In terms of everyday life, redox reactions occur all of the time around us. For example, the metabolism of sugars to CO_2, which stores energy in the form of ATP, is a redox reaction. Another example of redox is fire or combustion, such as in a car engine. In a car engine, hydrocarbons in the fuel are oxidized to carbon dioxide and water, while oxygen is reduced to water. Corrosion (i.e. the formation of rust on iron) is a redox reaction involving oxidation of a metal.



Different valence states of vanadium in acidic solution. From left to right the valence goes from +5 to +2. These four valencen states form the basis of the vanadium flow battery, a storage device for electricity generated from sunlight and wind.[1]

Oxidation-reduction reactions are important to understanding inorganic chemistry for several reasons:

- Transition metals can have multiple valence states
- Main group elements (N, halogens, O, S...) also have multiple valence states and important redox chemistry
- Many inorganic compounds catalyze redox reactions (which are especially useful in industrial and biological applications)
- Energy conversion and storage technologies (solar water splitting, batteries, electrolyzers, fuel cells) rely on inorganic redox reactions and catalysis
- Electrochemistry provides a way to measure equilibrium constants for dissolution/precipitation, complexation, and other reactions.
- Reaction mechanisms often involve changes in the valence states of metals.

Not all oxidizers and reducers are created equal. The electrochemical series ranks substances according to their oxidizing and reducing power, i.e., their standard electrode potential. Strong oxidizing agents are typically compounds with elements in high valence states or with high electronegativity, which gain electrons in the redox reaction. Examples of strong oxidizers include hydrogen peroxide, permanganate (Mn(VII)), and osmium tetroxide (Os(VIII)). Reducing agents are typically electropositive elements such as hydrogen, lithium, sodium, iron, and aluminum, which lose electrons in redox reactions. Hydrides (compounds that contain hydrogen in the formal -1 valence state), such as sodium hydride, sodium borohydride and lithium aluminum hydride, are often used as reducing agents.

6.3.4: Prelude to Redox Stability and Redox Reactions is shared under a not declared license and was authored, remixed, and/or curated by LibreTexts.

- **4.1: Prelude to Redox Stability and Redox Reactions** by Chemistry 310 is licensed CC BY-SA 4.0. Original source: https://en.wikibooks.org/wiki/Introduction_to_Inorganic_Chemistry.

6.3.5: Latimer and Frost Diagrams

There are a few different types of redox stability diagrams, two of which are known as Latimer diagrams and Frost diagrams. Each of these diagrams contains similar information, but one representation may be more useful in a given situation than the others.

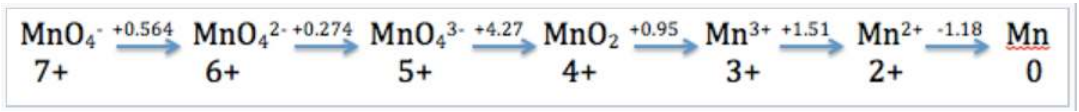
Latimer and Frost diagrams help predict stability relative to higher and lower valence states, usually at one fixed pH. A third type of diagram, a Pourbaix diagram, helps understand pH-dependent equilibria, which are often coupled to solubility equilibria and corrosion (which will be talked about more later).

Latimer diagrams:

Latimer diagrams are the oldest and most compact way to represent electrochemical equilibria for substances that have multiple valence states. Electrochemical potential values are written for successive redox reactions (from highest to lowest oxidation state), typically under standard conditions in either strong acid ($[H^+]$ = 1 M, pH 0) or strong base ($[OH^-]$ = 1 M, pH 14). The valence states of successive substances in a Latimer diagram can differ by one or more electrons. Valence states for the element undergoing redox are typically determined by difference; we assign the oxygen atoms a valence state of -2 and the hydrogen atoms avalence state of +1.

Example:

Mn in Acid



The Latimer diagram for Mn illustrates its standard reduction potentials (in 1 M acid) in valence states from +7 to 0.

The Latimer diagram compresses into shorthand notation all the standard potentials for redox reactions of the element Mn. For example, the entry that connects Mn^{2+} and Mn gives the potential for the half-cell reaction:

$\mathbf{Mn^{2+}_{(aq)} + 2\,e^- \longrightarrow Mn_{(s)}}$ $E_{1/2}° = -1.18V$

and the entry connecting Mn^{4+} and Mn^{3+} represents the reaction:

$\mathbf{MnO_{2\,(s)} + 4\,H^+_{(aq)} + e^- \longrightarrow Mn^{3+}_{(aq)} + 2\,H_2O_{(l)}}$, :$E_{1/2}° = +0.95V$

We can also calculate values for **multi-electron reactions** by first adding ΔG°(=-nFE°) values and then dividing by the total number of electrons

For example, for the 5-electron reduction of MnO_4^- to Mn^{2+}, we write

$$E^o = \frac{1(0.564) + 1(0.274) + 1(4.27) + 1(0.95) + 1(1.51)}{5} = +1.51V \quad (6.3.5.1)$$

and for the three-electron reduction of MnO_4^-(aq) to MnO_2(s),

$$E^o = \frac{1(0.564) + 1(0.274) + 1(4.27)}{3} = +1.70V \quad (6.3.5.2)$$

Remember to divide by the number of electrons involved in the valence number change (5 and 3 for the above equations).
Thermodynamically stable and unstable oxidation states

An unstable species on a Latimer diagram will have a lower standard potential to the left than to the right.

Example:

\(\ce{2MnO4^{3-} -> MnO2 + MnO4^{2-}}\ ) the MnO_4^{3-} species is unstable

$E^o = +4.27 - 0.274 = 3.997V$ (spontaneous disproportionation)

Which Mn species are unstable with respect to disproportionation?

MnO_4^{3-} 5+ → 6+,4+

Mn^{3+} 3+ → 4+,2+

So stable species are: MnO_4^-, MnO_4^{2-}, MnO_2, Mn^{2+}, and Mn^0.

But **MnO_4^{2-}** is also unstable - why?

$$\mathbf{MnO_4^{2-} \longrightarrow MnO_2}$$

$$\mathbf{2\,MnO_4^{2-} \longrightarrow 2\,MnO_4^{-} + MnO_2}$$ E° = 2.272 - 0.564 = +1.708 V

Moral: All possible disproportionation reactions must be considered in order to determine stability (this is often more convenient with a Frost diagram).

Note

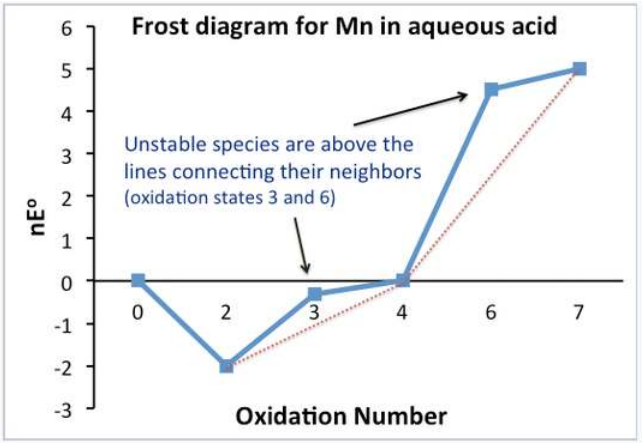
Thermodynamically unstable ions can be quite stable kinetically. For example, most N-containing molecules (NO_2, NO, N_2H_4) are unstable relative to the elements (O_2, N_2, H_2), but they are still quite stable kinetically.

Frost diagrams:

In a Frost diagram, we plot ΔG°/F (= nE°) vs. valence number. The zero valence state is assigned a nE° value of zero.[2]

Stable and **unstable oxidation states** can be easily identified in the plot. Unstable compounds are higher on the plot than the line connecting their neighbors. Note that this is simply a graphical representation of what we did with the Latimer diagram to determine which valence states were stable and unstable.

The **standard potential** for any electrochemical reaction is given by the **slope** of the line connecting the two species on a Frost diagram. For example, the line connecting Mn^{3+} and MnO_2 on the Frost diagram has a slope of +0.95, the standard potential of MnO_2 reduction to Mn^{3+}. This is the number that is written above the arrow in the Latimer diagram for Mn. Multielectron potentials can be calculated easily by connecting the dots in a Frost diagram.



A Frost diagram:

Contains the same information as in a Latimer diagram, but graphically shows stability and oxidizing power.

The lowest species on the diagram are the most stable (Mn^{2+}, MnO_2)

The highest species on diagram are the strongest oxidizers (MnO_4^-)

6.3.5: Latimer and Frost Diagrams is shared under a CC BY-SA license and was authored, remixed, and/or curated by LibreTexts.

- **4.4: Latimer and Frost Diagrams** by Chemistry 310 is licensed CC BY-SA 4.0. Original source: https://en.wikibooks.org/wiki/Introduction_to_Inorganic_Chemistry.

6.3.6: Pourbaix Diagrams

Pourbaix Diagrams plot electrochemical stability for different redox states of an element as a function of pH. These diagrams are essentially phase diagrams that map the conditions of potential and pH (most typically in aqueous solutions) where different redox species are stable. The lines in Pourbaix diagrams represent redox and acid-base reactions, and are the parts of the diagram where two species can exist in equilibrium. For example, in the Pourbaix diagram for Fe below, the horizontal line between the Fe^{3+} and Fe^{2+} regions represents the reaction $Fe^{3+}_{(aq)} + e^- = Fe^{2+}_{(aq)}$, which has a standard potential of +0.77 V. While we could use standard potentials for all these lines, in practice Pourbaix diagrams are usually plotted for lower ion concentrations (often 1 mM) that are more relevant to corrosion and electrochemical experiments.

Example: Iron Pourbaix diagram

Areas in the Pourbaix diagram mark regions where a single species (Fe^{2+}(aq), Fe_3O_4(s), etc.) is stable. More stable species tend to occupy larger areas.

Lines mark places where two species exist in equilibrium.

- **Pure redox** reactions are **horizontal** lines - these reactions are not pH-dependent
- **Pure acid-base** reactions are **vertical** lines - these do not depend on potential
- Reactions that are **both** acid-base and redox have a slope of -0.0592 V/pH x # H^+/# e^-)

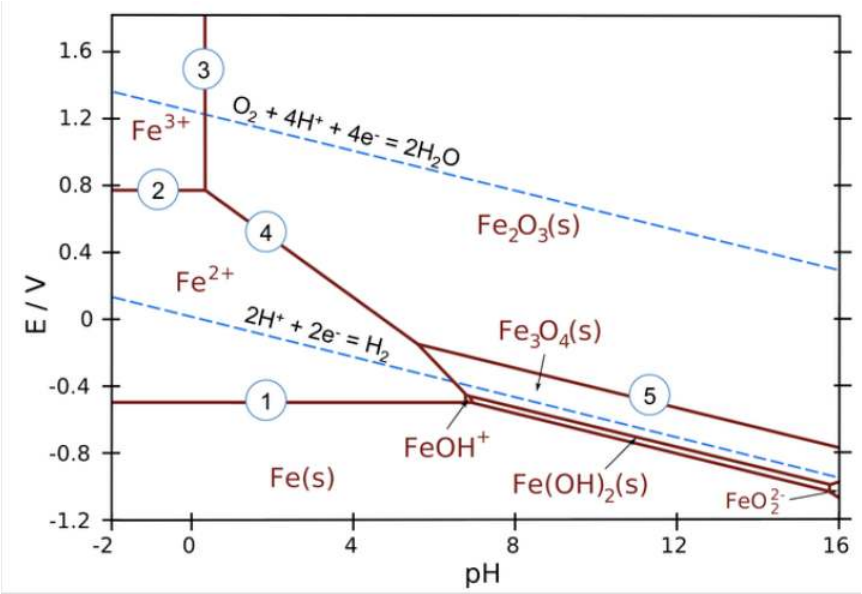


Figure **6.3.6.1**: Pourbaix diagram for iron at ionic concentrations of 1.0 mM. (CC BY-SA 3.0 Unported; Metallos via Wikipedia)

Examples of equilibria in the iron Pourbaix diagram (numbered on the plot):

1. $Fe^{2+} + 2e^- \longrightarrow Fe_{(s)}$ (pure redox reaction - no pH dependence)
2. $Fe^{3+} + e^- \longrightarrow Fe^{2+}$ (pure redox reaction - no pH dependence)
3. $2Fe^{3+} + 3H_2O \longrightarrow Fe_2O_{3(s)} + 6H^+$ (pure acid-base, no redox)
4. $2Fe^{2+} + 3H_2O \longrightarrow Fe_2O_{3(s)} + 6H^+ + 2e^-$ (slope = -59.2 x 6/2 = -178 mV/pH)
5. $2Fe_3O_{4(s)} + H_2O \longrightarrow 2H^+ + 2e^-$ (slope = -59.2 x 2/2 = -59.2 mV/pH)

The water redox lines have special significance on a Pourbaix diagram for an element such as iron. Recall that liquid water is stable *only* in the region between the dotted lines. Below the H_2 line, water is unstable relative to hydrogen gas, and above the O_2 line, water is unstable with respect to oxygen. For active metals such as Fe, the region where the pure element is stable is typically below the H_2 line. This means that iron metal is unstable in contact with water, undergoing reactions:

$Fe_{(s)} + 2H^+ \longrightarrow Fe^{2+}_{(aq)} + H_2$ (in acid)

$fe_{(s)} + 2H_2O \longrightarrow Fe(OH)_{2(s)} + H_2$ (in base)

Iron (and most other metals) are also thermodynamically unstable in air-saturated water, where the potential of the solution is close to the O_2 line in the Pourbaix diagram. Here the spontaneous reactions are:

$4\,Fe_{(s)} + 3\,O_2 + 12\,H^+ \longrightarrow 4\,Fe^{3+} + 6\,H_2O$ (in acid)

\(\ce{4Fe_{(s)} + 3O2 -> 2Fe2O3_{(s)} (in base)

Corrosion and passivation. It certainly sounds bad for our friend Fe: unstable in water, no matter what the pH or potential. Given enough time, it will all turn into rust. But iron (and other active metals) can corrode, or can be stabilized against corrosion, depending on the conditions. Because our civilization is dependent on the use of active metals such as Fe, Al, Zn, Ti, Cr... for practically everything, it is important to understand this, and we can do so by referring to the Pourbaix diagram.

The **corrosion** of iron (and other active metals such as Al) is indeed rapid in parts of the Pourbaix diagram where the element is oxidized to a soluble, ionic product such as Fe^{3+}(aq) or Al^{3+}(aq). However, solids such as Fe_2O_3, and especially Al_2O_3, form a protective coating on the metal that greatly impedes the corrosion reaction. This phenomenon is called **passivation.**

Draw a vertical line through the iron Pourbaix diagram at the pH of tap water (about 6) and you will discover something interesting: at slightly acidic pH, iron is quite unstable with respect to corrosion by the reaction:

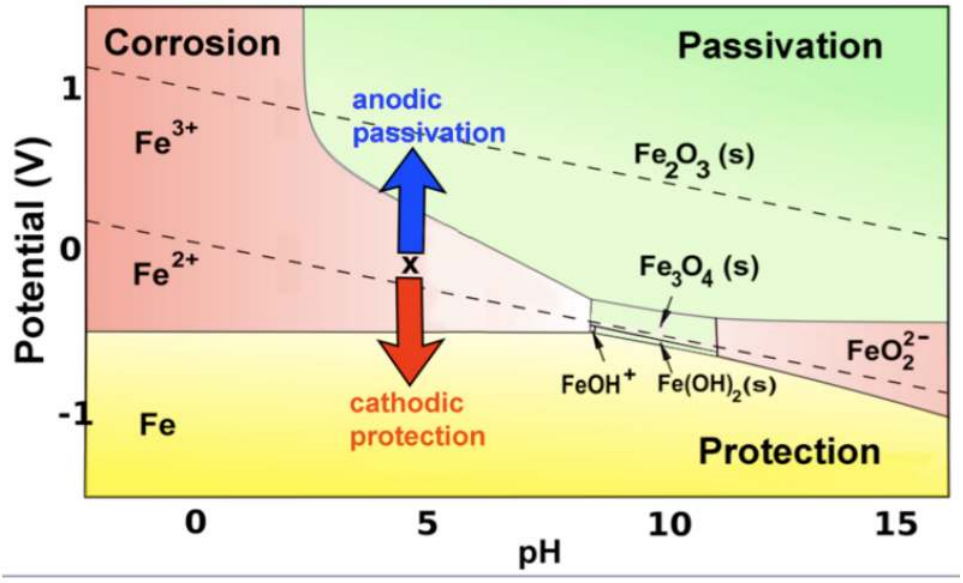
$$Fe_{(s)} + 2\,H^+ \longrightarrow Fe^{2+}{}_{(aq)} + H_2 \tag{6.3.6.1}$$

but *only in water that contains relatively little oxygen*, i.e., in solutions where the potential is near the H_2 line. Saturating the water with air or oxygen moves the system closer to the O_2 line, where the most stable species is Fe_2O_3 and the corrosion reaction is:

$$4\,Fe_{(s)} + 3\,O_2 \longrightarrow 2\,Fe_2O_{3\,(s)} \tag{6.3.6.2}$$

This oxidation reaction is orders of magnitude slower because the oxide that is formed *passivates* the surface. Therefore iron corrodes much more slowly in oxygenated solutions.

More generally, iron (and other active metals) are passivated whenever they oxidize to produce a solid product, and corrode whenever the product is ionic and soluble. This behavior can be summed up on the color-coded Pourbaix diagram below. The red and green regions represent conditions under which oxidation of iron produces soluble and insoluble products, respectively.

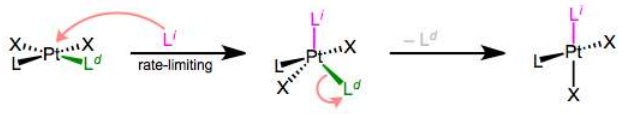


6.3.6: Pourbaix Diagrams is shared under a CC BY-SA license and was authored, remixed, and/or curated by LibreTexts.

- **4.6: Pourbaix Diagrams** by Chemistry 310 is licensed CC BY-SA 4.0. Original source: https://en.wikibooks.org/wiki/Introduction_to_Inorganic_Chemistry.

6.4: Associative Ligand Substitution

A very common reaction for metal complexes is ligand substitution in which one ligand is exchanged with another. There are two common mechanisms for ligand substitution reactions the first of which is called the associative mechanism. In this mechanism the incoming ligand approaches the complex before departure of the leaving ligand. How can we spot an associative mechanism in experimental data, and what are some of the consequences of this mechanism?



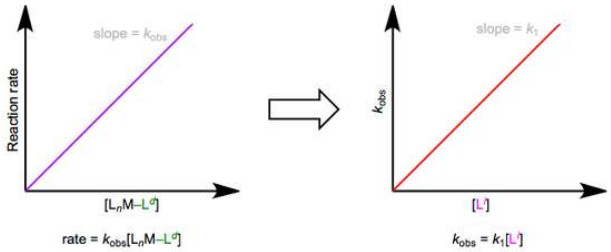
The prototypical mechanism of associative ligand substitution. The first step is rate-determining. A typical mechanism for associative ligand substitution is shown above. Let's begin by examining the kinetics of the reaction.

Reaction kinetics are commonly used to elucidate reaction mechanisms, and ligand substitution is no exception. Different mechanisms of substitution may follow different rate laws, so plotting the dependence of reaction rate on concentration of the species involved in the reaction often allows us to distinguish mechanisms. Associative substitution's rate law depends on the concentrations of both starting materials.

$$L_nM\text{–}L^d + L_i \rightarrow L_nM\text{–}L_i + L^d \tag{6.4.1}$$

$$\frac{d[L_nM\text{–}L^i]}{dt} = rate = k_1[L_nM\text{–}L^d][L^i] \tag{6.4.2}$$

The easiest way to determine this rate law is to use pseudo-first-order conditions. Although the rate law is second order overall, if we could somehow render the concentration of the incoming ligand unchanging, the reaction would appear first order. The observed rate constant under these conditions reflects the consistency of the incoming ligand's concentration ($k_{obs} = k_1[L^i]$, where both k_1 and $[Li]$ are constants). How can we make the concentration of the incoming ligand invariant, you ask? We can drown the reaction in ligand to achieve this. The small amount of the incoming ligand actually used up in the reaction has a negligible effect on the concentration of the "sea" of starting ligand we began with. The observed rate is equal to $k_{obs}[L_nM\text{–}L^d]$, as shown by the purple trace below. By determining k_{obs} at a variety of $[L^i]$ values, we can isolate k_1, the rate constant for the slow step. The red trace below at right shows the idea.



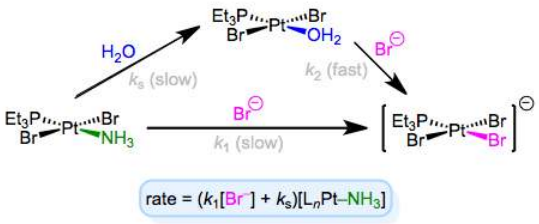
Associative substitution under pseudo-first-order conditions. The reaction is "swamped out" with incoming ligand.

In many cases, the red trace ends up with a non-zero y-intercept…curious, if we limit ourselves to the simple mechanism shown in the first figure of this post. A non-zero intercept suggests a more complex mechanism. We need to add a new term (called k_s for reasons to become clear shortly) to our first set of equations:

$$rate = (k_1[L_i] + k_s)[L_nM\text{–}L^d] \tag{6.4.3}$$

$$k_{obs} = k_1[L_i] + k_s \tag{6.4.4}$$

The full rate law suggests that some other step (with rate ks[LnM–Ld]) independent of incoming ligand is involved in the mechanism. To explain this observation, we can invoke the solvent as a reactant. Solvent can associate with the complex first in a slow step, then incoming ligand can displace the solvent in a fast step. Solvent concentration doesn't enter the rate law because, well, it's drowning the reactants and its concentration undergoes negligible change! An example of this mechanism iis shown below.



Associative substitution with solvent participation—a head-scratching mechanism for many an organometallic grad student!

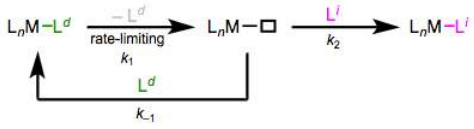
As an aside, it's worth mentioning that the entropy of activation of associative substitution is typically negative. Entropy decreases as the incoming ligand and complex come together in the rate-determining step.

Dr. Michael Evans (Georgia Tech)

This page titled 6.4: Associative Ligand Substitution is shared under a not declared license and was authored, remixed, and/or curated by Michael Evans.

6.5: Dissociative Ligand Substitution

The second mechanism for ligand substitution is the dissociative mechanism. In the slow step with positive entropy of activation, the departing ligand leaves, generating a coordinatively unsaturated intermediate. The incoming ligand then enters the coordination sphere of the metal to generate the product. The reverse of the first step, re-coordination of the departing ligand (rate constant k–1), is often competitive with dissociation.



A general scheme for dissociative ligand substitution. There's more to the intermediate than meets the eye!

Let's begin with the general situation in which k_1 and k_{-1} are similar in magnitude. Since k_1 is rate limiting, k_2 is assumed to be much larger than k_1 and k_{-1}. Most importantly, we need to assume that variation in the concentration of the unsaturated intermediate is essentially zero. This is called the steady state approximation, and it allows us to set up an equation that relates reaction rate to observable concentrations Hold onto that for a second; first, we can use step 2 to establish a preliminary rate expression.

$$\text{rate} = k_2[L_nM\text{–}\Diamond][Li] \tag{1}$$

Of course, the unsaturated complex is present in very small concentration and is unmeasurable, so this equation doesn't help us much. We need to remove the concentration of the unmeasurable intermediate from (1), and the steady state approximation helps us do this. We can express variation in the concentration of the unsaturated intermediate as (processes that make it) minus (processes that destroy it), multiplying by an arbitrary time length to make the units work out. All of that equals zero, according to the steady state approximation. Since Δt must not be zero, the other factor, the collection of terms, must equal zero.

$$\Delta[LnM\text{–}\Diamond] = 0 = (k1[LnM\text{–}L^d]\text{–}k\text{–}1[LnM\text{–}\Diamond][L^d]\text{–}k_2[LnM\text{–}\Diamond][Li])\Delta t \tag{2}$$

$$0 = k_1[LnM\text{–}Ld]\text{–}k_{-1}[LnM\text{–}\Diamond][Ld]\text{–}k_2[LnM\text{–}\Diamond][Li] \tag{3}$$

Rearranging to solve for [LnM–◊], we arrive at the following.

$$[LnM\text{–}\Diamond] = k_1\frac{[LnM\text{–}L_d]}{(k_{-1}[L_d] + k_2[Li]} \tag{4}$$

Finally, substituting into equation (1) we reach a verifiable rate equation.

$$\text{rate} = k_2k_1\frac{[LnM\text{–}Ld][Li]}{(k_{-1}[L_d] + k_2[Li]} \tag{5}$$

When k_{-1} is negligibly small, (5) reduces to the familiar equation (6), typical of dissociative reactions like S_N1.

$$\text{rate} = k_1[LnM\text{–}L_d] \tag{6}$$

Unlike the associative rate law, this rate does not depend on the concentration of incoming ligand. For reactions that are better described by (5), we can drown the reaction in incoming ligand to make $k_2[Li]$ far greater than $k_{-1}[Ld]$, essentially forcing the reaction to fit equation (6).

In general, introducing structural features that either stabilize the unsaturated intermediate or destabilize the starting complex can encourage dissociative substitution. Both of these strategies lower the activation barrier for the reaction. Other, quirky ways to encourage dissociation include photochemical methods, oxidation/reduction, and ligand abstraction.

Contributors and Attributions

- Dr. Michael Evans (Georgia Tech)

This page titled 6.5: Dissociative Ligand Substitution is shared under a not declared license and was authored, remixed, and/or curated by Michael Evans.

6.6: Biological Significance of Iron, Zinc, Copper, Molybdenum, Cobalt, Chromium, Vanadium, and Nickel

The transition metals and zinc are among the least abundant metal ions in sea water from which contemporary organisms are thought to have evolved.[1-5] For many metals, the concentration in human blood plasma, while still very low, greatly exceeds that in sea water (Table **6.6.1**). Such data indicate the importance of mechanisms for accumulation, storage, and transport of transition metals in living organisms.

Table 6.6.1. Concentrations of transition metals and zinc in sea water and human plasma.a*Data from References 1 - 5 and 12

Element	Sea Water (M) x 10^8	Human Plasma (M) x 10^8
Fe	0.005 - 2	2230
Zn	8.0	1720
Cu	1.0	1650
Mo	10.0	1000
Co	0.7	0.0025
Cr	0.4	5.5
V	4.0	17.7
Mn	0.7	10.9
Ni	0.5	4.4

The metals are generally found either bound directly to proteins, in cofactors, or in clusters that are in turn bound to proteins; the ligands usually have O, N, S, or C donor atoms. Proteins with which transition metals are most commonly associated catalyze the intramolecular or intermolecular rearrangement of electrons. Although the redox properties of the metals are important in many of the reactions, in others the metal appears to contribute to the structure of the active state, e.g., zinc in the Cu-Zn dismutases and some of the iron in the photosynthetic reaction center. Sometimes equivalent reactions are catalyzed by proteins with different metal centers; the metal binding sites and proteins have evolved separately for each type of metal center.

Iron is the most common transition metal in biology.[6,7] Its use has created a dependence that has survived the appearance of dioxygen in the atmosphere ca. 2.5 billion years ago, and the concomitant conversion of ferrous ion to ferric ion and insoluble rust. All plants, animals, and bacteria use iron, except for a lactobacillus that appears to maintain high concentrations of manganese instead of iron. The processes and reactions in which iron participates are crucial to the survival of terrestrial organisms, and include ribonucleotide reduction (DNA synthesis), energy production (respiration), energy conversion (photosynthesis), nitrogen reduction, oxygen transport (respiration, muscle contraction), and oxygenation (e.g., steroid synthesis, solubilization and detoxification of aromatic compounds). Among the transition metals used in living organisms, iron is the most abundant in the environment. Whether this fact alone explains the biological predominance of iron or whether specific features of iron chemistry contribute is not clear.

Many of the other transition metals participate in reactions equivalent to those involving iron, and can sometimes substitute for iron, albeit less effectively, in natural Fe-proteins. Additional biological reactions are unique to nonferrous transition metals.

Zinc is relatively abundant in biological materials.[8,9] The major location of zinc in the body is metallothionein, which also binds copper, chromium, mercury, and other metals. Among the other well-characterized zinc proteins are the Cu-Zn superoxide dismutases (other forms have Fe or Mn), carbonic anhydrase (an abundant protein in red blood cells responsible for maintaining the pH of the blood), alcohol dehydrogenase, and a variety of hydrolases involved in the metabolism of sugars, proteins, and nucleic acids. Zinc is a common element in nucleic-acid polymerases and transcription factors, where its role is considered to be structural rather than catalytic. Interestingly, zinc enhances the selectivity of the polymerization of nucleotides under reaction conditions designed to simulate the environment for prebiotic reactions. Recently a group of nucleic-acid binding proteins, with a repeated

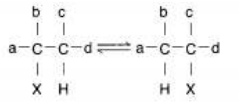
sequence containing the amino acids cysteine and histidine, were shown to bind as many as eleven zinc atoms necessary for protein function (transcribing DNA to RNA).[10] Zinc plays a structural role, forming the peptide into multiple domains or "zinc fingers" by means of coordination to cysteine and histidine. A survey of the sequences of many nucleic-acid binding proteins shows that many of them have the common motif required to form zinc fingers. Other zinc-finger proteins called steroid receptors bind both steroids such as progesterone and the progesterone gene DNA . Much of the zinc in animals and plants has no known function, but it may be maintaining the structures of proteins that activate and deactivate genes.[11]

Copper and iron proteins participate in many of the same biological reactions:

1. reversible binding of dioxygen, e.g., hemocyanin (Cu), hemerythrin (Fe), and hemoglobin (Fe);
2. activation of dioxygen, e.g., dopamine hydroxylase (Cu) (important in the synthesis of the hormone epinephrine), tyrosinases (Cu), and catechol dioxygenases (Fe);
3. electron transfer, e.g., plastocyanins (Cu), ferredoxins, and c-type cytochromes (Fe);
4. dismutation of superoxide by Cu or Fe as the redox-active metal (superoxide dismutases).

The two metal ions also function in concert in proteins such as cytochrome oxidase, which catalyzes the transfer of four electrons to dioxygen to form water during respiration. Whether any types of biological reactions are unique to copper proteins is not clear. However, use of stored iron is reduced by copper deficiency, which suggests that iron metabolism may depend on copper proteins, such as the serum protein ceruloplasmin, which can function as a ferroxidase, and the cellular protein ascorbic acid oxidase, which also is a ferrireductase.

Cobalt is found in vitamin B_{12} , its only apparent biological site.[12] The vitamin is a cyano complex, but a methyl or methylene group replaces the cyano ligand in native enzymes. Vitamin-B_{12} deficiency causes the severe disease of pernicious anemia in humans, which indicates the critical role of cobalt. The most common type of reaction in which cobalamin enzymes participate results in the reciprocal exchange of hydrogen atoms if they are on adjacent carbon atoms, yet not with hydrogen in solvent water:



Nickel is a component of a hydrolase (urease), of hydrogenase, of CO dehydrogenase, and of S-methyl CoM reductase, which catalyzes the terminal step in methane production by methanogenic bacteria. All the Ni-proteins known to date are from plants or bacteria.[13,14] However, about 50 years elapsed between the crystallization of jack-bean urease in 1925 and the identification of the nickel component in the plant protein. Thus it is premature to exclude the possibility of Ni-proteins in animals. Despite the small number of characterized Ni-proteins, it is clear that many different environments exist, from apparently direct coordination to protein ligands (urease) to the tetrapyrrole F430 in methylreductase and the multiple metal sites of Ni and Fe-S in a hydrogenase from the bacterium *Desulfovibrio gigas*. Specific environments for nickel are also indicated for nucleic acids (or nucleic acid-binding proteins), since nickel activates the gene for hydrogenase.[15]

Manganese plays a critical role in oxygen evolution catalyzed by the proteins of the photosynthetic reaction center. The superoxide dismutase of bacteria and mitochondria, as well as pyruvate carboxylase in mammals, are also manganese proteins.[16,17] How the multiple manganese atoms of the photosynthetic reaction center participate in the removal of four electrons and protons from water is the subject of intense investigation by spectroscopists, synthetic inorganic chemists, and molecular biologists.[17]

Vanadium and chromium have several features in common, from a bioinorganic viewpoint.[18a] First, both metals are present in only small amounts in most organisms. Second, the biological roles of each remain largely unknown.[18] Finally, each has served as a probe to characterize the sites of other metals, such as iron and zinc. Vanadium is required for normal health, and could act *in vivo* either as a metal cation or as a phosphate analogue, depending on the oxidation state, V(lV) or V(V), respectively. Vanadium in a sea squirt (tunicate), a primitive vertebrate (Figure 1.2B), is concentrated in blood cells, apparently as the major cellular transition metal, but whether it participates in the transport of dioxygen (as iron and copper do) is not known. In proteins, vanadium is a cofactor in an algal bromoperoxidase and in certain prokaryotic nitrogenases. Chromium imbalance affects sugar metabolism and has been associated with the glucose tolerance factor in animals. But little is known about the structure of the factor or of any other specific chromium complexes from plants, animals, or bacteria.

Molybdenum proteins catalyze the reduction of nitrogen and nitrate, as well as the oxidation of aldehydes, purines, and sulfite.[19] Few Mo-proteins are known compared to those involving other transition metals. Nitrogenases, which also contain iron, have been the focus of intense investigations by bioinorganic chemists and biologists; the iron is found in a cluster with molybdenum (the iron-molybdenum cofactor, or FeMoCo) and in an iron-sulfur center (Chapter 7). Interestingly, certain bacteria (*Azotobacter*) have alternative nitrogenases, which are produced when molybdenum is deficient and which contain vanadium and iron or only iron. All other known Mo-proteins are also Fe-proteins with iron centers, such as tetrapyrroles (heme and chlorins), Fe-sulfur clusters, and, apparently, non-heme/non-sulfur iron. Some Mo-proteins contain additional cofactors such as the Havins, e.g., in xanthine oxidase and aldehyde oxidase. The number of redox centers in some Mo-proteins exceeds the number of electrons transferred; reasons for this are unknown currently.

6.6: Biological Significance of Iron, Zinc, Copper, Molybdenum, Cobalt, Chromium, Vanadium, and Nickel is shared under a not declared license and was authored, remixed, and/or curated by LibreTexts.

SECTION OVERVIEW

6.7: Ferrodoxins, Hydrogenases, and Nitrogenases - Metal-Sulfide Proteins

Transition-metal/sulfide sites, especially those containing iron, are present in all forms of life and are found at the active centers of a wide variety of redox and catalytic proteins. These proteins include simple soluble electron-transfer agents (the ferredoxins), membrane-bound components of electron-transfer chains, and some of the most complex metalloenzymes, such as nitrogenase, hydrogenase, and xanthine oxidase. In this chapter we first review the chemistry of the Fe-S sites that occur in relatively simple rubredoxins and ferredoxins, and make note of the ubiquity of these sites in other metalloenzymes. We use these relatively simple systems to show the usefulness of spectroscopy and model-system studies for deducing bioinorganic structure and reactivity. We then direct our attention to the hydrogenase and nitrogenase enzyme systems, both of which use transition-metalsulfur clusters to activate and evolve molecular hydrogen.

6.7.1: Iron-sulfur Proteins and Models

6.7.2: Iron-sulfur Proteins and Models (Part 2)

6.7.3: Iron-sulfur Proteins and Models (Part 3)

6.7.4: Iron-sulfur Proteins and Models (Part 4)

References

1. F. Armstrong, in A. G. Sykes, ed., *Advances in Inorganic and Bioinorganic Mechanisms*, Vol. **I**, Academic Press, 1982.
2. H. Beinert and S. P. J. Albracht, *Biochim. Biophys. Acta* **683** (1982), 245.
3. A. V. Xavier, J. J. G. Moura, and I. Moura, in J. B. Goodenough *et al.*, eds., *Structure and Bonding*, Springer-Verlag, **43** (1981), 187-213.
4. D. C. Yoch and R. P. Carithers, *Microbiol. Rev*. **43** (1979), 384.
5. H. B. Dunford *et aI.*, eds., *The Biological Chemistry of Iron: A Look at the Metabolism of Iron and Its Subsequent Uses in Living Organisms*, Reidel, 1981.
6. R. K. Thauer and P. Schönheit, in Reference 8, p. 329.
7. A. Bezkorovainy, *Biochemistry of Nonheme Iron*, Plenum, 1980, pp. 343-393.
8. T. G. Spiro, ed., *Iron-Sulfur Proteins*, Wiley-Interscience, 1985.
9. W. Lovenberg, ed., *Iron-Sulfur Proteins*, Vol. I, Academic Press, 1973.
10. Reference 9, Vol. II, Academic Press, 1973.
11. Reference 10, Vol. III, Academic Press, 1977.
12. Nomenclature, *Eur. J. Biochem.* **93** (1979), 427.
13. Nomenclature, *Biochim. Biophys. Acta* 549 (1979), 101.
14. C. F. Yocum, J. N. Sadow, and A. San Pietro, in Reference 9, p. 112.
15. B. B. Buchanan, in Reference 9, p. 129.
16. T. P. Singer and R. R. Ramsay, in A. N. Martonosi, ed., *The Enzymes of Biological Membranes*, Plenum, 1985, pp. 301-332.
17. T. Yagi, H. Inokuchi, and K. Kimura, *Acc. Chem. Res.* **16** (1983), 2; Y. Higuchi *et al.*, *J. Mol. Biol.* **172** (1984), 109.
18. R. Lemberg and J. Barrett, *Cytochromes*, Academic Press, 1973.
19. H. Beinert, in Reference 9, p. 1.
20. K. K. Rao and D. O. Hall, in G. V. Leigh, ed., *Evolution of Metalloenzymes, Metalloproteins, and Related Materials*, 1977, p. 39.
21. D. O. Hall, R. Cammack, and K. K. Rao, *Nature* **233** (1977), 136.
22. T. Ohnishi and J. C. Salerno, in Reference 8, p. 285.
23. F. A. Cotton and G. Wilkinson, *Advanced Inorganic Chemistry*, Wiley, 1980.
24. D. E. McRee *et al.*, *J. Biol. Chem.* **261** (1986), 10277.

25. S. J. N. Burgmayer and E. I. Stiefel, *J. Chem. Educ.* **62** (1985), 943.
26. W. Lovenberg and B. E. Sobel, *Proc. Natl. Acad. Sci. USA* **54** (1965), 193.
27. E. T. Lode and M. J. Coon, in Reference 9, pp. 173-191.
28. I. C. Gunsalus and J. D. Lipscomb, in Reference 11, p. 151.
29. R. W. Estabrook *et al*., in Reference 9.
30. I. Moura *et al*., *Biochem. Biophys. Res. Commun*. **75** (1977), 1037.
31. I. Moura *et al*., *J. Biol. Chem.* **255** (1980), 2493. a) J. LeGall *et al*., *Biochemistry* **27** (1988), 1636.
32. K. D. Watenpaugh, L. C. Sieker, and L. H. Jensen, *J. Mol. Biol*. **138** (1980), 615.
33. E. T. Adman *et al*., *J. Mol. Biol.* **112** (1977), 113. a) C. D. Stout, in Reference 8, p. 97.
34. K. D. Watenpaugh *et al*., *Acta Cryst*. **B29** (1973), 943.
35. R. G. Shulman *et al*., *Proc. Natl. Acad. Sci. USA* **72** (1975), 4003.
36. R. G. Shulman *et al*., *J. Mol. Biol.* **124** (1978), 305.
37. W. D. Phillips *et al*., *Nature* **227** (1970), 574.
38. J. C. Rivoal *et aI*., *Biochim. Biophys. Acta* **493** (1977), 122.
39. D. E. Bennett and M. K. Johnson, *Biochim. Biophys. Acta* **911** (1987), 71. a) M. S. Gebhard *et al*.,*J. Am. Chem. Soc*. **112** (1990), 2217. b) K. D. Butcher, M. S. Gebhard, and E. I. Solomon, *Inorg. Chem*. **29** (1990), 2067.
40. M. C. W. Evans, in Reference 8, p. 249.
41. W. A. Eaton and W. J. Lovenberg, *J. Am. Chem. Soc*. **92** (1970), 7195.
42. M. K. Johnson, A. E. Robinson, and A. J. Thomson, in Reference 8, p. 367.
43. P. J. Stephens *et aI*., *Proc. Natl. Acad. Sci. USA* **75** (1978), 5273.
44. J. Peisach *et al*., *J. Biol. Chem.* 246 (1971), 5877.
45. P. M. Champion and A. J. Siever, *J. Chem. Phys.* **66** (1977), 1819; D. Coucouvanis *et al*., *J. Am. Chem Soc.* **101** (1979), 3392.
46. R. Cammack, D. S. Patil, and V. M. Fernandez, *Biochem. Soc. Trans.* **13** (1985), 572.
47. B. L. Trumpower, *Biochim. Biophys. Acta* **639** (1981), 129.
48. H. Beinert, *Biochem. Soc. Trans.* **13** (1985), 542.
49. G. Palmer, *Biochem. Soc. Trans.* **13** (1985), 548.
50. R. Malkin and A. J. Bearden, *Biochim. Biophys. Acta* **505** (1978), 147.
51. C. E. Johnson, *J. Inorg. Biochem.* **28** (1986), 207.
52. E. Münck and T. A. Kent, *Hyperfine Interactions* **27** (1986), 161.
53. K. K. Rao *et al*., *Biochem. J.* **129** (1972), 1063.
54. I. Bertini and C. Luchinat, eds., *NMR of Paramagnetic Molecules in Biological Systems*, Benjamin/ Cummings, 1986.
55. G. N. La Mar, W. D. Horrocks, Jr., and R. H. Holm, NMR *of Paramagnetic Molecules*, Academic Press, 1973.
56. M. T. Werth *et al*., *J. Am. Chem. Soc.* **109** (1987), 273.
57. T. G. Spiro *et al*., in Reference 8, p. 407. a) T. V. Long and T. M. Loehr, *J. Am. Chem. Soc.* **92** (1970), 6384.
58. G. Christou, B. Ridge, and H. N. Rydon, *J. Chem. Soc. Chem. Commun.* (1979), 20.
59. S. W. May and J.-Y. Kuo, *Biochemistry* **17** (1978), 3333.
60. S. W. May *et al*., *Biochemistry* **23** (1984), 2187.
61. P. Saint-Martin *et al*., *Proc. Natl. Acad. Sci. USA* **85** (1988), 9378.
62. R. W. Lane *et al*., *Proc. Natl. Acad. Sci. USA* **72** (1975), 2868.
63. R. W. Lane *et al*., *J. Am. Chem. Soc.* **99** (1977), 84.
64. D. G. Holah and D. Coucouvanis, *J. Am. Chem. Soc.* **97** (1975), 6917.
65. D. Coucouvanis *et al*., *J. Am. Chem. Soc.* **93** (1976), 5721.
66. M. Millar *et al*., *lnorg. Chem.* **21** (1982), 4105.
67. S. A. Koch and L. E. Madia, *J. Am. Chem. Soc.* **105** (1983), 5944.
68. M. Millar, S. A. Koch, and R. Fikar, *lnorg. Chim. Acta* **88** (1984), L15.
69. J. C. Deaton *et al*., *J. Am. Chem. Soc.* **110** (1988), 6241.
70. D. B. Knaff, *Trends Biochem. Sci.* **13** (1988), 461. a) T. Tsukihara *et al*., *J. Biochem.* **90** (1981), 1763.
71. D. R. Ort and N. E. Good, *Trends Biochem. Sci.* **13** (1988), 467.
72. V. Massey, in Reference 9, p. 301.
73. M. K. Johnson *et al*., *J. Biol. Chem.* **260** (1985), 7368.

74. J. C. Salerno *et al*., *J. Biol. Chem.* **254** (1979), 4828.
75. T. P. Singer, M. Gutman, and V. Massey, in Reference 9, p. 225.
76. H. Twilfer, F.-H. Bernhardt, and K. Gersonde, *Eur. J. Biochem.* **119** (1981), 595.
77. L. Petersson, R. Cammack, and K. Krishna Rao, *Biochim. Biophys. Acta* **622** (1980), 18.
78. B.-K. Teo and R. G. Shulman, in Reference 8, p. 343.
79. T. Tsukihara *et al*., in K. Kimura, ed., *Molecular Evolution, Protein Polymorphism and the Neutral Theory*, Japan Scientific Societies Press and Springer-Verlag, 1982, p. 299.
80. T. Tsukihara *et al*., *BioSystems* **15** (1982), 243.
81. D. Petering and G. Palmer, *Arch. Biochem. Biophys*. **141** (1970), 456.
82. J. F. Gibson *et aI*., *Proc. Natl. Acad. Sci. USA* **56** (1966), 987.
83. W. A. Eaton *et al*., *Proc. Natl. Acad. Soc. USA* **68** (1971), 3015. a) L. B. Dugad *et al*., *Biochemistry* **29** (1990), 2663.
84. J. Rawlings, O. Siiman, and H. B. Gray, *Proc. Natl. Acad. Sci. USA* **71** (1974), 125.
85. I. Salmeen and G. Palmer, *Arch. Biochem. Biophys.* **150** (1972), 767.
86. J. J. Mayerle *et al*., *Proc. Natl. Acad. Sci. USA* **70** (1973), 2429.
87. J. L. Markley *et al*., *Science* **240** (1988), 908. a) L. Banci, I. Bertini, and C. Luchinat, *Structure and Bonding* **72** (1990), 113.
88. V. K. Yachandra *et al*., *J. Am. Chem. Soc.* **105** (1983), 6462.
89. S. Hwa, R. S. Czernuszewicz, and T. G. Spiro, *J. Am. Chem. Soc*. **111** (1989), 3496.
90. S. Hwa *et al*., *J. Am. Chem. Soc.* **111** (1989), 3505.
91. J. R. Rieske, D. H. MacLennan, and R. Coleman, *Biochem. Biophys. Res. Commun*. **15** (1964), 338.
92. W. D. Bonner, Jr., and R. C. Prince, *FEBS Lett.* **177** (1984), 47.
93. J. F. Cline *et al*., *J. Biol. Chem.* **260** (1985), 3251.
94. H.-T. Tsang *et al*., *Biochemistry* **28** (1989), 7233.
95. R. C. Prince, S. J. G. Linkletter, and P. L. Dutton, *Biochem. Biophys. Acta* **635** (1981), 132.
96. J. G. Reynolds and R. H. Holm, *lnorg. Chem*. **19** (1980), 3257; **20** (1981), 1873. a) J. J. Mayerle *et al*., *J. Am. Chem. Soc*. **97** (1977), 1032. b) Y. Do, E. D. Simhon, and R. H. Holm, *lnorg. Chem.* **22** (1983), 3809. c) S. Han, R. Czernuszewicz, and T. G. Spiro, *lnorg. Chem.* **25** (1986), 2276. d) H. Strasdeit, B. Krebs, and G. Henkel, *lnorg. Chim. Acta* **89** (1989), LII.
97. P. K. Mascharak *et al*., *J. Am. Chem. Soc.* **103** (1981), 6110.
98. P. Beardwood *et al*., *J. Chem. Soc.* Dalton Trans. (1982), 2015.
99. D. Coucouvanis *et al*., *J. Am. Chem. Soc*. **106** (1984), 6081.
100. P. Beardwood and J. F. Gibson, *J. Chem. Soc. Chem. Commun.* **102** (1985), 490 and 1345.
101. L. C. Sieker, E. Adman, and L. H. Jensen, *Nature* **235** (1971), 40.
102. J. M. Berg, K. O. Hodgson, and R. H. Holm, *J. Am. Chem. Soc*. **101** (1970), 4586.
103. P. J. Stephens *et al*., *Proc. Natl. Acad. Sci. USA* **82** (1985), 5661.
104. M. W. W. Adams and L. E. Mortenson, in Reference 235a.
105. L. W. Lim *et al*., *J. Biol. Chem.* **261** (1986), 15 and 140.
106. J. C. Salerno *et al*., *Biochem. Biophys. Res. Commun.* **73** (1976), 833.
107. G. Strahs and J. Kraut, *J. Mol. Biol.* **35** (1968), 503.
108. C. W. Carter, Jr., *et al*., *Proc. Natl. Acad. Sci. USA* **69** (1972), 3526.
109. C. W. Carter, Jr., *et al*., *J. Biol. Chem*. **249** (1974), 4212.
110. K. Fukuyama, *J. Mol. Biol.* 199 (1988), 183. a) K. Fukuyama *et al*., *J. Mol. Biol.* **210** (1989), 383.
111. G. H. Stout *et al*., *Proc. Natl. Acad. Sci. USA* **85** (1988), 1020.
112. C. D. Stout, *J. Biol. Chem.* **263** (1988), 9256.
113. A. H. Robbins and C. D. Stout, *Proc. Natl. Acad. Sci. USA* **86** (1989), 3639.
114. E. T. Adman, L. C. Sieker, and L. H. Jensen, *J. Biol. Chem.* **248** (1973), 3987.
115. R. C. Prince and M. W. W. Adams, *J. Biol. Chem.* **262** (1987), 5125.
116. L. E. Mortenson, R. C. Valentine, and J. E. Carnahan, *Biochem. Biophys. Res. Commun.* **7** (1962), 448.
117. W. Lovenberg, B. B. Buchanan, and J. C. Rabinowitz, *J. Biol. Chem*. **254** (1979), 4499.
118. R. Mathews *et al*., *J. Biol. Chem.* **249** (1974), 4326.
119. A. J. Thomson, in P. M. Harrison, ed., *Metalloproteins, Part I: Metal Proteins with Redox Roles*, Verlag Chemie, 1985, pp. 79-120.

120. R. Cammack, *Biochem. Biophys. Res. Commun.* **54** (1973), 548.
121. M. J. Carney *et al.*, *Inorg. Chem.* **27** (1988), 346.
122. M. J. Carney *et al.*, *J. Am. Chem. Soc.* **110** (1988), 6084.
123. L. Noodleman, D. A. Case, and A. Aizman, *J. Am. Chem. Soc.* **110** (1988), 1001.
124. L. Noodleman, *Inorg. Chem.* 27 (1988), 3677.
125. J.-M. Moulis, J. Meyer, and M. Lutz, *Biochemistry* **23** (1984), 6605. a) W. D. Phillips and M. Poe, in Reference 10, p. 255. b) E. L. Packer *et al.*, *J. Biol. Chem.* **252** (1977), 2245. c) J. Bertini *et al.*, *Inorg. Chem.* **29** (1990), 1874. d) B.-K. Teo *et al.*, *J. Am. Chem. Soc.* **101** (1979), 5624.
126. T. Herskovitz *et al.*, *Proc. Natl. Acad. Sci. USA* **69** (1972), 2437.
127. B. A. Averill *et al.*, *J. Am. Chem. Soc.* **95** (1973), 3523.
128. J. M. Berg and R. H. Holm, in Reference 8, p. I.
129. G. B. Wang, M. A. Bobrick, and R. H. Holm, *Inorg. Chem.* **17** (1978), 578.
130. D. Coucouvanis *et al.*, *J. Am. Chem. Soc.* **104** (1982), 1874.
131. A. Müller and N. Schladerbeck, *Chimia* **39** (1985), 23.
132. A. Müller, N. Schladerbeck, and H. Bagge, *Chimia* **39** (1985), 24.
133. S. Rutchik, S. Kim, and M. A. Walters, *Inorg. Chem.* **27** (1988), 1513.
134. W. E. Cleland *et al.*, *J. Am. Chem. Soc.* **105** (1983), 6021.
135. M. G. Kanatzidis *et al.*, *J. Am. Chem. Soc.* **106** (1984), 4500.
136. M. G. Kanatzidis *et al.*, *Inorg. Chem.* **22** (1983), 179.
137. R. E. Johnson *et al.*, *J. Am. Chem. Soc.* **105** (1983), 7280.
138. M. G. Kanatzidis *et al.*, *J. Am. Chem. Soc.* **107** (1985), 4925. a) K. S. Hagen, J. G. Reynolds, and R. H. Holm, *J. Am. Chem. Soc.* **103** (1981), 4054. b) G. Christou and C. D. Gamer, *J. Chem. Soc. Dalton Trans.* (1979), 1093. c) M. J. Carney *et al.*, *Inorg. Chem.* **27** (1988), 346. d) P. Barbaro *et al.*, *J. Am. Chem. Soc.* **112** (1990), 7238.
139. E. J. Laskowski *et al.*, *J. Am. Chem. Soc.* **100** (1978), 5322.
140. E.1. Laskowski *et al.*, *J. Am. Chem. Soc.* **101** (1979), 6562.
141. T. O'Sullivan and M. Millar, *J. Am. Chem. Soc.* **107** (1985), 4096.
142. M. Millar, private communication.
143. T. D. P. Stack and R. H. Holm, *J. Am. Chem. Soc.* **110** (1989), 2484. a) T. D. P. Stack, M. J. Carney, and R. H. Holm, *J. Am. Chem. Soc.* **111** (1989), 1670. b) S. Ciurli *et al.*, *J. Am. Chem. Soc.* **112** (1990), 2654. c) P. R. Challen *et al.*, *J. Am. Chem. Soc.* **112** (1990), 2455.
144. L. Que, Jr., R. H. Holm, and L. E. Mortenson, *J. Am. Chem. Soc.* **97** (1975), 463.
145. N. R. Bastian *et al.*, in Reference 10, p. 227.
146. H. Beinert and A. J. Thomson, *Arch. Biochem. Biophys.* **222** (1983), 333.
147. M. H. Emptage *et al.*, *J. Biol. Chem.* **255** (1980), 1793.
148. W. W. Sweeney, J. C. Rabinowitz, and D. C. Yoch, *J. Biol. Chem.* **250** (1985), 7842.
149. B. A. Averill, J. R. Bal, and W. H. Orme-Johnson, *J. Am. Chem. Soc.* **100** (1978), 3034.
150. C. D. Stout, *Nature* **279** (1979), 83.
151. D. Ghosh *et al.*, *J. Biol. Chem.* **256** (1981), 4185.
152. D. Ghosh *et al.*, *J. Mol. Biol.* **158** (1982), 73.
153. M. K. Johnson *et al.*, *J. Am. Chem. Soc.* **105** (1983), 6671.
154. H. Beinert and A. J. Thomson, *Arch. Biochem. Biophys.* **222** (1983), 333.
155. M. R. Antonio *et al.*, *J. Biol. Chem.* **257** (1982), 6646.
156. E. Miinck, in Reference 8, p. 147.
157. C. E. Johnson, *J. Inorg. Biochem.* **207** (1986), 28.
158. B. H. Huynh *et al.*, *J. Biol. Chem.* **255** (1980), 3242.
159. J. J. G. Moura *et al.*, *J. Biol. Chem.* **257** (1982), 6259. a) H. Beinert and M. C. Kennedy, *Eur. J. Biochem.* **186** (1989), 1865.
160. C. R. Kissinger *et al.*, *J. Am. Chem. Soc.* **110** (1988), 8721. a) S. Ciurli and R. H. Holm, *Inorg. Chem.* **28** (1989), 1685.
161. T. A. Kent *et al.*, *J. Biol. Chem.* **260** (1985), 6871.
162. A. H. Robbins and C. D. Stout, *J. Biol. Chem.* **260** (1985), 2328.
163. M. K. Johnson *et al.*, *J. Biol. Chem.* **258** (1983), 12771.

164. M. C. Kennedy *et al.*, *J. Biol. Chem.* **258** (1983), 11098.
165. J. TeIser *et al.*, *J. Biol. Chem.* **261** (1986), 4840.
166. D. H. Flint, M. H. Emptage, and J. R. Guest, *J. Inorg. Biochem.* **36** (1989), 306. a) R. L. Switzer, *BioFactors* **2** (1989), 77.
167. H. Beinert *et al.*, *Proc. Natl. Acad. Sci. USA* **80** (1983), 393.
168. M. K. Johnson *et al.*, *J. Biol. Chem.* **256** (1981), 9806.
169. T. R. Halbert *et al.*, *J. Am. Chem. Soc.* **106** (1984),1849.
170. G. N. George and S. J. George, *Trends Biochem. Sci.* **13** (1988), 369. a) I. Moura *et al*., *J. Am. Chem. Soc.* **108** (1986), 349. b) K. K. Surerus *et al.*, *J. Am. Chem. Soc.* **109** (1987), 3805. c) R. C. Conover *et al.*, *J. Am. Chem. Soc.* **112** (1990), 4562. d) J. K. Money, J. C. Huffman, and G. Christou, *Inorg. Chem.* **27** (1988), 507.
171. B. H. Huynh *et al*., *Proc. Natl. Acad. Sci. USA* **81** (1984), 3728.
172. T. R. Hawkes and B. E. Smith, *Biochem. J.* 223 (1984), 783.
173. M. A. Whitener *et al.*, *J. Am. Chem. Soc.* **108** (1986), 5607.
174. K. S. Hagen and R. H. Holm, *J. Am. Chem. Soc.* **104** (1982), 5496.
175. K. S. Hagen, A. D. Watson, and R. H. Holm, *J. Am. Chem. Soc.* **105** (1983), 3905. a) J.-J. Girard *et al.*, *J. Am. Chem. Soc.* **106** (1984), 5941.
176. M. C. Kennedy *et al.*, *J. Biol. Chem.* 259 (1984), 14463. a) H. Strasdeit, B. Krebs, and G. Henkel, *Inorg. Chem*. **23** (1983), 1816.
177. M. G. Kanatzidis *et al.*, *J. Chem. Soc. Chem. Commun.* (1984), 356.
178. M. G. Kanatzidis, A. Salifoglou, and D. Coucouvanis, *J. Am. Chem. Soc.* **107** (1985), 3358; *Inorg. Chem*. **25** (1986), 2460.
179. S. Pohl and W. Saak, *Angew. Chem. Int. Ed. Engl.* **23** (1984), 907. a) S. A. AI-Ahmand *et al.*, *Inorg. Chem.* **29** (1990), 927.
180. F. Cecconi, C. A. Ghilardi, and S. Midolini, *J. Chem. Soc. Chem. Commun.* (1981), 640.
181. A. Agresti *et al.*, *Inorg. Chem.* **24** (1985), 689.
182. K. S. Hagen, J. M. Berg, and R. H. Holm, *Inorg. Chim. Acta* **45** (1980), L17. a) B. S. Snyder and R. H. Holm, *Inorg. Chem.* **27** (1988), 1816. b) B. S. Synder *et al.*, *Inorg. Chem.* **27** (1988), 595. c) M. S. Reynolds and R. H. Holm, *Inorg. Chem.* **27** (1988), 4494. d) B. S. Snyder and R. H. Holm, *Inorg. Chem*. **29** (1990), 274.
183. I. Noda, B. S. Snyder, and R. H. Holm, *Inorg. Chem.* **25** (1986), 3851. a) J.-F. You, B. S. Snyder, and R. H. Holm, *J. Am. Chem. Soc.* **110** (1988), 6589. b) J.-F. You *et al.*, *J. Am. Chem. Soc.* **112** (1990), 1067. c) W. R. Hagen, A. J. Pierik, and C. Veeger, *J. Chem. Soc., Faraday Trans. I* **85** (1989), 4083.
184. E. I. Stiefel *et al*., *Adv. Chem. Ser.* **162** (1977), 353. a) I. Moura and J. J. G. Moura, in Reference 5, p. 179. b) J. R. Lancaster, Jr., ed., *The Bioinorganic Chemistry of Nickel*, VCH Publishers, 1988. c) H. J. Grande *et al.*, in Reference 5, p. 193. d M. W. W. Adams, L. E. Mortenson, and J.-S. Chen, *Biochim. Biophys. Acta* **594** (1981), 105. e) J. LeGall and H. D. Peck, Jr., in Reference 5, p. 207. f) J. LeGall *et al.*, in Reference 8, p. 177. g) S. P. Ballantine and D. H. Boxer, *Eur. J. Biochem.* **156** (1986), 276. h) W. H. Onne-Johnson and N. R. Onne-Johnson, in Reference 8, p. 67.
185. B. Bowien and H. G. Schlegel, *Annu. Rev. Microbiol.* **35** (1981), 401.
186. C. R. Bowers and D. P. Weitekamp, *J. Am. Chem. Soc.* **109** (1987), 5541.
187. T. C. Eisenschmid *et al.*, *J. Am. Chem. Soc.* **109** (1987), 8089.
188. M. W. W. Adams *et al.*, *Biochimie* **68** (1986), 35.
189. R. Cammack, V. M. Fernandez, and K. Schneider, in Reference 184b, p. 167. 189a. M. W. W. Adams, *Biochem. Biophys. Acta* **1020** (1990),115.
190. H. J. Grande *et al.*, *Eur. J. Biochem.* **136** (1983), 201.
191. M. W. W. Adams and L. E. Mortenson, *J. Biol. Chem.* **259** (1984), 7045.
192. S. W. Ragsdale and L. G. L. Ljungdahl, *Arch. Microbial*. **139** (1984), 361.
193. C. R. Woese, *Microbial. Rev.* **81** (1987), 221.
194. M. W. W. Adams, E. Eccleston, and J. B. Howard, *Proc. Natl. Acad. Sci. USA* **86** (1989), 4932.
195. D. S. Patil *et al*., *J. Am. Chem. Soc.* **110** (1988), 8533.
196. A. T. Kowal, M. W. W. Adams, and M. K. Johnson, *J. Biol. Chem.* **264** (1989), 4342.
197. W. R. Hagen *et al.*, *FEBS Lett.* **203** (1986), 59.
198. I. C. Zambrano *et al.*, *J. Biol. Chem.* **264** (1989), 20974.
199. M. W. W. Adams, *J. Biol. Chem.* **262** (1987), 15054.
200. T. V. Morgan, R. C. Prince, and L. E. Mortenson, *FEBS Lett*. **206** (1986), 4.

201. W. R. Hagen *et al.*, *FEBS Lett.* **201** (1986), 158.
202. F. M. Rusnak *et al.*, *J. Biol. Chem.* **262** (1987), 38.
203. G. Wang *et al.*, *J. Biol. Chem.* **259** (1984), 14328.
204. J. Telser *et al.*, *J. Biol. Chem.* **262** (1987), 6589.
205. J. Telser *et al.*, *J. Biol. Chem.* **261** (1986), 15536.
206. H. Thomann, M. Bernardo, and M. W. W. Adams, *J. Am. Chem. Soc.* **113** (1991), 7044.
207. A. J. Thomson *et al.*, *Biochem. J.* **227** (1985), 333.
208. K. A. Macor *et al.*, *J. Biol. Chem.* **282** (1987), 9945.
209. G. N. George *et al.*, *Biochem. J.* **259** (1989), 597.
210. R. Cammack, *Adv. Inorg. Chem.* **32** (1988), 297.
211. J. J. G. Moura *et al.*, in Reference 5, p. 191.
212. J. R. Lancaster, *FEBS Lett.* **115** (1980), 285.
213. M. Teixeira *et al.*, *J. Biol. Chem.* **260** (1985), 8942.
214. J. W. Van der Zwaan *et al.*, *FEBS Lett.* **179** (1985), 271.
215. M. K. Eidsness, R. J. Sullivan, and R. A. Scott, in Reference 184b, p. 73.
216. M. K. Eidsness *et al.*, *Proc. Natl. Acad. Sci. USA* **86** (1989), 147.
217. P. A. Lindahl *et al.*, *J. Am. Chem. Soc.* **106** (1984), 3062.
218. R. A. Scott *et al.*, *J. Am. Chem. Soc.* **106** (1984), 6864.
219. S. P. J. Albracht *et al.*, *Biochim. Biophys. Acta* **874** (1986), 116.
220. A. Chapman *et al.*, *FEBS Lett.* **242** (1988), 134.
221. S. L. Tau *et al.*, *J. Am. Chem. Soc.* **106** (1984), 3064.
222. G. J. Kubas *et al.*, *J. Am. Chem. Soc.* **106** (1984), 451.
223. G. J. Kubas and R. R. Ryan, *Polyhedron* **5** (1986), 473.
224. G. J. Kubas *et al.*, *J. Am. Chem. Soc.* **108** (1986), 7000.
225. M. Rakowski DuBois *et al.*, *J. Am. Chem. Soc.* **102** (1980), 7456.
226. C. Bianchini *et al.*, *Inorg. Chem.* **25** (1986), 4617.
227. W. Tremel *et al.*, *Inorg. Chem.* **27** (1988), 3886.
228. W. Tremel and G. Henkel, *Inorg. Chem.* **27** (1988), 3896.
229. I. Dance, *Polyhedron* **5** (1986), 1037; P. J. Blower and J. R. Dilworth, *Coord. Chem. Rev.* **76** (1987), 121.
230. C. L. Coyle and E. I. Stiefel, in Reference 184b, p. 1.
231. M. Kumar *et al.*, *J. Am Chem. Soc.* **111** (1989), 5974.
232. M. Kumar *et al.*, *J. Am. Chem. Soc.* **111** (1989), 8323.
233. T. H. Blackburn, in W. E. Krumbein, ed., *Microbial Geochemistry*, Blackwell Scientific, 1983, p. 63.
234. J. R. Postgate, *Fundamentals of Nitrogen Fixation*, Cambridge University Press, 1982.
235. R. W. F. Hardy, *Treatise on Dinitrogen Fixation*, Wiley, 1979, Section I. a) T. G. Spiro, ed., *Molybdenum Enzymes*, Wiley-Interscience, 1985.
236. W. J. Brill, *NATO Adv. Sci. Inst., Ser. A* **63** (1983), 231.
237. R. Haselkorn, *Annu. Rev. Microbial.* **40** (1986), 525.
238. A. C. Robinson, D. R. Dean, and B. K. Burgess, *J. Biol. Chem.* **262** (1987), 14327.
239. P. J. Stephens, in Reference 235a, p. 117.
240. A. H. Gibson and W. E. Newton, eds., Current *Perspectives in Nitrogen Fixation*, Australian Academy of Science, 1981.
241. E. I. Stiefel, in W. E. Newton and C. Rodriquez-Barrucco, eds., in *Recent Progress in Nitrogen Fixation*, Academic Press, 1977, p. 69.
242. C. Veeger and W. E. Newton, eds., *Advances in Nitrogen Fixation Research*, Nijhoff/Junk, 1984.
243. H. J. Evans, P. J. Bottomley, and W. E. Newton, eds., *Nitrogen Fixation Research Progress*, Martinus Nijhoff, 1985. a) A. Braaksma *et al.*, in Reference 5, p. 223. b) B. H. Huynh, E. Münck, and W. H. Orme-Johnson, in Reference 5, p. 241.
244. E. I. Stiefel, in Reference 240, p. 55.
245. R. V. Hageman and R. H. Burris, *Proc. Natl. Acad. Sci. USA* **75** (1978), 2699.
246. V. Sundaresan and F. M. Ausubel, *J. Biol. Chem.* **256** (1981), 2808. a) R. P. Hausinger and J. B. Howard, *J. Biol. Chem.* **258** (1983), 13486. b) M. M. Georgiadis, P. Chakrabarti, and D. C. Rees, *SSRL Annual Report* (1989), p. 94.

247. L. E. Mortenson, M. N. Walker, and G. A. Walker, in W. E. Newton and C. J. Nyman, eds., *Proceedings of the First International Conference on Nitrogen Fixation*, Washington State University Press (1976), p. 117.
248. W. H. Orme-Johnson et al., in W. E. Newton, J. R. Postgate, and C. Rodriguez Barrucco, eds., *Recent Developments in Nitrogen Fixation*, Academic Press, 1977, p. 131.
249. G. D. Watt and J. W. McDonald, *Biochemistry* **24** (1985), 7226.
250. W. R. Hagen *et al.*, *FEBS Lett.* **189** (1986), 250.
251. L. Noodleman *et al.*, *J. Am. Chem. Soc.* **107** (1985), 3418.
252. G. D. Watt, Z.-C. Wang, and R. R. Knotts, *Biochemistry* **25** (1986),8156; J. Cordewener *et al.*, *Eur. J. Biochem.* **148** (1985), 499.
253. L. E. Mortenson and R. N. F. Thorneley, *Annu. Rev. Biochem.* **48** (1979), 387.
254. A. V. Kulikov *et al.*, *Dokl. Akad. Nauk SSR* **262** (1981), 1177.
255. R. N. F. Thorneley and D. J. Lowe, in Reference 235, p. 221. a) F. A. Schultz, S. F. Gheller, and W. E. Newton, Proc. *Int. Symp. Redox Mech. Interfacial Prop. Mol. Biol. Importance* **3** (1988), 203.
256. B. K. Burgess and W. E. Newton, in A. Müller and W. E. Newton, eds., *Nitrogen Fixation: The Chemical-Biochemical-Genetic Interface*, Plenum, 1983, p. 83.
257. E. I. Stiefel and S. P. Cramer, in Reference 235, p. 88.
258. V. Shah and W. J. Brill, *Proc. Natl. Acad. Sci. USA* **74** (1977), 3249.
259. S. D. Conradson *et al.*, *J. Am. Chem. Soc.* **109** (1987), 7507. a) P. A. McLean *et al.*, *Biochemistry* **28** (1989), 9402. b) D. A. Wink *et al.*, *Biochemistry* **28** (1989), 9407.
260. M. A. Walters, S. K. Chapman, and W. H. Orme-Johnson, *Polyhedron* **5** (1986), 561.
261. P. A. McLean and R. A. Dixon, *Nature* **292** (1981), 655.
262. P. A. McLean and B. E. Smith, *Biochem. J.* **211** (1983), 589.
263. T. R. Hawkes, P. A. McLean, and B. E. Smith, *Biochem. J.* **217** (1984), 317.
264. T. R. Hoover *et al.*, *Biochemistry* **27** (1988), 3647.
265. T. R. Hoover *et al.*, *Biochemistry* **28** (1989), 2768. a) J. Liang *et al.*, *Biochemistry* **29** (1990), 8377. b) M. S. Madden *et al.*, *Proc. Natl. Acad. Sci. USA* **87** (1990), 6517.
266. A. C. Robinson, D. Dean, and B. K. Burgess, *J. Biol. Chem.* **262** (1989), 14327. a) A. C. Robinson *et al.*, *J. Biol. Chem.* **264** (1989), 10088. b) D. J. Scott *et al.*, *Nature* **343** (1990), 188. c) H. M. Kent *et al.*, *Biochem. J.* **264** (1989), 257.
267. W. R. Hagen *et al.*, *Eur. J. Biochem*. **169** (1987), 457.
268. P. A. McLean *et al.*, *J. Biol. Chem.* **262** (1987), 12900.
269. P. A. Lindahl *et al.*, *J. Biol. Chem.* **263** (1988), 19442.
270. G. D. Watt, A. Burns, and D. L. Tennent, *Biochemistry* **20** (1981), 7272; G. D. Watt and Z. C. Wang, *Biochemistry* **25** (1986), 5196.
271. R. Zimmermann *et al.*, *Biochim. Biophys. Acta.* **537** (1978), 185.
272. D. M. Kurtz *et al.*, *Proc. Natl. Acad. Sci. USA* **76** (1979), 4986.
273. R. A. Venters *et al.*, *J. Am. Chem. Soc*. **108** (1986), 3487. a) J. Bolin, in P. M. Gresshoff, L. E. Roth, G. Stacey, and W. E. Newton, eds., *Nitrogen Fixation: Achievements and Objectives*, Chapman and Hall, 1990, p. 111.
274. B. M. Hoffman, J. E. Roberts, and W. H. Orme-Johnson, *J. Am. Chern. Soc.* **104** (1982), 860.
275. A. E. True *et al.*, *J. Am. Chem. Soc.* **110** (1988), 1935. a) A. E. True *et al.*, *J. Am. Chem. Soc.* **112** (1990), 651.
276. G. N. George *et aI.*, *Biochem. J.* **262** (1989), 349.
277. W. B. Mims and J. Peisach, in R. G. Shulman, ed., *Biological Applications of Magnetic Resonance*, Academic Press, 1980, p. 221.
278. W. H. Orme-Johnson *et al.*, in Reference 8, p. 79.
279. H. Thomann *et al.*, *J. Am. Chem. Soc.* **109** (1987), 7913.
280. H. Thomann *et al.*, *Proc. Natl. Acad. Sci. USA*, **88** (1991), 6620.
281. B. H. Huynh, E. Munck, and W. H. Orme-Johnson, *Biochim. Biophys. Acta* **527** (1979), 192.
282. B. H. Huynh *et aI.*, *Biochim. Biophys. Acta* **623** (1980), 124.
283. E. Münck *et al.*, *Biochim. Biophys. Acta* **400** (1975), 32. a) W. E. Newton *et al.*, *Biochem. Biophys. Res. Commun*. **162** (1989), 882.
284. S. D. Conradson, B. K. Burgess, and R. H. Holm, *J. Biol. Chem*. **263** (1988), 13743.

285. W. R. Dunham *et aI*., *Eur. J. Biochem.* **146** (1985), 497.
286. S. P. Cramer *et al*., *J. Am. Chem. Soc*. **100** (1978), 3398.
287. M. K. Eidsness *et al*., *J. Am. Chem. Soc*. **108** (1986), 2746.
288. S. D. Conradson *et aI*., *J. Am. Chem. Soc.* **107** (1985), 7935; Reference 259.
289. B. Hedman *et al*., *J. Am. Chem. Soc*. **110** (1988), 3798.
290. M. R. Antonio *et al*., *J. Am. Chem. Soc.* **104** (1982), 4703.
291. J. M. Arber *et al*., *Biochem. J.* **252** (1988), 421.
292. M. S. Weininger and L. E. Mortenson, *Proc. Natl. Acad. Sci. USA* **79** (1982), 378.
293. N. I. Sosfenov *et al*., *Dokl. Akad. Nauk. SSSR* **291** (1986), 1123.
294. T. Yamane *et al*., *J. Biol. Chem.* **257** (1982), 1221.
295. A. M. Flank *et aI*., *J. Am. Chem. Soc.* **108** (1986), 1049.
296. J. F. Rubinson *et aI*., *Biochemistry* **24** (1985), 273.
297. E. I. Stiefel, *Proc. Natl. Acad. Sci. USA* **70** (1973), 988.
298. K. L. Hadfield and W. A. Bulen, *Biochemistry* **8** (1969), 5103.
299. F. B. Simpson and R. Burris, *Science* **224** (1984), 1095.
300. B. K. Burgess *et al*., *Biochemistry* **20** (1981), 5140.
301. S. Wherland *et aI*., *Biochemistry* **20** (1981), 5132.
302. J. H. Guth and R. H. Burris, *Biochemistry* **22** (1983), 5111.
303. Z.-c. Wang and G. D. Watt, *Proc. Natl. Acad. Sci. USA* **81** (1984), 376.
304. B. E. Smith *et al*., *Phil. Trans. Roy. Soc. London* **B317** (1987), 131.
305. R. N. F. Thorneley, R. R. Eady, and D. J. Lowe, *Nature* **272** (1978), 557.
306. S. Wherland *et al*., *Biochemistry* **20** (1981), 5132.
307. B. K. Burgess *et al*., *Biochemistry* **20** (1981), 5140.
308. H. Bortels, *Arch. Mikrobiol*. **1** (1930), 333.
309. R. C. Bray, *Quart. Rev. Biophys*. **21** (1988), 299.
310. H. Bortels, *Zentbl. Bakt. Parasiten Abt. II* **95** (1935), 193.
311. C. E. McKenna, J. R. Benemann, and T. G. Traylor, *Biochem. Biophys. Res. Commun.* **41** (1970), 1501.
312. R. C. Burns, W. H. Fuchsman, and R. W. F. Hardy, *Biochem. Biophys. Res. Commun.* **42** (1971), 353.
313. J. R. Benemann *et al*., *Biochim. Biophys. Acta* **264** (1972), 25.
314. P. E. Bishop, D. M. L. Jarlenski, and D. R. Hetherington, *Proc. Natl. Acad. Sci. USA* **77** (1980), 7342.
315. P. E. Bishop *et al*., *Science* **232** (1986), 92.
316. B. J. Hales, D. J. Langosch, and E. E. Case, *J. Biol. Chem.* **261** (1986), 15301.
317. B. J. Hales *et al*., *Biochemistry* **26** (1987), 1795.
318. J. Morningstar *et al*., *Biochemistry* **26** (1987), 1795.
319. R. L. Robson *et al*., *Nature* **322** (1986), 388.
320. R. R. Eady *et al*., *Biochem. J.* **244** (1987), 197.
321. M. J. Dilworth *et al*., *Nature* **327** (1987), 167.
322. R. N. Pau, *Trends Biochem. Res.* **14** (1989), 186; P. E. Bishop and R. D. Joerger, *Annu. Rev. Plant Physiol. Plant Mol. Biol*. **41** (1990), 109.
323. J. E. Morningstar and B. J. Hales, *J. Am. Chem. Soc.* **109** (1987), 6854.
324. J. M. Arber *et al*., *Nature* **372** (1987), 325.
325. G. N. George *et al*., *J: Am. Chem. Soc.* **110** (1988), 4057.
326. R. R. Eady *et al*., *Recueil des Travaus Chim. des Pays-Bas* **106** (1987), 175.
327. M. J. Carney *et al*., *J. Am. Chem. Soc.* **108** (1986), 3519.
328. R. H. Holm, *Chem. Soc. Rev.* (1981), 455.
329. G. Christou and C. D. Gamer, *J. Chem. Soc. Dalton Trans.* (1980), 2354.
330. C. D. Gamer *et al*., *Phil. Trans. Roy. Soc. Land.* **A308** (1982), 159. a). R. H. Holm and E. D. Simhon, in Reference 235a, p. 1.
331. W. H. Armstrong, P. K. Mascharak, and R. H. Holm, *Inorg. Chem.* **21** (1982),1699.
332. R. E. Palermo and R. H. Holm, *J. Am. Chem. Soc.* **105** (1983), 4310. a) D. Coucouvanis, E. D. Simhon, and N. C. Baenziger, *J. Am. Chem. Soc.* **102** (1980), 6644. b) G. D. Friesen *et al*., *Inorg. Chem.* **22** (1983), 2203. c) P. Stremple, N. C. Baenziger, and D.

Coucouvanis, *J. Am. Chem. Soc.* **103** (1981), 4601. d) D. Coucouvanis *et al.*, *J. Am. Chem. Soc.* **102** (1980), 1732. e) A. Müller *et al.*, *Inorg. Chim. Acta* **148** (1988), 11. f) A. Müller *et al.*, *Angew. Chem. Int. Ed. Engl.* **21** (1982), 860. g) D. Coucouvanis *et al.*, *Inorg. Chem.* **27** (1988), 4066. h) P. A. Eldridge *et al.*, *J. Am. Chem. Soc.* **110** (1988), 5573. i) K. S. Bose *et al.*, *J. Am. Chem. Soc.* **111** (1989), 8953. j) J. A. Kovacs, J. K. Bashkin, and R. H. Holm, *Polyhedron* **6** (1987), 1445.

333. R. D. Sanner *et al.*, *J. Am. Chem. Soc.* **98** (1972), 8351. a) M. B. O'Regan *et al.*, *J. Am. Chem. Soc.* **112** (1990), 4331.
334. G. Pez, P. Apgar, and R. K. Crissey, *J. Am. Chem. Soc.* **104** (1982), 462.
335. K. Jones *et al.*, *J. Am. Chem. Soc.* **98** (1976), 74.
336. G. J. Leigh, *J. Mol. Catal.* **47** (1988), 363.
337. R. A. Henderson, G. J. Leigh, and C. J. Pickett, *Adv. Inorg. Chem. Radiochem.* **27** (1984), 198. a) M. Hidai and Y. Mizobe, in P. S. Braterman, ed., *Reactions of Coordinated Ligands*, Plenum, **2** (1989),53. b) T. Yoshida *et al.*, *J. Am. Chem. Soc.* **110** (1988), 4872. c) T. Yoshida, T. Adachi, and T. Ueda, *Pure Appl. Chem.* **62** (1990), 1127.
338. D. Sellmann *et al.*, *Angew. Chem. Int. Ed. Engl.* **28** (1989), 1271.
339. A. E. Shilov, in M. Gratzel, ed., *Energy Resources through Chemistry and Catalysis*, Academic Press, 1983, p. 533.
340. W. E. Newton *et al.*, *Inorg. Chem.* **19** (1980), 1997.
341. T. R. Halbert, W.-H. Pan, and E. I. Stiefel, *J. Am. Chem. Soc.* **105** (1983), 5476.
342. M. Rakowski DuBois *et al.*, *J. Am. Chem. Soc.* **101** (1979), 5245.
343. R. H. Crabtree, *Inorg. Chim. Acta* **125** (1986), 27.
344. W. B. Mims and J. Peisach, in J. Berliner and J. Reuben, eds., *Biological Magnetic Resonance*, Plenum, **3** (1981), 213.
345. T. Yamane *et al.*, *J. Biol. Chem.* **257** (1982), 1221.
346. D. C. Rees and J. B. Howard, *J. Biol. Chem.* **2587** (1983), 12733.
347. R. B. Frankel *et al.*, *J. de Physique* **37** (1976), C6.
348. C. E. Johnson, *J. Appl. Phys.* **42** (1971), 1325.
349. P. Middleton *et al.*, *Eur. J. Biochem.* **88** (1978), 135.
350. K. Tagawa and D. I. Amon, *Biochim. Biophys. Acta* **153** (1968), 602.
351. G. Palmer, R. H. Sands, and L. E. Mortenson, *Biochim. Biophys. Acta* **23** (1966), 357.
352. R. H. Sands and W. R. Dunham, *Quart. Rev. Biophys.* **4** (1975), 443.
353. R. Cammack, in M. J. Allen and P. N. R. Usherwood, eds., *Charge and Field Effects in Biosystems*, Abacus Press, 1984, p. 41.
354. J. Cardenas, L. E. Mortenson, and D. C. Yoch, *Biochim. Biophys. Acta* **434** (1976), 244.
355. R. Cammack, M. J. Barber, and R. C. Bray, *Biochem. J.* **157** (1976), 469.
356. R. C. Bray, in *The Enzymes*, 3d ed., **12** (1975), 299.
357. J. A. Fee *et al.*, *J. Biol. Chem.* **259** (1984), 124.
358. R. N. Mullinger *et al.*, *Biochem. J.* **151** (1975), 75.
359. R. Cammack *et al.*, *Biochim. Biophys. Acta* **490** (1977), 311.
360. F. A. Armstrong *et al.*, *FEBS Lett.* **234** (1988), 107.
361. W. R. Hagen *et al.*, *Biochim. Biophys. Acta* **828** (1985), 369.
362. E. deGryse, N. Glandsdorff, and A. Piérard, *Arch. Microbiol.* **117** (1978), 189.
363. V. M. Fernandez, E. C. Hatchikian, and R. Cammack, *Biochim. Biophys. Acta* **832** (1985), 69.
364. V. Niviére, *Biochem. Biophys. Res. Commun.* **139** (1986), 658.
365. M. Teixeira *et al.*, *Biochimie* **68** (1986), 75.
366. D. J. Lowe, B. E. Smith, and R. R. Eady, in N. S. Subba Rao, ed., *Recent Advances in Biological Nitrogen Fixation*, Arnold, 1980, p. 34.
367. R. C. Bums, R. D. Holsten, and R. W. F. Hardy, *Biochem. Biophys. Res. Commun.* **39** (1970), 90.
368. M. G. Yates and K. Planque, *Eur. J. Biochem.* **60** (1975), 467.
369. T. C. Huang, W. G. Zumft, and L. E. Mortenson, *J. Bact.* **113** (1973), 884.
370. P. C. Hallenback, P. J. Kostel, and J. R. Benemann, *Eur. J. Biochem.* **98** (1979), 275.
371. S. Norlund, U. Erikson, and H. Baltscheffsky, *Biochim. Biophys. Acta* **504** (1978), 248.
372. B. K. Burgess *et al.*, in Reference 242.
373. S. D. Conradson *et aI.*, *J. Am. Chem. Soc.* **109** (1987), 7507.
374. S. A. Vaughn and B. K. Burgess, *Biochemistry* **28** (1989), 419.
375. R. W. Miller and R. R. Eady, *Biochim. Biophys. Acta* **952** (1988), 290.

376. B. K. Burgess, in Reference 235a, p. 161.
377. B. J. Hales *et al.*, *Biochemistry* **25** (1986), 7251.
378. M. M. Georgiadis *et al.*, *Science* **257** (1992), 1653.
379. J. T. Bolin *et al.*, in P. M. Greshoff et al., eds., *Nitrogen Fixation: Achievements and Objectives*, Chapman and Hall, 1990, p. 117.
380. J. Kim and D. C. Rees, *Science* **257** (1992), 1677.
381. J. Kim and D. C. Rees, *Nature* **360** (1992), 553.
382. For allowing us to see and quote their work prior to publication, we are grateful to Prof. M. W. W. Adams, Prof. B. K. Burgess, Dr. R. Cammack, Prof. D. Coucouvanis, Prof. S. P. Cramer, Dr. S. J. George, Prof. J. N. Enemark, Prof. J. Lancaster, Dr. Michelle Millar, Prof. M. Maroney, Prof. W. E. Newton, Prof. D. C. Rees, Prof. Dieter Sellman, Prof. A. E. Shilov, Dr. Barry E. Smith, Dr. R. N. F. Thorneley, and Prof. G. D. Watt. We thank Pat Deuel for her superb efforts under difficult circumstances in the preparation of this manuscript.

Contributors and Attributions

- Edward I. Stiefel (Exxon Research and Engineering Company)
- Graham N. George (Exxon Research and Engineering Company)

6.7: Ferrodoxins, Hydrogenases, and Nitrogenases - Metal-Sulfide Proteins is shared under a not declared license and was authored, remixed, and/or curated by LibreTexts.

6.7.1: Iron-sulfur Proteins and Models

Iron sulfide proteins involved in electron transfer are called *ferredoxins* and *rubredoxins*.* The ferredoxins were discovered first, and were originally classified as bacterial (containing Fe_4S_4 clusters) and plant (containing Fe_2S_2 clusters) ferredoxins. This classification is now recognized as being not generally useful, since both Fe_2S_2 and Fe_4S_4 ferredoxins are found in plants,[14,15] animals,[2,6,16] and bacteria.[4] Ferredoxins are distinguished from rubredoxins by their possession of acid-labile sulfide; i.e., an inorganic S^{2-} ion that forms H_2S gas upon denaturation at low pH. Rubredoxins have no acid-labile sulfide, and generally have a single iron in a more or less isolated site. Despite their lack of acid-labile sulfide, rubredoxins are included in this chapter because they have sequences much like those of the ferredoxins, and because their simple mononuclear Fe^{2+} and Fe^{3+} sites provide convenient illustrations of key structural and spectroscopic features.

In most ferredoxins, and in all rubredoxins, the protein ligands are cysteines, which provide four thiolate donors to the 1Fe, 2Fe, or 4Fe center. Additionally, the existence of 3Fe centers and of Fe-S sites that contain a second metal (i.e., heteronuclear clusters) make the Fe-S class a broad and multifunctional one.

Simple cytochromes and simple iron-sulfide proteins are similar, in that both can undergo one-electron transfer processes that are generally uncoupled from proton-, atom-, or group-transfer processes. Some of these proteins, such as cytochrome c_3 from *Desulfovibrio* with four hemes[17] or ferredoxin from *Clostridium pasteurianum* with two Fe_4S_4 centers,[6] can transfer more than one electron, because they have multiple copies of a one-electron transfer group. The cytochromes were discovered in 1886 by McMunn,[18] and their role in metabolism was discovered in the 1920s by Keilin (Chapter 6). The intense optical absorbance of these heme-containing proteins contributed singularly to their discovery and biochemical characterization. In contrast, the iron-sulfur proteins, although red to red-brown, absorb far more weakly in the visible region than do the cytochromes. Their presence is sometimes obscured by the cytochromes, and their frequent air instability made their initial recognition and isolation more difficult. It was not until the early 1960s that discoveries by several research groups[19] led to the isolation, recognition, and characterization of the ferredoxins. The use of EPR spectroscopy and its application to biological systems had a profoundly stimulating effect on the field (see below).

Although cytochromes were discovered first, the ferredoxins are likely to be the older proteins from an evolutionary perspective.[20] Ferredoxins have relatively low-molecular-weight polypeptide chains, require no organic prosthetic group, and often lack the more complex amino acids. In fact, the amino-acid composition in clostridial ferredoxin is close to that found in certain meteorites.[21]

The various Fe-S sites found in electron-transfer proteins (ferredoxins) are also found in many enzymes,[6,11,22.23] where these centers are involved in intraor interprotein electron transfer. For example, sulfite reductase contains a siroheme and an Fe_4S_4 center,[24] which are strongly coupled and involved in the sixelectron reduction of SO_3^{2-} to H_2S. Xanthine oxidase (see Figure 7.1) has two identical subunits, each containing two different Fe_2S_2 sites plus molybdenum and FAD sites. In xanthine oxidase, the Mo(VI) site carries out the two-electron oxidation of xanthine to uric acid, being reduced to Mo(IV) in the process.[25] The Mo(VI) site is regenerated by transferring electrons, one at a time, to the Fe_2S_2 and flavin sites, thereby readying the Mo site for the next equivalent of xanthine. Although the Fe_2S_2 sites do not directly participate in substrate reactions, they are essential to the overall functioning of the enzyme system. The Fe_2S_2 centers in xanthine oxidase play the same simple electron-transfer role as the Fe_2S_2 ferredoxins play in photosynthesis.

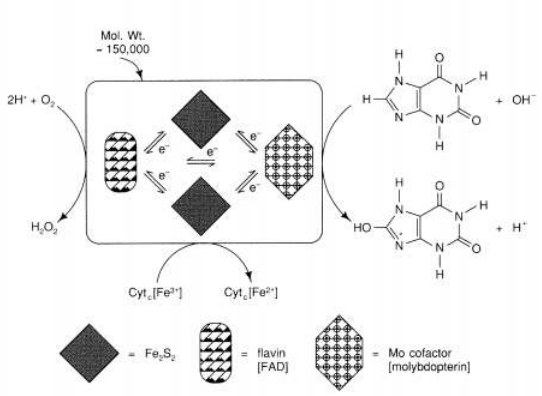


Figure 7.1 - A schematic drawing of xanthine oxidase illustrating the Mo, flavin, and Fe_2S_2 sites and interaction of the enzyme with substrate and oxidant(s).

Structurally, all the iron-sulfur sites characterized to date are built up of (approximately) tetrahedral iron units (see Figure 7.2). In rubredoxins the single iron atom is bound in tetrahedral coordination by four thiolate ligands provided by cysteine side chains. In two-iron ferredoxins the Fe_2S_2 site consists of two tetrahedra doubly bridged through a pair of sulfide ions, i.e., $Fe_2(\mu_2\text{-}S)_2$, with the tetrahedral coordination of each Fe completed by two cysteine thiolates. In four-iron or eight-iron ferredoxins, the 'thiocubane' Fe_4S_4 cluster consists of four tetrahedra sharing edges with triply bridging S^{2-} ions, i.e., $Fe_4(\mu_3\text{-}S)_4$, with each Fe completing its tetrahedron by binding to a single cysteine thiolate. Finally, for Fe_3S_4 clusters, which are now being found in more and more proteins, the well-established structure has one triply bridging and three doubly bridging sulfide ions, $Fe_3(\mu_3\text{-}S)(\mu_2S)_3$. The Fe_3S_4 unit can be thought of as derived from the 'thiocubane' Fe_4S_4 unit by the removal of a single iron atom.

In what follows we will introduce these structures in the order 1Fe, 2Fe, 4Fe, and 3Fe. For each, we will first discuss the physiological role(s) of the particular proteins, then the structural features, followed by the spectroscopic properties and model systems.

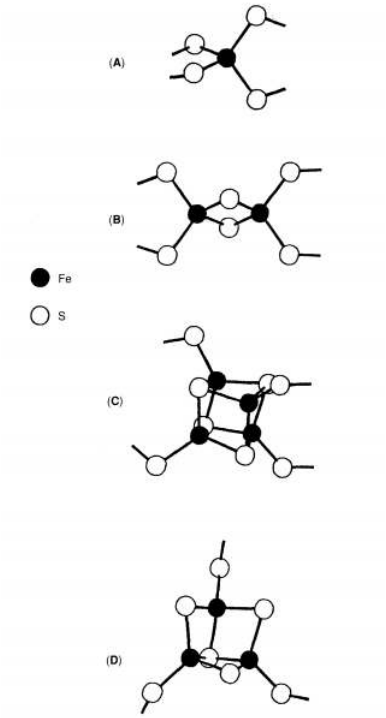


Figure 7.2 - Structural systematics of Fe-S units found in proteins: (A) rubredoxin single Fe center; (B) Fe_2S_2 unit; (C) Fe_4S_4 unit; (d) Fe_3S_4 unit.

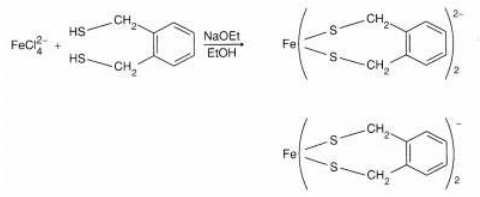
* For review articles, see References 1-11. For a discussion of nomenclature, see References 12 and 13.

6.7.1: Iron-sulfur Proteins and Models is shared under a not declared license and was authored, remixed, and/or curated by LibreTexts.

6.7.2: Iron-sulfur Proteins and Models (Part 2)

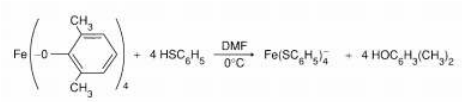
Rubredoxin Model Systems

The simple mononuclear tetrahedral site of Rd has been chemically modeled in both its reduced and its oxidized forms. The bidentate o-xylyl-α,α'-dithiolate ligand forms bis complexes of Fe(II) and Fe(III) that have spectroscopic features quite similar to those of the protein.[62,63] The preparative procedure is relatively straightforward (Equation 7.1).



The UV-visible-NIR spectra, Mössbauer spectra, and magnetic susceptibility differ only slightly from those of oxidized and reduced rubredoxins.

The monodentate benzenethiolate (thiophenolate) ligand, $C_6H_5S^-$, similarly forms the ferrous $Fe(SC_6H_5)_4^{2-}$ complex.[64,65] Although for some time it was felt that the oxidized form, $Fe(SC_6H_5)_4^-$, was inherently unstable, the sterically hindered monothiolate ligand 2,3,5,6-tetramethylbenzenethiolate was found to form[66-68] a stable, quite symmetric Fe(III) tetrathiolate anion. Armed with this information, the preparation of the tetrakis(benzenethiolate) Fe(III) complex was reinvestigated, and the complex successfully synthesized[67] (Equation 7.2).



The Fe(III) and Fe(II) tetrathiolate species now serve as excellent structural models for the Fe sites of both oxidized and reduced Rd.[69]

The structural parameters for the oxidized rubredoxin analogues are very similar to those of the oxidized Rd iron site. The reduced complexes reveal a lengthening of the average Fe-S bond from 2.27 to 2.36 Å, consistent with the change in oxidation state from ferric to ferrous. The addition of an electron has a more profound structural effect in this single-iron center than in some of the multiiron clusters, where electrons are more delocalized.

Clearly, for the single-Fe sites, the dominant structural feature is their near-tetrahedral tetrathiolate coordination. The dominant electronic structural feature is the presence of high-spin Fe^{3+} and Fe^{2+} sites. The important mode of chemical reactivity is a simple one-electron transfer. Each of these features carries over to the 2Fe, 4Fe, and 3Fe sites discussed below.

Fe_2S_2 Ferredoxins

The simple 2Fe-2S proteins are sometimes referred to as "plant" or "plant-type" ferredoxins. The protein from spinach, which serves as an electron acceptor in the photosynthetic apparatus,[14,15,50,70] was among the first to be wellcharacterized and widely studied, and could be considered the prototypical 2Fe-2S ferredoxin, However, 2Fe-2S proteins are also well-known in bacteria.[4] The protein from the cyanobacterium (blue-green alga) *Spirulina platensis* has been structurally elucidated by x-ray crystallography.[47] Putidaredoxin, from *Pseudomonas putida*, which serves as a donor to the P-450 camphor monooxygenase system, has been extensively studied.[28] Fe_2S_2 centers are also well-established in mammalian proteins. Adrenodoxin[29] serves as the electron donor to the P-450 monooxygenase system that carries out the 11-β-hydroxylation of steroids, The so-called "Rieske proteins" are found in the bc_1 complex of mitochondria[47] as well as in the bd complex of the photosynthetic apparatus of plants.[71] In addition, Fe_2S_2 centers are well-known constituents of such redox proteins as xanthine oxidase,[25,72] CO oxidase,[25] succinate dehydrogenase,[73-75] and putidamonooxin.[76] Table 7.1 lists some of the Fe_2S_2 proteins and their properties.

The x-ray crystal structure of only the single 2Fe-2S protein mentioned above has been determined;[70a] the 2Fe-2S ferredoxin from the blue-green alga Spirulina platensis[6,22,47,77,78] shows significant sequence identity with chloroplast ferredoxins typical of higher plants.[79,80] As Figure 7.8 shows, the Fe_2S_2 unit in this 11-kDa protein is bound by Cys-41, Cys-46, Cys-49, and Cys-79, The

binuclear iron cluster is found in a largely hydrophobic region of the protein, but is within 5 Å of the protein surface.[6] The sulfur atoms of the cluster, both inorganic and cysteinyl, are hydrogen-bonded to six peptide NH groups and one serine OH group, which presumably stabilize the cluster/protein complex, The serine involved in the H-bonding, Ser-40, is conserved in all plant and algal 2Fe-2S ferredoxins sequenced, which implies that it plays a crucial structural or functional role.

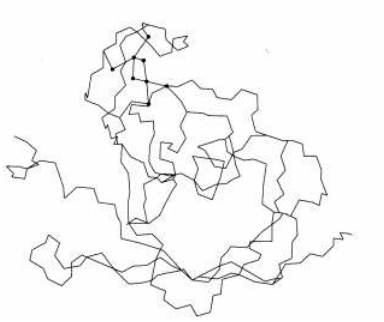


Figure 7.8 - The x-ray crystal structure of the Fe_2S_2 ferredoxin from Spirulina platensis.[70a]

The structure of the 2Fe-2S core in Figure 7.2 reveals a tetrahedron of S ligands surrounding each Fe atom. The two tetrahedra share an edge defined by the two bridging sulfide ions, and the core structure is designated $Fe_2(\mu_2\text{-}S)_2$. Fe-S distances and angles cannot be measured accurately in the structure at the present 2.5-Å resolution;[70a] so we will later discuss these details in terms of model compounds.

The Fe_2S_2 center shows nicely how spectroscopy can be used to deduce the structure of an active site. Indeed, in this case the now well-established active-site structure was deduced by a combination of chemical, spectroscopic, and magnetic methods, and the site was successfully modeled long before the first protein crystallographic study was reported. The presence of acid-labile, inorganic sulfide is a key feature of both the Fe_2S_2 and the Fe_4S_4 centers. The 1:1 stoichiometry between iron and acid-labile sulfide was eventually established analytically for Fe_2S_2 centers.[9-11] Care must be taken to ensure that both the protein and its active-site complement are homogeneous. Although protein homogeneity is usually established by electrophoretic methods, these methods may not distinguish between pure proteins and those with absent or incomplete active centers. Fortunately, absorption at 420 nm is due solely to the Fe_2S_2 cluster, whereas the 275-nm absorption is dominated by the protein. Therefore a good criterion for active-site saturation and homogeneity is the ratio of the absorbances at 420 and 275 nm, $A_{420\ nm}/A_{275\ nm}$, which is ~0.48 for pure spinach ferredoxin.[81] Once homogeneous protein is obtained, the Fe_2S_2 composition of the "plant" ferredoxins can be correctly deduced analytically.

The Fe_2S_2 center displays two redox states that differ by a single electron. The potential range for the couple is -250 to -420 mV, revealing the highly reducing nature of the ferredoxin. The correct structure of the Fe_2S_2 center was first proposed in 1966 based on EPR studies.[82] The reduced state of the cluster shows a rhombic EPR signal with g values of 1.88, 1.94, and 2.04 (Figure 7.6B) characteristic of an $S = \frac{1}{2}$ center. The oxidized state is EPR-silent. The weakness of the sulfur ligand field causes the iron atoms to be high-spin. But how can two sulfur-ligated iron atoms, each with a tendency to be high-spin, produce a state with a single unpaired electron?

The individual Fe atoms in the Fe_2S_2 cluster resemble those in rubredoxin quite closely. The two redox states of the Fe_2S_2 protein correspond to an Fe^{3+}-Fe^{3+} and an Fe^{3+}-Fe^{2+} pair, respectively, as shown in Figure 7.9. In the all-ferric oxidized state, the two Fe^{3+} sites are antiferromagnetically coupled; i.e., the spins of the five d electrons on the two iron atoms are oppositely aligned, such that their pairing produces an effective S = 0, diamagnetic ground state. In the reduced form, a single unpaired electron is present, because the $S = \frac{5}{2}$ Fe^{3+} and S = 2 Fe^{2+} sites are antiferromagnetically coupled, leaving one net unpaired spin and an $S = \frac{1}{2}$ ground state. The profound difference between the electronic properties of rubredoxin and Fe_2S_2 ferredoxin arises because the latter has two Fe atoms in close proximity, which allows for their magnetic coupling.

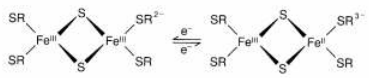


Figure 7.9 - Redox states of Fe_2S_2 proteins: (A) reduced; (B) oxidized.

Strong support for the spin-coupling model in Fe_2S_2 ferredoxins comes from a detailed analysis of their absorption and circular dichroism spectra.[83] As with rubredoxin (see Figure 7.5), we expect no low-energy spin-allowed d-d bands for the ferric site in either the oxidized or the reduced state. Indeed, the oxidized state containing all Fe^{3+} shows no low-energy bands; the reduced state containing a single Fe^{2+} displays low-energy, low-intensity bands in the region 4,000-9,000 cm^{-1}, in close analogy to the situation in reduced rubredoxin. The combined EPR and optical spectra leave little doubt about the structural assignment: two coupled high-spin ferric ions in the oxidized state, and coupled high-spin ferric and ferrous ions in the reduced state. Moreover, the spectra are consistent only with a localized model, i.e., one in which the Fe(II) site is associated with a single iron.[83,83a] The Fe_2S_2 site is inherently asymmetric, and inequivalence of the Fe(llI) sites is spectroscopically detectable in the all-ferric oxidized form.[84] In fact, the localized valence trapping is present in reduced model compounds that contain no ligand asymmetry.

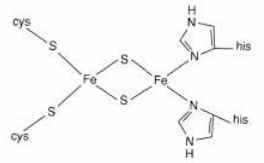
Mössbauer spectra provide additional and striking confirmation of the structural assignment. The spectrum of the oxidized ferredoxin (Figure 7.7) resembles strongly that of oxidized rubredoxin, indicating the presence of high-spin Fe^{3+}, even though the net spin is zero. In the reduced form, the Mössbauer spectrum involves the superposition of signals from a high-spin Fe^{2+} and a high-spin Fe^{3+}, i.e., a reduced and an oxidized rubredoxin, respectively. Clearly, the simplest interpretation of this result consistent with the S = $\frac{1}{2}$ spin state required by the EPR is the localized Fe^{2+}-Fe^{3+} antiferromagnetic coupling model discussed above.

NMR studies of oxidized Fe_2S_2 proteins reveal broad isotropically shifted resonances for the CH_2 protons of the cysteine ligands.[85] Despite the coupling of the irons, the net magnetism at room temperature is sufficient to lead to large contact shifts (-30 to -40 ppm downfield from TMS). The assignment of the resonance was confirmed with the synthesis and spectroscopic analysis of model compounds.[86] Extensive NMR studies of the Fe_2S_2 proteins have been reported.[87,87a]

Resonance Raman spectra of Fe_2S_2 sites[88,89,90] reveal many bands attributable to Fe-S stretching. Detailed assignments have been presented for the four bridging and four terminal Fe-S modes. A strong band at 390 cm^{-1}, which shifts on ^{34}S sulfide labeling, is assigned to the A_{1g} "breathing" mode; another band at 275 cm^{-1} is assigned to B_{3u} symmetry in point group D_{2h}.[57,88] Spectroscopic differences in the terminal, Fe-S(Cys) stretches between plant ferredoxins and adrenodoxin (which also differ somewhat in redox potential) seem to reflect different conformations of the cysteine ligands in the two classes. Evidence for asymmetry of the iron atoms is found in the intensity of the resonance enhancement of certain modes.

Rieske Centers

Within the class of Fe_2S_2 ferredoxins there is a subclass called the Rieske proteins, or the Rieske centers.[47,91,92] The Rieske iron-sulfur centers are found in proteins isolated from mitochondria and related redox chains.[47,92] In addition, the phthalate dioxygenase system from *Pseudomonas cepacia*[93,94] contains one Fe_2S_2 Rieske center as well as one additional nonheme Fe atom. Although the Rieske centers appear to contain an Fe_2S_2 core, there is extensive evidence for nonsulfur ligands coordinated to at least one of the Fe atoms. The proposed model in Scheme (7.3) has two imidazole ligands bound to one Fe atom. The nitrogen atoms are seen in ENDOR (Electron Nuclear Double Resonance) experiments,[93] and are manifest in EXAFS spectra, which are consistent with the presence of a low-Z (atomic number) ligand bound to iron.[94] The potentials for the Rieske proteins range from +350 to -150 mV,[47] in contrast to the plant-type Fe_2S_2 centers, which range from -250 to -450 mV. The strong dependence of redox potential on pH[95] suggests a possible role in coupling protonand electron-transfer processes.



Fe_2S_2 Models

Although spectroscopic studies led to the correct deduction of the structure of the Fe_2S_2 core, the synthesis of model compounds containing this core provided unequivocal confirmation. The model compounds allowed detailed structural analysis unavailable for the proteins. Moreover, by using a uniform set of peripheral ligands, properties inherent to the Fe_2S_2 core could be discerned.

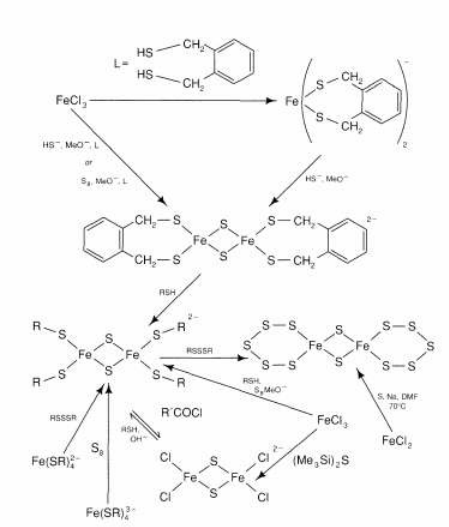


Figure 7.10: Preparative schemes leading to complexes containing the Fe_2S_2 core.[128]

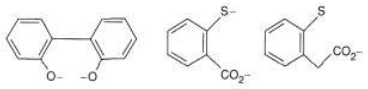
The Fe_2S_2 core has been synthesized by several routes[86,96a,b,c,d] (see Figure 7.10). For example, the reaction of $Fe(SR)_4^{2-}$, the ferrous rubredoxin model, with elemental sulfur produces the complex $Fe_2S_2(SR)_4^{2-}$. In this reaction the sulfur presumably oxidizes the Fe^{2+} to Fe^{3+}, being reduced to sulfide in the process. The Fe_2S_2 core has been prepared with a variety of peripheral S-donor ligands. Metrical details for $Fe_2S_2(SC_6H_4\text{-}p\text{-}CH_3)_4^{2-}$ are given in Table 7.3. Notable distances are the Fe-S (bridging) distance of 2.20 Å, the Fe-S (terminal) distance of 2.31 Å, and the Fe-Fe distance of 2.69 Å.

Table 7.3: Structural parameters for $Fe_2S_2(SC_6H_4-p-CH_3)_4^{2-}$. a) Data from Reference 211.

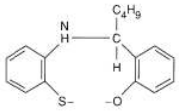
Atoms[a]	Distance Å	Atoms[a]	Angle[a]
Fe-Fe	2.691 (1)	Fe-S-Fe	75.3
Fe-S1 (bridge)	2.200 (1)	S-Fe-S	104.6
Fe-S2 (bridge)	2.202 (1)	S-Fe-S	115.1
Fe-S3	2.312 (1)	S-Fe-S	105.4

To date, all analogue systems structurally characterized contain the Fe^{3+}-Fe^{3+} fully oxidized form. Attempts to isolate the Fe^{3+}-Fe^{2+} form have so far failed. However, the mixed-valence Fe_2S_2 form can be generated and trapped by freezing for spectroscopic examination.[97,98] Mössbauer spectroscopy reveals the presence of distinct Fe^{2+} and Fe^{3+} ions, as found in the proteins, clearly showing that "trapped" valence states are an inherent characteristic of the $Fe_2S_2^{2+}$ core and are *not* enforced by the protein.[97,98]

The existence of noncysteine-bound Fe_2S_2 cores in Rieske-type proteins has led to attempts to synthesize complexes with oxygen and nitrogen ligands.[99-101] Characterized species include $Fe_2S_2(OC_6H_5)_4^{2-}$, $Fe_2S_2(OC_6H_4\text{-}p\text{-}CH_3)_4^{2-}$, $Fe_2S_2(C_4H_4N)_4^{2-}$, and $Fe_2S_2(L)_2^{2-}$, where L is a bidentate ligand.



The potentially tridentate ligand



acts in a bidentate fashion, binding through S and O but not N.

No Fe_2S_2 complexes containing mixed S,N terminal ligands, such as those suggested for the Rieske site, have been prepared. The Se^{2-} bridged analogue has been prepared for some of the complexes.[102,103]

6.7.2: Iron-sulfur Proteins and Models (Part 2) is shared under a not declared license and was authored, remixed, and/or curated by LibreTexts.

6.7.3: Iron-sulfur Proteins and Models (Part 3)

Fe_4S_4 Ferredoxins (including HiPIPs)

We now turn our attention to proteins containing the Fe_4S_4 center. Historically, within this class a strong distinction was made between the "ferredoxins," which are low-potential (as low as -600 mV in chloroplasts) iron-sulfur proteins, and the "HiPIPs" = High Potential Iron Proteins, which have positive redox potentials (as high as +350 mV in photosynthetic bacteria). Although the HiPIP designation is still useful, proteins of both high and low potential are considered ferredoxins, whose key defining feature is the presence of iron and acid-labile sulfide.[13]

The Fe_4S_4 proteins participate in numerous electron-transfer functions in bacteria, and in some organisms (such as *Clostridium*) are the immediate electron donors for the nitrogenase and/or hydrogenase enzymes. The function of the HiPIPs seems obscure at present. In addition, Fe_4S_4 centers have been shown or postulated to occur in numerous microbial, plant, and mammalian redox enzymes, including nitrate reductase,[104] sulfite reductase,[24] trimethylamine dehydrogenase,[105] succinate dehydrogenase,[73,106] hydrogenase, and, possibly, in altered forms, nitrogenase. Table 7.1 lists some of the Fe_4S_4 ferredoxins and their properties.

In the Fe_2S_2 ferredoxins, combined spectroscopic, analytical, and model-system work led to an unequivocal assignment of the structural nature of the active site long before the crystallography was done. In contrast, for Fe_4S_4 systems and in particular the 8Fe-8S = $2Fe_4S_4$ systems from bacteria, the initial chemical suggestions were fallacious, and even the number and stoichiometry of the clusters were in doubt. In these cases, crystallography provided the definitive structural information.

The first indication of the presence of the "thiocubane" structure came in 1968, when a 4-Å resolution study[107] indicated a compact cluster of potentially tetrahedral Fe_4 shape in the HiPIP from *Chromatium vinosum*. This finding did not lead to much excitement, since it was not yet appreciated that HiPIPs and ferredoxins were structurally similar. In 1972, the high-resolution structure solution of both *Chromatium* HiPIP[108] and the 8Fe ferredoxin from *Peptococcus aerogenes* (formerly *Microbacter aerogenes*)[101] confirmed the presence of virtually identical thiocubane clusters in the two proteins.[108] Moreover, the structures for both oxidized and reduced HiPIP were deduced, and these revealed that the Fe_4S_4 cluster remained intact during the redox interconversion.[109] Subsequently, four-iron clusters have been crystallographically confirmed in an Fe_4S_4 ferredoxin from *Bacillus thermoproteolyticus*,[110,110a] in *Azotobacter vinelandii* ferredoxin I (also previously called Shethna Fe-S protein II), which also contains a 3Fe-4S cluster,[111,112] in the active form of aconitase,[113] and in sulfite reductase, where the cluster is probably bridged by cysteine sulfur to a siroheme.

In all the proteins characterized to date, the Fe_4S_4 clusters adopt the thiocubane structure,[108] which is discussed at greater length in the section on models. The clusters are usually bound to their proteins by four cysteine residues. As shown in Figure 7.11, in the *P. aerogenes* protein the two Fe_4S_4 clusters are bound by cysteines numbered 8, 11, 14, 18, 35, 38, 41, and 45.[101,114] The presence of the Cys-x-x-Cys unit is again apparent. However, this sequence seems prominent in all Fe-S proteins, and so is not specific for a particular Fe-S site. At first glance one might expect one cluster to be bound by cysteines 8,11,14, and 18, the other by cysteines 35, 38, 41, and 45. Actually, one cluster is bound by cysteines 8, 11, 14, and 45, the other by cysteines 35, 38, 41, and 18. The binding of a given cluster by cysteine residues from different portions of the polypeptide chain apparently helps stabilize the tertiary structure of the protein and brings the two clusters into relatively close proximity, the center-center distance being 12 Å.[114]

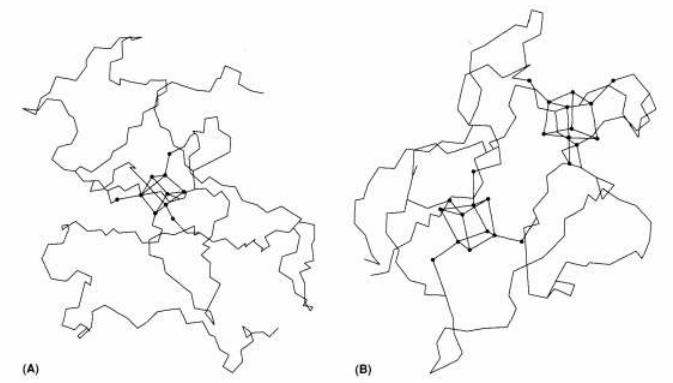


Figure 7.11 - The x-ray crystal structures of (A) *Chromatium vinosum* HiPIP[108] and (B) the 8Fe-8S ferredoxin from *Peptococcus aerogenes*.[101]

The *C. pasteurianum* protein displays weak magnetic coupling, which leads to an unusual EPR spectrum[115] consistent with the 12-Å cluster-cluster separation. However, the redox potentials for the two sites seem virtually identical at -412 mV, thus allowing the 8Fe ferredoxin to deliver two electrons at this low redox potential.[115] Significant sequence identity indicates the likelihood that other 8Fe ferredoxins, such as the well-studied one from *C. pasteurianum*,[116-118] have quite similar structures.

The thiocubane unit of Fe_4S_4 proteins can exist in proteins in at least three stable oxidation states. This so-called three-state model[74,109,119,120] contrasts dramatically with the situation for Rd(1Fe), Fe_2S_2, and Fe_3S_4 systems, in which only two oxidation states are accessible through simple electron transfer for each center. For the thiocubane structure, the three accessible states can be designated $Fe_4S_4^{3+}$, $Fe_4S_4^{2+}$, and $Fe_4S_4^{+}$, corresponding to $[Fe(III)_2Fe(II)]$, $[Fe(III)_2Fe(II)_2]$, and $[Fe(III)Fe(II)_3]$ valence-state combinations, respectively. It is crucial to note that, in sharp contrast to the Fe_2S_2 and Fe_3S_4 sites, the oxidation states are not localized in the Fe_4S_4 clusters. In most cases, each Fe atom behaves as if it had the same average oxidation level as the other Fe atoms in the cluster. The redox interconversion of the Fe4S4 sites is shown in Figure 7.12. The $Fe_4S_4^{3+} \rightleftharpoons Fe_4S_4^{2+}$ couple is the high-potential redox couple characteristic of HiPIPs; the $Fe_4S_4^{2+} \rightleftharpoons Fe_4S_4^{+}$ couple is responsible for the low-potential process characteristic of the classical ferredoxins. In any given protein under physiological conditions, only one of the two redox couples appears to be accessible and functional.

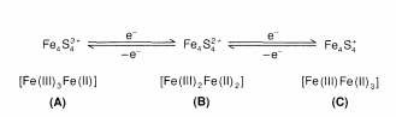


Figure 7.12 - The redox interconversions of Fe_4S_4 sites illustrating the three-state model. The states are found in (A) oxidized HiPIP; (B) reduced HiPIP and oxidized ferredoxin; (C) reduced ferredoxin.

Both the $Fe_4S_4^{+}$ and the $Fe_4S_4^{3+}$ states of the thiocubane cluster are paramagnetic and display characteristic EPR spectra (Figure 7.6C,D). The $Fe_4S_4^{3+}$ site in reduced ferredoxins[46,48,49,119] displays a rhombic EPR signal (Figure 7.6C) with g = 1.88, 1.92, and 2.06. The oxidized form of low-potential ferredoxins is EPR-silent, and attempts to "superoxidize" it to achieve the $Fe_4S_4^{3+}$ state invariably lead to irreversible cluster decomposition, probably through a 3Fe-4S structure. The $Fe_4S_4^{3+}$ signal is usually referred to as the HiPIP signal (Figure 7.6D) and shows distinct g values at 2.04($g_\perp$) and 2.10($g_\parallel$); it is present in oxidized HiPIP but absent in reduced HiPIP.[46,119] Reduction of HiPIP to a "super-reduced" state apparently occurs under partially denaturing conditions in aqueous DMSO.[108] The observed axial EPR signal with g = 1.94 and 2.05 is assigned to the $Fe_4S_4^{+}$ state characteristic of reduced ferredoxins. This result[108] is consistent with structural and spectroscopic identity of the HiPIP and Fd sites, as required by the three-state model of the Fe_4S_4 proteins (Figure 7.12).

In Fe_4S_4 centers at each level of oxidation, electronic transitions give rise to characteristic visible and UV spectra, although the delocalized nature of the electronic states makes detailed assignment difficult. MCD spectra of clusters in the three states of oxidation are clearly distinguishable from each other and from MCD of Fe_2S_2 clusters.[43,119] MCD, magnetic susceptibility, and Mössbauer spectra provide evidence that the S = $\frac{1}{2}$ state, whose EPR signal is so distinct in reduced ferredoxins, may coexist at higher T with S = $\frac{3}{2}$ and perhaps even higher spin states. Indeed, recent studies with model systems[121,122] and theoretical treatments[123,124] clearly support the ability of the Fe_4S_4 cluster to display a number of spin states that are in labile equilibria, which are influenced, perhaps quite subtly, by local structural conditions. The iron protein of nitrogenase also displays this behavior.

The Mössbauer spectra of Fe_4S_4 centers of ferredoxins reveal the equivalence of the Fe sites, and quadrupole splittings and isomer shifts at averaged values for the particular combination of oxidation states present.[3,51,52] Representative spectra are shown in Figure 7.7. Magnetic coupling is seen for the paramagnetic states.

Resonance Raman spectra (and IR spectra) have been extensively investigated in *C. pasteurianum* ferredoxin and in model compounds.[57,125] Selective labeling of either thiolate sulfur or sulfide sulfur with ^{34}S allows modes associated with the Fe_4S_4 core to be distinguished from modes associated with the FeSR ligands. The band at 351 cm^{-1} is assigned to Fe-SR stretching, and Fe_4S_4 modes occur at 248 and 334 cm^{-1} in reduced ferredoxin from *C. pasteurianum.* There is little difference between the oxidized and reduced spectra, although an extra band at 277 cm^{-1} seems present in the oxidized protein. The Fe_4Se_4 substituted protein has also been studied.[125]

As in the 1Fe and 2Fe proteins, ^1H NMR spectra reveal resonances from contact-shifted-CH_2-groups of cysteinyl residues.[125a] However, unlike the other proteins, where all states are at least weakly magnetic, only the reduced ferredoxin and the oxidized HiPIP states show contact shifts.[87a,125a,b,c]

EXAFS studies on proteins and on model compounds clearly identify the Fe-S distance of ~2.35 Å and an Fe-Fe distance of 2.7 Å. These distances, as expected, vary only slightly with state of oxidation.[125d]

Fe_4S_4 Models

Judging from the ease with which models of Fe_4S_4 are prepared under a variety of conditions and their relative stability, the $Fe_4S_4^{2+}$ core structure seems to be a relatively stable entity, a local thermodynamic minimum in the multitude of possible iron-sulfide-thiolate complexes. The initial preparation and structural characterization[126,127] of the models showed that synthetic chemistry can duplicate the biological centers in far-simpler chemical systems, which can be more easily studied in great detail.

The general synthetic scheme for Fe-S clusters is shown in Figure 7.13. Many different synthetic procedures can be used to obtain complexes with the Fe_4S_4 core.[126-138,138a,b] The multitude of preparative procedures is consistent with the notion that the $Fe_4S_4^{2+}$ core is the most stable entity present and "spontaneously self-assembles" when not limited by stoichiometric constraints.

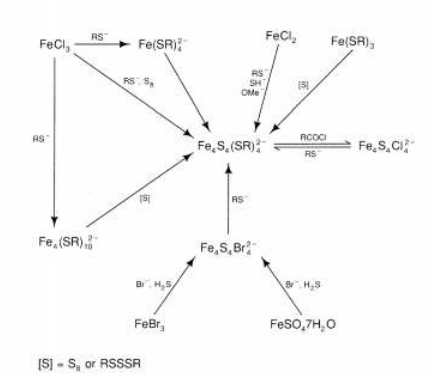


Figure 7.13 - Preparative schemes leading to complexes containing the Fe_4S_4 core.[128]

The thiocubane structure can be viewed as two interpenetrating tetrahedra of 4Fe and 4S atoms. The 4S tetrahedra are the larger, since the S-S distance is ~3.5 Å, compared with the Fe-Fe distance of ~2.7 Å. The S_4 tetrahedron encloses ~2.3 times as much volume as does the Fe_4 tetrahedron.[128] Key distances and angles for $Fe_4S_4(SCH_2C_6H_5)_4^{2-}$ given in Table 7.4 are extremely similar to those found in oxidized ferredoxin and reduced HiPIP centers in proteins.[127]

Table 7.4 - Structural parameters for $Fe_4S_4(SCH_2C_6H_5)_4^{2-}$.

a) Data from References 126 and 127.

Atoms[a]	Average Distances	Number of Bonds	Type
Fe(1)-S(3)	2.310 (3)	8	Sulfide
Fe(1)-S(2)	2.239 (4)	4	Sulfide
Fe(1)-S(5)	2.251 (3)	4	Thiolate
Fe(1)-Fe(2)	2.776 (10)	2	
Fe-Fe(other)	2.732 (5)	4	

Atoms[a]	Average Distances	Number of Bonds	Type
Fe-S-Fe	73.8 (3)	12	
S-Fe-S	104.1 (2)	12	Sulfide-Fe-Sulfide
S-Fe-S	111.7-117.3	12	Sulfide-Fe-Thiolate

The idealized symmetry of $Fe_4S_4^{2+}$ model systems is that of a regular tetrahedron, i.e., T_d. Though the distortion of the cube is quite pronounced, all known examples of the Fe_4S^{2+} core show distortion, which lowers the symmetry at least to D_{2d}. In most Fe_4S^{2+} core structures, this distortion involves a tetragonal compression, which leaves four short and eight long Fe-S bonds.

Complexes with non-S-donor peripheral ligands have been prepared and studied. The halide complexes $Fe_4S_4X_4^{2-}$ ($X = Cl^-, Br^-, I^-$) have been prepared, and serve as useful starting points for further syntheses.[129-133] The complex $Fe_4S_4(OC_6H_5)_4^{2-}$ can be prepared[134] from the tetrachloride (or tetrathiolate) thiocubane by reaction with $NaOC_6H_5$ (or HOC_6H_5). There are a few examples of synthetic $Fe_4S_4^{2+}$ cores in which the peripheral ligands are not identical. For example, $Fe_4S_4Cl_2(OC_6H_5)_2^{2-}$ and $Fe_4S_4Cl_2(SC_6H_5)_2^{2-}$ have structures characterized by D_{2d} symmetry.[135] The complexes $Fe_4S_4(SC_6H_5)_2[S_2CN(C_2H_5)_2]^{2-}$ and $Fe_4S_4(SC_6H_4OH)_4^{2-}$ are similarly asymmetric, containing both four- and five-coordinate iron.[136-138] The presence of five-coordinate iron in the Fe_4S_4 cluster is notable, since it offers a possible mode of reactivity for the cluster wherever it plays a catalytic role (such as in aconitase). Complexes with Fe_4Se^{2+} and $Fe_4Te_4^{2+}$ cores have also been prepared.[138c,d]

One structural analysis of $Fe_4S_4(SC_6H_5)_4^{3-}$, which contains the reduced $Fe_4S_4^+$ core, revealed a tetragonal elongation[139] in the solid state. In contrast, analysis of $Fe_4S_4(SCH_2C_6H_5)_4^{3-}$ revealed a distorted structure possessing C_{2v} symmetry.[102] It would appear that the $Fe_4S_4^+$ clusters maintain the thiocubane structure, but are nevertheless highly deformable. Interestingly, when the solidstate C_{2v} structure, $Fe_4S_4(SCH_2C_6H_5)_4^{3-}$, is investigated in solution, its spectroscopic and magnetic behavior change to resemble closely those of the $Fe_4S_4(SC_6H_5)_4^{3-}$ cluster,[140] which does not change on dissolution. The simplest interpretation assigns the elongated tetragonal structure as the preferred form for $Fe_4S_4^+$ cores with deformation of sufficiently low energy that crystal packing (or, by inference, protein binding forces) could control the nature of the distortions in specific compounds.[128] The elongated tetragonal structure has four long and eight short bonds in the core structure. The terminal (thiolate) ligands are 0.03-0.05 Å longer in the reduced structure, consistent with the presence of 3Fe(ll) and 1Fe(III) in the reduced form, compared to 2Fe(II) and 2Fe(III) in the oxidized form. There is no evidence for any valence localization.[128]

The oxidized $Fe_4S_4^{3+}$ core defied isolation and crystallization in a molecular complex prior to the use of sterically hindered thiolate ligands. With 2,4,6 tris(isopropyl)phenylthiolate, the $Fe_4S_4L_4^-$ complex could be isolated and characterized.[141] The structure is a tetragonally compressed thiocubane with average Fe-S and Fe-SR distances 0.02 and 0.04 Å shorter than the corresponding distances in the $Fe_4S_4L_4^{2-}$ complex. Again, there is no evidence for Fe inequivalence or more profound structural distortion in this 3Fe(III)-1Fe(II) cluster. Clearly, the Fe_4S_4 clusters have highly delocalized bonding.

Evidence from model systems using sterically hindered thiolate ligands indicates the existence of an $Fe_4S_4^{4+}$, i.e., all-ferric fully oxidized cube.[142] The existence of the complete series $Fe_4S_4[(Cy)_3C_6H_2S]_4^n$ (Cy =cyclohexyl; n = 0, -1, -2, -3) is implied by reversible electrochemical measurements. Clearly, five different states of the Fe_4S_4 core—including the (at least) transient fully oxidized state and the all-ferrous fully reduced state—may have stable existence. Although only the central three states have been shown to exist in biological contexts, one must not rule out the possible existence of the others under certain circumstances.

Recently, specifically designed tridentate ligands have been synthesized that bind tightly to three of the four Fe atoms in the thiocubane structure.[143,143a,b] The remaining Fe atom can then be treated with a range of reagents to produce a series of subsite-differentiated derivatives and variously bridged double-cubane units. These derivatives illustrate the potential to synthesize complexes that mimic the more unusual features of Fe_4S_4 centers that are bound specifically and asymmetrically to protein sites. The recently synthesized complex ion $[(Cl_3Fe_4S_4)_2S]^{4-}$, containing two Fe_4S_4 units bridged by a single S^{2-} ligand, illustrates the potential coupling of known clusters into larger aggregates.[143c]

The model-system work has made an important contribution to our understanding of the Fe_4S_4 centers. The existence of three states, the exchange of ligands, the redox properties, the metrical details of the basic Fe_4S_4 unit, and the subtleties of structural distortion can each be addressed through the study of models in comparison with the native proteins.

6.7.3: Iron-sulfur Proteins and Models (Part 3) is shared under a not declared license and was authored, remixed, and/or curated by LibreTexts.

6.7.4: Iron-sulfur Proteins and Models (Part 4)

Core Extrusion/Cluster Displacement Reactions

Synthetic model-system work led to the realization that the cluster cores can exist outside the protein and undergo relatively facile ligand-exchange reactions.[128] This behavior of the purely inorganic complexes allowed core extrusion reactions[128,144] to be developed. The basic assumption behind these reactions is that the cluster core retains its integrity when it is substituted by low-MW thiolates, especially aryl thiolates, which replace the cysteinyl ligands that bind it to the protein. In order to free the cluster from the protein, one must at least partially denature the protein, usually by using ~80 percent aqueous solution of a polar aprotic solvent, such as DMSO or HMPA. The resulting inorganic clusters can be identified and quantified by measurement of their characteristic electronic absorption or NMR spectra. An alternative approach involves transferal of the unknown cluster in question to an apoprotein that binds a cluster of known type.[145]

Since the 1Fe, 2Fe, and 4Fe sites are each usually bound to the protein by four cysteine residues, it is perhaps not surprising that there have been reports[58] of interconversion of cluster types bound to a given protein. Specifically, in 90 percent aqueous DMSO, the single Fe site in rubredoxin from *C. pasteurianum* is converted to an Fe_4S_4 cluster by the addition of sodium sulfide, ferrous chloride, and ferric chloride in ratio 4:2:1. Presumably the spacing and geometric disposition of the cysteines are suitable to bind a single Fe or the Fe_4S_4 cluster, which is readily formed under the reaction conditions. Another example of cluster rearrangement involves the three-iron center discussed below that does *not* extrude as an Fe_3S_4 center. Rather, at least under *certain* conditions, the Fe_{3Sx} center rearranges to form Fe_2S_2 centers.[146] The facile interconversion of the Fe clusters demonstrated the lability of Fe-S systems, and indicates that caution must be exercised in interpreting the results of cluster-displacement reactions.

Fe_3S_4 Centers

Three-iron centers are a comparatively recent finding,[119,146] and the full scope of their distribution is not yet known. Although they have now been confirmed in dozens of proteins, it often remains uncertain what physiological role these centers play. Indeed, since Fe_3S_4 centers can be produced as an artifact upon oxidation of Fe_4S_4 centers, it has been suggested that 3Fe centers may not be truly physiological, and could be side products of aerobic protein isolation. This caveat notwithstanding, the 3Fe sites are being found in more and more proteins and enzymes. Their physiological *raison d' être* may be more subtle than that of their 1, 2, and 4Fe cousins; we should certainly try to find out more about them. Some proteins containing Fe_3S_4 centers are listed in Table 7.1.

The 3Fe center was first recognized[147] in the protein ferredoxin I from the anaerobic nitrogen-fixing bacterium *Azotobacter vinelandii*. The protein is called *Av* FdI for short. It is instructive to sketch historically the evolution of our understanding of this protein. *Av* ferredoxin I was reported to have 6 to 8 Fe atoms and was first thought to resemble the clostridial 8Fe ferredoxins. However, unlike the clostridial protein, the *Av* FdI clusters appeared to have two quite different redox couples at +320 and -420 mV. Although it might have been thought that this protein contained one HiPIP-type and one Fd- or "ferredoxin"-type Fe_4S_4 cluster, the protein as isolated had an EPR signal with g = 2.01, which differed significantly (Figure 7.6) from that of an oxidized HiPIP or a reduced Fd.[148] Cluster extrusion reactions also seemed to indicate the presence of an unusual cluster type.[149]

Fortunately, the protein was crystallized, and could be studied by x-ray diffraction. Unfortunately, the initial conclusions[150] and subsequent revisions[151,152] of the crystal-structure analysis have proven to be wrong, teaching us in the process that protein x-ray crystallography, taken alone, does not always provide definitive results. Specifically, the first crystallographic report suggested the presence of a conventional Fe_4S_4 cluster and a smaller packet of electron density that was assigned as a 2Fe-2S center.[150] However, upon further refinement, and following the formulation of the 3Fe center by Mössbauer spectroscopy,[147] a 3Fe-3S center was identified and refined.[151,152] The "refined" Fe_3S_3 center was a six-membered alternating iron-sulfide ring with an open, almost flat, twistedboat conformation (Figure 7. 14). The Fe-Fe separation of 4.1 Å and the structural type was unprecedented, and did not agree with the results of resonance Raman spectroscopy,[153] with x-ray absorption spectroscopy on the native protein or on samples from which the Fe_4S_4 center was removed,[103] or even with stoichiometry, which eventually led to the reformulation[154] of the cluster as Fe_3S_4. The x-ray absorption studies (EXAFS) clearly led to the assignment of a 2.7-Å Fe-Fe distance for the 3Fe cluster.[103]

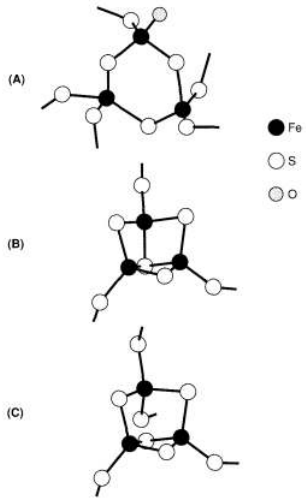


Figure 7.14 - Fe_3S_n structures: (A) open Fe_3S_3 structure proposed from initial x-ray studies (now shown to be in error); (B) the thiocubane fragment structure believed present in most Fe_3S_4 proteins; (C) open Fe_3S_4 structure (not found to date).

In parallel with the studies on *Av* FdI, two additional proteins played key roles in the resolution of the nature of the Fe_3 cluster. These are FdII from *Desulfovibrio gigas* and aconitase from beef heart. Each contains (under certain conditions) only Fe_3S_4 sites, thus enabling more definitive structural, stoichiometric, and spectral information to be acquired. Studies on these proteins using EXAFS,[155] Mössbauer,[52,156,157] EPR,[146] and resonance Raman (to which we will return briefly) clearly favor the closed structure shown in Figure 7.14C. Indeed, x-ray crystallography on aconitase by the same group that did the initial x-ray work on *Av* FdII revealed the compact structure in agreement with the spectroscopy.[20]

In 1988 the structural error in the crystallography of *Av* FdI was found by two groups, and a new refinement in a corrected space group led to a structure in agreement with the spectroscopy.[111,112] The Fe_3S_4 cluster has the apoFe thiocubane structure, with each iron atom bound to the protein by a single cysteinyl thiolate. Clearly, even x-ray crystallography is potentially fallible, and its findings must be critically integrated with the data from other techniques in arriving at full structural definition of metalloenzyme sites.

The studies on the ferredoxins from *D. gigas* present an interesting lesson on the lability of the Fe-S cluster systems. Two distinct proteins from *D. gigas*, FdI and FdII, contain the same polypeptide chain (6 kDa) in different states of aggregation,[158,159] Whereas FdI is a trimer containing three Fe_4S_4 clusters, FdII is a tetramer that contains four Fe_3S_4 clusters. The ferredoxins differ in their redox potentials and appear to have different metabolic functions in *D. gigas*. The oxidation of *D. gigas* FdI with $Fe(CN)_6^{3-}$ leads to FdII, and treatment of FdII with iron salts leads to FdI. The *D. gigas* system reveals the lability and interconvertibility of Fe-S clusters. The recently reported[160] crystal structure of *D. gigas* FdII shown in Figure 7.15 confirms the partial (apoFe) thiocubane Fe_3S_4 center. The iron atoms are ligated by three cysteinyl residues from protein side chains. The cube missing an iron is now firmly established as a viable structural type.

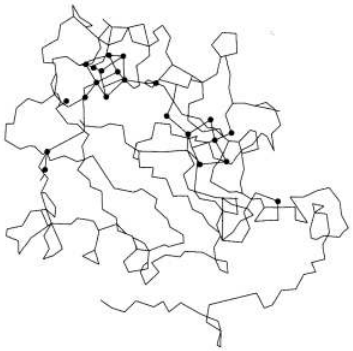
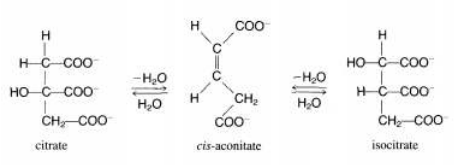


Figure 7.15 - The x-ray crystal structure of D.gigas FdII, illustrating the Fe_4S_4 and Fe_3S_4 centers in this protein.[160]

The aconitase system presents yet another fascinating story.[159a] Aconitase is a key enzyme in the Krebs cycle, catalyzing the conversion of citrate and isocitrate through the intermediacy of cis-aconitate, as shown in Equation (7.6).



This is a hydrolytic nonredox process, and for some time it was thought that aconitase was a simple Fe^{2+} protein wherein the ferrous iron was involved in the Lewis-acid function of facilitating the hydrolytic reaction. Indeed, aconitase is inactive when isolated from mitochondria, and requires the addition of Fe^{2+} to achieve activity.

Surprisingly, the isolated aconitase was found by analysis and Mossbauer spectroscopy to possess an Fe_3S_4 site in its inactive form.[161] Low-resolution crystallographic study supports the presence of an apo-Fe thiocubane, Fe_3S_4 structure in aconitase.[162] Resonance Raman[163] and EXAFS[103,155] studies clearly fingerprint the Fe_3S_4 cluster. The current hypothesis for aconitase activation involves the Fe_3S_4 thiocubane fragment reacting with Fe^{2+} to complete the cube, which is the active form of the enzyme.[164] Recent crystallographic studies[113] confirm the presence of a complete cube in the activated aconitase. The dimensions and positioning of the Fe_3S_4 and Fe_4S_4 centers in the cube are virtually identical. The added Fe^{2+} iron atom is ligated by a water (or hydroxide) ligand, consistent with the absence of any cysteine residues near the exchangeable iron. Since this water (or a hydroxide) is also present in the Fe_3S_4 system, one wonders whether a small ion such as Na^+ might be present in the Fe_3S_4 aconitase system.

Questions of detailed mechanism for aconitase remain open. ENDOR spectroscopy[165] shows that both substrate and water (or OH^-) can bind at the cluster. Does one of its Fe-atom vertices play the Lewis-acid role necessary for aconitase activity? Is the $Fe_3S_4 \rightleftharpoons Fe_4S_4$ conversion a redox- or iron-activated switch, which works as a control system for the activity of aconitase? These and other questions will continue to be asked. If aconitase is indeed an Fe-S enzyme with an iron-triggered control mechanism, it may be representative of a large class of Fe_3/Fe_4 proteins. Other hydrolytic enzymes containing similar Fe-S centers have recently been reported.[166,166a]

Spectroscopically, the Fe_3S_4 center is distinct and clearly distinguishable from 1Fe, 2Fe, and 4Fe centers. The center is EPR-active in its oxidized form, displaying a signal (Figure 7.6) with g = 1.97, 2.00, and 2.06 (*D. gigas* FdII).[158] The Mössbauer spectrum (Figure 7.7) shows a single quadrupole doublet with ΔQ = 0.53 nm/s and isomer shift of 0.27 nm, suggesting the now familiar highspin iron electronic structure.[158,159] In its reduced form, the center becomes EPR-silent, but the Mössbauer spectrum now reveals two quadrupole doublets of intensity ratio 2:1. The suggestion of the presence of a 3Fe center was first made based on this observation.[147] The picture of the reduced Fe_3S_4 state that has emerged involves a coupled, delocalized Fe^{2+}/Fe^{3+} unit responsible for the outer doublet, with a single Fe^{3+} unit responsible for the inner doublet of half the intensity. The oxidized state contains all Fe^{3+} ions, which are coupled in the trinuclear center.

EXAFS studies were consistent and unequivocal in finding an Fe-Fe distance of ~2.7 Å in all putative Fe_3S_4 proteins.[103,155,167] Resonance Raman spectra compared with those of other proteins and of model compounds with known structures[168,169] for other metals also favored the structure of Figure 7.14B. Clearly, what has been termed the spectroscopic imperative[170] has been crucial in the successful elucidation of the 3Fe structure. An interesting excursion has led to isolation of what are presumed to be $ZnFe_3S_4$, $CoFe_3S_4$, and $NiFe_3S_4$ thiocubane structures by adding Zn^{2+}, Co^{2+}, or Ni^{2+}, respectively, to proteins containing reduced Fe_3S_4 cores.[170a,b,c] These modified proteins provide interesting electronic structural insights and, potentially, new catalytic capabilities.

Fe_3 Model Systems

To date, the Fe_3S_4 center is the only structurally characterized biological iron-sulfide center that does not have an analogue in synthetic Fe chemistry. In fact, the closest structural analogue[21,170d] is found in the $Mo_3S_4^{4+}$ or $V_3S_4^{3+}$ core in clusters such as $Mo_3S_4(SCH_2CH_2S)_3^{2-}$, whose structure is shown in Figure 7.16.

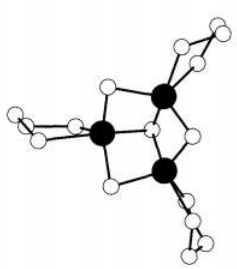


Figure 7.16 - The x-ray crystal structure of $Mo_3S_4(SCH_2CH_2S)_3^{2-}$. (From Reference 10a.)

The resonance Raman spectrum[169] of this complex bears a close resemblance to that of the *D. gigas* ferredoxin II. Since the vibrational bands responsible for the resonance Raman spectrum are not strongly dependent on the electronic properties, it is not surprising that an analogue with a different metal can be identified using this technique.

In synthetic Fe chemistry, although there is no precise structural analogue, it is instructive to consider three types of trinuclear and one hexanuclear center in relation to the three-iron biocenter.

The trinuclear cluster $Fe_3S[(SCH_2)C_6H_4]_3^{2-}$ is prepared[171,172] by the reaction of $FeCI_3$, $C_6H_4(CH_2SH)_2$, $Na^+OCH_3^-$, and p-CH_3-C_6H_4-SH in CH_3OH. As shown in Figure 7.17A, this cluster has, like the biocluster, a single triply bridging sulfide ion but, unlike the biocluster, it uses the sulfur atoms of the ethane 1,2-dithiolate as doubly bridging, as well as terminal, groups. The inorganic ring $Fe_3(SR)_3S_6^{3-}$ (X = CI, Br) has a planar $Fe_3(SR)_3$ core, which resembles the now-discredited structure for *Av* FdI[173] (Figure 7. 14A).

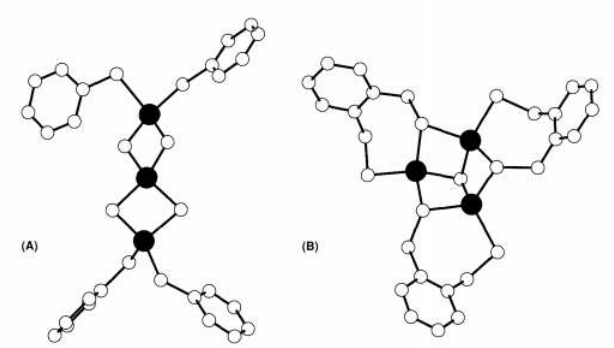


Figure 7.17 - The x-ray crystal structures of trinuclear Fe complexes: (A) $Fe_3S_4(SR)_4^{3-}$; (B) $Fe_3S[(SCH_2)_2C_6H_4]_3^{2-}$. (Data from References 171, 172, 174, 175.)

The complex $Fe_3S_4(SR)_4^{3-}$ is prepared[174,175] by reaction of $Fe(SR)_4^{2-}$ with sulfur. The x-ray-determined structure reveals two tetrahedra sharing a vertex with the linear Fe-Fe-Fe array shown in Figure 7.17B. This complex has distinctive EPR, Mössbauer, and NMR spectra that allow it to be readily identified[174,175,175a] Interestingly, after the complex was reported, a study of (denatured) aconitase at high pH (>9.5) revealed that the thiocubane fragment Fe_3S_4 site in that enzyme rearranged to adopt a structure that was spectroscopically almost identical with that of the linear complex.[176] Although the state may not have any physiological significance, it does show that Fe-S clusters different from the common (conventional) ones already discussed could be important in proteins under certain physiological conditions or in certain organisms; i.e., iron centers first identified synthetically may yet prove to be present in biological systems.

A synthetic cluster that displays features related to the biological Fe_3S_4 cluster is the hexanuclear cluster $Fe_6S_9(SR)_2^{4-}$ shown in Figure 7.18. This cluster contains two Fe_3S_4 units bridged through their diiron edges by a unique quadruply bridging S^{2-} ion (μ_4-S^{2-}) and by two additional μ_2S^{2-} bridges. The inability of synthetic chemists to isolate an Fe_3S_4 analogue may indicate that in proteins this unit requires strong binding. Significant sequestration by the protein may be needed to stabilize the Fe_3S_4 unit against oligomerization through sulfide bridges or, alternatively, rearrangement to the stable Fe_4S_4 center.

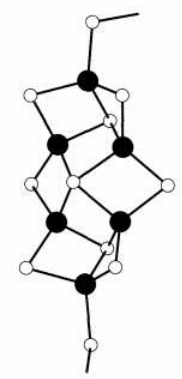


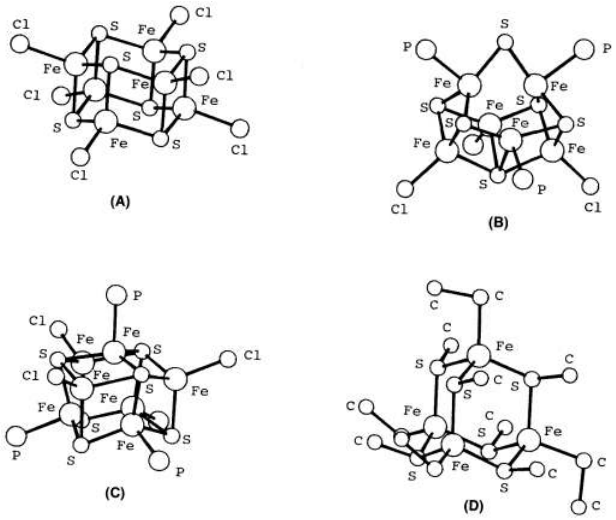
Figure 7.18 - The x-ray crystal structure[176a,b] of $Fe_6S_9(SR)_2^{4-}$.

Fe-S Chemistry: Comments and New Structures

The first successful model system for an iron-sulfur protein was an analogue of the Fe_4S_4 system, i.e., the system with the largest presently established biological Fe cluster. The reactions used to synthesize the cluster shown in Figure 7.13 are said to involve self-assembly, meaning that starting materials are simply mixed together, and thermodynamic control causes the cluster to assemble in its stable form. Interestingly, the Fe_4S_4-containing proteins, such as those of *C. pasteurianum*, are considered to be among the most ancient of proteins. Perhaps on the anaerobic primordial Earth, Fe-S clusters self-assembled in the presence of protein ligands to form the progenitors of the modem ferredoxins.

Much progress has been made in synthetic chemistry, and it is clear that both understanding and control of Fe-S chemistry are continuing to grow. New preparations for known clusters continue to be found, and new clusters continue to be synthesized, Although many of the new clusters appear to be abiological, we should not ignore them or their potential. They add to our understanding of Fe-S chemistry in general, and serve as starting points in the study of heteronuclear clusters, There is also the distinct possibility that one or more of these synthetic clusters represent an existing biological site that has not yet been identified in an isolated system.

Among the "nonbiological" structures that have been synthesized are complexes with $Fe_6S_6^{3+/2+}$ cores[177,178] including the thioprismanes,[108,109,177-179] the octahedron/cube $Fe_6S_8^{3+}$ cores,[180,181] the $Fe_6S_9^{2-}$ cores[176a,b] discussed above, the adamantane-like $Fe_6(SR)_{10}^{4-}$ complexes related to Zn and Cu structures in metallothioneins,[182] basket $Fe_6S_6^{2+}/Fe_6S_6^{+}$ cores,[182a,b,c,d] monocapped prismatic $Fe_7S_6^{3+}$ cores,[183] the cube/octahedron $Fe_8S_6^{5+}$ cores,[179] and the circular Na^+-binding $Fe_{18}S_{30}^{10-}$ unit.[183a,b] Representative ions are shown in Figure 7.19. Some of these cores are stabilized by distinctly nonbiological phosphine ligands. Nevertheless, one should not *a priori* eliminate any of these structures from a possible biological presence. Indeed, recently a novel, apparently six-iron protein from *Desulfovibio gigas* has been suggested[183c] to have the thioprismane core structure first found in model compounds.



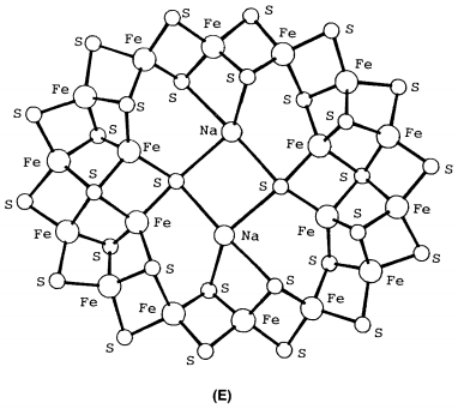


Figure 7.19 - Structures of "to date nonbiological" Fe-S clusters: (A) the thioprismane structure;[177] (B) basket-handle structure;[182a] (C) monocapped prismatic structure;[183] (D) adamantane structure;[182] (E) circular $Fe_{18}S_{30}^{10-}$ core unit.[183a,b]

Detection of Fe-S Sites

Several recent reviews have concentrated on the ways in which the various Fe-S centers can be identified in newly isolated proteins.[5,6,184] It is instructive to summarize the central techniques used in the identification of active sites. Optical spectra are usually quite distinctive, but they are broad and of relatively low intensity, and can be obscured or uninterpretable in complex systems. MCD spectra can give useful electronic information, especially when the temperature dependence is measured. EPR spectra, when they are observed, are distinctive, and are usually sufficiently sharp to be useful even in complex systems. Mössbauer and resonance Raman spectroscopies have each been applied with good effect when they can be deconvoluted, and NMR and magnetic susceptibility have given important information in some simple, lower-MW protein systems. X-ray absorption spectra, especially EXAFS, give accurate Fe-S and Fe-Fe distances when a single type of Fe atom is present. Analytical and extrusion data complement the spectroscopic and magnetic information. Extrusion data must be viewed with considerable caution, because of possible cluster-rearrangement reactions. Even x-ray crystallography has led to incorrect or poorly refined structures. In general, no one technique can unequivocally identify a site except in the very simplest systems, and there is continued need for synergistic and collaborative application of complementary techniques to a given system.

Redox Behavior

Figure 7.20 shows the ranges of redox behavior known for Fe-S centers. Clearly, the Fe-S systems can carry out low-potential processes. The rubredoxins cover the mid-potential range, and the HiPIPs are active in the high-potential region. The lack of extensive Fe-S proteins in the positive potential region may reflect their instability under oxidizing conditions and their preemption by Mn, Cu, or heme-iron sites (such as in cytochrome c), which function in this region.

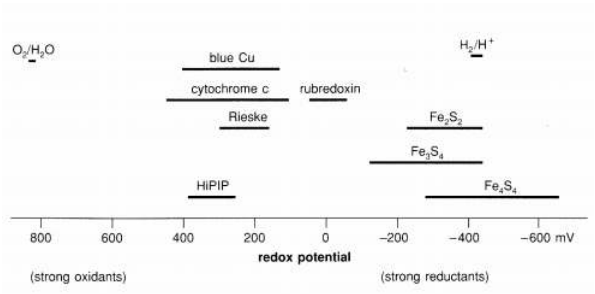


Figure 7.20 - A schematic diagram of the redox potential of the various FeS centers in comparison with other known redox centers.

6.7.4: Iron-sulfur Proteins and Models (Part 4) is shared under a not declared license and was authored, remixed, and/or curated by LibreTexts.

SECTION OVERVIEW

6.8: Overview of Hemoglobin and Myoglobin

6.8.1: Myoglobin, Hemoglobin, and their Ligands

6.8.2: Oxygen Transport by the Proteins Myoglobin and Hemoglobin

---

6.8: Overview of Hemoglobin and Myoglobin is shared under a not declared license and was authored, remixed, and/or curated by LibreTexts.

6.8.1: Myoglobin, Hemoglobin, and their Ligands

Hemoglobin:

- 1st. protein whose molecular weight was determined
- 1st protein to be assigned a specific function - dioxygen transport
- has a prosthetic group (non-amino acid) heme group (protoporphyrin IX with a ferrous ion) covalently attached to the protein. The heme group binds dioxygen.
- 1st protein in which a point mutation (single base pair charge) causes a single amino acid change in the protein, marking the start of molecular medicine
- 1st protein with high resolution x-ray structure
- theory for dioxygen binding explain control of enzyme activity
- the binding of dioxygen is regulated by binding of H^+, CO_2, and bisphosphoglcyerate which bind to sites (allosteric) distant from oxygen binding site.
- crystals of deoxy-Hb shatter on binding dioxygen, indicating significant conformational changes on binding.

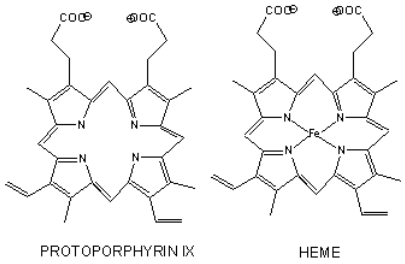


Figure 6.8.1.1. The heme group contains protoporphyrin IX, with four tetrapyrrole rings linked by methene bridges. Attached to the tetrapyrrole structure are four methyl, two vinyl, and two proprionate groups. These can be arranged in 15 ways, only one (IX) occurs in biological systems.

The heme fits into a hydrophobic crevice in the proteins with the proprionate groups exposed to solvent. The Fe^{2+} ion is coordinated to 4 N's on the 4 pyrrole rings, The 5th ligand is a supplied by proximal His (the 8th amino acid on helix F) of the protein. In the absence of dioxygen, the 6 ligand is missing. and the geometry of the complex is square pyramidal with the Fe above the plane of the heme ring. A distal His (E7) is on the opposite side of the heme ring, but too far to coordinate with the Fe. When dioxgen binds, it occupies the 6th coordination site and pulls the Fe into the plane of the ring, leading to octahedral geometry. CO, NO, and H_2S also bind to the 6th site, but with higher affinity than dioxygen, which can lead to CO poisoning. The distal His keeps these ligands (including dioxygen) bound in a bent, non-optimal geometry. This minimizes the chances of CO poisoning.

Myoglobin

- Myoglobin is a relatively small protein that contains 150 amino acids.
- Mb is extremely compact, and consists of 75% alpha helical structure.
- The interior amino acids are almost entirely nonpolar. The only polar amino acids found completely buried are the two His (proximal and distal) found at the active site of dioxygen binding.

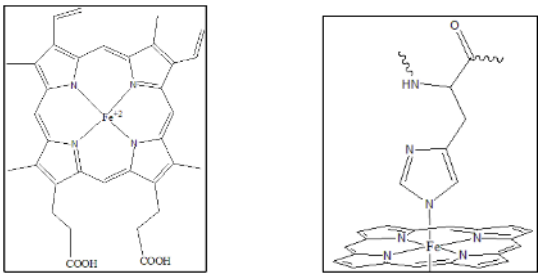


Figure 6.8.1.2. The skeletal structure of the heme prosthetic group found within the structure of myoglobin. The porphyrin ring contains four pyrrole nitrogens bound to a ferrous (Fe(II)) ion center. There are six coordination sites in the Fe(II) ion; four are occupied by the pyrrole nitrogens, one is occupied by a proximal histidine, one site can be occupied by a dioxygen molecule (not shown).

Difference between Hb and Mb

Hb is a tetramer of two α and two β subunits held together by IMF's (an example of quarternary protein structure), and 4 bound hemes, each of which can bind a dioxygen. In a fetus, two other subunits make up Hb (two zeta - ζand two epsilion - ε subunits - analogous to the two αand two β subunits, respectively). This changes in fetuses to two α and two γ subunits. Fetal Hb has higher affinity for dioxygen than adult Hb. Mb is a single polypeptide chains which has higher affinity for dioxygen than Hb.

The α and β chains are similar to Mb, which is unexpected since only 24 of 141 residues in the α and β chains of Hb are identical to amino acids in Mb. This suggests that different sequences can fold to similar structures. The globin fold of Mb and each chain of Hb is common to vertebrates and must be nature's design for dioxygen carriers. A comparison of the sequence of Hb from 60 species show much variability of amino acids, with only 9 identical amino founds. These must be important for structure/function. All internal changes are conservative (e.g. changing a nonpolar for a nonpolar amino acid). Not even Pro's are conserved, suggesting there are different ways to break helices. The two active site His are conserved, as is Gly B6 (required for a reverse turn).

This page titled 6.8.1: Myoglobin, Hemoglobin, and their Ligands is shared under a CC BY-NC-SA 4.0 license and was authored, remixed, and/or curated by Henry Jakubowski.

6.8.2: Oxygen Transport by the Proteins Myoglobin and Hemoglobin

Oxygen Transport

Many microorganisms and most animals obtain energy by respiration, the oxidation of organic or inorganic molecules by O_2. At 25°C, however, the concentration of dissolved oxygen in water in contact with air is only about 0.25 mM. Because of their high surface area-to-volume ratio, aerobic microorganisms can obtain enough oxygen for respiration by passive diffusion of O_2 through the cell membrane. As the size of an organism increases, however, its volume increases much more rapidly than its surface area, and the need for oxygen depends on its volume. Consequently, as a multicellular organism grows larger, its need for O_2 rapidly outstrips the supply available through diffusion. Unless a transport system is available to provide an adequate supply of oxygen for the interior cells, organisms that contain more than a few cells cannot exist. In addition, O_2 is such a powerful oxidant that the oxidation reactions used to obtain metabolic energy must be carefully controlled to avoid releasing so much heat that the water in the cell boils. Consequently, in higher-level organisms, the respiratory apparatus is located in internal compartments called mitochondria, which are the power plants of a cell. Oxygen must therefore be transported not only to a cell but also to the proper compartment within a cell.

Myoglobin and Hemoglobin

Myoglobin is a relatively small protein that contains 150 amino acids. The functional unit of myoglobin is an **iron–porphyrin complex** that is embedded in the protein (Figure 4.2.1). In myoglobin, the heme iron is five-coordinate, with only a single histidine imidazole ligand from the protein (called the proximal histidine because it is near the iron) in addition to the four nitrogen atoms of the porphyrin. A second histidine imidazole (the distal histidine because it is more distant from the iron) is located on the other side of the heme group, too far from the iron to be bonded to it. Consequently, the iron atom has a vacant coordination site, which is where O_2 binds.

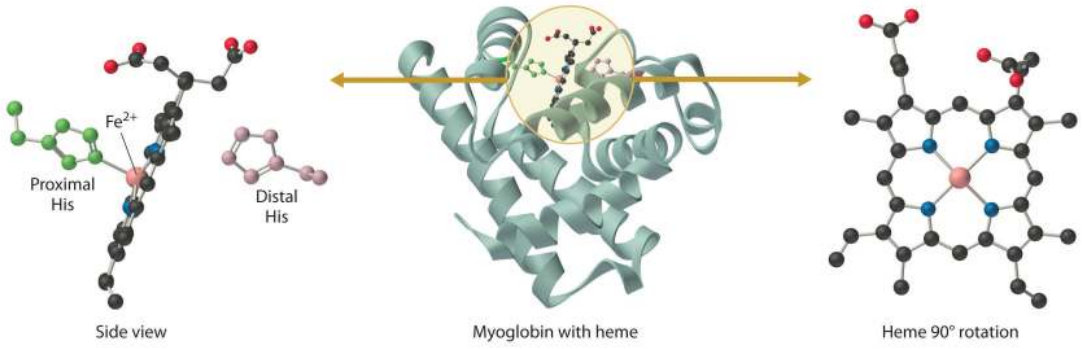


Figure 6.8.2.1. The Structure of Deoxymyoglobin, Showing the Heme Group. The iron in deoxymyoglobin is five-coordinate, with one histidine imidazole ligand from the protein. Oxygen binds at the vacant site on iron.

In the ferrous form (deoxymyoglobin), the iron is five-coordinate and high spin. Because high-spin Fe^{2+} is too large to fit into the "hole" in the center of the porphyrin, it is about 60 pm above the plane of the porphyrin. When O_2 binds to deoxymyoglobin to form oxymyoglobin, the iron is converted from five-coordinate (high spin) to six-coordinate (low spin; Figure 4.2.2). Because low-spin Fe^{2+} and Fe^{3+} are smaller than high-spin Fe^{2+}, the iron atom moves into the plane of the porphyrin ring to form an octahedral complex. The O_2 pressure at which half of the molecules in a solution of myoglobin are bound to O_2 ($P_{1/2}$) is about 1 mm Hg (1.3×10^{-3} atm).

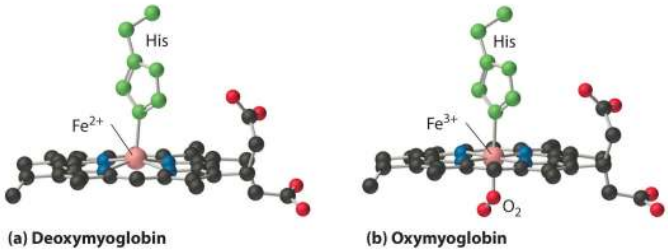


Figure 6.8.2.2. Oxygen Binding to Myoglobin and Hemoglobin. (a) The Fe^{2+} ion in deoxymyoglobin is high spin, which makes it too large to fit into the "hole" in the center of the porphyrin. (b) When O_2 binds to deoxymyoglobin, the iron is converted to low-spin Fe^{3+}, which is smaller, allowing the iron to move into the plane of the four nitrogen atoms of the porphyrin to form an octahedral complex.

Hemoglobin consists of two subunits of 141 amino acids and two subunits of 146 amino acids, both similar to myoglobin; it is called a tetramer because of its four subunits. Because hemoglobin has very different O_2-binding properties, however, it is not simply a "super myoglobin" that can carry four O_2 molecules simultaneously (one per heme group). The shape of the O_2-binding curve of myoglobin can be described mathematically by the following equilibrium:

$$MbO_2 \rightleftharpoons Mb + O_2 \tag{6.8.2.1}$$

$$K_{diss} = \frac{[Mb]\,[O_2]}{[MbO_2]} \tag{6.8.2.2}$$

The O_2-binding curve of hemoglobin is S shaped (Figure 4.2.3). As shown in the curves, at low oxygen pressures, the affinity of deoxyhemoglobin for O_2 is substantially lower than that of myoglobin, whereas at high O_2 pressures the two proteins have comparable O_2 affinities. The physiological consequences of unusual S-shaped O_2-binding curve of hemoglobin are enormous. In the lungs, where O_2 pressure is highest, the high oxygen affinity of deoxyhemoglobin allows it to be completely loaded with O_2, giving four O_2 molecules per hemoglobin. In the tissues, however, where the oxygen pressure is much lower, the decreased oxygen affinity of hemoglobin allows it to release O_2, resulting in a net transfer of oxygen to myoglobin.

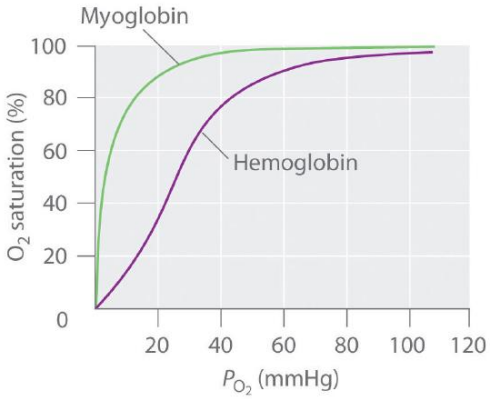


Figure 4.2.3: The O_2-Binding Curves of Myoglobin and Hemoglobin. Plots of Y (fractional saturation) vs L (pO2) are hyperbolic for Mb, but sigmoidal for Hb, suggesting cooperative binding of oxygen to Hb (binding of the first oxygen facilitates binding of second, etc).

The S-shaped O_2-binding curve of hemoglobin is due to a phenomenon called **cooperativity**, in which the affinity of one heme for O_2 depends on whether the other hemes are already bound to O_2. Cooperativity in hemoglobin requires an interaction between the four heme groups in the hemoglobin tetramer, even though they are more than 3000 pm apart, and depends on the change in structure of the heme group that occurs with oxygen binding. The structures of deoxyhemoglobin and oxyhemoglobin are slightly different, and as a result, deoxyhemoglobin has a much lower O_2 affinity than myoglobin, whereas the O_2 affinity of oxyhemoglobin is essentially identical to that of oxymyoglobin. Binding of the first two O_2 molecules to deoxyhemoglobin causes the overall structure of the protein to change to that of oxyhemoglobin; consequently, the last two heme groups have a much higher affinity for O_2 than the first two.

The affinity of Hb, but not of Mb, for dioxygen depends on pH. This is called the **Bohr effect**, after the father of Neils Bohr, who discovered it.

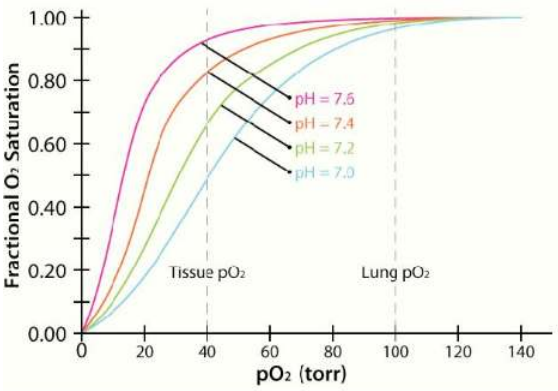


Figure 4.2.4: The Bohr Effect

Decreasing pH shifts the oxygen binding curves to the right (to decreased oxygen affinity). Increased [H^+] will cause protonation of basic side chains. In the pH range for the Bohr effect, the mostly likely side chain to get protonated is His (pKa around 6), which then becomes charged. The mostly likely candidate for protonation is His 146 (on the β chain - CH_3) which can then form a salt bridge with Asp 94 of the β(FG1) chain. This salt bridge stabilizes the positive charge on the His and raises its pKa compared to the oxyHb state. Carbon dioxide binds covalently to the N-terminus to form a negatively charge carbamate which forms a salt bridge with Arg 141 on the alpha chain. BPG, a strongly negatively charged ligand, binds in a pocket lined with Lys 82, His 2, and His 143 (all on the beta chain). It fits into a cavity present between the β subunits of the Hb tetramer in the T state. Notice all these allosteric effectors lead to the formation of more salt bridges which stabilize the T or deoxy state. The central cavity where BPG binds between the β subunits become much smaller on oxygen binding and the shift to the oxy or R state. Hence BPG is extruded from the cavity.

The binding of H^+ and CO_2 helps shift the equilibrium to deoxyHb which faciliates dumping of oxygen to the tissue. It is in respiring tissues that CO_2 and H^+ levels are high. CO_2 is produced from the oxidation of glucose through glycolysis and the Krebs cycle. In addition, high levels of CO_2 increase H^+ levels through the following equilibrium:

$$\mathbf{H_2O + CO_2 \rightleftharpoons H_2CO_3 \rightleftharpoons H^+ + HCO_3^-} \tag{6.8.2.3}$$

In addition, H^+ increases due to production of weak acids such as pyruvic acid in glycolysis .

Hb, by binding CO_2 and H^+, in addition to O_2, serves an additional function: it removes excess CO_2 and H^+ from the tissues where they build up. When deoxyHb with bound H^+ and CO_2 reaches the lungs, they leave as O_2 builds and deoxyHb is converted to oxyHb.

Contributors

Prof. Henry Jakubowski (College of St. Benedict/St. John's University)

Contributed by OpenStax, General Biology at OpenStax CNX

Dr. Kevin Ahern and Dr. Indira Rajagopal (Oregon State University)

6.8.2: Oxygen Transport by the Proteins Myoglobin and Hemoglobin is shared under a not declared license and was authored, remixed, and/or curated by LibreTexts.

Index

A

achiral
5.5.3: Stereoisomers - Optical Isomerism in Transition Metal Complexes
acidity
4.3: Acidity of the Hexaaqua Ions
active site
6.2: Introduction to Amino Acids and Proteins
ambidentate ligands
5.5.4: Structural Isomers - Linkage Isomerism in Transition Metal Complexes
amino acids
6.2: Introduction to Amino Acids and Proteins
ammine ligands
5.8: Ligand Exchange Reactions (Thermodynamics)
antibonding
2.5.5: Molecular Orbital Diagrams
aqua ligands
5.8: Ligand Exchange Reactions (Thermodynamics)
Associative Substitution
6.4: Associative Ligand Substitution

B

base peak
1.1: Mass Spectrometry
bent
2.3: The VSEPR Model
Berry pseudorotation
6.4: Associative Ligand Substitution
Bicapped square antiprism geometry
5.3: Coordination Numbers and Geometry
birefringence
3.14: Structures Related to NaCl and NiAs
Bohr Atom
1.2: Rutherford's Atom
Bohr model
1.2: Rutherford's Atom
bond angle
2.3: The VSEPR Model
bond order
2.5.5: Molecular Orbital Diagrams
bond polarity
2.5.1: Molecular Shape and Molecular Polarity
bonding molecular orbital
2.5.5: Molecular Orbital Diagrams
Bragg equation
3.9: X-ray Crystallography

C

Capped octahedron
5.3: Coordination Numbers and Geometry
Capped trigonal prism
5.3: Coordination Numbers and Geometry
chelate effect
5.8: Ligand Exchange Reactions (Thermodynamics)
Chemical Equivalence
2.8.2: Chemical Equivalence
chemical shift
2.8.5: The Basis for Differences in Chemical Shift
chiral
5.5.3: Stereoisomers - Optical Isomerism in Transition Metal Complexes
chiral center
5.5.3: Stereoisomers - Optical Isomerism in Transition Metal Complexes
Cis isomers
5.5.2: Structural Isomers - Geometric Isomerism in Transition Metal Complexes
complex ion
4.2: Lewis Acids and Bases
4.3: Acidity of the Hexaaqua Ions
compression
5.6.5: Jahn-Teller Distortions
conservative forces
1.2: Rutherford's Atom
coordinate compound
5.5.3: Stereoisomers - Optical Isomerism in Transition Metal Complexes
coordinate covalent bond
4.2: Lewis Acids and Bases
coordination complex
5.6.2: Colors of Coordination Complexes
coordination complexes
5.6.2: Colors of Coordination Complexes
Coordination Compounds
5.1: Introduction to Coordination Chemistry
coordination number
5.3: Coordination Numbers and Geometry
Coulombic force
1.2: Rutherford's Atom
crystal field splitting
5.6.3: Crystal Field Stabilization Energy
crystal field stabilization energy
5.6.3: Crystal Field Stabilization Energy
crystal field theory
5.6: Crystal Field Theory
5.6.2: Colors of Coordination Complexes
5.6.3: Crystal Field Stabilization Energy
6.5: Dissociative Ligand Substitution
Cube
5.3: Coordination Numbers and Geometry
Cube geometry
5.3: Coordination Numbers and Geometry
cuboctahedron geometry
5.3: Coordination Numbers and Geometry

D

Debye (unit)
2.5.1: Molecular Shape and Molecular Polarity
diamagnetic
2.5.5: Molecular Orbital Diagrams
diamagnetic anisotropy
2.8.5: The Basis for Differences in Chemical Shift
diamagnetic deshielding
2.8.5: The Basis for Differences in Chemical Shift
diamagnetic shielding
2.8.5: The Basis for Differences in Chemical Shift
dipole moment
2.3: The VSEPR Model
2.5.1: Molecular Shape and Molecular Polarity
Dissocative Substitution
6.5: Dissociative Ligand Substitution
dissociation
6.5: Dissociative Ligand Substitution
dissociation constant
4.2: Lewis Acids and Bases
Dissociative Ligand Substitution
6.5: Dissociative Ligand Substitution
Dodecahedron
5.3: Coordination Numbers and Geometry
Dodecahedron Geometry
5.3: Coordination Numbers and Geometry
Drago and Wayland's EC Model
4.5: Quantitative Measures of Hardness and Softness

E

electromagnetic spectrum
5.6.2: Colors of Coordination Complexes
electron ionization
1.1: Mass Spectrometry
electronegativity (Mulliken)
4.5: Quantitative Measures of Hardness and Softness
Electronic Configurations
5.6.5: Jahn-Teller Distortions
Electrospray Ionization
1.1: Mass Spectrometry
elongation
5.6.5: Jahn-Teller Distortions
enzymes
6.2: Introduction to Amino Acids and Proteins

F

fluorite (structure)
3.15: Tetrahedral Structures
formation constant
4.2: Lewis Acids and Bases
Formation Constants
5.8: Ligand Exchange Reactions (Thermodynamics)

G

geometric isomers
5.5.2: Structural Isomers - Geometric Isomerism in Transition Metal Complexes

H

Hexaaqua Ions
4.3: Acidity of the Hexaaqua Ions
Hexagonal bipyramid
5.3: Coordination Numbers and Geometry
Hexagonal bipyramid geometry
5.3: Coordination Numbers and Geometry
Hexagonal planar Geometry
5.3: Coordination Numbers and Geometry
high spin
5.6.3: Crystal Field Stabilization Energy
5.6.5: Jahn-Teller Distortions

hybrid orbital
2.4: Hybrid Orbitals
hybridization
2.4: Hybrid Orbitals
hydrate isomer
5.5.1: Structural Isomers - Ionization Isomerism in Transition Metal Complexes
hydration
5.6.3: Crystal Field Stabilization Energy

I
ionic radius
4.3: Acidity of the Hexaaqua Ions
ionization isomerism
5.5.1: Structural Isomers - Ionization Isomerism in Transition Metal Complexes
isomerism
5.5.4: Structural Isomers - Linkage Isomerism in Transition Metal Complexes
isomers
5.5: Isomers
5.5.2: Structural Isomers - Geometric Isomerism in Transition Metal Complexes

K
Kapustinskii equation
3.23: Kapustinskii Equation

L
Lancashire
5.3: Coordination Numbers and Geometry
5.6.5: Jahn-Teller Distortions
Lenz's Law
5.6.7: Magnetism
Lewis acid
4.2: Lewis Acids and Bases
Lewis base
4.2: Lewis Acids and Bases
ligand
4.2: Lewis Acids and Bases
6.4: Associative Ligand Substitution
6.5: Dissociative Ligand Substitution
Ligand Exchange Reactions
5.8: Ligand Exchange Reactions (Thermodynamics)
linear
2.3: The VSEPR Model
low spin
5.6.3: Crystal Field Stabilization Energy
5.6.5: Jahn-Teller Distortions

M
M+1 peak (mass spec)
1.1: Mass Spectrometry
M+2 peak (mass spec)
1.1: Mass Spectrometry
Magnetic Moment
2.8.1: The Origin of the NMR Signal
magnetic moments
5.6.6: Magnetic Moments of Transition Metals
magnetic permeability
5.6.7: Magnetism
magnetism
5.6.7: Magnetism
mass spectrometry
1.1: Mass Spectrometry
McLafferty rearrangement
1.1: Mass Spectrometry
metallic bonding
2.6: The Range of Bonding
miller indicies
3.10: Miller Indices (hkl)
Mirror Image Method
5.5.3: Stereoisomers - Optical Isomerism in Transition Metal Complexes
molecular geometry
2.2: Molecular Shapes
molecular ion peak
1.1: Mass Spectrometry
molecular ions
1.1: Mass Spectrometry
molecular orbital
2.5.5: Molecular Orbital Diagrams
Molecular orbital diagram
2.5.5: Molecular Orbital Diagrams

N
NMR
2.8.1: The Origin of the NMR Signal
2.8.2: Chemical Equivalence
2.8.3: The 1H-NMR experiment
2.8.4: Spin-Spin Coupling
2.8.5: The Basis for Differences in Chemical Shift

O
octahedral
2.3: The VSEPR Model
5.3: Coordination Numbers and Geometry
Octahedral Preference
5.6.3: Crystal Field Stabilization Energy
Octahedral Site Preference Energy
5.6.3: Crystal Field Stabilization Energy
Optical Isomers
5.5.3: Stereoisomers - Optical Isomerism in Transition Metal Complexes
optical isomers (complex ions)
5.5.3: Stereoisomers - Optical Isomerism in Transition Metal Complexes
organometallic
6.4: Associative Ligand Substitution

P
paramagnetic
2.5.5: Molecular Orbital Diagrams
parent peak
1.1: Mass Spectrometry
Pearson's absolute hardness
4.5: Quantitative Measures of Hardness and Softness
Pentagonal Bipyramid
5.3: Coordination Numbers and Geometry
Peptide bond
6.2: Introduction to Amino Acids and Proteins
Plane of Symmetry Method
5.5.3: Stereoisomers - Optical Isomerism in Transition Metal Complexes
polar covalent bond
2.5.1: Molecular Shape and Molecular Polarity
polarimeter
5.5.3: Stereoisomers - Optical Isomerism in Transition Metal Complexes
Polarimetry
5.5.3: Stereoisomers - Optical Isomerism in Transition Metal Complexes
Pourbaix diagrams
6.3.6: Pourbaix Diagrams
proteins
6.2: Introduction to Amino Acids and Proteins
proteomics
1.1: Mass Spectrometry

R
radical cation
1.1: Mass Spectrometry
radius
4.3: Acidity of the Hexaaqua Ions
rate law
6.4: Associative Ligand Substitution
reaction kinetics
6.4: Associative Ligand Substitution
6.5: Dissociative Ligand Substitution

S
seesaw
2.3: The VSEPR Model
soft ionization
1.1: Mass Spectrometry
solvents
2.8.3: The 1H-NMR experiment
sp hybrid orbital
2.4: Hybrid Orbitals
sp2 hybrid orbital
2.4: Hybrid Orbitals
sp3 hybrid orbital
2.4: Hybrid Orbitals
sp3d hybrid orbital
2.4: Hybrid Orbitals
sp3d2 hybrid orbital
2.4: Hybrid Orbitals
spectrochemical series
5.6.2: Colors of Coordination Complexes
spectroscopy
2.8.1: The Origin of the NMR Signal
2.8.2: Chemical Equivalence
2.8.3: The 1H-NMR experiment
2.8.4: Spin-Spin Coupling
2.8.5: The Basis for Differences in Chemical Shift
spin pairing energy
5.6.3: Crystal Field Stabilization Energy
Square antiprism
5.3: Coordination Numbers and Geometry
Square antiprism geometry
5.3: Coordination Numbers and Geometry
Square Planar Geometry
5.3: Coordination Numbers and Geometry

Square pyramid Geometry
5.3: Coordination Numbers and Geometry
square pyramidal
2.3: The VSEPR Model
Stability Constants
5.8: Ligand Exchange Reactions (Thermodynamics)
steady state approximation
6.5: Dissociative Ligand Substitution
stereochemistry
6.4: Associative Ligand Substitution
6.5: Dissociative Ligand Substitution
stereoisomers
5.5: Isomers
structural isomers
5.5: Isomers
5.5.4: Structural Isomers - Linkage Isomerism in Transition Metal Complexes
substitution
6.4: Associative Ligand Substitution
substrate
6.2: Introduction to Amino Acids and Proteins
symmetry elements
2.7.1: Symmetry Elements and Operations
symmetry operations
2.7.1: Symmetry Elements and Operations

T

tetrahedral
2.2: Molecular Shapes
2.3: The VSEPR Model
tetrahedral geometry
5.3: Coordination Numbers and Geometry
thermodynamics
5.8: Ligand Exchange Reactions (Thermodynamics)
Trans Isomers
5.5.2: Structural Isomers - Geometric Isomerism in Transition Metal Complexes
Transition Metal Complexes
5.5.1: Structural Isomers - Ionization Isomerism in Transition Metal Complexes
5.5.2: Structural Isomers - Geometric Isomerism in Transition Metal Complexes
5.5.4: Structural Isomers - Linkage Isomerism in Transition Metal Complexes
Trigonal Bipyramid Geometry
5.3: Coordination Numbers and Geometry
trigonal bipyramidal
2.3: The VSEPR Model
trigonal planar
2.3: The VSEPR Model
Trigonal planar Geometry
5.3: Coordination Numbers and Geometry
Trigonal prism Geometry
5.3: Coordination Numbers and Geometry
Trigonal pyramid Geometry
5.3: Coordination Numbers and Geometry
trigonal pyramidal
2.3: The VSEPR Model

U

Unsaturated Intermediate
6.5: Dissociative Ligand Substitution

V

valence bond theory
2.4: Hybrid Orbitals
valence shell electron pair repulsion theory
2.3: The VSEPR Model
VSEPR
2.3: The VSEPR Model

Glossary

Sample Word 1 | Sample Definition 1

Glossary

Sample Word 1 | Sample Definition 1

Detailed Licensing

Overview

Title: CHEM 211: Foundational Inorganic Chemistry (Nataro)

Webpages: 121

Applicable Restrictions: Noncommercial

All licenses found:

- Undeclared: 60.3% (73 pages)
- CC BY-SA 4.0: 25.6% (31 pages)
- CC BY-NC-SA 4.0: 11.6% (14 pages)
- CC BY-NC 4.0: 1.7% (2 pages)
- CC BY 4.0: 0.8% (1 page)

By Page

- CHEM 211: Foundational Inorganic Chemistry (Nataro) - *Undeclared*
  - Front Matter - *Undeclared*
    - TitlePage - *Undeclared*
    - InfoPage - *Undeclared*
    - Table of Contents - *Undeclared*
    - Licensing - *Undeclared*
  - 1: Atoms - *Undeclared*
    - 1.1: Mass Spectrometry - *CC BY-NC-SA 4.0*
    - 1.2: Rutherford's Atom - *Undeclared*
    - 1.3: Bohr's Atom - *Undeclared*
    - 1.4: Hydrogen Atom - *Undeclared*
    - 1.5: Slater Rules - *Undeclared*
  - 2: Molecules - *Undeclared*
    - 2.2: Molecular Shapes - *CC BY-NC-SA 4.0*
    - 2.3: The VSEPR Model - *CC BY-NC-SA 4.0*
    - 2.4: Hybrid Orbitals - *CC BY-NC-SA 4.0*
    - 2.5: Molecular Orbitals - *Undeclared*
      - 2.5.1: Molecular Shape and Molecular Polarity - *CC BY-NC-SA 4.0*
      - 2.5.2: Prelude to Molecular Orbital Theory - *Undeclared*
      - 2.5.3: Constructing Molecular Orbitals from Atomic Orbitals - *CC BY-SA 4.0*
      - 2.5.4: Orbital Symmetry - *CC BY-SA 4.0*
      - 2.5.5: Molecular Orbital Diagrams - *CC BY-SA 4.0*
      - 2.5.6: π Orbitals and Diatomic Molecules - *CC BY-SA 4.0*
      - 2.5.7: Orbital Filling - *CC BY-SA 4.0*
      - 2.5.8: δ orbitals - *CC BY-SA 4.0*
    - 2.6: The Range of Bonding - *CC BY-SA 4.0*
    - 2.7: Advanced Bonding - *Undeclared*
      - 2.7.1: Symmetry Elements and Operations - *Undeclared*
      - 2.7.2: Point Groups - *Undeclared*
        - 2.7.2.1: Other Groups - *Undeclared*
        - 2.7.2.2: Groups of Low and High Symmetry - *Undeclared*
      - 2.7.3: Ligand Group Orbitals and Generator Functions - *Undeclared*
      - 2.7.4: Expanded Octets and Molecular Orbitals - *Undeclared*
    - 2.8: Nuclear Magnetic Resonance (NMR) - *Undeclared*
      - 2.8.1: The Origin of the NMR Signal - *CC BY-NC-SA 4.0*
      - 2.8.2: Chemical Equivalence - *CC BY-NC-SA 4.0*
      - 2.8.3: The 1H-NMR experiment - *CC BY-NC-SA 4.0*
      - 2.8.4: Spin-Spin Coupling - *CC BY-NC-SA 4.0*
      - 2.8.5: The Basis for Differences in Chemical Shift - *CC BY-NC-SA 4.0*
    - Back Matter - *Undeclared*
      - Index - *Undeclared*
      - Glossary - *Undeclared*
      - Detailed Licensing - *Undeclared*
  - 3: Solid state - *Undeclared*
    - 3.1: Prelude to Metals and Alloys - *Undeclared*
    - 3.2: Unit Cells and Crystal Structures - *CC BY-SA 4.0*
    - 3.3: Crystal Structures of Metals - *CC BY-SA 4.0*
    - 3.4: Conduction in Metals - *CC BY-SA 4.0*
    - 3.5: Atomic Orbitals and Magnetism - *CC BY-SA 4.0*

- 3.6: Ferro-, Ferri- and Antiferromagnetism - *CC BY-SA 4.0*
- 3.7: Hard and Soft Magnets - *CC BY-SA 4.0*
- 3.8: Defects in Metallic Crystals - *CC BY-SA 4.0*
- 3.9: X-ray Crystallography - *Undeclared*
- 3.10: Miller Indices (hkl) - *Undeclared*
- 3.11: Powder X-ray Diffraction - *Undeclared*
- 3.12: Prelude to Ionic and Covalent Solids - Structures - *Undeclared*
- 3.13: Close-packing and Interstitial Sites - *CC BY-SA 4.0*
- 3.14: Structures Related to NaCl and NiAs - *CC BY-SA 4.0*
- 3.15: Tetrahedral Structures - *CC BY-SA 4.0*
- 3.16: Layered Structures and Intercalation Reactions - *CC BY-SA 4.0*
- 3.17: Ionic Radii and Radius Ratios - *CC BY-SA 4.0*
- 3.18: Structure Maps - *CC BY-SA 4.0*
- 3.19: Energetics of Crystalline Solids- The Ionic Model - *CC BY-SA 4.0*
- 3.20: Born-Haber Cycles for NaCl and Silver Halides - *CC BY-SA 4.0*
- 3.21: Lattice Energies and Solubility - *CC BY-SA 4.0*
- 3.22: Spinel, Perovskite, and Rutile Structures - *CC BY-SA 4.0*
- 3.23: Kapustinskii Equation - *CC BY-SA 4.0*

4: Acid-Base Theories - *Undeclared*

- 4.1: Bronsted-Lowry acids and bases - *Undeclared*
- 4.2: Lewis Acids and Bases - *CC BY 4.0*
- 4.3: Acidity of the Hexaaqua Ions - *CC BY-NC 4.0*
- 4.4: Hard-soft Acids and Bases - *Undeclared*
- 4.5: Quantitative Measures of Hardness and Softness - *Undeclared*

5: Coordination Chemistry - *Undeclared*

- 5.1: Introduction to Coordination Chemistry - *Undeclared*
- 5.2: Ligands and Nomenclature - *Undeclared*
- 5.3: Coordination Numbers and Geometry - *Undeclared*
- 5.4: Bonding with d-orbitals - *CC BY-SA 4.0*
- 5.5: Isomers - *Undeclared*
  - 5.5.1: Structural Isomers - Ionization Isomerism in Transition Metal Complexes - *Undeclared*
  - 5.5.2: Structural Isomers - Geometric Isomerism in Transition Metal Complexes - *Undeclared*
  - 5.5.3: Stereoisomers - Optical Isomerism in Transition Metal Complexes - *Undeclared*
  - 5.5.4: Structural Isomers - Linkage Isomerism in Transition Metal Complexes - *Undeclared*
- 5.6: Crystal Field Theory - *Undeclared*
  - 5.6.1: Crystal Field Theory - *CC BY-NC-SA 4.0*
  - 5.6.2: Colors of Coordination Complexes - *Undeclared*
  - 5.6.3: Crystal Field Stabilization Energy - *Undeclared*
  - 5.6.4: Factors That Affect the Magnitude of Δo - *Undeclared*
  - 5.6.5: Jahn-Teller Distortions - *Undeclared*
  - 5.6.6: Magnetic Moments of Transition Metals - *Undeclared*
  - 5.6.7: Magnetism - *Undeclared*
  - 5.6.8: Thermodynamics and Structural Consequences of d-Orbital Splitting - *CC BY-NC-SA 4.0*
- 5.7: Ligand Field Theory - *Undeclared*
- 5.8: Ligand Exchange Reactions (Thermodynamics) - *CC BY-NC 4.0*
- 5.9: Electronic Spectra of Coordination Compounds - *Undeclared*

6: Bioinorganic Chemistry - *Undeclared*

- 6.1: Biological Significance of Iron, Zinc, Copper, Molybdenum, Cobalt, Chromium, Vanadium, and Nickel - *Undeclared*
- 6.2: Introduction to Amino Acids and Proteins - *CC BY-NC-SA 4.0*
- 6.3: Redox Reactions - *Undeclared*
  - 6.3.1: Introduction to Redox Reactions - *CC BY-SA 4.0*
  - 6.3.2: Balancing Redox Reactions - *CC BY-SA 4.0*
  - 6.3.3: Electrochemical Potentials - *CC BY-SA 4.0*
  - 6.3.4: Prelude to Redox Stability and Redox Reactions - *Undeclared*
  - 6.3.5: Latimer and Frost Diagrams - *CC BY-SA 4.0*
  - 6.3.6: Pourbaix Diagrams - *CC BY-SA 4.0*
- 6.4: Associative Ligand Substitution - *Undeclared*
- 6.5: Dissociative Ligand Substitution - *Undeclared*
- 6.6: Biological Significance of Iron, Zinc, Copper, Molybdenum, Cobalt, Chromium, Vanadium, and Nickel - *Undeclared*
- 6.7: Ferrodoxins, Hydrogenases, and Nitrogenases - Metal-Sulfide Proteins - *Undeclared*
  - 6.7.1: Iron-sulfur Proteins and Models - *Undeclared*
  - 6.7.2: Iron-sulfur Proteins and Models (Part 2) - *Undeclared*
  - 6.7.3: Iron-sulfur Proteins and Models (Part 3) - *Undeclared*

- 6.7.4: Iron-sulfur Proteins and Models (Part 4) - *Undeclared*
- 6.8: Overview of Hemoglobin and Myoglobin - *Undeclared*
  - 6.8.1: Myoglobin, Hemoglobin, and their Ligands - *CC BY-NC-SA 4.0*
  - 6.8.2: Oxygen Transport by the Proteins Myoglobin and Hemoglobin - *Undeclared*
- Back Matter - *Undeclared*
  - Index - *Undeclared*
  - Glossary - *Undeclared*
  - Glossary - *Undeclared*
  - Detailed Licensing - *Undeclared*